NEW ZEALAND GEOTECHNICAL SOCIETY INC
www.nzgs.org

AUSTRALIAN GEOMECHANICS SOCIETY

14TH AUSTRALIA & NEW ZEALAND YOUNG GEOTECHNICAL PROFESSIONALS CONFERENCE

2ND – 5TH NOVEMBER 2022
ROTORUA, NEW ZEALAND

CONFERENCE PROCEEDINGS

THANK YOU TO OUR SPONSORS

PLATINUM SPONSOR

Stantec

GOLD SPONSOR

Beca

SILVER SPONSORS

GRIFFITHS DRILLING
RESULT DRIVEN GEOTECHNICAL SPECIALISTS

ENGEO

BRONZE SPONSORS

GEOBRUGG®
BRUGG
Safety is our nature

PERRY
GEOTECH

RILEY

pdp

SEEQUENT

EXHIBITORS

GEOTECHNICS

14TH AUSTRALIA AND NEW ZEALAND YOUNG GEOTECHNICAL PROFESSIONALS CONFERENCE

14YGPC
Rotorua, New Zealand, November 2022

ORGANISING COMMITTEE

Helen Loach	NZGS YGP / WSP	New Zealand
Sarah Barrett	Beca	New Zealand
Nima Taghipouran	WSP	New Zealand
Hannah Hadley	Terrane	New Zealand
Christoph Kraus	Beca	New Zealand
Nicola Manche	WSP Golder	Australia

MENTORS

Jen Smith	NZGS Treasurer / Tonkin + Taylor	New Zealand
Philip Robins	NZGS Past Chair / Beca	New Zealand
Darren Paul	AGS Past Chair / WSP Golder	Australia
Nina Levy	AGS Past Chair / Fugro	Australia
Brad Scott	GNS Science	New Zealand

TECHNICAL REVIEWERS

The 14YGPC Organising Committee would like to thank the following reviewers for the arduous task of undertaking reviews of papers presented at this Conference.

Geoffrey Farquhar	**Grant Maxwell**	**Ann Williams**	**Richard Young**
Andy Mott	**Joanna Petheram**	**Merrick Taylor**	**Brabha Brabhaharan**
Ayoub Ryman	**Mark Thomas**	**Phil Robins**	**Anna Punt**
Clauria Kayser	**Robert Hillier**	**Latasha Templeton**	**Neil Chaters**
Sally Hargraves	**Sam Glue**	**Jan Jupec**	**Paul Horrey**
Dora Avanidou	**Pedro Martins**	**Max Ervin**	**Klaus Thoeni**
David Airey	**Burt Look**	**Bindimadhava Aery**	**Vipman Tandjiria**
Mogana Z Sundaram	**Adam Kemp**	**Chaminda Gallage**	**Glen Burton**
Peter Fennell	**Rick Piovesan**	**Adrian Smith**	**Ian Shipway**
Stuart Masterson	**Mason Crumpton**	**Kam Choy Chew**	**Colin Mazengarb**
Mark Orr	**Ian Johnston**		

PUBLISHED BY:

New Zealand Geotechnical Society Inc.

WELCOME FROM 14YGPC ORGANISING COMMITTEE

The organising committee are delighted to welcome you to the 14th Australia and New Zealand (ANZ) Young Geotechnical Professionals Conference which is being held at the Millenium Hotel, Rotorua from 2nd to 5th November 2022. This is the first ANZ YGP conference following the global Covid19 pandemic, and we can't wait to reignite what has become a time honoured and traditional event for both the AGS and NZGS. Held every 2 years, the Young Geotechnical Professional Conference (YGPC) events are unique 3 day conferences facilitated by a joint initiative of Australian Geomechanics Society (AGS) and New Zealand Geotechnical Society.

The aim of the 14YGPC is to provide younger professionals both in industry and academia experience in technical paper preparation and conference presentation. We hope delegates not only gain technical knowledge but confidence in presenting, form new connections and enjoy the process. Presenting at this conference is the culmination of many months of paper preparation and peer review by senior professionals. Conference attendance is limited to only presenting authors with what is likely to be their first technical paper to their peers and a panel of senior industry professionals. It is important to note that 98 abstracts were received. Unfortunately, only 43 of them are accepted due to the limitation of the single-session conference and the desire to keep the audience small. The acceptance ratio is 44% and many of the rejected abstracts are very high quality.

We are pleased to have Nina Levy (Fugro & former AGS National Chair), Darren Paul (WSP Golder & former AGS National Chair), Phillip Robins (Beca & NZGS Past Chair) and Jen Smith (Tonkin and Taylor & NZGS Treasurer) as our senior industry mentoring panel. This panel not only has vast technical knowledge but also provides a direct link between the Young Professionals and both Trans-Tasman learned societies. We hope that delegates not only gain professional development but also learn more about the AGS and NZGS and the work they do to promote and advocate for our industry.

YGP events also include a field trip into the surrounding Rotorua region, and we are thrilled to have the assistance of Brad Scott (GNS New Zealand) to provide what will no doubt be an interesting, informative and entertaining commentary on the local geothermal and geological features of the area. No conference is complete without a number of social events to encourage interaction between the delegates, and this conference is no exception. We look forward to showcasing Rotorua during these events.

We wish to acknowledge the financial support provided by the Sponsors of this conference. Without their support and assistance this event could not occur and we thank each and every one of these organisations. We also thank the peer reviewers who gave their time and technical expertise to provide thorough and supportive reviews of the papers. Finally, I wish to acknowledge the hard work and commitment of the organising committee and guidance of both AGS and NZGS national steering committees. Without their efforts and the support of their respective home organisations this conference would not be possible.

Welcome to Rotorua, relax and most importantly enjoy the events and happenings planned in the next few days. I hope the 14YGPC provides an enjoyable and informative event aimed at the development of future leaders in the geotechnical profession.

Helen Loach
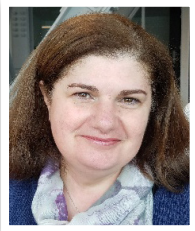14YGPC2022 Rotorua Organising Committee Chair / NZGS Young Geotechnical Professionals Representative

WELCOME FROM THE NZGS NATIONAL CHAIR

Welcome to the 14th Australia – New Zealand Young Geotechnical Professionals Conference 2022, in Rotorua, New Zealand (ANZ, YGP 2022). We are particularly happy to host the Conference in New Zealand this year, the first ANZ YGP after all the COVID disruptions of the last couple of years. I believe our industry and our communities are coming out of this adventure wiser and stronger, but I certainly hope that we will not experience enforced cancellations of our valued and enjoyable get-togethers ever again and for any reason.

The ANZ YGP Conference has a long history. The first was held in 1994 in Sydney, and since then the two Societies, AGS and NZGS, are collaborating to hold the two-yearly event seamlessly, recognising its value but also responding to the ongoing enthusiasm and strong support from the emerging geotechnical professionals in both countries. This Conference provides the unique opportunity for our younger colleagues to experience an international standard event, but in a familiar and supporting environment. The value of its format has been testified by many who attended in the past, including the current AGS Chair David Lacey, as noted in his introductory note.

The AGS and the NZGS are proud of their Young Geotechnical Groups. In New Zealand, the YGP Group is one of the most active of the NZGS. Their activities include the regional YGP Symposia throughout New Zealand every year, consistent representation in our local branches, initiatives for developing training material for YGPs and their international liaisons. Our YGP Groups make us confident that there is a bright future for the geotechnical profession "Down Under".

A large number of high-quality abstracts were submitted again this year, making the final selection of papers difficult for the organising committee. The proceedings include a fine selection of reference papers, spanning from project case histories from Australia, New Zealand and overseas, to research, thought-provoking pieces, and innovation.

I cannot thank enough our organising committee, Helen, Sarah, Christoph, Nima, Nicola and Hannah for their hard work bringing this event to reality. The Committee selected Rotorua for the Conference, known for its fascinating geology, bubbling mud pools, shooting geysers and abundant Māori history and culture. The Committee has put together a fantastic program of technical sessions, networking opportunities and social events, concluding the 3-day experience with an exciting field trip to explore the geothermal wonders of Rotorua.

I am grateful to our mentors Nina Levy and Darren Paul from AGS and Jen Smith and Philip Robins from NZGS, and to our Technical Reviewers. It is the mentorship and support of the experienced professionals from both countries that make this Conference unique. Also, my sincere appreciation to our sponsors, who kindly provided their support. Last, but not least, my warmest thanks to the AGS for our close collaboration once again this year on this event, and beyond. I am sure this wonderful team of people will continue working together for the best in our profession.

Eleni Gkeli,
Chair, New Zealand Geotechnical Society
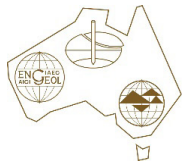
AUSTRALIAN GEOMECHANICS SOCIETY

WELCOME FROM THE AGS NATIONAL CHAIR

On behalf of the Australian Geomechanics Society (AGS) I am delighted to welcome you to the 14th edition of the co-branded AGS and NZGS' Young Geotechnical Professionals Conference (YGPC). The commencement of 14YGPC is especially heart-warming due to the repeated delay and eventual cancellation of 13YGPC event due to COVID-19 restrictions.

The ongoing ANZ YGPC series is, in my opinion, an outstanding example of how industry based technical societies can engage with early(ish) career geomechanics practitioners and provide an environment for both the dissemination of technical knowledge and networking between professionals that are at similar stages of their career. As a previous attendee at an ANZ YGPC event (9YGPC), I can personally attest to the professional relationships that are formed at these events can have enduring longevity – especially to continue to interact with colleagues that I would not otherwise get the collaborate with on a regular basis due to geographical constraints or slightly different focus' within the shared geomechanics community.

The YGPC events continue to be unique within the annual offering of the AGS, in that they are immersive environments where the participants are all required to make a significant contribution to the event. The absence of the presenter–attendee scenario common to most traditional conference events typically results in a 3-day experience in which all attendees can appropriately feel that they are all providing an equal contribution to the event. Based upon your varied backgrounds and career-to-date experiences, I have no doubt that by the conclusion of the conference you will all agree the YGPC model is a great example of how your active involvement within a professional society's community can widen your perception of the scope of the 'geomechanics' or 'geotechnical engineering' industries. I also hope the varied topics on which the presentations will ignite conversations that extend into the associated social events.

The AGS would like to thank the NZGS for taking on the hosting duties for the 14YGPC, and we are honoured to have been invited to provide two of the four members of the mentoring panel. Similarly, I would like to thank the Technical Reviewer team for their fundamental contribution to the conference and these excellent proceedings.

I would also like to personally thank Helen, Sarah, Nima, Hannah, Christoph and Nicola for working so diligently to organise this quality event. It is worth noting that, similar to the YGPC delegates whom are effectively preparing and presenting their first technical and peer-reviewed paper, it is traditional that these events represent the first exposure to conference event organisation for each YGPC's organising committee!

I sincerely wish you all the best for the conference and that you enjoy your time in Rotorua! Like the YGP conferences which have gone before, I hope that this event will be a memorable experience for all who attend.

David Lacey
National Chair, Australian Geomechanics Society

MENTORS
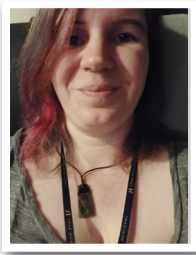
JEN SMITH
NZGS Treasurer and Vice Chair / Tonkin + Taylor

Jen is a Geotechnical Engineer working for Tonkin + Taylor and has worked in NZ since 2017, and prior to this worked in the UK. Jen is a Discipline Manager at T+T for the Auckland office, works in the natural hazards space and with local councils. Jen has been on the NZGS committee since 2019. In their role as Vice Chair, Jen is overseeing MBIE changes to occupational regulation as well as supporting the Chair with wider tasks and duties, and of course managing the NZGS finances and budget as Treasurer. Jen's current work has them working between Auckland and Nelson to coordinate the EQC and insurance response for T+T around the August storm event in Nelson and Marlborough.

In their free time, Jen plays the drums and loves doing creative things like quilting, leatherwork, and candle making.

PHILIP ROBINS
NZGS Past Chair / Beca

Philip is an acknowledged specialist in geotechnical engineering, high-seismicity engineering and design development, and is recognised by his peers as a Fellow of Engineering New Zealand. Trained as a civil engineer with a broad range of experience, locally and internationally, Philip has mixed his engineering skills with strong leadership in project delivery while developing key client relationships. Philip has experience in investigations, synthesis and analysis, slope stability, earthquake engineering, ground improvement works and detailed design and construction for large infrastructure projects.

Philip was the geotechnical team lead for the design and construction of the Mackays to Peka Peka (M2PP) Expressway project delivered through an alliance. The M2PP project includes 15 road bridges and several pedestrian bridges and has provided many geotechnical challenges due to the extent of peat and liquefiable ground. All bridges on the project required extensive ground improvements to cater for liquefaction to control ground

displacements at the bridge abutments. As part of M2PP Expressway Project, Philip also led the design and delivery of the Te Kākākura Retaining Wall, a 11m high split retaining wall which was recently awarded a 2017 Concrete Landscape Award Commendation in recognition of "a landscape project outstanding achievement in the advancement of concrete practice in design, construction, rehabilitation or research".

Philip was awarded a Bachelor of Engineering (Civil) from the University of Natal, Durban in 1990 and a Master of Sciences in Geotechnical Engineering from the University of California, Davis in 2000. He is a Chartered Member of Engineering New Zealand and Chartered Professional Engineer (CPEng) with Engineers Australia. Philip was Chair of the New Zealand Geotechnical Society from 2009 to 2010 and led the Technical subcommittee for the NZGS Symposium 2020, held in Dunedin May 2021. Philip has recently concluded his term as Vice President – Australasia on the Board of International Society of Soil Mechanics and Geotechncial Engineering (ISSMGE).

Philip has recently moved to Palmerston North with his family and enjoys walking to work.

NINA LEVY
AGS Past Chair / Fugro

Nina Levy is the immediate past chair of the AGS (2020 – 2021), having been involved with AGS committees for more than 15 years at a state (WA) and national level. Nina completed her undergraduate degrees (Engineering and Mathematics) at the University of Western Australia as well as a PhD in Geotechnical Engineering at the same institution. She has worked in Australia and the UK as a geotechnical engineer for more than 20 years, on a range of infrastructure and resources projects. Nina joined Fugro (formerly Advanced Geomechanics) 12 years ago and after spending more than 10 years working in the field of offshore geotechnics she is now the Service Line Manager for Marine Geotechnical and Geophysical Survey.

Nina lives in Perth with her family, where life is busy with sports and other activities. She is enjoying being able to travel again both for leisure and for Fugro and AGS business.

MENTORS

DARREN PAUL
**AGS Past Chair /
WSP Golder**

Darren is Technical Director of Engineering Geology at WSP Golder in Melbourne. He holds a Bachelor of Civil Engineering and Bachelor of Science in Geology, a combination which took him into the fields of geotechnical engineering and engineering geology. He also has an MSc in Engineering Geology from Imperial College London.

Darren's professional interests are in ground model development, the identification, assessment and management of geological uncertainty, landslide risk assessment and terrain evaluation. He has worked on many notable projects in Melbourne including the Burnley Tunnel, Eureka Tower, the Melbourne Metro Project and currently North East Link. He has also worked on large projects in Africa, the Middle East and PNG. In 2008 Darren was awarded the Young Professional Engineer Award for Victoria and in 2010 was awarded The Richard Wolters Prize from the IAEG. He was chair of the 2022 International Young Geotechnical Engineers Conference held in Sydney.

Outside of engineering geology, Darren was in the army reserve for 12 years and is currently an officer of army cadets. He enjoys travelling and getting outdoors with his wife and three young boys.

BRAD SCOTT
Volcanologist / GNS

Brad is a volcanologist with over 40 years' experience in monitoring, assessing and communicating on active volcanoes, geothermal systems and earthquake activity. During his career, Brad has been involved in a wide range of geological and geophysical investigations mostly involving monitoring, hazard assessment, rapid event response and communications. From 1992 to 2012, he took the lead role in coordination of volcano surveillance in New Zealand and since then has worked as a hazards and communications specialist for the GeoNet project.

PREVIOUS ANZ YOUNG GEOTECHNICAL PROFESSIONALS CONFERENCES

- 1st ANZ Young Geotechnical Professionals Conference, Sydney, Australia, 1994
- 2nd ANZ Young Geotechnical Professionals Conference, Auckland, New Zealand, 1995
- 3rd ANZ Young Geotechnical Professionals Conference, Melbourne, Australia, 1998
- 4th ANZ Young Geotechnical Professionals Conference, Perth, Australia, 2000
- 5th ANZ Young Geotechnical Professionals Conference, Rotorua, New Zealand, 2002
- 6th ANZ Young Geotechnical Professionals Conference, Gold Coast, Australia, 2004
- 7th ANZ Young Geotechnical Professionals Conference, Adelaide, Australia, 2006
- 8th ANZ Young Geotechnical Professionals Conference, Wellington, New Zealand, 2008
- 9th ANZ Young Geotechnical Professionals Conference, Melbourne, Australia, June 2012
- 10th ANZ Young Geotechnical Professionals Conference, Noosa, Australia, September 2014
- 11th ANZ Young Geotechnical Professionals Conference, Queenstown, New Zealand, 2016
- 12th ANZ Young Geotechnical Professionals Conference, Hobart, Australia, 2018
- 13th ANZ Young Geotechnical Professionals Conference, Cairns, Australia, 2021 (Cancelled)
- 14th ANZ Young Geotechnical Professionals Conference, Rotorua, New Zealand, 2022

CONFERENCE PROGRAMME

WEDNESDAY 2 NOVEMBER 2022: Welcome Function and Registration	
14:00	**Check-in opens – Millennium Hotel, Rotorua**
17:00	**Registration desk opens – Millennium Hotel Conference Room**
	Delegates to bring presentation on USB to upload
18:00	**WELCOME FUNCTION with refreshments (hosted by Beca)**
	Welcome on behalf of the organising committee, Helen Loach
	Welcome from the NZGS Chair, Eleni Gkeli
	Acknowledgement of sponsors
	Address from Beca
20:00	Registration desk closes, Welcome function concludes

THURSDAY 3 NOVEMBER 2022: First Day Presentations	
6:30	**Hotel breakfast**
8:15	Last chance for presentations to be uploaded
8:30	**Opening announcements (Helen Loach, Eleni Gkeli)**
	Introduction of mentors
9:00	**SESSION 1**
	Presentation of papers 1-6
	Mentor Summary
10:30	**MORNING BREAK AND REFRESHMENTS**
11:00	**SESSION 2**
	Presentation of papers 7-12
	Mentor Summary
12:30	**LUNCH**
13:30	**SESSION 3**
	Presentation of papers 13-18
	Mentor Summary
15:00	**AFTERNOON BREAK AND REFRESHMENTS**
15:30	**SESSION 4**
	Presentation of papers 19-24
	Mentor Summary
	Closing announcements
17:00	First Day Presentations conclude
18:00	Meet at reception to walk as a group to dinner
18:30	**DINNER AT PIG & WHISTLE HISTORIC PUB**
FRIDAY 4 NOVEMBER 2022: Second Day Presentations	

6:30	**Hotel breakfast**
8:30	**Opening announcements**
8.45	**SESSION 5**
	Presentation of papers 25-30
	Mentor Summary
10:15	**MORNING BREAK AND REFRESHMENTS**
10:45	**SESSION 6**
	Presentation of papers 31-36
	Mentor Summary
12.15	**LUNCH**
13:15	**SESSION 7**
	Presentation of papers 37-42
	Mentor Summary
14.45	**AFTERNOON BREAK AND REFRESHMENTS**
15:15	**SESSION 8**
	Presentation of papers 43-47
	Mentor Summary
	Field trip overview & H&S briefing (Brad Scott, GNS)
	Closing announcements
17:00	Second Day Presentations conclude
18:00	Meet at reception to board bus for dinner
18:30	**DINNER AT PATAKA KAI RESTAURANT (sponsored by Stantec)** Presentation of awards **Walk through the geysers at Te Puia** We have organised a 45-minute guided walk around Te Puia after the Friday night conference dinner so please bring appropriate footwear.

|	
SATURDAY 5 NOVEMBER 2022: Field Trip	
6:30	**Hotel breakfast**
	Check-out of Millennium Hotel by 8:30 – Hotel will store bag
8:50	Board bus from reception
9:00	**FIELD TRIP COMMENCES**
	Stop 1: Tihitonga Centennial Park
	Stop 2: Kuirau Park
	Stop 3: Stoney Point Reserve
12:00	**LUNCH**
13:00	**RETURN TO MILLENIUM HOTEL - CONFERENCE CONCLUDES**

TRAVEL GUIDE

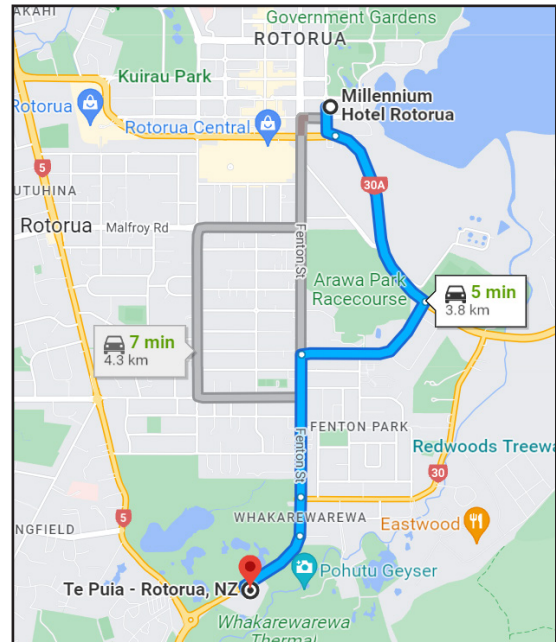## Rotorua Airport to Millennium Hotel Rotorua (1270 Hinemaru Street, Ohinemutu, Rotorua) - CONFERENCE VENUE

APPROXIMATELY 11 MINUTES TRAVEL TIME BY TAXI
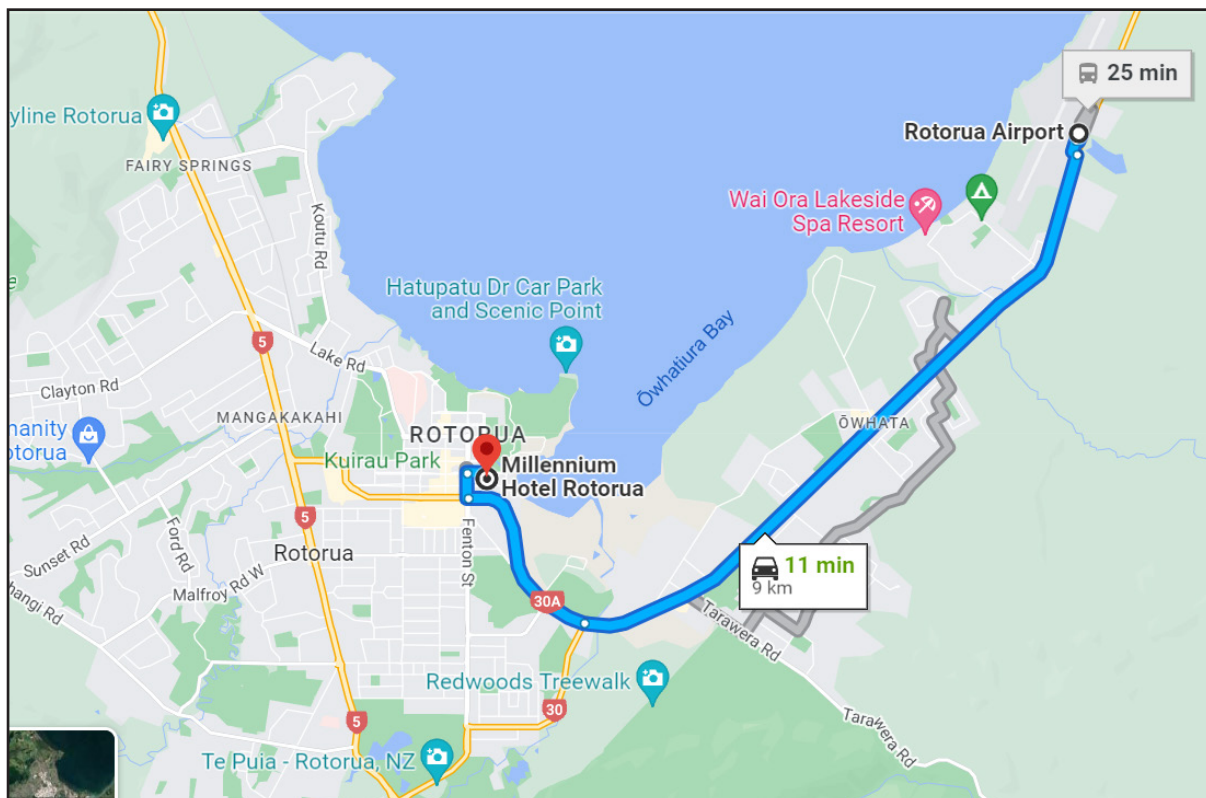
Pig & Whistle Historic Pub
(1182 Tutanekai Street)
– DINNER VENUE 3 NOVEMBER
Approximately 8-minute walk
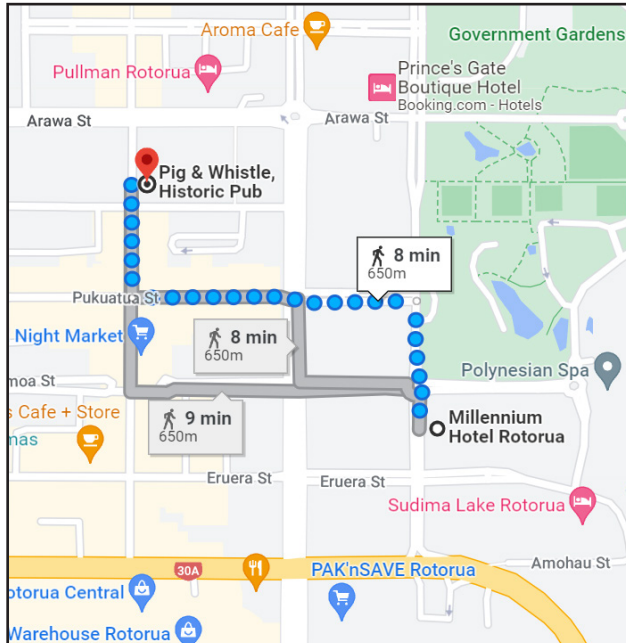
Pataka Kai Restaurant
– Te Puia (20 Hemo Road)
– DINNER VENUE 4 NOVEMBER
Approximately 5-minute bus charter

Tihitonga Centennial Park, Kuirau Park and Stoney Point Reserve
– FIELD TRIP 5 NOVEMBER Approximately 1-hour total travel time by bus charter

TABLE OF CONTENTS
TECHNICAL PAPERS
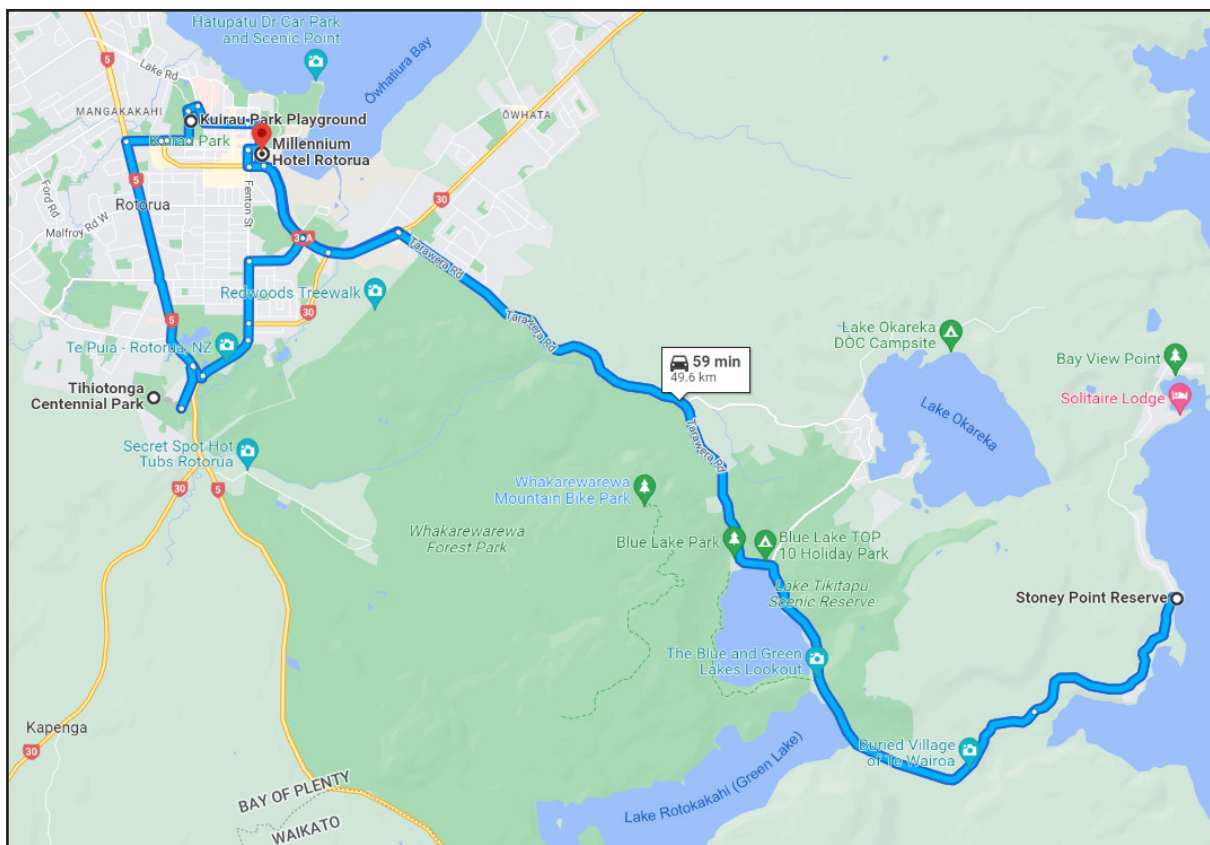
III TABLE OF CONTENTS

TECHNICAL PAPERS

Hydrogeological Model Development and Horizontal Drainhole Effectiveness for Slope Stability

L. D. Parsons[1]

[1] Pells Sullivan Meynink, 22 Delhi Street, West Perth, WA 6005, Australia; PH (61) 8-9462-8400; email: liam.parsons@psm.com.au

ABSTRACT

The presence of ground water, particularly pore pressures can have a significant detrimental effect upon slope stability. Successful open pit slopes, particularly in tropical environments, depend on a good understanding of the hydrogeological model and the development of appropriate depressurisation strategies. This paper presents the development of the hydrogeological model and depressurisation methods used at an open pit mine in Southeast Asia. The overall aim of the study was to reduce the number of horizontal drain holes installed while maintaining effective depressurisation objectives and achieving the projects economic and environmental goals.

A field observation program was conducted during wet season to support the study. The observations identified both lithology and structural controls on hydrogeological conditions within the open pit. This paper describes the resulting conceptual hydrogeological model, which is based on existing mine development data, recent groundwater monitoring and horizontal drain hole (HDH) installations. Preliminary model sectors were created to direct HDH design, including depth and spacing. These have then been tested against ongoing groundwater monitoring. This paper also presents the development of pore pressure trigger levels for areas where depressurization is insufficient and has implications for slope stability. Ongoing work is focused on the validation of the HDH design sectors.

Keywords: Open Pit Mining, Hydrogeological Model Development, Depressurisation, Horizontal Drain Hole, Slope Stability

1   INTRODUCTION

It is well understood that pore pressures contribute to most significant large scale slope failures (Read and Stacey, 2011; Beale and Read, 2013). Beale and Read (2013) describe the impact of ground water by the following: *"The presence of groundwater has a detrimental effect on slope stability. Water pressures acting in the pore spaces, fractures or other discontinuities in the materials comprising the pit slope will reduce the strength of those materials and may therefore have a large influence on the performance, safety, and economics of a mining operation".*

Open pit mines are commonly located in geologically complex environments in diverse climates around the world. To develop an adequate groundwater and surface water management plan, a degree of understanding is needed of the deposit's geology, structure, rock mass and hydrogeology to inform the conceptual hydrogeological model. The case study site is in Southeast Asia, a tropical environment wet seasons from May to October and dry seasons from mid-October to April. The deposit is situated in a mountain province and is positioned in a topographic low at a confluence of a regional river system.

This paper presents the application the development of a conceptual hydrogeological model and review of existing depressurisation performance. The aim of the study was to use the model to optimize Horizontal Drain Hole (HDH) design as the existing installation program is considered to have high human, environmental and financial costs.

2   EXISITING DEPRESSURISATION DESIGN

The existing site horizontal depressurisation hole (HDH) program is a grid design with 50 m spacings and typical lengths of 100 m to 150 m. A historic dewatering bore was also established prior to mine development in 2009, located in the northern sector of the pit, within a karstic limestone unit.

Depressurisation began in 2009 with the majority of HDH installed within volcanic tuff and siltstone units. Pit progression remained consistent from 2010 through to 2016 with total depressurisation drilling fluctuating between 5,000 m and 12,000 m annually. Mining progression accelerated from 2017 through to 2021 with the peak HDH installation occurring during 2020, with a total of 47,000 m.

3   METHODOLOGY

The open pit's geotechnical model was used to inform the basis of the hydrogeological model to optimise the HDH design. The characteristics of the geology, structure, rock mass and hydrogeology of the site were analysed to develop the model. The sections below present the key characteristics of the geotechnical model assessed.

3.1   Geology

The copper–gold (Cu-Au) deposit is described as a porphyry-skarn ore system, believed to be of Late Triassic age, related to subduction and island arc magmatism. The lithologies forming the primary geotechnical units are as follows:

1. Granite
2. Limestone
3. Interbedded calcareous siltstone-sandstone
4. Siltstone
5. Andesitic lapillic tuffs
6. Diorite intrusions, which are associated with faulting.

The distribution of the units are shown in Figure 1. Packer testing, where pressurised water is administered to the rock mass to ascertain hydraulic conductivity, was undertaken for each of these units.
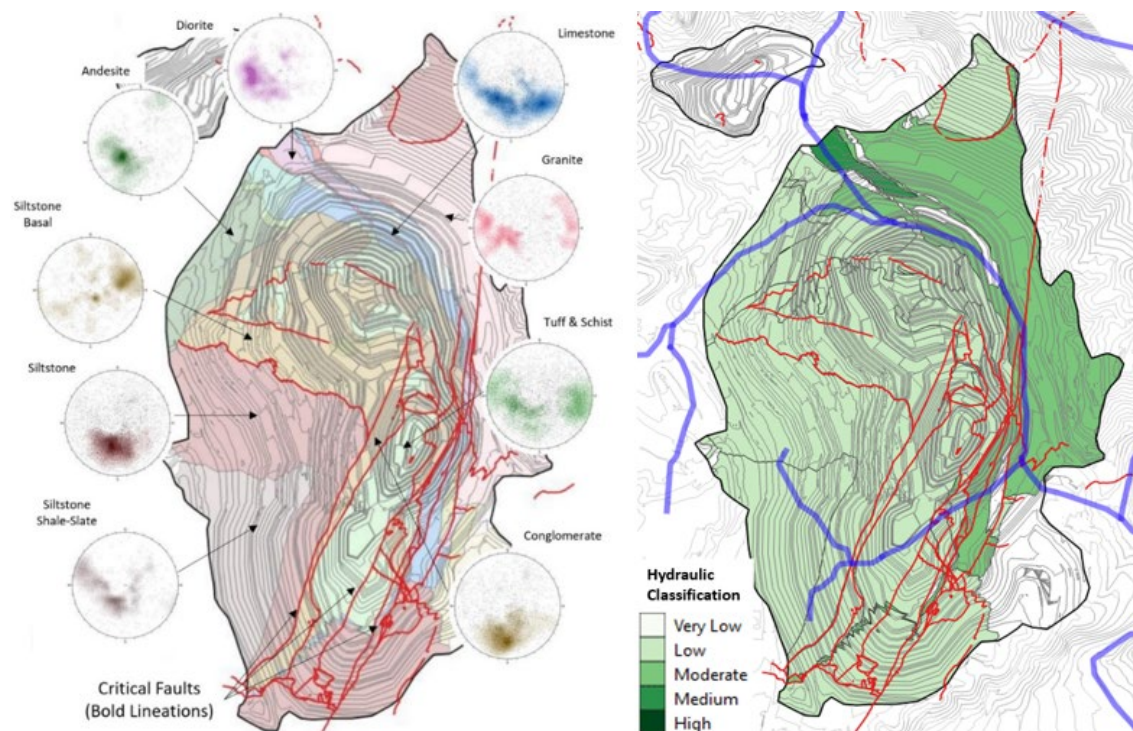
Figure 1. Lithology and the main structural elements of the case study site.

3.2   Structure

Geological structures were assessed to identify persistent anisotropic defects either consistent through the rock mass or defects that comprised a considerable reduction of the rock mass or material. Faults and shears were identified as reduction in rock mass, while bedding and foliation were identified as consistent anisotropic defects. Persistent structures such as faulting, shearing, bedding, or foliation were

PROCEEDINGS OF THE 14TH ANZ YOUNG GEOTECHNICAL PROFESSIONALS CONFERENCE
14YGPC ROTORUA, NEW ZEALAND, 2ND – 5TH NOVEMBER 2022

3

observed to be either a conduit (enhance permeability) or barriers (reduce permeability). Faults were further assessed based on geotechnical and hydrogeological importance and were classified based on four categories (Table 1). An over all rating was derived with faults achieving a rating over 12 being identified as a critical fault.

Table 1: *Critical Fault Criteria*

Rating	Fault Condition	Persistence (m)	Orientation	Confidence [a]
1	Healed	<100	>500m from pit	0
2	Narrow (<1m thick)	100 – 500	Perpendicular to the pit wall	2-3
3	Fragmented/Sheared	>500	Oblique to pit wall	>5
4	Clay/Gouge	N/A	Parallel to pit wall (>50m)	>5
5	N/A		Parallel to pit wall (<50m)	N/A

[a] Number of fault condition observations across a fault trace. Observed in either open pit mapping or boreholes.

3.3   Rock Mass

Understanding of the rock mass properties was imperative to the formation of the geotechnical model. To delineate the properties of the rock mass specific to the site, a review of existing literature and reports was undertaken. Site based data pertaining to the rock mass was reviewed. The rock mass was classified based on the level of oxidisation. Finally, the site-specific engineering properties of homogenous, heterogeneous, and anisotropic rock masses were identified.

3.4   Hydrogeology

Understanding the surface water and ground water characteristics was critical to implementing an effective HDH design. To identify surface water catchment and groundwater flow regimes, existing data relating to groundwater flow was assessed, including:

1. The paleo mining surface for post water drainage channels
2. Site specific recordings of ground water flows post heavy rainfall events
3. Flow readings from HDH's
4. Vibrating wire piezometer (VWP) measurements of pore pressures within the rock mass.

Finally, Hu values were derived from the VWP results whereby the Hu value was defined as a numerical assessment of the pore pressure behaviour irrespective of pressure head vs sensor depth. The assessment was conducted to identify confined aquifers that may be situated behind the pit wall and pose a risk to slope stability.

4   RESULTS

4.1   Geology

The lithologies at the case study site were characterised as a fractured rock aquifer, where most groundwater located in fresh rock is stored within fractures, joints, and cavities. Site based data included 103 packer tests were carried out within the surrounding rock mass through two campaigns. A 2014 campaign, consisting of 72 tests and another campaign in 2020 consisting of 31 tests, Figure 2.
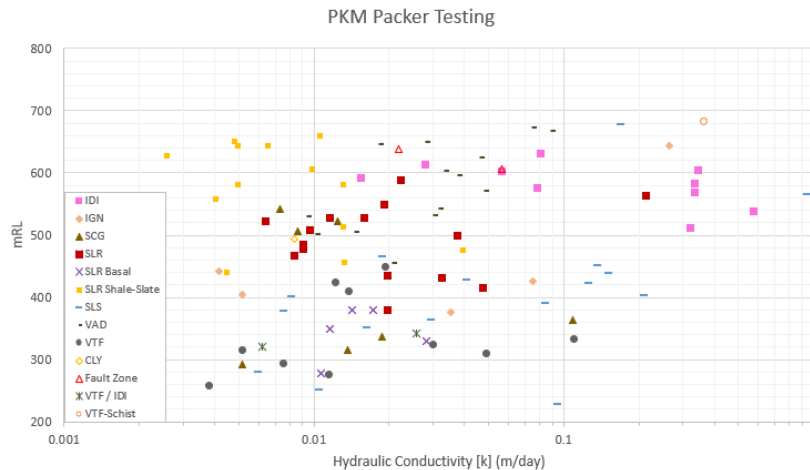
Figure 2. Packer testing results conducted between 2014 and 2020 at the Cu-Au deposit.

The packer testing indicated that most of the rock mass is of very low to low permeability. Diorite, granite, and limestone exhibited moderate to medium permeabilities associated with the eastern fault Corridor, (Figure 1). The limestone was karstic, with zones of solution cavities which provide the most significant groundwater aquifer. It is noted that the 2014 testing had limited information on the characteristics of rock mass tested, with most of the testing occurring along the eastern fault corridor.

4.2   Structure

Two main structural elements, also referred to as critical faults, were identified as important for the conceptual hydrogeological model and are shown on Figure 1. These are:

1. A series of northeast-dipping thrusts. The two primary surfaces are the North and South Thrusts. These are located to the west of the pit and separate the siltstones from the Tuff and Schist.

2. A series of north-northeast trending, steeply dipping structures that form a zone in the eastern part of the pit called the eastern fault corridor. These post-date and offset the thrust faults.

Analysis confirmed conduit faults were present along both the eastern fault corridor and along the siltstone/conglomerate faulted contacts. Assessment of core photos, logging descriptions and HDH flow rates indicated that barrier faults were present along the limestone faulted contacts between both the siltstone and granite.

4.3   Rock Mass

Three oxidisation zones were identified as relevant for the conceptual hydrogeological model: completely oxidised (CO), partially oxidised (PO) and fresh. The upper CO consists of silts and clays from completely weathered bed rock units . The unit was described as a porous medium (intergranular) clay alteration with low permeability. The PO zone was characterised by moderately weathered to slightly weathered parent rock. The unit was described as a fracture flow, high permeability rock mass.

Fresh rock mass was characterised by fresh parent rock and was divided into three subgroups for hydrogeological assessment. The subgroups identified were as follows:

1. Homogenous: comprises igneous, conglomerates and tuff units. Characterised as having preferential flow occurs through joints.
2. Heterogeneous: comprised of the limestone unit. Characterised as having preferential flow through the medium to highly permeable rock mass and along discrete defects. Karsts are characterised as discrete vertical features which act more as a surface water feature than groundwater feature.
3. Anisotropic: Bedded and foliated units including shales and schist. Preferential flow occurs along persistent defects (bedding or foliation).

PROCEEDINGS OF THE 14TH ANZ YOUNG GEOTECHNICAL PROFESSIONALS CONFERENCE
14YGPC ROTORUA, NEW ZEALAND, 2ND – 5TH NOVEMBER 2022

5

4.4 Hydrogeology

4.4.1 Hydrogeology - Surface water

The open pit is in a tropical climate where ground and surface water management have a large influence on mining operations, planning and management. The average annual rainfall from 1987 to 2019 was 2,525 mm where annual totals range from 1,547 mm (1992) to 3,738 mm (2005). The pre-mining water table was recorded between 4 mBGL and 9 mBGL. The deposit has a large surface water catchment located to the north to northwest of the pit and is estimated to be 5 km^2. The principal catchment for the area flows from the north-western corner of the pit and is then diverted along the north and eastern pit walls. Several tributaries converge with the principal catchment before exiting through the eastern pit wall. The principal stream was predominately unlined at the time of the study and flowed along excavated channels in transitional, faulted, medium permeable granite. The project concluded that surface water management has an important role in depressurisation at the site.

4.4.2 Ground Water and Hu Assessment

Since mining commenced about 160 VWP sensors have been installed across the various geotechnical units. The pit has been mined as a series of cutbacks resulting in many VWP's and HDH holes being destroyed between 2017 to 2019. Limited VWP data is available for the upper weathered (CO, PO zones).

Hu is a geotechnical pore pressure coefficient. It is a simple factor between 0 and 1, by which the vertical distance from a point in the soil of rock mass to a water surface is multiplied to obtain a pressure head. Hu values were derived for the site from the 160 VWP sensor readings. The results were able to directly compare with the assumptions used in the slope design. It was observed that for some units the VWP pore pressures exceeded both the assumed conditions and hydrostatic conditions (Hu =1), Figure 3.
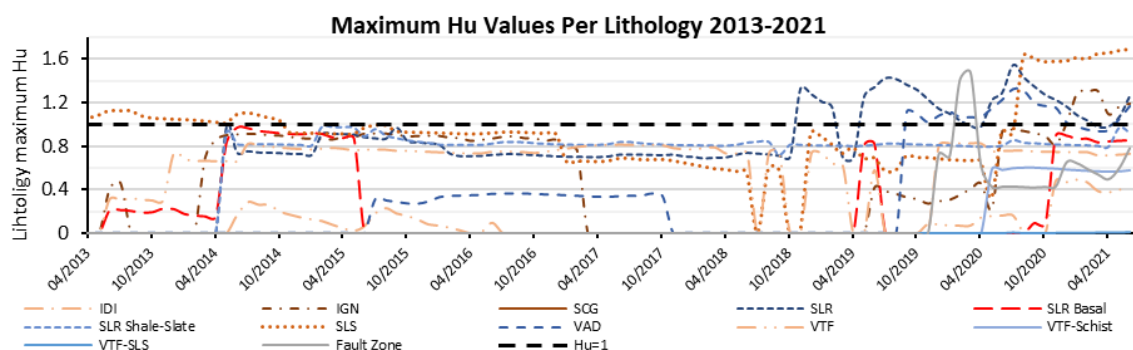
Figure 3. Maximum Hu values recorded per lithology from beginning of Mining to July 2022

For each VWP noted to exceed the slope design assumptions, a review on the location and consequence to slope stability was undertaken. No excessive pore pressure result had an immediate effect on slope stability. Further investigation was recommended to aid understanding of the increased pressures.

5 DISCUSSION AND CONCLUSIONS

This study found that the pre-existing HDH design achieved adequate depressurisation and groundwater conditions. However, the design required a large quantum of drilling, with substantial cost implications. In addition, there was inadequate monitoring of structurally complex locations such as the eastern fault corridor. The pre-existing design, with the unlined diversion drain allows surface water to infiltrate the moderately permeable rock mass units allowing recharge of pore pressures.

The hydrogeological model is presented in Figure 4 and considers specific components such as structure, anisotropy and surface water. The resulting HDH program included:

1. Completely Oxidized Zone: HDH spacing to remain at the 50 x 50m spacing with hole depth reducing to 100m. Recommendation of periodic flow ratings and observations.

2. Eastern Fault Corridor: HDHs only drilled to target Category 5 faults. Recommendation to increase monitoring behind these faults to confirm depressurisation targets are met.

3. West Wall Anisotropic Zone: Preferential flow along bedding. Targeted HDH drilling, perpendicular to bedding dip. Recommendation to continue monitoring through the West Wall hydrogeological units.
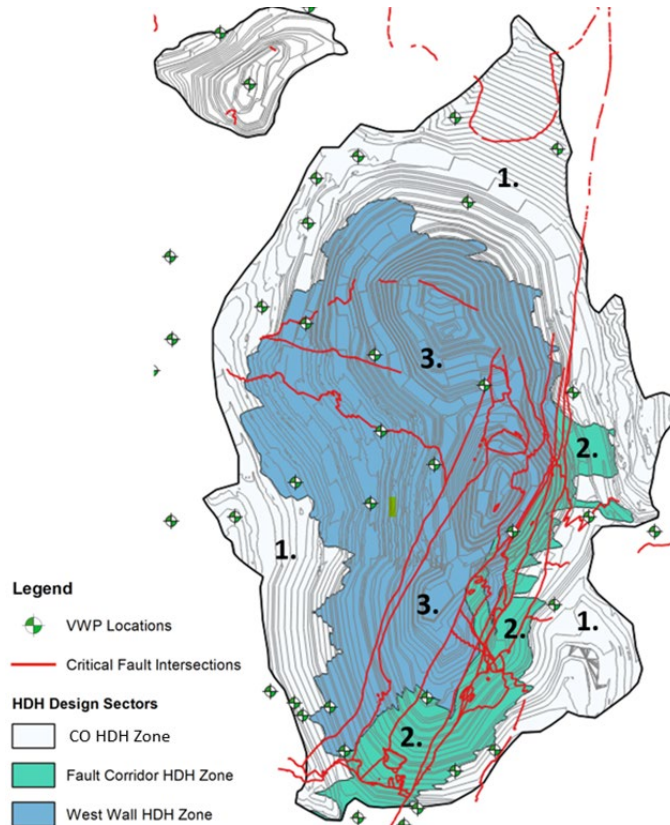
Figure 4. Hydrogeological depressurisation drilling sectors

Limitations to this model included restricted data regarding HDH flow rates and draw down responses unmonitored by VWPs. This led to difficulties in assessing the effectiveness of the HDH hole. Further work recommendations included:

1. VWP installation locations be selected along 2D cross-sections to understand pressure head gradients through various geological units.

2. Additional groundwater monitoring and permeability investigation be undertaken in the oxidised zones.

3. Ongoing permeability testing and installation of VWPs through the oxidised zones is warranted.

This study has illustrated that optimisation of specific components such as structure, anisotropy and surface water will greatly improve depressurisation outcomes whilst decreasing drilling requirements.

6   ACKNOWLEDGEMENTS

REFERENCES

Beale, G & Read, J 2013, *Guidelines for Evaluating Water in Pit Slope Stability*, CRC Press, Boca Raton.
Read, J & Stacey, P 2011, *Guidelines for Open Pit Slope Design*, CRC Press, Boca Raton.

PROCEEDINGS OF THE 14TH ANZ YOUNG GEOTECHNICAL PROFESSIONALS CONFERENCE
14YGPC ROTORUA, NEW ZEALAND, 2ND – 5TH NOVEMBER 2022

7

Site-Specific Probabilistic Seismic Hazard Assessment for a site in East Auckland

E. K. Gardiner[1] and L. Goldfarb[1]

[1]Jacobs, Wynn Williams Building Level 2, 47 Hereford Street, Christchurch 8013, New Zealand; PH (64) 3-940-49007; FAX (64) 3-940-4901; email: Emma.Gardiner@Jacobs.com

ABSTRACT

This paper presents a comparison of different methods to determine the seismic hazard for a site in East Auckland. A probabilistic seismic hazard assessment was used to evaluate the seismic hazard at bedrock and the ground surface, while a one-dimensional site response analysis determines the hazard at the ground surface. Seismic hazard results at bedrock and the ground surface are compared to their codified counterpart. The site-specific results (PSHA and SRA), and associated uncertainty, provide an indication of the expected range of responses at the site. Comparison of methods highlights the influence of subsurface soils on the ground motion response and the importance in considering the wider context when adopting seismic design loads.

Keywords: Probabilistic seismic hazard analysis, site response analysis, NZTA Bridge Manual, East Auckland

1 INTRODUCTION

Currently in New Zealand (NZ) there are two key design codes that define seismic hazard: New Zealand Standards 1170.5 (NZS1170.5) and the Waka Kotahi Bridge Manual (NZTA-BM). The NZ Building Code Clause, B1 Structure, refers to NZS1170.5 for seismic loading (MBIE, 2021). The NZTA-BM covers the design of transport related structures and a select range of geotechnical systems not covered in NZS1170.5. NZTA-BM refers to NZS1170.5 for seismic loading for structural design, whilst providing peak ground acceleration (PGA) and magnitude (M) values for geotechnical design. Design to the NZTA-BM is considered an 'Alternative Solution' in the context of compliance with the NZ Building Code.

For nearly 60 years, site-specific probabilistic seismic hazard analysis (PSHA) has been an internationally accepted scientific approach for the characterisation of seismic hazard (Cornell, 1968). As earthquakes cannot be reliably predicted, the PSHA method is adopted to quantify the probability that a ground-motion intensity level will be exceeded within a defined period (typically the building design life), at a particular location due to all possible future earthquakes. The principal output of PSHA is the seismic hazard curve, which shows the variation of the ground-motion intensity measure (e.g., PGA) with annual rate of exceedance (i.e., inverse of 'return period') at the site of interest. A secondary output of PSHA is the uniform hazard spectrum (UHS), which presents the spectral accelerations (SA) at vibratory periods of interest for structural design with an equal probability of exceedance. NZS1170.5 requires PSHA to be conducted for Importance Level (IL) four structures while NZTA-BM requires PSHA for projects valued at more than $7 million (as of December 2012). PSHA can be performed for different site conditions, generally considered in terms of the 30 m time averaged shear-wave velocity of the site, V_{s30}. Some consideration is given to the stratigraphy and stress-strain properties of the soil through V_{s30}; however, the site response is not properly characterised. Stratigraphy and stress-strain properties of the soil influence site response above bedrock (Baker et al., 2021). Alternatively, the effect of the soil deposit above bedrock on ground motions can be computed with site response analysis (SRA). SRA considers the stress-strain response of the soil under cyclic loading to compute the expected seismic hazard at the ground surface for a given bedrock input motion (Bradley, 2015).

A recent study by Cubrinovski et al. (2022) compared the seismic hazard predicted by the two aforementioned codes with a NZ wide regional PSHA study (Bradley et al., 2022). This study demonstrated significantly higher hazard compared to either code in several locations, notably the East Coast and Lower North Island and Upper South Island. Conversely, this study, along with several others, found that Auckland has a low risk from a M 7.5 earthquake, which was lower than the code specified values (Cubrinovski et al, 2022; Bradley, 2015). In NZ, if the results of a PHSA study provide lower hazard than the code minimum hazard, the minimums take precedence. NZS1170.5 provides a hazard factor (Z) to determine the seismic risk in an area. Minimum Z values are particularly relevant in low seismicity regions such as Auckland. This recognises that the adoption of seismic loads is an engineering decision, involving interpretation of the hazard analysis and wider societal and economic

8

PROCEEDINGS OF THE 14TH ANZ YOUNG GEOTECHNICAL PROFESSIONALS CONFERENCE
14YGPC ROTORUA, NEW ZEALAND, 2ND – 5TH NOVEMBER 2022

considerations. This paper presents a comparison of different methods to determine the seismic hazard for a site in East Auckland. First the seismic hazard for bedrock and surface conditions in the code was determined. Next, a PSHA was performed to determine the seismic hazard for bedrock and surface conditions. Finally, spectral rations (SRs) from a SRA were incorporated into the PSHA results at bedrock to estimate the hazard at the surface. The incorporation of the SRA in the PHSA was done in a deterministic manner (i.e., ignoring epistemic uncertainty or variability in the site response).

2   SEISMIC HAZARD IN NEW ZEALAND DESIGN CODES

This paper focuses on the elastic site hazard spectra defined in the NZTA-BM for structural loading. For structural loading, the NZTA-BM essentially uses the hazard spectra defined in NZS1170.5. The site of interest consisted of predominantly clays and silts underlain by the interbedded sandstone and siltstones of the East Coast Bays Formation (ECBF). According to NZS1170.5, the site can be classified as Soil Class C, while Site Class A/B was used to represent hazard at bedrock. The NZTA-BM code spectrum was derived with Z of 0.12 for Manakau City.

3   PROBABILISITIC SEISMIC HARAZRD ANALYSIS METHODOLOGY

The PSHA process is represented by equation (1), which gives the annual rate of exceedance of a target ground-motion level (z) and for the intensity measure of interest:

$$\gamma(Z > z) = \sum_{i=1}^{n_{sources}} v_i \int_{m_{min}}^{m_{max}} \int_{r=0}^{\infty} \int_{\varepsilon=\varepsilon_{target}}^{\infty} f_{mi}(M) f_{ri}(r) f_\varepsilon(\varepsilon) P(Z > z | M, r, \varepsilon) dM dr d\varepsilon \qquad (1)$$

where: $P(Z > z | M, r, \varepsilon)$ is the probability of the target ground motion being exceeded for a given magnitude-distance-epsilon scenario and is obtained from the ground motion characterisation (GMC) model, $f_{mi}(M)$, $f_{ri}(r)$ and $f_\varepsilon(\varepsilon)$ are the probability density functions for magnitude, distance and epsilon respectively. Epsilon (ε) is the number of standard deviations above the median needed in the GMM to reach the target ground motion (z) for a particular magnitude-distance scenario. v_i is the earthquake occurrence rate of events with magnitudes equal to or greater than m_{min} for source i. When this process is performed for different target ground-motion levels, a seismic hazard curve can be built up (McGuire, 2004). The PSHA process was conducted using the software R-CRISIS Version 18.4.2. The site was modelled as a single point with V_{s30} of 760 m/s at bedrock and V_{s30} of 250 m/s at the ground surface.

3.1   Seismic Source Model

The seismic source model (SSM) defines the spatial location and magnitude of future earthquakes, based on historical seismicity, geology and seismotectonic setting of the region surrounding the area of the project. The 2010 New Zealand National Seismic Hazard model (2010 NSHM) of Stirling et al. (2012) was used to inform the SSM. The 2010 NSHM model considers both mapped active faults, and faults not yet identified or unknown (background seismicity). Background seismicity was considered using a series of point source zones defined on a grid at a variety of depths. Seismic properties of the points were informed by the rates of seismic activity recorded by seismic instruments over preceding decades and characterised using the Gutenberg-Richter magnitude-recurrence relationship. Importantly, in low seismicity regions such as Auckland this relationship may be poorly constrained due to a lack of data. It is acknowledged there are continuous advancements in knowledge of seismic sources from geological and seismological studies; a revision of the NSHM is currently underway with a critical focus on the Hikurangi Subduction Zone, which is predicted to affect the modelled ground shaking from Auckland through to Wellington (Gerstenberger, 2021). The influence is expected to be small for Auckland. At large return periods (RPs) and longer vibration periods, the more distant regional faults, including the Hikurangi Subduction Zone, are expected to have more, but not dominant, contribution (Cubrinovski et al, 2022; Bradley, 2015). Until this model is released, the model of Stirling et al. (2012) forms the most recent national consensus. This approach was also adopted by Bradley et al. (2022) as the 2010 NSHM has significant advancements over those models used in the development of NZS1170.5 and NZTA-BM.

3.2   Ground Motion Characterisation Model

The GMC model predicted the expected ground shaking due to each earthquake scenario defined within the SSM and consists of multiple ground motion models (GMMs). Selected GMMs can have significant impact on the PSHA results therefore, a logic tree approach was considered to account for model

PROCEEDINGS OF THE 14TH ANZ YOUNG GEOTECHNICAL PROFESSIONALS CONFERENCE
14YGPC ROTORUA, NEW ZEALAND, 2ND – 5TH NOVEMBER 2022

9

uncertainty. The GMMs presented in this study are based on a revised, recent understanding compared to those used in the development of NZS1170.5. Three different seismotectonic regimes were identified for this study: active shallow crustal region (ASC), subduction region (SR), and Taupo volcanic zone (TVZ). A set of GMMs was selected based on the exclusion criteria proposed by Bommer et al. (2010). Suitability, and weightings, of selected GMMs to NZ conditions were informed by the work of Van Houtte (2017). For ASC, five models were models selected. Abrahamson et al. (2014), Boore et al. (2014) and Campbell and Bozorgnia (2014) were assigned equal weights of 0.25, while Bradley (2013) and Chiou and Youngs (2014) were assigned weights of 0.125. Bradley (2013) was derived using the same functional form and regression analysis as Chiou and Youngs (2008). Therefore, the two models cannot be considered entirely independent and consequently the remaining 0.25 weight was split. For the SR, the models selected were Abrahamson et al. (2006), Atkinson and Boore (2003), and Zhao at al. (2006) all assigned equal weights. For the TVZ, the only one model, Bradley (2013), was selected as it was developed to explicitly account for additional anelastic attenuation in the TVZ which other models do not explicitly account for. However, adopting only one GMM is not considered good practice as it fails to capture the epistemic uncertainty. A backbone model was developed by scaling the Bradley (2013) model up and down by applying a factor of ±20% to the logarithm of the predicted ground motions. This resulted in a three-branch logic tree where the median value of Bradley (2013) was assigned a weight of 0.6 and the adjusted models were each assigned a weight of 0.2.

4   SITE RESPONSE ANALYSIS METHODOLOGY

The SRA was performed using one dimensional equivalent linear (EQL) SRA for one soil profile using the software STRATA Version 0.8.1. EQL requires a relatively small number of input parameters, which helps avoid the introduction of supplementary parametric uncertainty. EQL is a computationally efficient method of analysis and has been found to give similar predictions to fully nonlinear SRA for strain levels less than 0.4% (Kaklamanos and Bradley, 2018). Three-time histories were used as bedrock input motions. Input motions were informed by the bedrock PSHA results and were selected and scaled in accordance with NZS1170.5. The shear wave velocity profile and characterized uncertainty (Figure 1) was informed by seismic cone penetration tests. Bedrock shear wave velocities were developed based on borehole data in conjunction with values reported in literature (Dawson et al., 2015). The bedrock horizon was defined at the top of the ECBF at approximately 19 m below ground level. The relationship of Darendeli (2001) established the nonlinear behaviour (shear modulus degradation and damping with shear strain) of the different soil layers. Empirical nonlinear curves were used due to the lack of site-specific advanced laboratory data. To account for aleatory variability in the spatial distribution of shear wave velocities at the site, and the lack of rigorous site-specific data, the randomization model of Toro (1995) was used. This model created a suite of statistically based randomised shear wave velocity profiles. It is acknowledged that this procedure may overestimate variability of the results at shorter periods while underestimating variability at longer periods (Stewart and Hashash, 2014). However, the results from SRAs using the three discrete profiles in Figure 1 are in reasonable agreement to the method used. Therefore, at this site, this methodology can reasonably indicate the range of expected responses. Additionally, using a randomisation procedure allowed uncertainty in the site amplification to be captured without the need to provide a weighting factor for different profiles which can lead to unintended distributions (Rodriguez-Marek et al., 2021). Moreover, there are more rigorous methods available for SRA and capturing uncertainty. However, as the input motions are low, and non-linearity effects are expected to be small, this simplified approach is expected to provide a good indication of the range of responses without the need for rigorous methods.

5   RESULTS

5.1   Bedrock

The hazard curves for PGA (Figure 2) at bedrock level shows the predicted site-specific (PSHA) hazard is less than its codified counterpart. The difference between the site-specific and code hazard curves decreases with increasing RP, indicating the code becomes less conservative as the RP increases. Figure 2 also shows the hazard curves by source for PGA for the five sources with the highest contributions to the hazard. The results indicated the hazard at the site was mainly controlled by the shallow background seismicity. This was expected as there are no major seismogenic features or subduction zones in the near region. Consequently, majority of the hazard predicted was from unknown or unmapped faults. This is similar to the perception of the seismic hazard at Christchurch prior to the Canterbury Earthquake Sequence in 2010 and 2011. Stirling et al. (2012) shows hazard disaggregation

at the 475-year RP for Auckland, Wellington, Christchurch, and Dunedin. However, neither NZS1170.5 nor NZTA-BM provide information regarding hazard disaggregation. Understanding the characteristics of the dominant seismic sources at a given site is useful in informing the selection of appropriate ground motions for use in dynamic structural and geotechnical analyses (Bradley, 2015). Consequently, the hazard disaggregation of the PSHA informed the ground motion time series selection for use in SRA. The UHS at bedrock for different RPs is presented in Figure 3. For all RP the site-specific UHS was less than the code spectra. This result is dependent on the location, RP, and IL of the structure. Herein, only the results for the 1000-year RP are considered.

5.2 Ground Surface

The SRs from the three methods are plotted in Figure 4. The codified curve shows little variation in SR, which is excepted as the Site Class curves are scaled versions of each other. The SRA curve shows high amplification between 0.4 -0.6 s, coinciding with the fundamental period of the site. Conversely, the
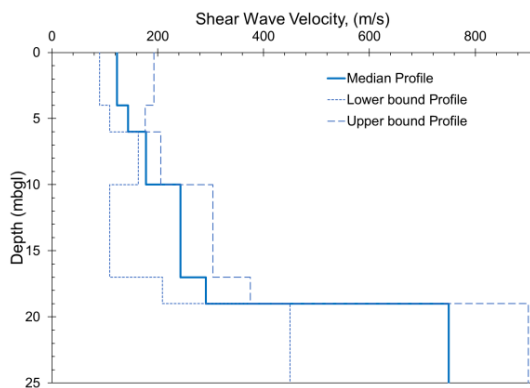
Figure 1. Shear wave velocity profile and associated uncertainty.
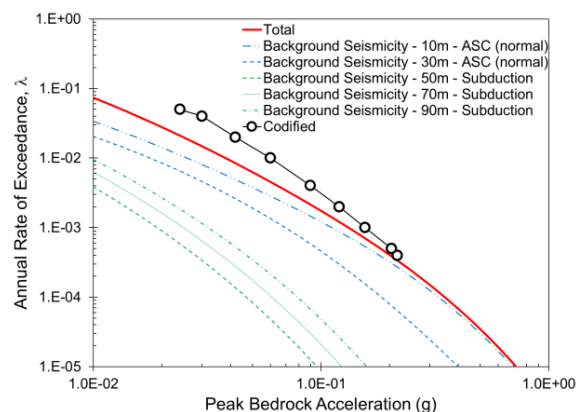
Figure 2. Hazard curve for peak bedrock acceleration.
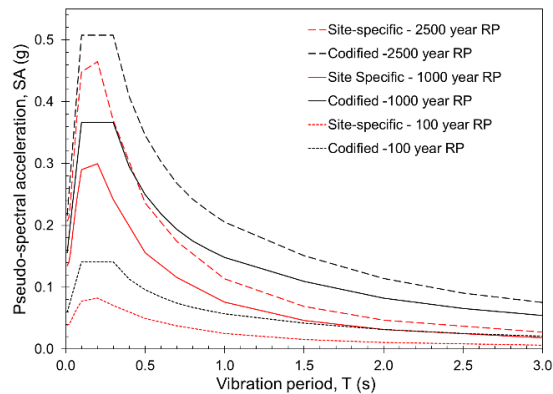
Figure 3. Bedrock UHS for three RPs.
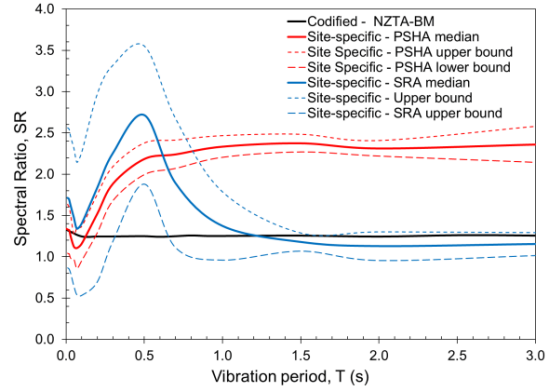
Figure 4. SRs at the 1000-year RP.
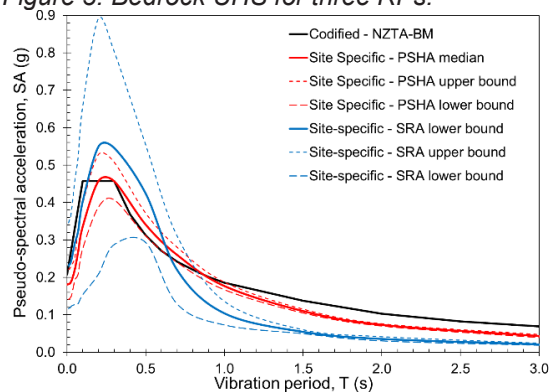
Figure 5. Ground surface UHS at the 1000-year RP.
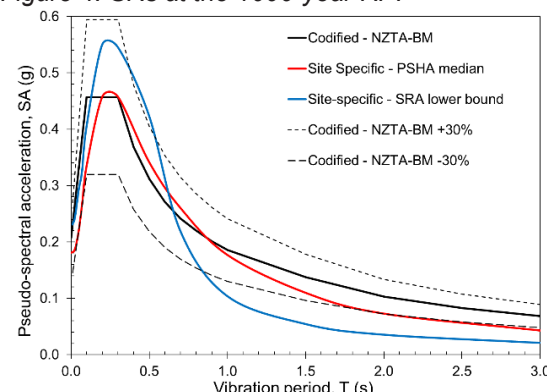
Figure 6. Ground surface UHS at the 1000-year RP compared to code limits.

PROCEEDINGS OF THE 14TH ANZ YOUNG GEOTECHNICAL PROFESSIONALS CONFERENCE
14YGPC ROTORUA, NEW ZEALAND, 2ND – 5TH NOVEMBER 2022

11

PSHA curves underestimate the amplification at the fundamental period and overestimates the amplification at longer periods. The PSHA curves miss the fundamental period, hence, fails to properly capture the site response. More variation is seen in the SRs of the SRA between 0.0 -1.5 s which may be due to the methodology used or better characterisation of the site response. The variation of the PSHA and SRA is similar for periods greater than 1.2 s. The UHS for the three methods are compared in Figure 5. The UHS for the SRA was determined by applying the SRs (Figure 4) to the PSHA bedrock UHS (Figure 3). The PSHA and code UHS are very similar. This is expected at the site response in both approaches is averaged out across a wide range of sites with different site response by similar V_{s30}. Conversely, the SRA curve shows amplification at short periods and attenuation at longer periods.

Differences between the site-specific (PSHA and SRA curves) and code-based spectra at both bedrock (Figure 3) and the ground surface (Figure 5) can be attributed to the functional methodology adopted by design codes which are intentionally conservative (McVerry, 2003). For this site, the code was unconservative for 0.2-0.7 s. The minimum Z factor in the code may have led to the higher code spectra for some period ranges. Moreover, code spectra are based on predefined piece-wise linear spectral shapes and aim to average the spectral shapes from many magnitude-distance scenarios. The NZTA-BM defines one spectral shape for each soil type across NZ (Bradley, 2015). Conversely, site-specific spectral shapes are defined by the site-specific controlling scenarios for the selected RP and can be influenced by the of proximity to potential seismic sources and soil conditions (Bradley, 2015). The findings presented here may vary for sites with softer or stiffer soil conditions which would affect the site-specific results at the surface. Additionally, sites that are subjected to higher amplitude input ground motions are likely to produce different results. This is due to the influence of these two factors on the nonlinear soil behaviour. This influence is likely to be greater for the SRA results as the nonlinear soil response is explicitly considered. No consideration of the stress-strain properties of the soils is given in PSHA determination at the surface (Baker et al., 2021). Despite low input ground motions, the SRA us properly characterising the site response while the PSHA is averaging the site response across many sites with similar V_{s30}. This is seen in the comparison of the code and PSHA results to the SRA results. Site response effects are much more complex than division into discrete soil classes in the NZTA-BM, or the average of the site amplification through V_{s30} in GMMs. More rigorous SRA methods may provide more insights into this influence and provide a better characterisation of uncertainty, compared to the simplified approach taken in this paper. Finally, the code-based spectra have been developed based on the 2002 NSHM (Stirling et al., 2002) which is the predecessor to the 2010 NSHM used in this study. This study used both an updated understanding of SSMs and GMMs based on the 2010 NSHM and more recently developed GMMs. This updated knowledge is not reflected in the code-based spectra.

For design recommendations, the NZTA-BM stipulates the adopted design spectra shall be within ±30% of the code UHS (Figure 6). The advantage of conducting site-specific studies is the ability to reflect a better estimate of the hazard reflecting latest knowledge on sources and ground motion estimation. However, an engineering interpretation of the results of a hazard analysis should be made before adopting the results of site-specific studies. Considering the importance level of the structure along with the soil conditions and intensity of input ground motions is needed in deciding if capturing nonlinear site response effects through more involved SRA is required, or the site amplification captured by PSHA is sufficient. Furthermore, adopting design hazard that is below code values, reduces the resilience of the structure to earthquake hazards. Alternatively, the results can indicate vibratory period ranges where higher seismic hazard is expected. Here, the SRA UHS is seen to exceed the code spectra between vibration periods of 0.2 -0.7 s. Caution should be taken if the period of the structure lies within this range. The IL, structural performance, and economic and social implications should be considered.

6   CONCLUSION

This study has compared the seismic hazard for a site in East Auckland determined from three different approaches: codified, PSHA and SRA. At this site, this study has demonstrated the code was conservative for the UHS at bedrock for Site Class A/B. The PSHA bedrock hazard calculations were valuable in understanding the seismic sources dominating the seismicity at the site, leading to a more-informed SRA. This information is not readily available in current design codes. The signification variation in SRs and spectral shape from the PSHA and code UHS, to the SRA UHS, highlighted the importance of properly characterising the effects subsurface soils on the ground motion response. This emphasises that site response effects are much more complex than division into discrete soil classes in the NZTA-BM, or the average of the site amplification through V_{s30} in GMMs. Even at low input ground motions, this complexity may be important to capture depending on the context of a project. Even after

the NZ codes have been updated, site-specific studies will offer more advanced characterisation of the seismic hazard through incorporation of the latest scientific knowledge and practices. While codes look at the hazard at regional level, site-specific studies focus on elements in the tectonic environment and soil conditions, providing an indication of the expect range of responses at a given period. However, the structural performance, IL of the structure and economic and social implications should be considered before adopting the results of site-specific studies for design.

7   ACKNOWLEDGEMENTS

The authors would like to acknowledge the support, contribution, and guidance from Guillermo Aldama-Bustos, Manuela Davi, Angeliki Lessi-Cheimarou and Chris Robson.

8   REFERENCES

Abrahamson, N., Silva, W., and Kamai, R. (2014). "Summary of the ASK14 ground motion relation for active crustal regions." Earthquake Spectra.

Abrahamson, N., Gregor, N., and Addo., K. (2016). "BC Hydro ground motion prediction equations for subduction earthquakes". Earthquake Spectra.

Atkinson, G., and Boore, D. (2003). "Empirical ground motion relations for subduction zone earthquakes and their application to Cascadua and other regions." Bulletin of the Seismological Society of America.

ASCE/SEI 7-16. (2017). "Minimum design loads and associated criteria for buildings and other structures." American Society of Civil Engineers.

Baker, J., Bradley, B., and Stafford, P. (2021). "Seismic Hazard and Risk Analysis". Cambridge University Press.

Bommer, J., Douglas, J., Scherbaum, F., Cotton, F., Bungum, H.,and Donat Fäh, D. (2010). "On the Selection of Ground-Motion Prediction Equations for Seismic Hazard Analysis." Seismological Research Letters, https://doi.org/10.1785/gssrl.81.5.783.

Boore D, Stewart J, Seyhan E and Atkinson G (2014). "NGA-West2 equations for predicting PGA, PGV, and 5% damped PSA for shallow crustal earthquakes". Earthquake Spectra, 30(3): 1057-1085.

Bradley, B. (2013). "A New Zealand-specific pseudo-spectral acceleration ground-motion prediction equation for active shallow crustal earthquakes based on foreign models." Bulletin of Seismological Society of America, doi:https://doi.org/10.1785/0120120021.

Bradley, B. (2015). "Benefits of site-specific hazard analyses for seismic design in New Zealand." Bulletin of the New Zealand Society for Earthquake Engineering, doi:https://doi.org/10.5459/bnzsee.48.2.92-99.

Bradley, B., Cubrinovski, M., and Wentz, F. (2022). "Probabilistic seismic hazard analysis of peak ground acceleration for major regional New Zealand locations". Bulletin of the New Zealand Society for Earthquake Engineering.

Campbell, K., and Bozorgnia, Y. (2014). "NGA-West2 ground motion model for the average horizontal components of PGA, PGV, and 5% damped linear acceleration response spectra." Earthquake Spectra.

Chiou, B., and Youngs, R. (2014). "Update of the Chiou and Youngs NGA Model for the Average Horizontal Component of Peak Ground Motion and Response Spectra." Earthquake Spectra, doi:https://doi.org/10.1193/072813EQS219M .

Cornell, C. (1968). "Engineering Seismic Risk Analysis". Bulletin of the Seismological Society of America.

Cubrinovski, M., Bradley, B., Wentz, F., and Balachandra, A. (2022). "Re-evaluation of NZ seismic hazard for geotechnical assessment and design." Bulletin of New Zealand Society for Earthquake Engineering.

Darendeli, M., Stokoe, K., Gilbert, R., Menq, F., and Choi, W. (2001). "Development of a New Family of Normalised Modulus Reduction and Material Damping Curves." University of Texas at Austin.

Dawson, H., Wotherspoon, L., Nelis, S., and Fraser, J. (2015). "Dynamic site characterisation of the Manakau Lowlands Region of Auckland, New Zealand. 6th International Conference of Earthquake Geotechnical Engineering, Christchurch, New Zealand.

Gerstenberger, M., and NSHM Team. (2021). "The 2022 New Zealand National Seismic Hazard Model Revision." Bulletin of the New Zealand Society for Earthquake Engineering.

Kaklamanos, J., and Bradley, B. (2018). "Challenges in predicting seismic site response with 1D analyses: Conclusions from 114 KiK-net vertical seismometer arrays." Bulletin of the Seismological Society of America, pp. 2816–2838.

McGuire, K. (2004). "Seismic hazard and risk analysis." Earthquake Engineering Research Institute.

Ministry of Business, Innovation and Employment. (2021). "Acceptable Solutions and Verification Methods: For New Zealand Building Code, B1 Structure." Wellington, New Zealand.

New Zealand Transport Agency. (2018). "Bridge Manual: SP//M/022. CH5 and CH6." Wellington, New Zealand.

Rodriguez-Marek, A., Bommer., J., Youngs., Robert., Crespo, M., Stafford, P., and Bahrampouri, M. (2021). "Capturing epistemic uncertainty in site response." Earthquake Spectra, doi: https://doi.org/10.1177/8755293020970975

Standards New Zealand. (2004). "NZS1170.5: Structural Design Actions. Part 5: Earthquake Actions-New Zealand." Standards New Zealand, Wellington, NZ.

Stewart, J and Hashash, Y. (2014). "Guidelines for Performing Hazard-Consistent One-Dimensional Ground Response Analysis for Ground Motion Prediction." Pacific Earthquake Engineering Research Centre, University of California at Berkely.

Stirling, M., McVerrry, G., and Berryman, K. (2002). "A new seismic hazard model of New Zealand." Bulletin of the Seismological Society of America.

Stirling, M., McVerry, G., Gerstenberger, M., Litchfield, N., Van Dissen, R., Berryman, K., Barnes, P., Wallace, L., Villamor, P., Langridge, R., Lamarche, G., Nodder, S., Reyners, M., Bradley, B., Rhoades, D., Smith, W., Nicol, A., Pettinga, J., Clark, K., and Jacobs, K. (2012). "National seismic hazard model for New Zealand: 2010 Update." Bulletin of the Seismological Society of America, doi:https://doi.org/10.1785/0120110170

Toro, G. (1995). "Probabilistic models of site velocity profiles for generic and site-specific ground-motion amplification studies." Brookhaven National Laboratory, Upton, New York.

Van Houtte, C. (2017). "Performance of Response Spectral Models against New Zealand data." Bulletin of the New Zealand Society for Earthquake Engineering, doi:https://doi.org/10.5459/bnzsee.50.1.21-38

Zhao, J., Zhang, J., Asano, A., Ohno, Y., Oouchi, T., Takahashi, T., Ogawa, H., Irikura, K., Thio, H., and Somerville, P. (2006). "Attenuation relations of strong ground motion in Japan using site classification based on predominant period." Bulletin of the Seismological Society of America.

Geotechnical Design of Non-Conventional Bridge Abutments at the Hakao Gully in Tauranga, New Zealand

K. D. Irmaputri[1]

[1]Geotechnical Engineer, Arup NZ Ltd (formerly Beca Ltd), 205/209 Queen Street, Auckland 1010, New Zealand; PH: +64 9 301 7000; email: khalista.irmaputri@arup.com

ABSTRACT

The Takitimu North Link (TNL) Stage 1 project delivers 6.8 km of new expressway: connection between State Highway 2 (west of Te Puna) to State Highway 29 (Takitimu Drive) and upgrade to the connecting stretch of State Highway 29 into Tauranga. The project is part of the government's New Zealand Upgrade Programme (NZUP).
The Minden Gully Bridges are a set of three separate structures designed and constructed for this project, comprising of mainline, on-ramp and off-ramps bridges, all located within the same 25-40 m high, steeply sloped Hakao gully. The bridge abutments were formed as piers, connected to the ground behind with settlement slabs bearing on reinforced soil slopes. The geology of the site was found to be highly variable between the east and west sides of the gully, as well as some variation from north to south. As such, various refinements and sub-layering were completed as part of the geotechnical design to adequately capture site soil conditions. The complex geology and topography of the site, together with the selected bridge abutment arrangements, called for specific geotechnical design for each bridge, including achieving compatibility between each geotechnical element and soil-structure interaction for the design of shear pile ground improvement.

Keywords: bridge, gully, abutment, shear piles, reinforced soil slope

1   INTRODUCTION

The TNL Stage 1 project is being delivered by Fulton Hogan Limited and HEB Construction Limited as a Joint Venture (JV) under a design and construct contract. The design of Takitimu North Link Stage 1 is being delivered by Beca Ltd (Beca), as lead designer, with Holmes Consulting Group Limited Partnership (Holmes) as a subconsultant. This project includes the design and construction of eight bridges, three million cubic metres of earthworks, 29 culverts, eight stream diversions, seven wetland areas, and a continuous and separate shared 'active mode path'. This project will significantly improve safety and ease congestion for the existing State Highway 2, in addition to supporting urban growth, providing more transport choices, and building resilience.
The Minden Gully Bridges are located adjacent to a full grade-separated interchange at Minden Road, designed to carry the mainline, an on-ramp lane and an off-ramp lane on three separate bridges over the Hakao gully. The bridges are typically 130-140 m long, three-span with foundations composed of 710 mm diameter driven steel pile casings, infilled with concrete. Refer Figure 1 for site plan.
Liquefaction assessments, slope stability assessments and pile design under seismic design loads were undertaken for the bridges as part of the design; however, this paper will focus on the discussion regarding performance of the bridges under static design criteria.

2   BRIDGE ARRANGEMENTS

2.1   Bridge Form

Balanced bridge forms and suitable lengths for the end spans were important for the structural design. As such, the abutments of all three bridges are composed of a piled abutment with 6-7.5 m long settlement slabs that extend back to a reinforced soil slope. With this arrangement, more detailed geotechnical design was required compared to conventional abutment design.
The abutments and piers are founded on 710 mm diameter driven steel pile casings infilled with concrete and partially reinforced. Oversized casings 5 m in length with a clear annulus between the sleeves and the piles were proposed for the abutment piles to reduce the demands caused from superstructure thermal and time dependent shortening strains, as well as reducing seismic demands. The abutment arrangement is shown diagrammatically in Figure 2.
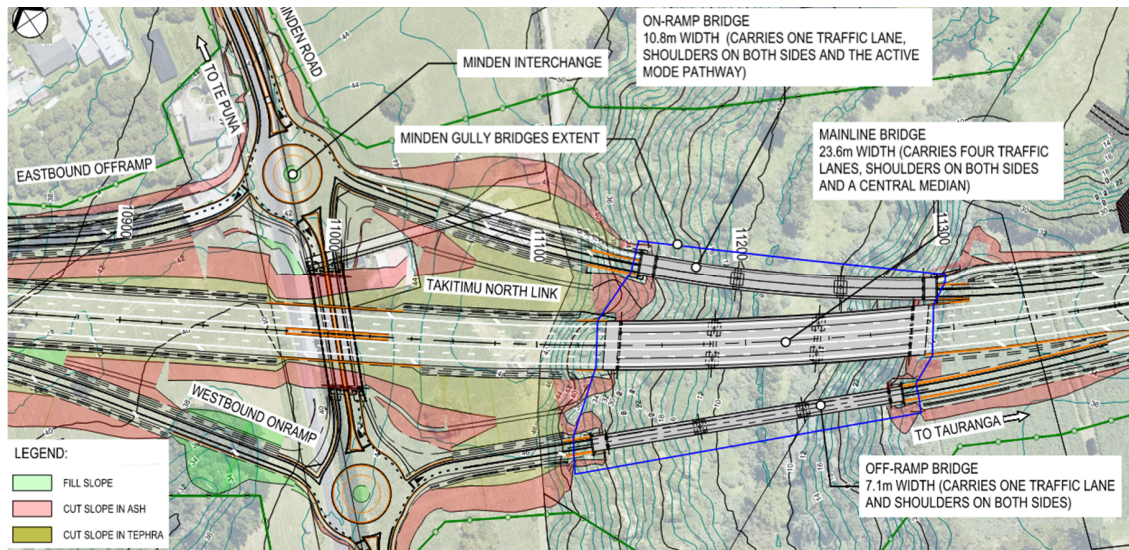
Figure 1: Site Plan

2.2   Settlement Slab Loads

The free end of the settlement slab rests on a concrete slab, with an expansion joint provided between these two elements. Through this arrangement, the reinforced soil slope is subject to axial and lateral loads from the settlement slab. These loads are provided by the structural engineer and comprise of:

- Axial – from the dead load of the concrete slab and settlement slab.
- Axial – from live loads (traffic on the settlement slab).
- Lateral – from thermal contraction of the bridge due to changes in temperature throughout the day. It arises from friction between the settlement slab and the abutment concrete slab. It is a component of the dead load and has a load direction out-of-the-slope (i.e., longitudinal to the bridges alignment).

Various load combinations for these loads are considered in the stability assessments and reinforced soil slope design. These load combinations are as follows:

- Static ULS (long-term) case
- Static SLS (short term): HO (overload) traffic case
- Static SLS (short term): elevated groundwater case
- Static SLS (short term): combined thermal effect and traffic case
- Seismic cases

Behind the settlement slab, typical traffic loads from the Bridge Manual (Waka Kotahi NZ Transport Agency, 2018) are applied: HN (normal) traffic loading of 12 kPa and HO (overload) traffic loading of 24 kPa. The arrangement of loads is shown diagrammatically in Figure 2.
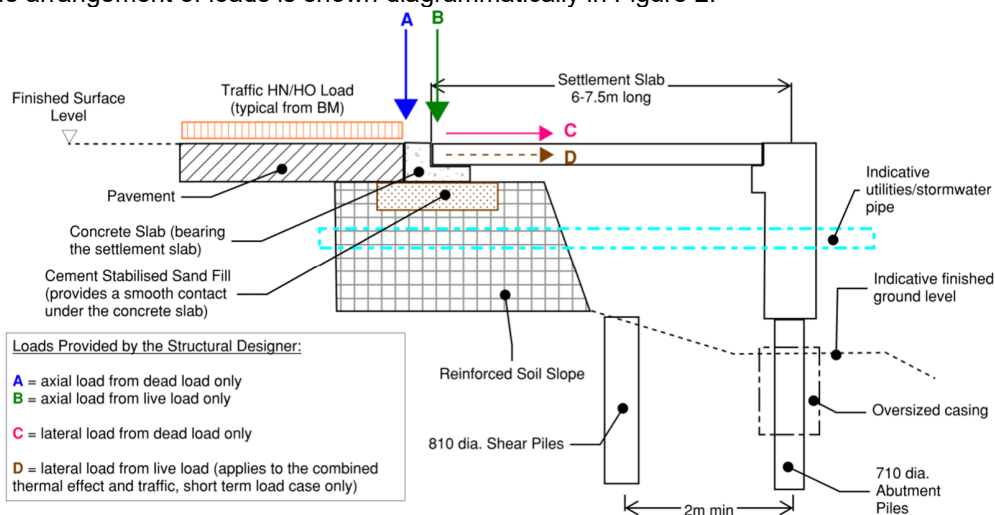
Figure 2: Typical abutment arrangement and settlement slab loads (shown diagrammatically)

3   GEOLOGY SETTING

The geology of the site generally comprises of Matua Subgroup - Interbedded (unit T3b) soils overlying Pakaumanu and Waiteariki Ignimbrite with surficial layers of Colluvium (unit T1b) on the gully slopes and Alluvium (unit T1a) deposits at the gully floor.

The Matua Subgroup - Interbedded is described as highly variable deposit comprising fluvial pumiceous and rhyolitic silts, sands, and gravels, lacustrine and estuarine muds, lignites, and peats, intercalated with airfall tephra and thin distal ignimbrites. The Pakaumanu Ignimbrite is described as non-welded to partially welded ignimbrite. The Pakaumanu Ignimbrite is divided into two units. The finer unit (unit T5a) is a completely weathered to highly weathered ignimbrite comprising firm to stiff clayey silt to silty sand, and the coarser unit (unit T5b) is a highly weathered ignimbrite comprising medium dense to dense silt to sand. In general, the finer unit typically underlies the coarser unit. Finally, Waiteariki Ignimbrite (unit T6) is typically highly to moderately weathered, partially welded to welded Ignimbrite (Briggs, 1996).

A series of ground investigations were undertaken in stages between 2011 and 2021, comprising of 15 machine boreholes (maximum depth of 55.7 m bgl), 10 CPTs, 4 sCPTs, 5 test pits, and 7 hand augers. Geological sections were generated from the three-dimensional site-wide ground model developed within the Leapfrog Geo software package. Longitudinal geological sections were taken along the bridge alignment and selected north and south edges of each of the three bridges, such that variation in topography and geology could be taken into consideration in the design. One of the longitudinal geological sections, located at the centreline of the mainline bridge, is shown in Figure 3.

4   ENGINEERING SOIL PROFILE

Varying soil strengths and behaviour within the same geology unit were encountered between the east and west sides of the gully. Refinements and sub-layering of these units were carried out to adequately capture site soil conditions therefore providing robust design for the lateral capacity of the bridge and shear piles, as well as slope stability assessments.

4.1   Matua Subgroup – Interbedded

The Matua Subgroup – Interbedded (T3b) was interpreted to have variable undrained shear strengths between the gully floor and slopes. Therefore, three different undrained shear strengths are assigned to the gully floor, east and west gully slope.

A pocket of Matua Subgroup – Interbedded was identified beneath the Pakaumanu Ignimbrite along the alignment of the on-ramp bridge. This soil sub-unit was described as predominantly sandy; hence this unit is interpreted as having "sand-like" behaviour and exhibits different behaviour to the shallower Matua Subgroup – Interbedded unit which mainly comprises of silts and clays. This unit was named Matua Subgroup – Interbedded – North (T3bN) and is only applicable at the on-ramp bridge. Although not discussed further within this paper, the presence of this material posed an interesting challenge to the piling works for the on-ramp bridge Pier B. It also provided further evidence of the complexities of ground conditions at this site.

4.2   Pakaumanu Ignimbrite

The Pakaumanu Ignimbrite – Coarse (T5a) unit was found to be variable across the gully. To account for this variability, the Pakaumanu Ignimbrite – Coarse was divided into three sub-units:
- Pakaumanu Ignimbrite – Coarse – Upper (T5a1): this sub-unit was identified at the west gully slope and interpreted as predominantly clayey, with relatively low strength (N-SPT ranges between 0 and 6) and interpreted to overlie a more competent unit of the T5a2. Consequently, this unit was modelled as exhibiting softer lateral soil springs compared to the other sub-units.
- Pakaumanu Ignimbrite – Coarse – Middle (T5a2): this sub-unit was identified as predominantly medium dense to dense silty sands with median N-SPT value of 35.
- Pakaumanu Ignimbrite – Coarse – Lower (T5a3): this sub-unit was interpreted as having similar behaviour with T5a2 with higher strength considering median N-SPT value of 50+. If T5a2 and T5a3 are not separated, the slip circle will pass through N-SPT=50+ layers. Separating this unit with T5a2 allows for higher soil parameters to be assigned, hence resulted in realistic slip shapes and sizes for the slope stability assessment. Therefore, a compatible solution between the design of bridge piles, shear piles, and the slope seismic displacements was achieved. Additionally, this sub-unit was targeted for the toe of the bridge abutment piles, providing adequate fixity as required by the structural design.

The Pakaumanu Ignimbrite – Fine (T5b) unit was found to have differing soil descriptions within the site and hence was divided into two sub-units:

- Pakaumanu Ignimbrite – Fine – West (T5bW): this sub-unit was interpreted as predominantly clayey with median N-SPT value of 20.
- Pakaumanu Ignimbrite – Fine – East (T5bE): this sub-unit was interpreted as predominantly sandy with median N-SPT value of 50+.

4.3   Waiteariki Ignimbrite

The Waiteariki Ignimbrite (T6) unit was found to have differing soil descriptions and strengths. Therefore, this unit was divided into two sub-units:

- Waiteariki Ignimbrite – West (T6W): this sub-unit was interpreted as having "clay-like" behaviour with a median N-SPT value of 19 and applicable to the west gully slope only. While the slip circle is unlikely to reach this sub-unit, separating this sub-unit allows for modelling soft lateral springs at depths and assigning lower end bearing and skin friction capacity for the abutment piles.
- Waiteariki Ignimbrite (T6): this sub-unit was interpreted as having "sand-like" behaviour with a median N-SPT value of 50+.

4.4   Engineering Long Section

Longitudinal engineering sections were developed from the geological long sections based on the refinements discussed above. Figure 4 shows the development from geological section to engineering section for the Mainline bridge at the centreline.
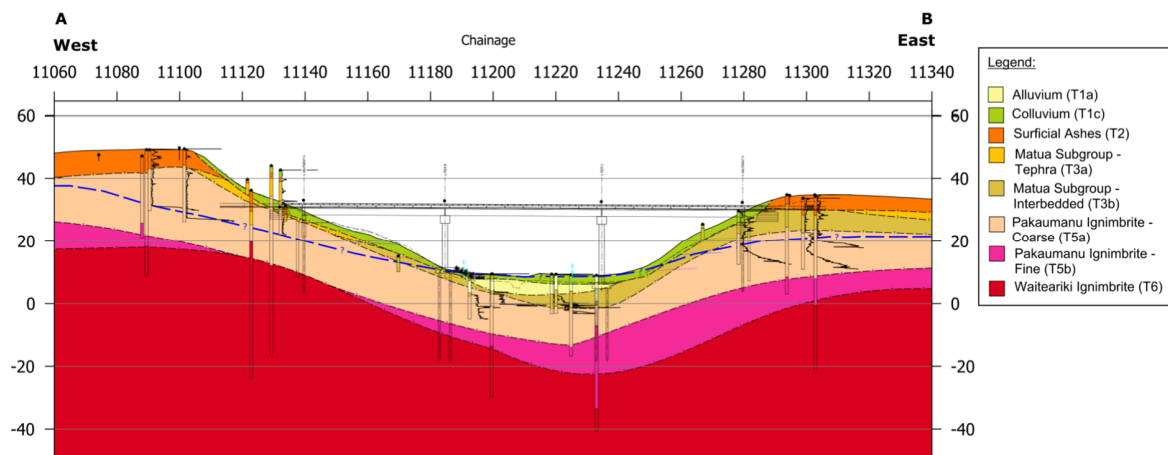
Figure 3: Geological Section of the Mainline Bridge, taken at the centreline
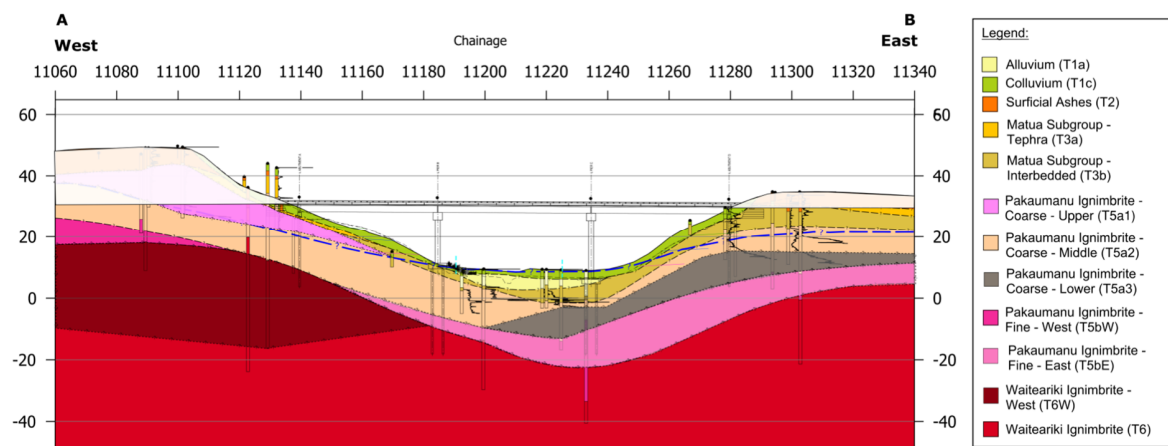
Figure 4: Engineering Section for the Mainline Bridge, taken at the centreline

PROCEEDINGS OF THE 14TH ANZ YOUNG GEOTECHNICAL PROFESSIONALS CONFERENCE
14YGPC ROTORUA, NEW ZEALAND, 2ND – 5TH NOVEMBER 2022

17

5   SLOPE STABILITY ASSESSMENT AND SHEAR PILES GROUND IMPROVEMENT

Stability analyses were carried for static, seismic, and post-seismic design cases using the Geostudio Slope/W software package to assess the performance following requirements described in the Bridge Manual. Different engineering long sections between the abutments were considered to capture variability in topography affecting the critical sections. Figure 5 shows an example where the critical slope stability assessment locations for each abutment are different for the Off-ramp bridge.
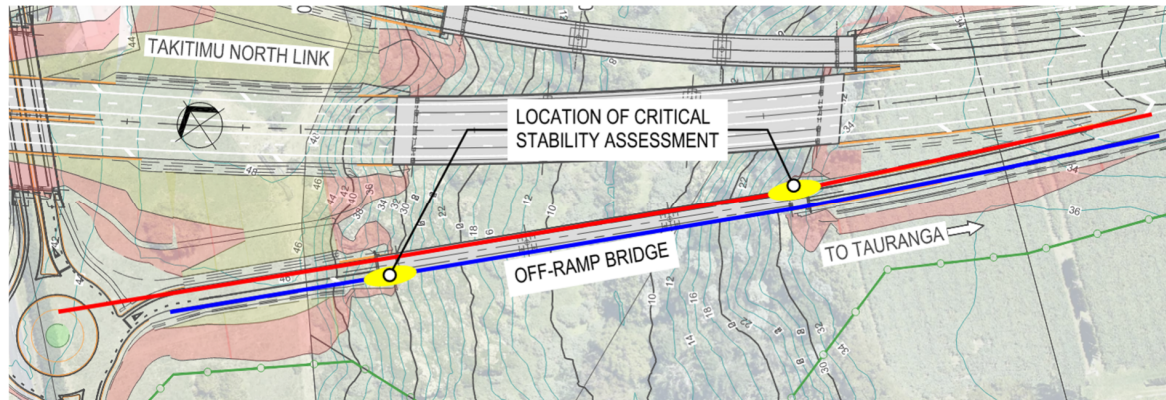
Figure 5: Location of critical stability assessment for the Off-ramp bridge

The settlement slab loads discussed in Section 2.2 are applied at the top of the reinforced soil slope.
A row of 810 mm diameter driven steel pile casings at each abutment is required as shear piles to increase the long-term static factor of safety of the slopes at the abutments to the required value of 1.5, noting that the bridge piles are not considered to provide any pinning effect onto the abutment soil. The slope stability analyses were used to determine the required shear capacity of the shear piles.
It is noted that the factor of safety of the slopes at the abutments under static long-term conditions, without the shear pile ground improvement, is 1.3 and the target factor of safety of 1.2 is achieved under all static short-term conditions without the shear pile ground improvement. Hence the static long-term case became the critical case for slope stability assessment.
Although, theoretically, no slope displacements are anticipated to develop for slopes with a minimum factor of safety of 1.5, a compatibility assessment was carried out in conjunction with the structural designers. Soil-structure interaction analyses was undertaken to consider the required shear resistance onto the structural model by applying a displacement to the shear piles, thus confirming a compatible solution. The required displacement was applied as individual displacements to the pinned ends of the soil link elements (i.e., below the slip circle). The shear piles were modelled by the structural designers in CSi Bridge software package, using nominal lateral soil spring values developed by the geotechnical design using LPile software package. Figure 6 shows illustratively the soil-structure interaction within the shear piles.
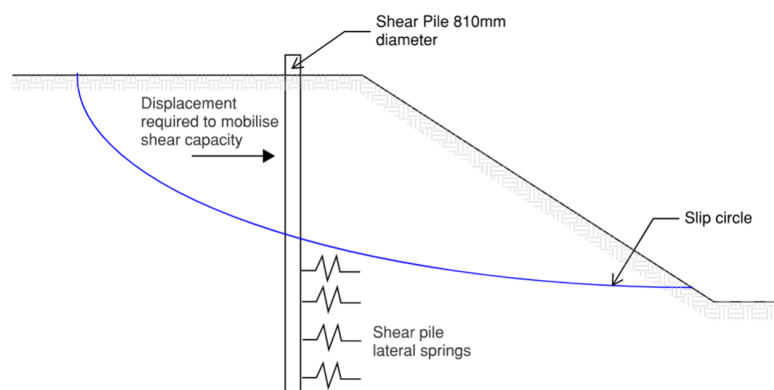
Figure 6: Soil-structure interaction in shear piles

An estimated displacement of 25-100 mm is required to mobilise the required ultimate shear capacity. Although it is considered unlikely that these displacements will occur (considering the static factor of

safety without shear piles is 1.3), this soil displacement profile was considered as a static demand for the abutment piles after the required shear resistance has been generated.

6 REINFORCED SOIL SLOPE

The reinforced soil slope runs for the full width of the settlement slab and returns parallel to the carriageway. It has a 70° face angle (from the horizontal) with a gabion basket finish on the face (achieved via Terramesh facing units infilled with rock). HDPE geogrids provide reinforcement to the slope. GAP65 hardfill (cement stabilised at the wrap arounds) was specified as backfill to provide a robust soil structure.

The reinforced soil slope design was carried out using MSEW+ software package. The relevant AASHTO (2020) load factors were applied onto the settlement slab loads discussed in Section 2.2, as well as traffic load behind the settlement slab and pavement fill. The short-term combined thermal effect and traffic case was found to be the critical case for the reinforced soil slope design due to high lateral force generated from the settlement slab. The direct sliding between geogrid and hardfill generally dictated the minimum geogrid length requirements. As such, cement stabilised sand fill (Refer Figure 2) was proposed to provide an even and homogeneous surface under the concrete slab to reduce the lateral load onto the reinforced soil slope. Additionally, the top two grids were proposed to be longer than the lower grids to support the loads from the settlement slab.

The set out proposed for the reinforced soil slopes are unique to each bridge due to the irregular interface with the existing gully slopes, presence of utilities and stormwater pipes crossing through the slopes, the longitudinal and transverse fall of the road, as well as the bridges' skew angle. Additional Terramesh blocks were proposed locally at some locations to manage these variabilities, hence the height of the reinforced soil slope varies between 3 m and 4.5 m.

Continuous reinforced soil slope was proposed for the mainline and on-ramp east abutments due to the limited space between two abutments. This design was achieved by taking into consideration the difference in elevations, potential clashes with the adjacent bridge structure, and the existing gully slope. The set out for the reinforced soil slope also influenced the set out for the shear piles. The shear piles were proposed to have minimum 2 m spacing from the bridge piles (Refer Figure 2), however at some location this is only achievable if the shear piles are below the toe of the reinforced soil slope due to limited room. The design identified the affected shear piles and proposed specific top of shear piles elevation for piles below the reinforced soil slope.

7 CONCLUSION

The geotechnical elements of the Minden Gully Bridges have been successfully designed by taking the variability of ground conditions, topography, and unconventional abutment form into consideration. Refinements of engineering soil profile and sub-layering were carried out to adequately capture site soil conditions for geotechnical design, particularly for achieving compatibility between the bridge pile design, shear pile design, and slope stability assessment.

The loads imposed by the settlement slab onto the reinforced soil slopes are considered for the slope stability assessment and reinforced soil slope design. Different critical cases were encountered between the two analyses, where static long-term was the critical case for the slope stability and the short-term combined thermal effect and traffic case for the reinforced soil slope design. Bespoke reinforced soil slope set out was provided for each abutment as part of the design to handle irregularities of the gully profile as well as various design constraints.

8 ACKNOWLEDGEMENTS

9 REFERENCES

American Association of State Highway and Transportation Officials. (2020). *LRFD Bridge Design Specifications.* Washington: American Association of State Highway and Transportation Officials.
Briggs, R. M. (1996). *Geology of the Tauranga area.* Hamilton: University of Waikato: Department of Earth Sciences.
Waka Kotahi NZ Transport Agency. (2018). *Bridge Manual SP/M/022* (3rd ed.). Wellington: Waka Kotahi NZ Transport Agency.

PROCEEDINGS OF THE 14TH ANZ YOUNG GEOTECHNICAL PROFESSIONALS CONFERENCE
14YGPC ROTORUA, NEW ZEALAND, 2ND – 5TH NOVEMBER 2022

19

The effect of confinement on rock failure behaviour under high-velocity impact

Jing Li[1], Qianbing Zhang[2], Chor Kin Tsang[1], Tong Joo SIA[1].

[1]SMEC Australia, Melbourne, VIC 3008, Australia; email: frank.li@smec.com; ck.tsang@smec.com; tongjoo.sia@smec.com.
[2]Civil Engineering, Monash University, VIC 3800, Australia; email: qianbing.zhang@monash.edu.

ABSTRACT

The result of redistributed quasi-static stress and/or dynamic sources can be serious underground disasters such as rock bursts. Rock failure characteristics are heavily affected by loading rates and confinement. A deep understanding of their roles has practical significance in evaluating the stability and the design of underground engineering. In this study, specimens were first confined under quasi-static uniaxial, biaxial and triaxial pre-stress conditions and then these were impacted by the launch of a high-velocity striker using a triaxial Hopkinson bar system. A high-speed imaging technique was used to record real-time deformation and fracturing processes. The rock dynamic behaviours such as stress-strain behaviours and energy evolutions were quantitatively investigated. The relationship between mechanical properties and fragmentation features was also presented.

Keywords: rock dynamic behaviours, confinement effects, fragmentation, triaxial Hopkinson bar

1   INTRODUCTION

Underground mining and tunnelling excavation significantly change the natural stress field of the surrounding rock mass. Rock will be damaged when the stress exceeds its strength limit. Analysis and prediction of rock failure is one of the key purposes of rock mechanics. Rock damage under quasi-static conditions have been extensively studied from failure criterion, energy evolution, micro-seismicity and so on (Hoek, 1964; Mogi, 1971, Lockner et al. 1991, Niandou et al. 1997, Hazzard and Young, 2000). These research findings have provided important guidance on engineering practices. Rock can also fail suddenly due to various dynamic/seismic loads from fault slip, roof breakage and blasting. Figure 1 shows an example of a coal burst hazard triggered by dynamic sources. Rock failure under dynamic loads has more complex characteristics due to strain rate effects. Numerous experimental studies have been carried out in this regard mainly using a split Hopkinson pressure bar (SHPB) system (Field et al. 2004; Kolsky, 1949). Comprehensive reviews on experimental techniques and mechanical behaviours of rock dynamic tests can be found in Zhang and Zhao (2014).
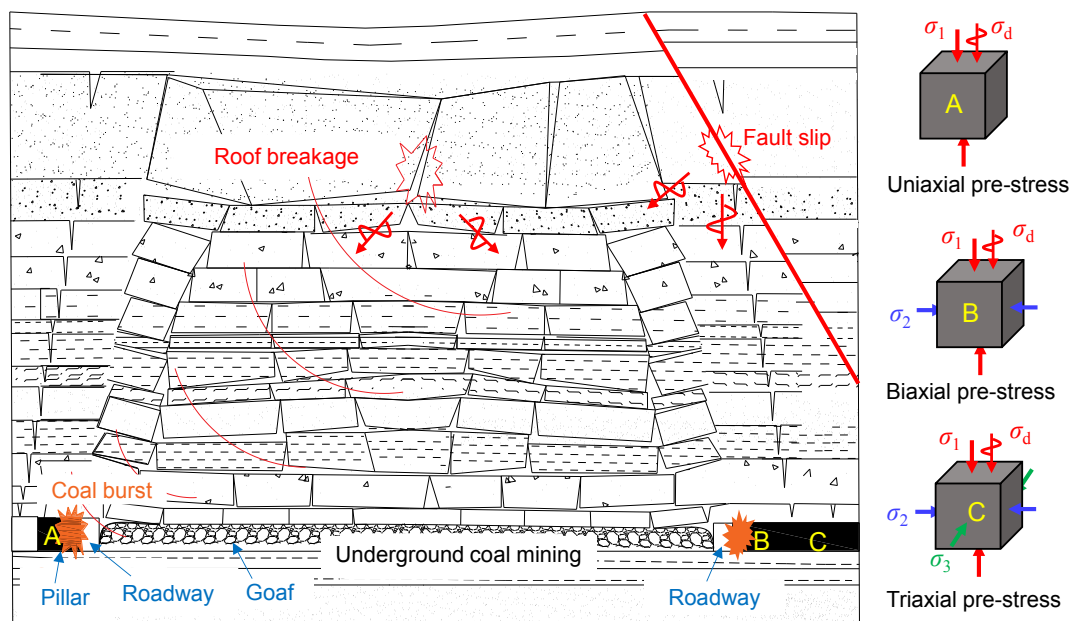
Figure 1: Coal stress states and coal burst hazards in mining. σ_1, σ_2 and σ_3 are maximum, intermediate and minimum principal stress, respectively. σ_d means dynamic loading.

Confinement is one of the most important factors affecting rock behaviour. The SHPB was also further improved so that confinement can be applied on the tested specimens (Christensen et al., 1972; Frew et al. 2010; Li et al. 2008). More recently, triaxial Hopkinson pressure bar was developed aiming to apply biaxial/true-triaxial pre-stresses and dynamic loads (Liu et al. 2019; Zhang et al. 2021; Li et al. 2021). Experimental results showed that improving confinement not only can significantly increase rock bearing capacity, but also change failure patterns. However, there is still a lack of research on dynamic mechanical and fracturing characteristics of rock under the coupled effect of strain rates and confinement. A comprehensive investigation of the coupled static and dynamic loads under different confinement types is of critical knowledge for the prevention of potential hazards and the improvement of underground engineering safety.

In this study, dynamic uniaxial, biaxial and triaxial tests were conducted on rock specimens by using a triaxial Hopkinson bar system, respectively. Real-time rock deformation and fracturing process were captured by high-speed cameras. The relationships among stress-strain response, peak stress, and failure patterns were explored and discussed in detail.

2   EXPERIMENTAL TESTS AND DATA ACQUISITION

Dynamic uniaxial, biaxial and triaxial compressive tests were conducted using a triaxial Hopkinson bar (Tri-HB) system, as shown in Figure 2. In the tests, a cubic specimen was placed in the loading cell where quasi-static confinement can be applied by movements of square steel bars aligned orthogonally in X, Y and Z directions. After the desired confinement was achieved, the dynamic loading was applied by the launch of the striker compressed by the gas gun. When the striker hits the incident bar, a compressive stress wave propagates towards the specimen and a transmission wave is generated in the transmission bar in the X direction. Meanwhile, the wave also propagates in the Y and Z bars. The velocity of the striker bar is measured by a laser-beam velocity measurement system. A detailed introduction to the Tri-HB system is provided in previous publications (Liu et al. 2019; Liu et al. 2020; Zhang et al. 2021). The dynamic stress σ, strain rate $\dot{\varepsilon}$ and strain ε can be obtained from incident, reflected and transmission waves recorded by strain gauges (Kolsky, 1949; Cadoni and Albertini, 2011). The energy carried in these waves can also be further calculated.

In this study, coal specimens with Uniaxial Compressive Strength (UCS) of 27.16 MPa and elastic modulus of 2.17 GPa were prepared for the tests. For the dynamic uniaxial compressive (UC) tests, the specimen was impacted without quasi-static confinement. In the dynamic biaxial compressive (BC) tests, the specimen was subjected to impacting under biaxial quasi-static pre-tress conditions. Biaxial pre-stresses σ_1 =10 MPa and σ_2 = 5 MPa were applied on the specimens in the X and Y directions, respectively. In the dynamic biaxial compressive (TC) tests, the specimen was impacted under triaxial pre-stresses σ_1 = 15 MPa, σ_2 = 10 MPa and σ_3 = 5 MPa in the X, Y and Y directions, respectively. For all the tests, impact was along the X direction.

(a)   (b)
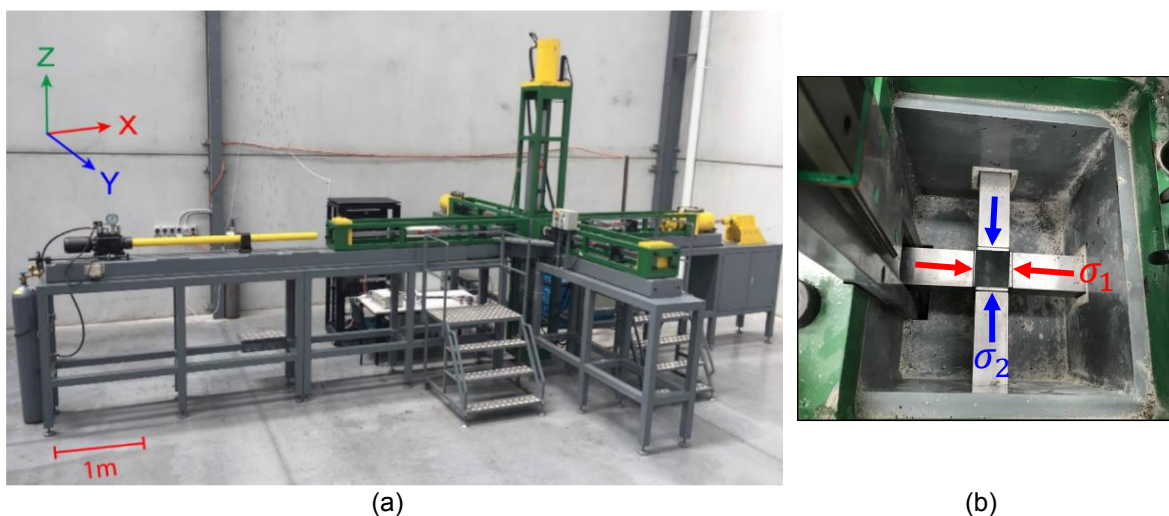
Figure 2: Triaxial Hopkinson bar at Monash University (a) and a standard cubic coal specimen placed between bars in the loading cell (b).

PROCEEDINGS OF THE 14TH ANZ YOUNG GEOTECHNICAL PROFESSIONALS CONFERENCE
14YGPC ROTORUA, NEW ZEALAND, 2ND – 5TH NOVEMBER 2022

21

3 RESULTS AND DISCUSSION
3.1 Stress-strain responses

Figure 3a-c shows the effect of strain rates on the dynamic stress-strain curves for specimens under uniaxial, biaxial and triaxial pre-stress conditions. Two types of stress-strain curve Class-I and Class-II can be observed according the evolution of strain and stress with loading process. For Class-I stress-strain curves, the dynamic strain continually increases to the peak and then decreases, while dynamic strain keeps increasing during the whole loading process for Class-II types. The strain recovery in the unloading stage of Class-I type prevents further failure of specimens, however continued deformation leads to the specimen failure for Class-II type curves. Experiments indicate that only Class-II type stress-strain curves were exhibited by specimens under uniaxial confinement. This means that specimens were damaged and did not have sufficient bearing capacity under this loading condition. Failure patterns also demonstrate that specimens were shattered into multiple fragments and the degree of fragmentation increased with increasing strain rates as shown in Figure 3a. For specimens under biaxial confinement, stress-strain curves gradually changed from Class-I to Class-II type as strain rate increased. At strain rates of 87.4 s^{-1} and 125.7 s^{-1}, specimens remained macroscopically or partially intact since the applied dynamic loading was insufficient to break specimens. The failure modes correspond to the Class-I stress-strain type, where the strain reduces gradually with the decrease of stress at post-peak stage. Specimens were pulverised into fragments when the strain rate exceeded the 188.4 s^{-1} as shown in Figure 3b. For specimens under triaxial confinements, the stress-strain curves always remained Class-I type when the strain rates increased from 107.5 s^{-1} to 191.2 s^{-1}. Failure patterns also show that specimens were not damaged as shown in Figure 3c. Figure 3d illustrates the relationships among peak stresses, strain rates and confinement. The peak stress exhibits an upward trend with the increasing strain rates under any confinement type. At the same strain rate, increasing restraints can improve specimen bearing capacity. Besides, strain rate sensitivity of peak stresses sees an increasing trend when the confinement type was changed from uniaxial to triaxial conditions.

(a)

(b)

(c)

(d)
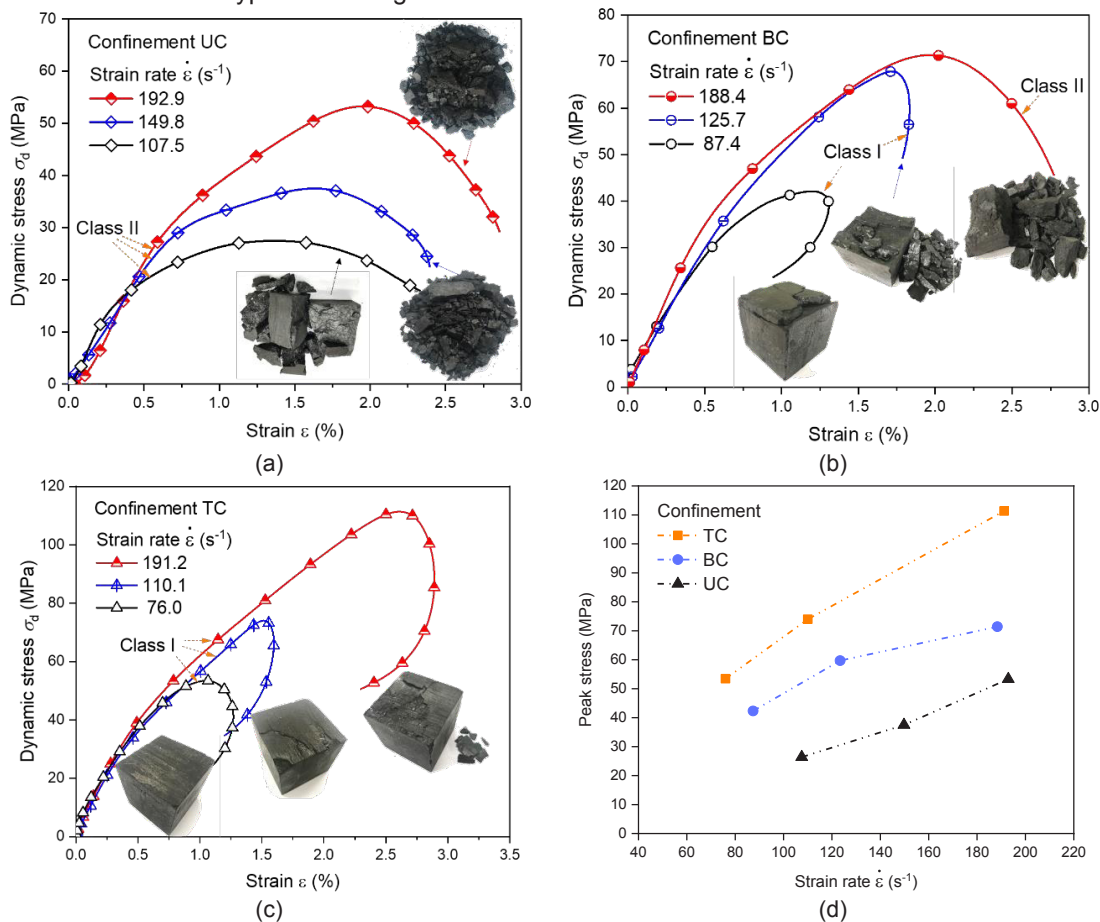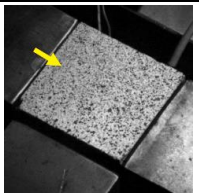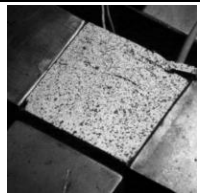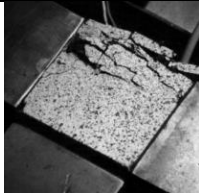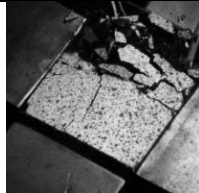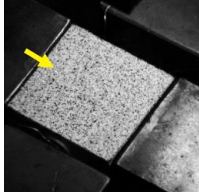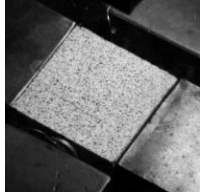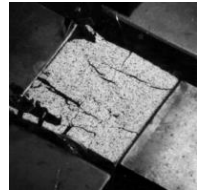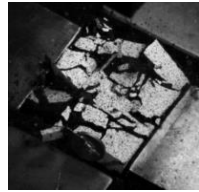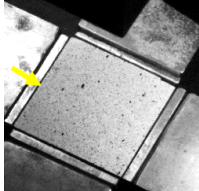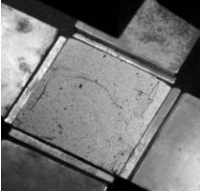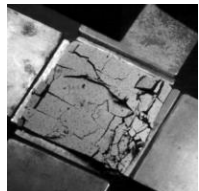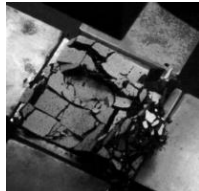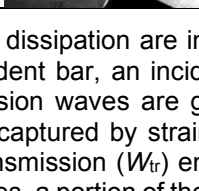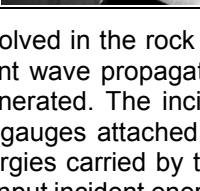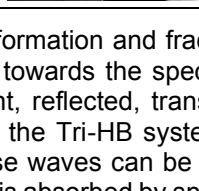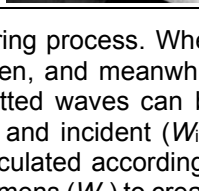
Figure 3: Stress-strain curves (a-c) and peak stresses (d) under the effect of strain rates and confinements.

3.2 Energy evolution

Table 1 compares the high-speed photography of rock dynamic failure process under uniaxial and biaxial confinement. Under UC conditions, the specimen deforms elastically without visible cracks on the surface at the initial loading stage, and several cracks parallel to impact direction emerge with further loading. These tensile cracks are caused by tension perpendicular to the impact direction. As the strain rate increases, more tensile cracks are produced, and the fragmentation degree is further improved. When the specimen is confined under BC conditions, biaxial prestresses cause the splitting failure of exposed surfaces, and flake surface into small fragments.

Table 1: Specimen failure patterns with the influence of strain rates and confinement. The yellow arrow indicates impacting direction.

Confinement	Strain rate/s	High-speed photographs of specimen fracturing processes			
		t = 0 *ms*	0.2 *ms*	1 *ms*	1.7 *ms*
UC	107.5				
UC	149.8				
BC	125.7				

Energy absorption and dissipation are involved in the rock deformation and fracturing process. When the striker hits the incident bar, an incident wave propagates towards the specimen, and meanwhile reflected and transmission waves are generated. The incident, reflected, transmitted waves can be extracted with signals captured by strain gauges attached on the Tri-HB system, and incident (W_{in}), reflected (W_{re}) and transmission (W_{tr}) energies carried by these waves can be calculated accordingly (Liu et al., 2020). Besides, a portion of the input incident energy is absorbed by specimens (W_s) to create fracture surface and micro-cracks. The amount of energy absorbed by rock specimens directly determines the damage severity.

Figure 4 presents the energy evolutions for specimens under uniaxial, biaxial and triaxial confinement at a strain rate of around 190 s^{-1}. For specimens under different pre-stress conditions, the evolution of various energies is similar in the deformation and fracturing stages. The energies increase slowly at the initial dynamic loading stage, while at 100 µs these energies increase sharply and growth rate slows down above 250 µs. Confinement plays a significant role in energy distribution. To achieve the same strain rate, the triaxially confined specimens require the highest input incident energy, while the lowest input energy is found for uniaxially confined specimens.

PROCEEDINGS OF THE 14TH ANZ YOUNG GEOTECHNICAL PROFESSIONALS CONFERENCE
14YGPC ROTORUA, NEW ZEALAND, 2ND – 5TH NOVEMBER 2022

23

(a) UC at strain rate of 107.5 s⁻¹

(b) UC at strain rate of 192.9 s⁻¹

(c) BC at strain rate of 188.4 s⁻¹

(d) UC at strain rate of 191.2 s⁻¹
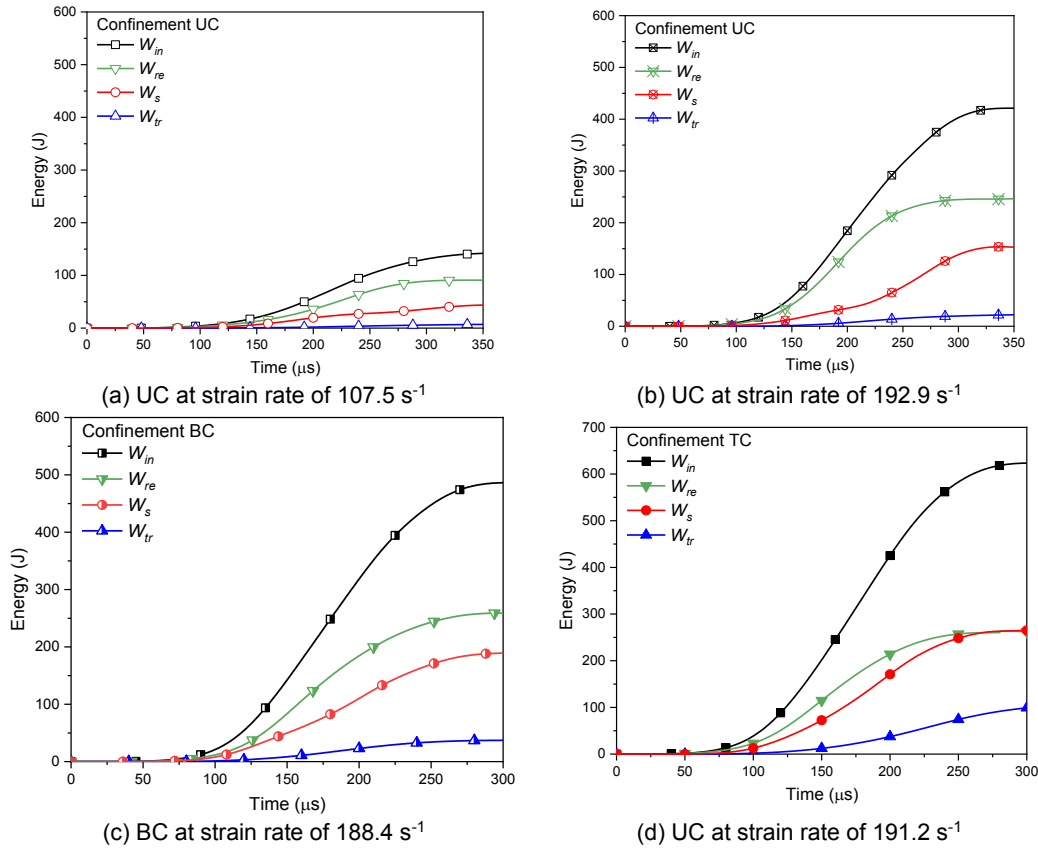
Figure 4: Energy evolutions for specimens under uniaxial, biaxial and triaxial confinements.

Figure 5 shows the effect of confinement type on the absorption energy at high-velocity impacting. Increasing strain rates or the input incident energy can make the specimen absorb more energy and meanwhile increase the fragmentation degree as indicated in Figure 3. At the same strain rate or incident energy, the largest absorption energy is observed when triaxially confined (TC) while the lowest value is found for Uniaxial confinement (UC). The varied energy absorption abilities are caused by difficulties in creating cracks. More energy will be consumed to create cracks with increasing confinement. To achieve the same fragmentation degree, specimens under TC consume the most amount of energy, while the minimum energy consumption is required to achieve the same damage degree for UC. This also offers an explanation why the specimen is failed at the strain rate of 107.5 s⁻¹, while triaxially confined specimens remain intact at a strain rate of 191.2 s⁻¹.

(a)

(b)
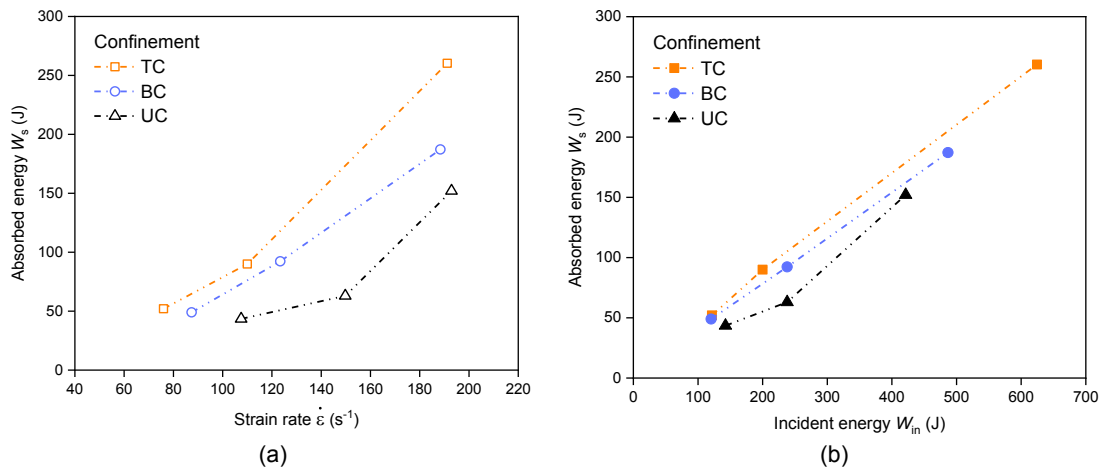
Figure 5: Correlation between specimen absorbed energy with strain rates (a) and incident energy (b).

24

PROCEEDINGS OF THE 14TH ANZ YOUNG GEOTECHNICAL PROFESSIONALS CONFERENCE
14YGPC ROTORUA, NEW ZEALAND, 2ND – 5TH NOVEMBER 2022

4   CONCLUSION

In this study, the effect of strain rate and confinement type on the rock mechanical and fracturing properties was investigated using a triaxial Hopkinson Bar system. Experimental results show that increasing strain rates improve the rock strength but also decrease its integrity. Increasing confinement can significantly reduce the fragmentation degree while increasing the ability of the rock to resist dynamic loads. Energy evolution analysis indicates that as the strain rate increases, more energy is absorbed to generate cracks. At the same strain rate, crack generation requires the minimum absorbed energy for uniaxial confinement, while the highest energy is absorbed in the triaxial case.

5   ACKNOWLEDGEMENTS

REFERENCES

Cadoni, E., and Albertini, C. (2011). "Modified Hopkinson bar technologies applied to the high strain rate rock tests." Adv Rock Dyn Appl. 79–104.

Christensen, R., Swanson, S., and Brown, W. (1972). "Split-Hopkinson-bar tests on rock under confining pressure." Experimental Mechanics 12, 508-513.

Field, J.E., Walley, S.M., Proud, W.G., Goldrein, H.T., and Siviour, C.R. (2004). "Review of experimental techniques for high rate deformation and shock studies." International Journal of Impact Engineering 30, 725-775.

Frew, D.J., Akers, S.A., Chen, W., and Green, M.L. (2010). "Development of a dynamic triaxial Kolsky bar." Measurement Science and Technology 21.

Hazzard, J.F., and Young, R.P. (2000). "Simulating acoustic emissions in bonded-particle models of rock." International journal of rock mechanics and mining sciences 37, 867-872.

Hoek, E. (1964). "Fracture of anisotropic rock." Journal of the South African Institute of Mining and Metallurgy 64, 501-518.

Kolsky H. (1949). "An investigation of the mechanical properties of materials at very high rates of loading." Proceedings of the Physical Society. Section B 62, 676-700.

Li, J., Zhao, J., Gong, S.Y., Wang, H.C., Ju, M.H., Du, K., and Zhang, Q.B. (2021). "Mechanical anisotropy of coal under coupled biaxial static and dynamic loads." International Journal of Rock Mechanics and Mining Sciences, 143, 104807.

Li, X.B., Zhou, Z.L., Lok, T.-S., Hong, L., and Yin, T.B. (2008). "Innovative testing technique of rock subjected to coupled static and dynamic loads." International Journal of Rock Mechanics and Mining Sciences 45, 739-748.

Liu, K., Zhang, Q.B., Wu, G., Li, J.C., and Zhao, J. (2019). "Dynamic mechanical and fracture behaviour of sandstone under multiaxial loads using a triaxial Hopkinson bar." Rock Mechanics and Rock Engineering 52, 2175-2195.

Liu, K., Zhao, J., Wu, G., Maksimenko, A., Haque, A., and Zhang Q.B. (2020). "Dynamic strength and failure modes of sandstone under biaxial compression." International Journal of Rock Mechanics and Mining Sciences 128.

Lockner, D.A., Byerlee, J.D., Kuksenko, V., Ponomarev, A., and Sidorin, A. (1991). "Quasi-static fault growth and shear fracture energy in granite." Nature 350, 39-42.

Mogi, K. (1971). "Fracture and flow of rocks under high triaxial compression." Journal of Geophysical Research 76, 1255-1269.

Niandou, H., Shao, J.F., Henry, J.P., and Fourmaintraux, D. (1997). "Laboratory investigation of the mechanical behaviour of Tournemire shale." International Journal of Rock Mechanics and Mining Sciences 34, 3-16.

Zhang, Q.B., and Zhao, J. (2014). "A Review of Dynamic Experimental Techniques and Mechanical Behaviour of Rock Materials." Rock Mechanics and Rock Engineering 47, 1411-1478.

Zhang, Q.B., Liu, K., Wu, G., and Zhao, J. (2021). "Dynamic Deformation, Damage, and Fracture in Geomaterials." Voyiadjis G.Z. (eds) Handbook of Damage Mechanics, 1-44.

PROCEEDINGS OF THE 14TH ANZ YOUNG GEOTECHNICAL PROFESSIONALS CONFERENCE
14YGPC ROTORUA, NEW ZEALAND, 2ND – 5TH NOVEMBER 2022

25

Streamlining Engineering Judgement in Emergency Scenarios

G. Crisp[1] and A. Riman

[1]ENGEO Ltd, 2-6 Gilmer Terrace, Wellington, 6012; PH (+64) 277 7585 60; email gcrisp@engeo.co.nz

ABSTRACT

ENGEO have been assisting Wellington City Council (WCC) with private land assessments of geological hazards, mainly landslides. WCC have used our recommendations to assist in the difficult decision of issuing danger notices when home occupants are at risk.

This paper outlines the three-zone classification system we are using on these projects to assist with making engineering judgement decisions on-site. The Red Zone is for Restricted Access, Yellow Zone for Controlled Access and Green Zone for No Controls. This classification system lays out clear parameters to be put in place that allow, in most cases, for occupants to continue living in the properties in a restricted manner. This both minimises disruption to the lives of those living on the property and mitigates risk of life safety in potential future events.

ENGEO have also used a cloud-based application to set up a template for future assessment projects. The template allows for reporting to be created quickly once key site features and the zones have been classified. This streamlines several processes and allows for fast communication between engineer, council entities, homeowners and home occupants.

The discussed process allows for the engineering judgement and assessment of short-term danger to be brought to the forefront of the project. It assists in changing the mindset of the engineer away from the typical design approach and towards assessing immediate life safety risk.

Keywords: Emergency, Classification System, Efficiency, Slope Instability

1   INTRODUCTION

ENGEO has been working with Wellington City Council in doing land assessments of geological hazards on private land. The role is to provide a fast and informative opinion on whether homeowners or tenants are safe to access the dwelling or property following a geological event occurring. WCC use this to issue danger notices where required, to inform the residents of the danger and require them to mitigate or reduce the hazard. These projects require important engineering judgement decisions to be made within hours with limited information.

We have created a three-zone classification system and report template for these projects. This allows for key decisions and reports to be mostly compiled on-site within a couple of minutes and relayed to WCC within hours.

2   BACKGROUND

2.1   Wellington City Slope Instability History

Wellington City is located in Central New Zealand and has a population of approximately 215,000. The city is well known for its hilly landscape and the majority of the suburban houses are founded on these steep slopes. The ground in the region is primarily in-situ Greywacke Sandstone, overlain by colluvial soils. Wellington also receives an average rainfall of 1250 mm per year, leading to a large number of landslides. According to Wellington City Council's Chief Infrastructure Officer Siobhan Proctor, Wellington typically records around 1,100 landslides annually.

2.2 Role of Councils

Geological Hazards that occur are the responsibility of private landowners. However, Section 124 of the Building Act states that if a territorial authority is satisfied that a building is dangerous, they may issue a danger notice. This can include any or all of the following:

- Putting up hoarding or fencing preventing people from approaching the building nearer than is safe.
- Attach a notice to the building that warns people not to approach the building.
- Issue a notice that requires the private owner to undertake work to be carried out to reduce or remove danger.
- Issue a notice restricting entry to the building for particular purposes or restricting entry to particular person or groups of persons.

The key word in the above is danger. It is our role to advise councils on whether we consider the geohazard to pose significant immediate danger to people present on the property. The council can then use our recommendations to decide whether any of the above actions are appropriate.

3 EMERGENCY CLASSIFICATION SYSTEM

The classification system works by assigning areas of the property into one of three hazard zones. The three hazard zones represent three different tiers of risk that the hazard poses to the land in this area. These locations of each of these zones are drawn on a site plan and represented by the colours Red, Yellow and Green.

Table 1 below outlines the three different hazard zone categories. This table contains the description of the geohazard risk each zone and our recommendations for appropriate controls to be placed on each zone while the risk is still present.

Table 1: Hazard Zone Description

Hazard Zone	Description	Recommendation
Restricted Access (Red)	This includes the geological hazard area and the potential areas, which could comprise future progressive failures. Immediate risk of endangering life is present.	Access to this zone should be restricted due to the likely risk of endangering life by ground loss or crushing from failing debris.
Controlled Access (Yellow)	The immediate risk of endangering life is considered to be low for these areas.	Precaution is required by not sleeping in these areas (should be always alert and conscious) and spend minimal time there.
No Controls or Restrictions (Green)	There are no current concerns for these areas.	These areas can continue to be used as intended.

The levels of controls range from recommending no access to the land or assets in this area to recommending that the areas can continue to be used as intended.

PROCEEDINGS OF THE 14TH ANZ YOUNG GEOTECHNICAL PROFESSIONALS CONFERENCE
14YGPC ROTORUA, NEW ZEALAND, 2ND – 5TH NOVEMBER 2022

27

4   EXAMPLE GEOHAZARDS

Figure 1 below shows three examples of geological hazard sites – where we have applied the three-zone hazard zone framework for emergency geological hazard assessments.

Figure 1:   Example landslide sites (Wellington)

5   PRACTICAL APPLICATION AND PROCESS

5.1   Site Visit

The most crucial aspect of making different judgement decisions within a short timeframe is the process of gaining a clear understanding of the hazard and the associated risk. This is done most effectively by visiting the site. Key aspects that we assess on site include distance from hazard to houses and other assets, the material type and slope angles of surrounding ground and evidence of potential ground movement in other locations surrounding the hazard. It is also commonplace and recommended to meet with council representatives on site who further provide context and background site information.

For one landslide site we had, key aspects to consider were the distance from the crest of the landslide to the deck and house piles and evidence of instability of surrounding ground. During the first visit to this site we noted separation in the driveway concrete, which indicated a possible future failure extent. This turned out to be the location of the regressed landslide crest after the further slippage.

Figure 2 below shows photos taken at the driveway of this site. These photos show the progression of the landslide within a five-month period, from the edge of the driveway to behind the garage door.

Figure 2:   Regression Landslide Crest Observed (two photos taken five months apart)

5.2   Site Plan

To produce the plan on which the hazard zones are outlined, ENGEO have utilised the software Datanest. Datanest is a commercially available, flexible tool for tailoring information input and reporting output for a wide range of environmental and geotechnical projects. This software allows for a GIS overlay map be made while out on site, using a tablet. The site plans show the different hazard zones relative to the hazard location, property boundaries and different assets, using the colour coordinated three-zone classification system. Datanest uses Nearmaps for background satellite images and simplified GIS tools to make the creation of the plans clear and efficient.

The plans created provide a clear outline to the council and homeowners to follow regarding the risk assessed on site.

Figure 3 below shows the examples of site plans from a site where the hazard zones changed as the crest of the landslide regressed.

5.3   Reporting

Datanest is also used to create a report that we issue for each site. The core elements of text that are the same for each site, such as the inclusion of Table 1 above, are programmed into an automated template.

Site specific details, such as on-site observations, photographs, and measurements, can be added to the Gather function on Datanest by using a table while still out of the office. Once back in the office, an automated Microsoft word document can be exported, which contains both the site-specific data and the core text elements that are the same for all sites. Once this has been done there is limited additional text that needs to be added to each memo before it is reviewed and issued to the client.

For each assessment the council receives the memo report and the site plan, both of which are mostly curated from Datanest. These products provide council with clearly communicated information to use for their own records, decision making and to provide to landowners if required.
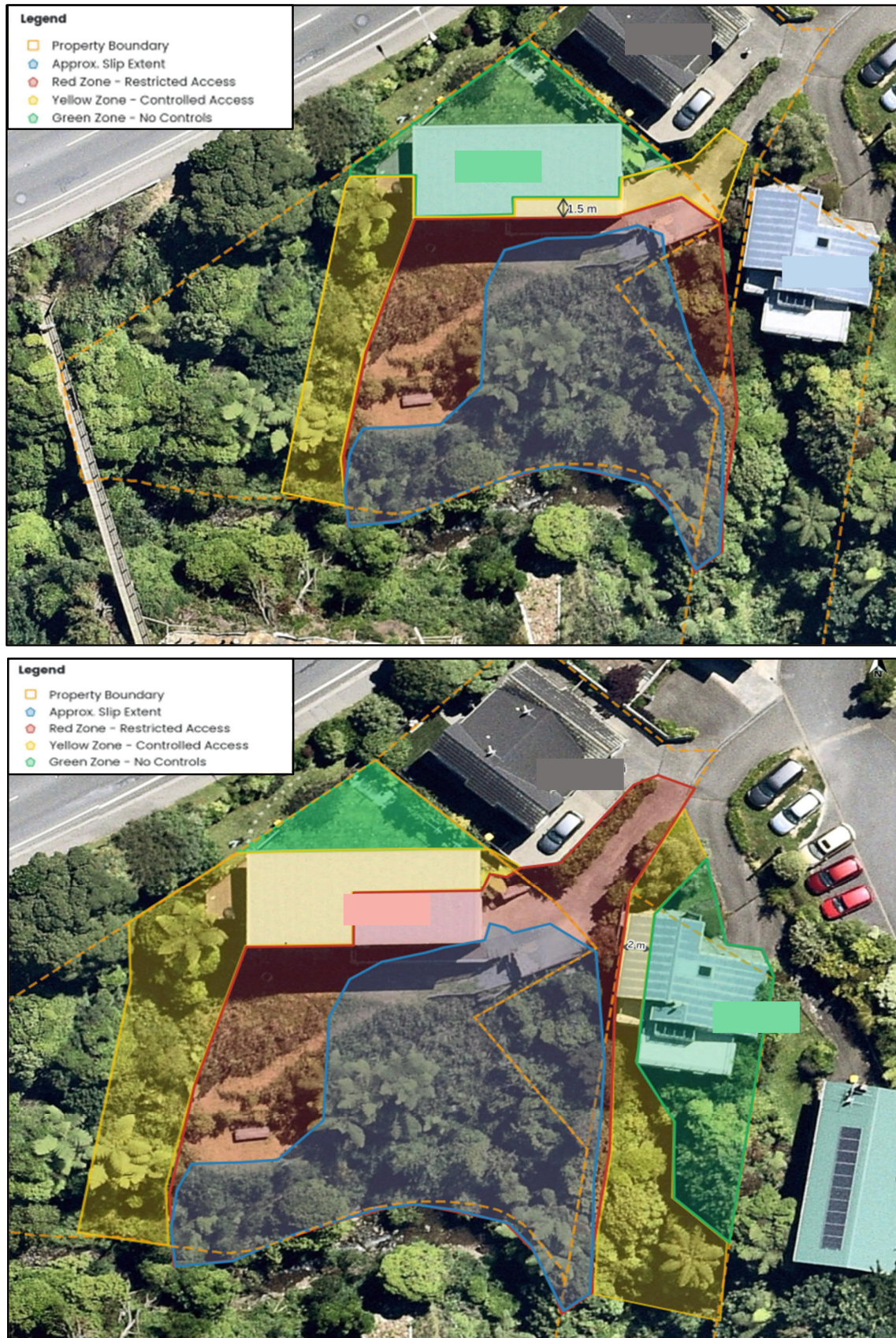
Figure 3: Hazard Zone Site Plans
(Examples showing geological hazard regression and reassessment)

6 ANALYSIS OF METHOD

6.1 Benefits

The main benefit of the three-zone classification system is that it provides a clear framework to communicate the risks of complex hazards. This is useful to both councils as it helps with their decision of whether or not to place certain restrictions on properties and landowners as it outlines the conditions of the restrictions simply.

The hazard zone boundaries can be easily changed overtime as the risk of a hazard changes, either for the better or the worse. Even if the zone boundaries move, the recommendations for each hazard zone category remain the same. This has the benefit of minimising confusion for council and landowners.

Using Datanest for both on site recording and reporting has the following benefits:

- All site data is stored together and is easily accessible with internet access.
- Outputs that the client receives have consistent recommendations and guidelines.
- Ability to record information on site without using paper.
- Fast transition from site visit to issued report.

6.2 Potential Additions to Process

For future projects we are looking to increase the amount of information that can be added to Datanest, both on site and in the automated memo template. The goal is to eventually be able to issue the site plan and memo to the client from site using Datanest from a tablet.

6.3 Potential Future Application

We have started using both the three-zone hazard classification system and the automation of site memos using Datanest on other types of projects. These tools have the potential to assist with efficient and informative assessment of all types of geological hazards, on both private and public land.

7 CONCLUSION

We consider the three-zone classification system to be effective at clearly relaying engineering judgement decisions in emergency scenarios. Feedback from WCC and homeowners has been positive, and we look forward to using this system on more projects in the future.

8 ACKNOWLEDGEMENTS

I would like to acknowledge John Davies, Ryan Cameron and Darrell Nichol from Wellington City Council for their guidance and cooperation with these projects. I would also like to thank Ayoub Riman for both his foresight to use the Datanest capabilities in this application and for his assistance with this paper.

PROCEEDINGS OF THE 14TH ANZ YOUNG GEOTECHNICAL PROFESSIONALS CONFERENCE
14YGPC ROTORUA, NEW ZEALAND, 2ND – 5TH NOVEMBER 2022

31

Central Interceptor - How does groundwater modelling and instrumentation stack up in the real world

H. Zhao[1] and P. Yee[2]

[1]Beca Limited, P.O. Box 6345, Victoria St West Auckland 1142; PH (64) 9-300-9000; email: hangjian.zhao@beca.com
[2]Ghella Abergeldie Joint Venture, 8 Gloucester Park Road Auckland 1061; PH (64) 9-953-5640; email: pyee@ga-jv.com

ABSTRACT
A new wastewater tunnel referred to as the Central Interceptor (CI) will collect stormwater and wastewater overflows from the Auckland isthmus area and transfer them to the Māngere Wastewater Treatment Plant. This will increase the wastewater network capacity by reducing the overflows and make the system more resilient. Numerical and analytical groundwater flow models representing the spatially varying geological settings and different construction methodologies were developed to assess the potential groundwater inflows and drawdown from the construction of the shafts and tunnels. Potential adverse effects arising from groundwater drawdown were assessed to demonstrate that the construction can meet the consented envelope of effects. The modelling results were also used to inform the construction planning in terms of groundwater inflow control and the setting of suitable trigger levels for groundwater drawdown and ground settlement that is part of a project wide monitoring network. Installed instrumentation includes real time data reporting and visualisation, that facilitates monitoring of the construction and consent compliance, and also provides feedback to the groundwater modelling should model updates be required. This paper highlights the lessons learnt during the construction of the CI through the eyes of installed instrumentation and how groundwater monitoring and modelling could complement each other, including:
1) Groundwater response during excavation of the Māngere Pump Station (MPS) in high permeability aquifers, and
2) Groundwater behaviour during launch of the tunnel boring machine in a confined, controlled environment.

Keywords: groundwater, modelling, dewatering, shafts, tunnels, monitoring

1 INTRODUCTION
1.1 Central Interceptor Project
Watercare Services Limited (Watercare) has obtained designations and resource consents for the construction and operation of a new wastewater tunnel, referred to as the Central Interceptor (CI). In the older parts of central Auckland, wastewater and stormwater currently flow into a combined network of pipes that were designed to direct overflows into nearby waterways. The CI is designed to reduce overflows in the city waterways, and also to enhance the resilience of the network for future urban growth in central Auckland region.

Delivery of the CI will involve construction of a mainline wastewater tunnel that will run between Māngere Wastewater Treatment Plant (MPS) and Grey Lynn, including multiple shafts, above ground facilities, and two link sewers. The mainline tunnel is 14.7 km long with an internal diameter (ID) of 4.5 m. The tunnel will be constructed at a depth of 21 m to 107 m below ground level (m bgl), including an approximate 1.5 km long crossing beneath the Manukau Harbour at about 15 m depth under the seabed. 16 working and connection shafts with depths ranging approximately between 12 m to 75 m will be constructed along the alignment. Link Sewer B is a 1.1 km pipeline (2.4 m ID) that runs from Rawalpindi reserve and connects to the mainline tunnel at the Mt Albert shaft. Located further south, Link Sewer C is a 3.2 km pipeline (2.1 m ID) that starts at Pump Station 25 and connects to the mainline tunnel at one of the May Road shafts.

1.2 Groundwater Modelling and Assessment
Construction of the CI will encounter groundwater during the excavation and completion of shafts, boring of the main tunnel and link sewers by tunnel boring machine (TBM) as well as mining of short sections of connecting adits. Groundwater control measures are therefore required to create workable conditions so that the excavation and construction works can be undertaken in a safe environment.

In order to prevent or minimise groundwater from entering into the shaft excavations, low permeability cut-off walls (e.g., secant piles, diaphragm walls, drilled casings etc.) will be constructed around the perimeter of the excavation, with walls normally penetrating down to the top of lower permeability rock

to form a lateral cut off to flow from higher permeability basalt and / or compressible sediments. This allows groundwater inflow to be managed via conventional sump pumping.

The mainline tunnel and Link Sewer B and C will be constructed using earth pressure balance (EPB) tunnel boring machines (TBM and Micro TBM) that can excavate the tunnels and simultaneously erect a gasketed precast concrete segmental lining or conventional pipe jacking support utilised for both link sewers. The tunnel sections are discretised into mandatory closed-mode zones and zones where "open-modes" of operation are allowed. During "closed-mode" tunnelling, the earth and groundwater pressures acting on the excavation face are balanced by the pressure of the conditioned soil stored inside the excavation chamber and therefore negligible groundwater inflows to the tunnels are expected. However, in other areas where open-mode is allowed, or at locations where cutter head intervention is required, the face pressure is lower than the hydrostatic pressure, some groundwater seepage into the tunnelling face is expected and will be managed as part of the soil conditioning process at the face, and then removed as slurry.

To understand groundwater inflows and to assess the potential effects that may arise (e.g., drawdown and associated risk of settlement or impacts on surface water bodies etc.), numerical groundwater modelling representing the spatially varying hydrogeological conditions and different construction methodologies was undertaken. In coordination with the overall construction programme, the models in some locations were developed to allow simultaneous excavations at multiple shafts, so the potential for cumulative effects could be considered.

Potential groundwater inflows are assessed to inform the construction planning in terms of groundwater inflow control, and the calculated groundwater drawdown is used for setting of suitable trigger levels for construction monitoring. The groundwater modelling work is complementary to the instrumentation and monitoring, which is then used to monitor the actual inflows and the effects to the receptors, and to confirm that effects are within the consented envelopes.

1.3 Compliance and Construction Monitoring

The regional resource consents for the CI project specify a range of conditions that are to be met. As one of the conditions, a Groundwater and Settlement Monitoring and Contingency Plan ('M&CP') is required to detail how groundwater and settlement effects arising from construction of the shafts and tunnels will be monitored and managed.

Construction monitoring has been undertaken utilising a combination of telemetered and manually read instruments, including vibrating wire piezometers to measure groundwater levels within varying lithological units, as well as settlement monitoring pins (SMP) and utility monitoring points (UMP) installed around each shaft and on critical assets. Additional inclinometers and extensometers have been installed immediately around the footprint of each shaft to measure lateral and vertical changes during each stage of shaft excavation. In addition, convergence prisms and ring convergence monitoring systems have been installed to measure convergence of the shafts and tunnels during excavation.

The instruments are used to monitor the influence of shaft and tunnelling activities and are set with trigger levels at 80% (green), 100% (amber), 120% (red) and 150% (black) of the modelled results. All data is collated and presented on a real-time data platform (Geoscope), that can instantly provide email notification when a trigger level exceedance occurs. During construction, data is reviewed on a weekly basis to validate the design assumptions and as a compliance requirement under the consent conditions. Where trigger levels are exceeded, the specific Trigger Action Response Plan (TARP) is adhered to.

2 SHAFTS CONSTRUCTION IN A HIGH PERMEABILITY AQUIFER AT MĀNGERE PUMPING STATION (MPS)

2.1 Design of Māngere Pumping Station

The MPS shafts were constructed as a dual cell (Figure 1), consisting of two adjacent and intersecting circular shafts, with a Diaphragm Wall (D-Wall) installed as the first element of support prior to the construction of the permanent shaft lining. The D-Wall was designed to leak and cope with the earth pressure, along with providing effective temporary support during shaft excavation. A length of approximate 133 linear metres of D-Wall was constructed for the two circular shafts. The two shafts are separated into the Inlet shaft (14.4 m ID) and the Main shaft as a Wet and Dry Well (28.4 m ID). The D-Wall provides at least 8 m to 10 m cut-off below the base of the deepest excavation, embedding into competent ECBF rock. Since completing the excavation, an internal cast in-situ wall (1.5 m thick) has been formed to restrain the full hydrostatic pressure.

PROCEEDINGS OF THE 14TH ANZ YOUNG GEOTECHNICAL PROFESSIONALS CONFERENCE
14YGPC ROTORUA, NEW ZEALAND, 2ND – 5TH NOVEMBER 2022

33
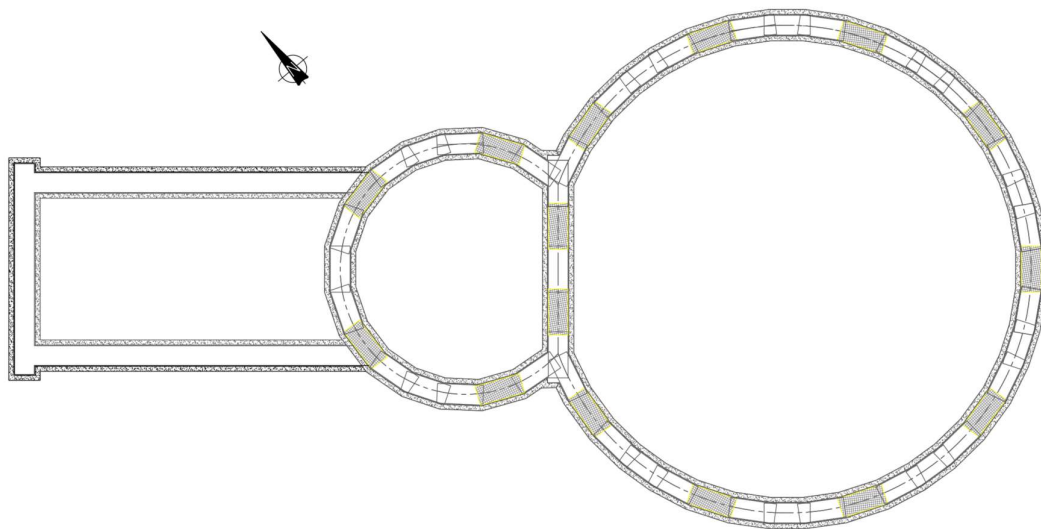
Figure 1: Māngere Pump Station shafts layout showing the temporary support diaphragm wall support and extended confinement box

2.2 Initial groundwater modelling

A 3 D finite difference groundwater flow model was developed, based on a purposely built geological model, to consider the impacts of construction on groundwater in a complex and variable geologic setting. The hydrostratigraphic units include volcanic tuff and basalt, Tauranga Group Alluvium (TGA), Kaawa Formation (newly named as Tāmaki Makaurau Formation[1]), Parnell Volcaniclastic Conglomerate (PVC) and East Coast Bays Formation (ECBF) (Figure 2).
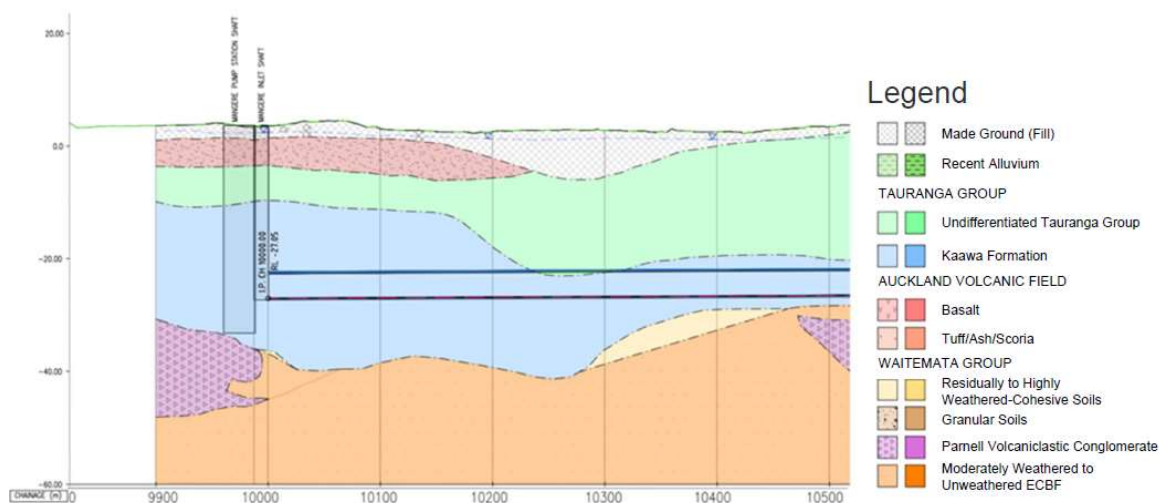
Figure 2: Māngere Pump Station geological cross section

Kaawa Formation is a regionally important water supply aquifer. A constant rate test in the Kaawa Formation was undertaken at 45 L/s and resulted with a drawdown at distance of up to 640 m away, and this confirms generally high permeability expected for this critical water supply aquifer. PVC that is interbedded in the ECBF consists of coarse debris flow deposits with volcaniclastic materials. The PVC is much stronger, but more brittle with a permeability that could be orders of magnitude higher than the host ECBF and these zones are likely to be preferential flow pathways which are challenging to model. The TGA generally has a lower permeability, i.e., not expecting significant groundwater flows, however, the compressible nature of the alluvium makes it critical to understand the drawdown response to assess the risk to the assets at surface.

---

[1] "Kaawa Formation" used herein as a more familiar name.

The model was calibrated to average groundwater levels and a transient pumping test undertaken in the Kaawa Formation. The modelling suggested peak groundwater inflows of up to 13 L/s, but typically less than 1 L/s for the base case scenario where the PVC was assumed to have the same permeability as the host ECBF (Beca, 2019). Because there was a risk of higher permeability in the PVC, modelling also considered an upper bound case with groundwater inflows to the shaft of 60 L/s. The project team took a proactive decision to increase the cut-off provided by the D-walls to help manage this, though modelling still suggested even in this case flows rates of 50 L/s could occur.

2.3 Construction challenges

A groundwater inflow of up to 26 L/s was observed during construction, that was followed by drawdown trigger exceedances at nine piezometers. The groundwater flow model was back calibrated to the observed pumping rate and drawdown observations recorded to date. The model, calibrated to the observed inflow rate, suggests a permeability of PVC (i.e., of the order of 10^{-5} m/s) that is higher than the original value adopted, but lower than the upper bound scenario presented in the initial modelling (Beca,2020).

The updated model was also utilised to assess the potential benefits of applying mitigation measures comprising a drainage blanket, with active sump pumping and passive relief wells within the shaft excavation. These mitigation measures, in conjunction with refined design analyses to confirm allowable pressure on the base slab, were expected to allow for some reduction in pumping rates as the construction staging allows. Modelling indicated a 25 to 50% reduction in pumping rates could be achieved at key stages.

2.4 Construction solutions

Excavation of the Māngere shafts commenced in August 2020, with approximately 35,000 m³ of material removed. The main shaft (28.4 m ID) extends 41.0 m bgl and the adjoining inlet shaft (14.4 m ID) extends to a depth of 38.0 m bgl. Final excavation levels were achieved in October 2020 for both shafts.

As excavation of the main shaft advanced to within 2.5 m of the final excavation depth a significant increase in groundwater inflow into the main shaft was observed (5th October 2020), initially in isolated areas flowing through at the base of the D-wall and with additional excavation, within the centre of the shaft. The groundwater inflow is anticipated from the Kaawa Formation via vertical fractures within the PVC providing a preferential flow path around the D-Walls, corresponding to groundwater drawdown observed in monitored piezometers installed within the deeper Kaawa Formation, PVC and ECBF (Figure 3) exceeding all respective trigger levels. The piezometers installed within the compressible TGA observed limited to no groundwater drawdown and remained within their trigger limits.The main shaft initially experienced groundwater inflows peaking at 26 L/s, reducing over time. Once the final excavation depth was reached, formation of the main shaft base slab was set with four 250 mm diameter relief wells and pumps installed, reducing the hydrostatic pressure exerted on the base slab. Continued pumping of groundwater is being undertaken at an average rate of ~16 L/s (lowering steadily) and is expected to continue around this rate until the permanent lining and dividing wall is installed and base slab can take full hydrostatic pressure.
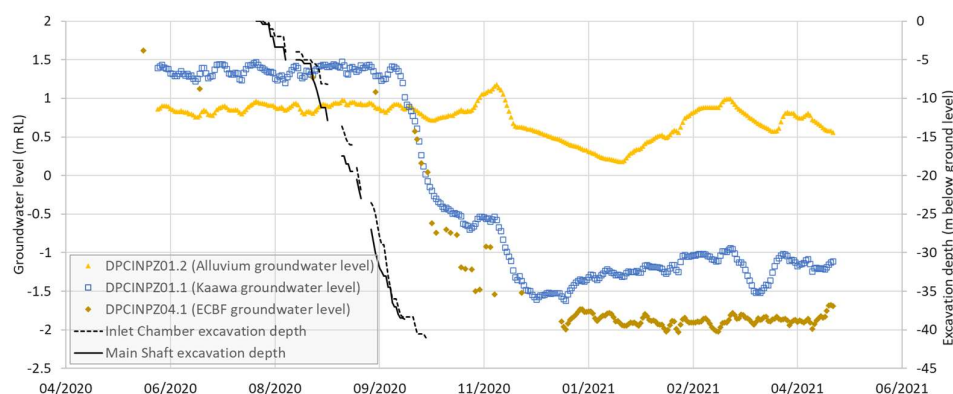
Figure 3: Monitored groundwater level of select piezometers surrounding the Māngere shafts in relation to the excavation depths of the inlet and main shaft

Additional vibrating wire piezometers and electrical conductivity instruments were installed in response to the large groundwater inflows and drawdown at MPS. Three shallow piezometers were installed within

PROCEEDINGS OF THE 14TH ANZ YOUNG GEOTECHNICAL PROFESSIONALS CONFERENCE
14YGPC ROTORUA, NEW ZEALAND, 2ND – 5TH NOVEMBER 2022

35

the site footprint to confirm the drawdown within the compressible alluvium, as an early warning for risk of ground settlement. Shallow groundwater levels remained stable upon review and mirrored the surrounding shallow piezometers installed. Two electrical conductivity monitoring instruments were also installed in shallow open standpipes and confirmed no change in groundwater salinity was occurring. Two deep piezometers were installed to the south and east of the site to get a better understanding of the magnitude and extent of the drawdown within the Kaawa Formation, this was particularly important as a number of private wells abstract water from the Kaawa Formation to the east and south of MPS shafts.

2.5 Monitoring observations
Figure 3 above provides an insight into the groundwater levels within the various geological units against the shaft excavation depth. The extensive groundwater drawdown of the Kaawa Formation and ECBF is in line with the groundwater inflows observed within the shaft. A delayed and limited groundwater drawdown of the upper compressible TGA is less extensive and in line with the settlement observed around the shaft. Monitored shaft array/building SMP's and the UMP's installed along a critical asset, the Western Interceptor located within 20 m of the shaft footprint, observed settlement within their trigger limits and differential settlement of no steeper than 1 / 10,000.

The groundwater drawdown observed to the east of the site was limited upon review and the southern deep piezometer was significantly influenced by the Māngere Waste Water Treatment Plant (MWWTP) activity, with groundwater drawdown not directly linked to the active dewatering at MPS.

Monitoring data is regularly reviewed and compared with modelling results to check the assumptions and provide additional observation datasets for model update.

3 GROUNDWATER CONTROL FOR TUNNEL BORING MACHINE LAUNCHING
3.1 Groundwater modelling
It is impractical and of little value to develop a groundwater model that encompasses the whole mainline tunnel alignment, instead, critical locations along the alignment were selected and modelled using a series of 2D analytical models and the existing 3D numerical groundwater flow models developed for the shafts. During "closed-mode" tunnelling, negligible groundwater inflows to the tunnels are expected. However, as a result of pressure reduction at the tunneling face (e.g., open-mode, or cutter head intervention), some groundwater seepage into the tunnelling face may occur, therefore a greater drawdown is expected at the tunnel invert. Particularly, this pressure control becomes more critical for the tunnel launch at MPS where there is greater potential for large inflows and associated risk of materials running into the face given the permeable and unconsolidated nature of Kaawa Formation.

3.2 Challenge and solution
The TBM was launched at MPS from the inlet shaft into the Kaawa Formation. The successful launch of the TBM commenced on 9th August 2021 and was initially within the confinement box shown in *Figure 2*. Soon after launching the TBM on 17th August, all New Zealand moved into alert level 4 lockdown restrictions.

The confinement box is a purpose designed and built 9.3 m x 17.6 m structure, contained by 1.2 m thick x 2.8 m long overlapping D-Wall panels that extend to an approximate depth of 47 m bgl. The purpose of the confinement box is to provide a complete groundwater cut-off, to allow the TBM to be launched in the "dry" and inadvertently provided a safe haven for the TBM during the lockdown restrictions.

Dewatering was undertaken within the confinement box via two dewatering wells below the tunnel invert level (i.e., -26.7 m RL) as the TBM exited the inlet shaft. With the surrounding groundwater level lowered below the tunnel invert level (-27.0 m RL), all checks for the TBM and concrete segments could be installed and verified safely within a controlled environment.

3.3 Monitoring Observations
Groundwater monitoring instruments were established within and beyond the confinement box. With the dewatering wells and the D-Wall acting as a cut-off to lateral groundwater inflows, the groundwater level in the Kaawa Formation within the confinement box was lowered, and it was observed to rapidly respond to pumping (i.e., pump shutdown test showing rapid rise and fall of levels when pumping stopped and resumed). The groundwater level outside of the confinement box (TBMCZPZ02.1) observed an initial depressurisation due to dewatering within the confinement box, but did not experience full groundwater drawdown, instead stabilised in March 2021 (Figure 4). As the TBM advanced beyond the confinement box, a short-term increase in pressure was also observed from the TBM face pressure (3 to 3.6 bar) as it passed within close proximity (10 m) of the vibrating wire piezometer (TBMCZPZ02.1_29.3 m bgl),

followed by a gradual descent in groundwater levels and stabilisation as the segment annulus is grouted in place immediately approximately 12 m behind the TBM face.

Figure 4 also shows induced fluctuation of the groundwater within the confinement box between September 2021 to February 2022, where the pumps were temporarily turned off to check and validate the segmental ring support performance.

Thereafter, the TBM advanced beyond the confinement box and has currently advanced over 2,500 m. Monitoring data are regularly reviewed on a weekly basis to monitor and confirm the effects rising from the tunnelling.
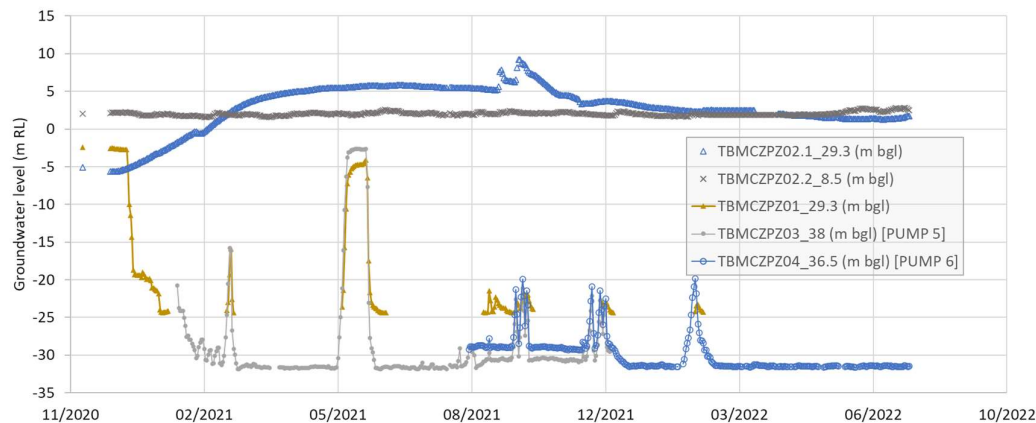
Figure 4: Groundwater level response to pumping in preparation for TBM launch.

4   CONCLUSION

With a robust understanding of the hydrogeological setting, groundwater modelling can be used in a systematic approach to understand the hydrogeological environment, quantify the potential effects that may arise and to help inform groundwater control measures. The models developed for CI have a focus of representing the hydrostratigraphic units and the understanding of the hydrogeological conditions on a regional scale. Test pumping and groundwater observations at Māngere site are of great use and importance to improve the understanding of the site-specific conditions. The more reliable model allows for a better estimation in groundwater inflows and drawdowns, also to adequately simulate the variation in groundwater control measures (i.e., increase the wall embedment depth) and assess the associated effects. Back calibrating the model to the observations also helps to provide the confidence that the proposed groundwater control measure would be effective.

Extensive and real-time monitoring network has been established at the shaft sites and along the tunnel alignments. Not only do they provide informative datasets for conceptualisation, model development, and calibration, but also serve as the eyes of the project to validate the modelling assumptions, to identify potential local variations, therefore providing feedback to the modelling and initial assessment. More importantly, it is an invaluable asset to monitor the effects from the construction and provide early warnings of risks that may potentially arise from the construction. Whilst modelling helps to quantify the groundwater inflows and potential effects on the environmental receptors, it isn't the end of the journey. Instead, it is the starting point. Being complementary to each other, groundwater modelling and monitoring work together as an effective tool to better understand the local conditions and therefore to respond to construction risks.

5   ACKNOWLEDGEMENTS

We would like to thank Beca Hydrogeology team for providing the technical support. We also thank Ghella Abergeldie Joint Venture for sharing the monitoring data and insights gained from the construction to help with the groundwater modelling and assessment. We thank Sixense for their timely assistance on Geoscope. We would like to extend our thanks to Watercare for the opportunity to be part of this project and their support on this paper to share the knowledge and lessons learnt. In the end, our thanks and appreciation also go to our colleagues who are always willing to help.

6   REFERENCES
Beca (2019). "Māngere Pump Station –Assessment of Groundwater Effects" Revision 1.
Beca (2020). "Māngere Pump Station – Revised Assessment of Effects" Revision 2.
Geoscope-Central Interceptor instrumentation online platform, Sixsense.

PROCEEDINGS OF THE 14TH ANZ YOUNG GEOTECHNICAL PROFESSIONALS CONFERENCE
14YGPC ROTORUA, NEW ZEALAND, 2ND – 5TH NOVEMBER 2022

37

A New Approach for Liquefaction Assessment of Pumiceous Sands

M. B. Asadi, M. S. Asadi, and M. Larisch

Jacobs New Zealand Limited, 12-16 Nicholls Lane, Carlaw Park, Auckland, 1010, New Zealand; email: Baqer.Asadi@jacobs.com

ABSTRACT

Sands consisting of pumice particles are a common soil type in several parts of the Waikato Basin and Bay of Plenty in the North Island of New Zealand. These pumice sands are highly crushable, compressible, and lightweight due to the vesicular nature of the particles. Pumiceous soils are often seen to be 'problematic' because their behaviour is considerably different compared to that of normal sands. Accordingly, the available empirical correlations for ordinary soils may not be applicable for the liquefaction assessment of pumiceous soils. Therefore, it is imperative to follow appropriate design recommendations for the liquefaction assessment of these soils. The development of several large-scale solar farms in the Eastern Bay of Plenty region requires more reliable approaches to assess the liquefaction susceptibility of pumiceous sands as some of the solar farm locations have thick layers of pumiceous deposits present across the site. The key geotechnical risk for solar farms in the Bay of Plenty is often related to soil liquefaction and the effects this may have on the foundations for various structures and the solar arrays. This paper will present a case study where several seismic cone penetration tests (sCPT) were performed and the obtained CPT and shear wave velocity (V_s) profiles were used for a site-specific liquefaction assessment. The results of the liquefaction assessment were made using the methods which reflect current good industry practice in New Zealand. In addition, a second assessment was carried out using recently developed pumice-specific correlations, which provided significantly improved cyclic resistance ratios (CRR) for pumiceous sands. In this paper, the important differences in using the newly developed and more advanced methods for liquefaction assessment of pumiceous deposits are discussed and presented.

Keywords: Pumice soil, particle crushing, liquefaction assessment, shear wave velocity

1 INTRODUCTION

Sands consisting of pumice particles are found in several parts of the Waikato Basin and the Bay of Plenty. These pumice sands are highly crushable, compressible, and lightweight, due to the vesicular nature of the particles, making engineering assessment of their properties complex and challenging. These unique characteristics of pumice particles significantly affect their behaviour under seismic conditions and are very different from the seismic response of 'normal' sand (Asadi et al. 2022a & b; Orense et al. 2020). The presence of crushable and porous pumice components in the naturally occurring pumiceous sands causes a softer response of those particles, and therefore, they have lower shear wave velocity (V_s). During seismic loading, pumice particle crushing results in significant increased particle-to-particle contacts. Subsequently, the irregularly shaped pumice particles can provide good interlocking between pumiceous sand particles, causing higher liquefaction resistance (Asadi et al. 2019). Following standard geotechnical engineering practice, pumiceous sands typically have lower V_s compared to the 'normal' sands; therefore, they are expected to have low liquefaction resistance which is not generally correct according to the comprehensive studies conducted by Asadi et al. (2022).

After the 1987 Edgecumbe Earthquake, manifestations of soil liquefaction, such as sand boils and ejected materials, have been reported for pumiceous deposits in many locations, including two sites reported by Orense et al. (2020), one in Whakatane and another in Edgecumbe. According to the case study of the 1987 Edgecumbe Earthquake published by Orense et al. (2020) at the above sites, the simplified empirical-based methods (for example, using CLiq software) would predict the occurrence of liquefaction for pumiceous deposits. However, while their assessments were consistent with the observed occurrence of liquefaction at the sites, the severity of liquefaction-induced damage, as indicated by the very low factor of safety against liquefaction, would not explain the minor-to-moderate degree of damage reported at the sites. This finding can be correlated to the conflicting response observed from pumiceous sands during dynamic testing as they typically have low V_s while providing relatively high liquefaction resistance. Accordingly, Asadi et al. (2022a) proposed a new methodology for the liquefaction assessment of pumiceous sands containing different pumice content (PC). This paper assesses a site-specific liquefaction assessment of the pumiceous deposits using advanced existing methods and the newly developed pumice-specific correlations.

2 PROJECT OVERVIEW AND SITE DESCRIPTION

Lodestone Energy Limited plans to develop several solar farms in the Eastern Bay of Plenty region. The projects generally rely on several thousands of foundation piles to support the solar PV modules and the associated infrastructure. In addition, other civil and infrastructure works are required such as earthworks, access roads, stormwater, power structures, and buildings and infrastructure such as buried cables. For the assessment, management and mitigation of key project risks, including ground risks, it is vital to develop site-specific ground models to better identify the potential geohazards for each site. The focus of this paper is the liquefaction assessment of the soil deposits present at one of the proposed solar farm sites (per client request, the name and the location of this site need to be kept anonymous).

2.1 Field testing

Various deep investigations, including borehole logs, test pits and cone penetration tests (CPT) were carried out to develop a site-specific ground model, to assign geotechnical design parameters and to provide recommendations allowing the assessment the geotechnical hazards. Further to the site investigation methods mentioned above, more advanced testing methods were performed to allow the assessment of the liquefaction potential of pumiceous soils, i.e., eight (8) seismic cone penetration tests (sCPT) to 20m depth. Such tests provide shear wave velocities for these soils, which are more suitable for a liquefaction assessment of pumiceous soils according to the MBIE Module 3 (2021).

2.2 Geological units

The proposed site is underlain by up to 2.5 km of volcanic, marine and non-marine sediments and significant ignimbrite deposits. The Holocene geology comprises sediments from marine incursion and non-marine sediments such as volcanic tephra, re-worked tephra, peat and back swamps and alluvium deposited by the Rangitāiki River. The geology from the site investigation has been interpreted into a geological model, and this is summarised in Table 1 (listed from youngest to oldest).

2.3 Assessment of pumiceous layers thickness and pumice content (*PC*)

The thickness of the pumiceous sand layers was estimated across the site by correlating the CPT tip resistance (q_c) to the known extent of pumice units in the nearby borehole logs, and therefore, using the tip resistance of CPT results to understand the extend of the pumiceous layers thickness for the investigated sCPT profiles. The estimated thickness of the pumiceous soil layers at the eight (8) sCPTs test locations are ranging from 1.5 to 2.5 m thickness for Unit 3 and 2.5 to 3.5 m thickness for Unit 4.

The method of Asadi et al. (2019) need to be followed to estimate the pumice content (*PC*) of the pumiceous sands found on site. However due to the in-depth experience of the author of this paper (also the same author of the Asadi et al. (2019) approach)) with the soils in the Bay of Plenty, the *PC* of the samples herein has been visually estimated using the borehole log material, as well as using the index properties of the soils (obtained from laboratory testing) to confirm the estimated values of the *PC of each sample*. These assessments indicate that the *PC* content in the granular Pumiceous (Unit 3) is about 40-50%, and about 50-60% in the Pumiceous Tephra (Unit 4)

Table 1:   Design engineering geotechnical units.

Unit No.	Name	Material Description
Unit 1	Recent Ashfall / Alluvium	Silt dominated, firm-stiff, caps the full extent of the site, encountered below the topsoil and typically extends 1.0 – 2.0 m bgl.
Unit 2	Swamp Deposits	Cohesive, fibrous peat and organic silt, thin (1-2m thickness), highly compressible, present across most of the site.0.5 to 1.0 m thick.
Unit 3	Granular Pumiceous	Loose to medium dense, fine to coarse pumice sand and gravel with varying silt, present across most of the site with 2 – 4m thickness.
Unit 4	Pumiceous Tephra	Very Stiff / medium dense to dense pumiceous medium-coarse silt and fine sand, moderately hard to dig with excavator. Non-plastic, liquefies when disturbed during drilling. Occurs in 3 - 5m thick layers across the entire site.
Unit 5	Non-Pumiceous Alluvial/Estuarine	Soft silt with minor clay, non-pumiceous and more plastic than above units. Predicted to underly the full site, minimum 2m thickness.

PROCEEDINGS OF THE 14TH ANZ YOUNG GEOTECHNICAL PROFESSIONALS CONFERENCE
14YGPC ROTORUA, NEW ZEALAND, 2ND – 5TH NOVEMBER 2022

39

2.4 Seismic design parameters

The seismic design parameters for liquefaction assessments are summarised in Table 2 for serviceability limit sate (SLS) and ultimate limit state (ULS) conditions. These parameters have been determined using the guidance provided in MBIE Module 1 (2021). Table 2 also presents the ground water level (GWL) used for the liquefaction assessment carried out in this paper.

Table 2: *Design input parameters for liquefaction assessment*

Seismic State Limit	Annual Probability of Exceedance (AEP)	Peak Ground Acceleration (PGA)	Moment Magnitude (M_w)	GWL (m bgl)
Scenario 1 (SLS1)	1/25	0.11g	6.1	1.0
Scenario 2 (ULS)	1/100	0.22g	6.1	1.0
Scenario 3 (ULS)	1/500	0.44g	6.1	1.0

3 METHODS OF LIQUEFACTION ASSESSMENT

3.1 Existing empirical methods

The primarily liquefaction assessment was carried out using GeoLogismiki software package CLiq (version 3.0.3.4) following two standardized methods as follows: (1) to analyse CPT profiles: Boulanger and Idriss (2014); and (2) to analyse V_s profiles: Andrus & Stokoe (2000), and Kayen et al. (2013).

3.2 Pumice-specific empirical method

Asadi et al. (2022a) proposed a step-by-step procedure, a newly developed V_s-based method, to assess the liquefaction susceptibility of pumiceous sands. The key aspects of this method are set as below:

- Determine the V_s profile of the soil deposit.
- Obtain disturbed soil samples, e.g., from borehole logs.
- Asses the thickness of pumiceous layers.
- Quantify / estimate pumice content - use Asadi et al. (2019) method or soil properties.
- Assess liquefaction resistance - use the liquefaction assessment chart shown in Figure 1 or alternatively use the empirical correlations presented in Equations 1 and 2.
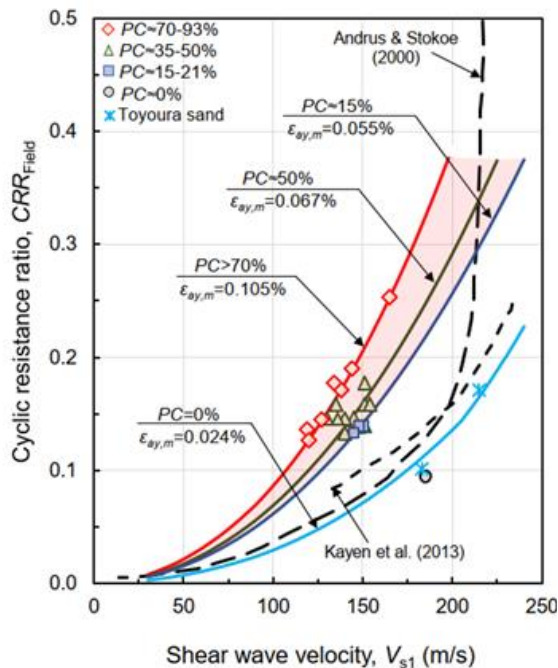
Figure 1. Liquefaction assessment chart for pumiceous sand and compared with the normal sand correlations (Asadi et al. 2022a).
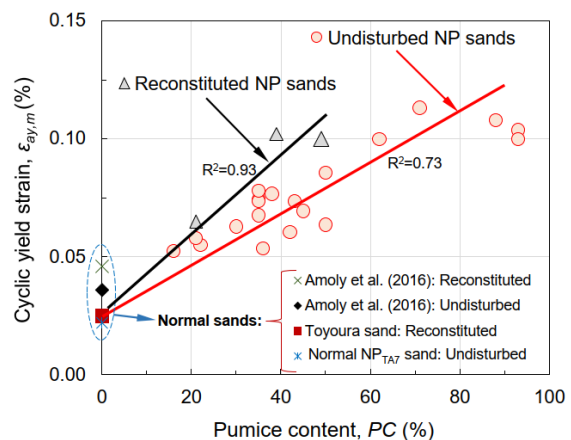
Figure. 2. The relation of cyclic yield strain factor with pumice content (Asadi et al. 2022b).

$$CRR_{(Field)} = \frac{3\rho}{(1+2K_0)\,P_a}\;\varepsilon_{ay,m\,(Field)}\,V_{s1}^{2} \tag{1}$$

where $CRR_{(Field)}$ is the liquefaction resistance of soils in field condition; ρ is soil's bulk density; K_0 is the lateral earth pressure coefficient (ranging 0.4 to 0.5); P_a is the referenced overburden pressure (= 100 kPa); V_{s1} is the normalised V_s with respect to P_a; and $\varepsilon_{ay,m\,(Field)}$ is cyclic yield strain factor (in field conditions). The investigated $\varepsilon_{ay,m}$ (in laboratory conditions) for different pumice contents is shown in Figure 2; next, use Equation 2 to convert the $\varepsilon_{ay,m}$ (from Figure 2) to $\varepsilon_{ay,m\,(Field)}$ to use in Equation1.

$$\varepsilon_{ay,m\,(Field)} = r_c\left(\frac{1+2K_0}{3}\right)^{2n+1}\varepsilon_{ay,m} \tag{2}$$

where r_c is a constant value to account for the multi-directional shaking effects in field (=0.95), and n is power coefficient of confining pressure (for $PC \le 5\%$ use $n = 0.25$; $5\% < PC \le 50\%$ use $n = 0.3$; and $PC > 50\%$ use $n = 0.35$). For further details see Asadi et al. (2022a) publication.

4   RESULTS AND DISSCUSSTION

Eight (8) seismic cone penetration tests (sCPT) were completed at the proposed solar farm site and have been used to determine the liquefaction susceptibility of the pumiceous soil layers (Unit 3 and Unit 4) following the procedures explained above.

4.1   CLiq analyses outputs (CPT-based results)

This section summarises the results of liquefaction analyses using CPT profiles only for the three seismic scenarios outlined in Table 2. The assessment of liquefaction induced free-field vertical settlements as the result of post-liquefaction volumetric reconsolidation strain is important to estimate the surface settlements for this project. Therefore, the post-liquefaction ground settlements, using CPT-based approaches, are estimated and reported in Table 3. These results are based on using the existing engineering methods (from CLiq) for the liquefaction assessment. The estimated settlements for Scenario 1 are significantly lower than those predicted for Scenario 2 and Scenario 3, predominantly due to the lower seismic design parameters, which are less than the estimated liquefaction triggering PGA value (the triggering PGA is at approximately 0.15g). The estimated ground settlements for Scenario 2 and Scenario 3 indicate comparable total settlements values. This similarity for Scenario 2 and Scenario 3 can be explained as the PGA values for both scenarios are much greater than the estimated liquefaction triggering PGA value where the Settlement-PGA curves tend to become horizontal, and the majority of liquefiable sediments have been liquefied by ground shaking. Note that the tabulated results under 'pumice-specific methods' shown in Table 3, will be explained in Section 4.4.

Table 3:   Summary of total vertical ground settlement for SLS and ULS events.

sCPT No.	Total estimated vertical free field surface settlements (mm)					
	CLiq outputs			Pumice-specific methods		
	Scenario 1	Scenario 2	Scenario 3	Scenario 1	Scenario 2	Scenario 3
sCPT101	12	70	86	Nil	45	86 (70%)
sCPT102	27	92	111	Nil	25	111 (70%)
sCPT103	7.5	86	127	Nil	40	127 (70%)
sCPT104	6	61	81	Nil	25	81 (70%)
sCPT105	18	137	155	Nil	20	155 (70%)
sCPT106	19	126	148	Nil	30	148 (70%)
sCPT107	5	50	74	Nil	25	74 (70%)
sCPT108	12	120	131	Nil	30	131 (70%)

4.2   CLiq analyses outputs (V_s-based results)

The CLiq software was also used for liquefaction assessments using the V_s profiles of the soil deposits based on the above stated seismic input parameters. The CLiq software is not able to directly estimate the free-field ground settlement using the V_s-based methods. Alternatively, the factor of safety (FoS) against liquefaction is presented instead to illustrate the severity level of liquefaction for the different scenarios. The $FoS = CRR/CSR$, where CRR is the 'cyclic resistance ratio' (liquefaction resistance), and CSR is the 'cyclic stress ratio' (the shear stress ratio induced in the soil deposit from an earthquake).

PROCEEDINGS OF THE 14TH ANZ YOUNG GEOTECHNICAL PROFESSIONALS CONFERENCE
14YGPC ROTORUA, NEW ZEALAND, 2ND – 5TH NOVEMBER 2022

41

The sensitivity of the liquefaction assessment results for the three seismic scenarios (Table 1) as well as alternative liquefaction assessment methods were assessed. The Andrus and Stokoe (2000) methodology estimated that the overall soil profiles (including pumiceous layers) are susceptible to liquefaction for all three seismic scenarios (with *FoS* < 1.0). Figure 3 shows the outputs of the Andrus and Stokoe (2000) method for sCPT102. In addition, the Kayen et al. (2013) method was applied, and it was estimated that these soil profiles are susceptible to minor liquefaction under Scenario 1 (1 < *FoS* < 1.1) and the site was assessed to be highly liquefiable under Scenarios 2 and 3 (*FoS* < 1).

4.3 Pumice-specific analyses outputs

Following the Asadi et al. (2022a) method, the sCPTs (*V*s profiles only) were analysed to assess their liquefaction susceptibility, considering the thickness of the pumiceous layers as well as their estimated *PC*. Figure 3 presents the liquefaction assessment results for sCPT102 for the three seismic scenarios. The plot also shows the comparison between the use of pumiceous-specific correlations and the more generic Andrus & Stokoe (2000) method. At the location of sCPT102 the pumiceous layers are present between 2.3 to 7 m bgl. Therefore, for these specific depths, pumiceous-specific correlations were applied while 'standard' correlations were used for non-pumiceous soil layers above and below this horizon (the pumice-specific correlations can still be used for non-pumiceous layers with input *PC* = 0%; see the comparison in Figure 3 between the two methods for non-pumiceous layers). As evident from Figure 3, under seismic Scenario 1 and 2, the pumiceous layers are not liquefiable with *FoS* ranging from 2.0 to 3.9 and 1.2 to 2.0, respectively, whereas the pumiceous layers are estimated to be liquefiable under Scenario 3 with *FoS* ranging from 0.6 to 0.9. It should be noted that while the pumiceous layers are liquifiable under seismic Scenario 3, they have much higher *FoS* compared to the results of Andrus and Stokoe (2000) as demonstrated in Figure 3 (c).
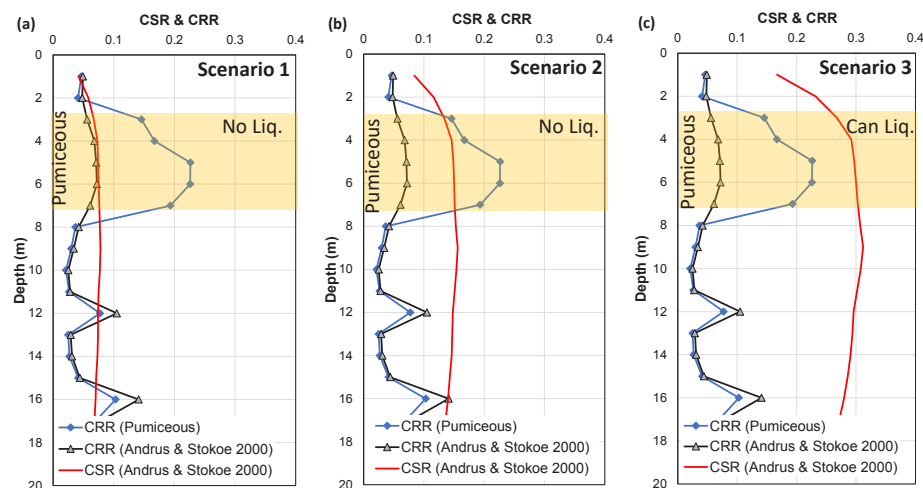
Figure 3. Liquefaction assessment results for sCPT102 profile: (a) Scenario 1, (b) Scenario 2, and (c) Scenario 3 (the shaded yellow zone represents the layers of pumiceous sand).

4.4 Design considerations

For sites with level ground conditions, the severity of ground damage caused by liquefaction is affected by the properties and thickness of the liquefied layers, and by the location (depth) of the liquefied layers within the soil profile. Ground displacements and liquefaction-induced settlements generally increase with the thickness of the liquefied layer, and with the proximity of the liquefied layer to the ground surface. The presence of a non-liquefiable crust at the ground surface may reduce the manifestation and damaging effects of liquefaction at the surface, as observed by Ishihara (1985) and more recently during the Canterbury earthquake sequence (Cubrinovski et al. 2019). Such beneficial effects of the surface crust should only be expected in cases where lateral spreading does not occur, and where the crust is sufficiently thick and robust to ensure reduced differential movements for relatively light structures. Ishihara (1985) developed criteria identifying conditions for the occurrence of liquefaction-induced free field settlements based on the thickness of the liquefied sand layer (H2) and the thickness of an overlying crust of non-liquefied soils at the ground surface (H1). These criteria are expressed in a chart comparing different thicknesses of H1 and H2 in which boundary curves for identification of 'liquefaction-induced ground damage'.

Since the overall crust thickness of the top four soil units (Table 1) is approximately 7 m to 9 m thick across the Solar farm area, and these geological units are identified as non-liquefiable material for both, Scenario 1 and 2 (based on the Asadi et al. (2022) method), and the solar arrays are light weight structures, the Ishihara chart (refer to MBIE Module 3 (2021)) is used herein for ground induced damage assessment. Using the Ishihara chart and considering about 7 m - 9 m of non-liquefiable layers, this solar farm is expected to have a low potential for 'liquefaction-induced ground damage' under seismic Scenario 1 and 2. Furthermore, considering that the pumiceous layers are not liquefiable (under Scenario 1 and Scenario 2), the total ground settlement would be mainly a function of the settlement of the liquified material at depths below Unit 4. The estimated settlement values (from CLiq) for the material below the pumiceous layers is used to estimate the total ground settlement under Scenario 1 and 2 (these values are summarised in Table 3). The estimated post-liquefaction settlements are expected to be negligible for Scenario 1 and approximately 20 mm to 45 mm for Scenario 2. Regarding seismic Scenario 3, the post-liquefaction settlements are expected to be lower than those estimated from CLiq because the pumiceous-specific correlations estimated much higher *FoS* for Scenario 3 (and yet *FoS* < 1.0). The settlement values from CLiq analysed for Scenario 3 are then reduced by about 30% to incorporate the effect of pumiceous layers; this is in accordance with the differences between the *FoS* estimated by CLiq and Asadi et al. (2022) methodologies.

5   CONCLUSIONS

The presence of crushable, angular, and porous pumice components in natural pumiceous sands can result in conflicting responses when compared to 'normal' sands during seismic shaking, as pumiceous typically have low shear wave velocity (V_s) whilst having high liquefaction resistance. Considering the above observations and findings, the currently available correlations to assess liquefaction resistance developed from 'normal' sands would significantly underestimate the liquefaction resistance of pumiceous sands. Instead, the new correlations, specifically developed for pumiceous sands, were used in this project for more reliable liquefaction assessments of these crushable material. The application of a new method (Asadi et al, 2022a) to assess the liquefaction potential of pumicous sands significantly reduced the estimated ground settlements caused by soil liquefaction for the proposed solar farm project (in contrast with the outputs from CLiq software), which reduced the overall ground risk.

6   ACKNOWLEDGEMENTS

REFERENCES

Andrus, R. D., and Stokoe, K. H. (2000). "Liquefaction resistance of soils from shear-wave velocity." Journal of Geotechnical and Geoenvironmental Engineering, 126(11), 1015-1025.

Asadi, M. B., Orense, R. P., Asadi, M. S., and Pender, M. J. (2022a). "Empirical assessment of liquefaction resistance of crushable pumiceous sand using shear wave velocity." Journal of Geotechnical and Geoenvironmental Engineering.

Asadi, M. B., Orense, R. P., Asadi, M. S., and Pender, M. J. (2022b). "A unified approach to link small-strain shear modulus and liquefaction resistance of pumiceous sands." Soils and Foundations.

Asadi, M. B., Asadi, M. S., Orense, R. P., and Pender, M. J. (2020). "Small-strain stiffness of natural pumiceous sand." Journal of Geotechnical and Geoenvironmental Engineering, 146(6): 06020006.

Asadi, M. S., Orense, R. P., Asadi, M. B., and Pender, M. J. (2019). "Maximum dry density test to quantify pumice content in natural soils." Soils and Foundations, 59(2), 532-543.

Boulanger, R. W., and Idriss, I. M. (2014). "CPT and SPT based liquefaction triggering procedures". Report No. UCD/CGM-14/01, Center for Geotechnical Modeling, Department of Civil and Environmental Engineering, University of California, Davis, CA,.

Cubrinovski M, Rhodes A, Ntritsos N and Van Ballegooy S (2019). 'System response of liquefiable deposits.' Soil Dynamics and Earthquake Engineering, 124: 212-229pp.

Ishihara, K. (1985). 'Stability of Natural Deposits during Earthquakes,' Theme lecture, Proc. 11th Int. Conf. on Soil Mechanics and Foundation Engineering, San Francisco, 2, 321–376pp.

Kayen, R., Moss, R., Thompson, E., Seed, R., Cetin, K., Kiureghian, A. D., Tanaka, Y., and Tokimatsu, K. (2013). "Shear-wave velocity-based probabilistic and deterministic assessment of seismic soil liquefaction potential." Journal of Geotechnical and Geoenvironmental Engineering, 139(3), 407-419.

NZGS/MBIE, 2021. Earthquake geotechnical engineering practice - Module 1: Overview of the guidelines. In: New Zealand geotechnical society (NZGS) and Ministry of business innovation & Employment (MBIE) guidelines for Earthquake geotechnical Practice in New Zealand. Wellington: s.n.

NZGS/MBIE, 2021. Earthquake geotechnical engineering practice - Module 3: Identification, assessment and mitigation of liquefaction hazards. In: New Zealand geotechnical society (NZGS) and Ministry of business innovation & Employment (MBIE) guidelines for earthquake geotechnical Practice in New Zealand. Wellington: s.n.

Orense, R. P., Asadi, M. B., Stringer, M. E., and Pender, M. J. (2020). "Evaluating liquefaction potential of pumiceous deposits through field testing: case study of the 1987 Edgecumbe earthquake." Bulletin of the New Zealand Society for Earthquake Engineering, 53(2), 101-110.

PROCEEDINGS OF THE 14TH ANZ YOUNG GEOTECHNICAL PROFESSIONALS CONFERENCE
14YGPC ROTORUA, NEW ZEALAND, 2ND – 5TH NOVEMBER 2022

43

Soft ground improvement – construction challenges and practical experiences from the field

A. D. Brunetti[1]

[1]SMEC Australia Pty Ltd, Level 5, 20 Berry Street, North Sydney NSW 2060, Australia; PH +61 2 9925 5555; email: Adrian.Brunetti@smec.com

ABSTRACT

The construction of highway infrastructure on soft ground presents unique geotechnical challenges that require solutions which fulfil the design objectives, account for site constraints, meet long-term maintenance requirements and provide a comfortable road user experience for motorists. This paper presents a case study of the construction challenges encountered during delivery of a recent NSW highway upgrade project and evaluates the implications of several construction issues on embankment performance throughout the entire project lifecycle. The project involved two major creek crossings with 5 m high bridge approach embankments overlying compressible ground between 10 m to 25 m thick. Ground improvement methods comprised of concrete injected columns (CIC) and driven concrete columns (DCC) in combination with wick drains and surcharge. Numerous technical and constructability challenges were met, including strict settlement and deflection tolerances; a narrow construction footprint near live traffic; adjacent existing bridge structures; and variable soft ground conditions. The practical application of soft soil engineering principles in solving these challenges is discussed, including mitigating the impact of CIC installation on existing structures by selection of an appropriate construction sequence to limit soil lateral displacement and ground heave; interpretation of wick drain installation records to assist planning and verification of DCC and CIC treatment extents; and the assessment of alternative construction methods to avoid CIC and bridge abutment interface clashes. Monitoring data from geotechnical instrumentation used to manage ground treatment performance is also presented.

Keywords: Ground improvement, soft soil, construction, concrete injected columns, installation effects

1   INTRODUCTION

The delivery of a recent highway upgrade project on the east coast of Australia involved the duplication of 1.5 km of the existing NSW highway network to dual carriageway. The works included the construction of two major creek crossings with associated bridge approach treatment works for embankments up to 5 m in height overlying soft compressible ground. The new bridges replaced existing bridges that were demolished, after being originally built in the 1960s, to form the southbound carriageway. Figure 1 shows the new southbound bridge and embankment under construction, adjacent to the recently constructed northbound carriageway at the second creek crossing.

The objectives of the ground improvement works were to control settlement at the bridge approaches to protect the new and existing bridge piles from excessive ground movements, meet pavement performance criteria that would require limited maintenance over 40 years and provide a smooth transition zone from the bridge to the embankments.

The author provided geotechnical advice to the project construction delivery team, acting as the Principal on behalf of the client, to oversee implementation of the geotechnical design in the field. Construction risks included the potential impact of the new works on the existing bridge abutment piles, which had strict tolerances for the allowable lateral movement imposed by the new works, cracking of the existing embankment pavement, working within a narrow construction footprint and a tight construction program.

2   SITE GEOLOGY

The highway alignment is underlain by highly compressible, Holocene-age soft to firm estuarine clay deposits over Pleistocene-age stiff clay, residual soils and weathered argillite. The Holocene clay thickness ranged from approximately 10 m to 20 m thick at the bridge abutments, extending up to 25 m thick where a paleochannel exists to the east of the second creek crossing. The underlying Pleistocene clay continued to approximately 40 m depth below ground level.

Figure 1: Southbound carriageway embankment and bridge construction at the second creek crossing

3 GROUND IMPROVEMENT DESIGN

The ground improvement design was completed by a third party geotechnical consultant engaged by the client under a design only contract. Interactions between the newly constructed embankments and existing highway were to be limited to mitigate the risk of significant settlement causing damage to adjacent bridge structures. Ground treatment methods using rigid ground inclusions were employed to support the embankments via load transfer to stiffer underlying materials, including concrete injected columns and driven reinforced concrete columns, in combination with wick drains and surcharge.

Concrete injected columns (CICs) with diameter of 450 mm at 1.8 m and 2.25 m spacing were to be installed by displacement auger techniques within the abutment zone adjacent to the bridge structures. The CICs were embedded 4 m into the stiff Pleistocene clays below the soft clay layer at the location of abutments, with gradually reducing embedment depth to 1 m away from the abutment in order to maintain a smooth transition gradient. Five rows of sacrificial 400 mm square driven concrete columns (DCCs) at 2.25 m spacing were installed immediately adjacent to the surcharge and wick drain area to protect the CICs from excessive lateral movement during fill placement.

4 CONSTRUCTION CHALLENGES

The following section presents a case study of the construction challenges encountered during delivery of the ground improvement works and evaluates the implications of these issues on embankment performance throughout the entire project lifecycle. The practical application of soft soil engineering principles in solving these challenges is discussed, which aimed to fulfil the design objectives, account for site constraints, meet long-term maintenance requirements and provide a comfortable road user experience for motorists.

4.1 Variable soft ground conditions

Geotechnical investigations completed for the project, including numerous boreholes, test pits and cone penetration tests (CPTs), revealed a highly variable ground profile with soft clay depths extending up to 25 m below ground level at discrete locations. The development of a 'live' geotechnical model during the construction phase, using additional information gathered from wick drain and geotechnical instrument installation records, provided an improved understanding of the ground conditions.

Wick drains, or prefabricated vertical drains, were installed to provide shorter drainage paths which enable faster pore water dissipation and accelerate the consolidation process. The drains were driven through the soft Holocene sediments using a vibrating mandrel mounted onto an excavator and anchored into the underlying stiffer Pleistocene deposits. A review of the penetration resistance over the depth of installation for 8,000 wick drains showed a distinct inflection point which indicated the inferred depths to the base of the soft soils. These depths were compared with information from CPTs adjacent to specific wicks. The interpreted depths were plotted spatially to map the varying soft soil thicknesses. This information assisted construction planning and verification of DCC and CIC lengths, which rely on site-specific termination criteria based on the depth to the Pleistocene clays. The data was also compared to the interpreted profiles used in the design and, where necessary, the ground treatment was refined to suit the actual ground conditions.

PROCEEDINGS OF THE 14TH ANZ YOUNG GEOTECHNICAL PROFESSIONALS CONFERENCE
14YGPC ROTORUA, NEW ZEALAND, 2ND – 5TH NOVEMBER 2022

45

An example of the output from this exercise is presented in Figure 2. The data indicated that the depth to the base of soft clay underlying the embankment footprint increased towards the east to approximate RL -23 m AHD, associated with a deep paleochannel. In comparison, the original design profile assumed that the base of soft clay was at approximate RL -14 m AHD. Consequently, the surcharge height at this location was increased to reflect the deeper soft soil profile and maintain a smooth transition gradient between the bridge treatments and adjacent low embankment zone.
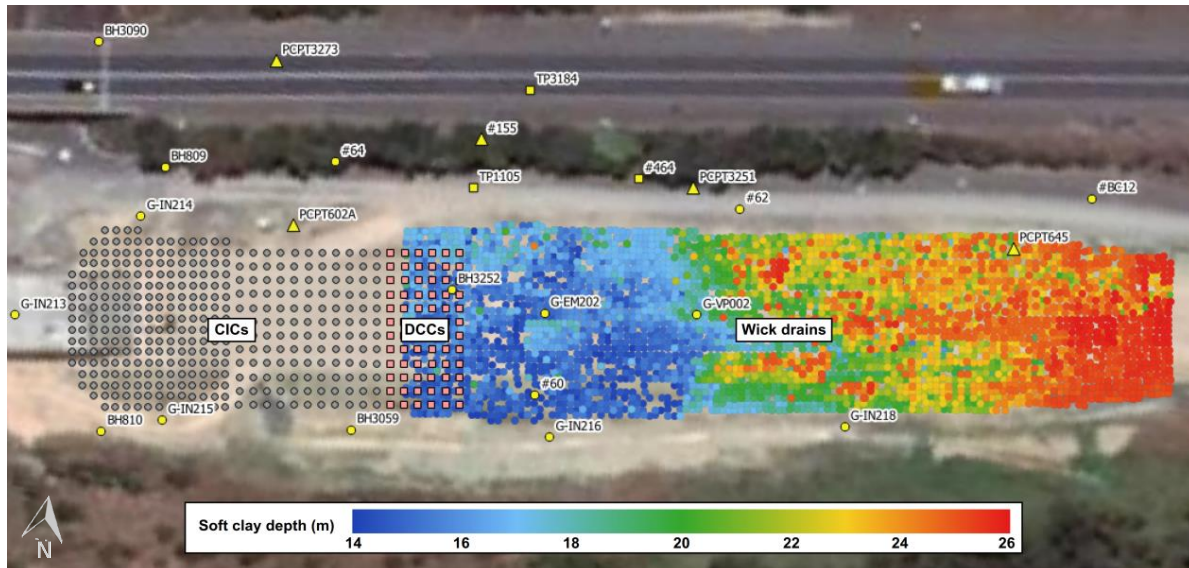
Figure 2: Estimated soft clay depths based on wick drain installation records (plotted using QGIS)

4.2   CIC installation effects

The presence of existing bridge structures directly adjacent to the ground improvement works imposed construction challenges on the concrete injected column (CIC) installation process. CICs, also known as drilled displacement columns, are rigid inclusions that are installed using piling rigs attached with displacement auger heads. The auger is rotated and pushed though the soil formation to the design depth, which displaces the soil laterally rather than excavating soil to the ground surface, followed by grout injection through the hollow stem while the auger is extracted to form the column in-situ. Vertical (heave) and horizontal soil movements occur as the volume of the installed element exceeds the volume of soil extracted and compressed, with the most significant effects observed in soft clays with low permeability which generate high excess pore water pressures (Zhang and Choi 2015).

Nguyen et al. (2016) note that when construction sites involving CICs are located in close proximity of existing sensitive structures such as an existing bridge foundation, the risk of damaging adjacent structures due to lateral soil movement can be high if a proper installation sequence is not considered, as demonstrated by several studies (Brown 2005, Hewitt et al. 2009 and Larisch et al. 2014).

Furthermore, Zhang and Choi (2015) report that the resulting soil displacement has the potential to adversely affect previously installed adjacent columns, with several recent projects in Australia recording damage to CICs during construction as well as ground deformations and soil heave. Larisch et al. (2014) conclude that this damage creates potential conflicts between contractors and clients during construction, and recommends that all stakeholders involved understand the consequences of soil deformations, which can be effectively managed provided the process of installation is well understood and the contractors are knowledgeable and experienced in the design and construction of CICs.

The risk of significant ground movements and damage to adjacent bridge structures caused by CIC installation effects was addressed by selection of a construction sequence that aimed to limit lateral soil displacement and ground heave. Interactions between the newly constructed embankments and existing highway were to be limited to an acceptable level, with lateral soil displacement due to CIC installation on the bridge piles estimated during the design phase to be up to 10 mm.

Figure 3: Concrete injected column (CIC) installation at the first creek crossing

The columns were proposed to be installed in a sequence which achieved a balance between preventing damage to columns already installed and the adjacent existing bridge structures. To limit installation effects, the preferred construction sequence was to start installing columns close to the existing bridge structures and then work away from the existing embankments, as described by Hewitt et al. (2009) and Nguyen et al. (2017). However, the installation process was constrained by site geometry, with the narrow construction footprint surrounded by the creek, existing highway and project boundary, as illustrated in Figure 3 at the first creek crossing.

An alternative sequence was proposed by the contractor to work outwards from the centre of the new embankment to protect the integrity of the columns and provide an exit point for the piling rig. Concerns were raised over the impact of this approach on the existing bridge piles, so a compromise was reached to install every second column in a 'hit and miss' sequence, similar to the staggered approach adopted by Zhang and Choi (2015). The presence of existing embankments that settled several metres also provided construction challenges and required pre-drilling to limit surface ground heave.

The CICs were installed using a Casagrande B250 piling rig with 250 kNm rotational torque capacity and an average concrete overconsumption of approximately 12%. Over 1,800 columns were installed with typical column lengths between 15 m to 25 m and a total combined length of 35,000 m. Monitoring data from geotechnical instrumentation was used to manage the ground treatment performance, with inclinometers installed within the soft soil formation to measure lateral soil deformations and displacement markers in the form of survey prisms placed on the adjacent bridge abutments to record lateral movement caused by CIC installation.

During the installation process, lateral soil movement of 60 mm (at a depth of 7 m) was identified in one inclinometer adjacent to an existing bridge abutment, with corresponding survey marker readings indicating that the structure had moved laterally by approximately 30 mm. This was caused by rapid installation of a small portion of CICs in a continual 'wet-on-wet' fashion due to miscommunication between the lead contractor and piling sub-contractor. The bridge was assessed for structural integrity and was found to be in an acceptable condition.

PROCEEDINGS OF THE 14TH ANZ YOUNG GEOTECHNICAL PROFESSIONALS CONFERENCE
14YGPC ROTORUA, NEW ZEALAND, 2ND – 5TH NOVEMBER 2022

47

Following this event, all remaining columns adjacent to bridge structures were mandated to be installed working outward from the bridge abutments using the 'hit and miss' sequence. With this adopted construction sequence and regular monitoring, the maximum lateral movement was limited to less than 10 mm during subsequent column installation. Monitoring indicated the existing bridges were not affected by ground movements during CIC installation.

Research work by Larisch (2014) and Larisch et al (2015) suggest that inadequate penetration rates may also be potential causes for excessive ground movements, with test results indicating that the depth of the heave cone and the diameter of the heave radius around the column depend on the penetration rate of the displacement drill tool. Inadequate penetration rates were found to cause disturbance of the clay to greater depth, leading to greater heave volumes of up to 60%. The study results highlight the importance of utilising adequately powerful piling rigs to provide sufficient installation energy to maintain the required penetration rates during installation.

The quality of each individual column and performance of the construction sequence was also controlled by continual review of installation records (including torque, auger penetration rate and down-thrust applied during advancement) to assess that the design objectives were met and limit the risk of longer than required socket lengths into stiff material. In one instance, close monitoring of these records, in combination with the development of the 'live' construction phase geotechnical model described earlier, assisted in identifying a dense sand deposit which was interbedded between the soft soil and stiff clay founding layer. This discovery, which was later confirmed during bridge pile excavation, allowed the column socket lengths to be terminated within the sand layer and avoided the need to penetrate the deeper stiff clay layer, limiting associated ground heave and lateral movement.

4.3 Bridge abutment interface clashes

Successful delivery of the ground improvement works required tailored construction solutions to avoid CIC and bridge abutment interface clashes, whilst satisfying long-term pavement performance criteria and providing a smooth transition zone to each bridge from the approach embankments.

The CIC foundation concept often requires the presence of a load transfer platform (LTP), comprising a geosynthetic reinforced gravel mattress beneath the supported embankment, to enhance load transfer to the columns through arching effects in the granular material (Filz and Smith 2006). The need for the LTP and reinforcement should be based on assessment of the differential settlement at road level, particularly for low embankments which do not have the ability to span between columns and require a minimum height of fill over the column heads (Zhang and Choi 2015) to prevent adverse localised deformations that present as dimpling of the pavement surface.

The original design assumed that the existing highway embankment would be stripped to natural ground level, or a level which provided sufficient clearance between the pavement and top of CICs (defined as a minimum height of 1.5 times the clear spacing between each column) to spread the load over a wide area, therefore avoiding the need for a geosynthetic reinforced LTP. However, during construction a decision had been made to retain the existing fill material to act as a working platform. A consequence of this change was that the minimum design requirement for adequate load transfer was not met. After review with the designer and client, a LTP with structural geofabric was placed on top of the CICs as a contingency measure to mitigate adverse localised differential settlement of the pavement, meet long-term maintenance requirements and provide a comfortable road user experience for motorists.

Further implications of this construction approach were that the CICs were constructed at a level higher than the base of the abutment headstock, and the piling platform would need to be lowered to allow construction of the bridge piles and superstructure. Several construction methods were considered to lower the column heads without causing damage. Direct use of an excavator bucket or saw cutting individual columns after localised excavation around the CICs were precluded due to the risk of uncontrolled cracking and time constraints. The adopted method was to 'post-bore' the CICs to the desired level by mixing the pre-injected concrete and platform material which typically resulted in a lower strength material similar to stabilised sand. After preloading, this material was removed by bulk excavation allowing rapid construction of the abutment piles and greatly benefitting the construction program. Figure 4 illustrates the constructed 'stepped' CIC transition profile following preload removal.
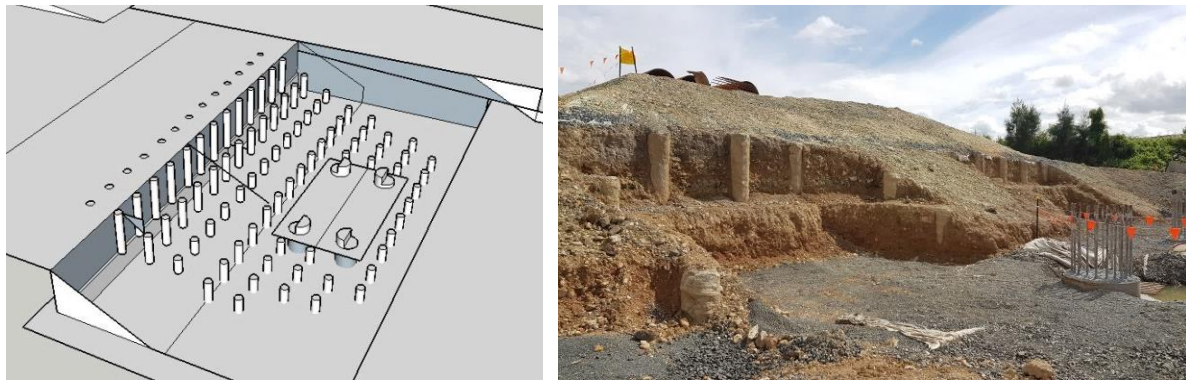
Figure 4: Proposed 'stepped' CIC transition (left) and constructed CICs following preload removal (right)

5 CONCLUSION

This paper presents a case study of the challenges encountered during construction of a recent highway upgrade project overlying soft ground and describes the geotechnical solutions which met numerous technical and constructability constraints. The key issues were associated with construction time limitations, strict settlement and deflection tolerances, a narrow construction footprint near live traffic, adjacent existing bridge structures and variable soft ground conditions.

The value of the practical application of geotechnical engineering principles in solving construction challenges is described, including the benefits of providing on-site technical support to manage the implementation of the geotechnical design. The highway upgrade is open to traffic and has displayed good operational performance, demonstrating the successful delivery of the ground improvement works.

Experienced geotechnical practitioners with expertise in the design and construction of highway infrastructure on soft ground should be consulted by all parties involved, including clients, contractors and sub-contractors so that that the finished product achieves the design objectives, accounts for site constraints, meets long-term maintenance requirements and provides a comfortable road user experience for motorists.

6 ACKNOWLEDGEMENTS

REFERENCES

Brown, D. A. (2005). "Practical considerations in the selection and use of continuous flight auger and drilled displacement piles." Advances in Deep Foundations: Geotechnical Special Publication No. 132, ASCE, Austin, 1-11.

Hewitt, P., Summerell, S. and Huang, Y. (2009). "Bridge approach treatment works on the Coopernook to Herons Creek section of the Pacific Highway Upgrade." Geosynthetics: New materials for modern infrastructure, AGS, Sydney, 51-60.

Filz, G. M. and Smith, M. E. (2006). "Design of bridging layers in geosynthetic-reinforced, column-supported embankments." Report No. VTRC 06-CR12, Virginia Transportation Research Council, Charlottesville

Larisch, M. D. (2014). "Behaviour of stiff, fine-grained soil during the installation of screw auger displacement piles." PhD thesis, The University of Queensland, Brisbane.

Larisch, M. D., Kelly, R. and Muttuvel, T. (2014). "Improvements of soft soil formations by drilled displacement columns", in Indraratna, B., Chu, J. and Rujikiatkamjorn, C. (eds), Ground Improvement Case Histories, Butterworth-Heinemann, Oxford, Chapter 21, 573-622.

Larisch, M. D., Williams, D. J. and Scheuermann, A. (2015). "Influence of pile installation techniques on ground heave in clays". 12th Australia New Zealand Conference on Geomechanics, Wellington, 143-150.

Nguyen, H. H., Khabbaz, H., Fatahi, B. and Kelly, R. (2016). "Bridge pile response to lateral soil movement induced by installation of controlled modulus columns." 3rd International Conference on Transportation Geotechnics, Guimarães, 475-482.

Nguyen, H. H., Khabbaz, H., Fatahi, B. and Hsi, J. (2017). "Effects of installing controlled modulus columns on previously installed columns." 19th International Conference on Soil Mechanics and Geotechnical Engineering, Seoul, 2611-2614.

Zhang, H. and Choi, B. (2015). "Controlled modulus column design and construction on a highway project on east coast of Australia." International Conference on Soft Ground Engineering, Singapore, 165-176.

PROCEEDINGS OF THE 14TH ANZ YOUNG GEOTECHNICAL PROFESSIONALS CONFERENCE
14YGPC ROTORUA, NEW ZEALAND, 2ND – 5TH NOVEMBER 2022

49

Assessment and Design Methodology for the Identification and Remediation of Rock Snagging Hazards on Road Cuttings – A Case Study from the Hervey Range Road Safety Upgrade Program Project

M. R. McLoughlin

Queensland Tunnelling and Ground Engineering, Townville Office, Jacobs Group (Australia) Pty Ltd; Suite 2, Level 7, 61-73 Sturt Street, Townsville City, QLD 4810; PH: (61+) 475 747 204; email: matthew.mcloughlin@jacobs.com

1. ABSTRACT

Hervey Range Developmental Road (83A) is a two-lane, two-way single carriageway rural road connecting Townsville to Hervey Range and outer suburban residential areas such as Alice River and Rangewood. As part of a safety upgrade program along Hervey Range Road, identification of rock snagging locations and design of value for money smoothing solutions were required to be undertaken due to the need for widening of the sealed road alignment and the proximity of the existing rock cuttings relative to the road. An assessment methodology for identifying what constitutes a rock snagging hazard in a quantitative sense is either not well defined or inconsistent when considering published literature (such as various state road authority specifications and other Australian road design guidelines). In light of this, a definition of a rock snagging hazard was developed for the project and can be qualitatively defined as a rough, sharp or jagged rock protrusion or depression which has the potential to constitute a hazard to vehicular navigation. This paper describes the qualitative and quantitative assessment criteria and design methodology that has been adopted to address the risks associated with rock snagging hazards on irregular and often jagged road cuttings that are close to the edge of the road using the Hervey Range Road Safety Upgrade Program project as a case study. The assessment of rock snagging hazards without the necessary budget for detailed field assessment and mapping, as well as fit for purpose detailed survey, can complicate the ability to provide cost effective remedial solutions to this type of problem. Two-dimensional analysis of survey can often prove problematic with regards to identification of the hazards. This paper discusses how interrogation of the available information through rendered three-dimensional survey assessment in conjunction with digital video recorder (DVR) footage and still imagery, as well as use of conventional two-dimensional analysis of cross-sections and long-sections, can be used to provide value for money smoothing solutions. An innovative design methodology incorporating the vertical extent of treatment on slopes to reduce the risk of safety in construction as well as reducing the construction costs was also implemented as part of the project.

Keywords: Rock Snagging, Rock Smoothing, Design Methodology, Range Road

2. INTRODUCTION

Rock snagging is a poorly defined safety hazard prevalent along range roads, where unremediated cuttings are common. These hazards present a considerable risk to motorists, whether due to the "can opening" effect of smaller protrusions, or possible collisions with larger protrusions or depressions. Various transport authorities identify the risk posed by rock snagging without providing an actual description or method of identification for what constitutes a rock snag. Consequently, a description and method of identification had to be produced to provide a basis for an assessment. Rock snagging was defined to be a rough, sharp or jagged rock protrusion or depression which has the potential to constitute a hazard to vehicular navigation. With an understanding of what rock snags were, a quantitative assessment to identify them was required.

3. PUBLICATIONS REGARDING THE IDENTIFICATION OF ROCK SNAGGING

The only publications from a transport authority that discussed quantitative values for rock snagging was Austroads – Guide to Road Design Part 6. Section 4.4.6, which stated that there were no guidelines available for the acceptable roughness of rock faces. However, reference to a Federal Highways Administration approval letter (referenced within Austroads) regarding the vertical relief on the face of rigid barriers states that the roughness tolerated is minimal, with a maximum height of 64mm for any irregularities in the surface of the barrier above where contact with the wheel would occur. This criterion was considered too stringent for rock cuttings and would be unfeasible to apply.

As the case study was a Department of Transport and Main Roads (DTMR) project, DTMR technical specifications (MRTS) and the geotechnical design standard (GDS) were considered. The only information applicable from these documents was from Section 16 of MRTS04, where there are to be no overhangs outside the edge of the table drain from rocks batters and the design shape of the finished batter is not to extend away from the design line further than the lesser of 300mm or one third the height of the batter. This supplied a more reasonable deviation from the design slope in comparison to Austroads but did not consider the increased risk of larger protrusions closer to the road level.

To further refine the assessment criteria, the New South Wales Roads and Maritime Services (RMS) Quality Assurance Specification R44 was also considered. R44 Section 3 specifies that cuttings must not have undulations in the general plane of the batter and that batter tolerances should be calculated regarding the height and steepness of the batter at any given point. This provided the consideration of increased risk for protrusions on lower sections of the slope and are detailed in Table R44.3, detailing the excavation tolerances for batters in cuttings.

4. ADOPTED METHODOLOGY

While RMS provided the most thorough criteria, conformance with DTMR technical specifications would allow a wider application of the methodology. This change meant that the maximum allowable tolerance away from the roadway for slopes steeper than 1H:1V would be limited to 300mm instead of 600mm. These values have been provided as part of Table 1.

Table 1: Adopted Tolerance Criteria for Rock Snagging

Location	Tolerance (mm) [a]	
	Slope 1H:1V or flatter	Steeper than 1H:1V
At the toe of the batter	+0 / -150	+0 / -200
0m to 2m above the toe of the batter	Interpolate	Interpolate
2m to 4m above the toe of the batter	+300 / -300	+300 / -300

[a] The "+" is the tolerance towards the roadway, while the "-" is the tolerance away from the roadway.

As DTMR and Austroads specifications do not specify whether the tolerance is to be taken as a vertical, horizontal or perpendicular to the slope plane, the RMS method was adopted where all tolerances shall be measured perpendicular to the slope plane.

Areas within the first 2m (vertical height) of the batter are considered the highest potential risk due to being the most important to prevent snagging. This is with consideration of the height of passenger vehicles, RMS R44 limiting the tolerances within this region and Austroads stating that the first 1m of the cutting is important when trying to prevent snagging. However, where significant heavy vehicle traffic is present, consideration should also be given for the potential of snagging above 2m. A vertical height of 4m is suggested as the upper extremity of potential treatments based off the height of heavy vehicles (i.e., type 1 and 2 road trains).

To ensure that treatments are not overly excessive, limiting the height of treatments based on the horizontal offset from the toe of the batter is suggested. As a result, steeper slopes will require a greater height of treatment in comparison to flatter slopes. As part of the adopted methodology, horizontal offsets greater than 1m away from the toe of the batter should be achieved before considering the rock snagging hazard outside the reasonable area to treat. A simplification of this that can be used is that slopes of 45°or less require a treatment height of 1m, slopes greater than 45° and up to 60° require a treatment height of 2m and slopes greater than 60° require a treatment up to 4m.

Rock snagging is also unable to be assessed in only a conventional cross-section analysis, with several issues arising due to the application of 2D analysis to a 3D problem. A significant issue is that undulating slopes, which are a potential collision hazard, are a type of rock snagging that may be unidentified without 3D assessment. Smoothing solutions also need to consider the risk posed to vehicles that may collide with the treated area and tapering the solution back towards the rock cutting is required. 2D analysis also presents an issue when considering the constructability, estimation of quantities and budgeting of costs for tendering purposes. As such, a 3D assessment is needed to accompany 2D analysis.

PROCEEDINGS OF THE 14TH ANZ YOUNG GEOTECHNICAL PROFESSIONALS CONFERENCE
14YGPC ROTORUA, NEW ZEALAND, 2ND – 5TH NOVEMBER 2022

51

5. APPLICATION OF METHODOLOGY TO DEVISE CASE STUDY TREATMENT OPTIONS

When applying the methodology, consideration is needed for the challenges presented by an irregular 3D slope face. Removing the hazard via scaling would be the simplest solution, however, the likelihood of uncovering even more problematic geology meant that this should be reserved for small scale locations. There was also the issue that scaling would not allow for the treatment of depressions, where an infill treatment is required. This was considered as Option 1 for treating rock snagging.

To effectively treat rock snagging where scaling was not feasible, a solution that can be applied over complex geometries including protrusions and depressions was required. Initially, a shotcrete solution with mesh was suggested, but it is difficult to adapt mesh reinforcement to adequately support the shotcrete around complex geometry with depressions often being found in conjunction with protrusions. This meant that alternative reinforcement solutions were required, and as such fibre-reinforced shotcrete or fibrecrete were selected as the preferred solutions. The weight of the fibrecrete would seldom be sufficiently supported by the slope and required dowels to act as supports for the treatment. To ensure that the dowels had adequate corrosion protection, as well as assist in transferring the weight of itself to the dowels, a minimum cover of 100mm was needed over protrusions. Consequently, the protrusion would be extended towards the road, which increases its severity. Tapering the protruded areas back into the slope at such an angle that it would not present a hazard to vehicles, would rectify this. To do this, reference to DTMR technical specifications and Austroads was needed to consider the effect of a vehicle impacting the treated slope, which requires the treatment to have similar considerations to concrete barriers. This is highlighted in Section 4.4.6 of Austroads – Part 6, where cuttings and rock faces should be designed to provide a smooth face that will act as a rigid barrier, allowing errant vehicles to slide along and stop gradually. To adhere to this, Section 5.3.5 of Austroads – Part 6, specifies a flare rate to be applied to the treatment, while limiting the encroachment angle to no greater than 25°. Section 5.3.14 of Austroads – Part 6 is used to assess the encroachment angle of a vehicle on straights relative to the design speed. The DTMR Road Planning and Design Manual (RPDM) Supplement to Austroads – Part 6, Table 6-4 (which supersedes Table 5.5 of Austroads – Part 6), specifies the minimum flare rate relative to the design speed and shy-line. The offset of the shy-line from the pavement edge is also specified in DTMR RPDM Supplement to Austroads – Part 6, in Table 6-3. Once these additional safety considerations had been applied, this was considered as Option 2 for treating rock snagging.

There were also locations where there were only depressions and did not require a treatment to further extend the slope face towards the road. In these cases, this meant that no taper was required as the edges of the treated area acted only as infill for the depression. However, it still required dowels to support the treatment. Given the simplification of treatment in comparison to Option 2, this was designated as Option 3 for treating rock snagging.

While Option 1, 2 and 3 covered the requirements of all situations along Hervey Range Road, there were instances where a significant volume of shotcrete would be required and consequently, a non-cost-efficient solution would be specified. To minimise these volumes, an extension to the considerations of Option 2 were adopted. Instead of a fibrecrete solution, the façade geometry of the treatment was adopted from precast concrete barriers as stipulated in DTMR Standard Drawing SD 1458, which limited the treatment to 1.05m high. This treatment would effectively operate in the same way as a concrete barrier but would infill the entire area behind the façade. Due to the limited height and consistent geometry of the façade, formwork can be made for the option, allowing for a poured concrete solution. Due to the same issues with reinforcement as Option 2, fibre-reinforced concrete was used to provide adequate reinforcement for the treatment, which also required support from dowels. This treatment was also required to consider the tapering requirements of Option 2 as it extended the slope face towards the road. Using this treatment significantly lowered the costs in several locations and was designated as Option 4 for treating rock snagging.

After considering potential drainage issues, including at least a 5° slope angle at the top of the structure for Option 2, 3 (where applicable) and 4 would allow for runoff to flow over the treatment while limiting the effects of erosion behind it. Typical sections depicting Options 2, 3 and 4 are provided in Figure 1, 2 and 3 respectively.
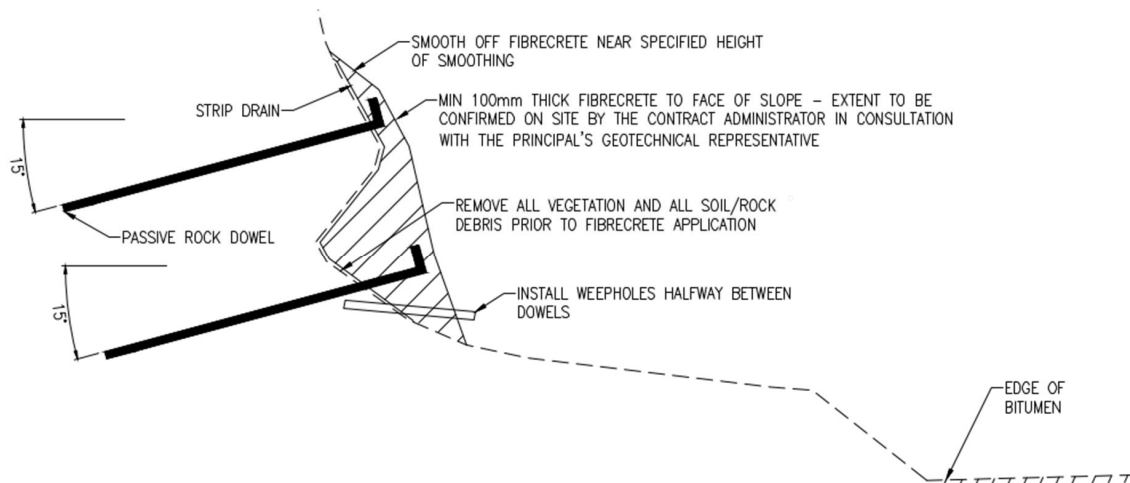
Figure 1: Typical section of Option 2.
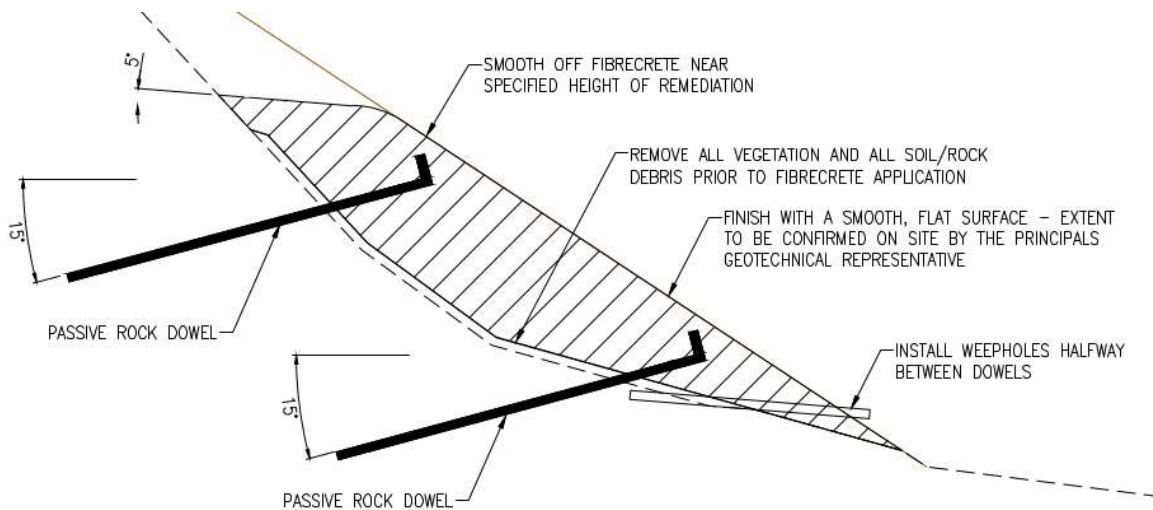
Figure 2: Typical section of Option 3.
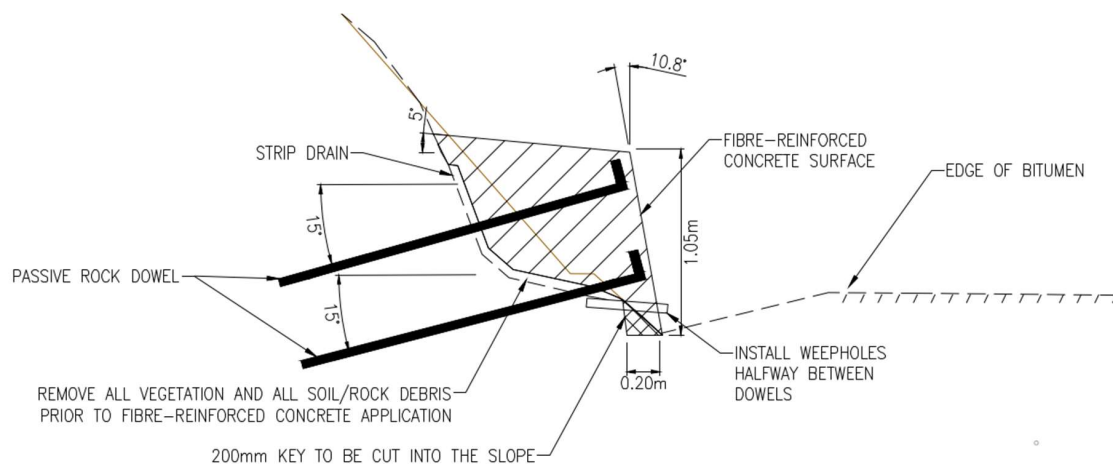
Figure 3: Typical section of Option 4.

PROCEEDINGS OF THE 14TH ANZ YOUNG GEOTECHNICAL PROFESSIONALS CONFERENCE
14YGPC ROTORUA, NEW ZEALAND, 2ND – 5TH NOVEMBER 2022

53

6. CASE STUDY: HERVEY RANGE DEVELOPMETAL ROAD

Hervey Range Developmental Road (83A) is a two-lane, two-way single carriageway rural road connecting Townsville to Hervey Range and outer suburban residential areas such as Alice River and Rangewood. As part of a safety upgrade program along Hervey Range Road, identification of rock snagging locations and design of value for money smoothing solutions were required to be undertaken due to the need for widening of the sealed road alignment and the proximity of the existing rock cuttings relative to the road. By applying the assessment methodology provided in Section 4, twenty-two (22) locations were identified that needed rock snagging treatments using the options provided in Section 5.

The basic parameters such as height and length can be estimated with 2D analysis and site imagery (i.e., DVR and Google Earth), but by utilising 3D assessments the tolerance at multiple locations could be assessed rapidly with more accurate information. The increase in accuracy also allows for better estimation of the slope and treatment heights, slope coverage, surface area and volume of materials, which is useful for generating a more cost-effective design. An example of which can be shown in Figure 4, where the dark areas on the slope correspond to depressions, with the light area in the depressions being greater than 600mm away from the design surface.
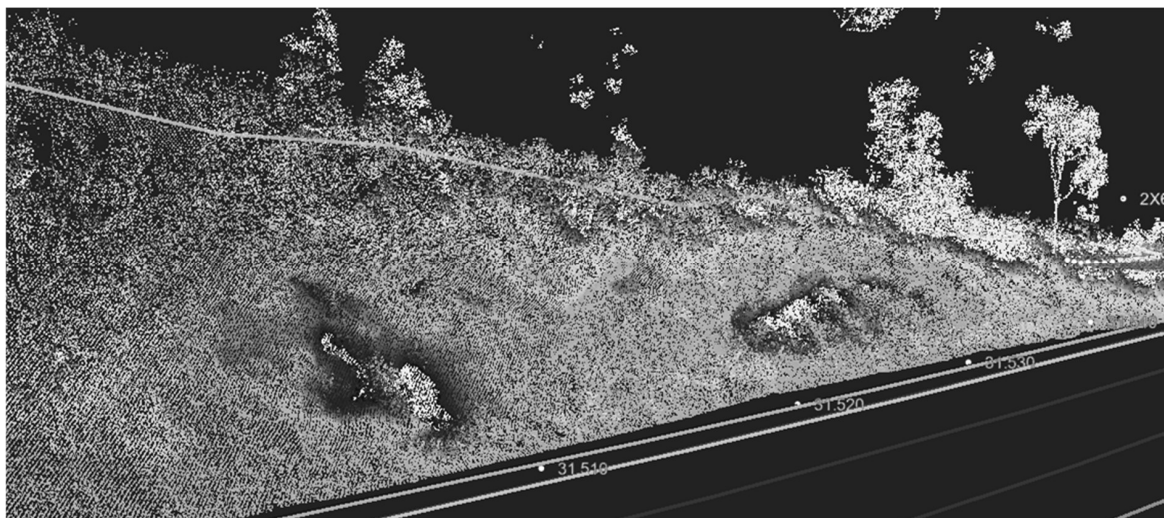
Figure 4: Example of 3D assessments from Ch. 31505 to 31535

Options were assigned based on the construction limitations and cost-effectiveness, which was performed by calculating the cost of the volume of material and considering the addition of other elements like dowels. Each option would result in varying thicknesses and the calculations of components like dowel length were dependent on the option chosen due to changes in parameters (i.e., average thickness and surface area). Table 2 outlines the chosen option for each location, as well as some basic information in regard to the slope.

Table 2: Designation of Options for Identified Rock Snagging Treatment Areas

Start Chainage (km)	End Chainage (km)	Height (m)	Length (m)	Angle (°)	Average Thickness (m)	Suggested Treatment
27.441	27.449	0.80	8.0	46	0.25	Option 1
27.449	27.454	0.96	5.0	40	0.20	Option 1
27.572	27.618	1.05	46.0	64	0.40	Option 4
27.869	27.953	1.00	84.0	44	0.45	Option 4 [a]
28.101	28.120	2.00	19.0	56	0.15	Option 3
28.477	28.519	1.05	41.6	46	0.25	Option 4
28.663	28.695	1.05	31.8	48	0.55	Option 4
28.718	28.726	1.00	8.0	26	0.70	Option 3

Start Chainage (km)	End Chainage (km)	Height (m)	Length (m)	Angle (°)	Average Thickness (m)	Suggested Treatment
28.897	28.915	0.58	18.9	47	0.15	Option 2
28.925	28.963	2.00	38.5	48	0.35	Option 4 [a]
29.165	29.258	2.00	93.0	57	0.40	Option 4 [a]
29.495	29.548	2.00	53.0	55	0.40	Option 4 [a]
29.645	29.656	1.00	11.0	35	0.35	Option 2
29.977	29.999	1.05	22.5	57	0.25	Option 4
30.130	30.145	1.05	15.0	60	0.40	Option 4
30.145	30.152	2.00	5.0	60	0.30	Option 2
30.232	30.262	1.05	30.0	47	0.55	Option 4
30.262	30.335	1.05	73.0	60	0.40	Option 4
30.360	30.418	1.05	57.5	55	0.45	Option 4
30.464	30.525	1.05	61.0	52	0.35	Option 4
31.505	31.535	1.05	30.0	46	0.40	Option 4
31.731	31.752	1.05	20.6	50	0.35	Option 4

[a] Scaling or splitting is required prior to implementation of the suggested treatment.

By scrutinising the results in Table 2, some trends can be noticed in the application of options:

- Option 1 was able to be applied due to the limited height of the slope and the rock snags being solely supported by a soil matrix.

- Option 2 is effective on slopes with lesser thickness, limited height, or relatively flat slope angles. Being a spraycrete, its application is versatile but more costly when considering the volume of material applied in comparison to the poured concrete of Option 4.

- Option 3 is limited by the presence of protrusions, but it is extremely effective at targeting shallower depressions regardless of the height at which they occur. Depending on the position of the depression, Option 3 is also able to out-perform Option 4 where thicker applications of concrete are required.

- Option 4 is the most adaptable option with the height of the slope not affecting the volume of material needed. The only instances where Option 4 is outperformed is where thinner applications of material are applied to steeper slopes, or on shallower slopes where a significant amount of material is required to infill behind the façade.

7. CONCLUSION

While rock snagging was initially poorly defined yet still considered a safety hazard, the combination of publications from different transport authorities allowed for quantitative and qualitative definitions to be provided. This allowed for the methodology to be combined with design considerations to provide treatment options for real-life application. This in turn allowed for the calculation of the most cost-effective option, which was best performed by including 3D assessments with conventional 2D analysis. This was due to 3D assessments helping better identify parameters for effective cost-estimation and also simplifying the identification of potential rock snagging hazards. As such, the definitions and methodology in this paper are considered not only feasible but effective at assessing the different design aspects required to treat rock snagging hazards.

8. ACKNOWLEDGEMENTS

Design of Controlled Modulus Columns without Load Transfer Platform

W. T. Eom[1], BE(Hons), MESc, CPEng, RPEQ and R. B. Kelly[2], BE, PhD, CPEng, PREQ,

[1]Tonkin + Taylor, Unit 11, 1 Metier Linkway, Birtinya, Queensland, 4575 Australia; PH (61) 430 633 012; email: WEom@tonkintaylor.com.au
[2]SMEC, Level 6, 480 St Pauls Terrace, Fortitude Valley, Queensland, 4006, Australia; PH (61) 7 3029 6625; email: DrRichard.Kelly@smec.com

ABSTRACT

Ground improvement by means of Controlled Modulus Columns (CMCs) usually involves the construction of a Load Transfer Platform (LTP) over the CMCs, especially for construction of low embankments over soft soil, to carry the overburden load and transfer to the CMCs, thereby not loading the surrounding soft soils, and avoiding excessive total and differential settlement. This paper provides a case study of a design undertaken for CMCs without an LTP, taking advantage of a relatively high embankment (4.5 m). Compacted fill and gravel working platform layers have been considered to be sufficient to dissipate any differential settlement at the surface of the embankment, without a need for an LTP. Available settlement monitoring data has confirmed the settlement to be within tolerable limits. Advantages of this method include time and cost savings, as well as environmental benefits.

Keywords: ground improvement, controlled modulus columns, finite element analysis

1   INTRODUCTION

With the increase in population especially in large cities, there is a corresponding increase in the need for additional buildings and infrastructure. Existing structures are likely to have been developed where the ground conditions are readily suitable, i.e. exhibiting high bearing capacity and low compressibility. Such areas are near depletion especially in large cities, and new structures are required to be constructed in remaining unsuitable ground conditions where typically additional construction measures are required to meet the functionality requirements of the structures. Some of these measures include ground improvement and piling, and a range of these construction measures are available, determined by considering several factors such as the cost, available time for construction, functionality requirements, availability of materials, and the applicability in the ground condition.

Controlled Modulus Columns (CMCs) are a ground improvement method that involves installation of rigid concrete columns in a grid pattern using a rotary displacement auger. They are typically used in areas where large embankments, such as bridge abutments, are constructed over soft soils that are too deep for some other ground improvement methods, and when some degree of settlement can be tolerated.

The intent of the CMCs is to transfer the majority of the vertical load of the embankment to the stiffer ground on which the CMCs are embedded in and minimise the vertical load on the overlying soft soil, thereby reducing settlement. They are different to piled embankments, where the piles are expected to support all of the vertical load. (Larisch et al, 2014)

To facilitate the load transfer to the CMCs, a load-transfer platform (LTP), generally comprised of a granular mattress and geogrids, is usually constructed over the CMCs. However, LTPs may be omitted where it is considered that the majority of the embankment load could be transferred to the CMCs via soil arching, which effectively serves the purpose of an LTP. A relatively thick embankment would be required for this to occur. The removal of the LTP reduces costs, construction time and environmental impact. (Wong and Muttuvel, 2012). It should be noted that this may be possible in certain situations and the discussions in this paper should not be interpreted as removal of LTP in *all* design cases.

The theory of soil arching is discussed in BS 8006:2010, based on Marston's formula and the Hewlett and Randolph method (1988). Partial arching and full arching are achieved when the height of the embankment is greater than 0.7 × clear spacing and 1.4 × clear spacing, respectively.

The spacing of the CMCs require careful consideration. Closer spacings would reduce settlement while increasing cost, and therefore the selection of the most effective spacing is an important part of CMC design. Wong and Muttuvel (2012) have shown in their numerical parametric analyses that the predicted embankment settlement increases rapidly beyond a spacing to column diameter ratio of about 4.
Due to the soils being laterally displaced during the installation, close spacings can affect the adjacent CMCs by either, depending on their condition, inducing cracking if the concrete has been set (Larisch et al, 2014), or induce heaving or necking if the concrete is still wet. The latter is referred to as wet-construction in this paper.

This paper discusses a design that was undertaken for CMCs without an LTP, using the wet-construction method, and some observations during construction and settlement monitoring.

2 GEOTECHNICAL GROUND MODEL

The design was undertaken for an area underlain by a 6.5 m thick soft estuarine layer, overlying residual soils and weathered material comprising stiff to hard clayey material. The proposed final embankment height was 4.5 m, comprising 1.5 m granular working platform to facilitate construction activities on the soft soil and 3.0 m engineered fill. The developed ground model is summarised in Table 1 and shown in Figure 2a. The adopted settlement parameters are summarised in Table 2. The groundwater level was adopted as 0.3 m below top of soft clay layer.

Table 1:   Ground model

Thickness (m)	Material	Unit Weight (kN/m^3)	Young's Modulus (MPa)	Undrained Shear Strength (kPa)	Drained Cohesion (kPa)	Drained Friction Angle (°)
3.0	Engineered fill	20	40	-	5	30
1.5	Working platform	20	60	-	1	45
6.5	Soft Clay	16	Refer Table 2	15	1	23
1.0	Stiff Clay	18	20	50	3	27
4.0	Very Stiff Clay	19	30	100	4	28
> 5.0	Hard Clay	20	40	200	5	30

Table 2:   Summary of settlement parameters

Compression Ratio $CR = C_c/(1+e)$	Compression / Recompression Ratio C_c/C_r	Secondary Compression Index C_α/C_c	Coefficient of Consolidation C_v (m^2/year)	Over-Consolidation Ratio
0.375	7.5	2.5%	10.0	Varies

3 ANALYSIS

The design was undertaken for a range of CMC centre to centre spacings between 4.0 × diameters and 5.5 × diameters in a square pattern, for an embedment depth into the Very Stiff Clay layer ranging between 0.5 m and 2.0 m.

The analysis was undertaken by a finite element software package, PLAXIS 2D (Version 22), using the axisymmetry model. Finite element modelling was adopted over conventional approaches, as some conventional approaches may underpredict the efficacy of columns and foundation soil (Yapage, *et al*. 2013).

The width of the axisymmetry model was determined based on the equivalent tributary area of a single CMC based on the spacing and square grid layout pattern. The CMC was modelled with the Linear Elastic model, with a diameter of 0.36 m and Young's Modulus of 12 GPa. The Soft Soil Creep model has been used to model the soft clay layer, and Mohr-Coulomb model was used for remaining materials.

The following analysis staging was adopted in PLAXIS, based on the proposed construction sequence:

PROCEEDINGS OF THE 14TH ANZ YOUNG GEOTECHNICAL PROFESSIONALS CONFERENCE
14YGPC ROTORUA, NEW ZEALAND, 2ND – 5TH NOVEMBER 2022

57

- Initial Phase (K0 Procedure)   Not applicable
- Construct Working Platform   14 days
- Hold Construction   14 days
- Install CMC   14 days
- Hold Construction   14 days
- Construct Fill Embankment   14 days
- Finalise Construction   30 days
- Design Life (Post-construction)   50 years

The assessed post-construction settlement results are summarised in Table 3 and Figure 1.

Table 3:   Summary of assessed post-construction settlement results

Spacing		Embedment (m)			
Diameter	m	0.5	1.0	1.5	2.0
4.0 D	1.44	39	40	25	22
4.5 D	1.62	145	140	70	64
5.0 D	1.80	179	177	75	75
5.5 D	1.98	237	230	218	214
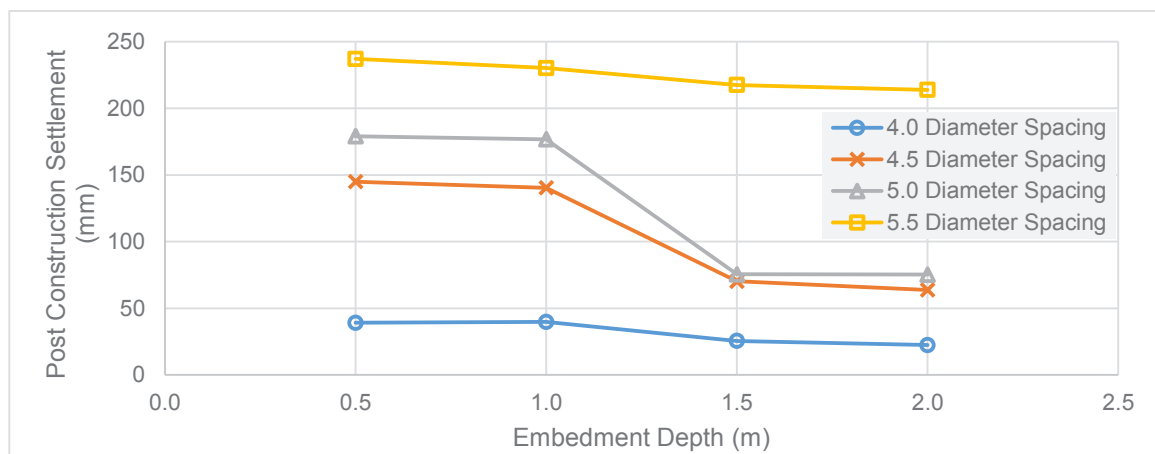
Figure 1:   Assessed post-construction settlement results

Figure 1 shows that the settlement is significantly lower for the spacing of 4.0 diameter, which is comparable to analyses by Wong and Muttuvel (2012). Based on BS 8006, only the spacing of 4.0 diameter achieves full soil arching, whereas other spacings only achieve partial soil arching, which agrees with the assessed values.

The adopted CMC spacing and embedment depth were determined based on the post-construction settlement criteria. For areas with 200 mm allowable settlement, CMC spacing of 5.0 × diameter and 1.0 m embedment depth were selected. For areas with 100 mm allowable settlement, the same spacing with 1.5 m embedment depth was selected. For areas with 50 mm allowable settlement, CMC spacing of 4.0 × diameter was selected. CMC spacing of 4.0 × diameter was also selected for areas where differential settlement criteria of 50 mm governed, for example, along pipe alignment or areas adjacent to piled structures.

Figure 2 shows a) the ground model, showing the CMC has been constructed from the top of the working platform and embedded into Very Stiff Clay; b) the principal stress directions showing soil arching within the embankment fill and working platform layers; and c) displacement contours, from the case analysed for 5 × diameter spacing and 1.5 m embedment (with selected values labelled on the contours for clarity). The displacement contours show the relative movement of the CMC to the soil. In the upper portion of the soft soil, or above the 'neutral plane', the soil moves more than the CMC, applying negative skin friction to the CMC. In the lower portion of the soft soil, or below the 'neutral plane', the soil moves less than the CMC. (Muttuvel and Wong, 2012)

The principal stress plots showing soil arching and sensitivity assessments with and without LTP were used to justify an LTP was not required. The latter are not part of the scope of this paper.
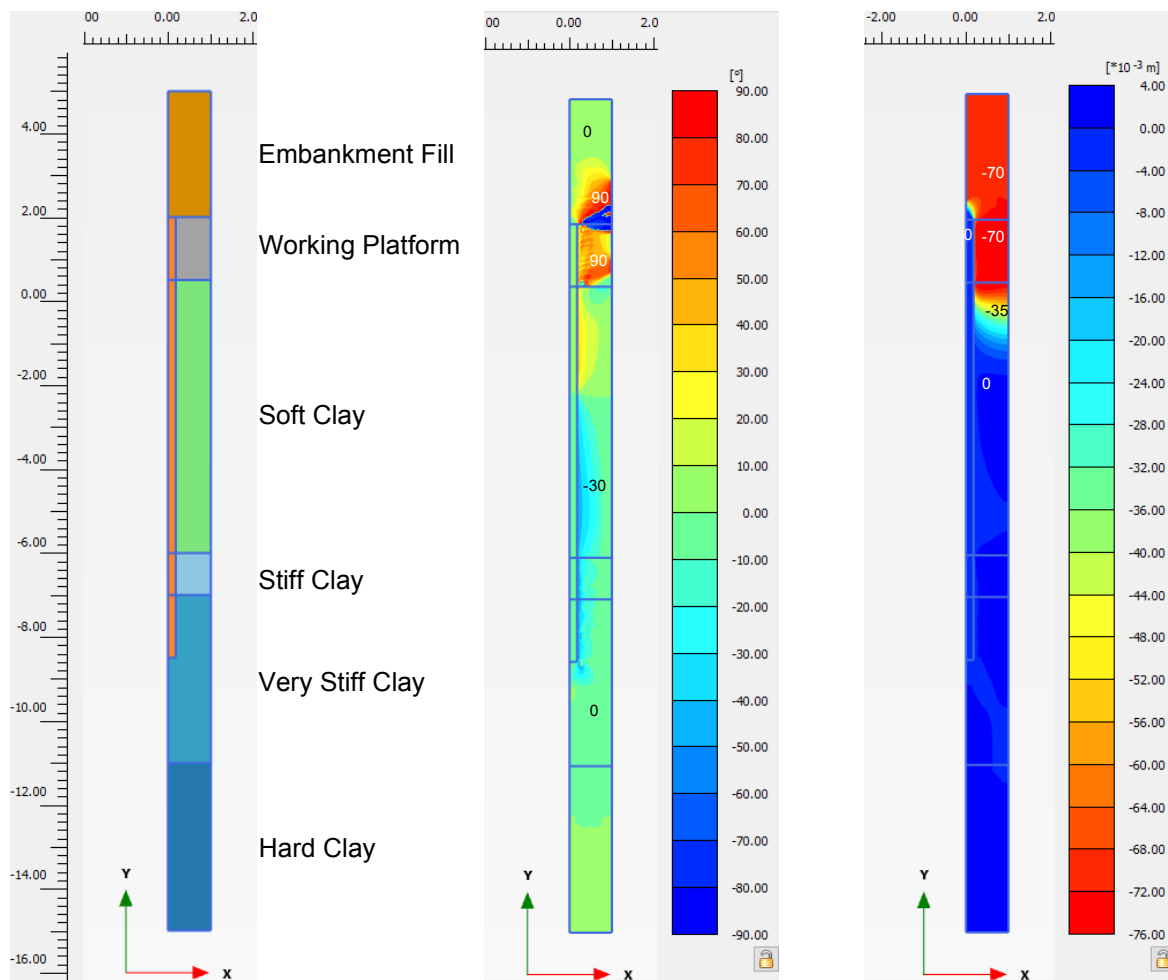
Figure 2: *PLAXIS Outputs: a) Model; b) Principal stress directions; c) Displacement Contours*

4 CONSTRUCTION

Prior to the installation of CMCs, a trial construction was undertaken to confirm applicability of the wet-construction method, using a group of 5 CMCs in two different areas. As anticipated, when a CMC was being installed adjacent to a freshly installed CMC, heaving was observed in the latter, creating a shallow puddle of wet concrete. However, based on the approximate volume of the displaced concrete, it was assessed that the reduction in diameter was relatively minor when the CMC spacing was no less than 4 × diameters. Figure 3 shows a CMC being installed on the left, with heaving of wet concrete observed in a previously installed CMC to its right.

When the purpose of the CMCs and surrounding structures were considered, it was decided that the presence of cracks would be more detrimental to the CMCs compared to having a slightly reduced diameter. The wet-construction method also reduced the construction time, as it was not necessary to wait until the concrete had fully set before an adjacent CMC was installed.

In other cases, it might be considered that the risk of having reduced diameter or necking are more critical the risks of having cracked CMCs. Careful consideration should be made before deciding which construction method should be adopted. There are benefits and risks associated with both methods. An increased spacing reduces the likelihood of forming cracks or having reduce diameter.

PROCEEDINGS OF THE 14TH ANZ YOUNG GEOTECHNICAL PROFESSIONALS CONFERENCE
14YGPC ROTORUA, NEW ZEALAND, 2ND – 5TH NOVEMBER 2022

59

Figure 3:   Heaving of wet concrete during installation of an adjacent CMC

5   SETTLEMENT MONITORING

Based on the assessment results, the anticipated amount of construction settlement was approximately 230 mm depending on the adopted CMC spacing and embedment, with 150 mm of settlement occurring prior to CMC installation, and 80 mm post CMC installation.

Settlement was monitored via settlement plates that were installed once the CMCs were installed. The settlement during working platform placement and CMC installation could not be monitored. The monitored data from settlement plate installation to two months after embankment construction showed that the actual settlements were less than 50 mm.

There are a few reasons that may have led to this difference between assessed and monitored values:

- Due to difficulties during construction, the settlement plates could not be installed before the working platform was constructed. Depending on the permeability, more settlement may have undergone than assessed. Sensitivity assessment showed that the assessed settlement during and post construction are highly sensitive to the adopted permeability values.
- The assessed construction sequence was longer than the actual construction staging.
- The CMCs were installed to target depths based on either the torque readings or the interpreted base level of the soft soil layer.
    i. If the torque measurement was not sensitive, the CMC may have been installed deeper than required.
    ii. This depth was measured from not the tip of the auger, but approximately 0.5 m above the tip, and therefore the actual embedment depth may be deeper than the proposed by 0.5 m.

6   CONCLUSION

This paper discussed the design of CMC without the use of an LTP, and observations made during the installation of CMCs while the adjacent CMC was still wet. Relatively thick layers of working platform and embankment, 1.5 m and 3.0 m, respectively, were proposed, and assessments were carried out to confirm soil arching was achieved to transfer the majority of the embankment loads to CMCs without an LTP, for a CMC spacing of up to 5.0 × diameter. A range of CMC spacings and embedment depths were assessed using PLAXIS 2D axisymmetry model to determine the most cost-effective configuration, based on the imposed settlement criteria.

Trial CMC installation was carried out to ensure the wet-construction method was not detrimental to the performance of the CMCs. Minor heaving was observed, and the assessed remaining diameter was considered to be adequate. The monitored settlement was less than the estimated settlement, which may be attributed a few factors during both design and construction.

REFERENCES

BS 8006-1:2010. "Code of practice for strengthened/reinforced soils and other fills". British Standards Institution, UK.

Hewlett, W.J., and Randolph, M.A. (1988). "Analysis of Piled Embankments". Ground Engineering, 21 (3), 12-18.

Larisch, M. D., Kelly, R., and Muttuvel, T. (2015). "Chapter 21 – Improvement of Soft Soil Formations by Drilled Displacement Columns." in Indraratna, B., Chu, J., and Rujikiatkamjorn, C. eds., "Ground Improvement Case Histories." Butterworth-Heinemann, 573-622.

Muttuvel, T. and Wong, P. (2012). "Design of Semi-Rigid Inclusions for Bridge Approach Embankments." in Indraratna, B., Rujikiatkamjorn, C., and Vinod, J. S. eds., International Conference on Ground Improvement and Ground Control, Wollongong, Australia.

Wong, P. K., and Muttuvel, T. (2012). "Economic Design of Controlled Modulus Columns for Ground Improvement." In Narsilio, G., Arulrajah, A., and Kodikara, J. eds., 11th Australia New Zealand Conference on Geomechanics, Melbourne, Australia.

Yapage, N. N. S., Liyanapathirana, D. S., Leo, C. J., Poulos, H. G., and Kelly, R. B. (2013). "Towards the Development of a New Design Guideline for Geosynthetic Reinforced Column Supported Embankments". Australian Geomechanics, 48 (3), 35-50.

PROCEEDINGS OF THE 14TH ANZ YOUNG GEOTECHNICAL PROFESSIONALS CONFERENCE
14YGPC ROTORUA, NEW ZEALAND, 2ND – 5TH NOVEMBER 2022

61

Numerical Modelling of Tiered Retaining Walls

C. J. B. Wright[1], CMEngNZ

[1]Riley Consultants Limited, P.O. Box 100253, North Shore, Auckland, 0745; PH (64) 9 489 7872; email: cwright@riley.co.nz

ABSTRACT

Tiered retaining walls tend to be constructed on property boundaries to address planning requirements with respect to excavations on the boundary, and/or for aesthetics (e.g., improve sunlight, reduce mass, etc.), and may be constructed independently as adjacent sites are developed. The interaction between tiered cantilevered pole walls is not well researched. This paper summarises the finding of the author's masters research, which consisted of numerical analysis of tiered retaining walls using two finite element analysis software programmes, RocScience RS2 (finite element analysis software) and WALLAP (pseudo-finite element software). The numerical analysis was undertaken in three parts. Analysis of single retaining walls to establish baseline results, utilising both RS2 and WALLAP to calculate the internal forces (bending moments and shear forces) and associated deflections; analysis of the variation in internal forces and deflections with changes to the in-plane spacing between tiered retaining walls utilising RS2; and analysis of equivalent tiered walls loads using WALLAP. The results showed that the effective retained height of the lower wall approaches the combined retained height of the tiered retaining walls as the spacing between the walls approaches zero. This increase in the effective retained height can be detrimental to the stability of the walls, particularly in situations where the interaction has not been considered.

Keywords: tiered cantilever pole retaining walls, overlapping earth pressure wedges, numerical modelling.

1   INTRODUCTION

This paper summarises research into the interaction between closely spaced cantilever pole retaining walls with vertical offsets (tiered retaining walls). There is minimal guidance for the design of tiered retaining walls, and architects and civil/structural designers tend to overlook the potential interaction and associated loads in concept designs.

Tiered retaining walls are commonly used on boundaries to address planning requirements with respect to boundary excavations or constructed independently as adjacent sites are developed. The research reviewed relevant literature and undertook numerical analysis using two finite element analysis software programmes (RocScience RS2 and WALLAP), and assessed the interaction between tiered cantilever pole retaining walls.

2   BACKGROUND AND LITERATURE REVIEW

2.1   Types of Retaining Walls

Retaining walls are structural elements used to support ground that is either cut or filled. They tend to be linear structures that are assessed in terms of plain strain. Retaining walls are therefore visualised by an in-plane cross section through the wall, although some walls approach axisymmetric situations such as relatively localised excavations/shafts (Das, 2010). There are a range of different retaining wall types that are based on variations or combinations of the following three main types, gravity walls, cantilever walls, and tied-back/anchored walls (US Army Corps of Engineers, 1989).

Gravity retaining walls use the mass of the structural element to resist the overturning forces from the soil being supported (Das, 2010). Larger retained heights therefore require heavier walls to resist the applied forces. They transfer the lateral forces applied to the wall into vertical pressure and require the founding soil to have sufficient bearing capacity. Therefore, the bearing capacity of the founding soil can limit the retained height. Typical examples of gravity walls are gabion baskets walls, mass block walls, and crib walls.

Cantilever retaining walls are detailed to resist internal bending moments and shear forces and use soil mass to counteract the overturning forces applied (Derucher, et al., 1978). There are two main forms, pole walls and concrete cantilever walls. Pole retaining walls utilise closely spaced piles with or without rails to distribute the force between piles. The pile embedment is selected based on the soil mass required in front (downslope) of the wall to resist the forces behind (upslope) of the wall, and the pile dimensions are sized and detailed to resist the bending moments and shear forces generated by the lateral forces on the wall. Concrete cantilever walls (i.e., masonry block or tilt slab) utilise a shallow footing and transfer the lateral forces into bearing pressures similar to gravity walls. This method reduces the mass of the structural elements that are required for gravity walls systems. The stem (vertical member) and base of the wall are sized and detailed to resist the bending moment, and shear forces generated.

Anchored or tied-back walls use horizontal forces from anchors/reinforcement to resist some or all the pressure applied to the wall (Federal Highway Administration, 1999). They can take forms similar to either gravity or cantilever type walls, such as reinforced soil walls (mechanical stabilised earth wall or soil nailed walls), or pile walls with one of more rows of anchors (the anchors can be attached to deadmen, bulkheads, embedded piles, or a rod/tendon grout bonded into the soil/rock) (Federal Highway Administration, 1999). The anchor(s) provide support to the pile, stem or face of wall which reduces the maximum moment and the mass of soil required in front of the wall, and therefore can reduce the section size and embedment depth of the pile.

2.1 Tiered Retaining Walls

Tiered walls are defined in this paper as two or more walls that are parallel, or near parallel, with a vertical offset between the walls. These are also called terraced retaining walls, parallel retaining walls, or twin retaining walls (if a pair of walls).

There are some design manuals for gravity-type tiered walls that discuss replicating the influence by utilising a surcharge equivalent to the weight of soil supported by the wall (NCMA, 2010). However, there was negligible literature on tiered cantilever pole retaining walls with vertical offsets identified during the research. The available information tended to be planning documents produced by local territorial authorities (LTAs), which were generally associated with planning limitations. The LTA documents did not tend to reference how to design for these walls or discuss potential for proximate walls to influence each other.

Research into closely spaced retaining walls is generally limited to parallel walls without a vertical offset, such as walls utilised for silos, wharfs, jetties, docks, and cut off walls such as those discussed by Onsa (2015) and others. These walls benefit from the reduced spacing between the walls, and these walls tend to move away from each other, and the overlapping active pressure wedges effectively share and reduce the active earth pressures acting on each wall.

2.1 Lateral Pressures

The forces on cantilever pole retaining walls are the result of the combination of several lateral (horizontal or near horizontal) pressures applied to the back of the wall, and these forces can also be partly or wholly resisted by lateral pressures applied to the front of a wall. The main lateral pressures comprise earth pressures, surcharge pressure, water pressure, and seismic pressure (Derucher, et al., 1978).

Lateral earth pressures are typically expressed as a triangular pressure distribution and is related to the vertical stress at a given depth within the soil and rock, soil parameters, stress history of the soil, shear stresses applied to the soil, slope and wall geometry, and wall friction (Das, 2010; Rankine, 1857; and Coulomb 1776). The lateral earth pressure in ground proximate to retaining wall (upslope and downslope) are dependent on and described by the relative movement of the wall as either at-rest (for no movement of wall), active (with movement of wall away from the soil), or passive (with movement of wall towards soil) pressure. Active and passive wedges are inferred to develop above and below the wall. The detrimental effects of overlapping passive pressure wedges are discussed for closely spaced piles by Broms (1964a; 1964b) and anchors FHWA (1999) and others. However, discussion of overlapping active and passive pressure wedges (which likely occur with closely spaced tiered retaining walls) was not identified during the literature review and is considered by the author to be a critical factor in the interaction of tiered retaining walls.

Surcharge pressures tend to be applied for an "infinite" width behind the retaining wall and treated as a rectangular pressure block (opposed to triangular soil pressure) to simplify the analysis (NCMA, 2010; and Derucher, et al., 1978). Alternatively, the stress from surcharge loads can be specifically calculated based on work by Boussinesq (1883).

Water can develop various pressures on retaining walls, which include hydrostatic, seepage, hydrodynamic, ice, and swelling pressures (Bellezza, et al., 2009; Derucher, et al., 1978; and NCMA, 2010).

Seismic accelerations from earthquake events can result in horizontal and vertical accelerations of the soil and wall (gravity wall), and the associated inertial forces can destabilise retaining walls. For rigid gravity walls the inertial force related to the weight of the wall is considerable and should be considered alongside soil seismic loads. Whereas, cantilever pole retaining walls tend to have relatively minimal mass and the acceleration of the soil wedge will be critical for the loading on the wall.

3   METHODOLOGY

To assess the potential interaction between tiered cantilever pole retaining walls, numerical modelling was undertaken in three stages:

1. Single Retaining Wall Modelling using RS2 and WALLAP
2. Tiered Retaining Wall Modelling Using RS2
3. Approximate Tiered Retaining Wall Modelling using WALLAP (not discussed in this paper)

3.1 Single Retaining Wall Modelling

A range of single retaining wall models (base and sensitivity scenarios) were set up to establish the baseline results for pole retaining walls for a range of soil and wall parameters and retained heights (between 1m and 4m heights). This enabled interaction to be assessed for the tiered retaining wall modelling which undertaken in the later stages, and allowed for comparisons to be made between modelling software. The base case and associated parameters are presented in Figure 1 (lower wall only).

The sensitivity models were set up by varying a single parameter from the base case. The following ten parameters were adjusted from the base model for the sensitivity scenarios: embedment depth, soil friction angle, cohesion, Youngs Modulus of soil, surcharge, ground slope, groundwater depth, and bending stiffness (EI) of wall.

PROCEEDINGS OF THE 14TH ANZ YOUNG GEOTECHNICAL PROFESSIONALS CONFERENCE
14YGPC ROTORUA, NEW ZEALAND, 2ND – 5TH NOVEMBER 2022

63

The results of each software (RS2 vs WALLAP) and sensitivity cases (sensitivity vs base) were compared to establish a relative percentage difference for the maximum bending moments (BM), shear forces (SF), and deflections (Δ).

3.2 Tiered Retaining Wall Modelling

The tiered retaining wall models have been developed utilising the single wall base case parameters for a range of retained height and proximity combinations. A sketch of the tiered walls is presented in Figure 1. The base case parameters have been maintained from the single retaining wall analysis.
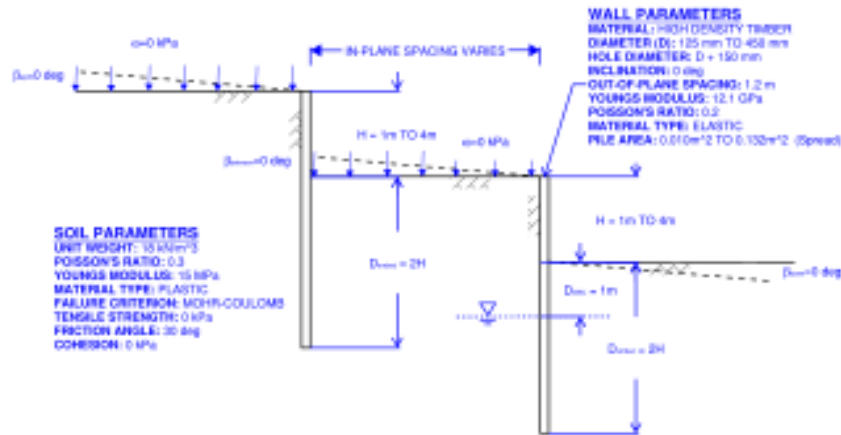
Figure 1: Tiered retaining wall base model and parameters

The retained height combinations have been developed based on 1 m retained height increments ranging between 1 m to 4 m. This enabled a six sets of various retaining wall combinations to be assessed. Each set was named based on the retained height of each wall (e.g., 2 m high upper wall and 3 m high lower wall was named 2-3).

Each set of retained height combinations has been modelled with six different in-plane spacings between the walls. The spacings range from remotely spaced (Model 1) to closely spaced (Model 6). The spacing between the walls are proportional to the retained height of the retaining walls being modelled. The in-plane retaining wall spacings for Models 1 to 6 are summarised below:

- **Model 1:** Developed so that lines projected at 45° and 60° from the bottom of each pole in the lower and upper wall (respectively) would touch (i.e., outside the influence if both walls were rotating about the base of the poles).
- **Model 2:** Developed as average spacing of Model 1 and Model 3
- **Model 3:** Developed so that an active wedge of the lower wall and a passive wedge of the upper wall, projected at 45° and 60° (respectively) from the retained height minus 0.5 m below the ground level at the toe would touch (i.e., rotation of each wall at the approximate depth of maximum moment).
- **Models 4, 5, 6:** Developed to be three-quarters, half, and quarter of the in-plane spacing of Model 3, respectively.

The results of each model were compared against the single wall and Model 1 results to establish a relative percentage difference for the maximum bending moments (BM), shear forces (SF), and deflections (Δ).

4 RESULTS

The maximum BM, SF, and Δ results for the single retaining wall base case has been presented in Figure 2, with 1%, 5% and 10% displacement of retained height for reference (dashed). The range of results for the lower walls has been presented based on the combined height for the tiered wall for comparison.

a) Maximum Bending Moment	b) Maximum Shear Force	c) Maximum Displacement
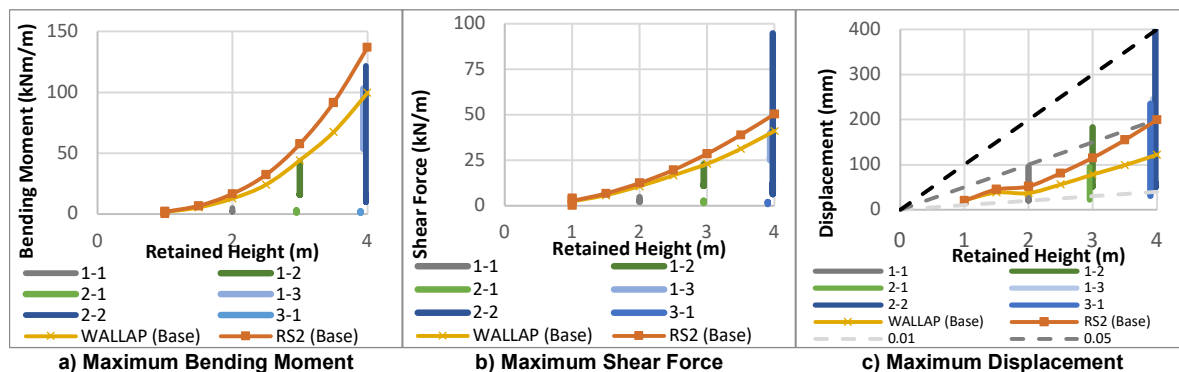
Figure 2: Comparison of Lower Wall results against the single wall baseline results for the lower tiered retaining wall

The selected total displacement outputs and variation of selected tiered wall model relative to Model 1 results have been presented below. The bending moment variations are presented on Figure 4, shear forces variations are presented on Figure 5, and displacement variations are presented on and Figure 6.

a) Model 1   **b) Model 3**   **c) Model 6**
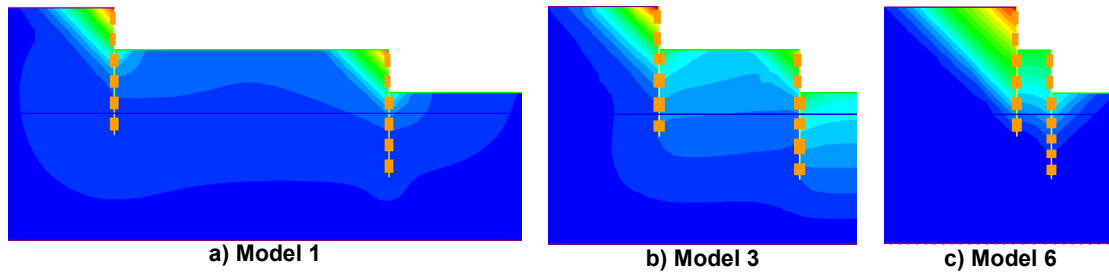
Figure 3: Selected RS2 total displacement outputs for Tiered Wall Scenario 2-2

a) **Consistent Lower Wall Height**   b) **Consistent Upper Wall Height**
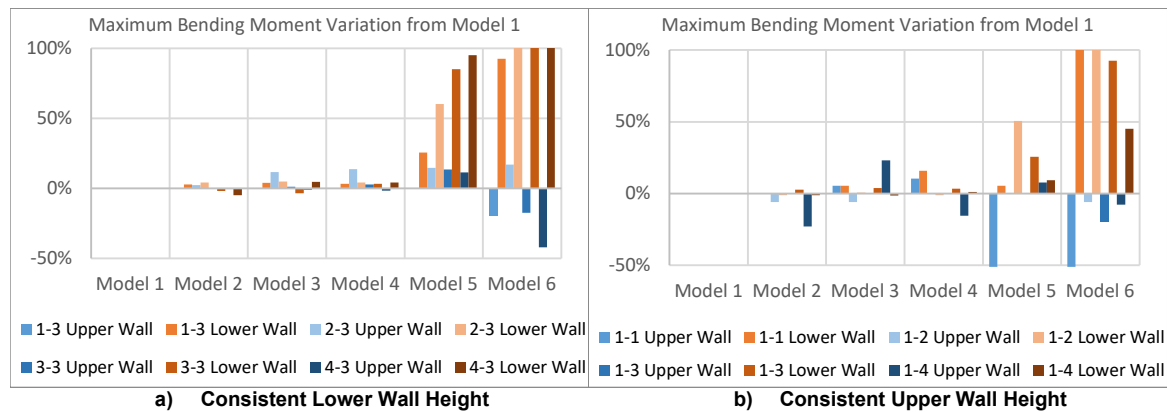
Figure 4: Selected tiered retaining wall bending moment variation relative to Model 1 with in-plane spacing

a) **Consistent Lower Wall Height**   b) **Consistent Upper Wall Height**
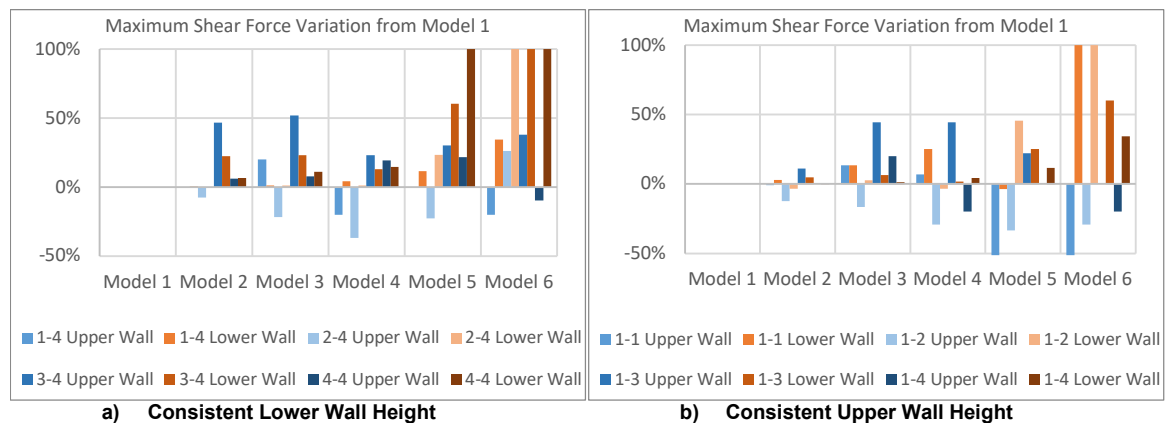
Figure 5: Selected tiered retaining wall shear force variation relative to Model 1 with in-plane spacing

a) **Consistent Lower Wall Height**   b) **Consistent Upper Wall Height**
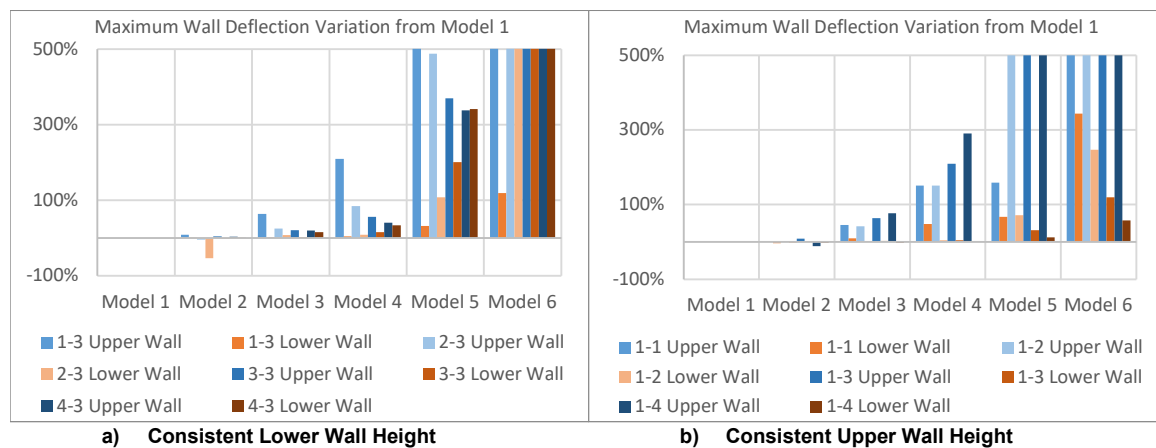
Figure 6: Selected tiered retaining wall displacement variation relative to Model 1 with in-plane spacing

PROCEEDINGS OF THE 14TH ANZ YOUNG GEOTECHNICAL PROFESSIONALS CONFERENCE
14YGPC ROTORUA, NEW ZEALAND, 2ND – 5TH NOVEMBER 2022

65

a) Upper Wall Displacement   **b) Lower Wall Displacement**
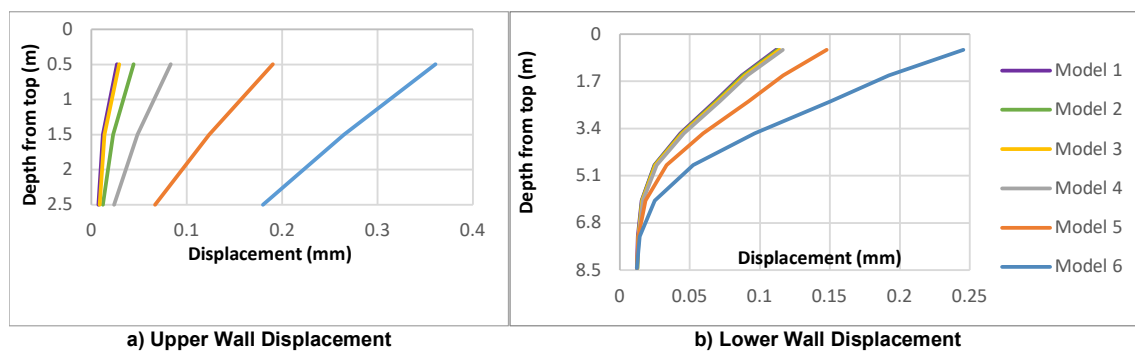
Figure 7: Deflection (Δ) results for Tiered Wall Scenario 1-3

5   DISCUSSION

5.1   Single Retaining Walls

The calculated BM, SF, and Δ results for the single wall modelling tended to be 22%, 15%, and 25% less respectively in WALLAP than RS2 (Figure 2). There was a similar trend for all of the sensitivity models (i.e., RS2 results were larger than WALLAP results), except for the models that included soil cohesion. The selection of the non-linear modulus (L_0) parameter in WALLAP appears to be the main parameter that results in the variation between the two software. Reduction to an L_0 to zero reversed the differences for BM and SF and resulted in the Δ calculated to be between 50% and 100% higher in WALLAP than RS2.

5.1   Tiered Retaining Walls

The graphical output from the modelling (Figure 3) showed most of the displacement of the soil occurred within apparent active and passive pressure wedges. These wedges approached in Models 1 to 3 and overlapped to varying degrees in Models 4 to 6. This overlap has resulted in additional load being transferred to the lower wall the displacement of the both walls. There was also slight displacement of the soil beyond these wedges, and this is attributed to the early displacement of the upper walls.

The overlap of lateral earth pressure wedges results in effective retained height of the lower wall approaching the combined height of both walls as in-plane spacing between the walls approaches zero. The embedment depth of each wall has been set as 2H for the height of the subject wall rather than the combined height of each wall, and embedment depths between 1H to 2H would be typical for independently developed walls. The increase of the effective retained height from the wall height to the combined height of the tiered walls results in a decrease of the ratio of embedment depth to retained height (from 2H). The corresponding deflection of closely spaced walls is excessive, which was also observed in the sensitivity results of the single wall with embedment depths between 0.5H and 1H.

There were also specific trends identified for the lower and upper retaining walls based on relative heights of each wall, which are discussed below.

5.1.1   Lower Retaining Wall

For a lower wall with a constant height, pile diameter, and embedment depth, the maximum BM (Figure 4a), SF (Figure 5a), and Δ (Figure 6a) of the lower wall tends to increase with an increase of the retained height of the upper wall. This is due to additional pressure from the upper wall which results in increased pole diameter and embedment depth requirements. An example is a comparison of Scenario 1-2 with 4-2, as the walls become more closely spaced, the retained height of the lower wall increases from 2 m to an effective (combined) retained height of 3 m for Scenario 1-2 and 6 m for Scenario 4-2. This leads to additional active pressure on the wall, which is observed by the increase of BM and SF. This also results in a decrease of the embedment ratio from 2H (for remotely spaced walls) to 1.33H (Scenario 1-2) and 0.67H (Scenario 4-2). The associated increase in Δ is related to both an insufficient embedment depth to generate resistance to overturning, and an insufficient pile diameter to limit the mechanical deflection of the wall. The deflections calculated would likely be detrimental to the stability of the walls and use of the land above the walls. Reducing the in-plane spacing between the wall should be compensated by an increase of the pile diameter and embedment depth of the lower wall to resist the increased forces, and the increase is dependent of the proximity of the walls and the combined retained height.

For an upper wall with constant height, the maximum BM (Figure 4b), SF (Figure 5b), and Δ (Figure 6b) for the lower wall tends to decrease with an increase of the retained height of the lower wall. An example is a comparison of Scenario 1-1 with 1-4. As the walls become more closely spaced, the retained height of the lower wall increases for Scenario 1-1 from 1 m to an effective (combined) retained height of 2 m (100% increase of H) and Scenario 4-1 from 4 m to 5 m (25% increase of H). Active pressures are positively related to height, so a smaller increase in H would typically result in a smaller proportional increase in BM and SF, as was observed. The proximity also results in a varied decrease of the embedment ratio from 2H (remotely spaced wall) to 1H (Scenario 1-1) and 1.6H (Scenario 1-4). The diminishing variation in Δ from the baseline with the increase of the lower wall height is suggested to be related to the decrease of the embedment depth ratio coupled with an increase in the pile diameter of the lower wall from 125 mm (Scenario 1-1) to 450 mm (Scenario 1-4).

5.1.2 Upper Retaining Wall

Unlike the lower wall, the trend for BM (Figure 4) and SF (Figure 5) for the upper wall relative to the baseline results is unclear. There is no variation of loading on the upper wall with the proximity of the walls, therefore, BM and SF increases are not expected. The variation observed is likely associated with variations in the deflection of the soil between the walls and associated lateral displacement (shorter upper walls) or bending (longer upper walls).

For a lower wall with a constant height (Figure 6a), the maximum Δ of the upper wall tends to decrease with an increase of the retained height of the upper wall. This is suggested to be due to the increase embedment depth (and pole diameter) of the upper wall which assists in minimising lateral displacement of shorter wall and the increase of bending stiffness as the pole diameter increases. Conversely, given the same height upper wall (Figure 6b), the Δ of the upper wall tends to increase with an increase of the retained height of the lower wall. This is suggested to be related to lateral displacement which is facilitated by increased displacement of the soil block between the walls and the lower wall, discussed above, the soil supporting the upper wall moves as the lower wall deflects and the total deflection of the wall increases with the increase in the combined retained height.

6   CONCLUSION

The baseline single wall models using RS2 and WALLAP identified slight to moderate differences in the calculation of internal forces and deflection of the wall, with RS2 generally calculating additional bending moments, shear forces and deflections than WALLAP. Nevertheless, the variation of the results for the analysis of eight sensitivity parameters relative to the baseline results was similar magnitude for each software, and resulted in variation of internal forces and deflection in agreement with the literature.

The modelling of cantilever pole tiered retaining walls showed that the internal forces (bending moment and shear forces) within the lower wall and associated deflections increased as the walls became more closely spaced, and the effective retained height of the lower wall approaches the combined height of both walls as in-plane spacing between the walls approaches zero. This is due to the transfer of load between the walls, and the variation of the relative depth of embedment and section capacity enabling larger the displacements (overturning and mechanical deflection).

There was no obvious trend with the internal forces for the upper wall, which is expected given there is no additional loading, and variations were dependent of the displacement of the soil between the walls and relative length of the wall, i.e., shorter upper walls were more likely to displace laterally. Deflection of the upper wall was shown to increase as the tiered walls became more closely spaced and as the soil supporting the wall displaced due to the additional loading and associated deflection of the lower wall.

The specific effects on each wall depend on the relative height and wall spacing, and should be assessed specifically when they are close enough for pressure wedges to overlap (i.e., Model 3 or closer). Displacement of the upper wall increasing initially and increases in internal loading increasing sharply with reduced proximity.

7   ACKNOWLEDGEMENTS

REFERENCES

Bellezza, I., Fentini, R., Fratalocchi, E. & Pasqualini, E., 2009. *Stability of waterfront retaining walls in seismic conditions.* Alexandria, 17th International Conference on Soil Mechanics and Geotechnical Engineering.

Boussinesq, J., 1883. *Application des Potentials a L'Equilibre et du Mouvement des Solides Elastiques.* Paris: Gauthier-Villars.

Broms, B. B., 1964a. Lateral resistance of piles in cohesive soils. *Journal of soil Mechanics and Foundation Engineering Division, ASCE,* Volume 90, pp. 27-63.

Broms, B. B., 1964b. Lateral resistance of piles in cohesionless soil. *Journal of Soil Mechanics and Foundation Engineering Division, ASCE,* Volume 90, pp. 123-156.

Coulomb, C. A., 1776. Essai sur une Application des Regles de Maximis et Minimis a quelques Problemes de Statique, relatifs a l' Architecture. *Mem. Roy. des Sciences,* Volume 3, p. 38.

Danish Geotechnical Institute, 1978. *Bulletin No. 32 - Code of Practice for Foundation Engineering,* Copenhagen: Geoteknisk Institut (Danish Geotechnical Institute).

Das, B. M., 2010. *Principals of Geotechnical Engineering.* 7th ed. Stamford(CT): Cengage Learning.

Derucher, K. N., Schelling, D. R. & Patel, V. B., 1978. Methods and Practice in Cantilever Retaining Wall Design. *Computers and Structures,* Volume 8, pp. 569-582.

Federal Highway Administration, 1999. *Geotechnical Engineering Circular No.4 Ground Anchors and Anchored Systems,* Washington: U.S. Department of Transportation.

Mononobe, N. & Matsuo, H., 1929. *On the determination of earth pressure during earthquakes.* s.l., Proc. World Engineering Conference, pp. 177-185.

NCMA, 2010. *Design Manual for Segmental Retaining Walls,* Herndon, VA: National Concrete Masonry Association.

Okabe, S., 1926. *General theory of earth pressure.* Tokyo, Japan, Japanese Society of Civil Engineers.

Onsa, E. H., 2015. Lateral Earth Pressure between two Parallel Rigid Retaining Walls. *Internatonal Journal of Scientific & Engineering Research,* 6(8), pp. 73-78.

Rankine, W. M. J., 1857. On Stability of Loose Earth. *Philosophic Transactions of Royal Society,* Issue Part I, pp. 9-27.

Sherif, M. A., Fang, Y. S. & Sherif, R. I., 1984. Ka and K0 Behind Rotating and Non-Yielding Walls. *Journal of Geotechnical Engineering, ASCE,* Volume 110, pp. 41-56.

US Army Corps of Engineers, 1989. *Engineering Design - Retaining and Flood Walls,* Washington: US Army Corps of Engineers.

PROCEEDINGS OF THE 14TH ANZ YOUNG GEOTECHNICAL PROFESSIONALS CONFERENCE
14YGPC ROTORUA, NEW ZEALAND, 2ND – 5TH NOVEMBER 2022

67

A Consideration of Compaction Pressures for Retaining Wall Design in a New Zealand Context

R. J. Reed[1], MEngNZ and Dr. M. Larisch[2], CPEng. CMEngNZ, CPEng. MIE Aust., RPEQ

[1]Jacobs New Zealand Ltd., 12-16 Nicholls Lane, Carlaw Park, Auckland, 1010, New Zealand; email: Ryan.Reed1@Jacobs.com
[2]Jacobs New Zealand Ltd., Level 8, 1 Grey Street, Wellington, 6011, New Zealand; email: Martin.Larisch@Jacobs.com

ABSTRACT

The permanent works design of retaining walls in New Zealand typically focusses on the assessment of seismic loading and its impact on the structure. This is also reflected in the emphasis of New Zealand design guidance on seismic engineering considerations for earth pressure loading of retaining walls. In contrast, there can often be an absence of detailed commentary on non-seismic aspects. Compaction pressures are one such phenomena that may dominate non-seismic loading. However, in the authors' experience, the underlying theory is often inconsistently applied by practitioners in New Zealand.

A literature review has been carried out, reviewing the theoretical derivation of compaction-induced lateral earth pressures on retaining walls. A summary is presented on the recommendations given by design standards and guidelines, and the application of these recommendation to typical construction in New Zealand. An opportunity for improved commentary from New Zealand specific guidance is identified and recommended.

Keywords: Retaining Walls*, Compaction Pressure, Lateral Earth Pressures

1 INTRODUCTION

Retaining walls are most easily classified as 'gravity', 'cantilever' and 'anchored' systems. Gravity systems typically involve rigid or stiff, inflexible elements, where the predominant direction of movement of the structure in yielding to soil pressure is translational (sliding). Cantilever systems often involve flexible wall elements, where the predominant direction of movement of the structure is rotational. The design of anchored systems is somewhat different and is not the focus of this paper.

Static earth pressures acting on retaining walls are primarily a function of the movement of the structure relative to the adjacent soil. Three primary states of static earth pressures are defined: active (relating to movement of the wall away from the soil), at-rest (no movement), and passive, (movement towards the soil). Where the wall is designed for no movement, it is described as 'rigid'. In contrast, if it is designed to permit deflections greater than ~0.5% of the retained height of the wall, it is described as 'flexible'. 'Stiff' walls are those designed for an intermediate degree of movement, typically in the order of 0.2% of the retained height of the wall (Wood and Elms, 1990).

Several classical theories were developed to determine the limiting values of the active and passive states. Coulomb (1776), Rankine (1857), and Caquot et al. (1948) are well-known examples. Defining these limiting active and passive pressure distributions is significant as, in either case, further movement would result in shear failure of the soil. In a limit equilibrium design, they are therefore intended to describe the maximum earth pressures that the wall could be expected to experience. The at-rest state differs meanwhile in that is does not have a limiting value; rather, it is an estimation of the pressure distribution when there is no relative movement between the soil and wall.

Since the 1930's testing has been undertaken on retaining walls with compacted backfill incorporated into their construction. These tests have consistently found that the measured lateral earth pressures can significantly exceed the limiting values of the classical theories (Coyle and Bartoskewitz, 1967; Ingold, 1979a; Duncan and Seed, 1986). These higher pressures remain until greater outward deflection of the wall occurs (Coyle and Bartoskewitz, 1967). Cohesive backfill has also been identified to present time dependent pressure distributions (Heidra-Cobo, 1986; Symons and Clayton, 1992).

Where that outward deflection is constrained, such as in the design for rigid or stiff walls, then the pressures to be resisted by the internal structure of the wall are higher than would otherwise be

calculated from classical theory. For flexible walls, where such outwards deflection isn't constrained, the magnitude of that deflection would instead be greater than otherwise anticipated. As such, careful consideration of the effects of compaction is warranted in retaining wall design.

2   COMPACTION EARTH PRESSURE THEORY

2.1   General

Compaction-induced earth pressure theory has developed as a means of describing the discrepancy between measured lateral pressure distribution and classical theory for retaining walls with compacted backfill. It has largely focused on the concept of such compaction being analogous to an over-consolidation of the backfill material. It is premised on the concept that the increased lateral stresses, developed from the compaction plant, remain elevated, in at least some proportion, after the compaction plant is removed. The theories are typically presented as a substitute to the classical pressure distributions, rather than as an excess pressure to be superimposed. A selection is discussed below.

2.1   Rowe (1954)

Rowe developed a modified at-rest earth pressure coefficient to be considered in the calculation of earth pressures acting on a rigid wall. This was based on experimental testing using a bi-directional shear box using granular fill. On the assumption that compaction should be considered as a transient surcharge pressure, Rowe noted negligible relaxation of stresses following removal of this surcharge. He therefore postulated that the full induced compaction pressures for rigid walls should be assumed to be retained following removal of the compaction plant.

2.2   Broms (1971)

Broms' assessment also focussed on the problem of rigid, smooth, vertical retaining walls. However, he applied the concept of a hysteretic stress path model in the derivation of an analytical solution. In this derivation, the soil was also assumed to be free draining and the backfill was assumed to have an at-rest pressure distribution prior to compaction. When the compaction plant acts on the backfill, it was assumed that the vertical stress was increased, following the elastic distribution with depth proposed by Boussinesq (1885). This was assumed to also bring a proportional increase in the lateral pressure distribution. Below a certain depth though, the soil stress remained unchanged, as the initial at-rest pressure distribution still governed.

After removal of the compaction plant, the vertical stress distribution largely returned to its initial values. The compaction induced plastic lateral strains in the soil though, leaving it over-consolidated. Broms proposed that the soil closest to the surface yields because of these high lateral stresses with removal of the compaction plant. He assumed that this reduced its lateral stress to a residual linear distribution, the slope of which was equal to the inverse of the at-rest earth pressure coefficient. Below a critical depth, this yielding was proposed not occur because the vertical confining pressures were greater. As such, below this critical depth, the soil retained its over-consolidated lateral stress distribution, and at a greater depth, still followed the initial at-rest pressure distribution.

On the expectation that the backfill was compacted in thin layers, he set out that the process described above was repeated. As the compaction effort was reapplied to the new backfill layer above, the vertical stress was predicted to again increase to the Boussinesq distribution; so too, a proportional increase in the lateral pressure. When the compaction plant was removed, only the soil closest to the new surface was assumed to yield to the residual linear distribution. This locked in the compaction pressures in the layers below as the backfill construction progressed up the wall. Simultaneously, with additional overburden placed through each subsequent layer, the at-rest earth pressure distribution that dominated at greater depth also followed the upwards migration of the backfill surface. Figure (1) describes the static lateral earth pressure distribution assumed to exist at the completion of this rigid wall construction.

2.3   Ingold (1979a; 1979b)

The analytical solution derived by Ingold (1979a) focussed on the problem of stiff, smooth, vertical walls with free draining backfill. Ingold largely followed the same methodology as that proposed by Broms

(1971), although he assumed that the initial stress distribution of the backfill followed that of an active state. Likewise, when the soil yielded following removal of the compaction plant, he assumed that the resulting residual pressure distribution was instead proportional to the inverse of the active earth pressure coefficient. Figure (1) also describes the static lateral earth pressure distribution assumed to exist at the completion of this stiff wall construction.
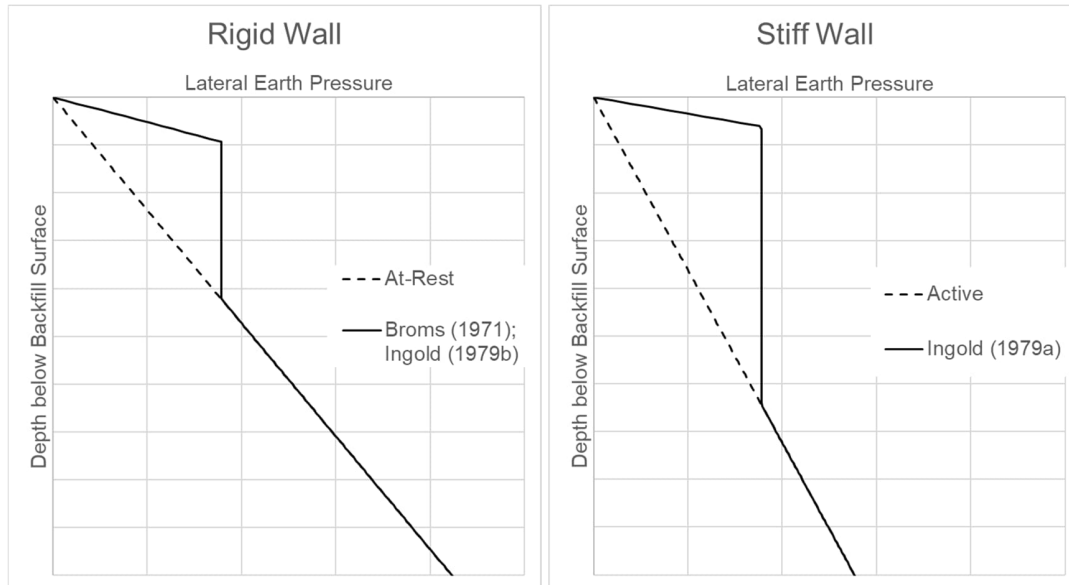
Figure 1. Lateral static earth pressure distribution with depth as proposed by Broms (1971) and Ingold (1979b) for rigid walls and by Ingold (1979a) for stiff walls.

Ingold (1979a) also presented a closed-form solution for this lateral pressure distribution with depth. To do so, he utilised an approximation for the compaction achieved by a dead-weight roller as originally proposed by Whiffen (1954). This assumed that the elastic stress distribution with depth during the compaction of a given layer was equivalent to that of an infinite line load. Whiffen (1954) found good agreement with this assumption from test results, even though the compaction plant itself was not infinite in length. Where vibratory rollers were utilised, Ingold (1979a) proposed that the uniform line load can be determined by "using an equivalent weight equal to the deadweight of the roller plus the centrifugal force induced by the roller vibrating mechanism." This followed earlier work by Forssblad (1965).

In a subsequent paper addressing the problem of rigid, smooth, vertical walls with free-draining backfill, Ingold (1979b) proposed that the closed-form solution presented in Ingold (1979a) could still be used, but where the active lateral earth pressure coefficient was substituted for the at-rest coefficient.

2.4 Duncan and Seed (1986), Duncan et al. (1991), and Clough and Duncan (1991)

Duncan and Seed (1986) further expanded on the hysteresis stress path by Broms (1971) for a rigid, smooth, vertical wall. Modifications included the consideration of cyclic loading and unloading of the soil elements for each compaction effort. The model continued to assume that this loading was described by at-rest lateral earth pressure but utilised a coefficient that was modified as the over-consolidation ratio of the soil element changed with compaction. Likewise, the reloading curve modified with ongoing compaction although was always bounded by a Mohr-Coulomb passive pressure failure criterion.

The model was also further expanded to consider the increase in horizontal stresses from a "transient, moving, surficial load of finite lateral extent" (Duncan and Seed, 1986). This contrasted with the uniform line load of infinite length assumed by Ingold (1979a; 1979b). Through following an iterative process that lends itself easiest to Finite Element Modelling (FEM), the compaction-induced pressure distribution over the height of the wall could be evaluated.

Duncan et al. (1991) utilised a software program to develop design charts for different construction plant following the method of Duncan and Seed (1986). The pressure distribution curves were nonlinear over the depth of backfill in which compaction pressures dominated. The charts included both cohesive and

cohesionless backfill, however, they noted caution regarding their adoption for cohesive material. Tables were also prepared to facilitate the modification of these pressure distributions for different variables.

Clough and Duncan (1991) stated that these charts should only be used for calculations when mechanical compaction equipment was anticipated within half the height of the wall, back from the wall. Likewise, they should only be applied to the design of vertical, rigid walls. For flexible walls, they noted that these pressures were likely to be conservative. Where movements as large as 0.4% were tolerable, they recommended that compaction-induced pressures be neglected for design.

2.5   Symons and Clayton (1992)

Symons and Clayton (1992) considered the application of existing compaction pressure theory on retaining walls with cohesive backfill. Utilising available test data, they concluded that the simplified methods of Ingold (1979a; 1979b) were in general inappropriate for cohesive material. This was due to the methods' fundamental assumption of free draining backfill. They did note though that the lateral pressure distributions after compaction of cohesive backfill were a function of the material's undrained shear strength. "Intermediate and high plasticity clay fills gave average horizontal total stresses on completion of filling of about 20% and 40% respectively of their undrained shear strengths" (Symons and Clayton, 1992). They also observed that reductions in this pressure distribution occurred with pauses in the backfilling operation because of stress relaxation.

Symons and Clayton (1992) also considered further the effect of time on these lateral earth pressures from cohesive backfill. In the case of rigid walls with intermediate plasticity backfill, these pressures were identified to reduce with time as the fill consolidated. The equilibrium distribution was concluded to be close to the at-rest state. Where swelling of cohesive backfill occurred, they recommended that the magnitude of these pressures must be determined experimentally. In the case of a rigid wall with high plasticity clay backfill, they noted that the equilibrium pressure distribution, following swelling, was close in magnitude to the limiting passive values. Lastly, they suggested that "problems due to swelling are likely to increase with the plasticity of the material" (Symons and Clayton, 1992).

3   DESIGN STANDARDS AND GUIDANCE

3.1   New Zealand

The primary compliance document for the design of structures in New Zealand, including retaining walls, is the New Zealand Building Code (MBIE, 2021a). It sets out that all buildings, building elements and sitework shall have a low probability of reaching an ultimate or serviceability limit state failure. The code requires that account shall be taken of all physical conditions that are likely to affect the design, including earth pressures (MBIE, 2021a). Compliance with this building code may be achieved through 'Acceptable Solutions', 'Verification Methods', or 'Alternative Solutions' although retaining wall design receives only brief coverage in Appendix C of Verification Method 4 (MBIE, 2021a). Hence, in demonstrating the compliance of retaining wall design, reference typically needs to be made to other design standards and guidance that discuss the topic of compaction pressures.

The authors are not aware of any New Zealand standards that specifically describe the determination of lateral earth pressures. However, recent design guidance is provided through the Earthquake Geotechnical Engineering Practice Module 6 (MBIE, 2021b) and the Bridge Manual (Waka Kotahi, 2022). The former specifically relates to earthquake resistant retaining wall design. Although it recommends consideration of surcharge loads in static design, no comment is made regarding compaction-induced pressures (MBIE, 2021b). The Bridge Manual does require the consideration of compaction earth pressures, although no specific prescription is made of how to determine them. However, a general reference is made to the Australian standard AS4678:2002 (Waka Kotahi, 2022).

An earlier New Zealand design guidance had commented on the use of compaction-induced earth pressures. The Works and Development Services Corporation (1990) recommended the adoption of the method of Broms (1971) and Ingold (1979a) for the calculation of compaction-induced earth pressures on rigid and stiff retaining walls respectively. The guide also made the distinction that "translations or rotations in the order of H/500, where H is the height of the wall, may reduce compaction-induced pressures to those of the active state." Hence "free standing relative flexible walls… on soil foundations

need only be designed for active pressures" (Works and Development Services Corporation, 1990). However, it also noted that due to the extent of wall displacement that occurs, a parabolic (rather than triangular) earth pressure distribution may result with a corresponding increase in bending moment of 50%. Nonetheless, the authors are not aware of continued widespread use of this guide in New Zealand.

3.2 International

Internationally, there are multiple standards and guidelines concerning the determination of lateral earth pressures for the design of retaining walls. AS4678-2002 Earth-Retaining Structures (Standards Australia, 2002), for example, includes a succinct commentary on the nature of compaction-induced earth pressures. The standard includes construction considerations such as the selection of compaction plant behind a retaining wall and recommends the method of Ingold (1979a; 1979b) for estimating these pressures for rigid and stiff walls. Likewise, the recommendations of the Hong Kong Geoguide 1 – Guide to retaining wall design (Government of the Hong Kong, 2000) are similar.

Eurocode 7 notes a requirement to consider the effects of compaction-induced earth pressures, although makes no mention of methods upon which this calculation should be based. Instead, it emphasises the specification of appropriate compaction procedures to avoid unacceptable movements (European Committee for Standardization, 2013). AASHTO recommends in the LRFD Bridge Design Specifications (2020) the use of the design charts prepared by Duncan et al. (1991) as presented in Clough and Duncan (1991).

4 APPLICATION TO NEW ZEALAND PRACTICE

Retaining walls in New Zealand commonly employ the use of compacted backfill in their construction. Generally, the backfill used is a well graded, cohesionless sandy gravel with back-of-wall drainage measures installed. An absence of detailed commentary from New Zealand standards and guidelines on compaction-induced earth pressures though means that practitioners require access to other design references. However, the international design standards and guidelines identified above are well-suited to this typical backfill construction.

In some regions of New Zealand access to such premium aggregates can be limited. There can instead be a desire to utilise more readily available, locally sourced finer grained backfill. Whilst this is unlikely to extend to high plasticity clays, the presence of an elevated fines content alone could introduce the potential for generating excess pore water pressures during construction. This desire may also increase in the coming years as carbon-reduction considerations grow in importance for civil engineering projects. A heightened awareness amongst practitioners of the consequences of such a decision is therefore required. In the authors' opinion, it is not immediately evident that the identified design standards and guidelines highlight these risks sufficiently.

Vibratory plates and rollers are common methods for the compaction of this backfill and hence have the potential to introduce significant lateral stresses and deflections into the constructed works. As noted by Forssblad (1965), the induced stresses from such vibratory plant are significantly greater than dead-weight plant. In the authors' experience, specification of limits to the proximity of these plant to these walls during construction is rare. So too, are recommendations to adopt smaller or non-vibratory plant in immediate proximity to the wall. The opportunity therefore exists to reduce the compaction-induced pressures requiring consideration through refinement of this construction practice. In such an absence, retaining wall designs in New Zealand should be considering the potential for use of large vibratory plant during construction.

For much of New Zealand, due to the presents of earthquake hazards, seismic considerations typically govern the design of moderate to high importance retaining walls. Nonetheless, to fully appreciate the consequences of seismicity on the structure, its condition under static loading also needs to be understood. Appropriate incorporation of the effect of compaction pressures is therefore necessary to ensure that the structure does not exceed its deflection tolerances or internal structural capacity when later subjected to the additional demands of seismic loading. This relationship does not appear to be strongly presented in the design standards and guidelines identified. Greater awareness amongst New Zealand practitioners of compaction-induced earth pressures is therefore recommended.

5   CONCLUSION

Testing over many decades has identified that the classical theories of lateral earth pressure often underestimate the measured values where backfill is placed and compacted behind retaining walls. Several models for this compaction-induced earth pressure have been developed by others. For rigid and stiff walls, where wall deflection is limited, the models present an increase in the stress distribution to be resisted by the structure. For flexible walls, where deflection is not constrained, the models present an increase in that deformation. It is evident from a review of existing literature that consideration of compaction-induced pressures can be critical in the static design of retaining walls. Where it isn't adequately considered in design, excessive deformation of the wall or internal structural failure may eventuate. This is also the case where the design is governed by seismic considerations, as the wall may be closer to its structural capacity or deflection tolerances, under static loading alone, than would otherwise be expected.

Commentary on the subject in current New Zealand standards and guidelines is limited and this should be addressed to promote consistency across the industry. Likewise, the recommendations of commonly used international design standards, such as AS4678:2002, are typically appropriate for the use of free draining backfill only. Whilst such a backfill is common for construction in New Zealand, there is limited guidance on compaction-induced pressures where cohesive backfill is selected. As such, there is a risk that these considerations are not fully understood by practitioners if they do compromise on backfill quality. This too should be addressed in updated New Zealand guidance. Furthermore, this updated guidance should promote opportunities to reduce these loads, such as through the specification of smaller non-vibratory compaction plant during construction in the immediate proximity of the wall.

REFERENCES

Boussinesq, J. (1885). "Applications of potentials to the study of equilibrium and motion of elastic solids." Gauthier–Villard, Paris, France

European Committee for Standardization. (2013). "Eurocode 7: Geotechnical design – Part 1: General rules."

Broms BB (1971). "Lateral pressure due to compaction of cohesionless soils." Proceedings of the 4th Conference on Soil Mechanics and Foundation Engineering, 373-384. Budapest, Hungary

Caquot, A., Kérisel, J., and Bec, M.A. (1948). "Tables for the calculation of passive pressure, active pressure and bearing capacity of foundations." Gauthier–Villard, Paris, France

Clough, G.W., Duncan, J.M. (1991). "Earth Pressures. In: Fang, HY. (eds) Foundation Engineering Handbook." Springer, Boston, MA, USA.

Coulomb C.A., (1776). "Essay on an application of the rules of maximis and minimis to some problems of statics relating to architecture." Memoires de l'Academie Royale pres Divers Savants, 7

Coyle, H.M. and Bartoskewitz, R.E. (1967). "Field Measurements of Lateral Earth Pressures and Movements on Retaining Walls." Engineering Practice 2nd Ed., 188-373. Wiley, New York, USA

Duncan, J.M., Seed, R.B. (1986). "Compaction-Induced Earth Pressures Under K0-Conditions." Journal of Geotechnical Engineering, 112 (1), 1-22

Duncan, J.M., Williams, G.W., Sehn, A.L., Seed, R.B. (1991). "Estimation Earth Pressures due to Compaction." Journal of Geotechnical Engineering, 117 (12)

Forssblad, L. (1965). "Investigations of soil compaction by vibration." Acta Polytechnica Scaninavica Ci, 34

Government of the Hong Kong. (2000). "Geoguide 1: Guide to Retaining Wall Design."

Hiedra-Cobo, J.C. (1986). "Lateral Pressures Induced by the Compaction of Clay against Rigid Retaining Structures (Thesis)." University of Surrey, UK

Ingold, T.S. (1979a). "The effects of compaction upon retaining walls." Géotechnique, 29 (3), 265-283.

Ingold, T.S. (1979b). "Lateral earth pressures on rigid bridge abutments." Journal of the Institute of Highway Engineering, 25 (12), 265-283.

Ingold, T.S. (1980). "Lateral earth pressures – a reconsideration." Ground Engineering, 39-43

Ministry of Business, Innovation and Employment [MBIE]. (2021a). "Acceptable Solutions and Verification Methods for New Zealand Building Code Clause B1 Structure: 1st Edition, Amendment 20."

MBIE. (2021b). "Earthquake Geotechnical Engineering Practice Module 6 - Earthquake resistant retaining wall design: Version 1."

Rankine, W. (1857). "On the stability of loose earth." Philosophical Transactions of the Royal Society of London, 147.

Rowe, P.W. (1954). "A Stress-Strain Theory for Cohesionless Soil with Applications to Earth Pressures at Rest and Moving Walls." Géotechnique, 4 (2), 70-88

Standards Australia. (2002). "AS4678 Earth-Retaining Structures."

Symons, I.F. and Clayton, C.R.I. (1992). "Earth pressures on backfilled retaining walls." Ground Engineering, 26-34

Waka Kotahi NZ Transport Agency. (2022). "Bridge Manual (SP/M/022): 3rd Edition, Amendment 4."

Whiffen, A.C. (1954). "The pressure generated in soil by compaction equipment." ASTM Symposium on the Dynamic Testing of Soil, 186-210

Wood, J.H. and Elms, D.G. (1990). "Seismic Design of Bridge Abutments and Retaining Walls." RRU Bulletin 84, Volume 2. Road Research Unit, Wellington, New Zealand

Works and Development Services Corporation. (1990). "Retaining Wall Design Notes (CDP702/D)."

PROCEEDINGS OF THE 14TH ANZ YOUNG GEOTECHNICAL PROFESSIONALS CONFERENCE
14YGPC ROTORUA, NEW ZEALAND, 2ND – 5TH NOVEMBER 2022

73

Undisturbed block sampling and its use in the investigation of very stiff to hard residual soils and extremely weathered rock

T. M. Youngberry[1]

[1]GHD, Level 9, 180 Lonsdale Street, Melbourne, VIC 3000; PH (617) 8687-8376; email: tom.youngberry@ghd.com

ABSTRACT

Undisturbed sampling of very stiff to hard residual soils and extremely weathered rock can be problematic due to difficulty in penetrating these materials and ensuing disturbance. Traditional methods for undisturbed sampling of very stiff to hard residual soils and extremely weathered rock are reviewed in this paper. Block sampling, while not commonly used, allows greater control over sampling and often leads to less disturbance and high-quality samples for testing. A method for taking undisturbed block samples is presented. This sampling method can be completed relatively cheaply with commonly available equipment and basic training. The size of the block sample allows a wide range of laboratory tests to be completed on material exhibiting similar properties and offers the possibility of better characterisation of the soil behaviour. The discussion presented herein includes the materials and equipment used, the time required for sampling and proposed safety measures.

Keywords: block sample, residual soil, undisturbed

1 INTRODUCTION

Very stiff to hard residual soils and extremely weathered rock (i.e. material with soil-like properties) are unique when compared with other soils in that they are formed in situ by weathering, rather than being transported. The weathering profile, degree of weathering and resulting soil properties is a function of parent geology, site geomorphology and climate, thus the behaviour of these materials is often difficult to predict (Hencher, 2012). They decompose from their parent rock through chemical, physical and biological processes to form structured, heterogenous materials which, along with their relatively high strength, makes sampling problematic. Additionally, gravel and weathered rock fragments in residual soils make them particularly difficult to penetrate.

Good geotechnical engineering design requires the collection of high-quality undisturbed soil samples for laboratory testing. However, many aspects of the sampling process, no matter how precise, alter the sample from its in situ condition - often referred to as disturbance. Relict structure in weakly bonded residual soils and extremely weathered rock makes them particularly susceptible to disturbance during sampling. Best practice requires that procedures be undertaken to mitigate disturbance during sampling, packaging and transporting and to obtain a sufficient number of representative undisturbed samples from each geological unit to enable characterisation of its physical properties. The latter point is particularly relevant when sampling relatively thin layers using drill holes.

Block sampling has been used historically (Brand 1985, USBR 1998), although much less frequently than other methods of undisturbed sampling. Its slow adoption as a conventional sampling method is partly due to the manual labour required to excavate samples in very stiff to hard residual soils and extremely weathered rock. The method described in this paper combines the use of hydraulic machinery, hand excavation and the use of readily available packaging materials making it both economic and viable in hard ground.

2 SAMPLE DISTURBANCE

Sample disturbance is often difficult to avoid and can occur at all stages in the sample life-cycle; i.e. during sampling, packaging, transportation, storage, laboratory preparation and testing. Clayton et al. (1995) classified four soil disturbance mechanisms: (1) changes in stress conditions, (2) mechanical deformation, (3) changes in water content and void ratio and (4) chemical changes arising from contact with drilling fluid and/or the sampler.

When a sample is exposed and removed from the ground it undergoes stress relaxation from in situ stresses to zero total stress through the removal of overburden material and horizontal confining stress.

This is not such an issue for saturated clay soils which can maintain sufficient matric suction to resist volumetric expansion. Residual soils however are often partially saturated and have relatively large voids, causing them to lose matric suction and expand when sampled, damaging the soil structure (Fookes, 1997).

Mechanical deformation refers to the rearrangement of soil particles within a soil structure. Mechanical deformation is most commonly caused by shear strains developing at the interface between the soil and the sampler. Shear strain during sampling is most prevalent in tube sampling, even if thin-walled samplers are used. Mechanical deformation can also occur from vibrations and shock during transportation, and from extrusion, saturation and consolidation procedures in the laboratory.

Changes in water content can occur during sampling, storage and laboratory preparation. Moisture changes during sampling is a problem in partially saturated residual soils, particularly when sampling using rotary core with a flushing medium. Chemical disturbance is not often considered in practice, especially since sample storage time is typically short. However, acid and alkali soils as well as saline pore water can react with sample packaging and change pore water chemistry. This can result in changes in the observed post-failure behaviour such as sensitivity (Clayton et al., 1995).

3 TRADITIONAL SAMPLING METHODS

3.1 Thin-walled tube sampling

Thin-walled tube sampling (a.k.a. Shelby tube or push tube) is used almost universally in site investigation as the principal method of obtaining undisturbed samples. Steel or stainless-steel tubes with an area ratio (defined as the ratio of the net projected area of the sampler and the projected area of sample core) < 10 % and a bevelled cutting edge are standard (Standards Australia, 2015). To collect a sample, the tube is pushed into the ground, typically from the base of a pre-drilled hole. In very soft to soft soils, piston tube samplers provide higher quality samples as they prevent water or loose soil from entering the tube when sampling, and the piston seal creates a vacuum preventing sample loss when retrieving. When retrieved, often only the lower end of the tube can be logged. Molten microcrystalline wax, mechanical seals, tightly fitting end caps or a combination of these methods are used to seal the tube against moisture loss. Tube sizes that are commonly used in site investigations are 50 mm, 63 mm and 75 mm diameter and collect samples up to 450 mm in length.

Although tube sampling is an appropriate method for sampling very soft to stiff transported cohesive soils, strains can still develop at the sample-tube interface. Computed tomography (CT) scans are being increasingly used to assess sample quality prior to testing (Pineda et al., 2016a). In residual soils, side shear strains are significant and can damage soil structure resulting in misrepresentation of in situ properties in the laboratory. Refusal of the tube is common in hard residual soils and extremely weathered rock due to the limited hydraulic push capacity of the drilling rig. This can lead to insufficient sample for testing. Gravel or weathered rock fragments in these materials can deform the tube cutting edge leading to mechanical disturbance and refusal.

3.2 Rotary coring

In rotary coring, a coring bit attached to the bottom of the core barrel cuts an annulus of material (kerf) while the central material remaining enters the core barrel as the coring bit advances. While the drilling bit rotates and advances, a flushing medium is pumped down the drill rods and out through holes in the drill bit to cool the bit and to flush out cuttings up the outside of the core barrel and rods. NQ3 size (45.1 mm core) is used as a minimum, although better recovery is experienced with PQ3 size (83.1 mm core) as there is less potential for erosion from drilling fluid. The larger core size also reduces the depth of moisture penetration into the sample.

Initially, single and double tube core barrels were used, however triple tube core barrels are now the method of choice due to their superior core recovery and better-quality samples. The triple tube configuration consists of an outer barrel, to which the drilling bit is attached, which rotates while the inner barrel containing a third liner remains stationary. The benefit of the triple tube system is that the inner barrel does not rotate with the drill rods and the flushing medium flows between the outer two barrels instead of between the sample and the inner barrel. The inner liner to the triple tube core barrel is typically a split steel liner, although cylindrical polycarbonate liners are used in softer materials.

PROCEEDINGS OF THE 14TH ANZ YOUNG GEOTECHNICAL PROFESSIONALS CONFERENCE
14YGPC ROTORUA, NEW ZEALAND, 2ND – 5TH NOVEMBER 2022

75

In very stiff to hard residual soils and extremely weathered rock, sample disturbance during coring can occur in many ways – principally by contact with the drilling fluid as the sample enters the inner barrels resulting in erosion or a change in moisture (Nicholls, 1990). The use of drilling foam as a flushing medium can be employed to reduce moisture changes (Fookes, 1997). In addition to contact with the drilling fluid, expansion of the sample can also occur as the inside diameter of the coring bit is slightly smaller than the inside diameter of the liner.

3.3 Specialist coring techniques

Numerous specialist coring techniques have been developed; one of which is the Mazier core barrel. The Mazier core barrel is a triple tube rotary coring apparatus with an inner retractor barrel and a heavy-duty cutting shoe that protrudes slightly beyond the end of the outer barrel. The amount of protrusion depends on the stiffness of the ground; further for soft soils and less in harder ground. Since the inner barrel protrudes beyond the cutting bit, the sample is protected from erosion by the flushing medium unlike conventional coring techniques. Sample recovery can be improved by using a foam flushing medium (Phillipson and Chipp, 1982). The advantage of this specialist coring technique is that samples of very stiff to hard ground and soft rock can be taken, where a conventional thin-walled tube would be damaged or refused. This specialist coring technique is useful for weathering profiles that decrease in weathering with depth. However, deposits with interbedded soft and hard layers such as metasedimentary formations can restrict the use of this method, as time-consuming alternating between conventional rotary coring techniques and Mazier sampling may be required (Haw and Seng, 1990).

3.4 Block sampling

Block sampling produces the highest quality samples of residual soils (Fookes, 1997). Block sampling (using the Sherbrooke sampler) has also been shown to produce the highest quality samples in soft clays due to less change to the micro and macrostructure when compared with samples taken using thin-walled tubes (Pineda et al., 2016b). The traditional block sampling method involves carefully carving a block of soil from an exposure or an excavation. Historically this has generally been completed using hand tools (USBR, 1998). Due to the effort required in taking a block sample, samples are usually taken when the material type and location are known, hence it is commonly completed as a supplementary activity to a site investigation program. Due to the size and near surface location of block samples (typically < 5 m depth) stress relaxation is typically far less than samples taken at depth from drill holes. As with all undisturbed samples, block samples are susceptible to moisture loss during and after sampling. Many techniques, including covering with wax and cheesecloth and packing with moist sawdust or damp sand have been proposed to minimise this problem (Fookes 1997, USBR 1998, Standards Australia 2015).

4 BLOCK SAMPLING METHODOLOGY

4.1 Overview

The following block sampling methodology is an effective technique to obtain high-quality undisturbed samples of very stiff to hard residual soils and extremely weathered rock. The block size enables multiple essentially similar samples to be cut from the block in a controlled laboratory environment and the selective nature of the sampling methodology enables relict features to be targeted or avoided. This method uses a combination of hydraulic machinery and hand digging, thereby minimising time and cost. Once excavated, the block sample must be carefully packaged to retain moisture and protect it from shocks and impacts during transport. While the method detailed below is for sampling from a test pit, it could easily be modified for sampling from an exposure or the floor of a larger excavation.

4.2 Materials and Equipment

Sampling materials and equipment are listed in Table 1. A schematic of the box showing materials and indicative dimensions is provided in Figure 1.

4.3 Procedure

The first step is to select an appropriate sample location. This requires an understanding of the site geology and is best undertaken once preliminary investigations have been completed and there is an

understanding of which materials require sampling and physical characterisation. Prior to commencing the block sampling, the packaging box should be partially assembled by securing the four sides together and fastening the handles. The pilot holes for the top and bottom lids should be drilled and countersunk along with the holes in each lid which are used to release excess expanding foam.

To begin, the excavator progressively removes material by scraping away thin layers with the excavator bucket. Once the target material is exposed, the engineer should inspect the material and select the location where the block sample will be taken. This can be done by entering the excavation but only after appropriate safety measures are in place. Finding suitable material to sample may require a large surface area to be exposed due to variable composition and weathering, the presence of core stones or relict discontinuities. Once the approximate location has been identified, the excavator then cuts two slots leaving a pillar approximately 600 mm wide and 600 mm high (Figure 2a). The pillar from which the block will be taken is then closely inspected for features that may require sampling (relict joints) or those that need to be avoided from the perspective of laboratory testing (rock fragments or gravel). In some instances, it may be necessary to cut deeper slots or move to the side and excavate a new slot.

Once the sample location has been selected, the remainder of the excavation is completed using hand digging tools. Two cuts are made in the pillar, leaving a column of material approximately 600 mm square. Material is progressively removed from the top and sides so that a column 300 mm square and approximately 450 mm high begins to take form (Figure 2b). This part of the exercise can be challenging when sampling gravelly or blocky materials so care should be taken not to over excavate. While cutting the sample, it is important to work quickly to reduce moisture loss. If possible, the block should be shaded from direct sunlight. The block should be carved so that there is approximately 15 mm between the block and the box on all sides – test the fit by sliding the partially assembled box over the block. Once sized correctly, the block should be logged and photographed from all sides before wrapping. Small disturbed samples of trimmings should be kept for initial moisture content and index testing.

Table 1: *Block sampling materials and equipment list (materials for 1 box)*

Item	Qty	Item	Qty
Formply 15 to 18 mm thickness (m²)	0.7	Cling wrap (450 mm roll)	1
Cordless drill	1	Aluminium foil (450 mm roll)	1
Countersinking bit	1	Expanding polyurethane foam (can)	2
Pilot hole drill bit (1.6 mm)	1	Paint scraper	2
Driver bit	1	Shovel	1
Auger drill bit (8 mm)	1	Fencing bar	1
Timber screws (8G x 50 mm)	28	Excavator / backhoe	1
Heavy duty box handles (with screws)	2		
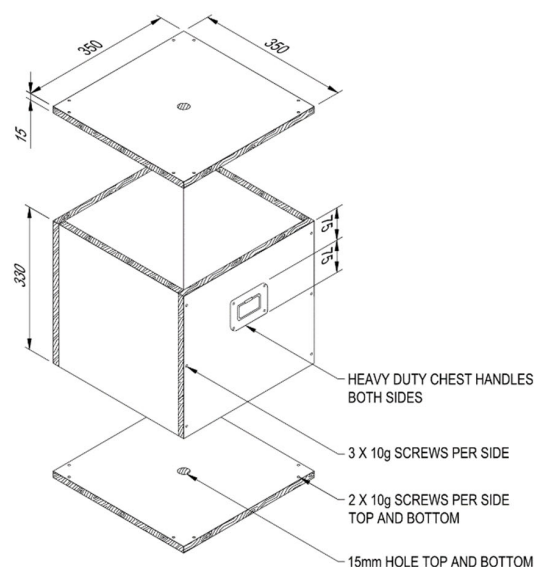
Figure 1: *Block sample box (dimensions are indicative only and could be modified to suit site conditions or materials)*

PROCEEDINGS OF THE 14TH ANZ YOUNG GEOTECHNICAL PROFESSIONALS CONFERENCE
14YGPC ROTORUA, NEW ZEALAND, 2ND – 5TH NOVEMBER 2022

77

(a)   (b)

Figure 2:   An excavated pillar (a) and a carved block (b)

The top and sides of the block are then carefully wrapped with alternating layers of cling wrap and aluminium foil. It is good practice to use three to four layers of each to protect against moisture loss through tear holes in the film or foil. The top of the block should be draped first before wrapping the sides to 'lock in' the top film and foil. When the block is sufficiently wrapped, the box is placed around the block. Loose soil is placed around the base of the box to elevate the top of the box approximately 15 mm above the sample (Figure 3a). The orientation of the box is marked on the sides. Polyurethane foam is then injected between the block and the sides of the box in accordance with the manufacturer's instructions. The top of the block is sprayed with foam before quickly securing the lid. Slight pressure should be applied to the lid of the box to avoid the box being lifted by the expanding foam while letting excess foam out of the release hole in the lid.

When the foam has set – something that may be affected by low temperatures, the block is very carefully undercut at its base and inverted. This step requires at least two people to ensure the block remains intact and it is not mishandled while inverting. Excess material at the base of the block is carefully removed to form a neat, flat base approximately 15mm below the top of the timber. The base is then wrapped with a similar alternate layering of cling film and aluminium foil, taking care to tie in the wrapping at the sides as much as possible. Any remaining gaps in the expanding foam can be filled from the base before spraying the wrapped base itself, quickly securing the bottom lid and, once the foam has set, restoring the block the right way up. The box should be labelled with relevant information. The block is now ready for transport (preferably on a pallet) together with the disturbed samples of trimmed material.

(a)   (b)

Figure 3:   Partially wrapped block prior to spraying foam (a) and the base of a block prior to final wrapping (b)

4.4   Safety

A risk assessment should be undertaken prior to commencing the block sampling and appropriate control measures implemented to manage any hazards. Typical hazards that need to be managed and controls are listed in Table 2.

Table 2:   Typical hazards and control measures

Hazard	Control
Engulfment	Excavations deeper than 1.5 m to be benched
Unsafe egress from excavation	Gently slope or step one side of the excavation to provide access
Working at heights	Barricade excavations deeper than 1.8 m
Heavy objects	Perform two-person lifts for heavy items, e.g. packaged blocks
Chemicals (polyurethane foam)	Follow instructions on the Material Safety Data Sheet (MSDS)
Manual excavation	Personal Protective Equipment (PPE) including gloves, safety glasses etc.
Working around heavy machinery	Establish exclusion zones, positive communication between operator and workers

4.5   Sampling Duration

The time taken to recover an undisturbed block sample depends on the depth of the sample, the difficulty in selecting a suitable block location and the difficulty in trimming a block. Provided the excavator is not required to create a bench to achieve the desired sampling depth, sampling takes between 2 and 4 hours. When scheduling an investigation program, a sampling rate of 2 blocks per day is a good estimate. The minimum number of workers required is 2; a machine operator and an engineer or engineering geologist. However, it is preferable to have 2 additional labourers to assist with hand digging and handling the box.

5   CONCLUSION

Traditional undisturbed sampling methods are reviewed and a current undisturbed block sampling method for very stiff to hard residual soils and extremely weathered rock is presented in this paper. Drawing on work by others on soft clays, the block sampling method presented has the potential to produce samples that exhibit less disturbance than other methods of undisturbed sampling in these materials. The block sample can be specifically selected by the geotechnical engineer or engineering geologist to be either representative of the bulk properties of the material under investigation or specific features. The size of the undisturbed block sample also allows sub-samples that are essentially similar to be taken for laboratory testing in a controlled laboratory environment. The undisturbed block sampling methodology presented in this paper minimises the labour-intensive methods of block sampling that have been used historically. In addition, the use of commonly available materials makes block sampling in hard ground both efficient and cost effective. While no sampling method eliminates sample disturbance entirely, if all steps involved are carried out with due care the highest quality undisturbed samples can be collected, enabling the first steps to be taken towards good engineering design.

6   ACKNOWLEDGEMENTS

REFERENCES

Brand, E. W. (1985). "Predicting the performance of residual soil slopes." 11th International Conference on Soil Mechanics and Foundation Engineering, San Francisco, 5: 2541-2578

Clayton, C. R., Matthews, M. C., and Simons, N. E. (1995). "Site Investigation." 2nd ed. Wiley-Blackwell, 592 pp.

Fookes, P. G. (1997). "Tropical Residual Soils: A Geological Society Engineering Group Working Party Revised Report." London: Geological Society, 184 pp.

Haw, C. C. and Seng, L. K. (1990). "Sampling with the Mazier core barrel." Proceedings of the Seminar on Geotechnical Aspects of the North-South Expressway, Kuala Lumpur, 31-35

Hencher, S. (2012). "Practical Engineering Geology." Spon Press, 464 pp.

Nicholls, R. A. (1990). "Sampling techniques in soft ground and residual soils." Proceedings of the Seminar on Geotechnical Aspects of the North-South Expressway, Kuala Lumpur, 1-7

Phillipson, H. B. and Chipp, P. N. (1982). "Air foam sampling of residual soils in Hong Kong. Proceedings of the ASCE Specialty Conference on Engineering and Construction in Tropical and Residual Soils, Honolulu, 339-356.

Pineda, J. A., Suwal, L. P., Kelly, R. B., Bates, L., Sloan, S. W. (2016a). "Characterisation of Ballina clay." Géotechnique 66, No. 7, 556-577

Pineda. J. A., Liu, X. F., Sloan, S. W. (2016b). "Effects of tube sampling in soft clay: a microstructural insight." Géotechnique 66, No. 12, 969-983

Standards Australia (2015). "Methods of testing soils for engineering purposes, Method 1.3.1: Sampling and preparation of soils-Undisturbed samples-Standard method." AS 1289.1.3.1:2015, viewed 16 December 2019, retrieved from SAI Global database.

USBR (1998). "Earth Manual." 3rd ed. Department of the Interior Bureau of Reclamation, 329 pp.

PROCEEDINGS OF THE 14TH ANZ YOUNG GEOTECHNICAL PROFESSIONALS CONFERENCE
14YGPC ROTORUA, NEW ZEALAND, 2ND – 5TH NOVEMBER 2022

79

GEOTECHNICAL ASSESSMENT OF PLEISTOCENE SOILS OF THE MULGRAVE RIVER DELTA, NORTH QUEENSLAND

C. Vincent and N. Murphy[1]

[1]WSP Golder, 900 Ann Street, Fortitude Valley, Queensland, Australia.

ABSTRACT

The Mulgrave River Delta is a Quaternary age fluvial system in tropical North Queensland. The near-surface geology of the area comprises the Quaternary age (Pleistocene to Holocene age) Mulgrave River Delta soils. The soils accumulated to form deep infill of a distinct valley that is tens of metres deep. Geotechnical borehole, cone penetration test (CPTu) and geotechnical laboratory testing data were collected for use in geotechnical design strength assessment for displacement (driven) piles design for structures associated with the Edmonton to Gordonvale (E2G) Bruce Highway upgrade project, south of Cairns. This study focuses on the Pine Creek Yarrabah Road (PCYR) overpass bridge specifically. It is planned for the bridge abutments and piers to be supported on driven precast pre-stressed concrete (PSC) piles. As part of the site investigation twelve boreholes were drilled enabling standard penetration testing (SPT) and sampling. The SPT data identified a lower strength layer at depth. This was considered to be inconsistent with the initially anticipated geology, where increasingly stiff to hard cohesive soils had been expected. Supplementary geotechnical investigations were completed, including cone penetration tests (CPTu) and additional laboratory testing was scheduled on 'undisturbed' tube samples (U_{50}). The aim was to assess implications (if any) of the identified lower strength layer on the design of PSC piles. Comparison of the field investigation and laboratory test data enabled greater confidence in the prediction of the soil strength profile and helped towards an optimised design for the PSC piles. To assist with the verification of geotechnical design strength, PDA testing (pile driving analyser – dynamic load testing) was completed during the driving of piles with CAPWAP analysis to help with confirming a prediction of shaft friction of the piles.

Keywords: Mulgrave River Delta, cohesive soils, undrained shear strength, shaft friction

1   INTRODUCTION

The Edmonton to Gordonvale (E2G) project will upgrade a 10.5 km section of the Bruce Highway between Gordonvale and Edmonton (south of Cairns) from a two-lane highway to a four-lane duplicated highway. The project will deliver significant safety improvements in this corridor which include signalised intersection and road upgrades, construction of overpasses (for vehicles and pedestrians), realignment of the Queensland Rail corridor, various cane rail relocations and construction of a separate cycle way adjacent to the new highway alignment.

The Maitland Road section of the E2G alignment (near Gordonvale) includes two new overpasses. The Pine Creek Yarrabah Road (PCYR) – North Coast Line (NCL) rail overpass is proposed over the existing rail alignment east of the Bruce Highway and the Pine Creek Yarrabah Road (PCYR) – Bruce Highway road overpass is proposed over the Bruce Highway. Both proposed bridges are located approximately 400 m south of the existing Maitland Road. This case study will focus on the PCYR road overpass which includes driven precast pre-stressed concrete (PSC) piles at the abutment and piers.

The site investigation included boreholes drilled at the piers and abutments where a thick layer of alluvium (up to 35 m) was identified overlying a layer of basalt at approximately 36 m depth. Between approximately 20 m to 26 m depth, standard penetration test (SPT) data identified a lower strength layer which was considered inconsistent with the anticipated geology.

Additional geotechnical investigations, comprising CPTs, were completed to help understand the impact (if any) of this perceived low strength layer on the proposed design of the PSC piles. During the pile driving, verification testing using PDA was used along with CAPWAP analysis to help confirm if the design geotechnical capacity was achieved. This case study details the findings of the geotechnical investigations carried out for the PCYR road overpass and the analysis of the data to create a design undrained shear strength model for driven PSC piles.

2   GEOLOGICAL SETTING AND STRATIGRAPHY

Reference to the published geological mapping (1:100,000 series Geological Map for Cairns Innisfail, by Queensland Government Department of Mines and Energy, 1989), indicates that the E2G corridor traverses a Quaternary age (Pleistocene overlain by Holocene age) alluvial flood plain, underlain at depth by the Hodgkinson Formation bedrock. The entire area represents a former delta of the Mulgrave River, where the Mulgrave River Delta soils represent deep infill of a down-cut gorge/valley that is tens of metres deep. The delta formed within the north to south oriented valley that is parallel to the coast, lying behind the coastal (former island) Malbon Thompson Range hills. The valley opens out both to the north and south, at the Trinity Inlet and the Mulgrave River respectively.

The alluvium is anticipated to be substantially deep. It formed as a series of prograding alluvial fans derived from the mainland during the Pleistocene period. Deltaic alluvial soils may comprise a series of coarsening upward sequences, where the higher energy (proximal to the source) deposits spilled forward over previously deposited finer grained (distal) deposits, that can also be conjectured to dominate towards the east, north and south. Periodic falls in relative sea level during the later Pleistocene and Holocene periods may have caused erosional downcutting into 'older' alluvium, only for these downcut valleys to become filled with lesser consolidated soils as the sea levels re-bounded.

During the later Pleistocene period, crustal extension enabled episodic eruptions of basaltic lava, today represented by Green Hill (the Meringa Basalt) that rises within the otherwise broad alluvial valley near Gordonvale. It is probable that the Meringa Basalt could overly older Pleistocene alluvium and potentially a cover of hillslope derived colluvium at the margins of the Mulgrave River valley corridor.

The surrounding and underlying geology is underlain by the Devonian age Hodgkinson Formation. The Hodgkinson Formation is dominated by folded and cleaved partly metamorphosed sediments and interspersed granite bodies. The bedrock surface was potentially eroded (scoured) during episodes of low relative sea level, such that a relatively thin (or absent) bedrock weathered profile may be anticipated under the alluvial deposits (W. F. Willmott, P. J. Stephenson, 1989).

2.1   Site Geology

The site geology (based on geotechnical investigation data) at PCYR road overpass typically comprises fine grained alluvial soils with beds of sand and gravel, underlain by a thin basalt (Meringa Basalt) flow (2.8 m to 4.1 m thick) at approximately 36 m depth (Golder Associates, 2020). Atterberg Limits test data and site observations (including SPT N values) indicate a layer of silt (typically 60-85% fines content) between approximately RL 1 m AHD and RL -6 m AHD. The inferred stratigraphy is illustrated in Figure 1.
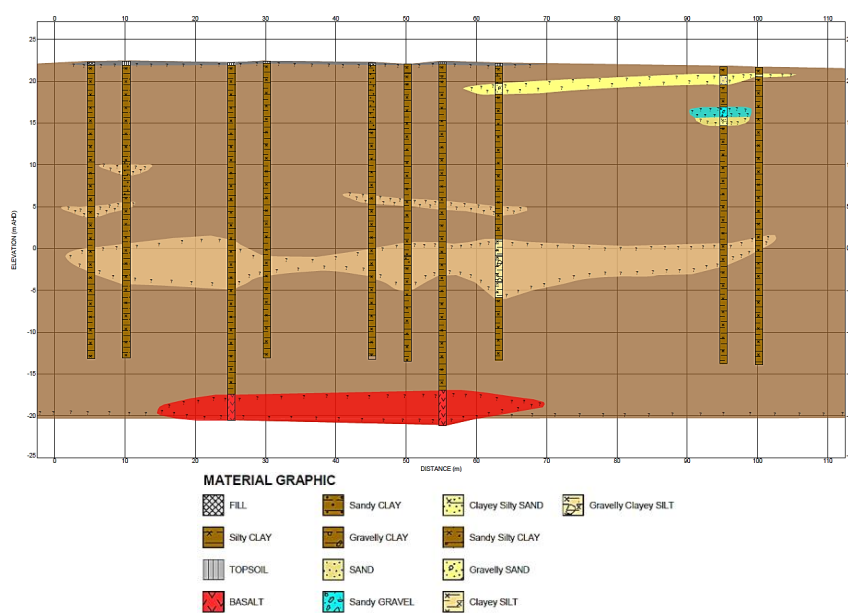
Figure 1: PCYR Road Overpass Inferred Stratigraphy

PROCEEDINGS OF THE 14TH ANZ YOUNG GEOTECHNICAL PROFESSIONALS CONFERENCE
14YGPC ROTORUA, NEW ZEALAND, 2ND – 5TH NOVEMBER 2022

81

3   GEOTECHNICAL SITE INVESTIGATION DATA

3.1   In-situ Testing (SPT and Vane Data)

The site investigation prior to and during the detailed design at the PCYR road overpass included borehole drilling and laboratory testing on disturbed and undisturbed soil samples (Golder Associates, 2020). SPTs were performed at 1 m intervals (commencing at 1 m depth) in all boreholes. Field SPT N values were corrected to N_{60} values to account for hammer efficiencies and equipment variables. The results are shown in Figure 2 below. Between about RL 1 m AHD and RL -6 m AHD, a layer of low SPT N values is evident (values as low as 0).
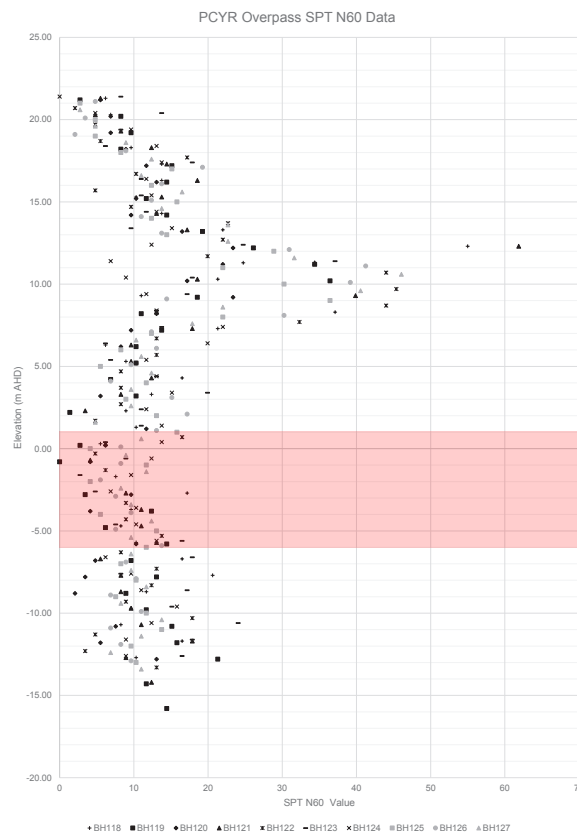
Figure 2: SPT N_{60} Data at PCYR Overpass

The SPT N_{60} values were used to estimate undrained shear strength values using a correlation factor of 7 ($s_u \approx 7 \times N_{60}$). Results are displayed in Figure 4 and where the inferred silt layer is present (between RL 1 m AHD and RL -6 m AHD), N_{60} values indicated the undrained shear strength varies from 25 kPa to 100 kPa (soft to firm).

In some undisturbed tube samples collected during the borehole investigation, vane shear tests were completed. These results indicated undrained shear strength values ranged between 40 kPa and 80 kPa (corrected for plasticity using the correction factor from Bjerrum, 1973) between RL 1 m AHD and RL -6 m AHD. Due to the low N_{60} values encountered within this layer, additional field investigation was completed comprising a CPT at the proposed abutment location (Golder Associates, 2020), discussed in Section 3.3 below.

3.2   Laboratory Test Data (Atterberg Limit, Particle Size Distribution and Triaxial Compression Test Data)

Atterberg Limit and Particle Size Distribution (PSD) tests were completed during the site investigation prior to the detailed design at the PCYR road overpass (Golder Associates, 2020). PSD and Atterberg Limit test results completed on samples collected between RL 1 m AHD to RL -6 m AHD are presented in Figure 3. Results indicate the soil at this elevation is predominantly low to high plasticity silt.
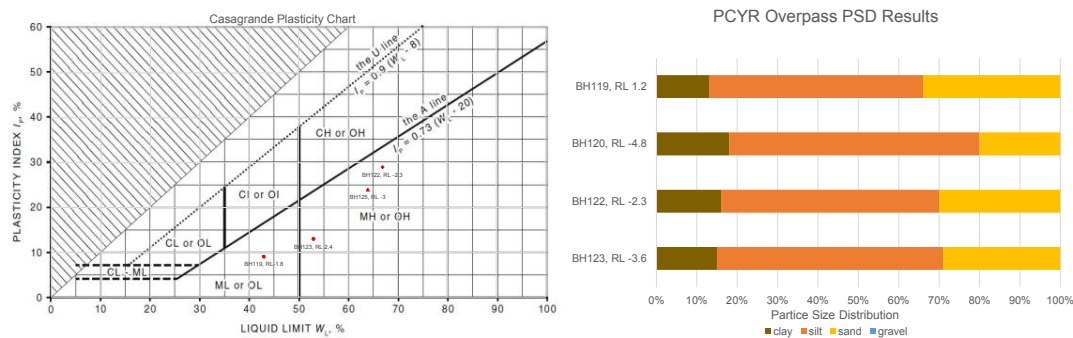
Figure 3: Atterberg Limit and PSD Test Data PCYR Road Overpass

Laboratory testing undertaken on undisturbed tube samples collected within the boreholes included single stage and multi-stage triaxial compression testing. The undrained shear strength at the select test locations (inferred from the test results) varied between 114 kPa and 398 kPa. The samples from BH120 to BH125 indicate the undrained shear strength of the soil between RL 1 m AHD and RL -6 m AHD is very stiff to hard. The triaxial test results are plotted in Figure 4.

3.3 CPT Data

Undrained shear strength was calculated from the CPT data using corrected cone resistance (q_t) and a N_{kt} factor of 15. The undrained shear strength inferred from in-situ test results (i.e. CPT data, SPT data, vane shear and pocket penetrometer tests) and from laboratory tests (i.e. triaxial tests) are presented in Figure 4. The CPT results correlate with the results from the triaxial compression tests and vane shear tests and indicate the soil strength between RL 1 m AHD and RL -6 m AHD varies from 50 to >200 kPa (stiff to hard). Note that CPT201 was pre-drilled from RL 15 m AHD to RL 5 m AHD (refer to Figure 4).

Figure 4: Undrained Shear Strength Data at PCYR Road Overpass

PROCEEDINGS OF THE 14TH ANZ YOUNG GEOTECHNICAL PROFESSIONALS CONFERENCE
14YGPC ROTORUA, NEW ZEALAND, 2ND – 5TH NOVEMBER 2022

83

4   DESIGN OF DRIVEN PSC PILES

Between RL 1 m AHD and RL -6 m AHD the results from CPT201 indicate the undrained shear strength varies from 50 kPa to > 200 kPa whereas the N_{60} results indicate the undrained soil strength ranges from <25 kPa to 100 kPa (soft to stiff). Triaxial compression test results correlated with the CPT results and indicates the soil is stiff to hard at this elevation. The low SPT values could have been caused by realignment of the soil structure due to repetitive shearing by the SPT hammer and appear to correlate with the zone of high silt content (illustrated in Figure 1). The design shear strength profile adopted for the piles at PCYR road overpass was estimated using CPT and triaxial compression test data. Design shaft friction was then developed using the adopted design shear strength profile and adhesion factors from Tomlinson and Woodward (2008). Table 1 below presents the adopted design parameters for alluvial cohesive soils at PCYR road overpass. The Unit 1B parameters were adopted within the silt layer between RL 1 m AHD and RL -6 m AHD.

Table1: Adopted Design Parameters

Unit	Unit General Description	γ_b (kN/m^2)	c_u (kPa)	f_s (kPa)*
1B	Stiff	19.0	80	40
1C	Very Stiff to Hard	19.5	140	80
1D	Hard	20.0	250	125

Note: * - f_s calculated based on adhesion factors from Tomlinson and Woodward (2008)

5   DESIGN SOIL STRENGTH PROFILE VERIFICATION

Verification testing using PDA was completed during the driving of piles with CAPWAP analysis to analyse the achieved shaft friction at Pier 3 for PCYR road overpass (Golder Associates, 2020). Pre-drilling to 7 m depth was carried out on site to assist with pile installation. Figure 5 presents the piles at Pier 3 achieved shaft friction results from the CAPWAP analysis along with the adopted design shaft friction for Pier 3. The CAPWAP results typically indicate a higher achieved shaft friction than the design shaft friction profile. The results indicate that shaft friction through the inferred silt layer below RL 1 m AHD decreases from approximately 100 kPa to as low as 30 kPa, but is still generally higher than the design shaft friction (40 kPa) for this layer. Note that the pile design was based on static analysis, adopting the full frictional resistance of the soil. This full friction resistance will occur over time (set-up) after pile driving and installation. The CAPWAP results below are presented for re-strike testing (at between 6 and 23 days post pile installation) and allow for some set-up.
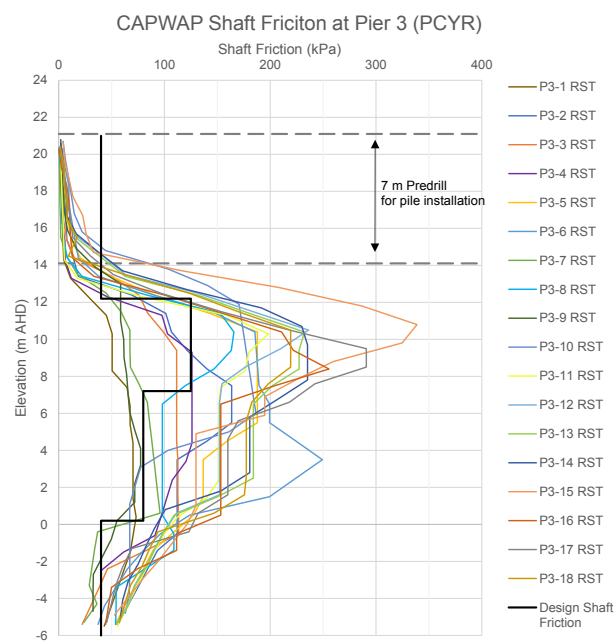
Figure 5: CAPWAP Shaft Friction Results

6   CONCLUSIONS

The Pine Creek Yarrabah Road (PCYR) Bruce Highway road overpass site investigation data (including laboratory test and SPT results) indicated a bed of silt was present between approximately RL 1 m AHD and RL -6 m AHD at PCYR road overpass. SPT results from borehole investigations indicated the undrained shear strength of the silt was much lower than the results of the triaxial compression test and CPT data. The low SPT results (and inferred undrained shear strength) are inferred to be caused by realignment of the soil structure due to repetitive shearing caused by the SPT hammer (i.e. cyclic loading).

The adopted undrained shear strength design profile (and later shaft friction profile) considered the results of the triaxial compression test data and CPT data. PDA results combined with CAPWAP analysis from driving of the PSC piles was used to help confirm the design shaft friction. The CAPWAP analysis indicated a lower achieved shaft friction at the elevation of the silt layer (compared to other alluvial layers in the profile), but still achieved close to the design skin friction for this layer.

The lower strength layer was identified during the site investigation, and the adopted design undrained shear strength relied on testing from CPT, vane shear tests and laboratory test data, rather than using correlations with SPT N_{60} values. Due to the sensitive nature of this layer at depth, SPT N_{60} values were considered not appropriate for the design. Furthermore, consideration must be given to site investigation methodology and laboratory testing when investigating Pleistocene soils of the Mulgrave River Delta. These soils are not consistent in nature over the entire depth of the profile, and some layers of 'sensitive' cohesive soils with high silt content may be present. The design methodology must consider different investigation techniques, including in-situ and laboratory testing. PDA testing is also crucial for confirmation of geotechnical resistance and confirmation of the design capacity of piles.

7   ACKNOWLEDGEMENTS

The authors would like to thank DTMR and AECOM for permission to produce this publication and acknowledge Wagstaff Piling for supply of pile driving data. The authors would also like to acknowledge the guidance of colleagues from WSP Golder, Australia in the preparation of this paper.

REFERENCES

Golder Associates (2020) Edmonton to Gordonvale Design Advice (200STBR04): Pine Creek Yarrabah Road – Highway Overpass (BR2310) Pile Capacity Assessment – Detailed Design. Report Ref. 1773248-032-TM-Rev0-Pine Creek Yarrabah Rd OP.

Golder Associates (2020) Geotechnical Factual Report – Cairns Southern Access Stage 3 (E2G), Report ref. 383276-HSA-000GEGE01-RPT-000001_0-stage3 factual report.

Martin, S. (2000, September). Wet Tropics Geology. Tropical Topics, volume 63, page2-page5. https://www.wettropics.gov.au/site/user-assets/docs/63WetTropicsGeology.pdf.

Queensland Government Department of Transport and Main Roads (2022). Bruce Highway, Cairns Southern Access Corridor (Stage 3), Edmonton to Gordonvale, construction. https://www.tmr.qld.gov.au/projects/bruce-highway-cairns-southern-access-corridor-stage-3-edmonton-to-gordonvale.

Queensland Government Department of Transport and Main Roads (2018) Preliminary Geotechnical Investigation Report R3642 – Bruce Highway Edmonton to Gordonvale (E2G) Upgrade Project, Maitland Overpass, Report ref. 02 Preliminary Geotechnical Investigation Report R3642 - E2G Maitland Overpass.

W. F. Willmott, P. J. Stephenson (1989). "Rocks and Landscapes of the Cairns District".

PROCEEDINGS OF THE 14TH ANZ YOUNG GEOTECHNICAL PROFESSIONALS CONFERENCE
14YGPC ROTORUA, NEW ZEALAND, 2ND – 5TH NOVEMBER 2022

85

The Geology of Omokoroa-Te Puna Region within the Tauranga Area: A Case Study from the Geotechnical Investigation of Stage 2 of the Takitimu North Link Project

Alexander Zohrab[1]

[1]CMW Geosciences, PO Box 13444, Tauranga Central 3141; PH (+64) 027-230-7167; email: alexz@cmwgeo.com

ABSTRACT

Stage 2 of the Takitimu North Link (TNL) project involves the proposed construction of a new 7 kilometre long four-lane expressway for State Highway 2, connecting in the east to the end of Stage 1 near Loop Road, extending approximately 900m west of the existing Omokoroa Intersection. It is to include several bridges and grade separated interchanges. The geology between Te Puna and Omokoroa is highly variable and complex and includes weathered and unweathered ignimbrite deposits at depth, which are overlain by reworked aged alluvial deposits. The landform along the TNL alignment consists of several broad terraces which are underlain by volcanic tephra deposits. The terraces are bisected by deeply incised gullies with steeply graded escarpments. Geologically recent very soft alluvial deposits are present within the base of these gullies. A Geotechnical Investigation for the specimen design of Stage 2 was undertaken between March and October 2021 to develop a ground model for the site and to provide design parameters and key geotechnical recommendations for the construction of the expressway. This paper presents the geotechnical investigation techniques used during the geotechnical investigation and describes the logistical challenges associated with accessing site locations. It focuses on presenting and discussing the complex ground model that was derived from the investigations and some of the key geotechnical design issues that will require resolving due to the difficult ground conditions anticipated.

Keywords: road, geotechnical, alignment, terrace, gully, geology

1. INTRODUCTION

Stage 2 of the Takitimu North Link (TNL) project is a Waka Kotahi project that involves the proposed construction of a new 7 kilometre long four-lane expressway for State Highway 2 (SH2), that connects to the end of TNL Stage 1 near Loop Road, Te Puna, in the east and extends approximately 900m west of the existing intersection between SH2 and Omokoroa Road. The project involves the construction of eight bridges in locations where the proposed expressway alignment intersects with arterial roads and traverses streams, gullies and wetland areas. To meet the geometric requirements set out in the New Zealand Transport Agency (NZTA) Bridge Manual version 3.3 (BM3.3), earthworks involving cuts of up to 30m deep and engineered fill embankments with heights of up to 15m are anticipated.

2. INVESTIGATION SCOPE

2.1 Introduction

The geotechnical investigations that were undertaken along the TNL Stage 2 road alignment commenced in March 2021 and were completed in September 2021. The investigation locations generally targeted locations where large cuts, fills and major structures were proposed. They also involved both soil sampling techniques and in situ tests.

2.2 Investigation Techniques

2.2.1 Soil Sampling Techniques

Soil sampling techniques included hand auger boreholes, machine excavated test pits, and rotary cored machine boreholes. The material that was recovered was logged in accordance with the New Zealand Geotechnical Society (NZGS) guidelines described in NZGS (2005) and the NZTA guidelines described in NZTA (2015).

In excess of 174 hand auger boreholes were drilled using a 50mm diameter auger to depths of up to 5m below the existing ground level. In excess of 48 machine excavation test pits were undertaken using 8 to 16-tonne excavators equipped with 1.2m wide mud-buckets and were extended to depths of up to 4m below the existing ground level. In situ shear strength measurements were recorded within cohesive soils using a handheld shear vane apparatus. Dynamic cone penetrometer tests were undertaken where granular soils were encountered to determine the relative density of the soils.

In excess of 39 rotary cored machine boreholes were drilled to depths of up to 60m below the existing ground level. Rotary drilling techniques included triple tube and push tubes at selected depth intervals in the boreholes. In locations where bridge foundations have been proposed, acid sulphate samples were selected and collected from the material that was recovered from the boreholes.

In excess of 25 standpipe piezometers were installed within some of the machine boreholes using a 50mm uPVC pipe, gravel and bentonite plug, and a flush cover. Within two of the machine boreholes, nested piezometers were installed using two 32mm uPVC pipes. In locations where bridge foundations have been proposed, groundwater samples were collected to determine the sulphate and chloride concentrations.

2.2.2 In Situ Tests

In situ tests included cone penetrometer tests (CPTs), seismic penetrometer tests (sCPTs), and standard penetration tests (SPTs). In excess of 114 CPTs and 39 sCPTs were advanced to depths of up to 30m below the existing ground level using a track mounted Geoprobe rig and 36mm diameter cone. At several of the CPT investigation locations, dissipation tests were completed. During the advancement of the sCPTs, downhole seismic testing was undertaken at 1.0m interval depths, using a single geophone. The SPTs were carried out at 1.5m intervals during the advancement of the machine boreholes.

2.3 Laboratory Testing

Within some of the locations where soil sampling techniques were undertaken, undisturbed bulk samples and push tube samples were collected and selected for laboratory testing. The laboratory testing involved Atterberg limits, particle size distribution, organic content, one dimension consolidation (oedometer), dynamic triaxial tests, unconfined compressive strength, standard compaction, California bearing ratio, consolidated undrained triaxial compression, soil field density nuclear densometer direct transmission, soil core samples, and moisture content tests. The laboratory tests were undertaken in an IANZ accredited laboratory in accordance with New Zealand Standards 4402: 1986 and 4407: 2015, and British Standard 1377-7: 1990.

2.4 Logistical Challenges

The majority of investigations were undertaken during the wet and winter seasons, and also within gullies and wetland areas. Accessing investigation locations within these areas involved the mobilisation of equipment and machinery over wet, slippery, very soft and uneven terrain, sometimes with steep gradients and dense vegetation. There were several cases where excavation works were required to provide safe access tracks with gently sloping gradients that were unobstructed by vegetation, fences, or streams, and were also overlain by competent ground to prevent machinery getting stuck.

The land underlying the proposed alignment is currently occupied by rural properties and is privately owned. Accessing and undertaking investigations within these properties required obtaining permission from the property owners, which in several cases was not granted until near the end of the investigation program or was only permitted for a limited time. This resulted in piecemeal site access into properties along the road alignment. Investigations were prioritised to be completed in properties where site access was granted for a limited period, as well as properties where site access was fully granted. To minimise disruption to property owners and leaseholders, investigations were planned to be completed within a single property at a time where possible.

PROCEEDINGS OF THE 14TH ANZ YOUNG GEOTECHNICAL PROFESSIONALS CONFERENCE
14YGPC ROTORUA, NEW ZEALAND, 2ND – 5TH NOVEMBER 2022

87

During August 2021, an outbreak of the COVID-19 pandemic resulted in a nationwide lockdown that lasted for two weeks within the Tauranga Area. No geotechnical investigation work was permitted during that time. After the lockdown restrictions were lifted, the investigation tests that were originally scheduled to be undertaken prior to the lockdown were prioritised to be completed. This enabled the initial geotechnical investigation testing schedule to be followed successfully.

The final investigation locations were undertaken in properties where access was not initially permitted, but eventually became granted after positive relationships between the consultants and the property owners had been developed. These remaining investigations were able to be completed. The proposed road alignment is also located along and near areas of Māori heritage, and investigations were required to not cause any destruction to Māori taonga. This was achieved by having an iwi monitor at each investigation location. Due to access restraints, seven test pit excavations and fourteen hand auger boreholes were abandoned.

3. GROUND MODEL

3.1 Geomorphology

The general landform within the Omokoroa-Te Puna region comprises a series of north-north-east trending terraces elevated at approximately between RL22m and RL62m (Moturiki Datum). The terraces are bisected by shallow gullies and deeper incised gullies that are associated with the Te Puna Stream. The gullies are located between Munro Road east and Ainsworth Road, and are also located at an inlet to the Tauranga Harbour approximately 700m to the south-east of the intersection between SH2 and Omokoroa Road. The elevations of the shallow gullies are at approximately RL8m to RL23m, and for the deeply incised gullies they are at approximately RL1m to RL18m. The transition between the gullies and terraces comprises moderately to steeply inclined escarpments that are inclined at gradients of 15 degrees to greater than 40 degrees. Relic landslide scarps are present on many of the escarpments.

3.2 Geological Setting

Omokoroa and Te Puna are located within the Tauranga basin, with the 2.09Ma Waiteariki Ignimbrite comprising the basement material (Briggs et al. 1996). The Tauranga basin has been subsequently infilled with late Pliocene and Pleistocene aged volcanic rocks and soils consisting of ignimbrites that are intercalated with estuarine and terrestrial deposits of the Matua Subgroup (Briggs et al. 1996). The Waiteariki Ignimbrite dips to the north-east as a result of uplift of the Kaimai Ranges (Briggs et al. 1996).

Within the Omokoroa-Te Puna region, the Te Puna Ignimbrite has previously been identified in locations to the east of the proposed TNL Stage 2 road alignment, where it overlies the Waiteariiki Ignimbrite and is underlain by soils of the Matua Subgroup, but it has not been identified in locations to the west of the road alignment (Briggs et al. 1996; CMW Geosciences 2021). It has a geological age of 0.93Ma, and is typically non-welded to partially welded and extremely weak (Briggs et al. 1996, 2005). The soils of the Matua Subgroup have a wide range of lithologies, and include fluvial deposits, estuarine and lacustrine muds, peats and lignites, and intercalated tephras (Briggs et al. 1996).

The peninsulas and terraces within the Omokoroa-Te Puna region are overlain by late Quaternary aged volcanic airfall deposits that originated from the Taupo Volcanic Zone, which comprise interbedded silts, sands and clays (Briggs et al. 1996). From oldest to youngest, these deposits include the Hamilton Ash, Rotoehu Ash, and Post-Rotoehu Ashes (Briggs et al. 1996). Within the gully features, the geology comprises Holocene and Late Pleistocene aged alluvial and peat deposits (Briggs et al. 1996). The current orientation of the terraces and gullies has been suggested to have been caused by a series of north-north-east striking faults that are regarded to be present in the Tauranga basin (Briggs et al. 1996).

3.3 Project Geology

The geological report created by Briggs et al. (1996) indicates that the proposed project alignment for TNL Stage 2 is underlain by units associated with the Waiteariki Ignimbrite and Matua Subgroup. This was later confirmed with the geotechnical investigations that were completed. The geological map of the area within which the road alignment comprises is presented in (Figure 1).
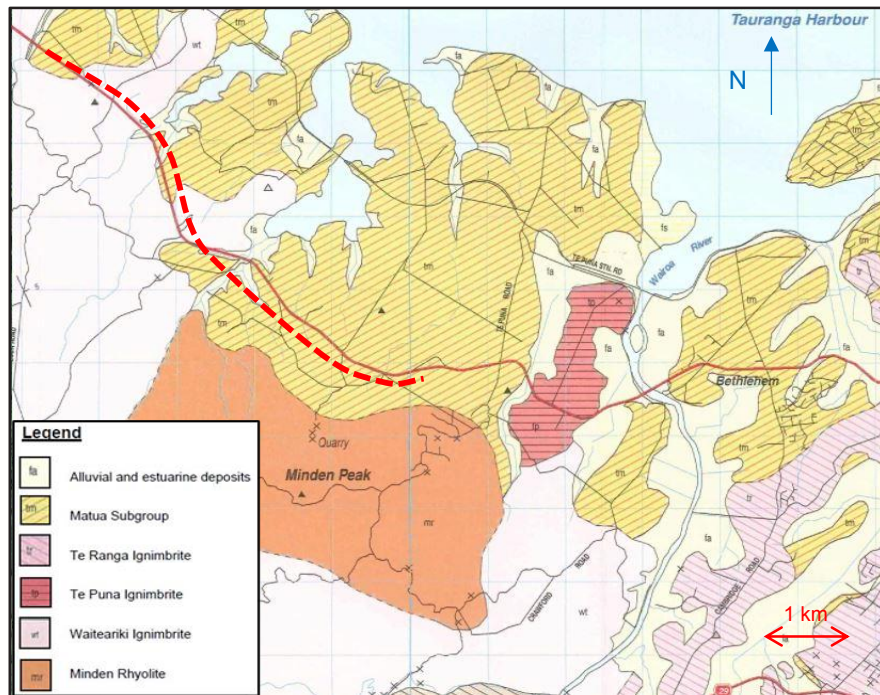
Figure 1: Geological map of the Te Puna-Omokoroa Region, with the extent of the road alignment for TNL Stage 2, modified from Briggs et al. (1996). The dashed red line indicates the approximate extent of the proposed road alignment. Units are described in the legend.

On the basis of the findings from the geotechnical investigation, the ground model for the road alignment for TNL Stage 2 includes seven geotechnical units. The units were determined based on having distinct engineering properties and are summarised in (Table 1) below:

Table 1: Summary of geotechnical units encountered underlying the road alignment for TNL Stage 2.

Geotechnical Units		Description
Unit	Name	
Holocene Alluvium	Recent Alluvium – Sands	Sand and silty sands. Light grey to grey in colour. Loose to medium dense.
	Recent Alluvium – Swamp Deposits	Interbedded alluvial silts, clayey silts, sandy silts, organic silts, and peat. Brown, grey, and bluish grey in colour. Very soft to soft in cohesive soils and very loose to loose in granular materials. Variable organic content.
Volcanic Ash	Late Quaternary Volcanic Airfall	Silt, sandy silt, silty sand, and sand layers. Orange-brown, brown, and grey in colour. Firm to very stiff. Moderately sensitive to sensitive.
Matua Subgroup	Matua Subgroup – Tephra	Interbedded silts, sandy silts, and clayey silts. Light orange, orange and brown in colour, often mottled. Firm to very stiff. Moderately sensitive to sensitive.
	Matua Subgroup – Tephra, Alluvium, and Intercalated Ignimbrite	Interbedded clayey silts, silts, sandy silts, silty sands, and sands. Wide range in colours. Firm to very stiff in cohesive soils. Loose to very dense in granular soils.
Ignimbrite	Non-welded Ignimbrite	Highly to completely weathered rock. Recovered as hard silts and medium dense to very dense sands. Consistency increases with depth.
	Partially welded, weathered Ignimbrite	Highly to completely weathered. Recovered as extremely weak to very weak rock.

PROCEEDINGS OF THE 14TH ANZ YOUNG GEOTECHNICAL PROFESSIONALS CONFERENCE
14YGPC ROTORUA, NEW ZEALAND, 2ND – 5TH NOVEMBER 2022

89

3.4 Groundwater

Groundwater table depths were determined from monitoring the water levels within the piezometers that were installed within the machine boreholes during the geotechnical investigation. Within the Omokoroa-Te Puna region, the groundwater level is known to fluctuate significantly, and perched groundwater has been found to form after a heavy rainfall event due to the geological units having contrasting permeabilities.

4. GEOLOGICAL DESIGN ISSUES

4.1 Introduction

The findings from the geotechnical investigation have revealed that significant ground improvements are required to be resolved for the design and construction of Stage 2 of TNL to have grades and transitions that meet the performance criteria outlined in BM3.3. Two of the key geotechnical design issues that will need to be addressed are discussed.

4.2 Earthworking of Matua Subgroup Deposits

Earthworks associated with construction of Stage 2 of TNL are anticipated to involve cuts up to 30m deep in the elevated terraces. In the locations along the road alignment where road cuts are proposed over elevated terraces that expose the soil profile below the upper 6m, soils of the Matua Subgroup units will be encountered. These soils generally have high in situ moisture contents and very high sensitivities, and therefore can be extremely difficult to earthwork.

Previous experience has indicated that earthworking of soils from the Matua Subgroup units can be successful where there is sufficient land area for the soil to be spread, disked and then dried in thin layers. However, this can be difficult to achieve on roading construction projects, where there is limited time and space available for earthworking the soils. Therefore, the suitability of soils from the Matua Subgroup units for the use as engineered certified fill structures is considered unlikely; however, they can possibly be used for non-permanent fill structures such as pre-loads. Due to the high sensitivity, care would still be required when handling these soils, even if they are to be used in non-certifiable fill structures.

4.3 Settlement in Alluvial Deposits

Engineered earth fill embankments with heights of up to 15m have been proposed to be constructed over the base of the gullies along the road alignment. The soils within the base of the gullies comprised very soft to soft organic and estuarine silts, clays, and peat within the Recent Alluvium – Swamp Deposits unit, and were assessed for settlement induced from earth fill embankment loading.

Within the Recent Alluvium – Swamp Deposits unit, the primary consolidation settlement values were determined in accordance with 1-dimensional consolidation theory described in Terzaghi et al. (1996), and secondary creep settlement values were determined based on Mesri et al. (1994). For the earth fill embankment, a design life of 100 years and construction period of 18 months were used, and locally sourced borrow materials were assumed to be used for the earth fill. It was found that, where the thickness of the Recent Alluvium – Swamp Deposits units was greater than 1.1m, primary consolidation static settlement values exceeded the BM3.3 serviceability limit state performance criterion of 50mm over a design life of 100 years.

Ground improvement techniques are required in order for the predicted settlement values within the Recent Alluvium – Swamp Deposits units to be compliant with BM3.3 performance criteria. In some locations along the alignment, the removal and replacement of these units with engineered fill would be considered cost exorbitant, environmentally unacceptable, and/or difficult to achieve within locations below the level of the groundwater table. Alternative ground improvement options may be required that would reduce the values of post-construction settlement within the Recent Alluvium – Swamp Deposits unit. Some options for this to be achieved could be in the form of the construction of a pre-load fill embankment, the use of lightweight geofoam for the earth fill embankment construction, and/or

undertaking ground improvement techniques within locations beneath where the earth fill embankment is proposed to be constructed.

Alluvial soils, such as the Recent Alluvium – Swamp Deposits units, have an inherent material composition that is influenced by the local depositional environment, that can be highly variable both laterally and at depth, and that can also be affected by the presence of sand lenses. This makes the time rates of settlement extremely difficult to estimate in alluvial soils. The settlement values that have been predicted for the Recent Alluvium – Swamp Deposits units were determined from the oedometer tests and prior back-analysis of settlement parameters from the TNL Stage 1 trial embankment, and are unlikely to account for the complete range of settlement values occurring across the entire length of the road alignment. Therefore, it is recommended that settlement monitoring instruments are installed at regular intervals along the road alignment where the earth fill embankment is proposed to be constructed, as this will enable back analysis of the resulting consolidation settlement parameters and allow for the subsequent geotechnical design to be progressively refined.

5. CONCLUSIONS

Based on the findings from the geotechnical investigation completed for TNL Stage 2, the following conclusions have been made:

- For major roading construction projects, significant challenges related to successfully completing a geotechnical investigation may arise if accessing investigation locations involves traversing difficult terrain, working within areas of archaeological significance, and/or requiring permission to enter private properties. These obstacles can be overcome with careful planning and by developing positive relationships with the stakeholders;
- Within deeper cuts along the TNL Stage 2 road alignment, soils within the Matua Subgroup unit are likely to be exposed, which are unlikely to be suitable for use as certifiable earth fill structures, and care should be used when handling those soils if they are to be used for non-permanent fill structures;
- Settlement values predicted from consolidation analysis indicates that earth fill embankment construction over the Recent Alluvium – Swamp Deposits units is likely to induce settlement that exceeds the BM3.3 performance criteria. Therefore, ground improvement in the form of construction of a pre-load fill embankment, the use of lightweight geofoam for the earth fill embankment construction, and/or undertaking ground improvement techniques within locations beneath where the earth fill embankment is proposed to be constructed, are likely to be required.

6. ACKNOWLEDGEMENTS

RERENENCES

Briggs, R.M.; Hall, G.J.; Harmsworth, G.R.; Hollis, A.G.; Houghton, B.F.; Hughes, G.R.; Morgan, M.D.; Whitbread-Edwards, A.R. (1996). "Geology of the Tauranga Area." Occasional Report No 22. Department of Earth Sciences, University of Waikato, Hamilton, New Zealand.

Briggs, R.M.; Houghton, B.F.; McWilliams. M; Wilson, C. J. N. (2005). "40Ar/39Ar ages of silicic volcanic rocks in the Tauranga-Kaimai area, New Zealand: Dating the transition between volcanism in the Coromandel Arc and the Taupo Volcanic Zone." New Zealand Journal of Geology and Geophysics, 48:3, 459-469.

British Standard 1377-7: 1990. "Methods of Test for Soils for Civil Engineering Purposes."

CMW Geosciences. (2021). "Geotechnical Interpretive Report, Takitimu North Link Stage 2, State Highway 2, Tauranga." Prepared for Bloxam Burnett & Olliver Ltd.

Mesri, G.; Kwan Lo D.; Feng, T. (1994). "Settlement of Embankments on Soft Clays, Chapter of Vertical and Horizontal Deformation of foundations and Embankments." A.T.Yeung & G.Y.Felio, ASCE, New York, 8-56.

New Zealand Geotechnical Society. (2005). "Field Description for Soil and Rock."

New Zealand Standard 4402:1986. "Methods of Testing Soils for Civil Engineering Purposes."

New Zealand Standard 4407:2015. "Methods of Sampling and Testing Road Aggregates."

New Zealand Transport Agency. (2015). "Technical Advice Note (TAN #15-13) Geotechnical testing and investigations."

New Zealand Transport Agency Bridge Manual, 3rd Edition, incorporating amendments to October 2018.

Terzaghi; Peck; Mesri. (1996). "Soil Mechanics in Engineering Practice." 3rd Ed, Wiley, NYC, Chapters 16.6-16.8, pg 106-113.

PROCEEDINGS OF THE 14TH ANZ YOUNG GEOTECHNICAL PROFESSIONALS CONFERENCE
14YGPC ROTORUA, NEW ZEALAND, 2ND – 5TH NOVEMBER 2022

91

An Assessment on Correlation between Dynamic Cone Penetration Blow Count and Liquid Limit of NSW Clays

M. T. Le[1], S. Pitawal[1] and B. Damirchi[1]

[1] Geotesta Pty Ltd, 6/20-22 Foundry Rd, Seven Hills, Sydney, NSW 2147, PH (61) 0280523953; email: info@geotesta.com.au

ABSTRACT

The Dynamic Cone Penetration (DCP) test is one of the simple and economical geotechnical tests used in the field, and its results are commonly used for practical applications, such as checking consistency with the results from borehole loggings or roughly estimating soil bearing capacity. Even though the test is widely used in practice, particularly in Australia, its relationships with clay moisture limits, such as Liquid Limit (LL), have not been extensively studied. Hence, this paper describes the energy-based behaviour of DCP in relationship with LL via the theoretical model of pore collapse and empirical correlation. As a result, the method predicts well the plasticity behaviour of NSW clays from 8 DCP blows per 100mm. Discussion on the method, testing results and relevant limitations are also provided.

Keywords: cone resistance, driving energy, dynamic cone penetration, Liquid Limit, NSW clays.

1 INTRODUCTION

Among field soil tests, dynamic cone penetration (DCP) test is one of the oldest geotechnical methods for soil characterisation and was originally developed in Australia by Scala (1956). This in-situ test is simple with quick set-up, low cost and applicable to all kinds of soils, particularly to evaluate the consistency of in-situ soil and assist soil-logging descriptions. Furthermore, the portable DCP apparatus can characterise soil in field, particularly granular materials, such as sandy soils or road subgrades and pavement (Mohammadi et al. 2008; Lee et al. 2019). Of the correlated parameters, relative density (D_r) and California Bearing Ratio (CBR) are so far intensively investigated in relationship with DCP index (DPI) (Lin et al. 2019; MacRobert et al. 2019; Sagar 2022). The investigation is inspired from the correlation of DCP driving energy with cone tip resistance and skin friction along the rod in cohesionless soils (Escobar et al. 2013; Gholami et al. 2020). However, the analysis can be affected by reading of observer, rod tiltation after DCP extension during penetration, and energy loss. This loss can be caused by the friction between hammer and guide rod, and transferring energy through upper rod of DCP equipment (Sadrekarimi and Seyyedi 2009).

To gain the more reliable and meaningful DCP results, the energy-based assessment on soil resistance values was performed with the inclusion of load cell and accelerometer on the anvil (Byun and Lee 2013). The parameters of cone resistance were proven to be consistent with DPI values and soil properties via using instrumented DCP for shallow soils (Byun et al. 2014, Navarrete et al. 2021). The result is in good agreement with the study on DPI in lime-treated clays, which was performed by Vakili (2021), mentioning that DPI-values can also be correlated with CBR, Unconfined Compressive Strength (UCS) and subgrade reaction coefficients (K_s). The authors indicated that apart from curing effects, moisture content apparently affects DPI, along with density and pore water pressure (Ampadu et al. 2017). Using DCP test to predict the moisture change in lateritic soil subgrade was also researched by Ampadu and Fiadjoe (2015), confirming that DPI is significantly dependent on the small changes in water content of sandy clay materials. In the changing range of water content, optimal moisture content (OMC) of the soil is the most concerning parameter since DPI tends to increase significantly when moisture is larger than OMC and the soil turns to wet state. Hence, soil state obviously affects DCP behaviour in soil.

Although the soil state of clay related to Liquid Limit (LL) is one of the most important parameters for soil classification, few studies have been conducted to research correlations between DCP results and LL of clayey soils. In a similar mechanism, another common field test, named Standard Penetration Test (SPT) has been revealed with a strong relationship between SPT blows (*N*) and relative void ratio (Mujtaba et al. 2018). Meanwhile, initial void ratio is closely related to moisture content and Atterberg limits of intact clays (Chung et al. 2016; Pineda et al. 2016), suggesting correlations between dynamic penetration parameters with these values. Furthermore, Rahim et al. (2004) formulated the relationship between DPI and porosity, resulting in a good agreement with experiment data. Therefore, it is possible to establish a relationship between DPI and moisture content in limit values from Atterberg's methods.

In this paper, this relationship will be investigated for clayey soil at 30 sites in and around Sydney City, New South Wales, named NSW clays. Field DCP and laboratory Casagrande tests were performed for samples at shallow depths. The analysis goes from theoretical to empirical analysis to produce the predicted curve between field DCP results and laboratory-based values of LL. The discussion on the results and limitations is also conducted to evaluate the analysis method.

2   ANALYSIS METHOD

2.1   DCP analysis and initial-void-ratio prediction

According to AS 1289.6.3.2 (1997), DCP test is a simple penetrometer test in which a hammer of 9kg falls from a height of 510mm, pushing a 20-mm diameter cone with apex angle θ of 30° into layers of ground. The amount of penetration in mm for each falling or blow is called Dynamic Cone Penetration Index, denoted as DPI (mm/blow). According to Australia Standard HB 160 (2006), there is also another parameter to express DCP result, named Dynamic Cone Penetration Blow Count (N). This count is the blow number of hammer to push the DCP rod penetrate 100mm into the ground. From this, it can obtain:

DPI (mm/blow) = 100 / N (blow)   (1)

In each blow, the energy to push the DCP cone penetrating into the ground is originated from the kinetic energy (E), which is produced by dropping the 9-kg hammer to the 16-mm diameter rod head from the height of 510mm. However, in DCP test, when the energy is transferred from the rod head to the cone tip, there is an amount of energy loss through the rod, which increases with an extension of the rod length (Odebrecht et al. 2005; Byun and Lee 2013). Assuming that this energy is totally turned into cone tip resistance (denoted as q_c, kPa), and rod friction in the ground is insignificant because the cone diameter is larger than the rod diameter (d=20 mm, compared with 16 mm), the energy of DCP test can yield as follows:

E = DPI.$A.q_c$ / LR (2)

Where, A (m²): cone tip area, A = $\pi d^2/4$
　　　LR: energy loss ratio, LR = 0.64 without extension rod (after Byun and Lee 2013)

Substituting Eq. (1), A, E and LR-value into Eq. (2), cone tip resistance (q_c) can be obtained:

q_c (kPa) = 917N (3)

Adopting the analysis of slip pattern under the DCP cone, conducted by Salgado et al. (1997), and assuming a slip shape of logarithmic spiral around the cone (Bolton 1979), the DCP cone resistance q_c can be computed as:

q_c = 2p $e^{\pi\tan\Phi}$ [(1+C)^m-mC-1] / [C²m(1-m)] + c.cotΦ($e^{\pi\tan\Phi}$-1)   (4)

Where, p (kPa): the limiting cavity expansion pressure from cone tip,
　　　c (kPa): soil cohesion, Φ (°): frictional angle,
　　　m=1+1/[tan (45+ Φ/2)]²
　　　C = $e^{(\pi/2)\tan\psi}$cot (θ/2), where ψ: the dilatancy angle [ψ=0 for normally consolidated clay (Vermeer and de Borst 1984)], and θ: DCP apex angle (θ = 30°).

Considering when the cone tip penetrates into the ground, it creates and widens a cavity in the cylindrical shape, the final porosity (n) of penetrated soil can be formulated with the limiting cavity expansion pressure (p). Based on the theoretical model of pore collapse, suggested by Rahim et al. (2004), p can be calculated as below:

p = c cotΦ c ($n^{1.34\sin\Phi/(\sin\Phi-1)}$ -1)   (5)

Substituting Eq. 3-5 and values, the final porosity n can be calculated from N, Φ and c as follows:

n = {1+ 13.93m(m-1) [458.5N-c.cotΦ($e^{\pi\tan\Phi}$-1)] / [c cotΦ $e^{\pi\tan\Phi}$(4.73^m-3.73m-1)]}$^{(\sin\Phi-1)/(1.34\sin\Phi)}$ (6)

PROCEEDINGS OF THE 14TH ANZ YOUNG GEOTECHNICAL PROFESSIONALS CONFERENCE
14YGPC ROTORUA, NEW ZEALAND, 2ND – 5TH NOVEMBER 2022

93

By using the model of pore collapse, it is assumed that the soil matrix is incompressible during pore collapse occurring. This means that very little or no change in material matrix volume occurs due to compression of the soil. In other words, the volume change is mostly caused by effective pore collapse during cone penetration. Therefore, with the pore collapse theory suggested by Rahim et al. (2004) and applied in DCP test, the final porosity (n) can be relative to initial porosity (n_0) as the following equation:

$$n^{1.34} = (n-n_0) / (n-1) \tag{7}$$

From the initial porosity (n_0), the initial void ratio (e_0) can be calculated as below:

$$e_0 = (n+n^{1.34}-n^{2.34})/(1-n-n^{1.34}+n^{2.34}) \tag{8}$$

Observing Eq. 6 and 8 and with assumed values of clay cohesion (c) and frictional angle (Φ), initial void ratio (e_0) of the soil can be predicted from DCP blows/100mm (N). By investigating the next possible relationship between the ratio and LL, one can obtain the bridging relationship between N and LL.

2.2   Empirical prediction of Liquid Limit (LL) from initial void ratio (e_0)

The relationship between void ratio and Liquid Limit is extensively investigated by intensive studies on both remoulded and intact soils. For disturbed samples, Komurlu (2020) studied the influences of soil void ratio on LL, which is determined by fall-cone and Casagrande method. Before the LL tests were performed, void ratios of specimens had been measured in volumes determined with particular specific gravities of studied soils. The experimental results show that void ratio has an important effect on LL-values determined by both fall-cone and Casagrande testing mechanisms. However, there is no unique correlation between the two parameters of various kinds of remoulded soils. Instead, the LL-e_0 relationship differs among various disturbed soils in wide ranges of LL; therefore, the good correlation should be adopted for each kind of studied soil (Komurlu 2020). This statement is also associated with the research conducted by Sridharan and Honne (2011), confirming that there is a relationship between LL and change in void ratio. Nevertheless, the correlation is poor, and it is related to compressibility of soil, particularly when the studied soils are remoulded with the low ratio of void ratio ($\Delta e/e_0$), indicating the high disturbance level of tested sample. Hence, it is in need to investigate whether there is a good correlation between LL and e_0 from in-situ samples by high-qualified sampling and with low levels of disturbance.

In this study, researching the relationship between LL and in-situ void ratio (e_0) is reasonable because DCP test is a kind of on-site experiment, and its results come from the behaviour of intact ground. The high quality of tested soil sample plays an important role to produce a good correlation of LL-e_0, on which DCP blows N can rely on predicting acceptable LL-values. From the literature review on intact samples at shallow depths, various studies of high-quality clay specimens were conducted to characterise their features in soil mechanics (e.g. stress-strain behaviour by Pineda et al. (2016) or penetration behaviour by Chung et al. (2017). In their sampling technique, advanced modified samplers were utilised, such as Osterberg-type or hydraulic fixed-piston sampler (Pineda et al. 2016) and Oil-operated fixed-piston sampler (Chung et al. 2017). From extracting relevant results of in-situ void ratio e_0 and LL, their correlation curve can be shown in Figure 1a, which results in a parabolic fitting equation with the coefficient of determination R^2=0.93, as follows:

$$LL =6.4e_0{}^2 + 10.3\ e_0 + 29 \tag{9}$$

It is noted that LL in Figure 1a is determined by fall cone method, while LL in this study is based on values from Casagrande testing mechanism. However, since the LL from fall cone tests is quite equal to those defined from Casagrande method (Christaras 1991; Grønbech et al. 2011; Spagnoli 2012), it is reasonable to consider LL-values in Eq. 9, determined by both methods. It is also notable in Figure 1a that most samples are medium to super high plasticity clay with LL-values ranging from 30 to 120%, according to Unified Soil Classification System (Grønbech et al. 2011). To cover a lower and higher range of LL-value, two boundary lines are depicted in Figure 1a, illustrating the variation of LL for possibly lower or higher plasticity of other clays.

Figure 1: (a) Empirical correlation between LL and e_0, (b) Predicted curve of N vs e_0
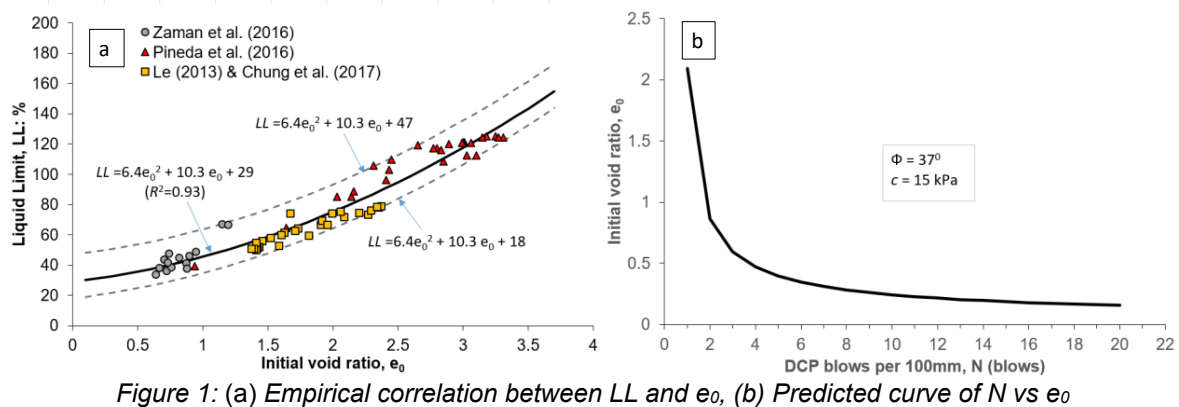
By adopting Eq. 9 into Eq. 6 and 8, *LL* at a specific depth can be predicted from *N*-values in DCP test at that depth with assumed values of cohesion (*c*) and frictional angle (Φ) (see Figure 1b). For studied NSW clays (e.g. Ballina clay), the average frictional angles of soil at the shallow depths can vary from 32° to 41° (Pineda et al. 2016). Therefore, a representative angle of 37° can be adopted, while clay cohesion can be averaged at around 15 (kPa). With these assumed values, the input blows (*N*) from in-situ DCP tests at a specific depth can roughly output the in-situ or initial void ratio at that depth. However, this rough estimation is based on the consideration that at the tested depth, the studied soil is homogeneous without any interference of impurity (e.g. rootlets, sandstone, gravel, ironstone or shale fragments). Furthermore, the depth should be shallow (up to just below 1.0m) since the extension can significantly reduce the energy loss ratio (Odebrecht et al. 2005; Byun and Lee 2013), which underestimates the values of initial void ratio (see Eq. 6 and 8), leading to the resulted *LL* smaller than expected in Eq.9.

3   EXPERIMENTAL VALIDATION

3.1   Testing sites and program

To investigate and verify the proposed relationship between DCP blow count (N) and LL at particular depths, DCP tests were conducted at thirty (30) different sites located in and around Sydney city, NSW, Australia (Figures 2a-b). There were totally 104 samples collected from the sites to bring them to Geotesta Laboratory for testing Liquid Limit (sample numbers shown on each pinpoint in Figures 2a-b). The sample depths are tabulated in Table 1 with NSW postcodes.
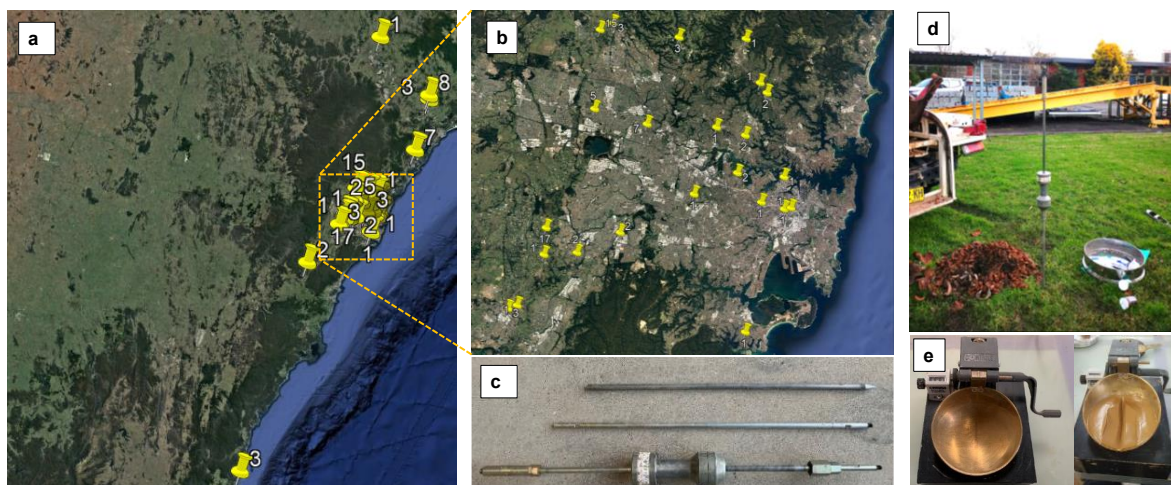
Figure 1: (a) NSW site, (b) Sydney site, (c) DCP equipment, (d) DCP test and (e) LL test

On the surveyed site, DCP tests were conducted following the guidance mentioned in Australian Standard AS 1289.6.3.2 (1997) for Determination of penetration resistance of a soil – 9 kg dynamic cone penetrometer test, while *LL* is determined by Casagrande method, following AS 1289.3.1.1 (2009). The photographs of equipment and tests are shown in Figures 2c-e.

PROCEEDINGS OF THE 14TH ANZ YOUNG GEOTECHNICAL PROFESSIONALS CONFERENCE
14YGPC ROTORUA, NEW ZEALAND, 2ND – 5TH NOVEMBER 2022

95

3.2 Testing results and discussion

Figure 3: Predicted curve and measured data of LL vs N
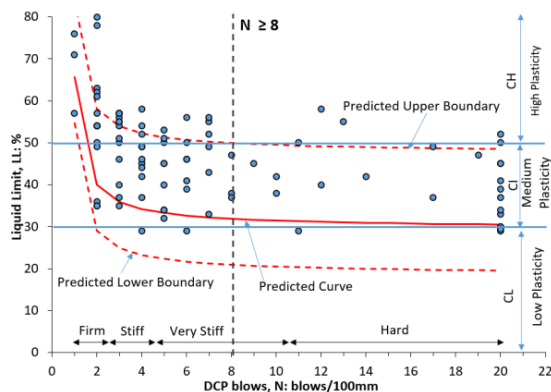
Table 1: Sample depths at sites in NSW postcodes

Postcode	2039	2042	2043	2072	2073
Depth (m)	1.0	1.2	0.8	0.6-0.8	0.9
Postcode	2077	2112	2114	2130	2137
Depth (m)	1.6	0.5-1.0	0.4	0.8	0.9
Postcode	2143	2145	2148	2155	2158
Depth (m)	0.8	0.5-1.2	0.8-1.3	0.4-0.9	0.5-0.7
Postcode	2170	2174	2179	2229	2259
Depth (m)	0.7-1.5	0.8-1.0	0.4-1.1	0.7	0.6-1.2
Postcode	2320	2321	2333	2546	2557
Depth (m)	0.5-1.4	0.5-0.8	0.6	0.8-1.2	0.5
Postcode	2565	2567	2575	2765	2800
Depth (m)	0.4	1.2-1.9	1.0-1.2	0.6-1.2	0.7-0.8

As a result of this study, Figure 3 illustrates the relationship between DCP blows per 100mm (N) and LL of NSW clays. It can be seen from this figure, most investigated clays are medium and high plasticity clays (LL>30%), equivalent to CI and CH, respectively (AS 1726: 2017). Furthermore, the predicted curve and upper boundary well cover measured points, which have a majority of N-values smaller than 8 with higher LL up to about 80%. With N larger than 8, most samples turn to be in medium plasticity (30%<LL<50%), and the predicted upper boundary reflects this tendency correctly by intersecting the medium-high-plasticity boundary (LL=50%) right at N = 8 (blows/100mm). According to Australian Standard No. HB160 (2006), the N-value of 8 indicates the clay consistency of Very Stiff, as shown on the horizontal axis in Figure 3. When considering the change of plasticity from medium-to-high (MH) to only medium (M) degree, very stiff NSW clays can be categorised into two levels, very-stiff-MH (5 < N < 8) and very-stiff-M (8< N <10).

From the investigation on testing postcode, the very-stiff-M to hard clays (N ≥ 8), indicating medium plasticity state (CI category), distribute in the areas with NSW 2039, 2072, 2077, 2145, 2155, 2158, 2170, 2229, 2259, 2320, 2321, 2546, 2567 and 2765. These postcodes mostly belong to the northern areas of testing Sydney and NSW sites (refer to Figures 2a-b). Based on the geological map of bedrock under very-stiff/hard clay in these areas, most of the surveyed sites are underlain by Wianamatta Group (Rh) with medium to coarse-grained quartz sandstone (DMRS 1983), corresponding to the very-stiff-M clay (medium plasticity). Meanwhile, to the south, the firm to very-stiff-MH clay (medium-to-high plasticity) is related to fine-to-medium-grained lithic sandstone (Rwb and Rwm) or black-to-dark shale (Rwa). This means that the differences in the grained level of bedrock between the northern and southern studied areas are in light with the categorisation in very-stiff clay based on plasticity degree; the predicted upper curve of DCP versus LL clearly demonstrates this categorisation.

However, using the prediction method has limitations. Firstly, the method analysis assumes that no skin friction occurs during penetration since cone diameter is larger than rod diameter and the depth is limited within shallow degrees. This leads to an overestimation of frictional angle value at 37^0, which is based on Ballina clay from the study of Pineda et al. (2016). Secondly, unexpected intervention of impurity in clay, such as ironstone, shale, gravel pieces, can significantly increase N-value, which may not reflect the right category of very-stiff-M clay. Likely, DCP test with the depths deeper than 0.8-1.0m (see Table 1) can remarkably increase the DCP blows due to further energy loss from rod extension. Future research is expected to consider these limitations to reflect better the correlation between DCP blows N and LL.

4 CONCLUSIONS

An analysis method was proposed to predict the correlation between dynamic cone penetration (DCP) blows per 100mm (N) and Liquid Limit (LL). The method is based on the theoretical model of pore collapse to build the relationship of N versus initial void ratio (e_0) and empirical curves between e_0 and LL. This correlation was investigated using the DCP tests at 30 sites in NSW, Australia and Casagrande tests for samples collected from these sites. The significant conclusions can be drawn as follows:

- Predicted curve and upper boundary reflect well the N-LL correlation: high LL with N-value lower than 8, and medium LL from 30% to 50% with N-value larger than 8. Therefore, the N-value of 8

can categorise very-stiff clay into two kinds: (i) very-stiff-M (medium plasticity) and (ii) very-stiff-MH (medium-to-high plasticity), which is in light of the discrepancies in geology origins of bedrock under the layer of studied clays.

- However, the study has limitations: assumptions with overestimated frictional angle, high DCP blows by extending rods and encountering unexpected intervention of impurity in NSW clays.

5 ACKNOWLEDGEMENTS

REFERENCES

Ampadu, S. I. K., & Fiadjoe, G. J. Y. (2015). The influence of water content on the Dynamic Cone Penetration Index of a lateritic soil stabilized with various percentages of a quarry by-product. Transportation Geotechnics, 5, 68-85.

Ampadu, S. I. K., Ackah, P., Nimo, F. O., & Boadu, F. (2017). A laboratory study of horizontal confinement effect on the dynamic cone penetration index of a lateritic soil. Transportation Geotechnics, 10, 47-61.

AS 1289.6.3.2 (1997). Methods of testing soils for engineering purposes, Method 6.3.2: Soil strength and consolidation tests - Determination of the penetration resistance of a soil - 9 kg dynamic cone penetrometer test. Australian Standard.

AS 1289.3.1.1 (2009). Method of testing soils for engineering purposes, Method 3.1.1: Soil classification tests – Determination of the liquid limit of a soil – Four-point Casagrande method. Australian Standard.

AS 1726 (2017). Geotechnical site investigations. Australian Standards.

Byun, Y. H., & Lee, J. S. (2013). Instrumented dynamic cone penetrometer corrected with transferred energy into a cone tip: a laboratory study. Geotechnical Testing Journal, 36(4), 533-542.

Byun, Y. H., Yoon, H. K., Kim, Y. S., Hong, S. S., & Lee, J. S. (2014). Active layer characterization by instrumented dynamic cone penetrometer in Ny-Alesund, Svalbard. Cold regions science and technology, 104, 45-53.

Chung, S. G., Lee, J. M., Kweon, H. J., & Singh, V. K. (2017). Penetration Behavior and Sample Quality of Hydraulically Activated Fixed-Piston Samplers. Journal of Geotechnical and Geoenvironmental Engineering, 143(3), 04016103.

Christaras, B. (1991). A comparison of the Casagrande and fall cone penetrometer methods for liquid limit determination in marls from Crete, Greece. Engineering Geology, 31(2), 131-142.

DMRS (1983). Geological Series Sheet 9130. Department of Mineral Resources, Sydney, Australia.

Escobar, E., Benz, M., Gourvès, R., & Breul, P. (2013). Dynamic cone penetration tests in granular media: Determination of the tip's dynamic load-penetration curve. In AIP Conference Proceedings (Vol. 1542, No. 1, pp. 389-392). American Institute of Physics.

Gholami, A., Palassi, M., & Fakher, A. (2020). Assessment of the effect of skin friction on the results of dynamic penetration testing in cohesionless soil. Iranian Journal of Science and Technology, Transactions of Civil Engineering, 44(2), 715-721.

Grønbech, G. L., Nielsen, B. N., & Ibsen, L. B. (2011). Comparison of liquid limit of highly plastic clay by means of Casagrande and Fall Cone Apparatus. Age (mil. Years), 40, 46.

HB160 (2006). Handbook for Soil Testing. Australian Standard.

Komurlu, E. (2020). An Investigation of Soil Void Ratio Effect on Liquid Limit Values Determined by Different Test Methods. GeoScience Engineering, 66(3), 150-161.

Lee, J. S., Kim, S. Y., Hong, W. T., & Byun, Y. H. (2019). Assessing subgrade strength using an instrumented dynamic cone penetrometer. Soils and Foundations, 59(4), 930-941.

Le, M.T. (2013). Consolidation behaviour of Busan clay by various methods. Master thesis, Dong-A University, Busan, South Korea.

Liang, Y., Cao, L., & Liu, J. (2015). Statistical Correlations between SPT N-Values and Soil Parameters. Department of Civil Engineering, Ryerson University.

Lin, L., Li, S., Liu, X. L., & Chen, W. W. (2019). Prediction of relative density of carbonate soil by way of a dynamic cone penetration test. Géotechnique Letters, 9(2), 154-160.

MacRobert, C. J., Bernstein, G. S., & Nchabeleng, M. M. (2019). Dynamic cone penetrometer (DCP) relative density correlations for sands.

Mohammadi, S. D., Nikoudel, M. R., Rahimi, H., & Khamehchiyan, M. (2008). Application of the Dynamic Cone Penetrometer (DCP) for determination of the engineering parameters of sandy soils. Engineering Geology, 101(3-4), 195-203.

Mujtaba, H., Farooq, K., Sivakugan, N., & Das, B. M. (2018). Evaluation of relative density and friction angle based on SPT-N values. KSCE Journal of Civil Engineering, 22(2), 572-581.

Navarrete, M. A. B., Breul, P., & Gourvès, R. (2021). Application of wave equation theory to improve dynamic cone penetration test for shallow soil characterisation. Journal of Rock Mechanics and Geotechnical Engineering.

Odebrecht, E., Schnaid, F., Rocha, M. M., & de Paula Bernardes, G. (2005). Energy efficiency for standard penetration tests. Journal of geotechnical and geoenvironmental engineering, 131(10), 1252-1263.

Pineda, J. A., Suwal, L. P., Kelly, R. B., Bates, L., & Sloan, S. W. (2016). Characterisation of Ballina clay. Géotechnique, 66(7), 556-577.

Sadrekarimi, J., & Seyyedi, S. (2009). Lessons learned during regular monitoring of in situ pavement bearing capacity conditions. In Bearing Capacity of Roads, Railways and Airfields, Two Volume Set (pp. 759-770). CRC Press.

Sagar, C. P., Badiger, M., Mamatha, K. H., & Dinesh, S. V. (2022). Prediction of CBR using dynamic cone penetrometer index. Materials Today: Proceedings, 60, 223-228.

Scala, A. J. (1956). Simple methods of flexible pavement design using cone penetrometers. New Zealand Engineering, 11(2), 34-44.

Spagnoli, G. (2012). Comparison between Casagrande and drop-cone methods to calculate liquid limit for pure clay. Canadian journal of soil science, 92(6), 859-864.

Vakili, A. H., Salimi, M., & Shamsi, M. (2021). Application of the dynamic cone penetrometer test for determining the geotechnical characteristics of marl soils treated by lime. Heliyon, 7(9), e08062.

Vermeer PA, De Borst R (1984) Non-associated plasticity for soils, concrete and rock. HERON 29(3).

PROCEEDINGS OF THE 14TH ANZ YOUNG GEOTECHNICAL PROFESSIONALS CONFERENCE
14YGPC ROTORUA, NEW ZEALAND, 2ND – 5TH NOVEMBER 2022

97

Analysing Tri-arch Cavern Supporting Mechanism with 3D Numerical Modelling

A. Z. CHEN[1] and T. J. SIA[2]

[1]SMEC Australia, Geotechnics & Tunnels, Melbourne, Victoria, Australia; email:albert.chen@smec.com
[2]SMEC Australia, Manager of Geotechnics & Tunnels, Melbourne, Victoria, Australia; email: tongjoo.sia@smec.com

ABSTRACT

Multi-arch caverns and tunnels are commonly adapted in underground metro station projects to meet the required cross-sectional span. The supporting mechanisms of such caverns/tunnels is very different from single-arch or circular tunnels/caverns, which have been studied by some researchers and engineers with numerical, analytical and experimental approaches. However, many of these works were only based on the cross-sectional analysis, and not able to provide a comprehensive support mechanism including all the related structures. In this paper, using the example of tri-arch underground station in Melbourne Metro project, the supporting mechanism is studied in detail, including the interactions between surrounding rockmass and key supporting structures (i.e. lining, crown, downstand beam & column). 3D numerical modelling with FLAC3D has been utilised for the study, hence the supporting mechanism at both transverse and longitudinal direction are analysed and proposed. Parametric studies have also been carried out to identify the role of key supporting elements. The key findings of this paper include identifying the central cavern crown as the critical structure, proposing a load transferring mechanism between different structures and suggesting the major supporting mechanism to be providing tensile restrain to the surrounding rock mass. The findings from this paper provide supplements to the supporting mechanism of such caverns/tunnels, which can be used as design theoretical basis for future projects.

Keywords: Multi-arch cavern, rockmass, underground station, 3D numerical modelling, FLAC3D.

1. INTRODUCTION

Melbourne Metro Tunnel project aims to upgrade the existing railway network with a pair of new nine-kilometre twin tunnels, which pass underneath the Melbourne CBD region. The project promised to enable 39,000 more passengers to use the railway system during each the peak period, and it would be the first step for Melbourne's 'metro style' rail network. For the State Library Station, a design of large-span tri-arch caverns is utilised for the underground station platform and the twin railway tunnels. With an average overburden of 25 m of soft rock, the general excavation method is of conventional NATM excavation, with primary ground supports including shotcrete, rockbolt and umbrella fore-pipe when encountering weak ground (Figure 1). The design of a tri-arch cavern makes it possible for the underground station to reach an overall cross-span of 30 m, as well as providing with adequate ground support. This type of 'multiple-arch' cavern have been studied by some researchers and engineers with numerical, analytical and experimental approaches (e.g. Lai et al. 2011, Yoo and Choi 2017, Cao et al. 2018, Zhu et al. 2019). Most of these works are mainly focusing on the estimation of rock load on the structure (Figure 2). In this paper, using the example of State Library Station, the supporting mechanism of a tri-arch is studied in detail by 3D numerical modelling method with FLAC3D.

2. METHODOLOGY

Most of the rock mass encountered at Melbourne Metro Project is known as Melbourne Formation (MF). Melbourne Formation consists of sandstone and siltstone, it is the basement rock through Melbourne region. Melbourne Formations are further classified in to four categories based on their weathering condition, namely MF1, MF2, MF3 and MF4. The conventional Mohr-Coulomb constitutive model has been utilised for all the Melbourne Formations, and these parameters are summarised in Table 1. The in-situ horizonal stresses are modelled as a factor to the vertical stresses (Table 2).

Modelling of ground supports is achieved by using FLAC3D build-in 2D Finite Element structure elements: the combining effect of shotcrete and lattice girder are modelled as shell elements; the steel columns are modelled by beam elements and rockbolts are modelled as cable elements. It is assumed that the connections between rock mass and linings, linings and columns are rigid, which means that all the components for velocity are fully transmitted between the target and source. The mechanical parameters of the supports are summarised in Table 3.

(a)   (b)
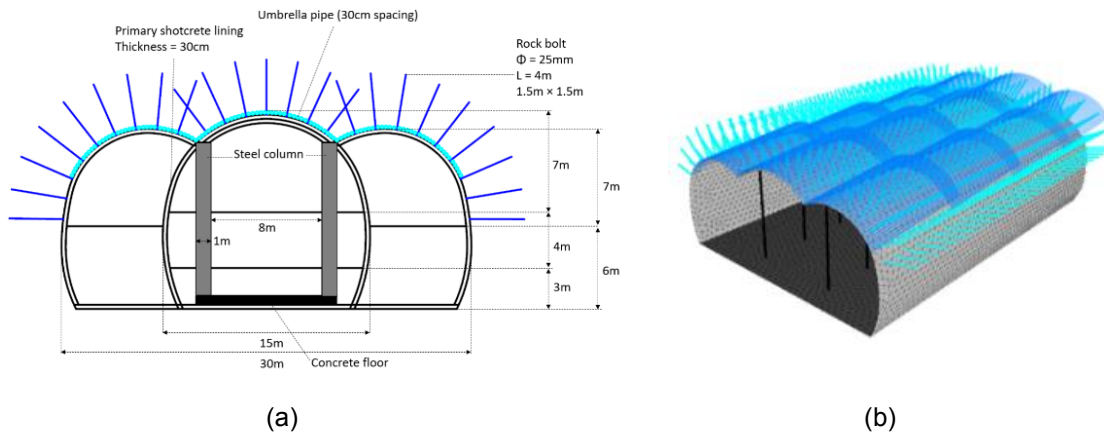
Figure 1. Ground supports of tri-arch cavern for State Library Station, cross-sectional (left) and perspective view (right).

(a)   (b)

(c)
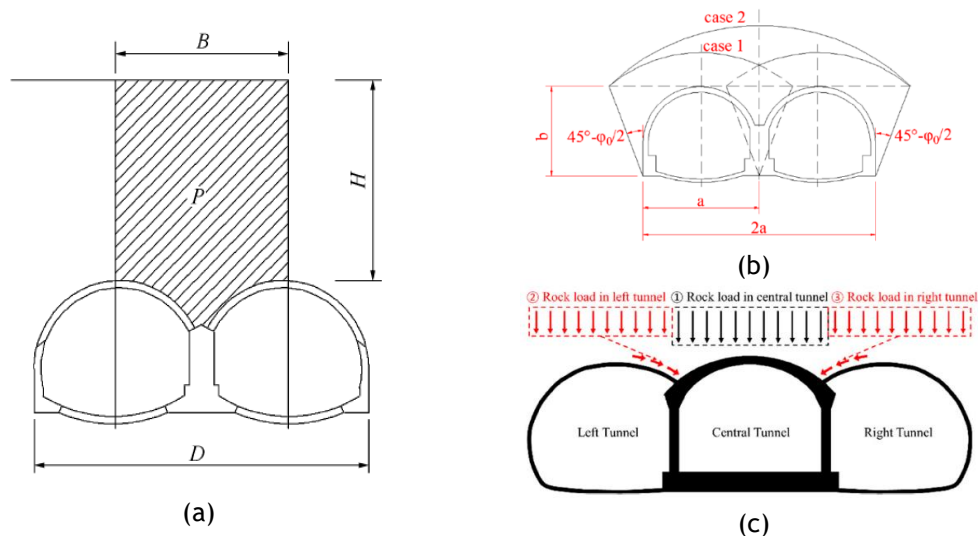
Figure 2. Theoretical ground load on multi-arch tunnels: (a) Matsuda, 1998, (b) Yan et al., 2017, (c) Lee et al., 2020.

Table 1. Ground parameters for Melbourne Formations.

	γ (kN/m³)	E_{rm} (MPa)	ν	ϕ (°)	c (kPa)	σ_t (kPa)
MF4	22.5	100	0.3	30	37	0
MF3	23	200	0.25	34	60	1
MF2	24	800	0.2	43	115	7
MF1	25.5	2500	0.2	54	270	50

PROCEEDINGS OF THE 14TH ANZ YOUNG GEOTECHNICAL PROFESSIONALS CONFERENCE
14YGPC ROTORUA, NEW ZEALAND, 2ND – 5TH NOVEMBER 2022

99

Table 2.In-situ horizontal stresses

	Major σ_h/σ_v	Minor σ_h/σ_v	Direction (to cavern axis)
MF4	0.6	0.6	45°
MF3	1.2	0.5	45°
MF2	1.5	0.75	45°
MF1	2.0	1.0	45°

Table 3.Ground support parameters

Supporting element	Properties
Shotcrete lining	γ = 25 kN/m^3, thickness = 30 cm, E = 3 GPa, v = 0.2
Concrete floor	γ = 25 kN/m3, thickness = 100 cm, E = 15 GPa, v = 0.2
Rock bolts	L = 4 m, E = 200GPa, Spacing: 1.5m x 1.5m
Steel column	H = 12.5 m, Cross-section: 1m x 2m, E = 200 GPa, v = 0.27

The 3D model of the studied area has a dimension of 150m x 36m x 70m. It has been divided in to four layers based on the geological models provided. Figure 3 shows the 3D model and the corresponded Melbourne Formations borehole core photos (MF4 at top and MF1 at bottom). The model has approximately 200,000 tetrahedral elements, with edge size varying from 1 m (at excavation zone) to 5 m (at boundary). The mesh size is set to 1 m to ensure best connection of lining (shell elements) and steel column (beam element). The modelling process has utilised a simplified excavation sequence for time saving purposes, as shown in Figure 4. Each excavation step is 1.5 meters, and the entire model is solved to equilibrium for each step.

(a)   (b)
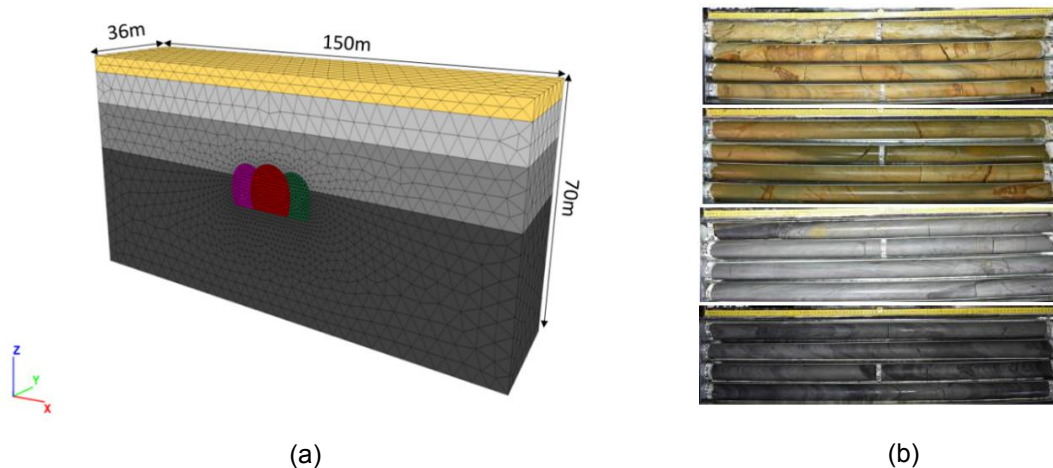
Figure 3. (a) FLAC3D model overview and (b) corresponded formation borehole core photos.

(a)   (b)
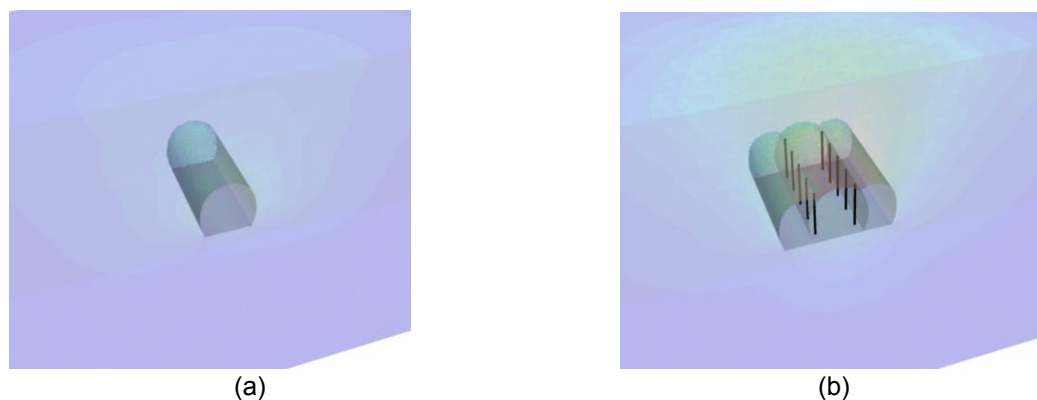
Figure 4. Simplified excavation sequence: (a) excavation of central cavern; (b) activating steel columns, excavation of both side cavern

3. RESULTS

3.1 Parametric study on factors affecting column loads

Since the proposed design has utilised a very conservative support strength, with a longitudinal twin column distance (S) of 6 m, the rock mass plasticity zone around excavation is of minimum and the maximum rock mass deformation is only 18 mm. Therefore, in order to study the supporting mechanism of the tri-arch cavern, a parametric study with numerical modelling has been performed. Firstly, an extreme case of a tri-arch cavern without any steel columns are modelled and calculated, and the cross-sectional view of rock mass plasticity zone is presented in Figure 5. It is obvious that the rock mass above the central cavern will experience potential shear and tension failure, and eventually form a natural 'rock arch' at the boundary of the plasticity zone.
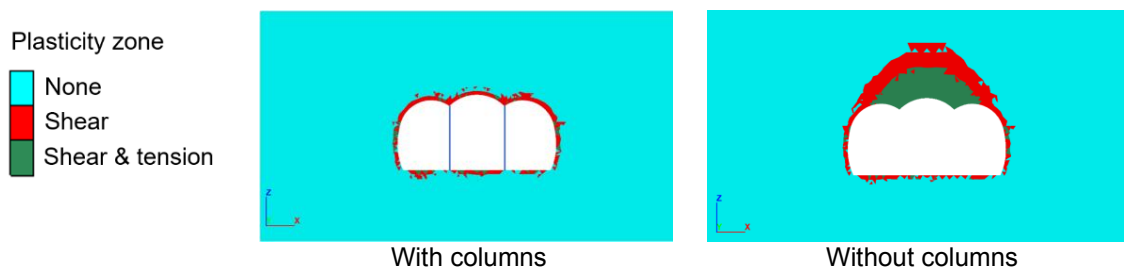
Figure 5. Comparing of rock mass plasticity zone: with columns vs without columns

Also, the effect of longitudinal column spacing (S) are being studied (Figure 6). By changing the column spacing, the total number of columns will also change. From the results in Figure 6, it is noticed that when the column spacing is greater than 6 m, arching zone of plasticity is also shown at longitudinal section, similar to the arching zone for cross-sectional section without columns. Hence, the central crown area (from Figure 4) and the region in-between columns at longitudinal direction (from Figure 5) are identified as key reinforcement area. To evaluate this hypothesis, four different ground supporting plans has been developed, which include:

- 3G30Sc : Control group, no extra reinforcement but only 30 cm shotcrete lining, E = 3 GPa
- 15G60Bm: 2m wide lining reinforcement (60 cm thick, E = 15 GPa) right above each role of column.
- 15G60Cr: Entire central crown reinforcement (60 cm thick, E = 15 GPa)
- 30G120Cr: Extreme case, very strong entire central crown reinforcement (120 cm thick, 30 GPa)

The efficiency of these ground supporting plans is evaluated by following factor:
Efficiency = Column load / S
Where Column load is the total load on one single column, S the longitudinal spacing between columns. The illustration of the four supporting plans and results of their efficiencies are presented in Figure 7.
For a high efficiency supporting plan, more load is taken by columns which will results in a higher value of Column load/S, and less load is taken by the rock mass itself thus ensures better ground stability; for a low efficiency supporting plan, less load is taken by columns which will results in a lower value of Column load/S, and more load will be taken by the rock mass itself which increase chances of rock mass failure (increased area of plasticity zone in modelling results). From results in Figure 7, it is noticeable that generally there is a great improvement of supporting efficiency when the central crown is reinforced. Also, 15G60Bm and 15G60Cr have almost identical results, which suggested the lining right above the columns are the most critical region. Furthermore, even though 30G120Cr has a huge increase in strength and thickness, the improvement of supporting efficiency is not very significant.

PROCEEDINGS OF THE 14TH ANZ YOUNG GEOTECHNICAL PROFESSIONALS CONFERENCE
14YGPC ROTORUA, NEW ZEALAND, 2ND – 5TH NOVEMBER 2022

101
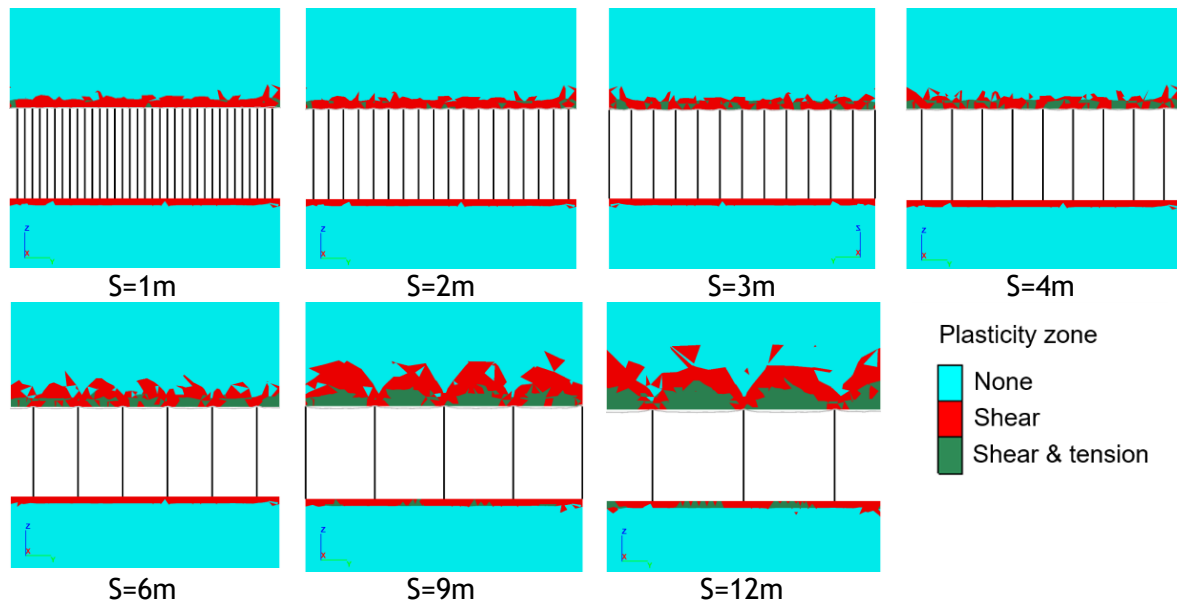
Figure 6. Effects of column spacing on rock mass plasticity zones, results taken from longitudinal section along the columns.
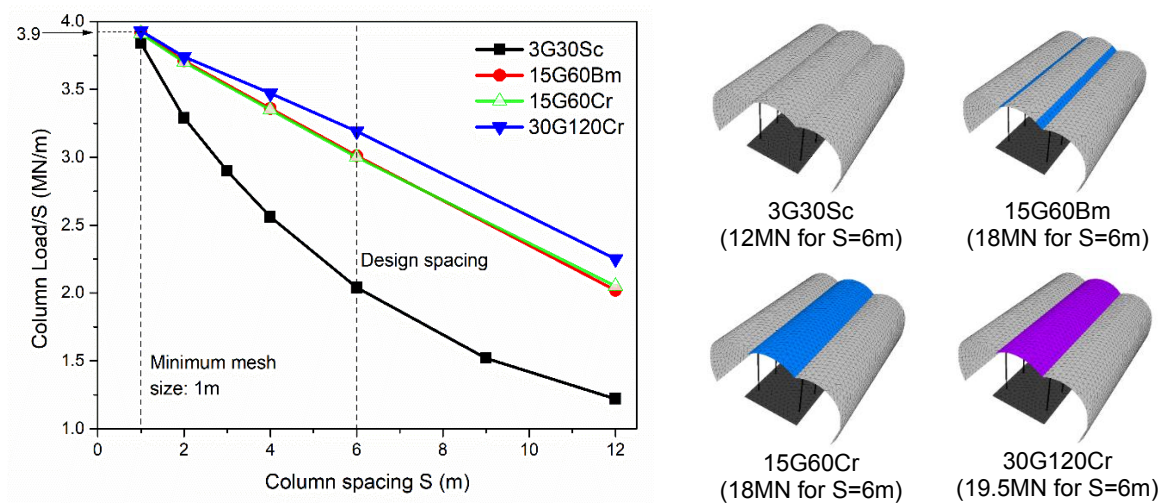
Figure 7. Illustrations of supporting plans and their modelling results for supporting efficiency.

3.2 Load transferring mechanism for tri-arch cavern

Based on results presented and discussed in Section 2.2, a load transferring mechanism is developed for tri-arch cavern, which is presented in Figure 8. It is concluded that the most significant load transferring mechanism taken place at the part of lining right above columns. The reinforcement of that part of lining will provide extra tensile restrain to the rock mass, thus limiting the deformation of rock mass and lining, resulting in higher load in the strong steel columns, and increasing the overall supporting efficiency.

(a) Central crown not reinforced   (b) Central crown reinforced
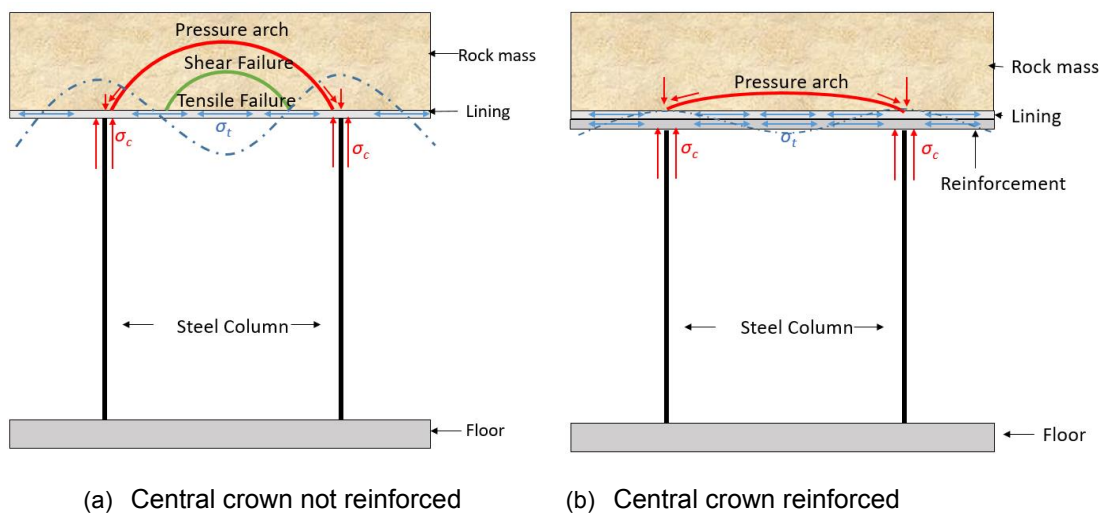
Figure 8. Illustration of load transferring mechanism between lining above columns and steel columns

By the time of submission of this paper, the primary support construction and monitoring of State Library Station has been completed. The actual steel column consists of six parallel steel elements and strain gauges are used to monitor the load on each single element. There is an extra "downstand beam" used as reinforcement between columns in longitudinal direction. From monitoring results, the load on each single element varies from 1.7 MN to 3.3 MN, which means for one column (six elements) the load varies from 10.2MN to 19.8MN. The modelled results are 12MN (3G30sc), 18MN (15G60Bm and 15G60Cr) and 19.5 MN (30G120Cr), which are highly comparable with the monitoring data. The presence of geological structure and uneven ground may have caused the uneven distribution of column loads.

4. CONCLUSION

In this paper, the supporting mechanism of tri-arch cavern is being evaluated using 3D numerical modelling approach. The modelling results are very comparable to monitoring results. The key findings of this paper include identifying the central cavern crown as the critical structure, proposing a load transferring mechanism between different structures and suggesting the major supporting mechanism to be providing tensile restrain to surrounding rock mass. The findings from this paper provide supplements to the supporting mechanism of such caverns/tunnels, which can used as design theoretical basis for future projects.

REFERENCES

Cao, L., Fang, Q., Zhang, D. and Chen, T. (2018). "Subway station construction using combined shield and shallow tunnelling method: Case study of Gaojiayuan station in Beijing". Tunnelling and Underground Space Technology, 82, 627-635.

Itasca. (2022). "FLAC3D 7.0 Documentation". URL: http://docs.itascacg.com/flac3d700/contents.html

Lai, H., Liu, M., and Xie, Y. (2011). "Study of Surrounding Rock Pressure Characteristics of Shallow Excavation Three-arch Metro Tunnel in Loess Region. Chinese Journal of Rock Mechanics and Engineering, 30, 9.

Lee, J.K., Yoo, H., Ban, H. and Park, W.-J. (2020). "Estimation of Rock Load of Multi-Arch Tunnel with Cracks Using Stress Variable Method." Applied Sciences, 10.

Matsuda, T. (1998). "Ground behavior and Settlement control of twin tunnels in soil ground" Tunnels and Metropolies, 1193-1198.

Yan, Q., Zhang, C., Lin, G. and Wang, B (2017). "Field Monitoring of Deformations and Internal Forces of Surrounding Rocks and Lining Structures in the Construction of the Gangkou Double-Arched Tunnel—A Case Study." Applied Sciences, 7.

Yoo, C. and Choi, J. (2014). "Three-Arch Tunnel Behavior – 3D Numerical Investigation." The 2017 World Congress on Advances in Structural Engineering and Mechanics (ASEM17). Ilsan (Seoul), Korea.

Zhu, Z.-G., Chen, M.-Z. and Sun, M.-L. (2019). "Calculation method of pressure of surrounding rock on double-arch road tunnel." Journal of Chang'an University (Natural Science Edition), 30, 4.

PROCEEDINGS OF THE 14TH ANZ YOUNG GEOTECHNICAL PROFESSIONALS CONFERENCE
14YGPC ROTORUA, NEW ZEALAND, 2ND – 5TH NOVEMBER 2022

103

Auckland Regulatory Review of Excavation Induced Ground Settlement

K. Lee[1], BA, BSc (Hons), MSc

[1]Auckland Council, Level 8 135 Albert Street, Auckland City 1010; PH (09) 301 0101; email: jin.lee@aucklandcouncil.govt.nz

ABSTRACT

Auckland is experiencing a surge in land development including high levels of intensification. As a result of intensification, developments involving deep excavations and both temporary and permanent retaining measures are more common. Where excavations are undertaken, ground settlement around the excavation can occur and is often caused by the combined effects of consolidation due to dewatering and mechanically induced settlement behind retaining structures.

The effects of combined settlement are the most critical where excavations are undertaken close to site boundaries, near existing structures and infrastructures. If not appropriately managed or designed, damage can occur and result in unforeseen costs for remediation and legal actions. Consequently, to understand and assess the effect of deep excavations, consolidation due to dewatering and mechanically induced settlement behind temporary and permanent retaining structures have been the subject of more focus by geotechnical specialists and Auckland Council.

Auckland Unitary Plan chapters E12 (Land disturbance - District) and E7 (Taking, using, damming and diversion of water and drilling) provide regulatory requirements for an assessment of effects as a result of ground settlement. This paper explores how consolidation and mechanically induced settlement are geotechnically assessed to fulfil these requirements in Auckland.

Keywords: regulatory requirements, resource consent, consolidation, mechanical settlement

1 INTRODUCTION

Auckland, like many other cities and towns around New Zealand, has been experiencing a significant increase in land development and intensification. As land becomes more costly to acquire, there is an incentive for land developers and homeowners to develop vertically and close to site boundaries to maximise the land available. This can also require trenching works for underground services which can be of significant depth. Consequently, developments with deep excavations are becoming more prevalent.

Deep excavations usually require significant retaining structures and often extend below groundwater level. This can result in ground settlement around the area of excavation because of mechanically induced settlement behind retaining structures and consolidation in areas where the excavations intercept groundwater levels and require a groundwater take (the removal of groundwater as part of land drainage) and/or diversion (rerouting groundwater flows). The settlement can cause neighbouring structures and services to be displaced, rotated and damaged. The severity of settlement is determined by the nature of the underlying geology (including its consolidation history and yield stress) the depth of excavation, the design of the proposed retaining structures, extent and depth of dewatering, and the proximity of the excavation to any nearby structures and services.

To manage the hazards of ground settlement associated with deep excavations, Auckland Council (Council) uses the Auckland Unitary Plan (AUP) chapters, E12 (Land disturbance - District) and E7 (Taking, using, damming and diversion of water and drilling) to provide a framework for the regulatory requirements and assessment of effects as a result of ground settlement.

2 REGULATORY FRAMEWORK AND REQUIREMENTS

The AUP provides two chapters which include sections addressing the potential for ground settlement induced effects within and off site – E12 and E7. Chapter E12 addresses district land disturbance under section 31 of the Resource Management Act 1991 (RMA) and Chapter E7 covers regional effects because of take or diversion of groundwater under section 14(1) and (3) of the RMA.

The RMA classifies activities into different classes as permitted, controlled, restricted discretionary, discretionary, non-complying and prohibited. These activities increase with Council discretion and

potential effects on the environment. Each category determines the criteria and level of assessment that Council considers as part of the consenting process and the nature of the conditions which may be imposed on the on any granted consent.

- Permitted activities do not require a resource consent; however, it may be needed to demonstrate compliance with general rules to show that the activity meets the requirements. If the activity exceeds permitted activity standards, it requires a resource consent and may be classed as a controlled, restricted discretionary, discretionary, or non-complying.
- Controlled activities typically are in keeping with the existing environment and anticipated effects are well understood and able to be mitigated by conditions. Therefore, controlled activities will be granted; however, Council may impose conditions of consent subject to the controlled activity status. If the activity exceeds the controlled activity standards, it may be considered as restricted discretionary.
- Restricted discretionary activities may be granted or refused and there is increased scope of discretion for assessment by Council relative to permitted and controlled activities.
- Discretionary activities allow Council to undertake a full assessment of relevant AUP provisions. This includes the restricted discretionary activity considerations.
- Non-complying activities are assessed by Council to determine if its adverse effects on the environment will be no more than minor or contrary to the objectives and policies of the AUP.
- Prohibited activities or proposals are expected to cause significant adverse effects on the environment which cannot be mitigated by conditions of consent, therefore will not be able to attain a resource consent without redesign to a lower activity status.

2.1 E12 (Land disturbance - District)

Any activity involving earthworks, irrespective of the area and volumes, must comply with E12.6.2 General Standards including E12.6.2(2) and E12.6.2(3) in the AUP. This includes the consequences of earthworks on neighbouring land or services.

This can include earthworks undertaken in a residential zone which are greater than 500 m^2 and/ or 250m^3. If the activity is found to be restricted discretionary, the Council has slightly different assessment criteria under E12.7.2(1)(c), E12.8.2(1)(c) and (j); however, the effects of instability on land, structures, and services remain critical to E12 assessment. One difference between the general standards and restricted discretionary, controlled or discretionary activity scope is that Council is no longer limited to the effects at or beyond the boundary of the property and assessment onsite can also be considered.

2.2 E7 (Taking, using, damming and diversion of water and drilling)

The requirement for a groundwater take or diversion can occur when excavations are at a depth which intercepts groundwater. The removal or diversion of groundwater from draining, piping or obstructing the flow of groundwater can trigger the requirement for a new regional consent issued under Chapter E7 rules, known as a water permit.

Any permitted activity must comply with E7.6.1.6 and E7.6.1.10 for the take and diversion of groundwater caused by an excavation. Excluding the items in E7.6.1.10(1), the activity must abide by the parameters outlined in E7.6.1.10(2) - (6). This includes the area of excavation, changes to groundwater levels, the duration of the water take/diversion and proximity to existing structures, other groundwater takes and sensitive overlays. Further, if the activity is permitted under E7.6.1.10, it must also meet the requirements in Section E7.6.1.6 for groundwater controls.

If found that the proposed deep excavations are not permitted, then Council has discretion to assess the consent in more detail under E7.8.2(4) and (10), including means of how the effects of groundwater induced settlement can be reduced on structures and services and requirements for monitoring.

The effects can therefore be generally segregated to mechanically induced settlement as a result of retaining wall deflection (under E12) and consolidation induced settlement as a result of dewatering (under E7). The conditions of consent (discussed below) can therefore be similar, as both Chapters are managing the effects of ground settlement, although serving different components of the RMA.

3 CONDITIONS OF CONSENT

Conditions of consent are regulatory tools used by Council to manage the risk of anticipated adverse effects on the environment and aid in certainty of outcomes expected as part of the Resource Consent process. Upon issue of a Resource Consent, conditions are included which adhere to the discretion

PROCEEDINGS OF THE 14TH ANZ YOUNG GEOTECHNICAL PROFESSIONALS CONFERENCE
14YGPC ROTORUA, NEW ZEALAND, 2ND – 5TH NOVEMBER 2022

105

under the AUP and may include conditions offered by the applicant following Section 108AA of the RMA. Common conditions of consent are discussed below to manage excavation induced ground settlement.

- **No instability offsite**

A condition of consent is included to ensure that should instability occur, it is rectified by the consent holder. This provides clarity around responsibility for potentially affected parties.

- **Supervision of Works**

Geotechnical reporting often includes recommendations for supervision or monitoring of works during earthworks and construction of geotechnical structures such as any retaining, counterfort drainage and foundations. This is considered standard practice as it serves not only for the geotechnical specialists to verify their ground conditions and assumptions but also to complete a producer statement and geotechnical completion report if required as part of project progression.

Supervision of works should be undertaken by a geotechnical specialist who is familiar with all geotechnical reporting, recommendations, engineering plans and codes of practice to ensure that the site is appropriately managed and supervised.

- **Settlement Monitoring Contingency Plan**

Predicting and then monitoring the effects of ground settlement form part of sound practices to reduce costly surprises and potential damage to property.

A Settlement Monitoring and Contingency Plan (SMCP) or Groundwater and Settlement Monitoring and Contingency Plan (GSMCP) are common means of managing the effects of ground settlement. The conditions including the settlement and groundwater monitoring, monitoring of the wall's deflection, screening of any potentially affected structures, services etc., visual inspections, surveys undertaken pre-, during and post-construction and remediation of any damages which may occur. This is supplemented with alert and alarm levels which are necessary to align observations and stipulate any contingency measures to be undertaken. The frequency of monitoring can be varied depending on the expected rates of movement, findings of the survey and subject to discussion between the geotechnical specialist and Council.

Monitoring is a useful tool to limit the effects of ground settlement, however, should not be relied upon as a standalone means of mitigation. SMCP and GSMCP are accompanied with other conditions or evidence to support management of deep excavations, such as a detailed construction methodology.

- **Detailed Construction Methodology**

While good structural design can minimise the effect of ground settlement, it cannot guarantee that some settlement will not occur. For the purposes of a Resource Consent only preliminary retaining wall design is required, as detailed design forms part of Building Consent processes. To provide flexibility with design and construction and account for available plant machinery and contractor experience, Council may accept that a detailed construction methodology is provided prior to the commencement of works onsite. This document should be written by or endorsed in writing by a Chartered Engineering Geologist or Chartered Geotechnical Engineer.

4   TYPICAL GEOTECHNICAL ASSESSMENT OF EFFECTS

Geotechnical specialists identify and assess geohazards and constraints in relation to land development. For deep excavations, this typically includes undertaking an assessment to quantify the level of anticipated total ground settlement, followed by an assessment of effects on surrounding land, structures, and services.

This can be effectively illustrated through a plot showing settlement, distance and any structures and services which may be affected. If it is found that the degree of settlement and potential damage are unacceptable, further protection measures are explored to reduce the risk. This is typically undertaken by reducing the scale of or relocating the excavation, changing the construction methodology or altering the preliminary retaining design e.g. top-down construction methodology, increasing retaining wall stiffness etc., such that the effects are considered acceptable or within the tolerable thresholds for the potentially affected structure or service.

The geotechnical specialist defines and justifies the parameters and assumptions used in their assessment. This includes the geotechnical parameters of soils subject to ground settlement, groundwater levels and regime, the excavation depths, any surcharges applied and preliminary retaining wall design and construction. Any chosen parameter should be representative of site conditions and be substantiated with intrusive testing and site observations to ascertain the ground model and potentially affected structures and services.

4.1 Mechanical Settlement Assessment

Mechanical settlement assessment can be undertaken using empirical methods, such as Clough and O'Rourke (1990), semi-empirical methods, e.g. WALLAP calculations of the wall deflection, numerical methods using finite elements analysis or other techniques.

Cases in which empirical data may be appropriate to be relied upon are those where the risk or the consequences of settlement are low e.g. smaller excavations and limited structures proximal to the excavation. Care should be taken when relying on empirical data and considerations given to underlying assumptions, applicability to Auckland geology, proposed retaining methods and any site constraints. In medium and higher risk cases, where excavations are significant, located close to existing structures, services or site boundaries, modelling software may be more suitable to verify empirical calculations and confirm the anticipated settlement with distance from excavation.

Common assumptions around the effects of ground settlement are often presented but are lacking in the context of the proposed works. The assumption that the effects are limited only up to a distance from the excavation equal to the height of the retaining wall is incorrect. Work undertaken by Clough and O'Rourke (1990) and Wang et al (2010) revealed that the influence zone of ground settlement effects can be found up to a distance of 2 – 3.5 times the retained height. Therefore, excavation depth is not the only parameter to affect the extent of the settlement influence zone. Ground deformation is generally greatest within a distance of approximately 0.5 times or equal to the retained height (Ou et al., 1993 and Moorman 2004); however, in soft soils, this can be up to two times the retained height (Moormann, 2004).

The shape of ground deformation can differ depending on the subsurface material, the type of retaining and its support system (see *Figure 1* below). The work undertaken by Hsieh and Ou (1998) reports that spandrel type ground settlement is attributable to sandy materials and stiff clays and produces the greatest ground settlement next to the retaining wall. Conversely, concave type ground settlement is attributable to soft clays, such as those found in recent marine muds. Cumulative movement can occur, initiating with spandrel type movement, then incremental deep inward movement with time and excavation depth. Therefore, the geometry of ground deformation can exhibit cantilever and deep inward movement characteristics as part of total horizontal displacement and ground settlement.
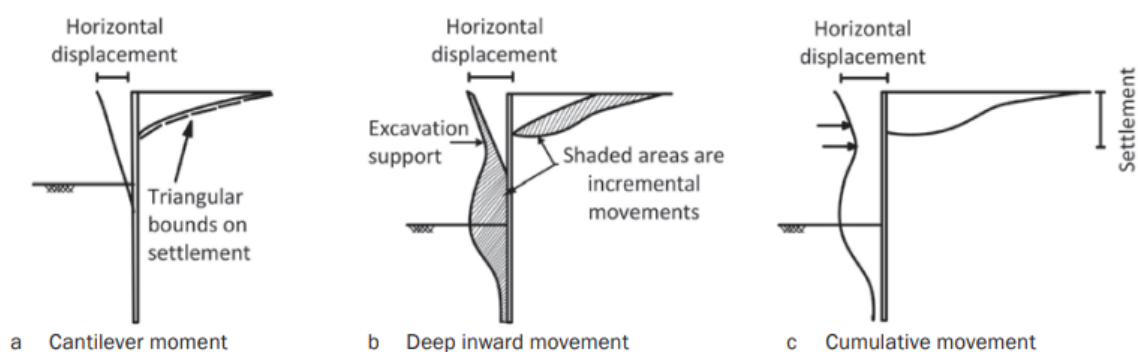
Figure 1. Typical ground settlement deformation as a result of retaining wall deflection and with time. (a) occurs with initial retaining wall construction can cause a spandrel type cantilever movement. As excavation continues with depth, excavation support is provided creating (b) deep inward movement occurs with incremental total settlement in a concave type ground settlement. Following the combination of (a) and (b) the cumulative movement and ground settlement shape is exhibited (c) and may vary depending on whether spandrel or concave type settlement was more dominant (CIRIA C760).

PROCEEDINGS OF THE 14TH ANZ YOUNG GEOTECHNICAL PROFESSIONALS CONFERENCE
14YGPC ROTORUA, NEW ZEALAND, 2ND – 5TH NOVEMBER 2022

107

4.2 Groundwater Drawdown and Settlement Assessment

The method of analysis used should be proportionate to the complexity of the geological and hydrogeological conditions including historical groundwater regimes and the nature and extent of the proposed groundwater take and diversion. In order to apply appropriate parameters, onsite intrusive testing and groundwater level monitoring is typically required. At a minimum, Council requires onsite intrusive investigations to at least the depth of anticipated excavation and the monitoring of groundwater levels e.g. dip test or automatic loggers at least 3 times over a 3 week period following drilling. If possible, groundwater level monitoring over a number of months is preferred to capture any seasonal variations. Deviations from this process will require justification from the applicant and subject to Council review under E7.

In complex conditions, numerical methods allow for finite element or finite difference analyses and models for consolidation and groundwater effects e.g. PLAXIS. These can provide insight in the ways which soils perform when undergoing consolidation settlement in three dimensions. Granular soils are typically more permeable and resistant to ground movements as a result in changes to pore water pressure and effective stress, in comparison to cohesive soils. Cohesive, soft soils such as alluvial clay and silt in Puketoka Formation soils can exhibit large consolidation settlement over time. Consolidation settlement can be complex and varies with subsurface geology. It is particularly sensitive to soil permeability and varying thicknesses and lithologies which can persist in unknown geometries below structures and services even in what is anticipated to be homogeneous material of uniform thickness. Numerical analyses can provide a high level of detail in their outputs, but their value is restricted by the input parameters. Where insufficient or questionable information is available, the outputs may not be reflective of consolidation effects and behaviour and should be treated with scrutiny (CIRIA 750).

Where the geologic setting is simpler, consolidation calculations can use analytical methods to estimate the time for groundwater drawdown. Analytical methods use a mathematical model to represent the geology and many assume a single value of permeability and assess flows in two dimensions in cross section e.g. Bear (1979) and Terzaghi and Peck (1948). With deep excavations, plane flow systems are commonly assessed, capturing the length of the excavation and radial flows at the corners of the excavation. This can be used to predict anticipated groundwater flows and settlement at the locations of any structures and/or services which may be affected.

Consolidation settlement may not be as significant contributor to total settlement in comparison to mechanical settlement, however, forms part of the total settlement effects.

4.3 Assessment of Effects

Assessment of effects is a description of all the environmental effects that an activity may impose on the environment. For ground settlement, this includes all anticipated adverse effects as a result of the excavation, temporary and permanent supports and the retaining wall construction process on adjacent properties, land, structures and services. The level of assessment should be equivalent to the risk and be undertaken in collaboration with Geotechnical and Structural Engineers. The assessment should include all potentially affected existing properties, structures and services, the maximum allowable horizontal deformation and induced total and differential settlement behind temporary and permanent supports to maintain serviceability of affected structures and services.

The assessment of effects can include empirical comparisons which classifies potential damage to a building into different categories of damage, based on estimated total settlement. One of the methods introduced by Burland (1995) is the Burland Scale, which is commonly used by geotechnical specialists. The Burland Scale groups building damages into aesthetics, serviceability and stability. These factors are all relevant when considering the effects of ground settlement in a regulatory assessment.

There are assumptions associated with using the Burland Scale that limits its use, but which are often overlooked. This includes the assumption that buildings have not endured any damage prior to ground settlement. In cases where a structure has historically endured damage or is a heritage building (and over 100 years old), relatively small ground settlement levels may result in more severe damage which may not be anticipated (Portugal et al. 2005). Therefore, considerations need to be made to the existing condition of any potentially affected structures or services.

Ground settlements occur behind the retaining wall and due to the groundwater drawdown generally reduces with distance from the excavation. The greatest ground settlement is expressed at the ground

surface; therefore, shallow foundations and paved surfaces commonly exhibit more obvious signs of cracking and damage. Underground services usually endure less ground settlement, being located at depth. That being said, underground services in Auckland include those of brittle construction type, such as clay, which can crack impairing serviceability, if the ground surrounding them is displaced. Therefore, consideration needs to be made for the age, condition, location, depth and construction type of structures and services.

5 CONCLUSION

There is an increase in deep excavations in Auckland to support land development and intensification. As a result of this trend, there is also increased risk of ground settlement.

AUP Chapters, E12 and E7 provide the regulatory requirements which Council uses to undertake an assessment of effects resulting from ground settlement. The discretion for assessment and conditions imposed on a Resource Consent is determined by the activity class and information provided by the applicant.

There are a number of methods which can be used to predict ground settlement. The chosen assessment approach should be proportionate to the level of risk and appropriate for the complexity of the geological and hydrogeological conditions. Once the mechanical, consolidation and total settlements have been quantified, an assessment of effects should be undertaken in collaboration with a geotechnical specialist and structural engineer. The effects of endured ground settlement should include potentially affected structures and services on neighbouring properties, their age, condition, location, depth and construction.

6 ACKNOWLEDGMENTS

REFERENCES

Bear, J. (1979). *Hydraulics of Groundwater*. New York: McGraw-Hill.

Burland, J. B. (1995). Assessment of risk of damage to buildings due to tunnelling and excavation. *Earthquake geotechnical engineering (3)*, 1189-1202.

Clough, G. W., & O'Rourke, T. D. (1990). Construction Induced Movements of Insitu Walls . *Design and Performance of Earth Retaining Structures*, 439-470.

Council, A. (2022, June 23). *Auckland Unitary Plan Operative in Part*. Retrieved from Auckland Council:
https://unitaryplan.aucklandcouncil.govt.nz/pages/plan/Book.aspx?exhibit=AucklandUnitaryPlan_Print

Gaba, A., Hardy, S., Doughty, L., Powrie, W., & Selemetas, D. (2017). *Guidance on embedded retaining wall design (C760)*. CIRIA.

Hsieh, P.-G., & Ou, C.-Y. (1998). Shape of ground surface settlement profiles caused by excavation. *Canadian Geotechnical Journal 35(6)*, 1004-1017.

Moormann, C. (2004). Analysis of Wall and Ground Movements Due to Deep Excavations in Soft Soil Based on a New Worldwide Database. *Soils and Foundations 44(1)*, 87-98.

Ou, C.-Y., Hsieh, P.-G., & Chiu, C.-C. (1993). Characteristics of ground surface settlement during excavation. *Canadian Geotechnical Journal 30*, 758-767.

Portugal, J. C., Portugal, A., & Santo, A. (2005). Excavation induced building damage . *Proceedings of the 16th International Conference on Soil Mechanics and Geotechnical Engineering*. Millpress Science Publishers/IOS Press.

Preene, M., Roberts, T. O., & Powrie, W. (2016). *Groundwater control: design and practice (second edition) (C750)*. CIRIA.

Terzaghi, K., & Peck, R. B. (1948). *Soil Mechanics in Enigneering Practice* . New York: Wiley.

Wang, J. H., Xu, Z. H., & Wang, W. D. (2010). Wall and Ground Movements due to Deep Excavations in Shanghai Soft Soils. *Journal of Geotechnical and Geoenvironmental Engineering 136(7)*, 985-994.

PROCEEDINGS OF THE 14TH ANZ YOUNG GEOTECHNICAL PROFESSIONALS CONFERENCE
14YGPC ROTORUA, NEW ZEALAND, 2ND – 5TH NOVEMBER 2022

109

PRACTICAL CULVERT DESIGN OBSERVATIONS IN QUEENSLAND

Dominic R. Jones[1] and Nicholas G. Lancashire[2]

[1]Jacobs Group (Australia) Pty Ltd, 32 Cordelia Street, South Brisbane, QLD 4101, PH +61490351802;
email: dominic.jones@jacobs.com
[2]Austserve Pty Ltd, PO Box 2623, New Farm, QLD 4005, PH +61424952343;
email: nlancashire@aseng.com.au

ABSTRACT

Buried underground drainage structures are used to satisfy the hydraulic requirements of a given site/environment and are typically manufactured of reinforced concrete. With the improvement of culvert inspection technology incorporating robotic camera inspection post installation, discovery of cracked culverts has been an increasing issue. Reinforced concrete pipe culverts are known to crack for various reasons including transport, handling, placement, backfill, foundation quality and vehicle over-loading during construction. A culvert's vulnerability to be adversely affected by these conditions can be a function of its design, particularly associated with installation conditions and strength class. This review focuses on these aspects from a geotechnical and structural perspective, for reinforced concrete culverts of rubber ring joint or flush joint type, with outside dimension greater than 375mm. The review highlights how the current culvert design process occurs and provides geotechnical and structural insight around the importance for designers to have a good working understanding of AS 5100.2:2017 and AS/NZS 3725:2007. Reference is also made to Queensland Road authority 'Transport and Main Roads' (TMR) Technical Specifications where modification to the Australian Standards has been made. The review also assesses, using finite element analyses, the accuracy of published methods used to determine vertical load from vehicle loading and soil overburden, and demonstrates how these findings may be relevant to the broader Australian and New Zealand region. Practical insights and suggestions on how analysis, selection of appropriate culvert class and detailed design information can be improved are also discussed.

Keywords: RCP, Culvert Cracking, Culvert Design Loading

1 INTRODUCTION

Common industry practice for calculation of concrete pipe culvert class in Queensland (QLD) continues to involve the use of design software 'Pipeclass' developed by the Concrete Pipe Association of Australasia (CPAA). On 19th August 2019, the State Road Authority for QLD, the Department of Transport and Main Roads (TMR) distributed a letter to detailing that CPAA Pipeclass software was not suitable for use on TMR projects based on the following information:

- The Road Drainage Manual (RDM) requires pipes to be designed in accordance with AS/NZS 3725, using the load distribution through fill from AS 5100.2.

Main Roads Technical Specification (MRTS) MRTS25 concurs with the RDM and specifies certain construction loads.
There are three Australian / New Zealand standards that designers need to have a working knowledge of for the design of reinforced concrete pipes:

- AS/NZS 3725 (2007) [Design for installation of buried concrete pipes].
- AS/NZS 4058 (2007) [Precast concrete pipes (pressure and non pressure)].
- AS 5100.2 (2017) [Bridge design loading standard, design load].

Additionally, for Transport and Main Roads (TMR) projects in Queensland, Technical Specification MRTS25 (January 2018) [Steel Reinforced Precast Concrete Pipes] provides further criteria over and above that outlined in the standards that designers are required to consider and design for.

The aim of this paper is to provide commentary on design for culvert class in Queensland, and highlight issues when navigating commonly used software and the Australian Standards that are applicable.

2   LIVE LOAD DISTRIBUTION THROUGH FILL

2.1   AS/NZS 3725 as augmented by AS 5100.2

Reinforced Concrete Pipes (RCP) are designed in accordance with AS/NZS 3725 with the exception that, in QLD on State Road projects, the method to calculate live load through fill is to be deleted (Clause 6.5) and replaced with the relevant AS 5100.2 method. There is a significant difference between the magnitude of the live loads calculated using the two methods. AS 5100.2 tends to result in the live loads being the governing load case for low cover scenario. To highlight this, Table 1 presents a comparison between the two methods with a first principles comparison using the Boussinesq Equation for live load distribution.

Table 1:   Live load distribution through fill comparison (Truck and Dog)

	AS/NZS 3725 method	AS 5100.2 method	Boussinesq Eq.
Wheel contact area at surface	$0.08 \ m^2$	$0.08 \ m^2$	$0.08 \ m^2$
Pressure[a] at surface	750 kPa	750 kPa	750 kPa
Calculated distribution area at 500 mm depth	$1.04 \ m^2$	$0.57 \ m^2$	N/A
Calculated pressure at 500 mm depth	57.7 kPa	105.3 kPa	93.5 kPa

[a] Dynamic load allowance not considered

As illustrated in Table 1, for this scenario the pressure calculated using AS 5100.2 is approximately 83% greater than that using AS/NZS 3725. Hand calculation checks using the Boussinesq equation were completed for comparative purposes with the pressure at 500 mm depth shown to be 93.5 kPa. Therefore, AS 5100.2 remains the governing method.

Notably, the difference between methods reduce as cover is increased and dead load becomes the critical load component. On this basis, designing in accordance with MRTS25, under shallow cover scenarios (during construction and shallow pavement subgrades), will likely be the most critical case.

3   DESIGN CONSIDERATIONS

3.1   Haunch And Bedding Zone

Correct design selection and site installation of the haunch and bedding material are critical to the performance of a buried RCP. The bedding layer serves to evenly distribute vertical pressure with the ground's reaction at the base of the pipe. A properly performing bedding layer will improve the functional life of the RCP by evenly distributing stresses in the pipe wall that could otherwise become concentrated, leading to increased risks of a variety of concrete cracking phenomena to occur (e.g. radial shear).

The importance of appropriate selection of the bedding material type on the culvert's structural performance is recognised under AS/NZS 3725. For calculation of load on a RCP at a given depth, determining the appropriate bedding factor to apply during design is critical. By virtue of the soil/structure interaction, RCPs can carry a greater vertical load buried in-situ than they could above ground. The distribution of load that occurs through the haunch zone most significantly impacts the load carrying capacity of the pipe. However, in determining a culvert's structural capacity (defined as 'class'), an above ground/unsupported three-edge bearing test is used to calculate the proof and ultimate load values. To account for the improvement in capacity of a buried RCP, the bedding factor serves to bridge analytically the relationship between the two different service conditions.

AS/NZS 3725 standard drawings include an uncompacted middle third bedding detail whereas TMR standard drawings (e.g. Standard Drawing 1359) do not. Loosely placed, uncompacted bedding directly under the invert of the pipe significantly reduces pipe stress concentrations. The intent is to allow a small amount of displacement to create a cradling effect that achieves an even load distribution along the longitudinal component of the culvert in the supportive spring zone, increasing the effectiveness of the haunch support. Incorrect compaction of the middle third or use of certain unsuitable material types in

PROCEEDINGS OF THE 14TH ANZ YOUNG GEOTECHNICAL PROFESSIONALS CONFERENCE
14YGPC ROTORUA, NEW ZEALAND, 2ND – 5TH NOVEMBER 2022

111

this zone can increase a risk of uneven load distribution, increasing likelihood of asymmetrical loading with circumferential or longitudinal cracking or other failure mechanism.

MRTS04 permits the following material types for bedding and haunch zones:

- well graded sand (in accordance with grading limits set by MRTS).
- 20 mm nominal free draining granular material.
- 10 mm nominal free draining granular material.

Success achieving a uniform and evenly distributed support using these materials is variable. There are constructability issues placing a well graded sand in a confined excavation and achieving compaction in the side zones while leaving a loose middle third that is level enough to provide even support across each cell. Commonly, contractors will use a single sized stone that is faster to place and eliminates compaction testing. Care must be taken when using 10mm stone to ensure it is a true screened high quality quarry product, free of fines (for example – decomposed granite) that can wash during high water table episodes, resulting in inadequate support.

3.2 Bedding Factor

In accordance with AS/NZS 3725, there are two Bedding Factors used in the calculation of the proof load (T_c):

- F, for fill and superimposed dead loads.
- Fq, for live loads.

The live loading Bedding Factor (F_q) is limited to 1.5 on the basis that it has been proven to be almost independent of the support type in a shallow cover live load scenario. The dead load Bedding Factor (F), ranges between 1 and 4 depending on the type of support selected.

Bedding Factor selection has significant bearing on the combined actions to be assessed against a culvert's proof load. AS/NZS 3725 allows for a denominator for Bedding Factor of up to 4 depending on the designer's assessment of the reliability of the bedding material and installation of the culvert. The authors' note that caution should be applied in the consideration of the appropriate Bedding Factor to utilise given the magnitude of the impact to loading it can have.

Where backfill grading does not meet AS/NZS 3725 requirement, there are penalising factors that are applied to the Bedding Factor that directly increase load induced on an RCP. The Bedding Factors shall be reduced if the fill in the bed or haunch zones have a grading curve that falls outside the limits given in AS/NZS 3725, as follows:

- Where the fraction passing the 0.6 mm sieve is outside the limits, and is not cement stabilised, the Bedding Factor shall be 1.5.
- For material outside of the limits of other sieve sizes, any maximum Bedding Factor shall be reduced by 15%.

The designer should exercise caution when selecting a dead load Bedding Factor, giving due consideration for the type and availability of backfill material, what material grading is permitted in accordance with the project specification and therefore, what penalising factor may be applicable for design.

3.3 Bedding Installation

Non-uniform support of an RCP can be a function of improper bedding installation. In particular, the method of placement of spigot and socket cells (also known as rubber ring jointed culvert type) on bedding material is critical. To reduce the risk of a stress-strain concentration forming at the critical section just beyond the bell end of a RCP, the bedding material requires local modification to account for the change in pipe geometry, see **Figure 1** and **Figure 2**. This can be easily achieved via hand or shovel excavation of some bedding material local to the pipe bell such that there is an improved uniformity of support along the change in pipe geometry.
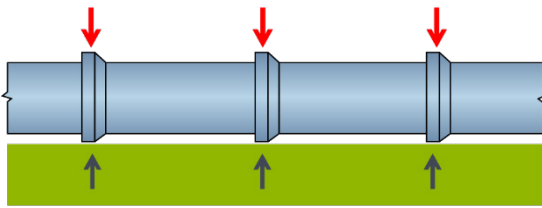
Figure 1: Incorrect bedding placement – no scuppering of material at bell end leading to stress concentration at critical zone (shear) beyond bell section
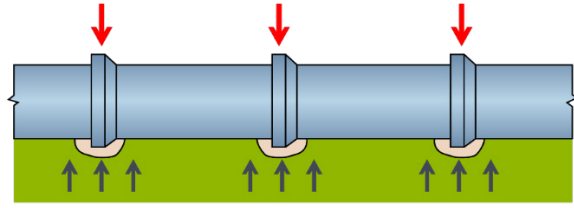
Figure 2: Correct bedding placement – scuppering of material at bell ends allowing for more even load dispersal at critical zone around bell end

It has been observed analytically that other vital considerations for installation of bedding material to yield in-field results comparable to calculated expectations include:

- (For trench installations) Careful excavation of the culvert trench line, with particular focus on not over excavating trench width, and the preparation of a smooth, homogenous base.
- Good preparation of the subgrade such that it is suitable for receiving an adjusted block load within the excavated trench zone. Typical ground preparation requirements include assessment of an influence zone, typically up to 1.5m beneath the culvert although this can be deeper depending on the ground conditions encountered and the type of culvert being installed, via dynamic cone penetrometer blow count assessment crudely converted to an estimated soil shear strength assessment, with typical acceptance ranges occurring between 50-100kPa (100-200 allowable bearing pressure at subgrade surface). Noting that it is vitally important the foundation is not 'over stiffened' (comparatively to the adjacent ground conditions) by excessive ground treatment.
- Properly confining the bedding material such that migration of bedding material away from the trench support zone does not occur. This is commonly and suitably achieved via introducing a geofabric/geotextile layer at the soil junction/excavation perimeter.

4   DISCUSSION

4.1   Finite Element Analysis Assessing the Impact of Ground Support Stiffness on Pipe Bending Moment

For working dead loads, the Bedding Factor is selected using AS/NZS 3725 Table 7 that considers varying bed / haunch zone depths and degrees of compaction in the backfill material. Generally, as depth of haunch zone increases along with the material's density, the Bedding Factor increases (up to a maximum of 4). The standard contends that as the stiffness of support is increased, the bending moment in the pipe is reduced and therefore can be subjected to higher levels of vertical stress. A PLAXIS 2D model was developed to demonstrate the importance of the bedding zone and to the resultant pipe bending moment, see **Figure 3** and **Figure 4**.
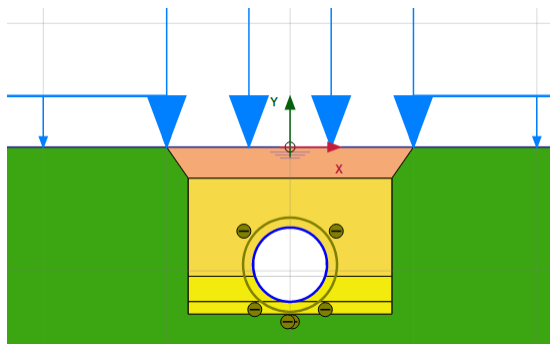
Figure 3: PLAXIS 2D Ground Model
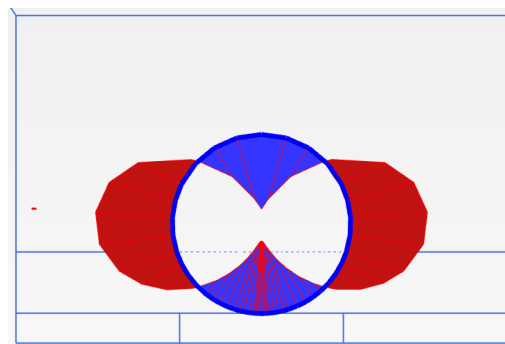
Figure 4: 600 dia. Pipe Bending Moment Diagram

Summary of findings:
- 50% reduction in bedding and haunch zone material stiffness results in a 15% and 9% increase to the bending moment and shear force, respectively.

- 50% asymmetrical material stiffness representing poor compaction on one side of the culvert and good compaction results in a 9% and 7% increase in bending moment and shear force, respectively.

Generally, there is agreement between the PLAXIS 2D assessment and AS/NZS 3725 that as density / stiffness of supporting material increases, the Bedding Factor utilised for working dead loads can be increased also, noting uniformity of support is critical.

4.2   Target Utilisation

Whilst it is structurally possible to design up to a Utilisation Factor of 1 (or 100% of proof load capacity), it is recommended designers target a lower Utilisation Factor with an appropriate risk adjusted value determined based on the consideration of a variety of factors. The authors are not aware of any publicly available design guidance for selection of an appropriate target utilisation as a percentage of proof load for RCPs. Based on anecdotal evidence collected in field, and sampling installation conformity with calculated design assumptions, it has been observed that a wide range of actual installation variables are present that would have a significant impact on a designer's assumed/calculated Utilisation Factor. **Table 2** presents a sensitivity assessment of a commonly observed as constructed variance in trench width excavation (trench installation technique) and the adverse (increased) impact this has on Utilisation Factor.

Table 2:   Sensitivity assessment of an as constructed variable – trench width – and its impact on the calculated utilisation factor in design (dead load assessment)

Culvert Size	+30% over excavation	Max Permitted Trench Width
450 (Class 6) *Impact to utilisation factor (averaged):*	1690mm *+2.50%*	1300mm *0.0*
600 (Class 6) *Impact to utilisation factor (averaged):*	2080mm *+10.86%*	1600mm *0.0*
1050 (Class 3) *Impact to utilisation factor (averaged):*	2730mm *+18.50%*	2100mm *0.0*
1200 (Class 3) *Impact to utilisation factor (averaged):*	2860mm *+10.63%*	2200mm *0.0*

Increase in utilisation beyond acceptable or pre-determined and assumed limits is one variable that can lead to cracking or other damage to the installed RCP.

4.3   Cracking in Concrete Culverts

RCPs are prone to cracking for various reasons, as a result of both design and non-design related actions including the aforementioned exceedance of utilisation for the culvert's designated loading class, transport, handling, placement, bedding (compaction, material grading, trench width), foundation quality (e.g. bearing capacity, expansive soils) and vehicle over-loading during construction. Culverts also crack when they approach proof load capacity. Per AS/NZS 4058:2007, the proof load capacity is determined by loading without developing crack width greater than the relevant test crack width (for example 0.25 mm). In other words, some types of cracking can be both expected and may be acceptable on a structural capacity and durability basis. Notwithstanding, MRTS25 mandates strict criteria for crack acceptability. Noting the various factors that cause cracking, it is not uncommon for crack widths to exceed limit criteria and require legitimate structural repair.

For determination of an appropriate utilisation percentage, designers may take a view that utilisation of 100% is acceptable given in some respects the proof load can be considered a serviceability case with the culvert having a greater ultimate capacity (ultimate capacity = 1.5 × proof load capacity). However, issues can arise when crack widths expected at 100% utilisation levels (e.g. test crack width) are classified as Type 2 defects and therefore are only acceptable after repair in accordance with MRTS25 Table 7(a). Further, there is no requirement to apply a loading Factor of Safety to AS/NZS 3725 calculations. To account for inherent variability in loading cand installation outcomes, a utilisation factor of 90% or less can offer an appropriate risk adjustment to the designer.

4.4 Culvert Inspection Technology

There is industry wide limitation with respect to the technology available that can be repeatably relied upon to provide accurate measurements of crack width. There is currently heavy reliance on operator experience, skill and judgement.

AS/NZS4058:2007 requires crack widths to be measured (and assessed) at 3 mm depth rather than at surface as is commonly undertaken from CCTV inspection. The only reliable and accepted method for achieving this is to physically insert various calibrated thickness feeler gauges into the crack to determine its width and depth. In most instances, confined space restrictions prevent this type of measurement being completed and the assessment is therefore commonly carried out via CCTV inspection with an estimate being made of crack width from photographic evidence by the CCTV robot operator. Notwithstanding, in accordance with AS/NZS 4058 Cl3.4.2.2, any crack greater than 0.10 mm (for cover ≤ 10 mm) is classified as a Type 2 defect and requires repair in accordance with MRTS25 Table 7(a). However, CCTV does not provide resolution to accurately measure width, and as such any observable crack is commonly reported discreetly as a crack less than, or greater than 1mm.

5 CONCLUSION

- Culvert supply, transport and handling, installation and construction loading are critical elements in early stage loading of a culvert.
- The authors' support TMR's requested amendments to AS/NZS 3725:2007, particularly that live load distribution is calculated in accordance with AS5100.2:2017. The authors' highlight that commonly used design software *Pipeclass* does not assess culvert loading performance in accordance with this requirement.
- The correct selection of both live and overall bedding factor (F, F_q) value is a critical factor in determining culvert suitability for applicable loading actions, and requires careful designer judgement and experience to ensure appropriate selection is made. Material selection and installation below the spring line (midpoint of culvert and below) of a buried RCP is fundamental to the loading performance in field. There is a correlation between support stiffness and loading performance, however this also relies (critically) on evenness of support.
- The sensitivity of a designer's calculation and assumptions to actual in field installation is significant. As such, designers should heed caution with utilisation factors approaching one (1).
- Current culvert CCTV inspection techniques for crack width are a crude means for designers to accurately determine structural relevance of cracking and recommend appropriate rectification methods, and risk either under or overestimating a culvert's actual structural condition. Appropriate rectification relies heavily on the designer's experience in this area.
- Improvements in CCTV inspection and reporting techniques could be made, such as higher resolution imagery, LIDAR or other higher accuracy point cloud scanning technique, and/or consideration of any correlation between surface crack width and crack depth measurement.

6 ACKNOWLEDGEMENTS

7 REFERENCES

Australian Standard (2017). Bridge Design Series, AS5100.2
Australian and New Zealand Standard (2007). Design for installation of buried concrete pipes, AS/NZS 3725
Australian and New Zealand Standard (2007), Precast concrete pipes (pressure and non pressure), AS/NZS 4058
Transport and Main Roads Specifications (2018), MRTS25 Steel Reinforced Precast Concrete Pipes
Transport and Main Roads Standard Drawing 1359 (2003), Installation, Bedding and Filling/Backfilling Against/Over Culverts
Transport and Main Roads Road Drainage Manual (3rd Edition) 2019

PROCEEDINGS OF THE 14TH ANZ YOUNG GEOTECHNICAL PROFESSIONALS CONFERENCE
14YGPC ROTORUA, NEW ZEALAND, 2ND – 5TH NOVEMBER 2022

115

The Use of A Geotechnical Constraint Map to Inform Subdivision Development: A Case Study

L. C. Foote[1], NZGS

[1]ENGEO Ltd (Wellington), P.O. Box 25-047, Wellington 6014; PH 04-472-0820; email: lfoote@engeo.co.nz

ABSTRACT

One of the biggest challenges faced by geo-professionals is how to convey complex information to non-technical end users. One method of conveying information in a straightforward manner is the use of geotechnical constraints mapping. A case study is presented for a site in the Maymorn Region of Wellington, New Zealand, where several geotechnical limitations for future subdivision were identified. The geomorphology of the site comprises level ground across the western side of the site, incised by a stream channel in the north; with hills present across the eastern side of the site. The flat area of the site has experienced historical filling of the stream channel and settling ponds associated with farming. The hill areas of the site have been extensively modified by forestry works. The geomorphology and past site works suggest a large number of geological hazards may affect future land use. These comprise liquefaction, lateral spreading and static settlements across the flat areas of the site; with landsliding (both shallow and deep seated), debris flows and rockfall across the sloping areas of the site. For each area of the site, we considered the risk posed by each hazard to the development and assigned it a rating class, from 1 (lowest) through 5 (highest). This was presented in a geotechnical constraints map with coloured zones reflecting each of the rating classes. The end result provided an easy and concise means of conveying extensive technical information to the end user who was readily able to apply it to their decision-making.

Keywords: geohazard, risk, constraints map, case study, Maymorn, Wellington

1   INTRODUCTION

The process of clearly and concisely convey complex geotechnical information to non-technical end users is a common problem faced by geo-professionals. While various different approaches exist, the use of constraints mapping presents an effective method in which to summarise this information while conveying implications for a specific project, in this case subdivision development.

This paper illustrates how numerous geological hazards can be summarised onto a single constraints map, based on a case study site located in the Maymorn region of Wellington, New Zealand. The intended use of the constraints map was to inform land development works, such that areas with low risk could be intensively developed while areas of higher risk could be avoided as much as practicable.

2   CASE STUDY

2.1   Site and Project Description

A geotechnical hazard assessment was required to inform development of an approximately 200 lot subdivision. The 74 ha site comprised relatively level ground across the western side, and sloping ground across the eastern side (Figure 1).

The flat area of the site is grass covered and used for cattle grazing. It is cut by a series of drainage channels which range from a steep sided natural meandering stream in the north-western portion of the site, to modified linear drainage features which flow into the natural stream channel and smaller drainage channels diverting water from the hills. The sloping area is currently vegetated, predominantly with pine forest. Generally, the ridgeline has a wide and relatively level crest. The adjacent slope angles typically range up to 35°, with isolated gullies where slope angles reach approximately 50°. Evidence of local areas of instability were observed through recent failures and bowing of tree trunks.

The Geological Q-map (Begg and Johnston, 2000) indicates that the flat areas are underlain by alluvial gravel, described as late Pleistocene poorly to moderately sorted gravel with minor sand or silt. The hills

are mapped as being underlain by grey sandstone-mudstone sequences and poorly bedded sandstone of the Rakaia Terrane (commonly termed Greywacke). The site is located in an area of active seismicity, with the Wellington Fault to the northwest (2 km) and the Wairarapa Fault to the southeast (11 km).

Figure 1:   Site Photographs: Left – Typical flat geomorphology of flat area with meandering stream channel; Right – View of sloping areas of site.

The site has been extensively modified over time. Prior to 2008 the flat area of the site was used as a pig farm, and a series of effluent ponds were present near the base of the hills. At that time, the meandering stream channel also extended further to the south. Both the ponds and stream channel were infilled as the piggery was decommissioned. The hill areas of the site have experienced modification, with the formation of forestry access tracks and successive rounds of logging and replanting altering the original terrain.

2.2   Ground Model

Critical to the assessment of site geohazards is the development of a detailed ground model. Across the hill area of the site, geomorphological mapping and logging of exposures in road cuts was undertaken. Across the flat areas of the site, where the geomorphology provides fewer clues to the nature of the ground conditions, a series of subsurface investigations were undertaken. The investigations comprised ten sonic machine boreholes to 19.95 m depth, and seven Cone Penetration Tests (CPT) to a maximum of 10.49 m depth.

Groundwater conditions varied across the site. Small streams were observed in the gullies across the hills, which may be seasonal in nature. Standing water was observed at the ground surface immediately adjacent to the base of the hills, with the depth to groundwater increasing to 3 m to 4 m below ground level around the stream channel in the northwest.

From the mapping and subsurface investigations, the site can be divided into several distinct areas. Across the hills, varying geological conditions were identified:
- Rock (Greywacke Sandstone), and shallow rock (areas with less than 3 m of soil cover).
- Colluvium (greater than 3 m in thickness).
- Alluvium (greater than 3 m in thickness).
- Landslide debris (both recent and historical).
- Fill, inferred to be associated with formation of forestry tracks.

Across the flat area, four geologically distinct areas were identified:
- Shallow dense gravels, located across the north-western side of the site.
- Fill associated with previous stream channel, extending up to 6.5 m thick.
- Fill associated with historical effluent ponds, extending up to 3 m thick.
- Interbedded silts and gravels of varying density across the remaining flat areas.

These geological conditions formed the basis for the hazard assessment described in the following section and are illustrated in Figure 2.

PROCEEDINGS OF THE 14TH ANZ YOUNG GEOTECHNICAL PROFESSIONALS CONFERENCE
14YGPC ROTORUA, NEW ZEALAND, 2ND – 5TH NOVEMBER 2022

117
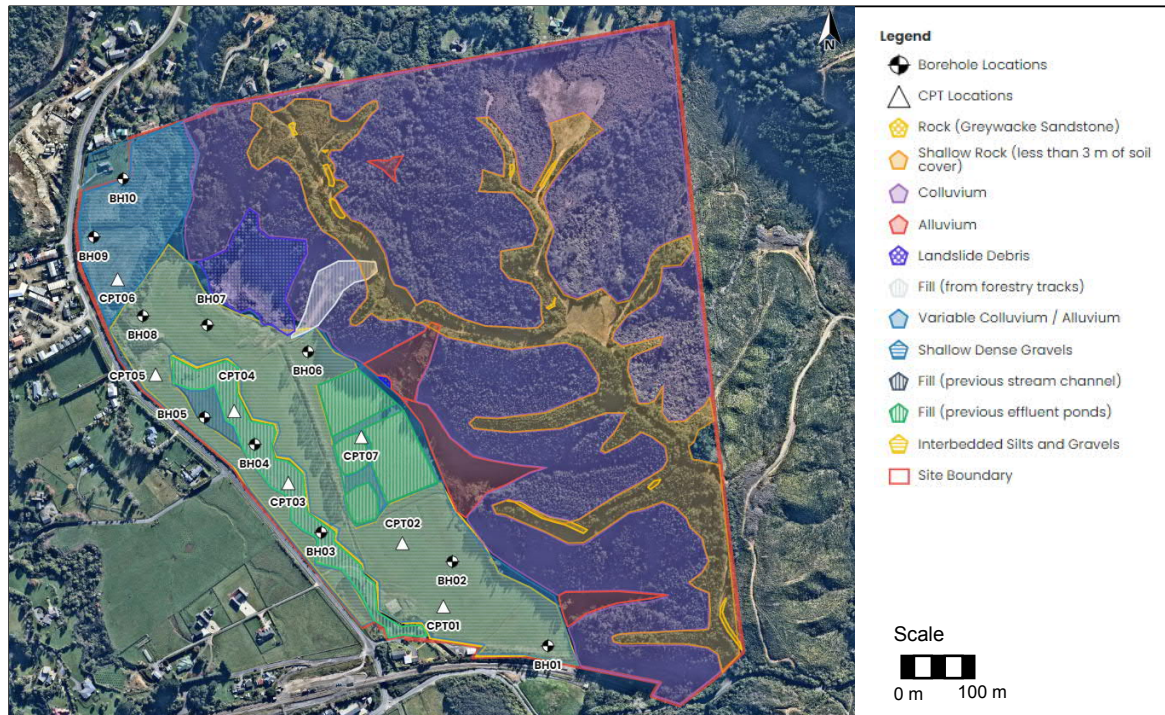
Figure 2:   Site Specific Interpretive Geological Mapping, with Subsurface Investigation Locations (street names not provided due to confidentiality)

3   HAZARD ASSESSMENT

Natural hazards were assessed against Section 106 of the Resource Management Act to inform subdivision suitability, as outlined below. This assessment excludes hazards associated with flooding.

3.1   Flat Area Hazards

3.1.1   Liquefaction

Liquefaction analysis was undertaken utilising the CPT data obtained for the flat areas of the site, following the methodology outlined within the Earthquake Geotechnical Engineering Practice Module 3 (2021), and groundwater from the surface as a conservative approach to reflect site observations. The analysis indicated very low levels of liquefaction induced vertical settlement under Serviceability Limit State (SLS) ground shaking conditions, with settlements due to thin lenses of potentially liquefiable material interspersed throughout the investigated soil profile. Under Ultimate Limit State (ULS) ground shaking conditions, higher settlements of up to 80 mm are indicated by the analysis, with individual layers of liquefiable material up to 2 m thick.

3.1.2   Lateral Spreading

Lateral spreading occurs when there are continuous and uniform liquefiable layers that are able to move towards a 'free face'. No lateral spreading was anticipated under SLS ground shaking conditions due to the lack of liquefiable layers of sufficient thickness in which to induce movement. While more of the ground profile is potentially liquefiable under ULS ground shaking conditions, the ground conditions are highly variable with no obvious evidence of a continuous and uniform liquefiable layer in which to trigger spreading. Accordingly, the potential for lateral stretch is considered to be low (stream bank regression is considered separately below). Lot specific analysis will be required to confirm this assessment when building platforms have been selected.

3.1.3   Static Settlement

The observed fill material within the infilled stream channel was generally very soft to firm or loose to medium dense and contained variable detritus (such as glass, metal, wood). These factors suggest that

the placed material was not cleanfill and was not placed to engineering standards. Static settlement in the form of consolidation is therefore possible under loads associated with further fill placement or the proposed residential development. In addition to settlement of the stream channel infill, there was potential that the soft fill materials used in the area of the past effluent ponds may statically settle over time or when loaded during development.

3.1.4 Stream Bank Regression

Where the meandering stream channel is present (those areas that were not previously filled), there was potential for stream bank regression over time. Stream bank heights varied from 3 m in the southeast to 12 m in the north, with some areas showing a clear slope break / crest, while others had a less distinct and rolling crest to the bank. Geomorphology of the stream banks suggested that there have been varied phases of instability over time.

3.2 Slope Hazards

3.2.1 Landslide Potential

Mapping presented within the Upper Hutt City Council proposed district plan identifies the sloping areas of the site as having a high slope hazard. Site observations and knowledge of the typical failure mechanisms that occur across Wellington slopes, suggests that the most likely form of landsliding would involve shallow sliding of the surface soils on the underlying rock surface. Owing to the relatively low nature of the hills and reasonably shallow expected depths to rock, it is considered that these will typically be of a localised and shallow nature; however, there is geomorphological evidence of at least one large scale failure across the north-western extent of the site. The large landslide does not appear to show any evidence of movement during the time frame of the available historical aerial photographs, suggesting movement prior to 1951.

As a preliminary means to characterise landslide potential, LiDAR available through the Greater Wellington Regional Council was used to group the site into areas of similar gradients. For each slope gradient, a likelihood of instability has also been assigned as follows:
- Less than 17.5°: instability unlikely.
- Between 17.5° and 25°: instability possible.
- Between 25° and 32.5°: instability likely under earthquake or rainfall events.
- Between 32.5° and 37.5°: instability likely.
- Greater than 37.5°: instability expected.

3.2.2 Rockfall Potential

The rock exposures were limited to those within formed accessways (forestry tracks and cuts), at the base of stream channels and along the broad ridge. No significant outcrops were observed on the side slopes and the potential for rockfall to be initiated was considered to be low. Further, the exposed rock comprised highly to completely weathered Greywacke sandstone which is highly fractured and more susceptible to localised frittering rather than large block release which is required for significant and damaging rockfall.

3.2.3 Debris Flow Potential

Historical alluvial fans suggested some potential for debris flows. The likely initiation of debris movement and style of flow has been assessed by morphometrical evidence, using the Melton ratio (R) outlined by Welsh and Davies (2010), which suggests a debris flood hazard rather than a debris flow. A debris flood is defined as a very rapid flow of water, in a steep channel. While debris floods can be heavily charged with debris, they do not have the same concentration of material as debris flows and are typically much less destructive. Accordingly, the risk to future development posed by impact from debris flow initiation was considered to be low.

4 GEOTECHNICAL CONSTRAINTS MAPPING

For this project, the developers aim was to identify areas of the site that could be readily developed in a cost-effective manner, compared to those areas which would require extensive engineering to form

PROCEEDINGS OF THE 14TH ANZ YOUNG GEOTECHNICAL PROFESSIONALS CONFERENCE
14YGPC ROTORUA, NEW ZEALAND, 2ND – 5TH NOVEMBER 2022

119

suitable building platforms. Accordingly, a visual summary of the hazards in the form of a constraints map was considered to be the most useful approach to conveying this information. This approach combines our knowledge of past and present site conditions with a visual aid to guide future works.

In its simplest form, the constraints map considers interactions between site geology, geomorphological conditions and topographic conditions, and how this will impact the proposed development. The complexity of the constraints map can be varied based on the known site history and stage of proposed development.

For this case study, the geotechnical assessment was completed at a very early stage of the project, and accordingly the constraints map was tailored to provide a broad overview of the limitations to future development. Five risk classes were identified, ranging from areas with little to no limitations to future development; through to areas where complex engineering would be required in conjunction with development and consideration could be given to avoiding those areas. Site properties were identified for each of the five categories, considering both flat land and hill slope characteristics based on the hazard assessment. The risk classes are summarised in Table 1.

Table 1:   *Risk Classes*

Development Risk Class	Flat Site Characteristics	Hill Slope Characteristics	Limitations to Development
1	Areas of natural ground Little to no liquefaction induced settlements	Low slope gradients (less than 17.5°) No obvious evidence of instability	Little to no limitations to residential development (subject to foundation suitability)
2	Areas of minor filling (up to 1 m thick) Liquefaction induced settlements of up to 25 mm under SLS conditions	Areas of moderate slope gradient (17.5° to 25°) Areas of minor filling (up to 1 m thick) May be evidence of instability following heavy rainfall or large earthquake events No obvious evidence of instability	May require shallow earthworks to form a suitable building platform
3	Areas of moderate filling (up to 3 m thick) Liquefaction induced settlements over 50 mm under SLS conditions.	Moderate to steep slope gradients (25° to 32.5°) Instability is likely under earthquake or rainfall events (includes potential for inundation from upslope) or Some evidence of small scale instability	Will likely require specific engineering design to form a suitable building platform
4	Areas of moderate to major filling (up to 8 m thick) Liquefaction induced settlements over 50 mm under SLS conditions.	Steep slope gradients (32.5° to 37.5°) Instability is likely under earthquake or rainfall events (includes potential for inundation from upslope) or Evidence of large-scale inactive or relict slope instability	Will require specific engineering design and substantial foundations and / or earthworks to form a suitable building platform
5	Areas where liquefaction induced settlements are likely to be over 100 mm under SLS conditions	Steep slope gradients (greater than 37.5° from horizontal) and indications of recent instability or Evidence of large-scale, active slope instability	Complex or large-scale engineering works required to develop. Consideration should be given to avoiding these other areas owing to severe physical limitations that are likely to be difficult to overcome

The risk classes were then mapped for the site, and the preliminary lot layout plan was overlain so that lots with a low risk to development can be clearly distinguished from those with greater risks, as shown in Figure 3.
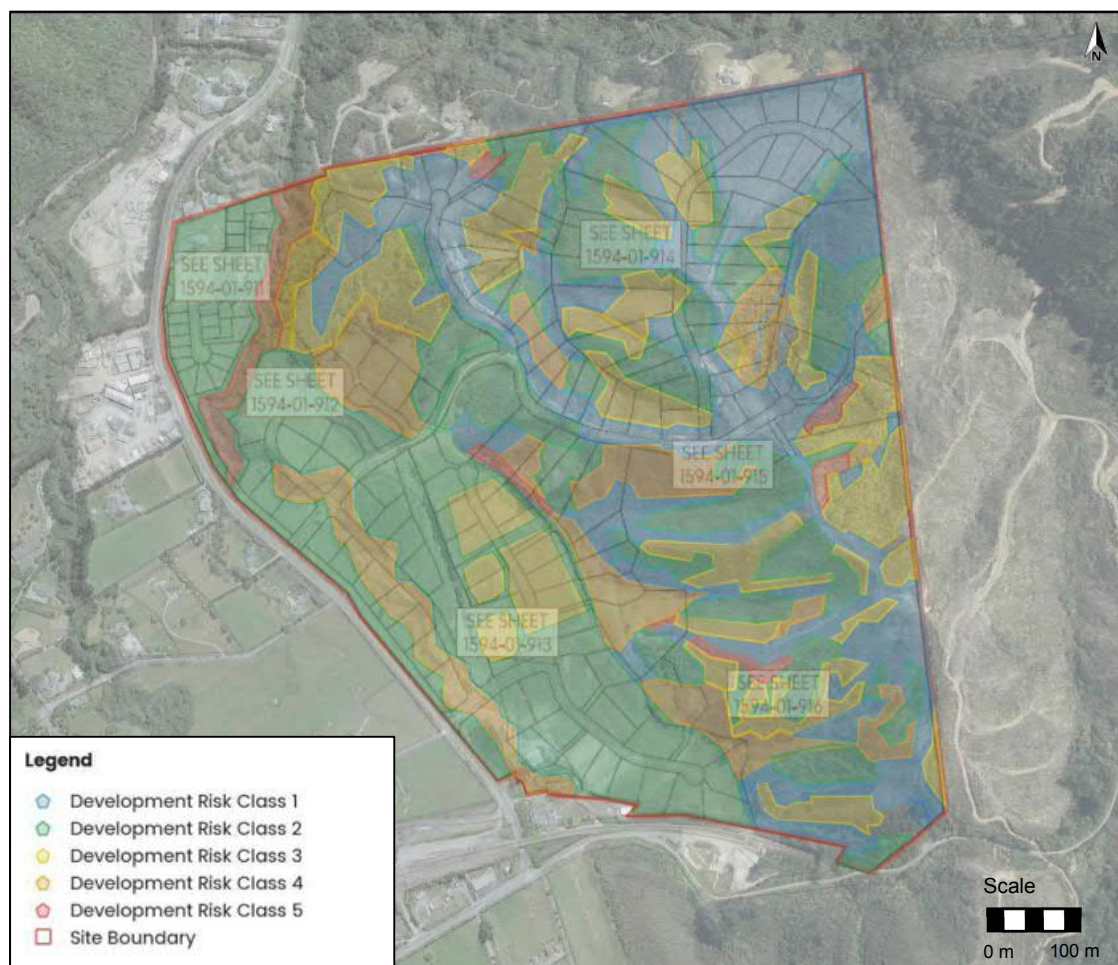
Figure 3: *Geotechnical Constraints Map*

In some areas the constraints map indicates higher development risk classes immediately adjacent to a lower risk category. Where that occurs, a lot-specific geotechnical investigation was recommended on the lower risk site to take into consideration the risk posed by the adjacent area.

5   CONCLUSION

Complex sites with many interacting geo-hazards require careful consideration as to the method of communicating associated risk to development works to avoid any hazards being overlooked. The use of constraints mapping provides a concise, typically single page, summary that can be readily interpreted by those without technical backgrounds. In this case study, the constraints map was found to be an invaluable tool for rapid assessment and re-evaluation of the subdivision lot layout.

6   ACKNOWLEDGEMENTS

REFERENCES

Begg, J.G. and Johnston, M.R. (2000). "Geology of the Wellington area". Institute of Geological and Nuclear Sciences. 1:250,000 geological map 10.
Ministry of Business, Innovation and Employment and the New Zealand Geotechnical Society (November 2021). Earthquake Geotechnical Engineering Practice, Module 3: Identification, assessment and mitigation of liquefaction hazards.
Welsh, A. and Davies, T. (2010). Identification of alluvial fans susceptible to debris-flow hazards.

Strength and Microstructural Developments in Magnesia-GGBS Stabilised Biochar-Sequestered Acid Sulphate Soil

Xue Le[1] and Asadul Haque[2]

[1]Keller Pty Ltd, 62 Mills Road, Braeside, VIC 3195, Australia; email: xue.le@keller.com.au; telephone: +61 3 9590 2600
[2]Department of Civil Engineering, Monash University, Melbourne, VIC 3800, Australia; email: asadul.haque@monash,edu

ABSTRACT

This study assessed the effectiveness of magnesia (MgO) and ground granulated blast-furnace slag (GGBS) in improving the strength of acid sulphate soil (ASS) and the feasibility of sequestering biochar carbon in stabilised ASS. To fulfil the objective of this study, ASS was treated with reactive MgO at 5 to 15%, GGBS at 10 to 20% and biochar at 10%. A range of testings, including pH, uniaxial compressive strength (UCS) test, scanning electron microscopy (SEM) and X-ray diffraction (XRD) analysis, was carried out to investigate strength and microstructural development of the treated ASS over a 180-day curing period. The results of this study showed that MgO-activated GGBS could effectively improve the strength of ASS with an optimum MgO to GGBS ratio of 1:4. Inclusion of biochar can lead to a slight reduction of approximately 10% in strength development of the MgO-GGBS treated ASS. The reduction is due to the porous structure of biochar.

Keywords: acid sulphate soil, soil stabilisation, MgO, GGBS, UCS, carbon sequestration

1 INTRODUCTION

In Australia, there are extensive deposits of acid sulphate soils (ASS), with some 95,000 km^2 (Fitzpatrick et al., 2008) underlying coastal areas. ASS in Australia usually has low strength and high compressibility. To improve the strength of ASS, Portland cement (PC) is commonly used; however, manufacturing PC generates a large amount of CO_2 emissions (0.95 t of CO_2/t of PC) (Yi et al., 2014). In order to reduce the carbon footprint, some industrial by-products, such as ground granulated blastfurnace slag (GGBS) and fly ash, have been adopted as supplementary additives. These supplements are latent-hydraulic materials which typically require alkaline activators to promote their hydration reaction. Recently, reactive magnesia (MgO) has been proposed as a more carbon-effective alternative (0.35 t CO_2/t reactive MgO) to PC in soil stabilisation (Jegandan et al., 2010, Yi et al., 2012); however, its performance in stabilisation of ASS requires further investigation.

To further incorporate sustainability into geotechnical engineering, the concept of sequestering carbon into urban soils, thus reducing atmospheric CO_2, needs to be considered seriously. One possible technology could be sequestration of carbon with biochar through soil mixing process (Haque et al., 2014). Biochar is an alkaline, recalcitrant and highly carbonaceous material produced from the thermal decomposition of biomass (e.g., green waste) (Lehmann, 2007, Renforth et al., 2011, Haque et al., 2014); however, to date, there is limited investigation on the engineering benefits and risks of adding biochar into soil stabilisation.

To reduce the CO_2 emission associated with stabilising ASS, this study investigated the effectiveness of MgO and GGBS in improving the strength of ASS and the feasibility of sequestering biochar carbon in stabilised ASS. A range of testings, including pH, uniaxial compressive strength (UCS) test, scanning electron microscopy (SEM) and X-ray diffraction (XRD) analysis, was carried out to investigate strength and microstructural development of the treated ASS over curing periods of up to 180 days.

2 MATERIALS AND METHODS

2.1 CIS and binders

The ASS was collected from the corner of Batman Hill Drive and Brentani Way in Docklands, Melbourne. In geological terminology, the soil is known as Coode Island Silt (Gill, 1967). The ASS had a liquid limit of 69%, plastic index of 46%, and pH of 8.2. The bulk density and specific gravity of the ASS were approximately 1.6 g/cm^3 and 2.54, respectively. The composition of GGBS (from Building Product Supplies, Australia) and reactive magnesium oxide MgO (XLM Magnesia from Causmag, Australia)

used in this study are shown in Table 1. The biochar used in this study was the pyrolysis product of abandoned rail sleepers. The pH of the biochar was 8.3. Before being added to the sample, the biochar was oven dried for 24 hrs and sieved through 425 µm.

Table 1. Mineralogical composition (% by weight) of GGBS and MgO

Material	SiO_2	Al_2O_3	MgO	CaO	Fe_2O_3	SO_3	MnO	Specific gravity
GGBS	35-37	13.5	5.9	41-43	0.3	2.9	0.4	2.83
MgO	1.3	0.3	97.0	1.3	0.2	-	-	3.24

MgO from 5 to 15% and GGBS from 10 to 20% were mixed with ASS to investigate the optimum MgO-GGBS combination. The MgO-GGBS combinations were each split in two and a fixed 10% of biochar was added to one of the sub-samples. All percentages were by weight of dry soil. In total, 18 binder combinations were adopted in this study, i.e., 5M10S0B, 5M15S0B, 5M20S0B, 5M10S10B, 5M15S10B, 5M20S10B, 10M10S0B, 10M15S0B, 10M20S0B, 10M10S10B, 10M15S10B, 10M20S10B, 15M10S0B, 15M15S0B, 15M20S0B, 15M10S10B, 15M15S10B, and 15M20S10B, where M, S and B represent reactive MgO, GGBS and biochar, respectively, while the number represents the percentage of the additive. In addition, control testing of ASS treated with 20% GGBS only was also carried out as a baseline. A water content of 130% by dry weight of ASS and additives was used to prepare the treated ASS samples. The high water content was adopted to ensure good workability and quality of samples.

2.2   Sample preparation

Due to moisture loss during the transportation and storage process, ASS sourced from the construction site was too stiff to be mixed with additives. Thus, the soil was pre-mixed with a good amount of water in a bench-top mixer for half an hour to break up large soil clumps and obtain a homogeneous soil slurry. At the end of mixing, the slurry was covered with plastic film to minimise any interaction between pyrite and air. After standing overnight, the soil slurry was mixed with additives in the dry form. The mixture was then stirred for 15 minutes in a bench-top mixer. Extra water was added during mixing to achieve a total water content of 130%. The mixture was then cast into cylindical PVC moulds in three layers to prepare samples 60 mm in height and 30 mm in diameter. At the end of placement of each layer, a hand vibrator was used to expel any trapped air bubbles. Both ends of the moulds were sealed with plastic sheets to prevent moisture loss. Samples were subsequently placed in a humidity chamber at 19°C and 100% relative humidity until ready for testing. The stabilised ASS samples were demolded after 7, 28, 90 and 180 days of curing.

2.3   Testing procedure

The pH of stabilised ASS was determined using a MW102 pH metre by mixing 1 part of treated ASS with five parts of deionised water (i.e., weight ratio of treated ASS to water=1:5). The strength of the stabilised ASS was determined through UCS testing in triplicates in accordance with ASTM D2166-06 (ASTM, 2006) at a constant displacement rate of 0.5 mm/min. SEM and XRD analyses were also carried out to examine the microstructure and mineralogical changes of the stabilised ASS. Crushed UCS samples were oven dried overnight at 105°C. Soil flakes with a diameter of no more than 2 mm were selected from the fractured surface of the dried UCS samples for the SEM analysis with a JEOL 7001F microscope. For the XRD analysis, the oven dried samples were ground in an agate mortar, sieved through 425 µm, and subsequently mixed with ethanol (99.7%). The samples were further pulverised with a McCrone Micronising Mill for 5 min. The pulverised samples were then placed in a fume hood for at least 24 hrs to thoroughly volatilise excessive ethanol before the XRD analysis. The XRD analysis was carried out with a Bruker D8 Advance X-ray with Cu-Kα radiation of wavelength λ = 1.5418 Å. The scanning was operated at 40 kV input voltage and 25 mA current with a continuous scan mode from 2θ = 3° to 80°, a step size of 0.02° 2θ, and a counting time of 2 s per step.

3   RESULTS AND DISCUSSION

3.1   pH

The pH variations of the various MgO-GGBS stabilised ASS samples are depicted in Figure 1. The initial pH of all samples was generally in the range 11.6 to 11.9. The pH variations of samples with 10% and 15% GGBS were similar. The pH generally dropped to 90 days and remained at a constant level afterwards. Nevertheless, the pH of ASS with 20% GGBS increased slightly for the first 7 days and

PROCEEDINGS OF THE 14TH ANZ YOUNG GEOTECHNICAL PROFESSIONALS CONFERENCE
14YGPC ROTORUA, NEW ZEALAND, 2ND – 5TH NOVEMBER 2022

123

dropped sharply afterwards until 28 days. The increase in pH may be due to the higher amount of GGBS undergoing hydration, releasing more hydroxyls to the pore solution. It is noted that regardless of the GGBS content, the pH of the ASS with 5% MgO dropped more significantly during the first 28 days when compared to counterparts with 10% or 15% MgO. The more significant decrease in pH probably resulted from a greater abundance of cementitious reactions, as evidenced by the higher 28-day strength of soils treated with 5% MgO (as discussed in section 3.2).

Despite the MgO and GGBS content, the pH values of soils with biochar were generally close to those of their counterparts without biochar and the trend of the pH variation was also similar. Although it was previously reported that the pH of a soil was elevated from 4.5 to 6 by the addition of 6% biochar (Chintala et al., 2013), in a strongly alkaline (pH>10) environment, it can be considered that biochar has insignificant influence on the pH of the whole system.
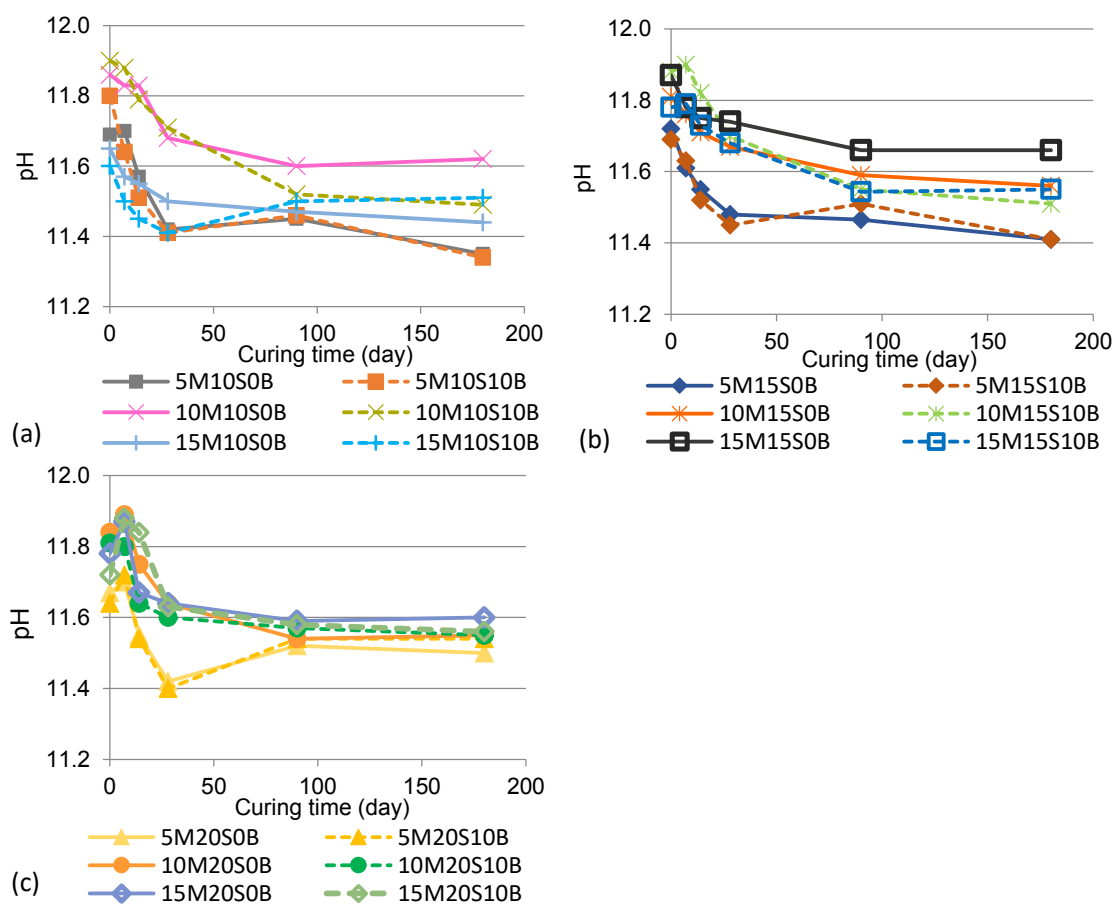
Figure 1. pH of ASS treated with MgO and (a) 10% GGBS, (b) 15% GGBS, and (c) 20% GGBS

3.2   Unconfined compressive strength

The control samples of ASS treated with 20% GGBS only were too soft for UCS testing at the end of a 28-day curing period. At 90 days, the samples registered a strength of 190 kPa. The improvement in the strength is ascribed to the hydration of GGBS. The presence of pyrite and its oxidation products in the mix probably assisted the hydration of the GGBS. Oti et al. (2008) reported that Lower Oxford Clay (LOC) mixed with 20% GGBS alone developed considerable strength at 28 days. They explained that the improvement could be ascribed to the sulphate in the LOC which facilitated the hydration of GGBS.

Figure 2 summarises the UCS results of the MgO-GGBS treated ASS. At 90 days, all samples with 20% GGBS developed more than four-fold of the UCS of the ASS with 20% GGBS only. This implies that MgO significantly enhanced the hydration of GGBS as well as the cementitious reactions. For ASS treated with 20% GGBS, the strength decreased with the increase in MgO content throughout the 6-month curing period. For ASS treated with 10 or 15% GGBS, the strength was also observed to decrease with the increase in MgO content over the first 28 days. However, at 90 and 180 days, increasing MgO

from 5 to 15% had negligible impact on the strength of ASS with 10 to 15% GGBS. It is also evident from Figure 2 that the UCS increases with the increasing GGBS content. The test results suggest that addition of 5% MgO was sufficient to activate up to 20% GGBS in the ASS. It is demonstrated that increasing the MgO content was not necessarily beneficial to the strength development. At higher GGBS content, increasing the MgO amount resulted in the reduction in both short- and long- term strength while at lower GGBS content, the increase in MgO content also decreased the short-term strength. The reduction in the short-term strength may be attributable to the activation limit of reactive MgO to GGBS. It is generally perceived that the rate of hydration of GGBS is faster at higher alkalinity levels (Lothenbach and Gruskovnjak, 2007, Song et al., 2000); however, increasing MgO content from 5% to 15% did not provide a much stronger alkaline environment as shown in the initial pH values (Figure 1). Increasing the MgO to 10 or 15% only resulted in excessive MgO, which was subsequently verified by the XRD analysis. Since the MgO itself did not possess strength or cohesion, the residual MgO only led to a decrease in the short-term strength.
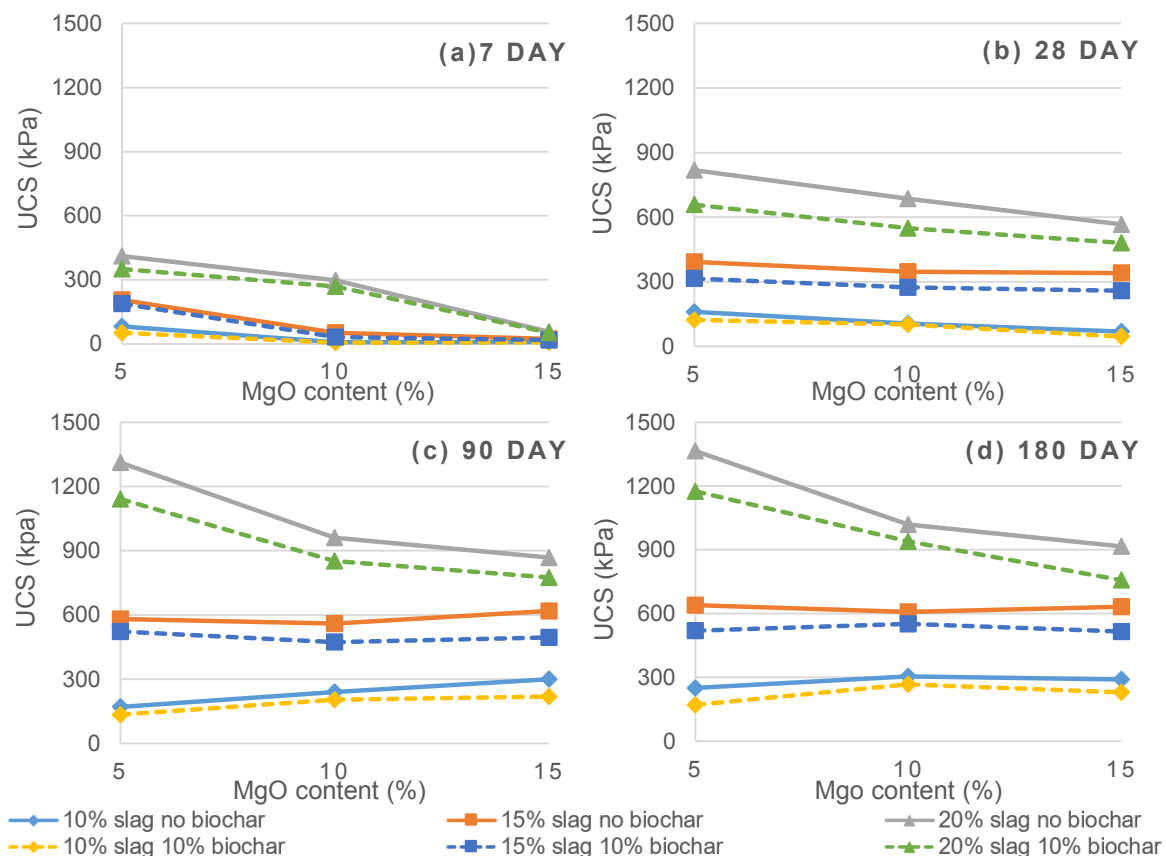
Figure 2. Effects of MgO and GGBS contents on the strength development of ASS at various curing time

It can also be seen from Figure 2 that ASS treated with 10% biochar generally developed slightly lower strength, by approximately 10%, in comparison to the counterparts without biochar. Other than the slight strength reduction, biochar did not influence the trend of strength development. These phenomena show that the biochar probably did not participate in the cementitious reactions but only results in an adverse impact on strength.

3.3   X-Ray diffraction and scanning electron microscopy

The mineralogy of ASS treated with 5% to 15% MgO and 20% GGBS is illustrated in Figure 3. Common minerals including illite, kaolinite, quartz, feldspar and pyrite were identified, reflecting the nature of ASS. The major diagnostic peak of MgO at $2\theta= 42.87°$ appears in the 1-month XRD trace as shown in Figure 3 (a), (b), (e) and (g). The peak of MgO in ASS with 5% MgO has a very low intensity compared to the peaks of MgO in ASS with 10% and 15% MgO, implying more residual MgO in the system with higher MgO contents. The broad peak in the 1-month XRD pattern at $2\theta=29.2°$ is ascribed to the development

PROCEEDINGS OF THE 14TH ANZ YOUNG GEOTECHNICAL PROFESSIONALS CONFERENCE
14YGPC ROTORUA, NEW ZEALAND, 2ND – 5TH NOVEMBER 2022

125

of calcium silicate hydrates (C-S-H). The intensity of the peak increased with time from 1 month to 6 months. This correlated to the great increase in strength over the 6 months. It is noted that at each curing period the intensity of C-S-H peak did not differentiate significantly among ASS with different MgO contents. This suggests that there were probably similar amounts of C-S-H formed in ASS, regardless of MgO contents. The XRD results show that increasing the MgO content from 5 to 15% seemed not to promote the formation of C-S-H but only resulted in more residual MgO and brucite. Thus, it can be concluded that 5% MgO was sufficient for activating up to 20% GGBS. Figure 3 (b) and (d) illustrate the mineralogy of ASS with biochar. At both 28 and 90 days, the XRD patterns of ASS with and without biochar were almost identical. This implies that inclusion of biochar neither altered cementitious products nor promoted/hindered the hydration reactions in both short and long term.
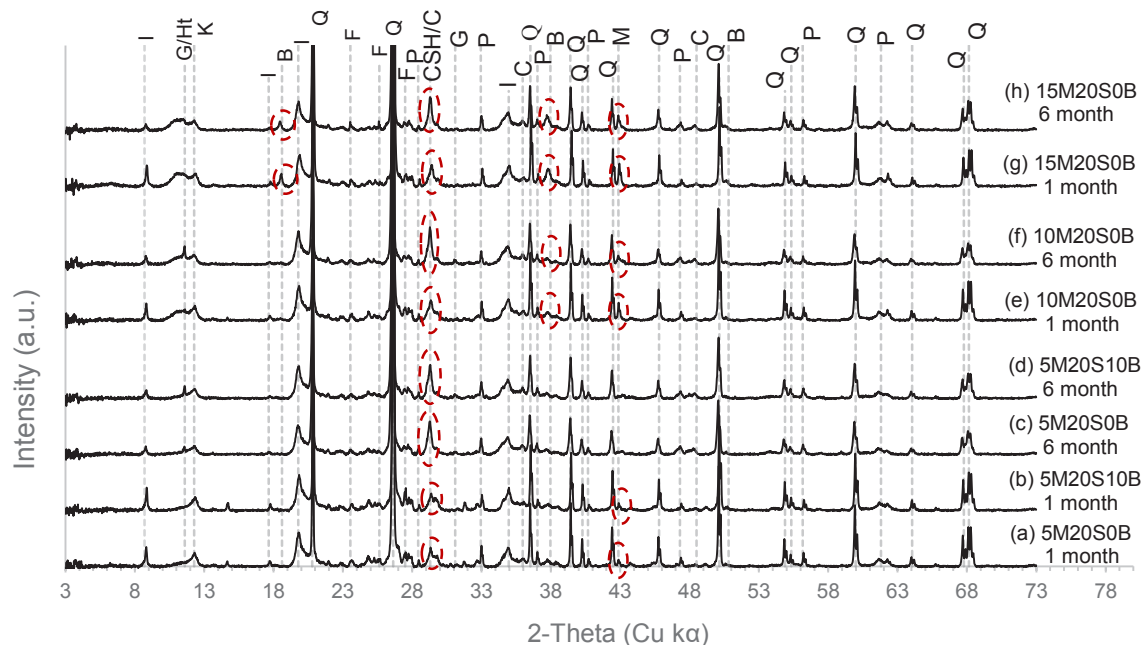
Figure 3. XRD patterns of ASS treated with MgO and 20% GGBS (I-illite, G-gypsum, Ht-hydrotalcite, K-kaolinite, B-brucite, Q-quartz, F-feldspar, C-calcite, P-pyrite, M-MgO)
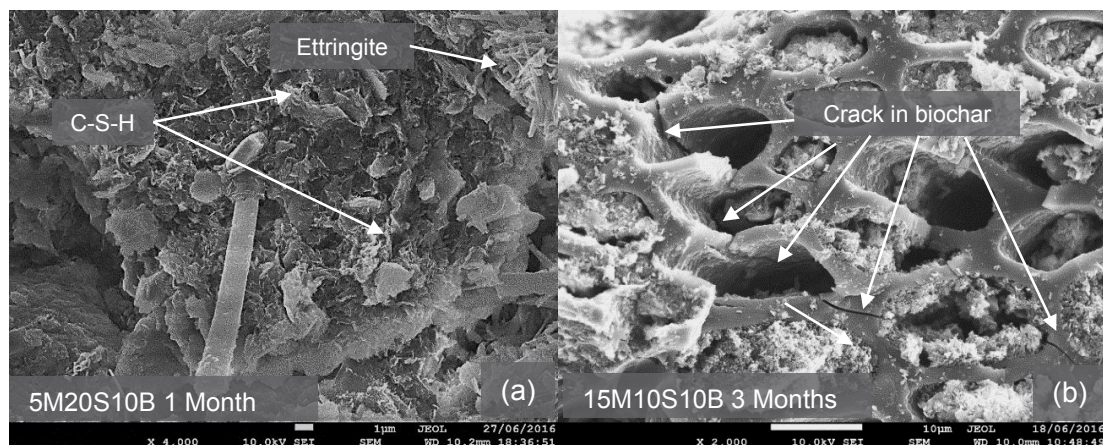
Figure 4. SEM images of ASS treated with MgO-GGBS-biochar binders

Figure illustrates the microstructure of MgO-GGBS-biochar treated ASS. Both C-S-H and ettringite were found in the soil as they are the common hydration products of cementitious reactions. Biochar fragments were found embedded in the ASS-binder matrix with some pores filled with mixtures of soil and cementitious materials. The soil and cementitious materials were also found depositing on part of the biochar surface as shown in Figure 4 (b). Cracks were found propagating across the pores in biochar, particularly in the pores that were left unoccupied or partially occupied as shown in Figure 5 (b). This explains the reason for the lower strength of ASS with biochar. Although biochar did not hinder the

cementitious reactions, cracks tended to propagate across biochar that had unfilled or partially filled pores when subjected to loading. In addition, the smooth surface of biochar with no soil and cementitious material caused lack of bonding between the soil matrix and biochar, which subsequently reduced the cohesion of the treated ASS.

4   CONCLUSION

The pH of all treated ASS test samples underwent a considerable decrease at the early curing stage and the inclusion of biochar had little influence on the pH of the treated ASS. All ASS samples treated with 5 to 15% of MgO and 10 to 20% of GGBS developed signifcant strength over a 180-day curing period, demonstrating that MgO-activated GGBS is an effective binder to improve the strength of ASS. For a GGBS content of 10 to 20%, increasing the MgO content from 5 to 15% generally led to decrease in strength. This implies that 5% MgO is sufficient to activate up to 20% GGBS and thus, the optimum MgO-to-GGBS ratio for strength development of ASS is 1:4 in this study. The XRD and SEM results indicated that the common cementious products of ASS stabilised with MgO-actived GGBS are C-S-H and ettringite.

The XRD and SEM results show that the additon of biochar has negligible impact on the cementitious reactions; however due to its porous structure, inclusion of biochar may lead to a slight reduction in strength. With 10% biochar the reduction is approximately 10%. Nevertheless, inclusion of biochar can offset CO_2 emissions generated by the construction activity and thus, the slight reduction in strength can be justified by the environmental benefits brought by biochar.

5   ACKNOWLEDGEMENTS

REFERENCES

ASTM 2006. Standard Test Method for Unconfined Compressive Strength of Cohesive Soil. Pennsylvania: ASTM International.

FITZPATRICK, R. W. Overview of acid sulfate soil properties, environmental hazards, risk mapping and policy development in Australia. Advances in Regolith. Proceedings of the CRC LEME Regional Regolith Symposia, CRC LEME, Bentley, WA, 2003. 122-125.

CHINTALA, R., MOLLINEDO, J., SCHUMACHER, T. E., MALO, D. D. & JULSON, J. L. 2013. Effect of biochar on chemical properties of acidic soil. Archives of Agronomy and Soil Science, 60, 393-404.

Gill, E.D., 1967, Keilor Excursion No. 40. IN McAndrew J., Marsden M.A.H.(eds) 'Geology excursions handbook for Section C - geology. ANZAAS 39th Congress, Melbourne, January 1967, ANZAAS, 207-208

HAQUE, A., TANG, C. K., ISLAM, S., RANJITH, P. G. & BAI, H. 2014. Biochar Sequestration in Lime-Slag Treated Synthetic Soils: A Green Approach to Ground Improvement. Journal of Materials in Civil Engineering, 06014024-1-06014024-5.

JEGANDAN, S., LISKA, A., OSMAN, A. A.-M. & AL-TABBAA, A. 2010. Sustainable binders for soil stabilisation. Proceedings of the ICE-Ground Improvement, 163, 53-61.

LEHMANN, J. 2007. A handful of carbon. Nature, 447, 143-144.

LOTHENBACH, B. & GRUSKOVNJAK, A. 2007. Hydration of alkali-activated slag: thermodynamic modelling. Advances in Cement Research, vol. 19, pp. 81-92.

OTI, J. E., KINUTHIA, J. M. & BAI, J. 2008. Using GGBS for unfired-clay masonry-bricks. Proceedings of the Institution of Civil Engineers - Construction Materials, 161, 147-155.

RENFORTH, P., EDMONDSON, J., LEAKE, J. R., GASTON, K. J. & MANNING, D. A. C. 2011. Designing a carbon capture function into urban soils. Proceedings of the ICE - Urban Design and Planning [Online], 164. Available: http://www.icevirtuallibrary.com/content/article/10.1680/udap.2011.164.2.121.

SONG, S., SOHN, D., JENNINGS, H. M. & MASON, T. O. 2000. Hydration of alkali-activated ground granulated blast furnace slag. Journal of Materials Science, vol.35, 249-257.

YI, Y., LI, C., LIU, S. & AL-TABBAA, A. 2014. Resistance of MgO-GGBS and CS-GGBS stabilised marine soft clays to sodium sulfate attack. Géotechnique [Online], 64. Available: http://www.icevirtuallibrary.com/content/article/10.1680/geot.14.T.012.

YI, Y., LISKA, M. & AL-TABBAA, A. 2012. Initial Investigation into the Use of GGBS-MgO in Soil Stabilisation. Grouting and Deep Mixing 2012, 444-453.

PROCEEDINGS OF THE 14TH ANZ YOUNG GEOTECHNICAL PROFESSIONALS CONFERENCE
14YGPC ROTORUA, NEW ZEALAND, 2ND – 5TH NOVEMBER 2022

127

Case Study on the Geotechnical Seismic Design for Lateral Flow Effects on a Single Span Bridge in Pumiceous Deposits

K. Chew[1], M. Taylor[1], R. Wessel[1] and P. Robins[1]

[1]Beca Limited, New Zealand; corresponding email: kevin.chew@beca.com

ABSTRACT

This paper presents a practical application of pseudo-static analysis methods to assess the impact of liquefaction and lateral spreading effects on a single spanned bridge and its foundation. The case study presented includes the assessment of seismic ground response using shear wave velocity testing to inform the kinematic loading of pile foundations. Some limitations encountered with the current guidance are discussed, specifically when flow failure is expected during or immediately following intense earthquake shaking. Insights into the assessment and modelling processes are also presented, including the different soil-structure loading scenarios for the whole bridge analysis and the incorporation of uncertainty in the assessment procedures.

Keywords: soil-structure interaction, pumiceous deposits, lateral spreading, site response analysis

1 INTRODUCTION

Bridges present both significant investments and potential weak points in transportation networks if structures fail to provide functionality following a natural disaster. The design of bridge foundations for the impact of liquefaction and lateral spreading effects is a highly complex problem. This paper presents a case study from a recent project where seismic ground response analysis was used to inform the kinematic loading of piles foundations, a key step in the assessment of the existing bridge performance, and in the design of suitable retrofit solutions. Waka Kotahi (New Zealand Transport Agency) provides relevant guidance in the Bridge Manual and published guidelines to undertake pseudo-static analysis of the bridge structure subjected to liquefaction and lateral spreading effects. Some limitations encountered with the current guidance are discussed, specifically when flow failure is expected during or immediately following intense earthquake shaking. Insights into the assessment and modelling processes are presented, including the incorporation of uncertainty in the assessment procedures, to develop a robust engineering design solution.

2 NZ DESIGN STANDARDS AND GUIDELINES

The engineering design of KiwiRail bridges and foundations is often undertaken in accordance with the Waka Kotahi/ New Zealand Transport Agency (NZTA) Bridge manual ('Bridge Manual') as per clause 6.3 of the KiwiRail railway bridge design brief W201 (KiwiRail 2010). The Bridge Manual adopts a performance-based design philosophy with a comprehensive set of requirements for the design and assessment of bridge foundations as well as soil structures supporting bridge abutments and approach embankments. The performance-based design is reflected in a series of seismic design limit states with varying hazard levels and corresponding performance requirements in terms of tolerable damage and operational continuity requirements.

The assessment of bridge performance when subjected to liquefaction-induced lateral spreading is a complex and technically challenging problem requiring consideration of both the seismic inertial loading of the bridge in response to ground shaking, as well as kinematic loading due to ground movement. Key uncertainties include the nature and intensity of seismic loading that a bridge may experience during its design life; the uncertainty in characterising and predicting the soil response and liquefaction triggering; and the uncertainty in characterising consequent effects – i.e. the loss of strength and stiffness and the resulting ground movements that may occur during or post-shaking; and finally the interaction of the structure to resist these movements with consequent impacts on the bridge performance.

Reflecting the complexity of the problem, NZTA provides, in addition to the requirements stipulated in the Bridge Manual, guidance documents on the analysis of bridges for lateral spreading effects in the form of the NZTA Research Note 553 ('R-533') (Murashev et al. 2014), with example design problems also provided (Keepa et al. 2018). These documents help inform suitable assessment procedures for the analysis of bridge foundations subject to liquefaction and lateral spreading effects in New Zealand.

128

PROCEEDINGS OF THE 14TH ANZ YOUNG GEOTECHNICAL PROFESSIONALS CONFERENCE
14YGPC ROTORUA, NEW ZEALAND, 2ND – 5TH NOVEMBER 2022

Recognising that the design methods commonly adopted in engineering practice are pseudostatic, and unable to assess the complex time-dependent nature of seismic loads and effects, R-553 (and Bridge Manual clause 6.3.5) propose three load cases to consider, corresponding to different distinct phases of response: (1) peak seismic inertial loads occurring in the absence of liquefaction; (2) degradation of stiffness and strength of the soils due to generation of excess pore water pressure during shaking causing cyclic ground displacement (kinematic loads) to be considered simultaneous with structural inertial loads; and (3) lateral spreading displacement typically occurring post-shaking with minor to no consideration of structural inertial loads. R-553 also provides guidance on the different methods of analysis ranging from the simplified pseudo-static approach (PSA) to dynamic numerical analysis. The PSA method is most commonly used as it is relatively simple to implement and carry out the required sensitivity studies, however it does suffer from significant uncertainties due to the gross approximation of a dynamic problem. The two PSA methods recommended are those of Cubrinovski et al. (2009) ('CEA09'), and Ashford et al. (2011) ('PEER').

The CEA09 method broadly consists of a Winkler-type beam-spring model using simple bilinear p-y curves as lateral soil springs connected to vertical beam elements forming the pile, with a conceptual three-layer soil model (i.e. non-liquefied soil crust, over liquefied soil, over deeper competent founding strata). The three-layer model considers the significant difference in the stiffness and yield strength of the soil springs in liquefied and non-liquefied layers, to address the design scenarios (2) and (3) presented earlier. The Winkler-type PSA model can also be used to assess scenario (1) without liquefaction effects. The PEER method is conceptually similar to the CEA09 method but considers non-linear p-y curves and provides guidance on accounting for pile-pinning effects for restraining seismically induced embankment movements (see also Boulanger et al. 2007; Caltrans 2012).

The complementary report to R-553 by Keepa et al. (2018) presents worked examples for liquefaction assessment and PSA of piled bridges to demonstrate the application of R-553 recommended methods in engineering practice. This report also provides guidance on how to consider varying combinations of kinematic and inertia loading at different piers and abutments on the whole-bridge seismic response.

3 BRIDGE 83 ECMT CASE STUDY

3.1 Background

The existing Bridge 83 is located on the East Coast Main Trunk (ECMT) Line between Tauranga and Te Puke in the Bay of Plenty Region. It is situated on a straight section of track crossing the Kopuaroa Canal immediately east of Te Puke Highway. The site is underlain by Tauranga Group Alluvium which comprises alluvial and colluvial sands and gravels dominated by pumice clasts, silts, and clay with local peat beds (Leonard et al. 2010). A site investigation was conducted to characterise the ground conditions at the bridge, consisting of two machine boreholes to a depth of 40+ metres and a seismic cone penetration test (sCPT) to 25m (Beca 2022). The site was found to be underlain by approximately 10m of weak Holocene alluvium (loose sands and soft silts) overlying ignimbrite deposits of increasing density with depth. The Matua Subgroup, an ignimbrite unit dating from the Pleistocene was encountered at a depth of around 45m below the existing ground level. The ground profiles were relatively similar at both abutments and the surrounding topography is relatively flat.

3.2 Liquefaction and Cyclic Softening Assessment

An initial liquefaction hazard assessment was undertaken using the SPT- and CPT-based empirical liquefaction triggering assessment methods (Boulanger & Idriss 2014) from the results of the site investigation. The findings indicated a risk of extensive liquefaction triggering in response to design-level seismic shaking, followed by wide-spread lateral spreading and associated ground displacements. However in contrast, the shear-wave velocity-based (Vs) liquefaction triggering assessment method (Kayen et al. 2013) exhibited a significantly lower extent of liquefaction. Figure 1 presents the Vs profile as *measured* by sCPT, compared to the *estimated Vs* using a CPT-based empirical correlation (Robertson, 2009). The discrepancy has been plotted adjacent as a ratio (referred to as the 'measured to estimated velocity ratio' (MEVR) after Andrus et al. 2007), with values above 1 indicating under-estimation, and values below 1 over-estimation compared to direct Vs measurement. The plot shows that the CPT-based correlation over-estimates the Vs for the soft clay (3 to 6m depth), but more significantly under-estimates the Vs for the pumiceous sands and deeper ignimbrite layers.

PROCEEDINGS OF THE 14TH ANZ YOUNG GEOTECHNICAL PROFESSIONALS CONFERENCE
14YGPC ROTORUA, NEW ZEALAND, 2ND – 5TH NOVEMBER 2022

129
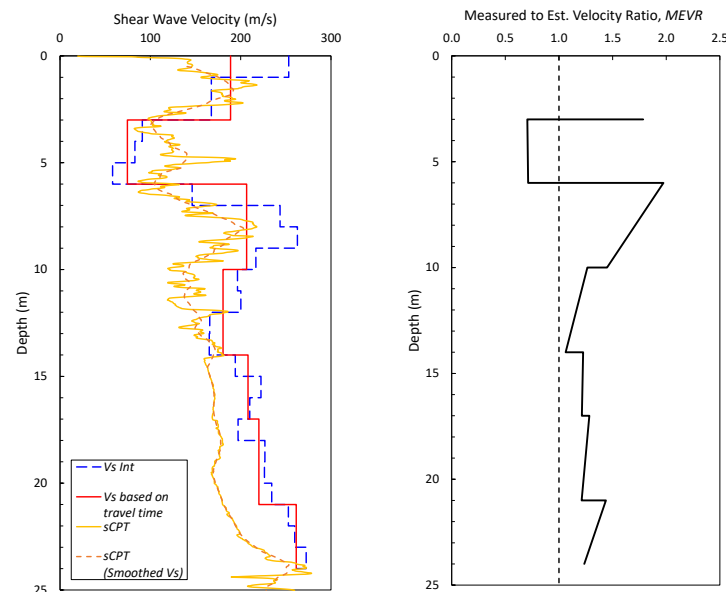
Figure 1. Comparison plots of shear wave velocity (Vs) measurements and CPT-based estimates of Vs (per CPeT-IT after Robertson, 2009). (Beca, 2022)

Problems with assessing the liquefaction hazard of pumiceous sand deposits using penetration-based testing (i.e. CPT, SPT) have been well documented in previous studies (MBIE/ NZGS Module 3, 2021; Orense et al. 2020; Clayton et al. 2019) and have not been discussed in this paper for brevity.

While clays are not susceptible to liquefaction, they may soften temporarily in response to cyclic loading, potentially leading to slope instability. The cyclic softening assessment method of Boulanger et al. (2007) was followed which is based on the results of cyclic testing of soft clays. Cyclic resistance of the clay is defined relative to the development of a specified level of strain, and for simplicity is related to the monotonic shear strength as 0.8 x s_u. Once the cyclic strength has been exceeded, potentially large displacements may occur if slope instability is precipitated, and further strain softening may occur towards residual strength values.

3.3 Bridge Substructure Analysis

The PSA method was adopted in the seismic design of the bridge piles. Non-linear soil springs were derived using commercial software LPile (Ensoft, 2019) for input into the SAP 2000 (CSI, 2021) structural software package. For sensitivity checks, upper and lower bound spring stiffness values were considered at 50% and 200% of the best estimate to account for variability of soil material response. The passive resistance provided by the existing stream banks in front of the piles has been ignored as the banks will not be stabilised. These soil springs were combined with a 3D substructure model in SAP 2000 to undertake a whole bridge analysis. Three different loading conditions/response phases were considered in the design of the piles in accordance with the Bridge Manual (section 6.3.5).

Loading Condition 1 – Prior to liquefaction triggering
In the pre-liquefied phase, permanent ground displacements of abutments were considered in combination with peak inertia loads on the bridge, with the kinematic loads modelled by applying the displacements to the back of the soil springs. The ground movements for a non-liquefied or cyclically softened abutment / embankment were estimated using the co-seismic ground displacement prediction equation of Jibson (2007), which was developed from curve fitting to the results of extensive Newmark's sliding block analyses. The equation required earthquake Peak Ground Acceleration (PGA), Magnitude, and the slope yield acceleration (k_y) as input.

Loading Condition 2 – After liquefaction triggering
After liquefaction is triggered (but prior to any flow failure occurring), cyclic oscillation of the ground surface may impose kinematic demands on the piles simultaneously with inertia loads. An 80% structural inertia load was considered during this interim cyclic phase with reduced soil stiffness and strength. The cyclic ground displacement profile was estimated from the results of 1D non-linear site response

analysis (SRA) summarised in Section 3.4. The kinematic and inertial loads were assessed in a whole bridge setting and assumed to act in the same direction (in-phase) given the short span of the bridge.

<u>Loading Condition 3 – Lateral spreading</u>

Based on a slope stability analysis, with softened strengths applied to units predicted to undergo liquefaction or cyclic softening, the abutments are expected to undergo a flow failure with large lateral spreading displacements following a design seismic event. This condition is identified to occur when a slope with no ground acceleration applied and with softened strength parameters for affected units, exhibits a factor of safety, FS < 1.0. The (free field) ground displacement under flow failure has been estimated to be in the order of 0.5m to 2.0m (Caltrans 2012). Given that large soil movements are expected, an effectively "unrestrained" ground displacement is characterised, and localised failure around the foundation is expected to displace regardless of the presence of piled foundations (Caltrans 2012). As a result of this, pile pinning effects have been ignored.

Different loading combinations as below were considered as part of this scenario, in combination with 25% structural inertia loads as recommended in the Bridge Manual:

- **Symmetrical Abutment Failure:** Flow failure at both abutments with full passive soil pressure mobilised in the non-liquefied soil crust, which acts as a load on the bridge abutment wing walls, and with kinematic loads from soil flowing around piles in the liquefied soil layers. The passive pressure from the non-liquefied crust was determined using the log spiral earth pressure theory.
- **Non-Symmetrical Abutment Failure:** Flow failure at only one abutment occurs, with a reduced / residual soil strength in cyclically softened layers, while reduced soil resistance is considered at the opposing abutment.

3.4 Cyclic Kinematic Loading

For Loading Condition 2, kinematic loads during ground oscillation are required to be characterised. The cyclic ground displacements for a liquefied soil deposit can be estimated from the maximum cyclic shear strains in the liquefied layers (i.e., Tokimatsu and Asaka 1998; Zhang et al. 2004). As highlighted above, liquefaction predicted under large seismic events was limited in a few thin sand horizons with ground failure mostly attributed to cyclic softening of soft clay layers. Consequently, a total stress-based 1D non-linear site response analysis (SRA) was undertaken to characterise the cyclic kinematic loads.

The SRA was undertaken using software DEEPSOIL (Hashash et al. 2020), with the soil column defined using a combination of the Vs measurement from the sCPT and SPT-Vs based correlations by Wair et al. (2012). While the MBIE/ NZGS guidelines do provide detailed requirements for SRA, the requirements in ASCE 7-16 (2017) were followed. This Standard requires that the uncertainty in the Vs profile be considered in the analysis. Therefore, best estimate, upper and lower bound Vs profiles were developed. Due to a lack of statistical test data for the site (1 sCPT, 2 Boreholes), the upper- and lower-bound profiles were characterised by adopting an assumed log-normal standard deviation, $\sigma_{\ln(Vs)}$ of 0.35 (Ulmer et al. 2021).

The non-linear soil model adopted in DEEPSOIL was that of Groholski et al. (2016) which enables calibration of the model to empirical strain-dependent dynamic shear modulus and damping properties, as well as the shear strength of the soil layer at large strains. A selection of seven input ground motions were obtained from the PEER NGA2West database (Ancheta et al. 2014). Ground motion selection and matching were undertaken in accordance with NZS 1170.5:2004, using a site-subsoil Class D target spectrum for Te Puke corresponding to the 1 in 1000yr return period hazard. The ground motions were applied at the top of the stiff ignimbrite layer at the base of the profile.

Figure 2(a) presents the site amplification ratios (i.e., ratio of surface to input motion response spectra) from the three 1D SRA models - i.e., best estimate Vs profile (BE), and upper and lower bounds (UB, LB respectively) compared to the spectral ratio between Site Class E and D spectral shape factors in NZS1170.5. There was relatively good agreement between the 1D SRA all things considered. The non-linear analysis is modelling more soil damping resulting in de-amplification (spectral ratio SR < 1) at low periods, and at the natural period of the soil profile (T ~ 1s) we see amplification (SR > 1), typically to levels expected from the NZS1170.5 spectral ratios. The results suggest the profile is behaving like a Class E profile, which was initially assumed for design. Depending on the period of the bridge structure, the Class E spectra in NZS1170.5 may be conservative (short periods *T* < 0.3s), about right (*T* 0.3 – 2s), or a bit unconservative (*T* 2 - 4s).

PROCEEDINGS OF THE 14TH ANZ YOUNG GEOTECHNICAL PROFESSIONALS CONFERENCE
14YGPC ROTORUA, NEW ZEALAND, 2ND – 5TH NOVEMBER 2022

131

(a) (b)
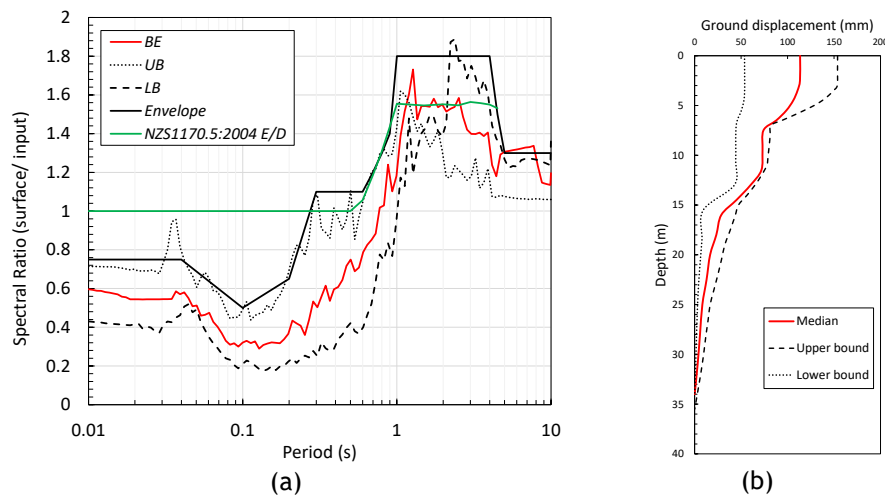
Figure 2. (a) Plot of spectral ratio for the three-site response analysis stiffness profiles considered (BE = best estimate, UB and LB upper and lower bound respectively), compared to NZS1170.5 spectral ratios based on Site Class D. (b) Ground displacement profile derived from the 1D SRA; lower bound displacement profile determined from the upper bound Vs profile and vice-versa.

The 1D SRA analysis also provides the peak ground displacement profile, which was used to characterise the cyclic oscillation loading of the bridge piles for the PSA analysis of Scenario 2 as shown in Figure 2(b). It is worth noting that the ground displacement may extend to the full depth of the foundation depending on the soil stiffness defined and the location of the rigid boundary assumed. Imposed displacements in the non-liquefying layers at depth can often lead to high soil pressures applied to the pile and can result in more onerous loading when compared to Scenario 3. This highlights the importance of considering Scenario 2, especially in soft soil sites where relatively low stiffness soils prevail. More advanced dynamic analyses can help to remove potential conservatisms in a PSA, with the trade-off being more complexity and time to undertake analyses that may not be justified.

4 STRUCTURAL-GEOTECHNICAL COLLABORATION

Good communication and collaboration between the structural and geotechnical engineer is key in modelling the soil-structure interactions of the bridge elements as noted below:

- Have a clear understanding of how the geotechnical inputs are translated in the structural model (i.e., how are the soils springs defined in the structural model).
- Be clear on how the ground displacements should be applied. Relative movement between the pile and the soil is what causes the soil springs to be loaded.
- For whole bridge analyses, consider the direction and magnitude of ground movements (i.e., in-phase or out of phase between the different abutments and piers). There is currently no consensus about what proportion of ground displacements at different bridge supports should be considered together with the inertial loads from the bridge. This requires engineering judgement and can lead to many design cases for multi-span bridges (Keepa, et al. 2018).
- It is often unclear what a conservative loading case is. An upper bound spring stiffness may provide better lateral resistance to the pile in response to inertial loads but will also apply higher soil pressures on the pile in response to kinematic movement.
- Undertake a sensitivity analysis. This can help identify the critical design scenarios / parameters.
- Consider the compatibility of the soil spring stiffness and the imposed displacements. Higher displacements often correspond to a lower-bound stiffness soil considered within sensitivity analyses, while lower displacements correspond to a higher stiffness soil case. It can be tempting to adopt upper bound stiffness with upper bound displacement combination, which would be incompatible and overly conservative.

5 CONCLUSIONS

The authors have presented a practical application of pseudo-static analysis methods to assess the liquefaction and lateral spreading effects on a single spanned bridge. The proposed procedures to

assess these effects under the design seismic event together with their limitations are presented. Commonly used tests (i.e., SPTs and CPTs) for liquefaction assessment can lead to an unreliable assessment of liquefaction susceptibility, especially in pumiceous deposits. Shear wave-based testing is often beneficial and should be paired with conventional penetration tests to provide a comparison for assessing the liquefaction potential. The use of shear wave velocity testing also helped characterise the 1D site response analysis, which informed the magnitude of kinematic loads during cyclic ground oscillations for sites undergoing predominantly cyclic softening. The loading conditions listed in the NZTA Bridge Manual require further and careful considerations to define the design scenarios for a whole bridge analysis. This involves assessing different combinations of magnitude and direction of kinematic and inertial loadings on the bridge support elements to address the associated uncertainties and approximation of a dynamic problem in the context of a pseudo-static approach.

6   ACKNOWLEDGEMENTS

REFERENCES

American Society of Civil Engineers (ASCE) (2017). "ASCE/SEI 7-16: Minimum Design Loads and Associated Criteria for Buildings and Other Structures.", ASCE: Reston VA.

Ancheta, T., Darragh, R., Stewart, J., Seyhan, E., Silva, W., Chiou, B., Wooddell, K., Graves, R., Kottke, A., Boore, D., Kishida, T., and Donahue, J. (2014). NGA-West2 database. Earthquake Spectra. 30. 10.1193/070913EQS197M.

Andrus, R.D., Mohanan, N.P., Piratheepan, P., Ellis, B.S., and Holzer, T.L. (2007). "Predicting shear-wavevelocity from cone penetration resistance." Proc., 4th Int. Conf. on Earthquake Geotechnical Engineering, Thessaloniki, Greece.

Ashford, S.A., Boulanger, R.W., and Brandenberg, S.J. (2011). "Recommended design practice for pile foundations in laterally spreading ground." Berkeley, California: Pacific Earthquake Engineering Centre.

Beca 2022. "Bridge 83 ECMT replacement – design features report."

Boulanger R.W. and Idriss, I.M. (2014). "CPT and SPT Based Liquefaction Triggering Procedures." Report No. UCD/CMG–14/01, Dept. of Civil & Environmental Engineering, University of California at Davis.

Boulanger, R.W. and Idriss, I.M. (2007). "Evaluation of Cyclic Softening in Silts and Clays." J. Geotech. Geoenv. Engng, 133 (6): 641–652.

Boulanger, R.W., Chang, D., Brandenberg, S.J., Armstrong, R.J., and Kutter, B.L. (2007). "Seismic design of pile foundations for liquefaction effects." Proc. 4th Int. Conf. on Eq. Geotech. Engng. KD Pitilakis (Ed). The Netherlands: Springer. pp277–302.

California Department of Transportation (Caltrans) (2012). "Guidelines for Foundation Loading and Deformation Due to Liquefaction Induced Lateral Spreading." Sacramento, CA.

Clayton P.J., de Graaf K.L., Yong I., and Green, R.A. (2019). "Comparison of assessments of liquefaction potential in selected New Zealand pumiceous soils." Proc. 7th Int. Conf. on Earthquake Geotechnical Engineering (7ICEGE), June 2019, Rome.

Computers & Structures Inc. (CSI) (2011). SAP2000 software. Version 23.

Cubrinovski, M., Ishihara, K., and Poulos, H. (2009). "Pseudo static analysis of piles subjected to lateral spreading." Special issue, Bulletin of the New Zealand Society for Earthquake Engineering 42(1): 28–38.

Ensoft Inc. (2019). LPile software. Version 11.

Groholski, D., Hashash Y., Kim, B., Musgrove, M., Harmon, J., and Stewart, J. (2016). Simplified Model for Small-strain Nonlinearity and Strength in 1D Seismic Site Response Analysis. J. Geotech. Geoenviron. Engg. 142(9): 14pp.

Hashash, Y.M.A., Musgrove, M.I., Harmon, J.A., Ilhan, O., Xing, G., Numanoglu, O., Groholski, D.R., Phillips, C.A., and Park, D. (2020). "DEEPSOIL 7, User Manual". Urbana, IL, Board of Trustees of University of Illinois at Urbana-Champaign.

Jibson, R.W. (2007). "Regression Models for Estimating Co-seismic Landslide Displacements." Eng. Geol., 91: 209–218.

Kayen, R.E., Moss, R.E.S, Thompson, E.M., Seed, R.B., Cetin, K.O., Der Kiureghian, A., Tanaka, Y., and Tokimatsu, K. (2013). "Shear-wave velocity-based probabilistic and deterministic assessment of seismic soil liquefaction potential." Journal of Geotechnical and Geoenvironmental Engineering 139(3): 407–419.

Keepa, C., Adhikari, G., Murashev, A., Novakov, D., Cubrinovski, M., and Haskell, J. (2018). "Analysis of piled bridges at sites prone to liquefaction and lateral spreading in New Zealand." Wellington: NZ Transport Agency, 161pp.

KiwiRail. (2010). "Railway bridge design brief." Structures Code Supplement, Issue 6, 28pp.

Leonard, G.S., Begg, J.G., and Wilson, C.J.N. (2010). "Geology of the Rotorua area." Institute of Geological & Nuclear Sciences 1:250 000 geological map 5. 1 sheet + 102 p. Lower Hutt, New Zealand. GNS Science.

Murashev, A., Kirkcaldie, D., Keepa, C., Cubrinovski. M., and Orense. R. (2014). "The development of design guidance for bridges in New Zealand for liquefaction and lateral spreading effects". NZ Transport Agency research report 553, 142pp.

New Zealand Geotechnical Society (NZGS) (2021) "Module 3 – guideline for the identification, assessment and mitigation of liquefaction hazards." Earthquake Geotechnical Engineering Practice in New Zealand, Rev1.

New Zealand Standard (NZS) (2004). "NZS1170.5 structural design actions, part 5: earthquake actions – New Zealand."

Orense, R.P., Asadi, M.B., Stringer, M.E., and Pender M.J. (2020). Evaluating liquefaction potential of pumiceous deposits through field testing: Case study of the 1987 Edgecumbe earthquake. *Bulletin NZ Society Earthquake. Engineering.* 53(2): 101-110

Robertson, P.K. (2009). "Interpretation of Cone Penetration Tests — a Unified Approach." Canadian Geotech. J. 46: 1337–1355.

Tokimatsu, K. and Asaka, Y. (1998). "Effects of liquefaction-induced ground displacements on pile performance in the 1995 Hyogoken-Nambu earthquake." Special Issue of Soils and Foundations, no.2: 163–177.

Ulmer, K.J., Rodriguez-Marek, A., and Green, R.A. (2021). "Accounting for Epistemic Uncertainty in Site Effects in Probabilistic Seismic Hazard Analysis." Bulletin of the Seismological Society of America 202, 111(4): 2005–2020.

Wair, R.B., DeJong, J.T., and Shantz, T. (2012). "Guidelines for Estimation of Shear Wave Velocity Profiles." PEER Report 2012/08, Pacific Earthquake Engineering Research Centre, University of California, Berkeley, CA

Waka Kotahi NZ Transport Agency (NZTA). (2022). "Bridge manual SP/M/022 3rd Edition, Amendment 4." 374pp.

Zhang, G., Robertson, P.K., and Brachman, R.W.I. (2004). "Estimating liquefaction-induced lateral displacements using the standard penetration test or cone penetration test." J. Geotech. Geoenv. Engng 130(8): 861–871.

PROCEEDINGS OF THE 14TH ANZ YOUNG GEOTECHNICAL PROFESSIONALS CONFERENCE
14YGPC ROTORUA, NEW ZEALAND, 2ND – 5TH NOVEMBER 2022

133

Different approaches to predict the ground settlements reinforced by rigid inclusions

Farbod Yarmohammadi[1], Ondrej Synac[2], Kostas Lontzetidis[3]

[1]CMW Geosciences, A3/63 Apollo Drive, Rosedale, Auckland 0632; PH (+64) 09 4144 632; email: FarbodY@cmwgeo.com
[2]CMW Geosciences, Level 3.17, 55 Miller Street, Pyrmont, NSW 2009; PH (+61) 02 9054 1243; email: OndrejS@cmwgeo.com
[3]CMW Geosciences, A3/63 Apollo Drive, Rosedale, Auckland 0632; PH (+64) 09 4144 632; email: KostasL@cmwgeo.com

ABSTRACT

Excessive ground settlements associated with building loads in highly compressible soils are among the most challenging geotechnical engineering problems, which can adversely affect the performance of the structures. Improving the performance of the soil using rigid inclusions is one of the most innovative methods to reduce the differential and overall settlements under the buildings. Rigid inclusions are not connected to the structures but are separated by a load transfer platform, usually consisting of a dense-graded aggregate layer with or without geogrids. Due to the complex nature of the load transfer mechanism and the interaction between the soil and the rigid element, there are still significant challenges to predict the settlements of the rigid inclusions. This paper draws a comparison between the possible methods including finite element modelling and analytical approaches for predicting the settlement of the ground improved by rigid inclusions. The results of the analyses are compared against the field measurements from a static load test in a site located in Auckland, New Zealand. This comparison between the predicted and measured settlements aims to assist the engineers to choose the appropriate approach for designing rigid inclusions.

Keywords: Numerical Modelling, Ground Improvement, Rigid Inclusions, PLAXIS, RATZ, RSPile

1 INTRODUCTION

Soft compressible soils can undergo significant settlements under an external surcharge. A classical solution to this problem is to use deep foundations under structures to transfer loads to the competent layers (Das & Sivakugan, 2018). However, due to the significant cost and time required for deep foundations, researchers and engineers have proposed different techniques to improve the performance of existing ground to support structural loads. Han (2015) classified the soil ground improvement methods into six main categories: 1) densification, 2) replacement, 3) drainage and consolidation, 4) chemical stabilisation, 5) reinforcement, and 6) thermal and biological treatment. Rigid inclusion is one of the recent techniques of soil reinforcement to increase the bearing capacity of the shallow soft soil and decrease the building settlements (Cirión et al., 2013). Early applications of rigid inclusion consisted of wooden piles pushed into the ground to increase the overall soil stiffness under the foundations (Auvinet & Rodríguez, 2006). However, with the recent advancements in technology, engineers have started to use concrete inclusions, which showed significant improvement compared to the timber columns (Cirión et al., 2013). These columns are not connected to the superstructure as their purpose is to improve the bearing capacity of the soft ground and reduce the anticipated settlements. A load transfer platform (LTP) consisting of a sandy or gravelly layer, is usually placed on top of the reinforced soil to help the efficient transfer of the load from the superstructure to the rigid inclusions (Auvinet & Rodríguez, 2006; Han & Gabr, 2002; Russell & Pierpoint, 1997; van Eekelen et al., 2013).

Several researchers have proposed different methods for rigid inclusions modelling (Bhasi & Rajagopal, 2015; Blanc et al., 2014; Combarieu, 1990; Mánica Malcom et al., 2016; Pérez & Melentijevic, 2015; Raithel et al., 2008). However, due to the complex interaction between the concrete columns, the soil, the LTP and the superstructure, there is still considerable uncertainty about the most efficient way to model the inclusions, especially for typical commercial solution such as warehouses. This paper draws a comparison between five possible approaches including finite element (FE) modelling and analytical approaches for predicting the settlements of the ground improved by rigid inclusions. The results of the analyses are compared against the field measurements from a static load test in a site located in Auckland, New Zealand, to assess the accuracy of the predictions. Furthermore, the ability of the different approaches to capture the ultimate capacity of the rigid inclusions will be analysed. This study aims to assist the designers in choosing the most efficient approach for designing the rigid inclusions.

2 SUMMARY OF THE PROJECT

CMW Geosciences undertook the detailed design of a ground improvement system in July 2021 to provide permanent support to a proposed single storey commercial development located at Papakura, Auckland, New Zealand. The ground improvement system comprises concrete rigid inclusions installed beneath the proposed footings and slab to limit the ground settlements. Post-construction load tests were performed on a test pile by putting a steel plate on top of the rigid inclusion and applying the pressure on it using a jack. Additionally, the piling rig was placed directly above the jack to apply the counterbalancing force. Three gauges were placed on different sides of the plate to monitor the vertical displacement of the rigid inclusions. The results of these tests are used in this paper to assess the predictions of different modelling approaches.

2.1 Ground model

Figure 1 and Table 1 present the ground model and the material properties used in the numerical modelling, respectively. 11m long unreinforced rigid inclusions with 450mm diameter and variable centre to centre spacings (i.e. from 2.5m to 6m) were designed to mitigate the large settlements in the soft material due to the bearing pressure of the proposed building (around 125mm under a 10kPa load).
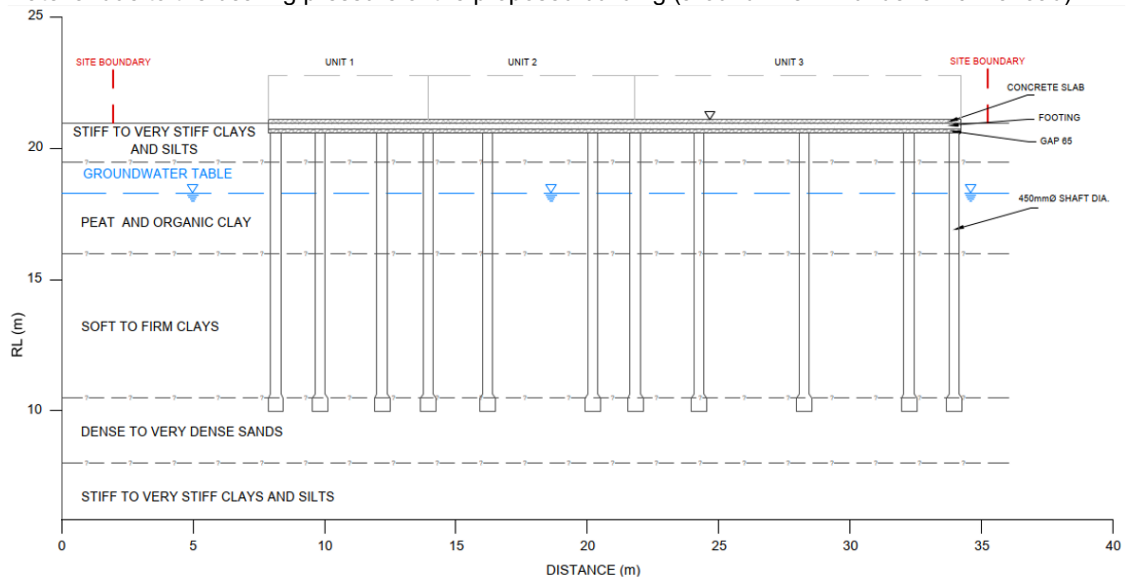
Figure 1 – The proposed ground model for the site

Table 1 –Material properties

Soil Layer	Thickness (m)	γ (kN/m)	S_u (kPa)	E (MPa)	Mohr-coulomb		HS/HS Small				HS Small	
					c' (kPa)	φ' (°)	E_{50}^{ref} (MPa)	E_{oed}^{ref} (MPa)	E_{ur} (MPa)	m	γ0.7	G_0^{ref} (MPa)
Stiff to Very Stiff Clays and Silts	1.50	18	80	28	5	28	22.4	17.92	67.2	1	$8×10^{-4}$	25
Organic Clays and Peat	3.50	17	10	1.5	1	25	1.2	0.96	3.6	1	$5×10^{-5}$	5
Soft to Firm Clays	5.50	17	20	3	1	25	2.4	1.92	7.2	0.8	$7.5×10^{-5}$	11
Dense to Very Dense Sands	3.50	18	-	40	1	35	32	25.60	96.0	0.5	$1.5×10^{-4}$	100
GAP65	0.15	20	-	100	0	40	-	-	-	-	-	-
Rigid Inclusion	-	22	-	$16.67×10^3$	-	-	-	-	-	-	-	-
Concrete Slab	0.18	23	-	$25.70×10^3$	-	-	-	-	-	-	-	-

PROCEEDINGS OF THE 14TH ANZ YOUNG GEOTECHNICAL PROFESSIONALS CONFERENCE
14YGPC ROTORUA, NEW ZEALAND, 2ND – 5TH NOVEMBER 2022

135

Five different numerical modelling approaches are used in this study: 1) FE modelling using Mohr-Coulomb model in PLAXIS 2D (Brinkgreve et al., 2017), 2) FE modelling using the Hardening Soil model (Schanz et al., 2019), 3) FE modelling using Hardening Soil model with small strain stiffness-HS-small (Benz, 2007; Schanz et al., 2019) in PLAXIS, 4) analytical analyses using RATZ software (Randolph, 2003), and 5) analytical analyses using t-z/Q-z curves (API, 2000) in RSPile software (Rocscience Inc., n.d.).

3.1 PLAXIS models

Unit cell axisymmetric models were developed in PLAXIS 2D to predict the settlement of the reinforced ground during the load tests. Undrained soil properties were used to model the load tests as they are done in short-term. Ballam and Booker (1981) recommendations were used to determine the dimensions of the unit cell. Mohr-Coulomb, Hardening Soil (HS) and HS-Small models were considered in the analyses to investigate the importance of the change in soil stiffness with strain in studying rigid inclusions. 15-node triangular elements with "very fine" global coarseness were chosen for the model (Figure 3). Furthermore, solid elements were used to model the soil, rigid inclusion and the overlying slab. Finally, an interface strength reduction factor of $R_{inter} = 0.6$ was chosen for the interface between the soil and the rigid inclusion. To properly model the testing condition, the loads from the tests were applied as point loads on top of the inclusions consecutively to calculate the corresponding displacements at the top of the piles for each soil model.
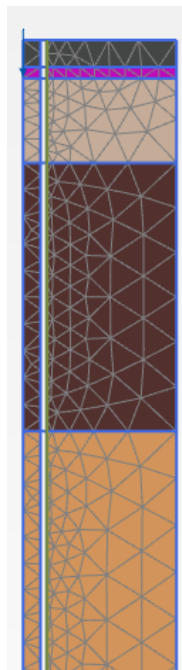
Figure 2 – Generated mesh for the FE model

3.2 Other models

Additional analyses were performed to estimate the rigid inclusion settlements using two different approaches including modelling of the rigid inclusion as a pile in RSPile and RATZ computer programs. RSPile uses the t-z/Q-z curves to take into account the skin friction and end bearing acting on the rigid inclusion and calculate its settlement under different loads. This is consistent with the approach recommended by the American Petroleum Institute (API, 2000) to model embedded piles.

RATZ is a software developed for non-linear 1-dimensional multi-segment modelling of piles. It considers the interaction between the soil and the rigid inclusion using the modified t-z/Q-z curves according to the soil properties. RATZ is also able to consider the group effects, cyclic load effects and thermal effects on the pile, which are beyond the scope of this paper.

4 RESULTS

4.1 Comparison with the load test

Figure 3 presents the settlement predictions of different modelling approaches compared to the experimental results from the load tests. Moreover, Table 2 summarises the root mean square (RMSE) values of the numerical modelling approaches with respect to the experimental data. From Figure 3 and

Table 2 it can be concluded that the HS Small model is the best model for predicting the settlement of the rigid inclusions during the loading and unloading events. Additionally, although the RATZ software decently captures the rigid inclusion settlements during the loading period, the unloading process was not modelled in this software, which led to a higher RMSE value compared to the HS Small model. Figure 3 also shows an example of the improved performance of the HS Small model in capturing the soil response, especially in small strains compared to the HS model. Finally, Figure 3 demonstrates that all the non-linear models performed better than Mohr-Coulomb, which significantly overestimates the rigid inclusion settlements, especially in larger loads that lead to more non-linearity in soil behaviour.
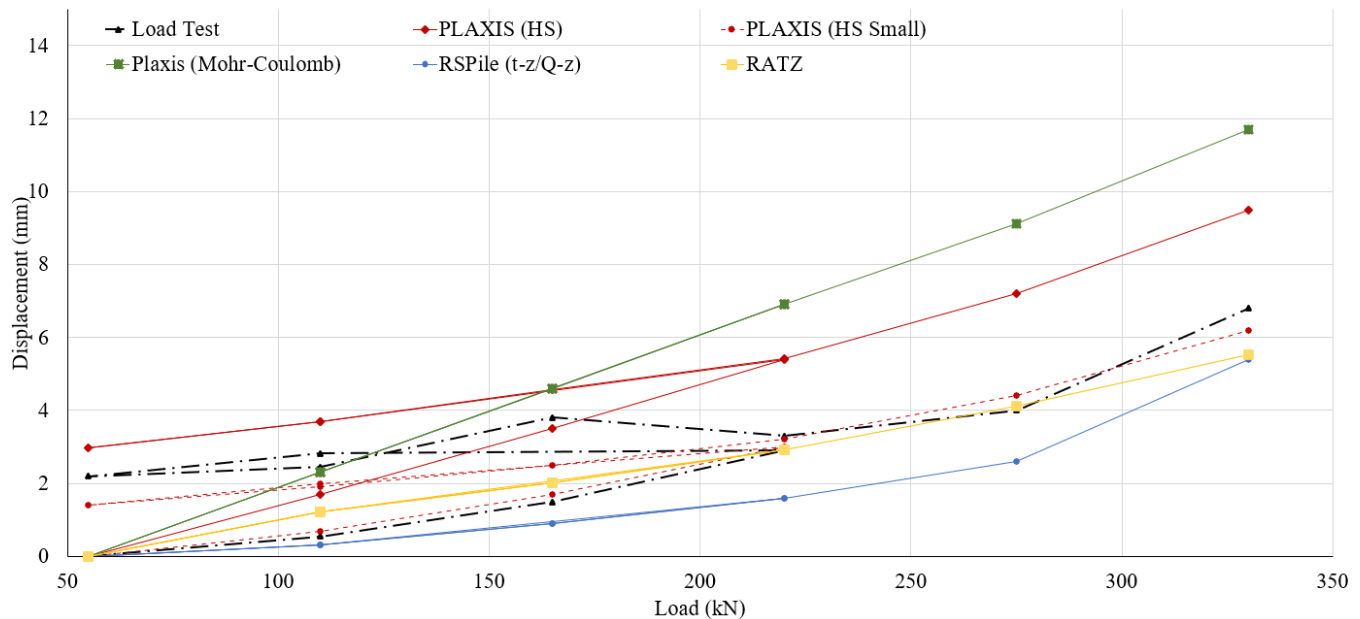
Figure 3 – The results of different modelling approaches compared to the load test

Table 2 – Comparison between the RSME values of different approaches

Modelling approach	PLAXIS (Mohr-coulomb)	PLAXIS (HS)	PLAXIS (HS Small)	RSPile	RATZ
RMSE (mm)	3	1.8	0.6	1.7	1.2

After validating the developed models against the experimental data from the load tests, additional analyses were performed to compare the ability of the models in estimating the ultimate capacity of the inclusions. The results of these analyses are presented in the next section.

4.2   Ultimate capacity of the piles

API recommends the point where the pile settles more than 10% of its diameter as its failure point and the load corresponding to this point as the ultimate capacity of the pile (API, 2000). Therefore, for the rigid inclusion considered in this study, the ultimate capacity is the load that leads to 45mm settlement in the column. However, due to the lack of experimental data and the ability of the PLAXIS HS Small model to accurately capture the pile displacements, this model was chosen as a reference to assess the other models' predictions. It should be noted that the load tests were done to a maximum displacement of around 6mm ($\approx$ 13% of the ultimate load) and therefore are not included in this section. According to Table 3, most modelling approaches significantly underestimate the ultimate capacity of the rigid inclusions mainly due to the overestimation of the displacements. On the other hand, RATZ has the closest prediction to the PLAXIS-HS Small model while slightly overestimating (i.e. around 5%) the ultimate capacity.

Table 3 – Predicted ultimate capacity of the piles using different numerical approaches

Modelling approach	PLAXIS (HS Small)	PLAXIS (Mohr-coulomb)	PLAXIS (HS)	RSPile	RATZ
Ultimate capacity (kN)	892	430	635	405	935

PROCEEDINGS OF THE 14TH ANZ YOUNG GEOTECHNICAL PROFESSIONALS CONFERENCE
14YGPC ROTORUA, NEW ZEALAND, 2ND – 5TH NOVEMBER 2022

137

5   CONCLUSIONS

This paper drew a comparison between five numerical modelling approaches to estimate the settlement and ultimate bearing capacity (based on the measured settlement) of rigid inclusions: 1) FE modelling using Mohr-Coulomb model in PLAXIS 2D, 2) FE modelling using the Hardening Soil model, 3) FE modelling using Hardening Soil model with small strain stiffness-HS-small in PLAXIS, 4) analytical analyses using RATZ software, and 5) analytical analyses using t-z/Q-z curves in RSPile software.

The results of the analyses were compared to the experimental data from a load test performed for a project in Auckland, New Zealand to validate the developed models and assess the quality of the predicted settlements. The results of these analyses showed that although most of the models could decently predict the rigid inclusion settlements during the loading period, only a proper non-linear model (i.e. HS Small) could predict the pile performance during the unloading event. Moreover, a comparison between the RSME values of the predicted settlements showed that the PLAXIS HS Small models could estimate the results of the load test better than other models (i.e RSME value of 0.6mm). The analyses performed in the RATZ software also showed a decent performance with an RMSE value of 1.2mm. On the other hand, the results showed that an elastic-plastic model like PM4Sand cannot consider the complex behaviour of the reinforced soil during the load tests.

Further analyses were performed to assess the ultimate capacity of the inclusions using the aforementioned approaches. Since the HS Small model produced the most accurate results in the previous section, the results of this model were chosen as reference to assess the performance of the other models in capturing ultimate capacity of the piles. These analyses showed that similar to the settlements, RATZ has the closest prediction to the PLAXIS-HS Small model with around 5% difference. All other models significantly underestimated the ultimate capacity of the rigid inclusions mainly due to the overestimation of their settlements.

This paper can help the engineers to choose the most efficient approach when modelling the rigid inclusions for real world applications. It also shows the importance of choosing the proper soil model for analysing the complex behaviour of rigid inclusions. It should be noted that the results of this study are limited to the soil type and the piles included in these analyses. Further studies are required to generalize the findings of this paper.

REFERENCES

API. (2000). *Recommended Practice for Planning, Designing, and Constructing Fixed Offshore Platforms-Working Stress Design: Upstream Segment. API Recommended Practice 2A-WSD (RP 2A-WSD): Errata and Supplement 1, December 2002*. American Petroleum Institute.

Auvinet, G., & Rodríguez, J. F. (2006). Rigid inclusions in Mexico City soft soils: history and perspectives. *Proc. of the Symposium Rigid Inclusions in Difficult Subsoil Conditions ISSMGE TC36*.

Balaam, N. P., & Booker, J. R. (1981). Analysis of rigid rafts supported by granular piles. *International Journal for Numerical and Analytical Methods in Geomechanics*, *5*(4), 379–403.

Benz, T. (2007). *Small-strain stiffness of soils and its numerical consequences* (Vol. 5). Univ. Stuttgart, Inst. f. Geotechnik Stuttgart.

Bhasi, A., & Rajagopal, K. (2015). Numerical study of basal reinforced embankments supported on floating/end bearing piles considering pile–soil interaction. *Geotextiles and Geomembranes*, *43*(6), 524–536.

Blanc, M., Thorel, L., Girout, R., & Almeida, M. (2014). Geosynthetic reinforcement of a granular load transfer platform above rigid inclusions: comparison between centrifuge testing and analytical modelling. *Geosynthetics International*, *21*(1), 37–52.

Brinkgreve, R. B. J., Engin, E., & Swolfs, W. M. (2017). Plaxis 2D manual. *Rotterdam, Netherlands, Balkema*.

Cirión, A., Paulín, J., Racinais, J., & Glandy, M. (2013). Displacement rigid inclusions. *Proceedings of the 18th ICSMGE, Paris, France*.

Combarieu, O. (1990). Fondations superficielles sur sol amélioré par inclusions rigides verticales. *Revue Française de Géotechnique*, *53*, 33–44.

Das, B. M., & Sivakugan, N. (2018). *Principles of foundation engineering*. Cengage learning.

Han, J. (2015). *Principles and practice of ground improvement*. John Wiley & Sons.

Han, J., & Gabr, M. A. (2002). Numerical analysis of geosynthetic-reinforced and pile-supported earth platforms over soft soil. *Journal of Geotechnical and Geoenvironmental Engineering*, *128*(1), 44–53.

Mánica Malcom, M. Á., Ovando-Shelley, E., & Botero Jaramillo, E. (2016). Numerical study of the seismic behavior of rigid inclusions in soft Mexico City clay. *Journal of Earthquake Engineering*, *20*(3), 447–475.

Pérez, R. G., & Melentijevic, S. (2015). Comparative analysis of analytical and numerical calculation methods for soil improvement by rigid inclusions. In *From Fundamentals to Applications in Geotechnics* (pp. 1859–1866). IOS Press.

Raithel, M., Kirchner, A., & Kempfert, H. G. (2008). German recommendations for reinforced embankments on pile-similar elements. In *Geosynthetics in civil and environmental engineering* (pp. 697–702). Springer.

Randolph, M. F. (2003). RATZ manual version 4.2: Load transfer analysis of axially loaded piles. *RATZ Software Manual*.

Rocscience Inc. (n.d.). *RSPile* (No. 2021).

Russell, D., & Pierpoint, N. (1997). An assessment of design methods for piled embankments. *Ground Engineering*, *30*(10).

Schanz, T., Vermeer, P. A., & Bonnier, P. G. (2019). The hardening soil model: formulation and verification. In *Beyond 2000 in computational geotechnics* (pp. 281–296). Routledge.

van Eekelen, S. J. M., Bezuijen, A., & van Tol, A. F. (2013). An analytical model for arching in piled embankments. *Geotextiles and Geomembranes*, *39*, 78–102.

PROCEEDINGS OF THE 14TH ANZ YOUNG GEOTECHNICAL PROFESSIONALS CONFERENCE
14YGPC ROTORUA, NEW ZEALAND, 2ND – 5TH NOVEMBER 2022

139

A tool for soil nail wall design optimisation using Slide2 and Python

M. P. Crisp[1], O. Davies[2]

[1]Mott MacDonald, 22 King William St, Adelaide, Australia; PH (08) 7325-7325; email: michael.crisp@mottmac.com
[2]Mott MacDonald, 383 Kent St, Sydney, Australia; PH (02) 9098-6800; email: owen.davies@mottmac.com

ABSTRACT

Optimised soil nail wall designs can result in reduced material costs, reduced construction program and reduced construction risk. Optimisation through assessing a large number of models manually has, in the past, been practically unfeasible due to the user time involved in model development and interrogation. The use of interfacing tools with the python scripting language, either through an included Python API or through modifying text-based models directly, has the potential to significantly reduce the time required for rigorous optimisation. This time reduction through digital tools, will lead to realisation of all the benefits design optimisation allows.

To demonstrate the above, this paper presents a python tool for assisting in the optimisation of soil nail wall design. It is implemented through the 2D limit equilibrium method software, Slide2, although may be applied to other software. Using the tool, an engineer can determine optimal soil nail lengths for a given slope angle, soil nail inclination, nail spacing, nail location (offset), and number of nails. Combinations of these parameters may also be assessed automatically to find a globally optimal solution. An example is given where a design was optimised simultaneously across multiple scenarios with different safety factors (e.g. flooding, earthquake, etc.). The use of this tool allows the engineer to identify the influence of key variables and quickly calibrate the optimised design to the specific constraints of the project.

Keywords: limit equilibrium method, soil nail wall, optimisation, python

1 INTRODUCTION

Geotechnical engineering software is becoming increasingly capable of interfacing with programming languages such as Python. This interfacing allows for extended software capabilities beyond that implemented by the core software, such as design optimisation and sensitivity analysis. The benefit of such an approach is that bespoke solutions can be developed which greatly speed up design, or even optimise designs to a degree that may not have been previously feasible due to time limitations.

For context, a number of programs have an Application Programming Interface (API) whereby a programming language can interact directly with the program, with Python (Python Software Foundation, 2021) being used in several applications.. However, there are other methods for integrating languages with software as well. For any program that stores its model information in a text-based format, code can be created to read, modify, and write these models. In essence, the user can create models that are modified in desired ways, such as alternate soil properties, load placement or magnitude etc. With sufficient coding, a model could be created entirely from scratch according to user inputs.

Further, these model modification tools can be combined with optimisation techniques in order to optimise designs. For example, there are a collection of evolutionary algorithms, such as the genetic algorithm, which use iterative population-based techniques to minimise a value (such as cost), and that can optimise several parameters simultaneously. Here, population-based means that within a given iteration, a large number of assessments are performed using different inputs, which collectively inform the population for the next iteration.

There's at least one example of finite element method (FEM) software Plaxis (Bentley, 2022) being used to optimise parameters of a soil nailed vertical cut using and comparing various evolutionary optimisation algorithms (Benayoun, et al., 2021). The downsides of these methods are that:

1. They are largely a black box, whereby the optimisation process is opaque.
2. They are not necessarily guaranteed to find a globally-optimal solution, particularly when complex solution surfaces exist with multiple local optima. A degree of randomness is involved.
3. A large number of analyses can be required (the number of iterations multiplied by the size of the population). Essentially, these methods can be "overkill" for simpler problems.

This paper presents an example of a tool being developed through integration with established software, in the form of a soil nail configuration optimiser for the 2D Limit Equilibrium Method (LEM) (Bishop, 1955)

software Slide2, a Rocscience program (Rocscience, 2022). Historically, designing soil nails for a retaining wall or cut slope could be fairly time-consuming due to:

- multiple geological sections
- construction stages
- multiple scenarios (earthquake; flooding; over-excavation etc.)
- different safety factors for each scenario

Each of these must be checked against the design to ensure the design requirements are satisfied. The tool, described within, solves this problem by determining a soil nail design by optimising across all scenarios and cases simultaneously, and on a row-by-row basis.

Here, optimisation means to minimise soil nail length for a given wall configuration. Other metrics, such as cost, are not considered. The optimisation methods discussed in this paper are well-established in literature, and as such are not the main focus of this paper. Rather, the novelty here lies in its application to multiple wall sections in a global and efficient manner, and as a proof-of-concept for enhancing established geotechnical software with scripting, regardless of the presence of a scripting API.

2   SOIL NAIL OPTIMISATION TOOL

The steps involved in the soil nail optimisation process are given in the flow chart in Figure 1. Note that this flow chart includes steps for multi-parameter optimisation, whereby variables such as vertical and horizontal nail spacing, and nail angle can be optimised. If the user wishes to simply optimise the lengths of nails that are already in the models, then the "optimise next combination" loop can be ignored.

2.1   Interaction with Slide2

Interaction with the Slide2 software is done through modification of the saved files. As is typical with Rocscience software, the models are text-based. There are various file types available, including the pure text .sli format. The alternative .slim format is simply zipped (compressed .zip) text files, with the ".zip" renamed to ".slim". The user will most often work with multi-doc files which are not supported by this optimisation tool. However it is a straightforward process to export the multiple models into a collection of individual .slim files. Python is well-equipped for both reading and writing .zip files.

Custom functions were written for interpreting the Slide2 model information, as well as for creating and manipulating soil nails. The only modification needed to the model file is to delete the lines containing existing soil nail geometry, and save the new/updated nails in an identical format. Into-the-page spacing is modified by changing the relevant parameter value in the list of soil nail properties.

The safety factor, also known as the factor(s) of safety (FoS) is obtained by running the model files through the slide2 compute program (aslidew.exe) and reading the text-based results file. The ability to both interact with the Slide2 model using python, and to read in the resulting FoSs, is the key part of this software, regardless of the optimisation algorithm employed.

2.1   Optimisation algorithm

The bisection method is a robust single-parameter optimisation method, as it is guaranteed to converge on the solution within a consistent timeframe when the solution lies between a specified upper and lower bound (Khoury & Harder, 2016). In this case, nail length is being optimised. The method starts by the user defining an upper and lower bound nail length (i.e. a maximum nail length (L_{max}) based on property boundaries, construction constraints etc. and minimum nail length (L_{min}) which well be zero for most cases). To find this optimal length it is assumed longer nails will achieve a higher FoS and shorter nails a lower FoS. An iterative procedure is then used whereby the nail length is continually bisected until the shortest nail length which satisfies the target FoS is found.

The bisection method consistently halves the search space in each iteration. There are other methods which can eliminate more than half of the search space in each iteration, and can potentially converge faster. These speed improves either rely on assumptions (i.e. Regular Falsi assumes the function is approximated by a straight line), or on additional information (Newton-Raphson method uses the derivative of the solution space) (Khoury & Harder, 2016). However, the former type are vulnerable to choke conditions, which could cause significant slowdowns. The latter type could fail to converge entirely. For these reasons, the bisection method is deemed most suitable.

The LEM method used for calculating FoS is also is fast enough not to require advanced approaches to minimise iterations and run times. Multi-parameter optimisation methods were also not considered due

PROCEEDINGS OF THE 14TH ANZ YOUNG GEOTECHNICAL PROFESSIONALS CONFERENCE
14YGPC ROTORUA, NEW ZEALAND, 2ND – 5TH NOVEMBER 2022

141

to reasons discussed in the introduction. However, the reader may read more about a range of evolutionary optimisation algorithms in (Omid, et al., 2017).

The algorithm assumes that the bottom-most nail will be longest and as such, the bottom row (adjusted in length with all above rows) is optimised first. This process is elaborated in a later example. In general this is a valid assumption. Although there may be cases where soil around the base of the cut is sufficiently long that the bottom-most nail can be removed entirely. This case is currently not accounted for, and the engineer should consider this possibility when reviewing the results. In the future this can be overcome by reversing the order in which rows are optimised, such that the top ones are first.
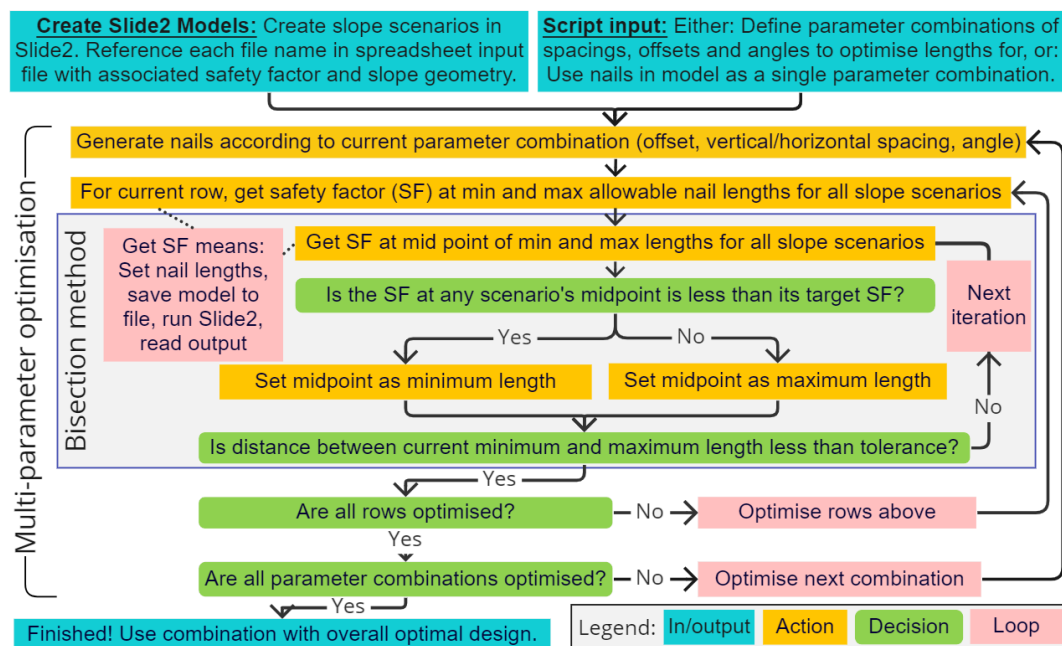
Figure 1: Flow chart describing the process of optimising soil nails.

2.2 Limitations

At present a number of limitations exist for the soil nail optimisation tool, as follows:

- All soil nails within any given model must all be of the same nail type (although different models can have different nails). Here, nail type refers to a set of material properties, such as tensile capacity, bond strength etc. Note, all Slide2 support types are supported (e.g. end-anchored, geosynthetic etc, including bond strength based on embedment material).
- A given soil nail row must have a constant head elevation, as this is how rows are identified across different models. However not all rows need to be present in all models.
- Multi-parameter optimisation involving vertical nail spacing, can not properly account for soil lift (excavation) stages. This is because the excavation levels are often dependant on the nail elevations, and the slope geometry cannot be changed in the tool.
  - This largely restricts vertical spacing optimisation to the final slope profile. The engineer should subsequently confirm that the design is valid during construction stages.
- Probabilistic analyses and transient water conditions are unsupported. In the case of transient water there is an additional file and solver program that the script is not yet hooked into.

3 EXAMPLE

An example of a slope section is considered. The geology and dimensions of the profile are shown in Figure 2. The slope is excavated from ground level at the top of the fill layer. Each lift (excavation for a nail row) is taken to 0.5m vertically below the nail head elevation. Nail lengths were fixed to a minimum and maximum of 0m and 10m respectively and with optimisation intervals at 0.5 m. Multiple scenarios for the profile are considered in the optimisation, as listed in Table 1. As such, the tool should produce a design that is not only valid and safe for the profile, but globally optimal as well.

In other words, multiple construction stages, and loading/water conditions are assessed within each optimisation iteration. Different geologies, soil or nail parameters could easily be added as additional cases in the optimisation, meaning that the results would not be sensitive to such variations, however this is not the current focus of this paper. In each iteration, the soil nail lengths are changed once across each case, based on the previous iteration. The nail lengths of each row are the same across all cases. Each case's FoS is calculated to check whether it satisfies its corresponding target value in that iteration. This means that all FoS are satisfied for all cases in the final result.

Due to space constraints within this paper, multi-parameter optimisation is not used here. Instead, the four nails, placed in the model by the user, have their length optimised. Nail location, inclination and spacing (both horizontal and vertical) are not modified within this example. As mentioned previously, this means the "optimise next combination" loop in Figure 1 can be ignored.

3.1   Conditions and material properties

The soil/rock material properties, and the soil nail properties are included in Figure 2. In addition, the soil nail bond strength is 23.3 kN/m in the "Fill" and "Residual soil" layers, and 58.3 kN/m in the remaining layers. A Mohr-coulomb strength model is used. The punching shear capacity of the shotcrete facing is not considered here.
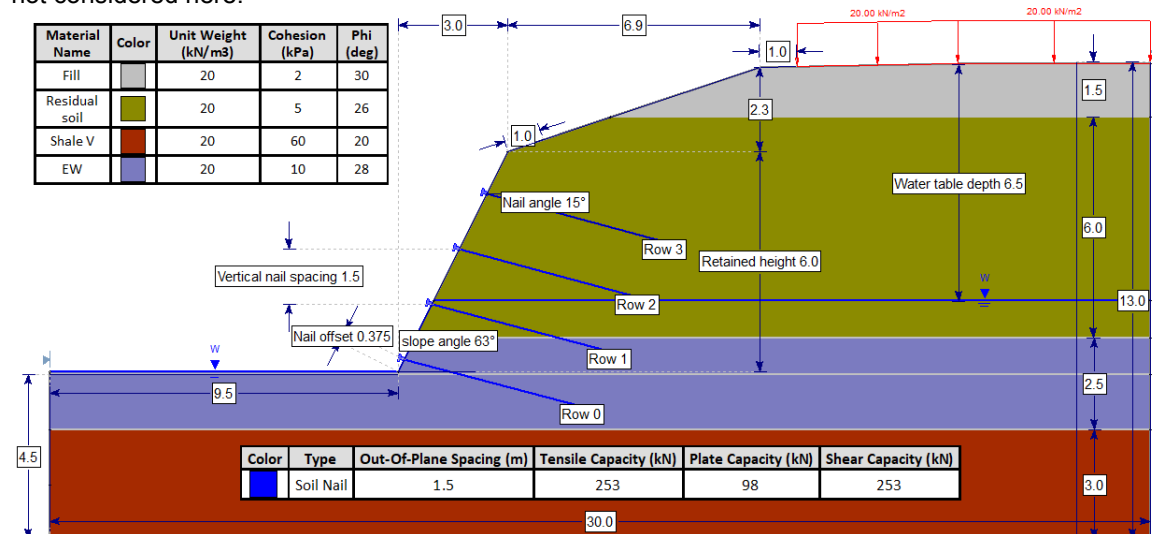
Figure 2: Dimensions and properties of the slope model.

The soil is considered undrained during the first lift, and during the earthquake analyses. For the earthquake case a horizontal seismic load coefficient of 0.09 has been adopted. In the flooding scenario, the water table within the soil is raised to 5.5 m below ground level. During all construction stages, including overcut, a surcharge of 10 kN/m^2 extended to 1 m from the crest of the retained slope.

3.2   Safety factor calculation

The FoS was determined from examining circular slip-surfaces, using the Morgenstern-Price method and a half sine interslice force function (Morgenstern & Price, 1965). The worst case slip surface was found using Slide2's "Auto Refine Search" method, which is a robust iterative search method (Rocscience, 2022). Note that all LEM and slip surface search methods, that are supported in Slide2, can be used. Multiple LEM methods can be used simultaneously, where the lowest FoS is taken.

Non-circular slip surfaces can also be used. However, care must be taken to ensure that small shallow slips (e.g. in the weak fill layer) don't define the global FoS. If such slips have a FoS that is below the target, then the slope is incorrectly considered "infeasible" and cannot be optimised.

3.3   Results

The design converged in 23 iterations, which comprised a total of 207 individual FoS calculations (23 x 9 scenarios). This is a relatively quick analysis, taking less than 30 minutes to complete. The final design lengths are given in Figure 4 Furthermore, the final FoS for each scenario is given in Table 1, along with the target FoS, and an indication of which section(s) was critical in the design of each nail row. This latter detail is useful as it informs the engineer which sections and/or slope elements to focus on in order to refine the design. These tables are taken from a CSV file produced by the tool.

PROCEEDINGS OF THE 14TH ANZ YOUNG GEOTECHNICAL PROFESSIONALS CONFERENCE
14YGPC ROTORUA, NEW ZEALAND, 2ND – 5TH NOVEMBER 2022

143

The results confirm that an optimal solution has been achieved, for this number and spacing of nails, and for this slope profile. This is evident by the final minimum FoS being equal to the target value of 1.5, i.e. shorter nails would result in an invalid value. An exception to this would be if higher nails could be longer than lower ones. As mentioned previously, this can be accounted for by reversing the order that rows are optimised in. Note that the rows being optimised in a specific order, as opposed to having rows of arbitrary, independent length, serves to constrain and greatly simplify the optimisation problem.

Table 1: Final FoS for each case, along with which case(s) were critical for each nail row.

Scenario	Lift 1	Lift 2	Lift 3	Lift 4	0.5 m Overcut	Drained	Un-drained	Earth-quake	Flood
Final SF	2.28	1.36	1.37	1.34	1.41	1.50	2.29	1.84	1.43
Target SF	1.30	1.30	1.30	1.30	1.30	1.50	1.50	1.30	1.30
critical at nail(s):		3	2	0, 1		0, 1			

The "Lift 1" case notably has no soil nails present, as the critical stage occurs prior to the installation of the first nail. As such, its safety factor does not change across iterations. The case was included for the script to determine that the slope was viable, although an engineer could conceivably do this manually before hand then exclude it from optimisation. Nail 3 (the top nail) first appears in the "Lift 2" case.

Furthermore, the tool also produces a PDF showing how the design evolved across iterations for all sections. An example of this, for a different model where all nail rows have different lengths, is shown in Figure 3 for the first two rows. Row 1 optimisation begins after row 0 is optimised.
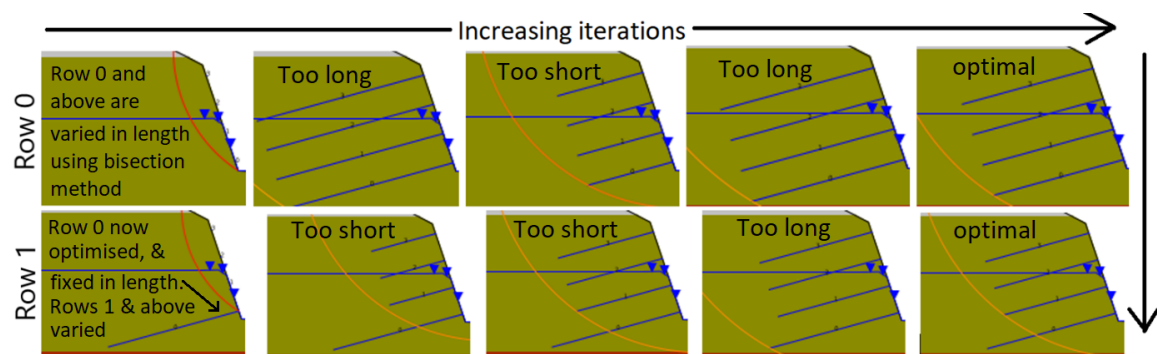
Figure 3: Selected iterations from the optimisation of the first two rows (starting from bottom row).

The final design and worst case circular slip surface (the "Drained" scenario) is shown in Figure 4, along with soil nail lengths. Upon comparison with Figure 2, which is a screenshot of the same model from the Slide2 modeller program, a lot of similarities are noted. The applied loads and water table are correctly shown, along with the geology and nails using the correct colour. This is achieved automatically as part of the tool's interpretation of the model file. Inspection of the full PDF (not shown here) can give the engineer further insight into how the design was achieved, and what the controlling factors were.
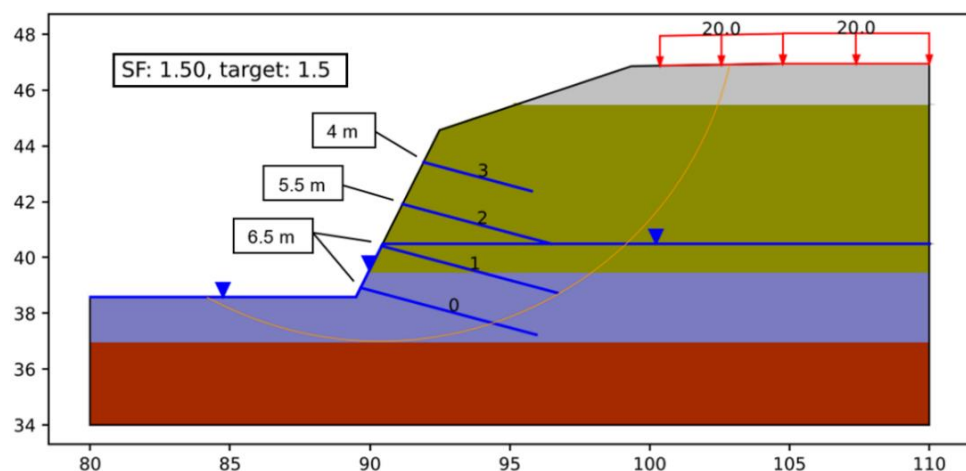
Figure 4: Tool-produced output section showing the optimised design and worst-case slip surface for the final drained scenario, along with soil nail lengths for each row.

3.1   Potential further analysis with existing tool features

Only one section was considered here, with a single set of soil properties. Soil nail designs can be sensitive to soil variability. As such, additional sections can be added with different geological profiles or alternate soil or nail material properties. There is no limit to the number of cases that can be accounted for in the optimisation of a single design. For example, each of the sections shown in the long section of Figure 5 could be incorporated, with the nail lengths being consistent within each row across all sections. Since vertical and horizontal soil nail spacing can also be optimised with the tool, using the multi-parameter optimisation mode, soil nails can effectively be designed in "3D"; i.e. optimal soil nail locations in the longitudinal and vertical directions can be identified. Alternatively, each of the sections could be optimised individually, such that nail lengths also vary longitudinally along the wall. Currently, non-horizontal rows (i.e. parallel to base cut) are not currently supported, but can be in the future. Analysis of the iteration history can provide insight into the FoS sensitivity of the final design.
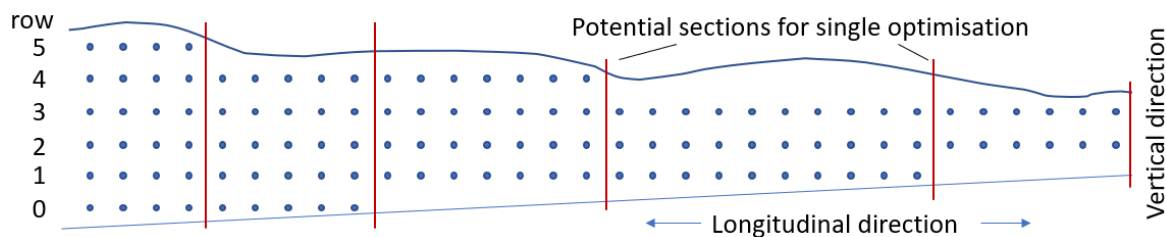
Figure 5: Example sections that can be used to optimise a wall along its entire length.

4   CONCLUSION

This paper has demonstrated a methodology and python tool to assist in optimising the design of soil nail walls using the Limit Equilibrium method. The optimisation tool accounts for a wide range of scenarios, including those related to construction, and extreme conditions such as earthquakes and flooding. This tool serves as a proof-of-concept for enhancing functionality of commercial geotechnical software with scripting, regardless of whether the software has a scripting interface.

The application of such tools is not intended to produce a finalised design. The designer remains responsible for ensuring any design meets design scope and code requirements. These tools are intended to hasten the optimisation process. A quicker process allows the designer to consider more scenarios and understand the benefits / drawbacks of design changes. This leads to the potential for more robust and economic designs with all the incumbent economic societal and sustainability benefits.

REFERENCES

Benayoun, F., Boumezerane, D. & Bekkouche, S., 2021. Techniques for Optimizing Parameters of Soil Nailed Vertical Cut. *Journal of Civil Engineering,* 16(1), pp. 131-145.

Benayoun, F., Boumezerane, D., Bekkouche, S. & Ismail, F., 2021. Optimization of geometric parameters of soil nailing using response surface methodology. *Arabian Journal of Geosciences,* Volume 14.

Bentley, 2022. *Plaxis 2D - Complete 2D Geotechnical Analysis Software.* [Online] Available at: https://www.bentley.com/en/products/product-line/geotechnical-engineering-software/plaxis-2d

Bishop, A., 1955. The use of the Slip Circle in the Stability Analysis of Slopes. *Geotechnique,* 5(1), pp. 7-17.

Khoury, R. & Harder, D., 2016. *Numerical Methods and Modelling for Engineering.* 1 ed. Berlin/Heidelberg: Springer.

Morgenstern, N. & Price, V., 1965. The analysis of the stability of general slip surfaces.. *Geotechnique,* 15(1), pp. 79-93.

Omid, B., Solgi, M. & Loiciga, H., 2017. *Meta-Heuristic and Evolutionary Algorithms for Engineering Optimization.* 1 ed. Newark: John Wiley & Sons.

Python Software Foundation, 2021. *Python Language Reference.* [Online] Available at: http://www.python.org/

Rocscience, 2022. *Auto Refine Search.* [Online] Available at: https://www.rocscience.com/help/slide2/documentation/slide-model/slip-surfaces/circular-surfaces/auto-refine-search [Accessed 28 July 2022].

Rocscience, 2022. *Slide 2 - 2D Limit Equilibrium Analysis for Slopes.* [Online] Available at: https://www.rocscience.com/software/slide2

PROCEEDINGS OF THE 14TH ANZ YOUNG GEOTECHNICAL PROFESSIONALS CONFERENCE
14YGPC ROTORUA, NEW ZEALAND, 2ND – 5TH NOVEMBER 2022

145

Tairāwhiti Roads Storm Damage: Determining factors for the best remediation solution to a mass number of slope failures

L. Parker[1], D. L. Fellows[2]

[1] GHD Limited, Level 3, 138 Victoria Street, Christchurch Central, 8013. PH (03) 378 0935; email: luke.parker@ghd.com

[2] GHD Limited, Level 3, 27 Napier Street, Freemans Bay, Auckland 1011. PH (09) 370 8165. email: Debra.Fellows@ghd.com

ABSTRACT

In 2017 and 2018 the Tairāwhiti Region was subject to multiple extreme rainfall events resulting in widespread damage to the regions roading network. Geotechnical assessment of the storm damage has found most failures were underslips resulting in loss of road width to the outside lane or road shoulder. The appropriate remedial solution for a site was determined by the following three fundamental engineering geology factors: geometry, geology, and water. Other varying factors included traffic volume/road importance level, expected level of resilience post repair, client budget, and construction material availability. Three geotechnical solutions were typically applied: bench and fill or mass stabilised earth walls (MSE), cantilever retaining wall (with or without anchors), and minor upslope road cut or full road retreats. Applying such fundamental engineering geological factors in a simple assessment template assisted the remediation of multiple sites in a rapid timeframe. This process highlighted the important role of an engineering geologist undertaking good geological observations, mapping, photography, record keeping, and understanding the wider context of the site. Including understanding the likely failure triggers such as leaking and blocked culverts, aging stormwater infrastructure, and forest harvesting.

Keywords: Engineering geology, slope stability, storm damage assessment.

1 INTRODUCTION

In 2017 and 2018, the Tairāwhiti region experienced three significant rainfall events and two cyclones. The extensive rainfall led to widespread damage to the Gisborne District Council's roading network, with 5,200 roading faults recorded. High levels of rainfall caused many road culverts to be overwhelmed resulting in downslope scour and saturation of the surficial soils and fills triggering slope failure. The failures caused loss of road carriageway or road shoulder. Rapid assessment was undertaken to assist in the resolution of the road damage across the network. This paper summarises the fundamental factors that resulted in the final remedial design solution for each site and the role of the engineering geologist. Having a strong understanding of such factors allowed for an effective repair solution to a significant number of storm damage sites across the Tairāwhiti local roading network.

1.1 2017/2018 rainfall intensity and deforestation

It is not unusual that the Tairāwhiti Region is exposed to frequent large rainfall events. The most notable event was Cyclone Bola in 1988. After this event much of the damaged steep land was planted into exotic forestry with a harvesting lifecycle of approximately 25-30 years. Consequently, many of these plantations are now mature and are being harvested. This is a notable factor in the widespread land damage within the region from recent storm events. The increase in deforestation in some areas and associated traffic results in increased pressure on Gisborne District Council roading infrastructure. After the June 2018 rainfall event, landslip damage was proven to be highest in areas that had been logged within the last 3 years, with 46% resulting from forestry infrastructure such as logging roads, haul sites and landings (Rosser et al. 2019). The specific details of the 2017 and 2018 rainfall events are outlined in Table 1.

Table 1: 2017-2018 Damaging rainfall events

Event	Rainfall	Time period
5 April 2017 (Cyclone Debbie)	85 mm	16 hours
12 April 2017 (Cyclone Cook)	80 mm	3 hours
13-16 & 20-24 July 2017	50-80 mm	Peak
3-4 June 2018 (Queens Birthday Storm)	266 mm	24 hours
4-9 September 2018	100 mm	Peak

Information sourced from (Fellows and Barker, 2021).

2 REGIONAL GEOLOGY AND GEOMORPHOLOGY

The geology of the Tairāwhiti Region has been broadly simplified into two geological terranes as illustrated in Figure 1. Much of the region comprises of the Tertiary terrane of less deformed massive to bedded sandstones and mudstones of early to middle Miocene age (Ministry for Primary Industries, 2018). The second is the Cretaceous terrane with variably indurated, extensively sheared, alternating siliceous mudstone; and sandstone of late Cretaceous to Palaeocene age comprising part of the East Coast Allochthon (Mazengarb & Speden 2000). Rhyolitic ash deposits are also present across the region up to 10 m thick. The upper weathered rock profile and volcanic ash material is prone to sliding on the underlying bedrock when steep or saturated.

The difference in the two geological terranes result in different geomorphology. The Cretaceous terrane is subdued slopes (15-25°) and prone to gullying, deep-seated earthflow, and slumping, while the Tertiary terrane is steep and prone to storm-initiated shallow land sliding and gullying (Ministry for Primary Industries, 2018). The steepness of this topography is a significant factor in defining the most appropriate remedial solution to the storm damage sites. This is an ongoing maintenance challenge for Gisborne District Council roading assets with 26% of the Tairāwhiti Regions land being prone to significant erosion compared to the national average of 8% (Ministry for Primary Industries, 2018).

3 DETERMINING FACTORS TO REMEDIATION OF ROADING INFRUSTRCUTRE

Of the 5,200 roading faults reported, 381 sites were classified as needing engineering assessment on the local roading network (Fellows and Barker, 2021). Figure 2 illustrates the significant number of design sites spread across the region. Numerous factors summarised below had to be considered in defining the best remediation solution for each site.
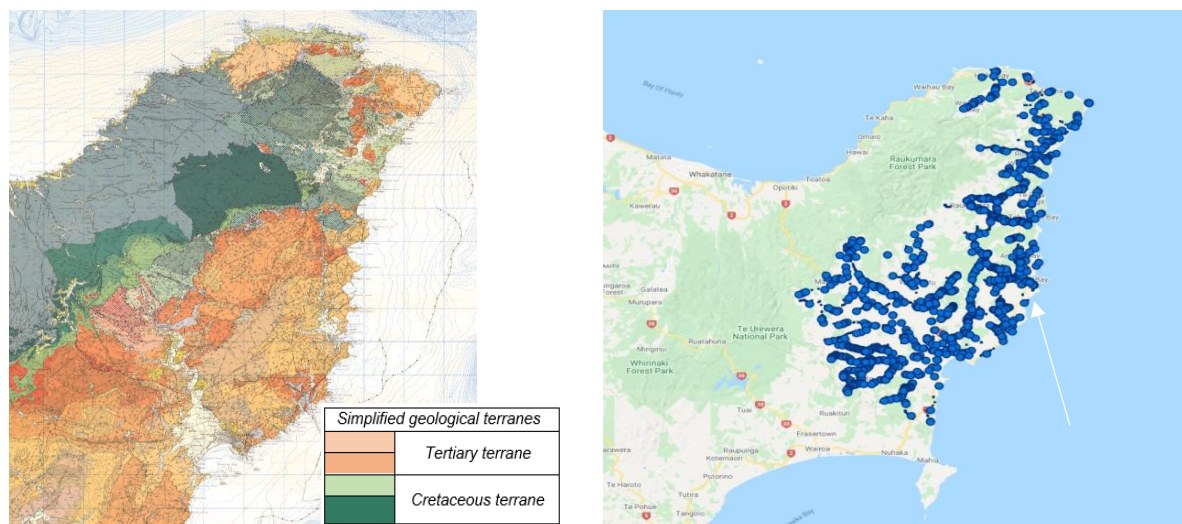

Figure 1 (Left): Geological map of the East Cape (Source Mazengarb and Speden, 2000)
Figure 2 (Right): Geographical spread of storm damage across Gisborne District Council roading network

PROCEEDINGS OF THE 14TH ANZ YOUNG GEOTECHNICAL PROFESSIONALS CONFERENCE
14YGPC ROTORUA, NEW ZEALAND, 2ND – 5TH NOVEMBER 2022

147

3.1   CLIENT FACTORS

Understanding the client's appetite for a repair solution for each site was the first step. Due to the large number of damaged sites and limited budget the client and consultant worked together to agree low-cost repair approaches that allowed the road to remain functional short term. This approach had limited engineering design and often did not meet typical New Zealand design standards. The approach considered returning the road to an operational level by the following decision factors summarised in Table 2**.**

Table 2: Client agreed design factors

Design feature	Client requirements
Downslope shoulder	Reinstatement of the downslope road shoulder to a minimum of 1.0 m width.
Functioning drainage	Repair the site with adequate drainage. Minimal to no storm water design or catchment analysis was to be undertaken by engineers.
Resilience post repair	Limited design life. This included a reduced seismic design life of 15 years.
Large scale global failure	Large scale global failure was not addressed.
Construction supervision	Limited to no construction supervision during construction.

As discussed in section 2, the highly erodible geology means natural construction materials such as hard crushed aggregate or gabion rock is scarce in the region and often needs to be sourced from large distances at an increased cost. This was a major factor in defining the types of repair solutions. The ease of construction in a short timeframe was also a client priority. The design solutions needed to be cost-effective and to be undertaken by local contractors from easily available materials. The three remedial options typically applied are summarised in Table 3.

Table 3: Client agreed remediation solutions

Remedial Option 1	Bench and fill or mass stabilised earth walls (MSE).
Remedial Option 2	Timber or steel pole cantilever retaining wall (with or without anchors).
Remedial Option 3	Minor upslope road cut or full road retreats.

3.2   ENGINEERING GEOLOGY FACTORS

As standard with the engineering geology discipline, the site geology, geometry, and the impact of water were the three fundamental factors needing to be understood for each site. Site assessment to understand the failure type (e.g., translational, circular or flow) and the movement triggers are crucial to defining the most appropriate solution. Undertaking geological mapping of these site factors with detailed sketches and observations in a simple site template enabled the design engineers and client to have a comprehensive understanding of the site. A breakdown of what fundamental site factors were recorded are summarised in Table 4.

Table 4: Key site factors recorded during site assessment

Geology	Geometry	Water
Depth, weathering, composition, and strength of • Road fill • Underlying soil • Upslope/downslope rock	• Existing carriageway width • Upslope/downslope angles • Failure height • Extent/length of failure • Inside/outside shoulder width • Road width suitable for lane closure to support construction	• Control of surface water, such as upslope table drain and cut off drains • Nearest culvert and condition including inlet/outlet culvert condition • Depth of ground water • Proximity to a stream or river

This process highlighted the importance of thorough use of the observational approach, good note taking, measurements, geological mapping, sketches, site photography and ground model development. Robust walkover of both above and below the failed section of road and thorough inspection of all stormwater infrastructure at the failure was essential. Having this information on hand during the remedial options review enabled the designers and client to make knowledgeable decisions, option adjustments or redesign without having to go back to site.

3.2.1 Geology and Geometry

Although the triggers and failure mechanisms are similar for many sites, the geology and geometry were always different. Every remedial option had to be tailored to fit the site. Experience from assessing many sites enabled the field team to understand the key geologic and geometric factors which influence the remedial options. Figure 3 shows a general schematic of what geometric and geological factors helped form the best fit remedial option. Option 1 relies on the underlying material to provide a suitable bench for an MSE/bench foundation. The depth to solid founding soil or rock coupled with slope angle on the downslope side strongly influences the choices for Options 2 and 3. A steeper downslope often arises in longer poles and/or multiple anchors, resulting in Option 2 becoming uneconomical. Remedial Option 3 was often the preferred solution by the client due to the short-term economic benefit.
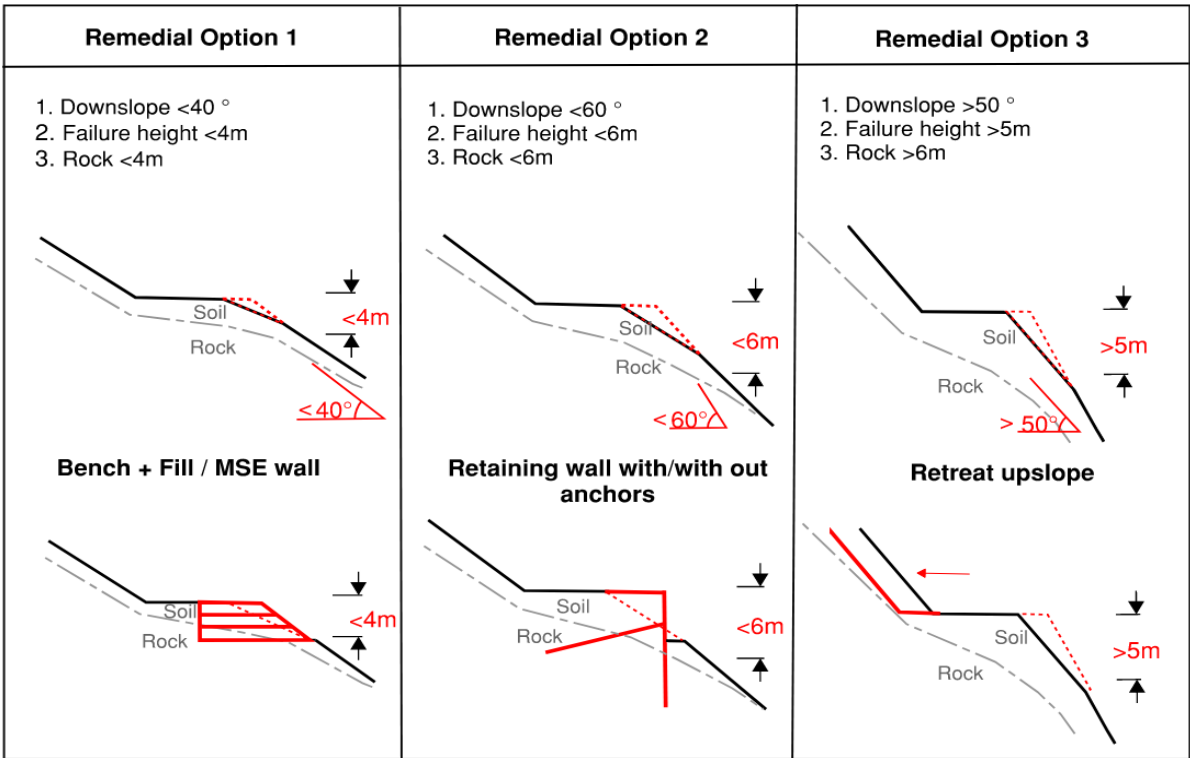
Figure 3: Generic schematic of the geometric and geological factors that helped determined the remedial option.

3.2.2 Water

As stated previously water is a fundamental driver of failure. Uncontrolled storm water or a high ground water table resulted in translational failure of saturated soils on the underlying bedrock and scour of the downslope sidling fill. Understanding the condition on site of the table drain or nearest culvert and how to better control storm water was essential for long term stability of the slope. Figure 4 shows a typical scour failure resulting from undersized and ailing storm water infrastructure.

PROCEEDINGS OF THE 14TH ANZ YOUNG GEOTECHNICAL PROFESSIONALS CONFERENCE
14YGPC ROTORUA, NEW ZEALAND, 2ND – 5TH NOVEMBER 2022

149

Figure 4: Anaura Road RP6.18 – Example site of scour from uncontrolled stormwater.

4   SELECTION PROCESS OF SOLUTION

The three typical remedial options were provided to the client together with the associated risk profile and estimated rough order cost. The three solutions were defined into the following categories for the client.

- High risk – Low-cost option
- Medium risk – Medium-cost option
- Low risk - High-cost option

Each solution was assessed on a case-by-case basis with several outside factors impacting the final solution. These factors included consenting, iwi, property boundaries, land purchase, client preference, utility locations and construction factors e.g., construction time and road closure needs. The site geology and geometric conditions usually resulted in the initial remediation selection, other factors gave rise to option changes or adjustments to best suit the above requirements. Figure 5 shows an example of each remedial solution before and after construction.

Figure 5: Examples showing the initial storm damage and final constructed design for each remedial option.

5 FUTURE STORM ASSESSMENT

Many learnings from the early 2017-2018 storm damage works have been adopted by both the client and consultant and applied to more recent storm events. A consistent design philosophy has been adopted by Gisborne District Council in 2020 for any ongoing storm damage. This philosophy has enabled a tiered approach to the importance level of the road and the required engineering design for remediation. Field assessment templates have since been digitised, with site assessment now being undertaken directly onto tablets enabling the data to be more readily accessible by the consultant and client. Initial reporting is now more stream lined and rough order cost estimate can become more automated.

6 CONCLUSION

Significant rainfall events over 18 months between 2017 and 2018 caused widespread damage to the Tairāwhiti Region and the Gisborne District Councils local road assets. Engineering geological assessment found most failures to be caused by uncontrolled stormwater resulting in slope instability and scour of the outside live lane or road shoulder. Several factors influenced the outcome of the final design solution. Understanding these factors were fundamental in selecting the preferred design solution to each location. These factors included.

- Geology and geomorphology of the Tairāwhiti Region
- The geometry and geology at the failure locations
- Ground and surface water including aged stormwater assets such as culverts or table drains
- Client factors such as limited budget, risk appetite and agreed design remediation factors
- Other varying factors such as traffic volume, consenting and construction material availability

Understanding these factors allowed the application of three typical remedial options based on risk and rough order cost. Key to the successful outcome of the process has been good engineering geological field practice and observations. The importance of the fundamentals such as the observational approach, geomorphic mapping, robust walkover, good note taking, accurate measurements, sketches, site photography and ground model development cannot be underestimated as key tool in the remedial option decision process. In addition, engineering geological assessment must be undertaken jointly with observation of the roading and stormwater infrastructure state.

7 REFERENCES

Fellows, D., & Barker, N. (2021). Slope Failures, scour and infrastructure damage: - Tairāwhiti road network response to multiple severse weather events. *Good grounds for the future*. Dunedin: NZGS Symposium 2021.

Mazengarb C, Speden IG 2000. Geology of the Raukumara area. Institute of Geological and Nuclear Sciences 1:250 000 geological map 6. 1 sheet and 60 pp.

Ministry for Primary Industries. (2018). *Best options for land use following radiata harvest in the Gisbone District under climate change: Lliterature review*. Wellington: Ministry for Primary Industries.

Rosser BJ; Ashraf S; Dellow S. 2019. Assessment of the use of differencing satellite imagery as a tool for quantifying landslide impacts from significant storms – a case study in the Uawa catchment, Tolaga Bay. Lower Hutt (NZ): GNS Science. 51 p. Consultancy Report 2019/ 93.

PROCEEDINGS OF THE 14TH ANZ YOUNG GEOTECHNICAL PROFESSIONALS CONFERENCE
14YGPC ROTORUA, NEW ZEALAND, 2ND – 5TH NOVEMBER 2022

151

Improvements to void hazard management for an active open pit mining through an old underground mine

M. Farmer[1] and J. Hancox[2].

[1]Pells Sullivan Meynink, 56 Delhi Road, North Ryde, Sydney, Australia; PH (+61) 449078499; email: michael.farmer@psm.com.au
[2]Glencore, Australia; email: joseph.hancox@glencore.com.au

ABSTRACT

McArthur River Mine (MRM) in the Northern Territory, Australia is one of the largest Zn-Pb deposits in the world. The ore body was initially mined with an expansive underground network of room and pillar and stopes, many of which remain open. The operation transitioned to open pit mining in 2006. Due to the extent and location of underground workings under the pit floor, void hazard interaction and management is an important part of the day-to-day pit operations.

The Void Management Procedure and Plans provide a framework to manage the risks to personnel and equipment from interaction with underground workings. More specifically, Void Management Plans provide a review and operational management plan for a particular void hazard area, considering the cost, timing and equipment access prior to works commencing. Due to variation in ground conditions and void geometry, management solutions are often not a straightforward problem. Prioritisation of safe management options may cause delays or changes to mine schedule.

This paper presents an overview of the operational strategies as well as recent improvements to void management, which involve a focus on a more rigorous and robust review of ground and void conditions. These improvements include a grid based Catastrophic Failure Analysis (CFA) check, which was developed to provide a rapid assessment of areas that require targeted investigation. The development of specific Q values to refine Scaled Span Analysis (SSA) results are also presented. The paper also presents an updated probe and monitor approach for stope management.

Keywords: underground, void, interaction, open pit, operations, geotechnical.

1   INTRODUCTION

McArthur River Mine (MRM) in the Northern Territory, Australia is one of the largest stratiform sediment hosted Zn-Pb deposits in the world. The eastward dipping orebody was initially mined with an expansive underground network of room and pillar and stopes, many of which remain open (Figure 1). Typical development drives are 5 m high by 8 m wide. Stopes are much larger, up to 40 m wide, 100 m long and 30 m high. The operation transitioned to open pit mining in 2006, with staged cutbacks progressing towards the east. The underground workings (referred to as "voids" at MRM) constitute an area of approximately 1.0 km by 1.5 km and will largely be mined out by the final life of mine (LOM) open pit. Due to the extent and location of voids under the pit floor, void hazard interaction and management is an important part of the day-to-day pit operations and will continue to be so throughout the life of the open pit.

This paper first presents a brief overview of the operational management plans for underground void interaction at MRM. Void interaction is managed through two primary documents: (1) the Void Management Procedure (Procedure) and (2) Void Management Plans (VMPs). The Procedure documents the general site guidelines for void hazard classification and management strategies (Smith and Bertuzzi, 2021). In contrast, the VMPs provide a detailed review and analysis of a specific void hazard and the operational management strategy for that area. VMPs typically include: a desktop study to assess current ground and void conditions, field investigation including probe drilling, analysis including Catastrophic Failure Analysis (CFA) and Scaled Span Analysis (SSA) and finally, the formulation of a management plan including delineation of specific voids to target for collapse or filling and addition/removal of void hazard exclusion zones. This paper presents recent improvements to the void analysis process, which provide a more rigorous and robust review of ground and void conditions.
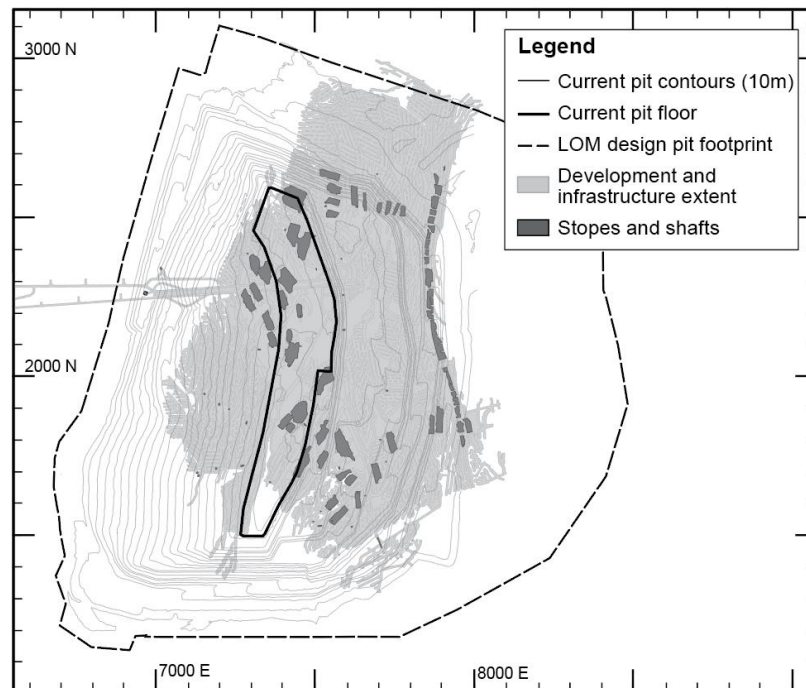
Figure 1: Extent of underground workings under the McArthur River Mine open pit.

Catastrophic Failure Analyses (CFA) are undertaken to assess the required crown thickness to safely operate over a void of a given height (Smith and Bertuzzi, 2021). The CFA equation is:

$$V = x (1 + 1/SF) \tag{1}$$

The analysis calculates the maximum possible vertical caving extent (V) of a void of given height (x) assuming that the caved material expands by a bulking factor (SF) and chokes the void such that no further caving can occur. This paper presents a grid-based CFA method that was developed to provide a rapid assessment of areas that require targeted investigation and reduce the time-consuming process of initial void analysis during the desktop study.

Scaled Span Analysis (SSA) is an empirical assessment of crown pillar stability against a series of case studies to determine the probability of failure (PoF) (Carter, 2014). It is routinely undertaken at MRM to compare against CFA results. The SSA considers the crown pillar rock mass quality (Q) and the void geometry, plotting results graphically. Q is calculated using the following formula:

$$Q = RQD/Jn \times Jr/Ja \times Jw/SRF \tag{2}$$

Where RQD is the rock quality designation, Jn is the number of defect sets, Jr is the defect roughness, Ja is the defect alteration, Jw is the defect water reduction factor and SRF is the strength reduction factor. This paper presents the site-specific Q values that were developed to refine Scaled Span Analysis (SSA). Lastly, this paper presents a proposed probe and monitor approach for stope interaction management.

2 VOID MANAGEMENT PLANS

Two common forms of VMPs at MRM are (1) Blast Master VMPs, which address all voids for the upcoming mining floor elevation and (2) Stope VMPs, which focus on specific voids with an elevated hazard, such as stopes or vertical shafts. The following sections detail the VMP process for both forms.

2.1 Blast Master Void Management Plans

Due to the extensive distribution of voids at MRM, Blast Master VMPs consider development drives for a given mining floor elevation. The workflow for a typical Blast Master VMP is as follows:
1. Assess current ground and void conditions, including:
    a. Overview of underground workings present in area under review
    b. Review of all previous probing drilling to determine caving extent

PROCEEDINGS OF THE 14TH ANZ YOUNG GEOTECHNICAL PROFESSIONALS CONFERENCE
14YGPC ROTORUA, NEW ZEALAND, 2ND – 5TH NOVEMBER 2022

153

      c. Review of production blast patterns to delineate areas of broken ground vs intact and collapsed voids

      d. Preliminary void analysis including CFA and SSA

      e. Development of field investigation program to address data gaps.

2. Field investigation including probing and 3D scanning.
3. Analysis of field investigation results including CFA and SSA.
4. Formulation of void management plan including:

      a. Targeting specific voids or areas for collapse or filling

      b. Create draft void hazard exclusion zones for both post-blast and post-excavation to the next pit floor elevation to assist with mine planning

      c. Any other area specific recommendations.

5. Review and implementation of management plan.

VMPs need to consider the potential cost, timing and equipment access for different management options. Due to the extent and complexity of underground workings at MRM, safe management options may cause delays or changes to mine schedule. Examples of this include where changes to blast pattern extents are required to collapse certain voids, where void hazard exclusion zones are extensive in a certain area requiring cranes for personnel to load blast patterns and where access for LVs and personnel is blocked to certain areas of the pit due to void hazard zones.

2.2 Stope Void Management Plans

Approximately 44 bulk stopes and 35 bench stopes were mined utilising a mine and retreat method which leaves the stopes open. Interaction of the open pit with the bench stopes is not anticipated for another 10 years. For the bulk stopes, 22 have been historically managed through a combination of filling and collapse. Many of the remaining bulk stopes require management in upcoming pit cutbacks. Due to the large stope void height (typically 30 m) the stopes require management from higher pit floor elevations than typical development drives. The workflow for a typical Stope VMP is as follows:

1. Analysis of the surveyed stope geometry, using CFA and SSA to determine the maximum possible caving extents
2. Development and implementation of probe investigation program
3. 3D scanning of open stope geometry to determine caving extent
4. Development and implementation of filling program
5. Further scanning and probing to determine the success of the filling program and resultant void hazard classification (generally a reduction in exclusion extent).

Due to the large void height, CFA results often mean that a void hazard exclusion zone would be implemented before site drill rigs were able to reach the stope crown for filling. This poses a substantial operational problem due to the required size of the exclusion zone and the locations of stopes, often under major haul road routes. Recent strategies to manage this issue are discussed in Section 3.3.

3 RECENT IMPROVEMENTS TO VOID ANALYSIS AND MANAGEMENT PRACTICES

3.1 Grid-Based Catastrophic Failure Analysis

CFA is typically utilised in void hazard assessments by spot checking areas of concern or relevance to upcoming operational works. Spot checks are undertaken by site engineers, and input into a spreadsheet, using equation (1). This form of the assessment relies on the diligence of the site engineer to identify areas that require analysis and can be very time consuming considering the number of voids present at MRM.

To streamline part of the analysis process, a grid-based CFA check was developed, allowing for a rapid assessment of broad areas. 3 x 3 m grids were created for the top and bottom of each development using "Vulcan", a 3D mine visualisation and modelling software developed by Maptek. The grid nodes were imported into a spreadsheet and the CFA calculated for corresponding top and bottom nodes for different pit floor elevations. The results were then imported back into Vulcan for visualisation. By progressively loading in CFA grid layers corresponding to different floor elevations, the engineer can rapidly assess large areas visually, with the CFA grids highlighting areas that fail CFA as the pit floor progresses downwards (Figure 2).

The grid-based approach provides an extremely useful tool for rapid, broad void hazard assessment. It has also substantially improved the robustness of the assessment in terms of detection. It is noted

however that the CFA assumes solid ground in the crown above the top of the development. In some cases, this does not represent the actual ground conditions, particularly where overlying developments have already been collapsed by blasting. The grid-based CFA assessment is therefore useful for assessments such as in the initial desktop study stages of void management plan development. However, it does not replace the need for detailed review of the ground conditions and void hazard prior to operations commencing in an area of risk.
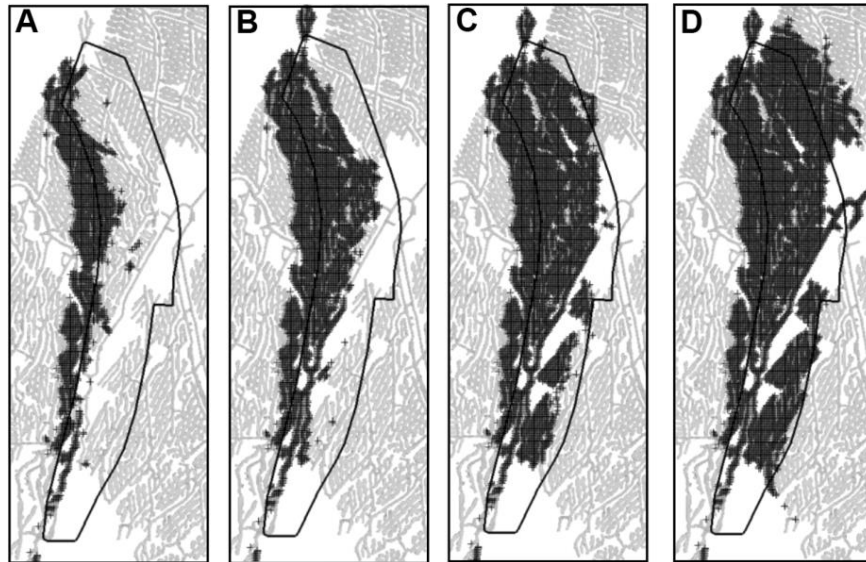
Figure 2: Example of grid-based CFA assessment for 2 Orebody Development (light grey). Dark Grey developments are areas that fail CFA for pit floor elevations A) 9840RL, B) 9816RL, C) 9800RL, D) 9784RL. The current pit floor extent is shown as a black polygon for reference.

3.2 Q Value Assessment for Scaled Span Analysis

An assessment of ground conditions was undertaken to develop site specific Q values for use in SSA. Previous analyses had assumed a Q value of 4.5, which was potentially conservative in typical rock mass conditions and unconservative where unfavourably oriented faults were present in the crown pillar.

Three rock mass/ structural domains were defined for the Q value assessment: (1) typical, (2) folded and (3) faulted. The 'typical' domain is the most common at MRM, characterised by uniform, moderately dipping bedding with two orthogonal joint sets. The 'folded' domain is where large to small-scale folds are present in the crown pillar. The 'folded' rock mass is likely to have a slightly reduced quality when compared to the 'typical' domain. The 'faulted' domain is applicable where a major or minor fault is modelled in the crown pillar and its orientation would promote chimneying and a higher degree of caving. The 'faulted' domain has significantly lower quality rock mass compared with the other two domains.

The equation (2) inputs to calculate a Q value for each domain are listed in Table 1. Most parameters were assessed based on mapping and available borehole data. The adopted Jw value considers that the underground workings have a significant dewatering impact on the pit. Consequently, the crown pillars for voids near the pit floor are likely to be largely dry, with only minor inflow during rain events. SFR was assessed by running a finite element (FE) analysis in the "RS2" software by Rocscience. The analysis section represents a typical distribution of development drives at MRM and parameters follow those used in previous site analysis. The results show that a SRF value of 0.5 – 2 is appropriate for the Q value assessment for typical and folded cases. A slightly higher SRF value of 5 was adopted for the faulted domains.

Table 1:   Q Value Assessment Input

Domain	RQD	Jn	Jr	Ja	Jw	SRF
Typical	70 - 93	9 - 12	2 - 3	1	0.66 - 1	1
Folded	83 - 90	9 - 12	1 - 3	1	0.66 - 1	1
Faulted	65 - 83	9 - 12	1 -1.5	15	0.66 - 1	5

PROCEEDINGS OF THE 14TH ANZ YOUNG GEOTECHNICAL PROFESSIONALS CONFERENCE
14YGPC ROTORUA, NEW ZEALAND, 2ND – 5TH NOVEMBER 2022

155

Due to variability of conditions within the three domains, a range of input parameters were assessed. This resulted in a range of Q values for each domain as shown in Figure 3. The average Q value for each domain has been adopted for SSA.

Summary of Assessed Q Range	Faulted	Folded	Typical
Upper Bound	0.2	30.0	31.0
Average	0.1	17.3	19.4
Lower Bound	< 0.1	4.6	7.7
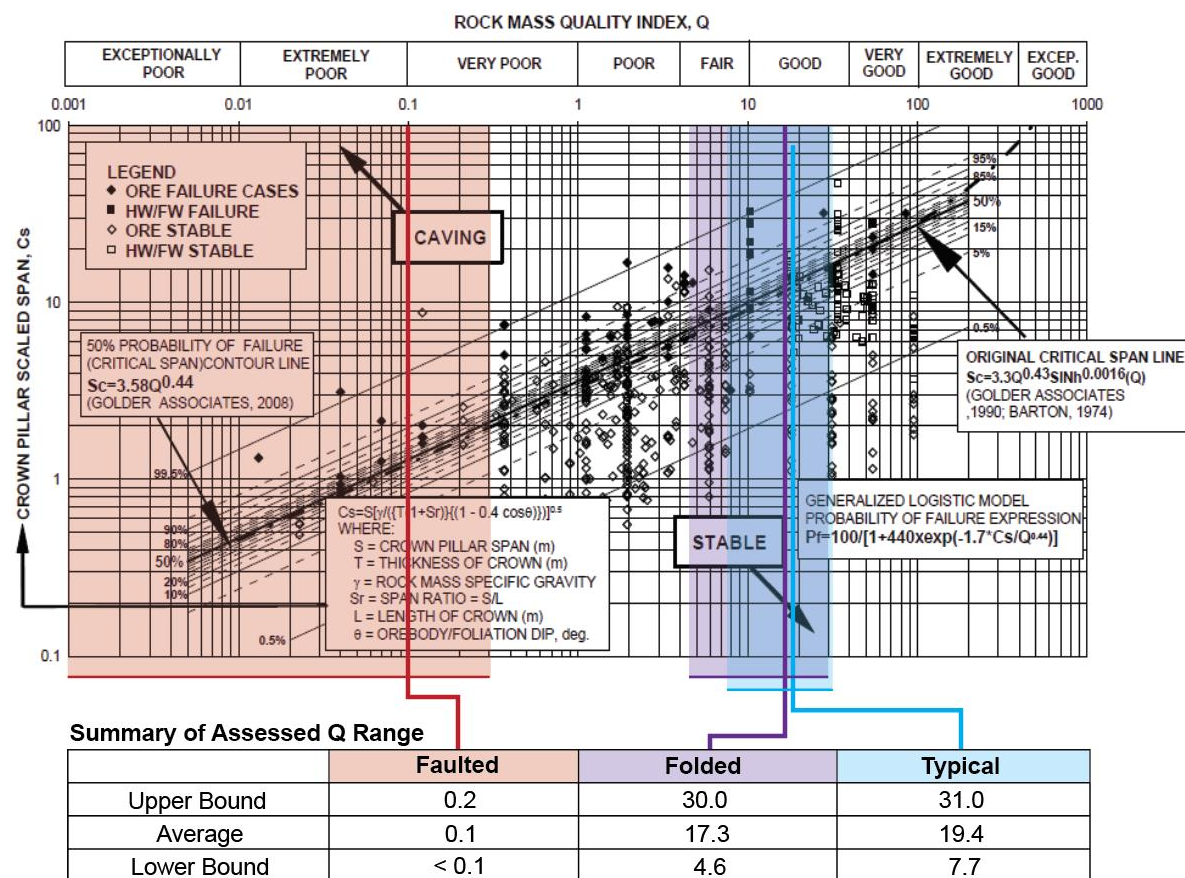
Figure 3: Summary of assessed Q values for MRM (modified from Carter, 2014).

3.3 Operational Stope Management

The upcoming open pit cutbacks are expected to intersect a number of large open stopes (Figure 1). SSA show that the stope crowns could be unstable as mining approaches and possibly experience caving conditions. CFA analysis for the surveyed stopes shows that current site drill rigs will be unable to intersect the stope crowns to fill and reduce the void height without operating below the CFA failure level. Consequently, a total exclusion zone would be triggered when the pit floor transitions below the CFA failure level of the open stope. The largest stopes are about 40 m wide by 100 m long. An exclusion zone of this size becomes unmanageable from an operational perspective, unable to be effectively blasted and excavated, and would potentially leave a large intact pillar as the rest of the pit floor progresses down. In addition to this, the stopes are sometimes located under major haul ramps, which would require major pit redesigns to maintain pit floor access.

An investigation was undertaken to assess different approaches and controls to manage the bulk stopes safely to reduce the impact to the operations and the mine schedule. Three main components were considered: (1) exclusion zones, (2) proving that the crown pillar is intact and (3) monitoring. In the absence of drilling capability to confirm the caving extent of the stopes and assuming that caving occurs progressively overtime as the open pit operations progress closer to the stope, a probe and monitor approach was proposed, as shown in Figure 4.

Several crown pillar monitoring options of varying complexity were assessed. Sub-surface monitoring options included resistance wire or rod extensometers, wireless crown monitoring systems typically used in block cave mining and geophones. Surface monitoring options would utilise the existing site slope stability radar and prism systems. Cost, timing, interaction and complexity were considered for

each option. Preference was given to less complex options leading to a simple manual extensometer being chosen.

The proposed updated process for operational stope management is as follows: Stage A) vertical probe holes drilled from above the CFA failure level to the maximum depth that site drill rigs can achieve (70 m). Once 70 m of intact crown pillar is confirmed, the floor is blasted to the next bench elevation, with an exclusion zone being triggered post blast as per the void management procedure guidelines. Stage B) Inclined probe hole(s) are drilled from outside of the exclusion zone to prove that the stope has not caved within ~60 m of the surface. Once this is confirmed, a vertical hole is drilled to 70 m depth and an extensometer installed. The extensometer extends above the hole collar with an easy to see, large displacement scale that corresponds to a Trigger Action Response Plan (TARP). Should the extensometer indicate that the displacement threshold has been reached, then a total exclusion zone is triggered pending further investigation. Stage B is repeated iteratively bench by bench until the stope crown is intersected by probe holes. Stage C) once the crown is intersected a fill plan can be implemented aiming to reduce the total open void height. Stage D) once the fill program has been completed, and filling success confirmed, a revised CFA level can be implemented with consideration to the reduced void height. Lastly, the void hazard exclusion zone can be removed.
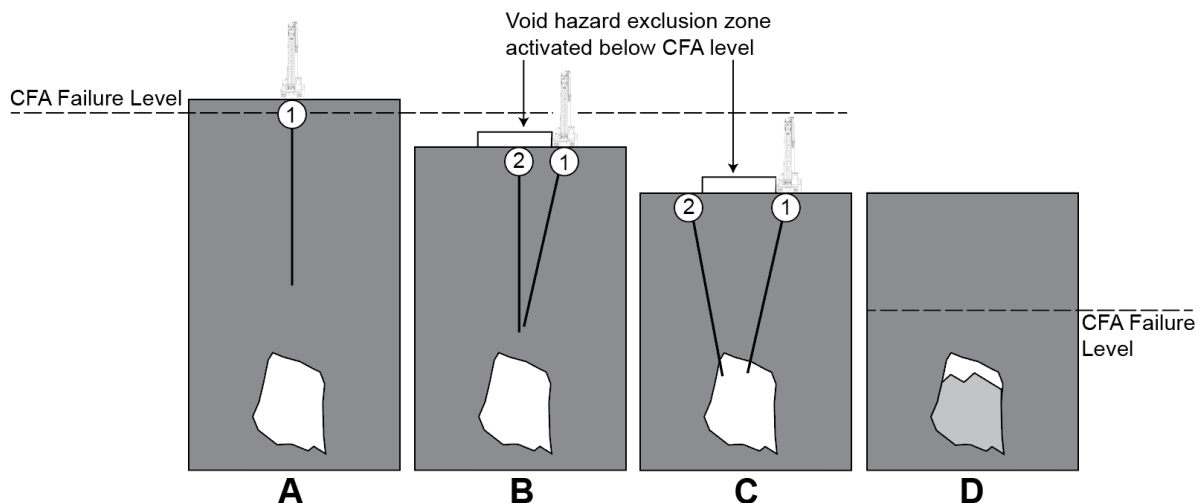
Figure 4: Schematic of updated management strategy for bulk stopes.

4   CONCLUSIONS

This paper has presented several recent improvements to the void hazard management at McArthur River Mine. The development of a grid-based CFA check has drastically reduced the amount of time required and improved robustness for preliminary void hazard assessments on a broad-scale. The development of site-specific Q values has improved the application of the SSA. The improvements to void analysis will ensure that void hazards are safely managed while reducing delays and impacts to mine scheduling. Lastly, a new probe and monitor stope management approach was presented. This process aims to reduce impacts to mine operations while safely managing the void hazard presented by large open stopes.

5   ACKNOWLEDGEMENTS

REFERENCES

Carter, T.G. 2014. "Guidelines for use of the scaled span method for surface crown pillar stability assessment". *Proceedings of the 1st International Conference on Applied Empirical Design Methods in Mining*, International Society for Rock Mechanics and Rock Engineering.

Smith, W, Bertuzzi, R. 2021. "Mining through historic underground workings and systematic void management processes at McArthur River Mine" in PM Dight (ed.), *SSIM 2021: Second International Slope Stability in Mining*, Australian Centre for Geomechanics, Perth, pp. 277-286, https://doi.org/10.36487/ACG_repo/2135_17.

PROCEEDINGS OF THE 14TH ANZ YOUNG GEOTECHNICAL PROFESSIONALS CONFERENCE
14YGPC ROTORUA, NEW ZEALAND, 2ND – 5TH NOVEMBER 2022

157

Dewatering effects on the Richmond South Trunk Main – geotechnical considerations for design and construction

M. Burrows[1], K. Clapcott[2] and E. Gkeli[3]

[1]Stantec New Zealand, Hazeldean Business Park, Level 2/2 Hazeldean Road Road, Christchurch, New Zealand PH (03) 341-4701; email: marcus.burrows@stantec.com
[2]Stantec New Zealand, 66 Oxford Street, Richmond, New Zealand PH (03) 546-0568; email: ken.clapcott@stantec.com
[3]Stantec New Zealand, Stantec House, Level 15, 10 Brandon Street, Wellington, New Zealand PH (03) 438-15771; email: eleni.gkeli@stantec.com

ABSTRACT

The Richmond South bulk water main construction project comprised installation of approximately 1km of DN450 PE pipe and associated infrastructure, including rammed steel conduits beneath state highways, and stream crossings in Richmond, Tasman, New Zealand. The conventional cut and cover pipe installation methodology required dewatering, and subsequent discharge and treatment of the water after extraction from the coarse grained Holocene alluvium. A dewatering assessment for an assumed pipe ram launch pit was undertaken in the design stage, and information added to the contract documents.

The construction works began in June 2021 and encountered lithology preventing deeper well pointing, higher groundwater level, and inflows of water into excavations in excess of that anticipated by the design. The higher groundwater level, the different hydraulic conductivity of the soils than those initially assumed in the design, and the timing of the works in the calendar year are identified as key causes of the excessive inflow. The ability of the Contractor to adapt their methodology, then extract and discharge large volumes of sediment laden water in an urban environment became critical for the completion of the works, incurring additional time, cost, and engineering effort to address.

This paper discusses the adequacy of geotechnical investigations and detail of dewatering assessment including sensitivity to input criteria. The implications of unforeseen geotechnical and groundwater conditions, primarily their effect on the practicality of pipe installation works, cost, and contractual arrangements are also discussed.

1   INTRODUCTION

The Richmond South bulk water pipeline project comprised investigation, design and construction of approximately 1km of DN450 PE pipe and associated infrastructure, including, two 600mm rammed steel conduits below State Highways 6 and 60, and two stream crossings. The pipeline is located in Richmond, Tasman, and crosses land of various uses, including state highways, urban residential roads, and green field rural properties.

Geotechnical investigations comprising machine excavated test pits were excavated prior to design in order to obtain an understanding of the near surface ground conditions. A dewatering assessment was undertaken for one of the pipe ram launch pits and anticipated groundwater inflow rates and dewatering effort were developed. A qualitative assessment of potential settlement was undertaken and concluded that dewatering activities would not result in settlement with potential to adversely affect adjacent buildings or infrastructure. Construction of the infrastructure was observed by the designer and geotechnical engineer.

This paper outlines all phases of the project and follows the impact of dewatering considerations throughout the project lifecycle. While details of this case study are specific to the Richmond South works, the intent is to present the considerations and outcomes for a wider engineering application.

2   PRE-CONSTRUCTION

2.1   Geotechnical Assessment and Design

2.1.1   Geological setting

158

PROCEEDINGS OF THE 14TH ANZ YOUNG GEOTECHNICAL PROFESSIONALS CONFERENCE
14YGPC ROTORUA, NEW ZEALAND, 2ND – 5TH NOVEMBER 2022

Published geological mapping at the Richmond South site (Geological and Nuclear Sciences Geological Map 9) shows Holocene age Q2a deposits comprising clay-bound gravel with minor fan deposits, commonly known as Hope gravels, in the Nelson, Tasman area.

2.1.2   Investigations and reporting

A geotechnical investigation programme comprising five test pits was undertaken across the site. Test pits were evenly spaced across the alignment and were typically advanced 2-3m below existing ground surface to the proposed pipe invert level and deeper in most instances. Subsurface material was consistent across the alignment and comprised silty coarse gravel with some cobbles and boulders, consistent with the unit description of Hope Gravels description identified in geological mapping.

Four test pits were undertaken in December 2018 (TP1-4), and one test pit in October 2020 (TP5). Groundwater was observed at 2.8m below ground surface in TP5 only and the others were dry. TP5 was located immediately adjacent to the pipe ram launch pit for the SH6 crossing.

The test pit investigation method was selected due to the expected gravelly and cobbly soils, and proposed pipe ram installation methodology. Test pits were limited to 3m in depth due to proximity to highway, commercial and residential infrastructure, and the highly trafficked urban environment. A deep borehole investigation with piezometric monitoring was proposed, however this was deferred to the construction programme rather than prior to design.

2.1.3   Pipe ram launch pit dewatering assessment

The dewatering assessment undertaken aimed to predict the rate of groundwater abstraction required to dewater an assumed 15m long, 3m wide excavated launch pit adjacent to SH6. The analysis used a transient analytical flow model to calculate groundwater inflow rates to a long narrow pit excavated into an unconfined aquifer, after Hazel 2009.

The model required five main inputs: the thickness, hydraulic conductivity and specific yield of the aquifer, the dimensions of the pit, and the water table drawdown in the excavation. Values for each input are summarised as:

1. A saturated zone modelling the assumed aquifer thickness of approximately 10m was used.
2. The hydraulic conductivity of the aquifer was estimated from soil descriptions from TP5. For sand and gravel mixtures, Kruseman and de-Ridder (2000) provide hydraulic conductivity values ranging from 5 to 200 m/d. A sensitivity analysis was undertaken using hydraulic conductivity values of 10 m/d, 100 m/d and 200 m/d to model the impact of various flowrates, which are included in Table 1.
3. An aquifer specific yield of 0.1 was adopted as suggested by Kruseman and de-Ridder (2000). This is a typical value for unconfined sand and gravel aquifers.
4. A pit dimension of 15 m long by 3 m wide was assumed.
5. Water table drawdown ranging from 0.42m (optimistic case) to 1.12m (conservative case). The range of groundwater levels was selected to allow for seasonal and weather influences. The best and conservative cases were noted to be an estimate; it was highlighted that the groundwater level in the conservative case may potentially not be the worst case.

The output of the assessment identified a range of possible flowrates for the excavated pit and are presented in Table 1.

Table 1. Dewatering assessment outputs

Scenario	Groundwater drawdown in excavation (m)	Groundwater inflow (L/s) for range of aquifer hydraulic conductivities (m/day)		
		10	100	200
Optimistic Case	0.42	2	11	19
Expected Case (based on water level observed in TP5)	0.62	2.5	14	25
Conservative Case	1.12	4	23	42

The assessment estimated that the inflow rates in the launch pit excavation could range from 2-42 L/s and a reasonable prediction of 10-20 L/s was provided.

PROCEEDINGS OF THE 14TH ANZ YOUNG GEOTECHNICAL PROFESSIONALS CONFERENCE
14YGPC ROTORUA, NEW ZEALAND, 2ND – 5TH NOVEMBER 2022

159

2.2   Contract Documents

2.3   Summary of contract documents

The full dewatering assessment was included in the contract documents for the project, and multiple references to the requirement for dewatering of excavations were made in the technical specification. The output and recommendations from the dewatering assessment were used as a basis of estimating a price during direct appointment of the Contractor. It was agreed during appointment of the Contractor that a reasonable allowance for dewatering works for the duration of the contract was one 150mm pump typically capable of pumping up to approximately 50 L/s, and associated pipes and conventional settlement tank treatment setup. This would allow for the conservative scenario of the assessment.

2.3.1   Resource Consent

Resource consent for the construction works included dewatering requirements, notably two key clauses as follows:
1. An initial drawdown phase shall be allowed at a rate of 106 L/s, with continuous dewatering allowed at a rate of 30 L/s. Continuous pumping rates exceeding these limits are subject to the approval of the local authority's Senior Resource Scientist.
2. Sediment control and/or treatment measures shall be adequate to ensure the visual clarity of any receiving waterway is not reduced by more than 40%, at a point measured 50m downstream of any discharge point, as a result of the dewatering activities.

3   CONSTRUCTION

3.1   Dewatering Methodology and Groundwater Observations

3.1.1   Launch Pit Dewatering

Construction works at the pipe ram launch pit area began in July 2021. The Contractor's initial dewatering methodology for the launch pit excavation comprised the installation of a dewatering well and initiating pumping for a sufficient length of time to draw down groundwater to the required level. The Contractor installed a 150mm diameter dewatering well to 9m below ground surface, with a slotted intake approximately 5m long below the excavation invert.

On installation of the well casing, the Contractor's driller attempted to develop the bore, however, was unable to extract water. The Contractor's driller was experienced in advancing bores for groundwater take in the area. Well pumping was abandoned on the realisation it would not be effective. The Contractor then installed two 0.3m diameter PVC sumps within the excavation to approximately 0.5m below the excavation invert. Groundwater was allowed to equalise within the excavation showing a static groundwater level of 1.6m below ground surface. The final launch pit excavation dimensions were approximately 15m long, 2m wide, and 3m deep. This required a groundwater drawdown of 1.4m to dewater the launch pit excavation.

3.1.2   Trench Dewatering

The typical detail for installation of the DN450 water main required excavation up to 2m depth across the alignment. Prior to the work starting, the trench excavation was anticipated to be largely dry with some areas requiring minor dewatering, as indicated by the water level observed in the test pit investigations. Cut and cover trenching was undertaken with approximately 50m lengths open at any one time. Groundwater was consistently observed between 1.6m to 2m below ground surface and was removed by sump pumping from two 0.3m diameter PVC sumps installed at each end of the trench length.

3.1.3   Stream Dewatering

Dewatering of stream crossings employed an over-pumping diversion of surface water from upstream to downstream and similar sump pumping to the trench installation. Pipe specials with prefabricated PE bends were used as opposed to utilising the pipe deflections to pass under the streams. Pipe specials

comprise a "special" configuration utilising fabricated bends to deviate around an obstruction, rather than using the pipes flexibility or joint articulation tolerance to achieve the deviation. In the case of the Richmond South works, this means the length of trench below the groundwater level could be significantly shortened reducing the dewatering required.

3.2   Ground Conditions Encountered

Ground conditions encountered site-wide to the depth of 2-3m typically comprised coarse GRAVEL with some cobbles and varying silt content to a depth of 3m below ground surface. Layers of clean gravel and cobbles were prevalent throughout the site. Significantly greater groundwater inflow was observed in clean gravel and cobble layers than in silty gravel layers. Ground conditions below 3m were not observed as geotechnical oversight was not present for the advancing of the dewatering bore, and no drillers logs were recorded.

Groundwater conditions observed at the site were significantly different than observed during geotechnical investigations. Groundwater inflow was observed from approximately 1.6 to 2.0m below ground surface across the alignment.

3.3   Effects and Impacts during Construction

3.3.1   Launch Pit Dewatering

When pumping was initiated within the launch pit excavation at SH6 it required three 150mm pumps operating at full capacity of approximately 55 L/s, and two smaller 50mm pumps at full capacity of approximately 8 L/s to effectively draw the water down to the excavation invert level. Total groundwater extraction flowrate during dewatering was assessed to be in excess of 170 L/s for the duration of the pumping.

Groundwater extracted from the excavation was extremely turbid and the Contractor was unable to meet the water clarity discharge requirements set out by the resource consent using conventional settlement tanks. A system of flocculent dosing using purpose-built plant referred to as a "silt-buster" was utilised to treat and discharge water in order to allow dewatering to continue.

Impact to the construction activities primarily comprised a fundamental change of dewatering methodology from bore extraction to sump pumping, this in turn required significant increase in plant including additional pumps, sumps and pipes, treatment of extracted water to meet resource consent requirements, extended duration of the works, and additional cost associated with the time and plant.

3.3.2   Pipe Trench Dewatering

Groundwater inflow during excavation of the pipe trench was common and also noted to rise quickly after rain events. Pumping out of 0.3m diameter sumps within the pipe trench was required. Up to two 150mm pumps operating at full capacity were required to effectively draw down water inflows, corresponding to a total discharge of over 100 L/s.

Where pipe trenches were in an urban area, treatment of the water by flocculent dosing was required, however in rural areas discharge of water to an infiltration pit a suitable distance from the work area was found to be effective. Impact to the construction activities again comprised additional plant including additional pumps, sumps and pipes, treatment of extracted water to meet resource consent requirements, an extended duration of the works, and additional cost associated with the time and plant.

3.3.3   Stream Dewatering

Using prefabricated PE bends instead of relying on pipe deflections to get below the stream crossings allowed the size of the excavations to be minimised. The final excavation was required to be approximately 3m below ground surface and achieve a groundwater drawdown of approximately 1.0m. Even with the reduction in size, up to 100 L/s of water was recorded for the stream excavations.

4   DISCUSSION

PROCEEDINGS OF THE 14TH ANZ YOUNG GEOTECHNICAL PROFESSIONALS CONFERENCE
14YGPC ROTORUA, NEW ZEALAND, 2ND – 5TH NOVEMBER 2022

161

4.1 Investigations and Dewatering Assessment

The analytical dewatering assessment comprised two key assumptions for this site, 1) a conversative maximum groundwater level of 2.3m below ground surface, and 2) hydraulic conductivity of the aquifer ranging between 10 to 200 m/day (5×10^{-5} m/s to 2×10^{-3} m/s). The assessment concluded that for a 15m x 2m x 3m excavation, a groundwater inflow rate of 10-20 L/s was considered reasonable.

During construction, groundwater was observed to range from 1.6m to 2.0m below existing ground surface, corresponding to up to 1.4m depth of water to be drawn down from excavations. Using the same assessment methodology and assumptions, and increasing the effective drawdown to 1.4m, a hydraulic conductivity of 1000 m/day or 1×10^{-2} m/s is required to match the observed inflows at the site.

The higher groundwater level at the site does contribute to the increased excavation inflows, however using the assessment methodology, a 0.3m water level increase within the excavation (from 1.12m to 1.42m) results in a modest 10 L/s increase in water inflow. Modification of the hydraulic conductivity of the gravel aquifer to 5 times greater than the conservative case was required to match the water inflows recorded.

4.2 Construction and Contractual Implications

Implications to the construction works of the pipeline were multiple, and these had contractual implications which included:

1. The elimination of borehole investigations prior to design and advancing test pits to 3m only meant the deeper aquifer conditions were unknown prior to construction. The dewatering methodology had to be adapted from well pointing to sump pumping during construction. This incurred additional time and effort for the contractor to procure plant and install the required system. The change in methodology also introduced more turbid water extraction. The well point system was anticipated to return clean water after a short period of pumping. Changing to sump pumping meant a much greater surface area for water inflow and potential to carry fine material from the gap graded silty gravel, resulting in significant fines migration and discoloured water.
2. The greater than anticipated groundwater inflows required additional pumping effort and significant treatment of discoloured water was required to meet resource consent requirements. The Contractor needed to procure more pumps and treat extracted water by addition of flocculants. This increased the plant required, as well as the duration, and cost of the works.
3. The extracted water rate exceeded the resource consent maximum peak extraction rate of 106 L/s. While in this case the increased extraction rate was accepted by the regional authority, the increased extraction rate had the potential to halt work.
4. The change in dewatering methodology and procurement of plant and treatment resulted in a three-week extension of the construction programme.
5. The additional time and materials resulted in a variation cost to the project of 15% of the original contract value.

4.3 Geotechnical and Contractual Risk

Geotechnical risk present from the outset for the Richmond South project had a follow-on effect through the design and construction. The key risk items identified by the case study are:

1. The suitability of investigations to inform not only the permanent works requirements, but also for the adequate consideration of the temporary dewatering works. For the Richmond South works this was understanding the ground conditions to a depth of 9m below ground surface and how these may affect dewatering.
2. Understanding of how a change in soil material properties may affect the proposed works. For the Richmond South works the key items were the sensitivity of hydraulic conductivity with changing soil types and how this in turn affects groundwater take volumes for the proposed excavations.
3. Understanding of the fluctuation of groundwater levels both seasonally and with significant rain events. The Climate and Weather of Nelson and Tasman produced by NIWA (Macara, 2016)

states mean monthly rainfall for the area in July and August to be 78mm and 82mm, respectively, mean monthly rainfall is taken from historical data from 1985 to 2010. Total rainfall of 189mm and 166mm was recorded for July and August 2021, respectively (NIWA, 2021). Rainfall of 2021 was exceptionally high, more than double the mean historical monthly totals. The rise in extreme weather events may become more prevalent because of climate change.

4. Inclusion of appropriate information in the contract to allow the contractor to price geotechnical risks identified, and sufficiently detailed contract clauses to ensure the Principal is sufficiently protected from programme extension and cost escalation.

5   CONCLUSION AND RECOMMMENDATION

In conclusion, there were multiple opportunities throughout the Richmond South project where additional information and consideration of risk may have directed decision making to improve the project outcome. The authors are aware of the process that exists in some regions of New Zealand, and recommend the Geotechnical Protocols set out in the Wellington Water Global Dewatering Consent (Wellington Water, 2017) as a good base for decision making and risk management for projects considering dewatering.

For brevity, the protocol is not included in full in this paper however a general flow of decision making in these types of projects, with some adaption from the protocol, could be as follows.

1. Project Planning
   a. Desktop review by a suitably qualified geo-professional.
   b. High level risk assessment for the works identifying key unknowns and potential impacts. This may include potential for settlement, volume and rate of groundwater take, discharge of extracted groundwater, seasonal, tidal, or storm event fluctuations, contaminates, or other as identified.
   c. Categorisation of risk profile of the proposed site into low, medium and high risk.
   d. Consideration of advanced monitoring i.e., installation of groundwater monitoring systems months or years before the works are planned to take place.
2. Geotechnical Investigation
   a. Execution of investigations suitable for the identified risk level, considering;
      i. A suitable ground monitoring method and duration
      ii. Specific technical inputs required for the design
      iii. Permanent and temporary works requirements for the proposed work
3. Design
   a. Determination of the level of design suitable for the site, this may comprise
      i. Engineering judgement review by an experienced engineer (low risk)
      ii. Quantitative assessment based on simplified methodologies (medium risk)
      iii. Numerical model assessment (high risk)
4. Contract Documents
   a. Review of contract documents by the geotechnical designer to incorporate an appropriate level of detail for temporary and permanent works
   b. Drafting of a groundwater management plan to be adopted by the Contractor

6   ACKNOWLEDGEMENTS

The authors acknowledge and thank the Tasman District Council for their agreement for the publication of this paper.

REFERENCES

Hazel, C.P. (2009). Groundwater Hydraulics, Second Edition. June 2009.

Kruseman, G.P & de Ridder, N.A. (2000). Analysis and Evaluation of Pumping Test Data. 2nd Edition, International Institute for Land Reclamation and Improvement.

Macara G.R. (2016). The Climate and Weather of Nelson and Tasman, 2nd Edition. NIWA Science and Technology Series Number 71. ISSN 1173-0383.

NIWA (2021). Climate Database Statistics Report July 2021.

NIWA (2021). Climate Database Statistics Report August 2021.

Rattenbury, M.S., Cooper, R.A., Johnston, M.R. (1998). Geology of the Nelson area. Institute of Geological and Nuclear Sciences 1:250,000 geological map 9. ISBN 0-478-09623-2.

Wellington Water (2017). Global Dewatering Consent Geotechnical Protocols. October 2017.

PROCEEDINGS OF THE 14TH ANZ YOUNG GEOTECHNICAL PROFESSIONALS CONFERENCE
14YGPC ROTORUA, NEW ZEALAND, 2ND – 5TH NOVEMBER 2022

163

GEOCHEMICAL AND COMPACTION-BREAKAGE CHARACTERISTICS OF WEATHERED AIR-FALL TEPHRAS

Shaurya Sood[1] and Gabriele Chiaro[2]

[1]PhD Candidate, Department of Civil and Natural Resources Engineering, University of Canterbury, Private Bag 4800, Christchurch, 8140; email: shaurya.sood@pg.canterbury.ac.nz
[2]Associate Professor, Department of Civil and Natural Resources Engineering, University of Canterbury, Private Bag 4800, Christchurch, 8140; email: gabriele.chiaro@canterbury.ac.nz

ABSTRACT

The North Island of New Zealand is a region of high volcanic activity with eruptions occurring every few years. Past events suggest that future volcanic eruptions may produce considerable amounts of air-fall tephra or tephric soil deposits (both ash and granular), which raises issues of disposal and storage. The use of such deposits in geotechnical applications is a viable solution, but it requires a full understanding of their physical, geochemical, mineralogical and mechanical properties in their fresh and weathered state. That is, when tephra deposits undergo weathering, their grains become more crushable, compromising their mechanical response. Aimed at providing useful insights, in this study, selected heterogeneous weathered tephras from Rotorua and Auckland regions were characterized. Specifically, compaction-induced particle breakage was evaluated by means of standard Proctor compaction test and sieve analyses, while elemental and mineralogical properties were attained by X-ray Fluorescence Spectroscopy (XRF) and X-ray Diffraction (XRD) techniques. The test results confirmed that the higher the degree of weathering is, the higher the degree of particle breakage is. Yet, the degree of weathering and, thus the associated particle breakage, is linked to the quartz and feldspars contents. It was seen that reworked volcanic deposits, having high silica (quartz) content and/or low feldspars content due to their mode of deposition, were generally more weathered and showed higher particle breakage.

Keywords: air-fall tephra, degree of weathering, weathered tephra, compaction, breakage

1 INTRODUCTION

The North Island of New Zealand has witnessed volcanism of every kind, including eruptions leading to the generation of air-fall tephra deposits in the adjoining areas. The central North Island including Taupo-Rotorua regions is mainly active and explosive due to being subduction driven, whereas northern North Island being primarily magmatic is currently dormant and less explosive (Hopkins et al., 2021). Over a period of time, these undergo changes in their physical and chemical composition depending on their mode of deposition and surrounding environment, commonly known as weathering. A weathered tephra or tephric soil deposit can be commonly used as a filling material for building sites or embankments due to its abundance and local availability near the construction sites. These tephra deposits to be used should be compacted well enough to satisfy the criteria of the engineering application. As these deposits can be products of different times and eruptions (Tarawera 1300 & 1886, Lowe & Balks 2019), their material properties are bound to be different and duly influenced by mode of deposition, imposed weathering conditions and further by loading conditions. Also, as a weathered tephra is susceptible to breakage, its particle breakage should be monitored during loading condition. Accordingly, this paper addresses the material-load characteristics of different air-fall tephras using their physical & chemical compositions and loading condition of compaction. The compaction behaviour and post compaction breakage values of studied air-fall tephras seem to be dependent on their mode of deposition and weathering state. It is imperative to mention that breakage here is defined as the change in percentage of particle sizes post compaction and weathering as the stabilization of the erupted tephra according to the physical and chemical conditions. The degree of weathering induced upon a particular tephra is evaluated using the following tests: physical (particle size distribution by sieving and hydrometer tests), chemical – XRF and Weathering Index of Parker WIP (Parker 1970), mineralogical (XRD) and post compaction breakage levels using sieve tests.

The WIP is a chemical method used to estimate the degree of weathering. It is the most appropriate weathering index applicable to a wide range of tephra types. The WIP seems useful chemical weathering index in the sense that it permits comparison between tehpra samples present at different locations, on different parent materials and on weathering profiles of different ages (Price and Velbel 2003). This method can be utilized for distinguishing differently weathered tephras in geology and geotechnical

engineering fields. However, the shortcomings of WIP are that it requires special equipment and non-application to highly weathered materials.

The preliminary characterization of any material can provide useful insights for its applicability in a particular geotechnical application. In this study, the material characterization of air-fall deposits was performed with respect to their weathering state using physical, chemical and mechanical methods. The post compaction breakage levels were compared with the results by XRD and WIP using XRF and as a result of the analyses, the breakage level and degree of weathering were correlated indicating higher breakage in reworked deposits than non-reworked tephras. Since the developed method can be performed with only basic laboratory tests such as sieve analysis test and compaction test, the developed equations can be useful for easy and quick evaluation of relative weathering between different tephra types and identify breakage levels of different tephras upon load implication.

2   MATERIAL PHYSICAL PROPERTIES AND METHODOLOGY

2.1   MATERIAL PHYSICAL PROPERTIES

The disturbed tehpras were sampled from quarry sites and roadside cuttings around Mt. Tarawera (Rotorua) and Mt. Maungataketake (Auckland) regions in the North Island of New Zealand (Fig. 1a). The tephras have been named successively from associated eruptions: White Kaharoa Ash (WKA), Golden Kaharoa Ash (GKA), Tarawera Basalt and Kaharoa Ash (TBKA) & Rotomahana Mud (RM) from Mt. Tarawera (Rotorua) eruptions (Lowe & Balks 2019); Pupuke Basalt (PB) and Maungataketake Ash (MA) from Auckland eruptions (Lindsay et al., 2011). Table 1 and Figure 1 show their physical properties.

Table 1 – Physical properties of tephra deposits

Tehpra Sample	Gravel (%)	Sand (%)	Fines (%)	PI (%)	Soil Classification (ASTM D2487-17e1)	G_s bulk sample (ASTM D4318-17e1)
WKA	5.0	81.2	13.8	NP	Silty Sand (SM)	2.238
GKA	0.3	77.6	22.1	NP	Silty Sand (SM)	2.325
TBKA	11.3	67.4	21.3	NP	Silty Sand (SM)	2.444
RM	0.1	35.7	64.2	11.3	Sandy Lean Clay (CL)	2.574
PB	8.9	90.7	0.4	NP	Poorly-Graded Sand (SP)	2.819
MA	0.0	48.3	51.7	3.7	Sandy Silt (ML)	2.736
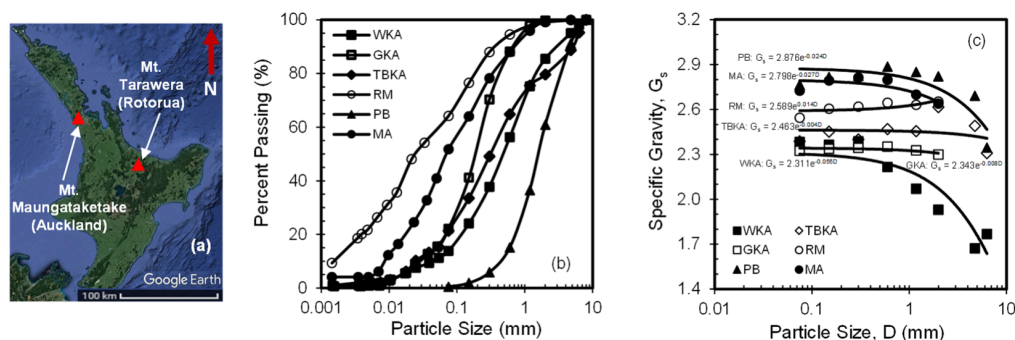
Fig. 1 – Sample locations, particle size distributions and specific gravity G_s of studied tephra deposits

While PB constitutes uniformly graded particles; WKA, GKA & TBKA contain appreciable amount of fines making them silty sandy and RM & MA predominantly fine grained with a slight plasticity in them. The specific gravity G_s values were measured (using water pycnometer and vacuum) over the entire investigated particle sizes and a decreasing G_s trend with increase in particle size due to internal voids was observed (Wesley 2001, Cecconi et al., 2010) for all tephras except slight deviations for RM at 4.75mm size and TBKA at 2 – 4.75mm size range (Fig. 1c). On physical observation, it was seen that TBKA and RM included basaltic and lithic fractions respectively in them in that range, which accounts for the respective higher G_s values around those sizes. For practical applications, the bulk G_s is calculated considering the entire particle size range and used further for compaction calculations.

2.2   METHODOLOGY

After the collected samples were oven-dried and pulverized, the tephras were analysed for elemental and mineralogical compositions using XRF and XRD techniques. The equation developed by

PROCEEDINGS OF THE 14TH ANZ YOUNG GEOTECHNICAL PROFESSIONALS CONFERENCE
14YGPC ROTORUA, NEW ZEALAND, 2ND – 5TH NOVEMBER 2022

165

Parker (1970) is used to estimate the degree of weathering of each sample:

$$WIP = 100 \times [(2Na_2O/0.35) + (2K_2O/0.25) + (CaO/0.70) + (MgO/0.90)] \quad (1)$$

The XRD scans for the tephra deposits show a certain hump in the 15 - 34° range, which is referred to as the amorphous or glassy phase. Using Rietveld (1969) analysis, the weight percentages of the crystalline and amorphous phases respectively were calculated using the following equation:

$$W_{Amo} = 100 - \sum(S_i \, \rho_i \, V_i^2 \, \mu \, / \, G) \, (\%) \quad (2)$$

where S_i is the scale factor, ρ_i the density, V_i the volume, μ the mass attenuation coefficient and G as the specific gravity of each crystalline phase. The tephra deposits were compacted using standard Proctor compaction, by ASTM 698-12e2, and then the particle size distribution of the samples were obtained after oven-drying. In the present study, the relative breakage defined by Hardin (1985) is used to evaluate the amount of particle crushing post compaction. The relative breakage (B_r.) defined as

$$B_r = (B_t \, / \, B_p) \times 100 \, (\%) \quad (3)$$

where B_p is the breakage potential, which is equal to the area between the line particle size D = 0.075mm and the part of the particle size distribution curve for which D > 0.075mm; and B_t is the total breakage, which is calculated as the difference between original breakage potential and breakage potential after compaction.

3   RESULTS AND DISCUSSIONS

3.1   GEOCHEMICAL COMPOSITIONS AND WEATHERING STATE ESTIMATION BY WIP

The major oxides and WIP of tephras were estimated by XRF (Table 2). The Rotorua tephras WKA, GKA, TBKA and RM categorize as rhyolites and dacites (higher SiO_2 & Na_2O+K_2O) and Auckland samples PB and MA as basalt and basalt andesitic (lower SiO_2 & $Na_2O + K_2O$) in the total alkalis ($Na_2O + K_2O$) vs silica (SiO_2) diagram (Fig. 2a). In addition, the higher G_s for TBKA around 2 – 4.75mm is due to the basaltic particles (TBKAc), indicating intermixing with rhyolitic (TBKAm) and dacitic (TBKAf) fractions in the sand (4.75 – 0.075mm) and finer (< 0.075mm) sized fractions. In the A (Al_2O_3) – CN ($CaO+Na_2O$) – K (K_2O) plot (Fig. 2b), the studied tephra samples lie in the slightly weathered region, indicating lesser mechanical breakdown into clayey minerals located at the upper end of the CIA plot (Nesbitt et al., 1997).

Table 2 – XRF results and calculated WIP values of all tephras

Tephra Sample	Major Oxide (Wt. %)											WIP
	SiO_2	TiO_2	Al_2O_3	Fe_2O_3	MnO	MgO	CaO	Na_2O	K_2O	P_2O_5	LOI	
WKA	75.1	0.2	12.3	1.3	0.1	0.2	1.1	3.9	3.4	0.0	2.0	5116.7
GKA	70.7	0.2	13.9	1.8	0.1	0.2	1.1	3.6	2.8	0.1	5.5	4443.0
TBKAc (2 - 8mm)	53.8	0.8	16.7	9.4	0.2	5.5	10.1	2.3	0.9	0.2	0.2	4117.2
TBKAm (0.075 - 1.18mm)	72.2	0.3	12.8	2.5	0.1	0.9	2.6	3.7	2.5	0.1	2.1	4561.8
TBKAf (<0.075mm)	68.5	0.3	12.3	2.0	0.1	0.4	1.5	3.3	3.0	0.1	8.1	4597.6
RM	68.2	0.4	14.9	3.9	0.1	1.2	2.6	2.3	2.8	0.1	3.6	4052.7
PB	45.7	2.3	11.7	13.8	0.2	13.2	8.3	2.5	0.9	0.5	0.6	4796.5
MA	57.3	1.4	12.3	8.3	0.1	5.2	6.6	2.4	1.6	0.4	4.0	4230.3

Note: TBKA shown here in three size fractions to show intermixing, WIP of TBKA is considered from the relative contributions of the three fractions
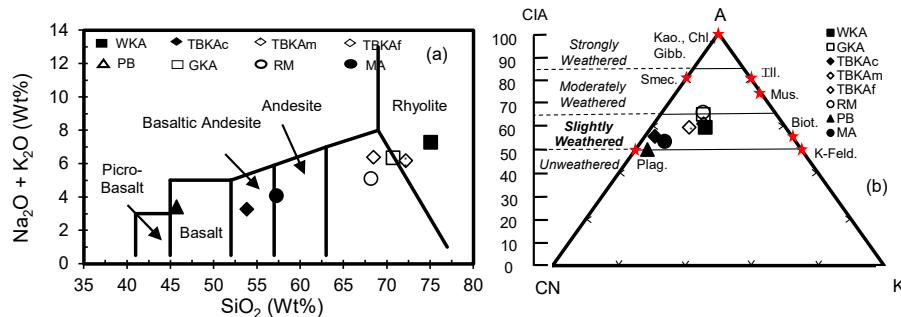
Fig. 2 – Elemental composition and weathering state by XRF

From the WIP values, the WKA is the least weathered tehpra followed by PB, TBKA (m & f), GKA, MA, TBKAc and lastly RM (higher the value of WIP, lower is the degree of weathering). Fig. 3 shows the XRD scan of WKA constituting amorphous and identified crystalline phases. As seen in this figure, silica (Qz & Crs), plagioclase feldspars (Ab, Ol), alkali feldspars (Sa) and accessories (Aug, Bt) are

identified crystalline mineral phases of WKA. The relative percentages of all these constituents for each tephra are shown in Table 3. From the relative abundances of these minerals, the GKA, RM and MA are silica rich in comparison to the remaining tephras WKA, TBKA(c, m and f) and PB. The values of WIP and wt. % of silica & feldspars are used further against post compaction breakage levels to assess the degree of weathering in the studied tephras.
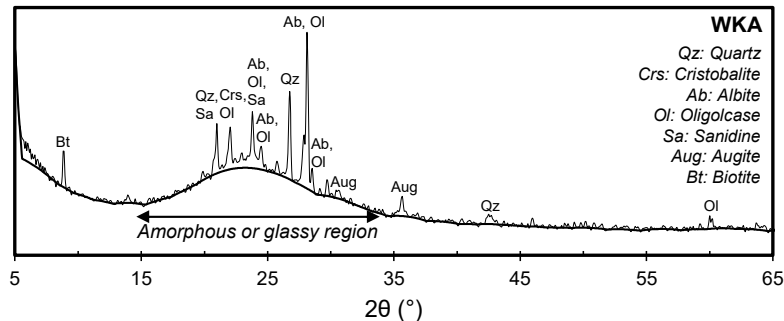

Fig. 3 – XRD scan of White Kaharoa Ash (WKA)

Table 3 – XRD - Rietveld results of all tephras

Mineral (Wt. %)	Tephra Sample							
	WKA	GKA	TBKAc	TBKAm	TBKAf	RM	PB	MA
Glass	78.3	86.2	59.4	67.3	79.6	13.9	31.5	38.5
Quartz	3.7	3.3	1.0	7.1	5.1	26.2	1.3	26.6
Cristobalite	0.6	0.7	2.2	0.4	0.2	2.1	-	1.1
Alkali Feldspars	2.9	1.2	3.3	5.1	1.3	12.3	3.7	5.4
Plagioclase Feldspars	13.5	8.1	24.2	18.9	13.8	31.0	27.6	19.3
Accessories	1.0	0.5	9.9	1.3	-	13.2	35.8	9.2
Quartz + Cristobalite	4.3	4.1	3.2	7.5	5.3	28.4	1.3	27.7
Feldspars	16.4	9.2	27.5	24.0	15.1	43.3	31.4	24.7
Total Crystal Content	21.7	13.8	40.6	32.7	20.4	86.1	68.5	61.6

Note: The Wt.% all three fractions of TBKA are used later for breakage level vs weathering state prediction, Qz + Crs = Silica

3.2 COMPACTION CURVES AND POST-COMPACTION BREAKAGE CHARACTERISTICS

Compaction test to provide load effect was carried out with each tephra and the effect of particle breakage was analysed at the respective water contents. In addition, the sieve analysis test was performed to characterize the breakage occurring post compaction by comparing the particle size distribution before compaction with the gradation obtained after compaction. Fig. 4a - d shows the results of compaction tests. The ρ_{dmax} and w_{opt} vary from 1.32 to 1.71g/cm^3 and 10.61 – 24.89% (low range) for the investigated tephras. The low range water content is attributable to the slightly weathered nature and non-presence of highly plastic fines or clayey fractions. The tests yielded three types of compaction curves – one and a half peak (for WKA, GKA and TBKA), parabolic or single peak (for RM and MA) and gentle peak (for PB). The respective shapes are due to the role played by water levels in respective tephras (Lee and Richard 1972). For silicate rich sand dominant tephras such as WKA, GKA and TBKA, anti-lubrication effects at lower water contents and lubrication effects at higher water contents control density changes. The latter phenomenon also holds for low-plasticity fine grained siliceous tephras RM and MA. On the contrary, the density of coarser basaltic lower silica PB remains unaffected by water as no effective particle contacts are generated due to the absence of fines. Fig. 4e –f show the grain size distribution curves of WKA and MA following the compaction tests. For the shown and remaining tephras, with the same original curve and different water contents compaction curves, the differences in positions of the grain size distribution curves after compaction are very small. This meant that the amounts of particle crushing during the compaction in the tested tephras, with the same original curve and different water contents curves, are very similar. The average of the breakages post compaction at different water contents is therefore used to define the breakage level of each tephra. The average breakage values ranged between 1.3 – 7.6% (< 10%), with noticeably higher values for GKA, RM and MA tephras (Fig. 4a). The measured higher breakages in these tephras are explained w.r.t. their weathering state in section 3.3.

PROCEEDINGS OF THE 14TH ANZ YOUNG GEOTECHNICAL PROFESSIONALS CONFERENCE
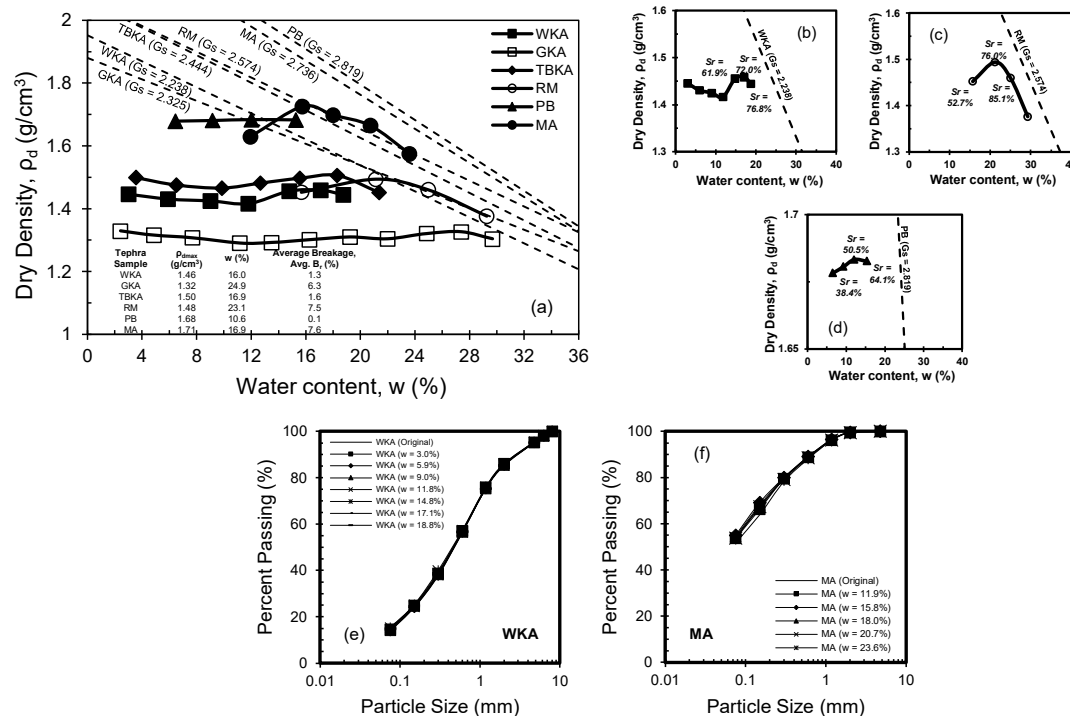14YGPC ROTORUA, NEW ZEALAND, 2ND – 5TH NOVEMBER 2022

167

Fig. 4 – Compaction curves and post compaction breakage characteristics

3.3 CHEMICAL COMPOSITIONS AND WEATHERING MECHANISMS INFLUENCING BREAKAGE OF WEATHERED TEPHRAS

The degree of weathering of each tephra evaluated using WIP was correlated with the breakage levels post compaction and internal silica (SiO_2 = quartz + cristobalite) and feldspars minerals (Fig. 5). Silica and feldspars are essential primary components of all tephric soils, which change relative to weathering undergone by tephra (Nesbitt and Young 1997). The lower WIP values of GKA, RM and MA in comparison to PB, WKA and TBKA tephras indicates higher degree of weathering in the former samples, which also accounts for their higher breakage. The abundance of feldspars and lower silica in TBKA, GKA and WKA indicates lesser chemical weathering - internal breakdown of minerals and mechanical breakdown, which explains their less weathered nature (Table 3). It might be worthwhile to mention here that although TBKA contains physical intermixing of basaltic fractions in the 2 – 8mm range, the overall compaction load and breakage response is governed from predominant high silica sand and fine fractions (as seen from close proximity XRF values of TBKAm and TBKAf to that of WKA). On the other hand, higher silica and lower feldspar levels in RM and MA can be explained due to their depositional nature – phreatomagmatic and phreatic with inclusions from secondary lithic fragments and plastic fines in coarser and finer fractions respectively (Lowe and Balks 2019, Lindsay 2011). This also further explains weathering state of GKA, elementally similar but also silica rich and feldspar deficient in comparison to WKA, which was pulverized by the deposition of RM tephra falling directly above it. Therefore, while assessing the material - load characteristics of natural redisturbed tephra deposits of heterogeneous compositions, it might be worthwhile to look into the way of deposition (direct like WKA or reworked like GKA and RM), weathering degree value (using WIP) and the relative abundances of minerals which collectively can then help represent the degree of weathering of tephras for further usage in engineering applications. This is represented in the equations 4, 5 and 6 as follows:

$$Br. (\%) = -0.008 \times WIP + 39.14 \tag{4}$$
$$Silica (\%) = -0.026 \times WIP + 145.53 \tag{5}$$
$$Feld. (\%) = 0.021 \times WIP - 38.40 \tag{6}$$

Considering the diverse nature of air-fall tephra deposits in this study (and as expected in the field) due to processes like intermixing and weathering, these equations allows inclusion of a wider array of deposits from low silica basalts to high silica rhyolites (using their geochemical state) and enable prediction of parameters such as particle breakage upon load implication as seen during standard compaction tests.
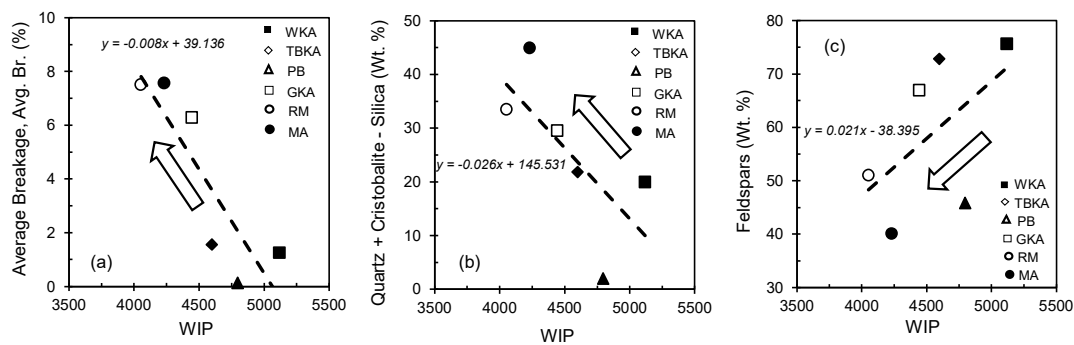
Fig. 5 – Degree of Weathering vs Breakage levels and Mineral compositions (arrows indicating higher weathering progression)

4 CONCLUSIONS

This study provided insights regarding the relationships between material (physical and chemical properties) and mechanical (compaction) characteristics of different non/slightly plastic (or slightly weathered) air-fall tephra deposits for usage as fill materials in geotechnical applications. The test results indicate that despite different grain size distributions and chemical compositions, the breakage level changes slightly with the varying water contents of a compaction test and are reportedly higher for reworked tephras - RM, GKA and MA than non-reworked WKA, TBKA and PB tephras. This is accountable to the relative abundances of quartz and feldspar minerals and corresponding higher degree of weathering (as collectively represented in the form of equations) in the former samples. The post compaction breakage values lie below 10%, therefore encouraging usage of these deposits as structural fills, although post-shear performance will be needed to be looked into.

5 ACKNOWLEDGEMENTS

REFERENCES

ASTM D2487-17e1, Standard Practice for Classification of Soils for Engineering Purposes (Unified Soil Classification System), ASTM International, West Conshohocken, PA, 2017.

ASTM D854-14, Standard Test Methods for Specific Gravity of Soil Solids by Water Pycnometer, ASTM International, West Conshohocken, PA, 2014.

ASTM D698-12e2, Standard Test Methods for Laboratory Compaction Characteristics of Soil Using Standard Effort (12 400 ft-lbf/ft^3 (600 kN-m/m^3)), ASTM International, West Conshohocken, PA, 2012, www.astm.org.

Cecconi, M., Scarapazzi, M., & Viggiani, G.M. (2010). On the geology and the geotechnical properties of pyroclastic flow deposits of the Colli Albani. *Bulletin of Engineering Geology and the Environment, 69*, 185-206.

Hardin, B. O. 1985. Crushing of soil particles. Journal of Geotechnical Engineering 111 (10):1177–92.

Hopkins, J.L., Smid, E.R., Eccles J.D., Hayes, J.L., Hayward J.L., Mcgee, L.E., van Wijk, K., Wilson, T.M., Cronin, S.J., Leonard, G.S., et al., 2021. Auckland Volcanic Field magmatism, volcanism, and hazard: a review. New Zealand Journal of Geology and Geophysics 64(2–3):213–234.

Lee, D. Y., and Suedkamp, R. J. (1972), Characteristics of irregularly shaped compaction curves of soil, *Highway Research Board*, 381, 1-9.

Lindsay, J.M., Leonard, G.S., Smid, E.R., & Hayward, B.W. 2011. Age of the Auckland Volcanic Field: a review of existing data, New Zealand Journal of Geology and Geophysics, 54:4, 379-401.

Lowe, D.J. & Balks, M.R. 2019. Introduction to tephra-derived soils and farming, Waikato-Bay of Plenty, North Island, New Zealand. University of Wisconsin-Platteville Education Abroad Program: Winterim Field Trip (15-17 January, 2019). School of Science (Earth Sciences), University of Waikato, Hamilton. pp. 82.

Nesbitt, H., Fedo, C. & Young, G. (1997). Quartz and Feldspar Stability, Steady and Non-Steady-State Weathering, and Petrogenesis of Siliciclastic Sands and Muds. The Journal of Geology. 105. 10.1086/515908.

Parker, A. (1970). An Index of Weathering for Silicate Rocks. Geological Magazine, 107(6), 501-504.

Price, J. R., & Velbel, M. A. (2003). Chemical weathering indices applied to weathering profiles developed on heterogeneous felsic metamorphic parent rocks. Chemical geology, 202(3-4), 397-416.

Rietveld, H. M. (1969). A profile refinement method for nuclear and magnetic structures. J. Appl. Cryst. 2, 65-71.

Wesley, L. D., 2001, Determination of Specific Gravity and Void Ratio of Pumice Materials, Geotechnical Testing Journal, Vol. 24, pp. 418–422.

PROCEEDINGS OF THE 14TH ANZ YOUNG GEOTECHNICAL PROFESSIONALS CONFERENCE
14YGPC ROTORUA, NEW ZEALAND, 2ND – 5TH NOVEMBER 2022

169

Use of a Rammed Aggregate Pier Ground Improvement trial to improve understanding of liquefaction potential in geologically aged soils

K. Brown[1] and K.Lontzetidis[2]

[1]CMW Geosciences, P.O. Box 12026, Rotorua South, Rotorua 3010, PH (07) 975 0916; email: kirstinb@cmwgeo.com
[2]CMW Geosciences, P.O. Box 300203, Albany, Auckland 0752, PH (09) 4144 632; email: kostasl@cmwgeo.com

ABSTRACT

CMW Geosciences (CMW) with the support of CLL Service & Solutions Ltd (CLL) have carried out an in-house research and development (R&D) exercise involving a Rammed Aggregate Pier (RAP) ground improvement trial within Pleistocene-aged sand deposits that have been assessed using conventional methods to be susceptible to liquefaction. Although the results of the trial demonstrated that the Pleistocene-aged alluvial sands densified following RAP installation, shear wave velocity measurements following RAP installation were much lower than those undertaken prior to installation indicating that the high energy vibratory hammer used to install the piers had disturbed the soil microstructure. The results of our trial have highlighted an interesting effect of dynamic ground improvement techniques in geologically older soil deposits.

The updated MBIE guidelines in Earthquake Geotechnical Engineering Practice released in November 2021 have acknowledged that although the age of a deposit is an important factor to consider when undertaking a liquefaction assessment, it is often challenging to quantify the effects ageing has on the liquefaction resistance of soils with no widely accepted methods to do so. As a result, the guidelines have recognised the limitations of the methods and have outlined an approach for evaluating the ageing effects incorporating the use of shear wave velocity measurements and advanced lab testing. This provides the New Zealand geotechnical industry further guidance when assessing liquefaction potential on geologically aged soils.

Keywords: Rammed Aggregate Pier, liquefaction, ground improvement, aged soils

1   INTRODUCTION

A Rammed Aggregate Pier (RAP) ground improvement trial was undertaken by CMW Geosciences (CMW) with the support of CLL Service & Solutions Ltd (CLL) to determine if RAPs were a suitable ground improvement option to mitigation liquefaction for a significant infrastructure project located within the Bay of Plenty region. The design of high importance infrastructure in the Bay of Plenty region attracts high seismic demands, that in turn can generate significant liquefaction induced settlements and lateral displacements beneath structures where ground improvement is typically required to achieve settlement and displacement limits.

RAP ground improvements have been used for liquefaction mitigation on projects around the world. Using these projects together with recent RAP ground improvement trials conducted around the world as guidance, three different triangular arrays, representing three different area replacement ratios were constructed to assist in determining the most appropriate arrangement. Considering the results of other trials, conventional large strain Cone Penetrometer Testing (CPT) in conjunction with small strain shear wave velocity testing methods, using the seismic cone penetrometer (sCPT), were carried out prior to and following RAP installation to assist in evaluating the effectiveness of the ground improvement.

2   GEOLOGICAL SETTING

The RAP ground improvement trial was situated over elevated terrace topography at the foothills of the Tauranga basin. The terraces in this region are typically mantled by 2m to 3m of late quaternary volcanic ash comprising silty sand, sands and sandy silts overlying Pleistocene alluvium differentiated based on CPT trace characteristics. The upper 2m to 3m of the Pleistocene alluvium directly beneath the volcanic ash comprises sensitive silts followed by pumiceous sands with silt lenses that progressively increase in density with depth. The groundwater table was encountered approximately 4.0m to 5.5m below existing ground level.

The Pleistocene-aged volcanic derived pumiceous sands encountered below the groundwater table, have been assessed using conventional methods to be susceptible to liquefaction.

3 RAMMED AGGREGATE PIER TRAIL

The RAPs were installed by CLL using the Geopier Impact Pier System and comprised 600mm diameter aggregate columns installed through a pre-driven 250mm diameter mandrel using a proprietary impact action to densify the columns and dilate them into the surrounding soil, as shown in Figure 1a. The aggregate comprised clean screen 40/20 gravel from a local quarry with a particle size ranging from 20mm to 40mm.

Three RAP arrangements were installed, with the piers spaced at 1.25m, 1.5m and 1.8m triangular centres to represent area replacement ratios (ARR) of 20%, 15% and 10% respectively. The piers were installed to depths of approximately 15m below the ground surface, the limit of the machinery used.

Both conventional large strain Cone Penetrometer Testing (CPT) and small strain shear wave velocity testing methods, using the seismic cone penetrometer (sCPT), were carried out prior to and following RAP installation. Prior to installation a CPT in combination with a sCPT was undertaken at each of the arrays, targeting the location of one of the priers.

RAP installation was completed in early June 2021, with the post installation CPTs and sCPTs completed early August 2021. A series of three CPTs in combination with sCPTs were carried out at each array following installation, one in the centre of the array, one adjacent to the pier and one at equal distance between the centre and the edge of the pier, as shown in Figure 1b.
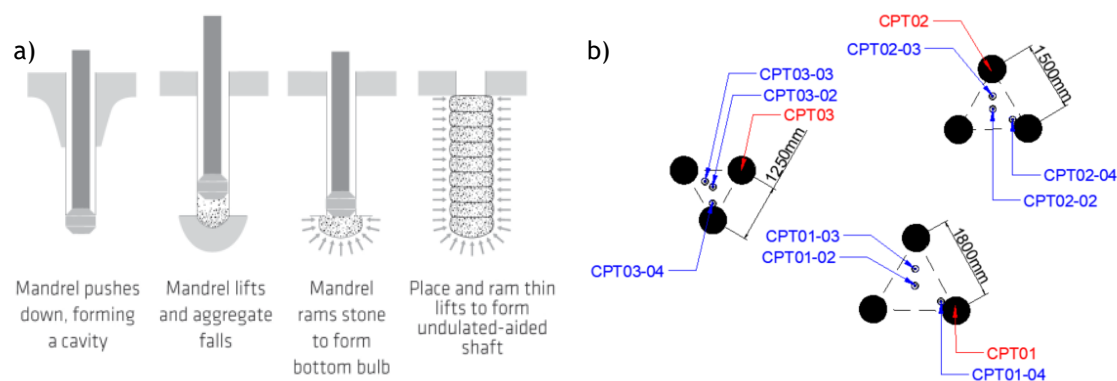
Figure 1: a) RAP construction methodology (Wissmann et al. 2015) b) Schematic of pre (red) and post (blue) installation CPT/sCPTs relative to the RAP arrays

4 POST RAP INSTALL EVALUATION

4.1 Performance Assessment

RAP ground improvements have been used for liquefaction mitigation on projects around the world, with various studies demonstrating their effectiveness in mitigating liquefaction in clean sands and more recently silty sands (Wissmann et al. 2015 & Smith and Wissmann, 2018). The effectiveness of the RAP ground improvement in various soil types is generally assessed by comparing pre and post installation CPT data such as cone tip resistance and corresponding soil behaviour type index.

The effectiveness of the RAP ground improvement is often assessed over time with CPTs and sCPTs completed at different time intervals following RAP installation. Studies like that of Saftner et al. (2018) have demonstrated time-dependent strength gain occurs with a further increase in CPT tip resistance observed one month following RAP installation and the initial post installation CPT.

Other methods incorporating shear wave velocity data have also been used to assess the effectiveness of the RAP ground improvement (Wissmann et al. 2015), with the view that the small strain stiffness (reflected in the shear wave velocity) may increase as a result of the ground improvement. Given the

geological setting (ie. age and composition), seismic CPTs were also considered more appropriate with researchers noting that conventional CPT based liquefaction analysis methods can over-estimate liquefaction potential in geologically older soils and pumiceous soils (Orense & Pender, 2013).

It is acknowledged that laboratory testing of soil samples prior and following the RAP ground improvement would have also assisted in assessing the performance of the ground improvement (Orense et. al 2020). However due to constraints, soil samples were unable to be retrieved.

4.2 Standard Cone Penetration Data

4.2.1 Cone Tip Resistance

The Pleistocene-aged alluvial sands considered to be susceptible to liquefaction were typically encountered 6m to 8m below the ground surface. The densification of these deposits was assessed by comparing the uncorrected cone tip resistance (qc) values pre and post installation. Generally, the data shows that the RAP's have resulted in an increase in qc in these soil layers, with increase in qc more significant in the arrays with higher area replacement ratios, as shown in Figure 2.
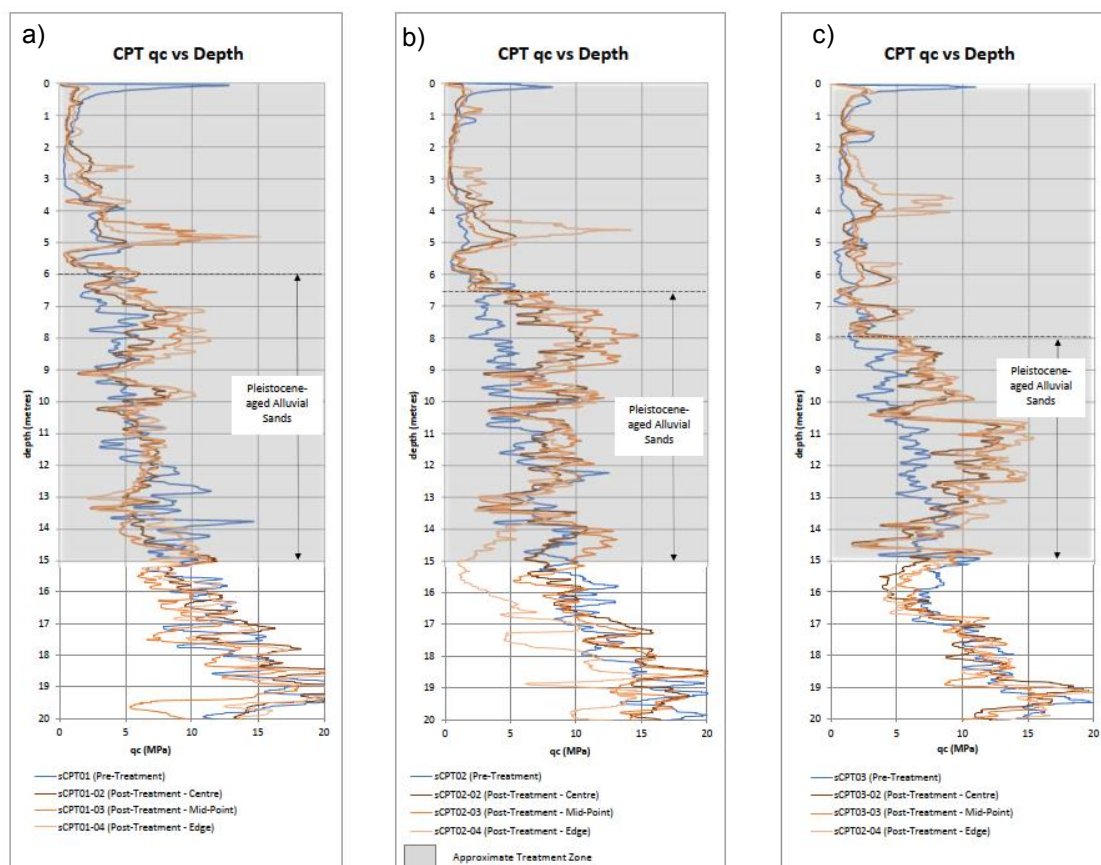
Figure 2: Pre and post installation CPT qc vs depth a) 1.8m spacing (ARR = 10%), b) 1.5m spacing (ARR = 15%), c) 1.25m spacing (ARR = 20%)

4.2.2 Improvement Ratio

Vautherin et al. (2017) suggested an improvement ratio (Qc), as a method of assessing the improvement of the soil, with the improvement ratio being compared to various influencing factors such as soil behaviour type and area replacement ratio. The improvement ratio is the ratio between the post improvement qc and the pre improvement qc. Typically for studies with large data sets this is done for each select layer, in this case Qc was determined for the full depth of the trace at 1cm intervals.

A comparison of the improvement ratio as a function of pre improvement qc with respect to the Robertson (1990) soil behaviour type index, Ic, was carried out for each array. The CPT undertaken in the centre of each array was used for the post improvement qc, as this demonstrates the most conservative improvement ratio.

For the soils considered susceptible to liquefaction (Ic < 2.6), higher pre improvement qc showed the least improvement, with a portion of the soil profile showing a reduction in qc following RAP installation with Qc values less than 1, as shown in Figure 3.

The overall trend of higher pre improvement qc showing the least improvement is similar to Vautherin et al. (2017) study which was undertake in Christchurch following the 2010 and 2011 earthquake (ie. geological young soils). However, Vautherin et al. (2017) generally observed improvement following RAP installation with the Qc greater than 1.

ARR of 20% showed the most improvement for the soils with high pre improvement qc. This is consistent with Vautherin et al. (2017) with higher ARR showing greater improvement. Although it is noted that their study had a limited data set for ARR greater or less than 8%.
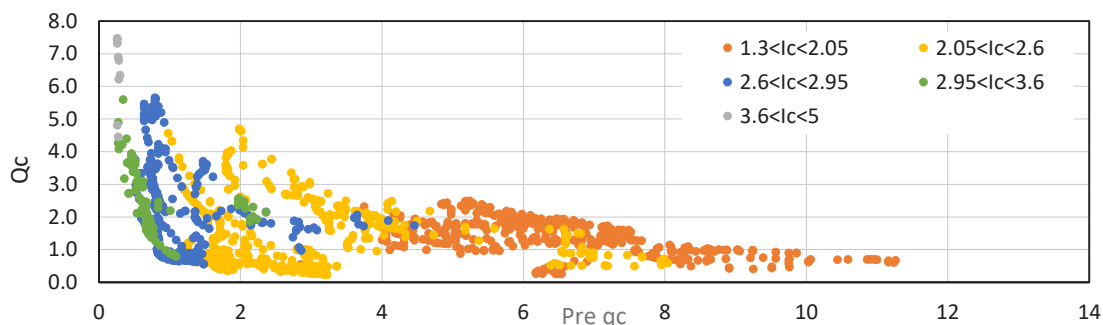
Figure 3: Improvement ratio (Qc) as a function of pre qc for ARR = 20%

4.3   Seismic Cone Penetrometer Data

4.3.1   Shear Wave Velocity

Comparison of the small strain shear wave velocity data obtained from the sCPTs pre and post RAP installation showed no improvement to the soil layers following installation. In fact, the shear wave velocity measurements post installation were lower than those record prior to installation, with average 20% reduction in shear wave velocity across the treated soil profile.

These results were unexpected, with a similar trial (Wissmann et al. 2015) showing a slight increase in shear wave velocity following ground improvement. In light of this, the authors used the shear wave velocity data to further evaluate the effects of the ground improvement on the soil properties / parameters, as discussed in the following sections.

4.3.2   Rigidity Index

The normalised rigidity index (K_G) has been proposed by Robertson (2015) as a parameter that combines Vs and normalized CPT tip resistance (Q_{tn}), to detect and quantify the presence of microstructure. The K_G of the Pleistocene-aged alluvial sand prior to RAP installation typically ranged between 250 and 360, with a clear reduction in K_G, to between approximately 110 and 150, following RAP installation. Generally, the lower K_G were observed within the sCPT carried out at the edge of the pier.

Schneider and Moss (2011) indicated that soils with no microstructure (ie. geologically young soils with no bonding), have rigidity index values which range between 110 and 330, average 215. Considering these values, it appears the RAP ground improvement has result in soil microstructure consistent with that of a geological "younger" soil.

PROCEEDINGS OF THE 14TH ANZ YOUNG GEOTECHNICAL PROFESSIONALS CONFERENCE
14YGPC ROTORUA, NEW ZEALAND, 2ND – 5TH NOVEMBER 2022

173

4.3.3   Strength Gain Factor

This observation is further supported when comparing the strength gain factors for the soil profile prior and following installation of the RAP's.

Using the MEVR (ratio of measured to estimated shear wave velocity) method proposed by Andrus and Hayati (2009) a strength gain factor of between 1.1 and 1.4 was determined for the Pleistocene-aged alluvial sands encountered at depths below 6m to 7m, prior to the installation of the RAP's. Following RAP installation this reduced to between 0.8 and 1.0

The MEVR method was compared with the one proposed by Robertson (2015) using the rigidity index. This demonstrated that the Robertson (2015) method is more conservative, with strength gain factors in the order of 1.1 to 1.4, pre treatment and in the order of 0.7 and 0.8 following installation of the RAP's.

The reduction in strength gain factors following RAP installation, also suggests that the ground improvement has change the microstructure of the Pleistocene-aged alluvial sands with a soil microstructure which now appears consistent with that of a geological "younger" soil.

4.3.4   Shear Wave Velocity Improvement Ratio

Recent studies demonstrated that shear wave velocity ratio typically increases with increase in ARR for ground improvement using columnar inclusions (Boulanger and Shao 2021 and Rahmani and Baez 2020). However, as discussed above this was not observed during the RAP ground improvement trial, with a reduction in shear wave velocity observed post treatment.

Plotting the shear wave velocity improvement ratio as a function of pre improvement shear wave velocity, showed an increase in shear wave velocity ratio with an increase in ARR. However, the shear wave velocity ratios are generally below 1 (refer to Figure 04) indicting no improvement post treatment.
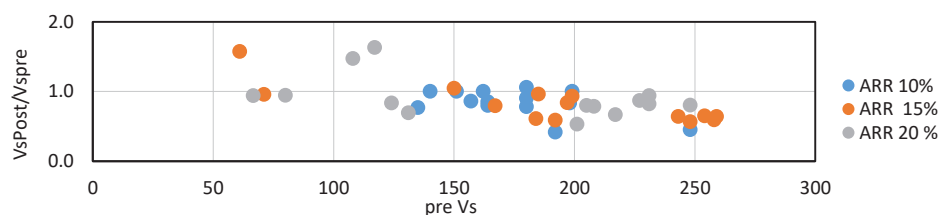
Figure 4: Shear wave velocity improvement ratio as a function of pre improvement shear wave velocity

5   DISCUSSION

The RAP ground improvement trial identified that the microstructure of the soil has been disturbed as a result of the high energy vibratory hammer associated with installing the piers. Although the RAPs had densified the soil, the soil microstructure now appears consistent with that of a geological "younger" soil. These observations are not consistent with similar ground improvement studies (Wissmann et al. 2015).

It is noted that current in-situ testing methods and subsequent analysis methods used in evaluating liquefaction potential of soils are generally based on a large database of case histories involving very young, silica-rich soils which have no bonding/cementation (Robertson, 2015). Therefore, there are limitation associated with assessing geologically aged soils as well as those with a high pumice content.

Following RAP installation, it has been acknowledged that the soils "heal" over time with verification testing typically undertaken a few months following installation (Saftner et al. 2018). Although, this has typically been observed with an increase in tip resistance, opposed to shear wave velocity. Further research into the time-dependent strength gain aspect of this trial is required, with further testing to assess whether there has been a change in the microstructure since the testing in August 2021.

Based on a number of ground improvement trial undertake in Christchurch following the 2010 and 2011 earthquakes the MBIE suggested that a ARR of 8% is reasonable to achieve the required densification

to provide resistance to the effect of liquefaction. However, this RAP ground improvement trail suggests a higher ARR may more suitable. Although, this is likely to be attributed to the microstructure of the soil as well as the pumice content, it highlights the importance in understanding the soil properties when assessing liquefaction potential and associated ground improvements options.

6   CONCLUSION

Although the trail was not successful in providing an appropriate ground improvement option for the project, it raises some interesting questions about the microstructure present in geologically aged soils and how this may change over time.

This RAP ground improvement trial further supports the use of "ageing" when assessing liquefaction potential. However, as with recent studies, it demonstrates that the "age" of soils can be reset following a seismic event with the microstructure (ie. bonding / cementation) of the soil being disturbed. As such the use of empirical formulas based on the geological of the soil are not considered appropriate when assessing liquefaction potential of geologically aged soils as these give no consideration the time since the last critical disturbance.

This is consistent with the updated MBIE guidelines which have recognised the limitations of the methods used to quantify the effects ageing on the liquefaction resistance and have outlined an approach for evaluating the ageing effects incorporating the use of shear wave velocity measurements and advanced lab testing.

REFERENCES

Andrus, R. D. and Hayati, H. (2009). "Updated Liquefaction Resistance Correction Factors for Aged Sands." J. Geotech. Geoenviron. Eng., 135(11), 1683–1692.

Boulanger, R. W., and Shao, L. (2021). "Liquefaction mitigation with deep mixing." Proceedings, Deep Mixing 2021, Deep Foundations Institute, 1146-1202.

Ministry of Business, Innovation and Employment (MBIE) (November 2021) "Earthquake Geotechnical Engineering Practice, Module 3: Identification, assessment and mitigation of liquefaction hazards"

Orense, R.P. and Pender, M.J. (2013) "Liquefaction characteristics of crushable pumice sand", 18th International Conference on Soil Mechanics and Geotechnical Engineering, Paris.

Orense, R.P., Asadi.M.B., Stringer M.E, and Pender, M.J. (2020) "Evaluating liquefaction potential of pumiceous deposits through field testing: Case study of the 1987 Edgecumbe Earthquake. Bulletin of the New Zealand Society for Earthquake Engineering, Vol 53. No. 2.

Rahmani, A. and Baez, J.I., 2020. New Approach to Determine Composite Shear Wave Velocity of Improved Ground Sites. Journal of Geotechnical and Geoenvironmental Engineering, 146(10), p.06020017.

Robertson, P.K. 1990. Soil classification using the cone penetration test. Canadian Geotechnical Journal, 27(1): 151–158.

Robertson, P. K.   (2015). "Comparing CPT and Vs Liquefaction Triggering Methods", Journal of Geotechnical and Geoenvironmental Engineering.

Saftner, David & Zheng, Junxing & Green, Russell & Hryciw, Roman & Wissmann, Kord. (2018). Rammed aggregate pier installation effect on soil properties. Proceedings of the Institution of Civil Engineers - Ground Improvement. 171. 63-73.

Schneider, J. A., and Moss, R. E. S. (2011). "Linking cyclic stress and cyclic strain based methods for assessment of cyclic liquefaction triggering in sands." Geotech. Lett., 1, 31–36.

Smith, M.E., and Wissmann, K.J. (2018). "Ground improvement Reinforcement Mechanisms Determined for the Mw7.8 Muisne, Ecuador, Earthquake", Geotechnical Earthquake Engineering and Soil Dynamics V GSP 290: 286-295.

Vautherin, E., Lambert, C., Barry-Macaulay, D., and Smith, M. 2017. "Performance of Rammed Aggregate Piers as a Soil Densification Method in Sandy and Silty Soils: Experience from the Christchurch Rebuild." Proceedings of 3rd International Conference on Performance-based Design in Earthquake Geotechnical Engineering

Wissmann, K.J., van Ballegooy, S., Metcalfe, B., Dismuke, J.N., and Anderson, C.K. (2015). "Rammed Aggregate Pier Ground Improvement as a Liquefaction Mitigation Method in Sandy and Silty Soils". 6th International Conference on Earthquake Geotechnical Engineering, Christchurch

PROCEEDINGS OF THE 14TH ANZ YOUNG GEOTECHNICAL PROFESSIONALS CONFERENCE
14YGPC ROTORUA, NEW ZEALAND, 2ND – 5TH NOVEMBER 2022

175

Co-Seismic Slope Displacements; A Comparative Case Study

J. L. Thomas[1], MEngNZ

[1]Holmes NZ LP, P.O. Box 6718, Upper Riccarton, Christchurch 8442; PH (+64) 3-345-9152;
email: Jamie.Thomas@holmesgroup.com

ABSTRACT

Estimation of co-seismic slope displacements remains an area of discussion and uncertainty in geotechnical design. While there are several available methods, with varying applicability to site conditions and design scenarios, it is relatively commonplace within New Zealand engineering practice for the same three methods to be used for legacy reasons, namely the rigid block methods described by Ambraseys & Srbulov (1995), Jibson (2007), and Bray & Travasarou (2007). The objective of this paper is to discuss the importance of applying the right analysis method for the site conditions. An assessment of the most appropriate co-seismic displacement method at three bridge sites was carried out, with a different method ultimately used for each. At Site 1 a simplified Newmark-type displacement method was deemed appropriate. For Site 2, a coupled analysis using selected time history records was used due to the slope height and depth of predicted failure surfaces from pseudo-static analyses. For Site 3, Newmark displacement methods were not considered appropriate due to the presence of deep liquefiable deposits. As a result, finite element analyses were used to better estimate potential seismic displacements.

Keywords: seismic, displacements, slope stability

1   INTRODUCTION

Estimation of co-seismic slope displacements for geotechnical design presents a challenge, with upwards of ten available methods of calculation. These methods have varying degrees of conservatism and applicability to site conditions. Careful consideration is needed to determine the most appropriate method to provide realistic results. It is commonplace in New Zealand engineering practice for simplified Newmark sliding block methods to be used, and this often consists of the same three. These are the rigid block methods described by Ambraseys & Srbulov (1995), Jibson (2007), and Bray & Travasarou (2007). These methods have a narrow range of applicability, typically limited to shallow surficial slides along a well defined failure plane. Discussion of the applicability of these methods has been presented in previous literature (Bray, 2007) and this case study is intended to serve as a comparative discussion only. The cut-off values that were considered for rigid methods are therefore summarised as follows:

Rathje & Bray (1999;2000) present the ratio of T_s/T_m as an indicator of whether a rigid block approach is applicable, where T_s is the fundamental site period, calculated according to Eq. 1 for a one dimensional failure, and T_m is the average period of the ground motion.

$$T_s = 4H/V_s \tag{1}$$

where H = the average height of the sliding mass and V_s = the weighted average shear wave velocity of the sliding mass.

Rigid block methods are indicated to be applicable where $T_s/T_m \leq 0.1$.

The Bray & Travasarou (2007) method presents a modification for a rigid sliding mass which is applicable for $T_s \leq 0.05s$.

It should also be noted that more recent methods have been published by Bray & Macedo (2018) and Bray et al. (2019), which provide less conservative results than the Bray & Travasarou (2007) equations.

As this case study is intended to provide a comparative assessment, the examples provided will focus on the Damage Control Limit State (DCLS) design scenario only. Project details are subject to confidentiality, therefore a simplified description of the site setting and geology is utilised.

2 SITE SETTING

2.1 General Geological Setting

All three sites are located in close proximitly to each other and are within a volcanic region of the North Island of New Zealand, with bedrock deposits comprising Quaternary ignimbrite associated with the Taupo Volcanic Zone. Within lower lying areas, the volcanic deposits are overlain by a highly variable unit of interbedded weathered ignimbrite, tephra and alluvial sediment. This interbedded material is typically capped by a thick layer of tephra and recent surficial ash deposits at higher elevations, and Holocene alluvial deposits in the low-lying valleys.

Design parameters were derived on a site-by-site basis, and the range of values considered for each stratum is summarised in Table 1 along with the stratigraphic sequence. All modelling was undertaken using undrained parameters where appropriate.

Table 1: Summary of design parameters

Layer Name	Layer ID	ϕ' (°)	c' (kPa)	Su (kPa)	Section Colour
Recent Alluvium (Cohesive)	RAc	25	1	10 - 27	
Recent Alluvium (Granular)	RAg	33	0	n/a	
Quaternary Airfall	QA	30 - 32	5 - 8	50 - 81	
Tephra	Tep.	33	5	82	
Interbedded Material	Int.	33 - 34	3 - 5	42 - 43	
Ignimbrite	Ign.	38 - 40	0	n/a	

2.2 Seismic Setting

The seismic design parameters used for analysis were based on a site-specific seismic hazard assessment, and are summarised in Table 2.

Table 2: Summary of DCLS seismic design parameters

Design Scenario	Mw	PGA
DCLS	5.9	0.27

3 SITE 1

3.1 Overview of Bridge and Geomorphological Setting

The first site provides an example for which simplified Newmark sliding block methods were deemed appropriate for calculating co-seismic displacements. The surficial site geology comprises QA at elevations above approximately RL+10m (NZVD 2016), and RAc below this level. These units are underlain by the Int. and Ign. The site geology is indicated in Figure 1.
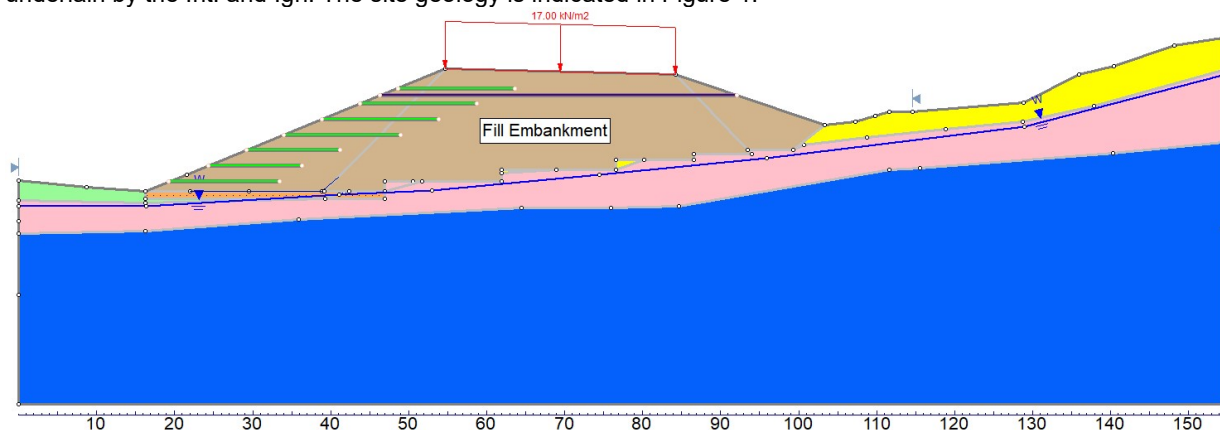

Figure 1: Transverse section through Site 1 western approach embankment

PROCEEDINGS OF THE 14TH ANZ YOUNG GEOTECHNICAL PROFESSIONALS CONFERENCE
14YGPC ROTORUA, NEW ZEALAND, 2ND – 5TH NOVEMBER 2022

177

The bridge abutments and approach embankments are to be constructed on the northern side of a shallow alluvial valley with the road mainline roughly parallel to the valley floor. The approach embankment is to be benched into the existing hillslope as shown in Figure 1.

3.2 Calculation of Seismic Displacements

A pseudo-static slope analysis was carried out for four transverse slope sections using Rocscience's *SLIDE2* software. A section was modelled through each MSE abutment, and each approach embankment. The MSE abutments were found to have a DCLS factor of safety (FoS) >1.0 so no calculation of seismic displacements was required. The approach embankments both indicated a FoS of <0.7 at the DCLS event, with minimum failure surfaces through the interbedded deposits.

The critical seismic coefficient (Ky) for Embankment A was calculated as 0.12g. This value was used to undertake DCLS displacement calculations using the methods noted above. The *Ts* value was calculated to be 0.29s which suggested a flexible method is more appropriate than a rigid method. Both variations of the Bray & Travasarou equations were therefore checked as well as the more recent Bray & Macedo, and Bray et al. methods. The calculated 50th percentile values are shown in Figure 2.
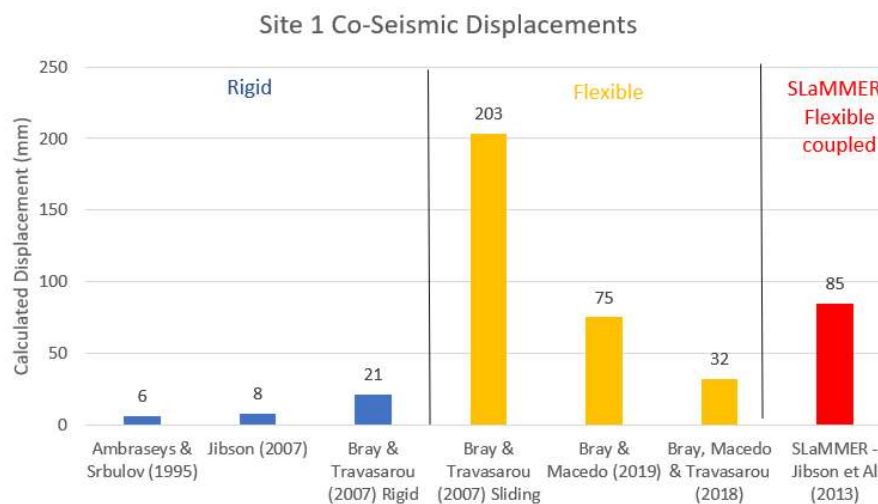
Figure 2: Summary of Site 1 co-seismic displacements to various methods

With the exception of the Bray & Travasarou method, all of the above displacement values were found to be within the DCLS performance criteria for the bridge and did not pose a design risk to the structure.

As can be seen in Figure 2, the Bray & Travasarou (2007) sliding block method predicts significantly higher displacements than the more recent publications so was eliminated from consideration.

Based on the above assessment, a conservative design value of 75mm displacement was adopted recommended using the Bray & Macedo (2019) method.

For the purpose of comparison, analysis was also undertaken using the SLaMMER module (Jibson et al., 2013) inbuilt in *SLIDE2* using ten time history records which were scaled to the site PGA.

The SLaMMER analysis indicated an average displacement of 85mm across the ten seismic records, and is also presented in Figure 2 for comparison. This value was still within the design criteria and further confirms the design value as being a reasonable estimate for this site.

From the assessment of Site 1, it is evident that use of the rigid block methods where not appropriate would significantly underestimate the likely seismic displacements of the structure, in this case by roughly a factor of 3. The impact in this particular case of an approach embankment is not significant, as the worst-case outcome would likely be a relevel of the road and surficial work to the embankment. However, once these values became critical to design of the structural elements, method selection became a key design choice as discussed for Bridge 2.

4   SITE 2

4.1   Overview of Bridge and Geomorphological Setting

The second site is characterised by a steep slope of up to 30m in height. The bridge pier columns are to be founded on piled foundations at the base of the slope. Transverse sections were assessed at the upper abutment, and through each of the pier locations. The critical section was found to be at Pier B, which will form the basis of this example. A cross section indicating the slope geometry, geology, and location of the pier column is shown in Figure 3.

The surficial geology of the slope comprises QA, underlain by Tep. and Ign. at depth.
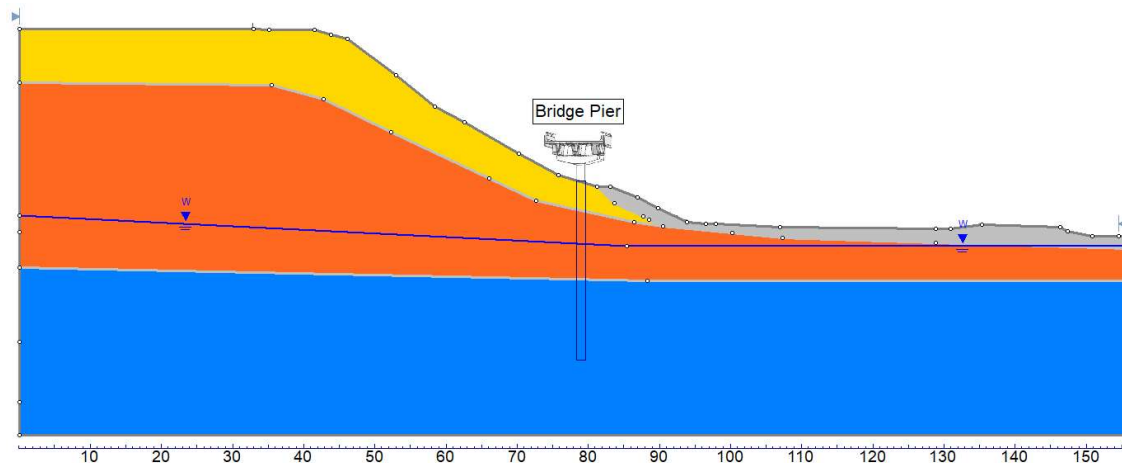
Figure 3: Transverse section through Site 2

4.2   Calculation of Seismic Displacements

Pseudo-static analysis of the slope indicated FoS <0.7 at the DCLS design event. The minimum failure surfaces indicated were global in nature. The sliding mass was assessed to have a *Ts* value of 0.6s and a *Ts/Tm* ratio of 1.2 which precluded use of rigid block methods. The calculated displacements for the flexible methods are presented in Figure 4, alongside the rigid method displacements for comparison.
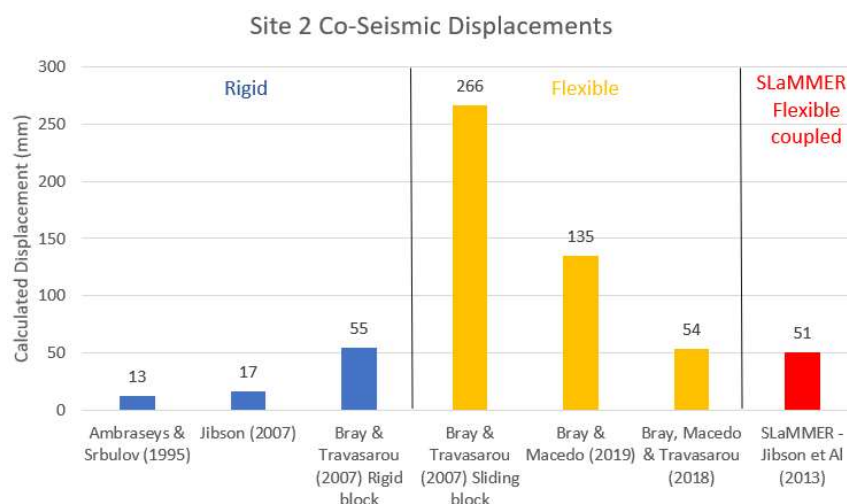
Figure 4: Summary of Site 2 co-seismic displacements to various methods

As noted for Bridge 1, the Bray & Travasarou (2007) sliding block method calculates high displacement values even where *Ky* approaches PGA, and is considered to be highly conservative. The Bray & Macedo (2019) method also calculated displacements in excess of 130mm which were anticipated to be intolerable by the bridge structure. As a result, a more advanced coupled analysis using selected time history records was undertaken to try and further constrain the likely seismic displacement.

PROCEEDINGS OF THE 14TH ANZ YOUNG GEOTECHNICAL PROFESSIONALS CONFERENCE
14YGPC ROTORUA, NEW ZEALAND, 2ND – 5TH NOVEMBER 2022

179

Ten ground motion records were selected from the Pacific Earthquake Engineering Research Centre (PEER) ground motion database and scaed to the site PGA. The coupled analysis was undertaken using the SLaMMER module (Jibson et. al. 2013) inbuilt into Rocscience's Slide software.

The SLaMMER analysis calculated displacement values ranging between 19mm and 161mm, with an average value of 51mm. The average value was adopted as the design value as per AASHTO guidelines (2010b).

The resultant reduction in the design displacement facilitated successful structural design of the piles.

5   SITE 3

5.1   Overview of Bridge and Geomorphological Setting

The third bridge is a ten-span piled structure with the abutments constructed on approximately 8m high approach embankments.

The surficial geology of the slope comprises deep RA to around 20m BGL, underlain by Int. and Ign. at depth. A typical longitudinal section through the western approach and the site geology are shown in Figure 5.
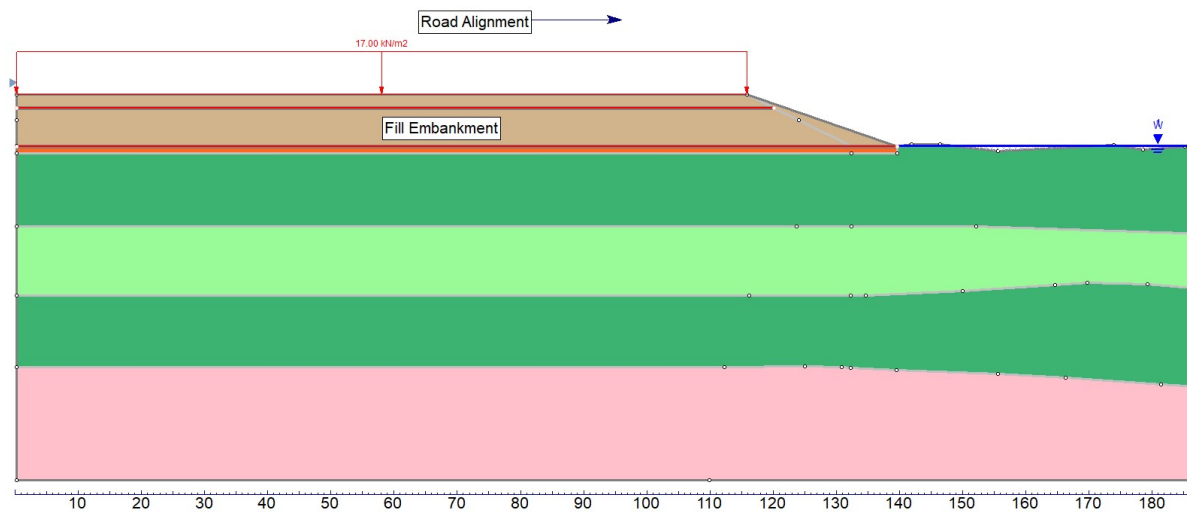
Figure 5: Longitudinal section through Site 3 western approach embankment

As shown in Table 1, the RAc consists of very soft material which was found to be subject to cyclic softening. The RAg and areas of the Int were also found to be susceptible to liquefaction. Given this significant depth of soft/liquefiable soils, failure surfaces from pseudo-static analysis were found to extend to depths of around 20m BGL, with a *Ky* = 0.06g. When dealing with a highly complex site such as this, calculation of seismic displacements can no longer be characterised as a simple rigid or flexible block, particularly when the failure mode is more of a bearing/lateral spread type failure than slope failure.

5.2   Calculation of Seismic Displacements

Due to the high complexity of the site, it was deemed necessary to undertake a dynamic finite element analysis to accurately characterise the seismic response of the system as a whole. This analysis was undertaken using seven of the time history records used for Site 2.

The range of maximum horizontal displacements across the 10 seismic records was found to be 155mm – 225mm, with an average displacement of 200mm.

For comparison, the seismic displacements calculated using Newmark methods are summarised in Figure 6.
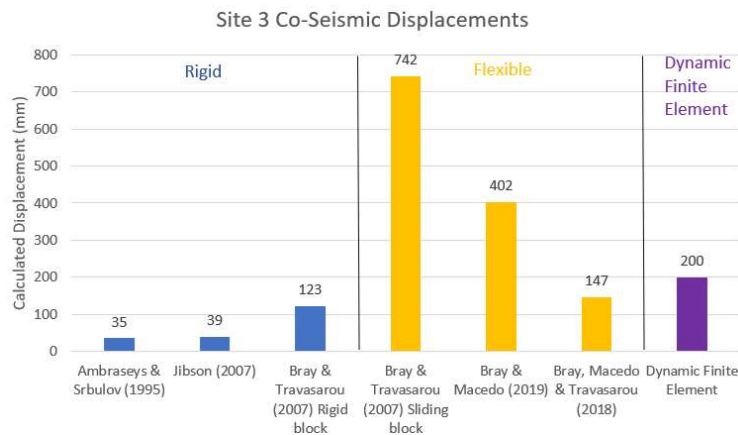
Figure 6: Summary of Site 3 co-seismic displacements to various methods

As with the previous two sites, the rigid methods are shown to significantly underestimate the likely displacement and were discarded as not being relevant to the site. The flexible methods, if considering the two worst case values of 742mm and 402mm, would render the preferred solution unworkable and were deemed inappropriate given the site complexities. The use of dynamic finite element modelling facilitated successful structural design of the bridge where simplified methods would have either drastically underestimated displacements, or over-estimated to the point of requiring a far costlier solution.

6   CONCLUSION

The case study provides an overview of three very different problems and the challenges faced in accurately characterising seismic displacements for design. Were simplified rigid methods to be used for all three as is not uncommon in geotechnical design practice, the risk of significantly underestimating the potential for seismic displacement is shown to be very apparent. Sites 2 and 3 also provide examples of where more advance analysis beyond simplified Newmark type calculations facilitate structural design of elements which would otherwise require significant additional engineering to meet performance criteria. The key message is to avoid complacency and use the right tool for the job, with careful consideration of the limitations and benefits of each.

REFERENCES

AASHTO, 2010b, LRFD Bridge Design Specifications, American Association of State Highway and Transportation Officials, Washington, D.C.

Ambraseys, N., Srbulov, M. (1995). "Earthquake Induced Displacements of Slopes." Soil Dynamics and Earthquake Engineering, Vol. 14, 59-71.

Bray, J.D. (2007). Simplified Seismic Slope Displacement Procedures. In: Pitilakis, K.D. (eds) Earthquake Geotechnical Engineering. Geotechnical, Geological and Earthquake Engineering, vol 6. Springer, Dordrecht.

Bray, J. D., Travasarou, T. (2007). "Simplified Procedure for Estimating Earthquake-Induced Deviatoric Slope Displacements." Journal of Geotechnical and Geoenvironmental Engineering,133(4), 381-392pp.

Bray, J. D., Macedo, J., Travasarou, T. (2018). "Simplified Procedure for Estimating Seismic Slope Displacements for Subduction Zone Earthquakes." Journal of Geotechnical and Geo-environmental Engineering 144 (3) : 381-392

Bray, J. D., Macedo, J. (2019). "Procedure for Estimating Shear-Induced Seismic Slope Displacement for Shallow Crustal Earthquakes." Journal of Geotechnical and Geo-environmental Engineering 145(12)

Jibson, R. W. (2007). "Regression Models for Estimating Coseismic Landslide Displacement." Engineering Geology, Vol 91, Issues 2-4, pp. 209-218.

Jibson, R.W., Rathje, E.M., Jibson, M.W., Lee, Y.W. (2013). "SLAMMER—Seismic LAndslide Movement Modeled using Earthquake Records (ver.1.1, November 2014)." U.S. Geological Survey Techniques and Methods, book 12, chap. B1, unpaged.

Rathje, E.M., Bray, J.D., 1999. An examination of simplified earthquake-induced displacement procedures for earth structures. Canadian Geotechnical Journal 36, 72-87.

Rathje, E.M., Bray, J.D., 2000. Nonlinear coupled seismic sliding analysis of earth structures. Journal of Geotechnical and Geoenvironmental Engineering 126, 1002-1014.

PROCEEDINGS OF THE 14TH ANZ YOUNG GEOTECHNICAL PROFESSIONALS CONFERENCE
14YGPC ROTORUA, NEW ZEALAND, 2ND – 5TH NOVEMBER 2022

181

Predicting Free Field Lateral Ground Movements due to Pile Driving in Soft Clay in Melbourne, Australia

S. J. Goodall[1], MIEAust and R. S. Merifield[2], FIEAust

[1,2]Douglas Partners Pty Ltd, 15 Callistemon Close, Warabrook, NSW 2295; PH (612) 4960 9600; email: Sean.Goodall@douglaspartners.com.au.

ABSTRACT

It is widely known that driving piles and pile groups into soft saturated clay can lead to substantial ground movements. Such movements can have serious implications for brownfield sites where existing infrastructure, such as inground services or existing pile groups, may be located nearby. It is important to be able to confidently predict the associated ground movements due to pile driving in these situations so the proposed pile or pile group can be optimised, or controls implemented, to mitigate potential impacts on existing assets. This paper presents two methods of analysis, namely the Shallow Strain Path Method (SSPM) and Plaxis 3D, applied to compute free field lateral ground movements associated with driving large pile groups in soft clay at a site in Melbourne, Australia. A brief discussion is also provided on the response of a pile to the estimated ground movements. The methods of analysis are compared with site data and overall good agreement is observed between both methods of analysis and the site observed data.

Keywords: soft clay, pile driving, lateral ground movement, finite element method, shallow strain path

1 INTRODUCTION

Driven precast concrete piles are displacement piles (AS2159 2009), meaning their installation causes soil displacement equivalent to the entire embedded volume of the pile. Where piles are driven into soil profiles which typically comprise a granular or cohesive soil of appreciable strength, the displaced soil tends to densify or compact locally to the pile, and the geotechnical design of the pile can take advantage of this by adopting higher design parameters. However, when piles are driven into soft saturated clays, no densification occurs in the clay and the volume of soil displaced is far greater, potentially leading to appreciable ground movements adjacent to and surrounding the pile. At brownfield sites, the impact these ground movements can have on adjacent existing infrastructure can be serious and must be considered in design. This paper presents two methods that were successfully applied to predict lateral ground movements associated with pile driving in soft clay at a brownfield site in Melbourne, Australia.

2 LITERATURE REVIEW

Pile driving in soft saturated clayey soil and the impacts it can have on surrounding infrastructure has been well documented in many laboratory tests and case studies (Hagerty and Peck 1971, Poulos 1994, Sagaseta et al. 1997, Sagaseta and Whittle 2001, Edstam and Kullingsjo 2010, Nenonen and Ruul 2011, Rainer Massarch and Wersall 2013, Hernquist and Nguyen 2016, Edvardsson and Melin-Nyhom 2018, and Attari et al. 2018). From the available case studies and laboratory tests it is observed that ground movement in soft clay due to pile driving is a complex phenomenon, and consequently can be difficult to predict accurately. However, of the available data and case studies, it has been shown that the magnitude and overall trend of lateral ground movement may be estimated by combining engineering judgement and existing published methods of analysis.

There are many methods of analysis available to estimate ground movements associated with pile driving in soft clay. The methods vary from: simple empirical methods such as Rehman's method (after Olsson and Holm 1993 as cited in Edstam and Kullingsjo 2010); analytical methods such as cavity expansion theory (Carter et al. 1979); semi analytical methods such as the Strain Path Method (SPM) (Baligh 1985) or the Shallow Strain Path Method (SSPM) (Sagaseta et al. 1997, Sagaseta and Whittle 2001); and numerical methods such as the finite element method (FEM). Various authors have investigated these methods (Poulos 1994, Xu et al. 2006; Edstam and Kullingsjo 2010, Nenonen and Ruul 2011, Hernquist and Nguyen 2016, Edvardsson and Melin-Nyhom 2018, Attari et al. 2018) and have shown that satisfactory estimates of the magnitude and trend of lateral ground movement due to pile driving in soft clay can be obtained. Of these available methods, the SSPM and FEM (eg Plaxis 3D Bentley Systems) tend to be more prevalent in the literature, albeit with some level of calibration or

modification to the method. These two methods, and one such modification, are described in more detail in the following sections of this paper. Two case studies that have applied the SSPM and / or 3D finite element analysis (FEA) compared with observed lateral movements are presented in Figure 1.
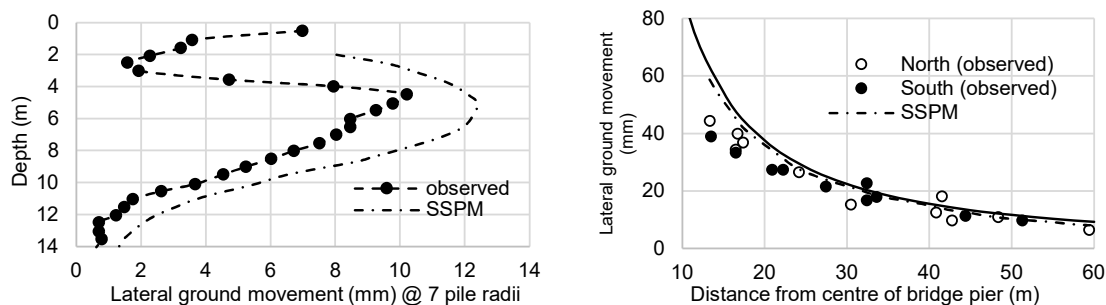

Figure 1: Selected Case Studies: LEFT – Single Shanghai 1.02 m diameter steel tube pile (Xu et al 2006). RIGHT – Partihallen highway bridge, 60 pile group 16.2 m x 6.4 m (Edtsam and Kullingsjo 2010).

2.1 Shallow Strain Path Method (SSPM)

The SSPM is used for predicting ground movements caused by driven or jacked piles in clay (Sagaseta et al. 1997 and Sagaseta and Whittle 2001). To simulate a pile being installed the method adopts a spherical point source that penetrates an inviscid fluid over the full length of a pile and a point sink is introduced to account for the incompressibility of the clay. The method has been developed assuming the clay behaviour is undrained, the surface of the clay layer is stress free and the piles are floating piles (Sagaseta et al. 1997 and Sagaseta and Whittle 2001). The solution for a cylindrical pile from Sagaseta and Whittle (2001) is given in Equation 1, as follows:

$$\delta_r (r,0) = (A_p/2\pi) \, L \, / \, (r \, \sqrt{(r^2 + L^2)}) \tag{1}$$

Where A_p is the cross-sectional area of the pile, L is the length of the pile and r is the radial distance from the pile.

Where end bearing piles are present a solution can be found by considering the relative displacement between the ground surface and incompressible layer (Sagaseta and Whittle 2001). Alternatively the method can be supplemented with numerical methods. The effect of driving numerous piles can be incorporated into the SSPM by using the principle of superposition.

A limitation of the SSPM is that the closed form solutions do not provide a profile of lateral ground movement with depth, and typically require numerical tools to solve for the lateral ground movement profile. However, if site specific data is available, the distribution of lateral ground movement profiles may be approximated using simple mathematical expressions. For example, some case studies from Sweden where the soil surface is relatively stress free and the soil is a deep homogeneous clay profile, a 6th order polynomial has been shown to provide a satisfactory approximation of the lateral ground movement profile with depth (Edstam and Kullingsjo 2010 and Nenonen and Ruul 2011).

2.2 Finite Element Analysis (Plaxis 3D)

Plaxis 3D (Bentley Systems) is a general purpose geotechnical finite element package used for deformation and stability analyses in geotechnical engineering. An advantage of Plaxis 3D is that it can handle complex geometry and interaction effects that cannot be accounted for in methods such as the SSPM. One limitation of Plaxis 3D is the potentially significant time required to setup a model, run the calculations, and extract and rationalise the results of the analysis.

It is generally not necessary to model the entire penetration process of driving a pile from the soil surface in Plaxis 3D, and to simulate the effect of driving piles in soft clay in Plaxis 3D it is common practice to apply a positive volumetric strain to the cross section of a pile to simulate the effect of the volume of the pile displacing the soft clay.

Of the available case studies (Edstam and Kullingsjo 2010, Nenonen and Ruul 2011, and Hernquist and Nguyen 2016), sensitivity analyses have shown the adoption of a linear elastic soil model in Plaxis 3D generally provides satisfactory estimates of the free field lateral ground movements due to pile driving.

PROCEEDINGS OF THE 14TH ANZ YOUNG GEOTECHNICAL PROFESSIONALS CONFERENCE
14YGPC ROTORUA, NEW ZEALAND, 2ND – 5TH NOVEMBER 2022

183

2.3 The Equivalent Pier Modification to the SSPM and Plaxis 3D

The equivalent pier concept in geotechnical engineering is widely known and is routinely adopted to estimate the settlement of a pile group (Poulos 1993). This concept has also been applied to estimating ground movements due to pile driving in soft clay using both the SSPM and Plaxis 3D, and has been shown to compare favourably with observed ground movements, and in this instance is more commonly referred to as a 'Super Pile' in the literature (Edstam and Kullingsjo 2010, Nenonen and Ruul 2011, Hernquist and Nguyen 2016, Edvardsson and Melin-Nyhom 2018, and Attari et al. 2018). When applying this modification to the SSPM or Plaxis 3D, the general approach is to replace a group of piles with a single equivalent pier or several smaller equivalent piers, having the same cross-sectional area and volume as the overall group, and is positioned at the centroid of the cluster of piles it replaces. The method has been verified against numerous cases studies where both methods exhibit similar predictions and compare well with observed data (Edstam and Kullingsjo 2010, Nenonen and Ruul 2011, Hernquist and Nguyen 2016, Edvardsson and Melin-Nyhom 2018, and Attari et al. 2018).

3 CASE STUDY AT A BROWNFIELD SITE IN MELBOURNE, VICTORIA, AUSTRALIA

3.1 Project Background and Geology

The project site is located within the Yarra Delta geological group, about 1 km west of Melbourne. Ground conditions typically comprise 3 m to 6 m of dredged sandy / gravelly fill, overlying a soft normally to slightly over consolidated silty clay, locally referred to as Coode Island Silt (CIS), to a depth of up to 15 m. Underlying the CIS, is the Fishermens Bend Silt (FBS) and / or Quaternary Aged Alluvium (Qha) which comprises mixtures of firm to very stiff / medium dense clay, silty clay, sand and silty sand, which is further underlain by the Moray Street Gravels (MSG) which typically comprise dense sands / gravels and / or the Melbourne Formation (MF). A summary of the geotechnical properties adopted for the Plaxis 3D analysis is given in Table 1.

Table 1: Geotechnical properties adopted in Plaxis 3D analysis

Geotechnical Unit	Unit Weight (kN/m^3)	Drained Elastic Modulus (MPa)	Poisson's Ratio
Dredge Fill	18	10 to 15	
Coode Island Silt	16	2 to 5	
Fishermens Bend Silt	18	10 to 30	
Quaternary Aged Alluvium	18	10 to 15	0.3
Morary Street Gravel	20	35 to 70	
Melbourne Formation	21	≥ 60	

The project comprised the construction of numerous large pile groups (typically between 12 to 25 piles per group) in close proximity to existing pile foundations and other surface infrastructure. Due to the presence of contaminated and / or acid sulfate soils, the preferred option was to use 400 mm square precast concrete driven piles to construct the pile groups. Owing to large loads each pile group would be required to support, the piles were designed to be driven to refusal on the MSG or MF.

3.2 Field Measurements and Observations

Field measurements were obtained from three inclinometers during early piling operations of a square 12 no. pile group at the site, shown in Figure 2.

In the right of Figure 2 it can be seen that in the upper 4 m within the predominantly granular fill, the movements are small or negative, however, large positive movements with depth are observed and are a result of the piles being driven through the CIS and upper portions of the FBS and Qha. The maximum ground movements within the CIS were: about 90 mm but more typically 80 mm at IPI1; about 40 mm at IPI2; and about 20 mm at IPI3. It can also be seen that unlike some of the case studies (Edstam and Kullingsjo 2010 and Nenonen and Ruul 2011), the trend of lateral ground movement with depth is not comparable to a 6th order polynomial but tends to be better approximated by a gaussian distribution, albeit with minor variation and scatter indicated by the inclinometers. The difference between the case studies and the site observations is likely to be attributed to the presence of the overlying dredged

granular fill materials not undergoing appreciable lateral movement during pile driving but also providing some overburden / confining stress to the surface of the soft clay.
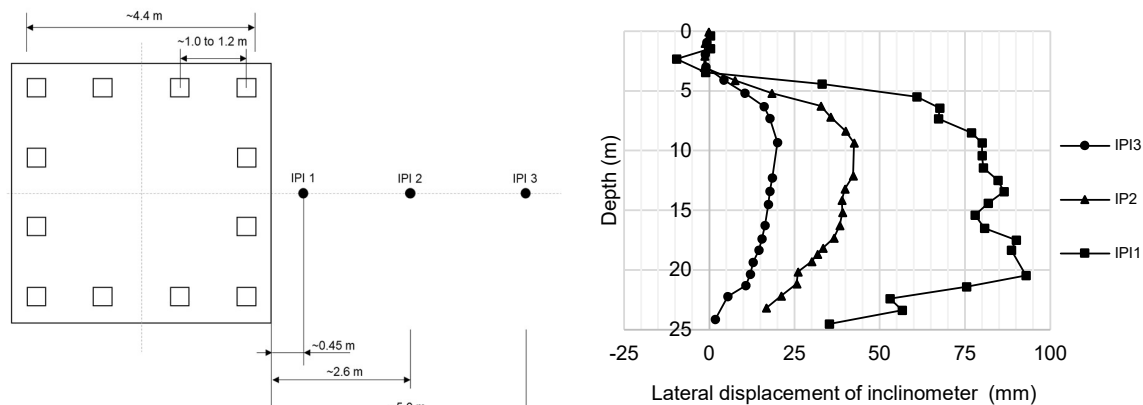

Figure 2: LEFT – Schematic of pile group and inclinometers IPI1, 2 and 3 (not to scale). RIGHT – Lateral displacement of inclinometers after pile group installation

3.3 Results and Discussion of Analysis Methodologies and Comparisons with Field Measurements

The SSPM and Plaxis 3D were applied to predict the lateral ground movements due to the installation of the 12 no. pile group. Based on the findings of Edstam and Kullingsjo (2010), Nenonen and Ruul (2011) and Hernquist and Nguyen (2016), a linear elastic soil model has been adopted for the Plaxis 3D analysis using the typical properties in Table 1. The analysis using Plaxis 3D and the SSPM included modelling individual piles and the replacement of them with a single equivalent pier. The equivalent pier method considered a positive volumetric expansion of 10% in Plaxis 3D and an equivalent pier diameter of 1.41 m in the SSPM. The lateral ground movement profile with depth ($U_x(z)$) for the SSPM has been derived from a gaussian distribution as defined in Equation 2:

$$U_x(z) = [U_{x,max} \exp(-(a^2)/(2(Kx_0)^2)] \qquad (2)$$

Where $U_{x,max}$ is the lateral soil displacement/movement estimated from the SSPM, "a" is the distance from the mid-point of the soft clay layer, x_0 is the distance from the centre of the pile / pile group being driven and K is an empirical factor and is estimated to be between 0.25 to 0.5 of the thickness of the soft clay layer (in Equation 2, Kx_0 is the distance to the point of inflexion of the lateral ground movement profile from the centre of the soft clay layer). It is of importance to highlight that a gaussian distribution is a well-established tool in geotechnical engineering, where it has been routinely adopted in tunnelling engineering (Mair et al. 1996) and also mine subsidence (Holla 1987) to estimate the distribution of surface settlement troughs.

Some results of the analysis compared with observed data have been presented in Figure 3.
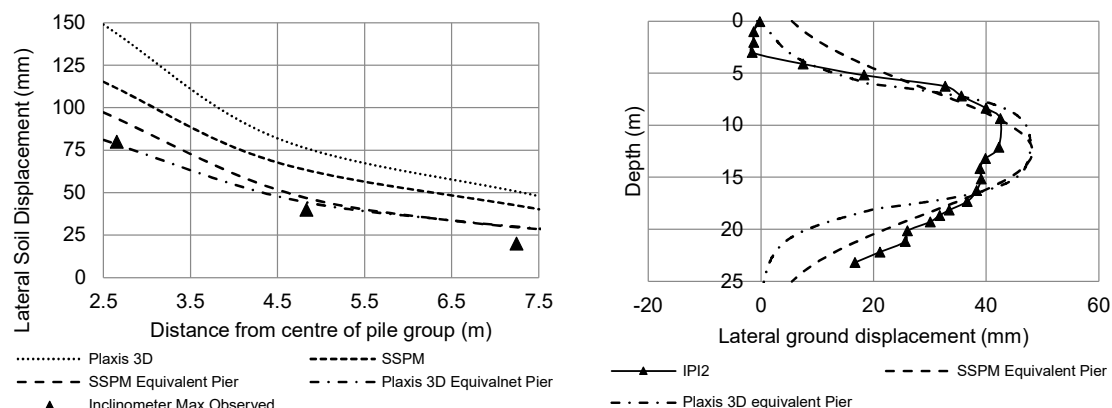

Figure 3: Comparison of observed and predicted lateral displacements. LEFT: Lateral ground movements vs distance from centre of pile group. RIGHT: Lateral ground movement profile for IPI2.

PROCEEDINGS OF THE 14TH ANZ YOUNG GEOTECHNICAL PROFESSIONALS CONFERENCE
14YGPC ROTORUA, NEW ZEALAND, 2ND – 5TH NOVEMBER 2022

185

The left of Figure 3 presents the maximum observed and predicted lateral movement from the inclinometers and analysis. When adopting the equivalent pier modification, the predictions compare well with observed data. However, when the individual piles are modelled the methods do not compare well, and exceed the observed data by about 1.5 to 2 times.

Additional analyses were performed in Plaxis 3D to assess the effect of the piles being modelled in a single stage or individually activated in consecutive stages. The difference between activating the piles in a single stage or adopting individually activated piles in consecutive stages did not provide an appreciable difference in the overall magnitude or trend of lateral ground movements. It should also be noted when considering the SSPM with an equivalent pier, the estimated movements closer to the source of movement are unlikely to yield realistic estimates of movement since the SSPM is more applicable to small strain applications. These behaviours are generally consistent with many of the available case studies (Edstam and Kullingsjo 2010, Nenonen and Ruul 2011, Hernquist and Nguyen 2016, Edvardsson and Melin-Nyhom 2018, and Attari et al. 2018).

The right of Figure 3 presents the comparison of observed and predicted lateral ground movement profiles based on the equivalent pier concept for IPI2. It is evident that the overall trend of lateral ground movement compares reasonably well between the observed and predicted movements. It should be noted that the predictions presented in Figure 3 were based on the nearest available borehole, which was some 40 m from the installed inclinometers, and it is possible that there is some variation in the actual and assumed thickness of the CIS. The SSPM and lateral ground movement profile derived using a gaussian distribution was further validated against additional pile driving undertaken in connection with the project and also other pile group geometries in Plaxis 3D.

4   A NOTE ON FREEFIELD LATERAL GROUND MOVEMENTS AND ITS EFFECT ON EXISTING PILES

An important consideration beyond predicting free field lateral ground movement is the effect that the lateral ground movement can have on existing piles / pile groups. The actual effect is a complex soil-pile interaction problem that depends on the stiffness and strength of the soil, pile stiffness, head fixity of the pile and the distribution of ground movement. The impacts can be readily assessed using numerical methods such as Plaxis 3D, however, it is useful to have an alternative methodology to check more sophisticated methods of analysis or as a preliminary assessment tool.

A theoretical study of a pile group comprising 19 x 450 mm square concrete driven piles has been undertaken. The study has been based on typical ground conditions encountered at the project site from Section 3 and assumes a single existing 30 m long square 450 mm concrete pile 4.5 m away from the pile group. The general methodology proposed by Poulos (1994) has been adopted, where the free field lateral ground movement due to pile driving is computed, in this instance using the SSPM and gaussian distribution, and a pile-soil interaction analysis is undertaken for the existing pile subjected to the computed free field lateral ground movement. The PY software LAP (Geocalcs) was used to undertake the pile-soil interaction. The results of the analysis have been presented in Figure 4 along with results from Plaxis 3D and the simplified chart solutions of Chen and Poulos (1997).
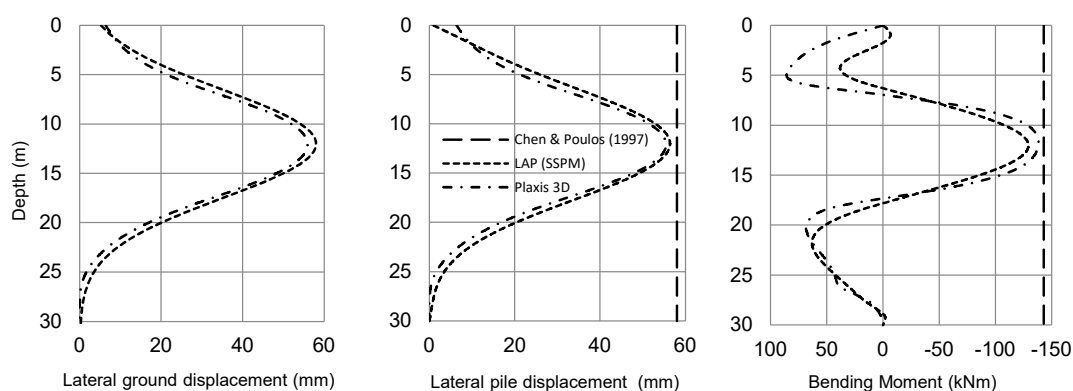

Figure 4: Theoretical study of lateral ground movement effects on a pile.

Figure 4 shows that the ground movements, and resulting maximum pile deflection and bending moment, derived from the SSPM compare well with the results of the Plaxis 3D analysis and the simple chart solutions of Chen and Poulos (1997). It is also worthy to highlight that the pile deflection is similar

to the free field lateral ground movement and is due to the slenderness of the existing pile and soft ground conditions, indicating that the relative stiffness of the ground and pile is an important factor when considering the effects of lateral ground movements on existing piles.

5   CONCLUSION

The analysis methods presented in this paper can be used to establish an understanding of the resulting lateral ground movement due to pile driving in soft clay. The methods showed similar predictions and also compared well with observed site data. This is generally consistent with many of the available case studies in the literature which concluded these methods capture overall magnitude and trend of lateral ground movement due to pile driving in soft clay. This is with the exception of the profile of lateral ground movement with depth, which based on the available site data, was better approximated by a gaussian distribution. This highlights the importance of site-specific data and/or a monitoring program to compare predictions with. Particularly since the resulting ground movement profile effects the curvature and bending moment of an existing pile.

Notwithstanding the above, review of the many case studies within the literature indicates there is appreciable scatter in the observed lateral ground movements, which indicates that regardless of the analysis method adopted, it should be applied cautiously in conjunction with good engineering judgement. In many practical applications it would be considered appropriate to use both methods since they are expected to converge to a similar magnitude and trend of free field lateral ground movement.

Further work is underway to better establish the empirical factor K, the effect of overburden and how intermediate strong layers within the soft clay may affect the lateral ground movement profile.

6   ACKNOWLEDGEMENTS

The authors acknowledge the support from Douglas Partners Pty Ltd.

REFERENCES

AS 2159. (2009). "Piling - Design and Installation". Standards Australia.

Attari, Y., Quigley, P., Doherty, P., and Lusack, N. (2018). "Predicting Pile Driving Induced Movements in Gothenburg Soft Clay". Proceedings of the 26th Young Geotechnical Professional Engineers Conference, 153-160.

Baligh, M. N. (1985). "Strain Path Method". Journal of Geotechnical Engineering, ASCE, 111 (9), 1108-1136.

Carter, J. P., Randolph, M. R,. and Wroth, P. C. (1979). "Some Aspects of the Performance of Open and Closed End Piles". Proceedings of the International Conference on Numerical Methods in Offshore Piling, ICE London, 137-142.

Chen, L. T., and Poulos, H. G. (1997). "Piles Subjected to Lateral Soil Movements". Journal of Geotechnical and Geoenvironmental Engineering, ASCE, 123 (9), 802-811.

Edstam, T., and Kullingsjo, A. (2010). "Ground Displacements Due to Pile Driving in Gothenburg Clay". Numerical Methods in Geotechnical Engineering, 625-630.

Edvardsson, G., and Melin-Nyholm, P. (2018). "Mass Displacement Due to Pile Driving Installation in Soft and Sensitive Clay". The Influence of Pile Installation with Precast Concrete Displacement Piles has on Adjacent Areas. Gothenburg: Chalmers University of Technology.

Hagerty, J. A., and Peck, R. B. (1971). "Heave and Lateral Movements Due to Pile Driving". Journal of the Soil Mechanics and Foundations Division, ASCE, 97 (11),1513-1532.

Hernqvist, H., and Nguyen, D. (2016). "Analysis and FE-Modelling of Soil Displacement Associated to Pile Driving". A Case Study of Pile Installation at Gamlestadstorget. Gothenburg: Chalmers University of Technology.

Holla, L. (1987). "Mine Subsidence in New South Wales – Surface Subsidence Protection in the Newcastle Coalfield". Department of Mineral Resources.

Mair, R. J., Taylor, R. N., and Burland, J. N. (1996). "Prediction of Ground Movements and Assessments of Risk of Building Damage due to Bored Tunnelling". Geotechnical Aspects of Underground Construction in Soft Ground. 713-718.

Nenonen, P., and Ruul, J. (2011). "Environmental Impact of Pile Driving. An FE-Analysis of the Displacements of the Skaran Bridge". Gothenburg: Chalmers University of Technology.

Poulos, H. G. (1993). "Settlement Prediction for Bored Pile Groups". Proceedings of Deep Foundations on Bored and Auger Piles, Volume 2, 103-117.

Poulos, H. G. (1994). "Effect of Pile Driving on Adjacent Piles in Clay". Canadian Geotechnical Journal, 31 (6), 856-867.

Olsson, C., and Holm, G. (1993). Piled Foundations (Original Swedish title Pålgrundläggning). Swedish Geotechnical Institute.

Rainer Massarsch, K., and Wersall, C. (2013). "Cumulative Lateral Soil Displacement Due to Pile Driving in Soft Clay". Sound Geotechnical Research to Practice, Geotechnical Special Publication Honouring Robert D. Holtz II, ASCE, 463-480

Sagaseta, C., and Whittle, A. (2001). "Prediction of Ground Movements Due to Pile Driving in Clay." Journal of Geotechnical and Geoenvironmental Engineering, ASCE, 127 (1), 55-66.

Sagaseta, C., Whittle, A. J., & Santagata, M. (1997). "Deformation Analysis of Shallow Penetration in Clay". International Journal for Numerical and Analytical Methods in Geomechanics, 20 (10), 687-719.

Xu, X. Lehane, B. M., and Liu, H. (2006). "Pipe Pile Installation Effects in Soft Clay". Proceedings of Geotechnical Engineering, ICE, 159 (4), 258-296.

PROCEEDINGS OF THE 14TH ANZ YOUNG GEOTECHNICAL PROFESSIONALS CONFERENCE
14YGPC ROTORUA, NEW ZEALAND, 2ND – 5TH NOVEMBER 2022

187

Preparing for Intelligent Compaction – The Importance of Degree of Saturation when Measuring Dry Density with Stiffness Indexes

R. Latimer[1], BEng, D. Airey[2], PhD

[1]Higher Degree by Research Candidate, University of Sydney, School of Civil Engineering (Geotechnical), Sydney, Australia, email: rlat5653@uni.sydney.edu.au
[2]Professor, University of Sydney, School of Civil Engineering (Geotechnical), Sydney, Australia, email: david.airey@sydney.edu.au

ABSTRACT

Increasingly, the earthworks industry seeks to assess compaction through stiffness indexes, as it is both easier to measure, and is relatable to road design parameters such as soaked CBR. This interest in stiffness is not addressed in a conventional Proctor based approach to compaction. Furthermore, there is an often-held misconception that additional compaction improves stiffness. However, as shown in this paper, and by others, it is clear that stiffness is not related to density in a simple way.

During a recent compaction study undertaken at the University of Sydney, it has been shown that monitoring degree of saturation (S_r) is essential for understanding the relationship between small shear modulus (G_o) and dry density (ρ_d). Silty sand samples were prepared at differing moisture ratios before undergoing multi-staged compaction. First arrival shear wave velocity was measured via Bender Element (BE) to produce G_o at a range of ρ_d. Results presented in this paper show G_o increases with increasing ρ_d at a constant S_r rather than constant water content (w). Analysis indicates that additional compaction past the critical S_r range of 50% will reduce stiffness response G_o at constant w, and that when compacting across the typical range of S_r of 40-70% G_o is nearly constant and largely independent of ρ_d.

Keywords: compaction, degree of saturation, S_r, bender elements, shear modulus, G_o

1   INTRODUCTION

The compaction of soil embankments is a crucial component to major infrastructure projects. While the mechanics behind compaction are relatively well understood (such as Proctor, 1933), there is a desire within the earthwork's community to better control the engineering properties of the embankment, and also to automate the quality control and assurance process of its construction (Kodikara, 2018). The emerging field of Intelligent Compaction (IC) has been heralded as the long-awaited step change to earthworks' practices. IC involves the combination of compactor mounted global positioning systems (GPS) and stiffness index measuring devices making use of accelerometers to produce complete coverage and pass-by-pass stiffness index maps in real-time for an earthworks' lot. However, counter to expectations, during a recent field trial conducted in Australia, a common IC unit Compaction Meter Value (CMV) was found to have scattered and independent relationship to density and compaction.

The motivation for the work described in this paper has been to understand the soil mechanics responsible for the constant stiffness observed in the field data. There has been almost thirty years of research, such as Sandström (1994), White (2011), and Pistrol and Adams (2021), showing that CMV can produce a reliable, but noisy, stiffness index with a properly implemented construction method. But, given CMV has been found to be largely independent of ρ_d during compaction, what is the explanation? This paper presents findings from a compaction study undertaken at the University of Sydney and explores what factors affect stiffness as soil is compacted.

1.1   The case for S_r and the stiffness / density relationship

Due to the consistent increase of ρ_d during compaction, the expectation is that IC measurement values should also increase with compaction. This has been shown to be not the case (Latimer et al, 2022).

The work of Tatsuoka et al (2021) offers an updated framework for compaction, one in which stiffness is controlled by S_r and ρ_d, rather than solely ρ_d. To test this framework, a consistent and controlled approach for measuring compaction and stiffness is required. Measuring of shear wave velocity through bender elements (BE) has been shown to be one of the simplest, non-destructive ways to measure small strain shear modulus (G_o) (Heitor, 2013; Airey and Mohsin, 2013). The general relationship between shear wave velocity (V_s in m/s) to elastic shear modulus (G_o in kPa) where ρ_b is the bulk density (kN/m^3) is shown in Equation 1.
.

Equation 1: Go relationship to Vs

$$G_o = V_s^2 . \rho_b$$

2 LABORATORY TRIAL: THE EFFECT COMPACTION HAS ON SHEAR MODULUS G_O

To compare the effects S_r and ρ_d have on G_o, and to test the framework developed by Tatsuoka et al. (2021), a test apparatus was constructed to statically compact soil at various moisture contents while taking shear wave velocity using bender elements at regular intervals.

2.1 Methodology

All works have been conducted in general accordance with AS1289 (2017) Methods of Testing Soils for Engineering Purposes, unless otherwise stated. Due to its current popularity in earthworks' projects around Sydney (NSW) (Sutton et al. 2018), a tunnel sourced crushed Hawksbury Sandstone, sieved to 1.18mm, was selected as the test soil. Typical particle size distribution (PSD) curve from wet sieve and hydrometer is shown in Figure 1. Specific gravity of the soil was G_s = 2.65.

Samples were moisture conditioned to desired levels and homogenised by mixing thoroughly. The prepared sample was rained loosely into a PVC mould and placed into the test set up as shown in Figure 2. The sample was compacted in stages using the triaxial ram. Bender elements were mounted in the top and bottom platens to monitor the shear wave velocity throughout the experiment. Soil was compressed one-dimensionally, and displacement of the upper platen used to update ρ_d and S_r. Compaction proceeded in stages: the soil was compressed to a target dry density, the shear wave velocity and load recorded, and then the stress was then reduced to zero and the shear wave velocity measured again. Soil relaxation during unloading was found to have a negligible impact on ρ_d. The process was then repeated for progressively higher target densities until the limiting stress of 5 MPa was reached.

The PVC mould was not sealed at the top, allowing moisture to be expelled from soil once optimum S_r was passed. The soil was compacted slowly and controlled by a combination of stress and displacement to prevent pore water pressure build up and ensure drained conditions. When water was expelled from the soil due to approaching the nil air voids line, this displaced water was captured and measured, adjusting the soil moisture accordingly. The PVC mould diameter was 16 cm and compacted sample thickness typically 5-10 cm. This aspect ratio is such that friction on the sides is not expected to be significant.

G_o was calculated from shear wave velocity measured by Bender Elements using the first arrival method (Heitor, 2013). It was checked against cross-correlation method (Airey and Mohsin, 2013) and found to give essentially the same V_s.
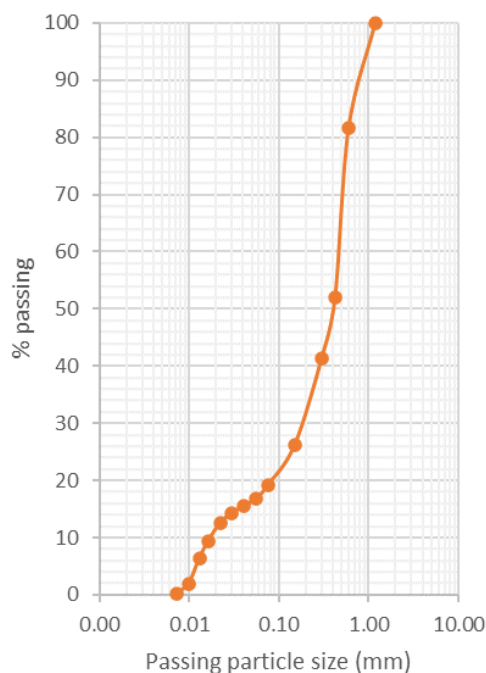

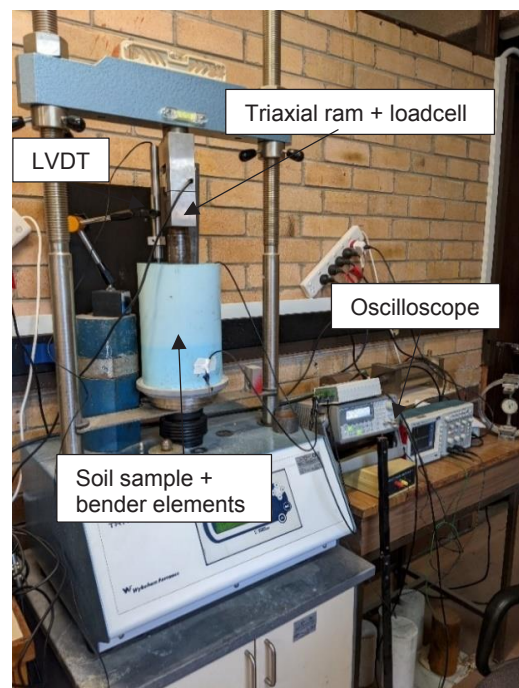*Figure 1: Typical particle size distribution of trial soil*

Figure 2: University of Sydney bender element compaction test apparatus set-up

PROCEEDINGS OF THE 14TH ANZ YOUNG GEOTECHNICAL PROFESSIONALS CONFERENCE
14YGPC ROTORUA, NEW ZEALAND, 2ND – 5TH NOVEMBER 2022

189

A total of 16 test iterations were completed at varying moisture contents from dry, partially saturated and saturated conditions.

3 RESULTS

Because V_s is strongly dependant on stress level, a consistent stress is needed to enable comparison of the effects of density and moisture content. To achieve this, the soil was unloaded to zero vertical applied stress and the results presented below are only from this zero applied stress state. It is noted that G_o measured while under load increased by an order of magnitude compared to unloaded G_o during final stages of compaction approximately when Sr > 50%. The relevancy of comparing unloaded G_o to CMV (which essentially a stiffness measurement taken while under load from the roller drum) is not addressed by this paper, however, the effects of density and moisture are expected to be qualitatively similar.

A sample of the data captured during the test is presented in Figure 3 and Figure 4 below. Figure 3 shows that for a constant w, G_o increases as ρ_d increases, and the rate appears to be increasing with density. However, as shown in Figure 4, this increasing trend does not continue indefinitely, and as the soil approaches the no air voids line, further change can only occur if moisture drains from the soil. This w=10-15% result shows the relationship between G_o and ρ_d for a fixed w ratio is not unique. It can also be noted on Figure 3 that as the soil is compressed, S_r is increasing because of the reduced void space while the volume of water remains constant.
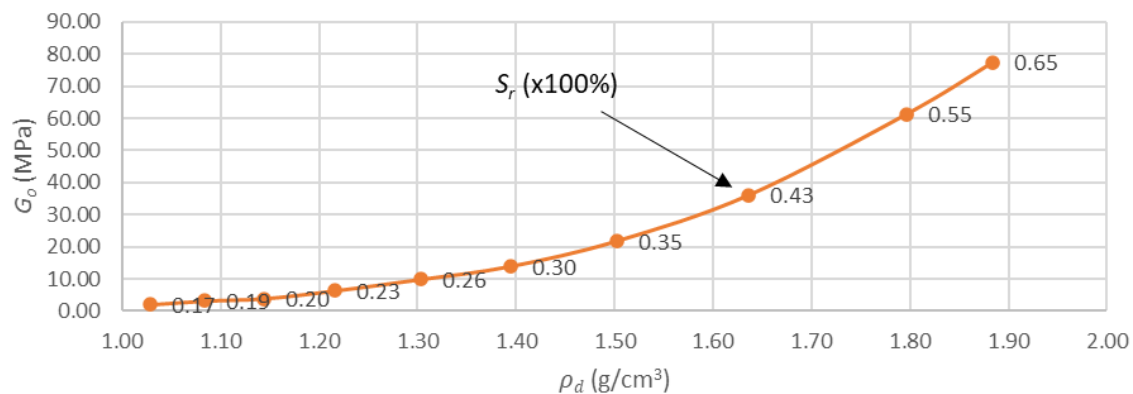

Figure 3: Typical G_o to dry density correlation seen during compaction in trial (w= 10%, under zero confining pressure conditions)

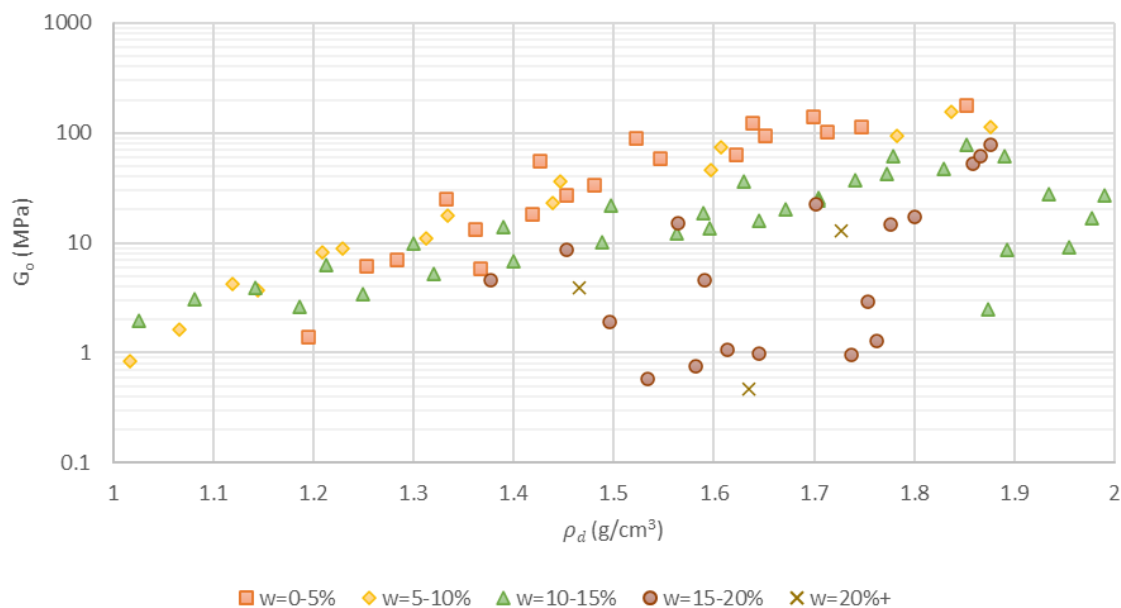
Figure 4: G_o to dry density correlation seen across all compaction trials (zero confining pressure)

190

PROCEEDINGS OF THE 14TH ANZ YOUNG GEOTECHNICAL PROFESSIONALS CONFERENCE
14YGPC ROTORUA, NEW ZEALAND, 2ND – 5TH NOVEMBER 2022

Figure 5 shows a distinct and unique relationship where G_o is increasing exponentially with increasing ρ_d when sorted by S_r. Broadly Figure 5 shows G_o is increasing with ρ_d for fixed S_r, and in Figure 6 G_o decreasing with S_r for fixed ρ_d. R^2 trend between G_o and S_r when sorted by ρ_d in Figure 6 are convincing at 0.56 to 0.84. These results are similar to those of Tatsuoka et al. (2018 and 2021).
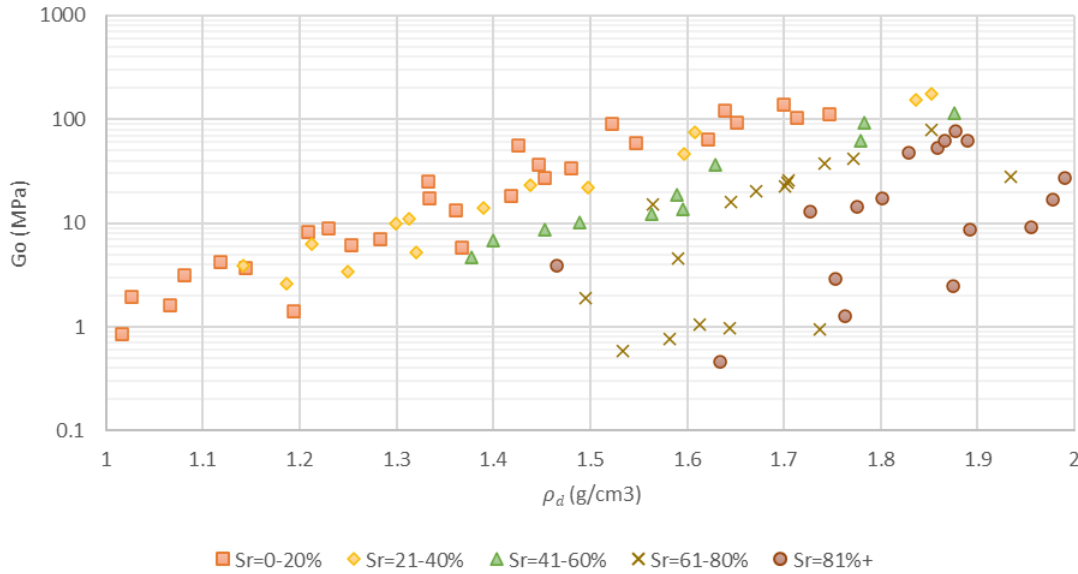
Figure 5: Increasing relationship between G_o and ρ_d for fixed S_r[1]

[1]Note: data variation seen above optimum S_r (around 80%) and at high water content is likely due to miscalculations of S_r and slight variation in ρ_d as water and small amounts of soil particles are expelled from the mould. Improving the testing method to produce a higher quality data set is part of an ongoing research effort.
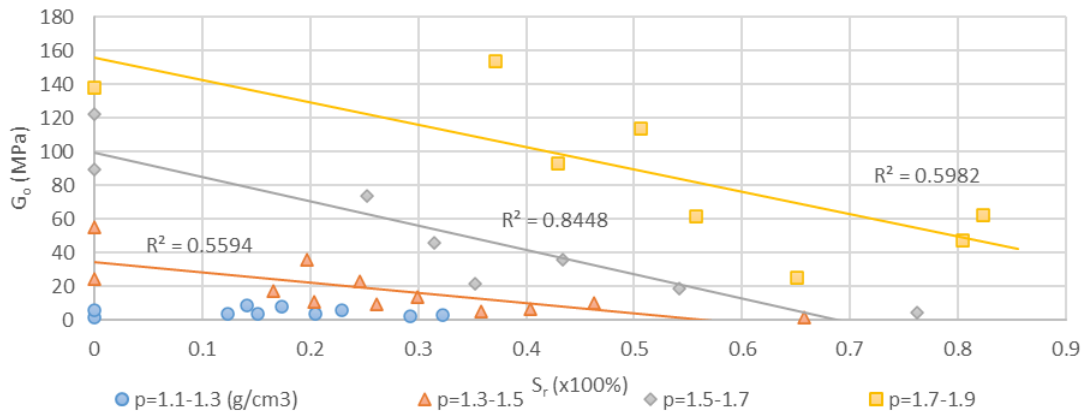
Figure 6: Decreasing relationship between G_o and S_r for fixed ρ_d

4 DISCUSSION

Building upon empirical framework developed by Tatsuoka et al. (2021) and assuming a relationship for G_o described in Equation 2, where soil specific variable *a* is a function of S_r, and soil specific parameters *b* and *c* are a fixed function of ρ_d.

Equation 2: Empirical G_o relationship to S_r and ρ_d (Tatsuoka et al. 2021)

$$G_o = a * (\frac{\rho_d}{\rho_w} - b)^c$$

A series of best fit graphs such as Figure 7 have been plotted to empirically estimate variables *a*, *b* and *c*. Variable *a* has then been plotted to produce a best fit Boltzmann equation for a generalised function relating G_o to S_r in Figure 8. The Boltzmann fit for data from this BE trial fits the theoretical framework of Tatsuoka et al. (2021), it is noted that it also fits a polynomial trend.

PROCEEDINGS OF THE 14TH ANZ YOUNG GEOTECHNICAL PROFESSIONALS CONFERENCE
14YGPC ROTORUA, NEW ZEALAND, 2ND – 5TH NOVEMBER 2022

191
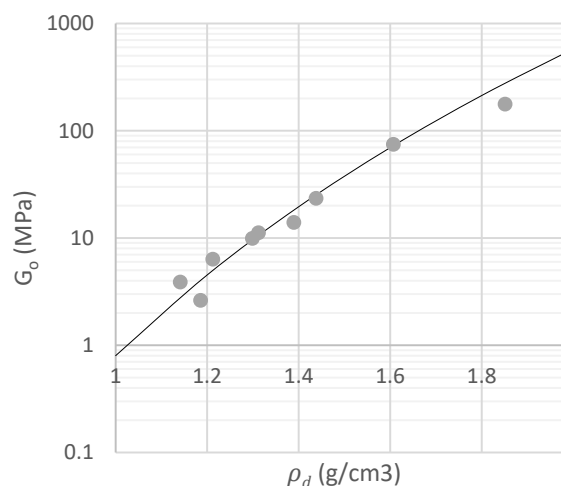
Figure 7: Sample correlation of Sr 21-30% relating ρ_d to G_o, the fitted equation is $G_o=0.8(\rho_d/ \rho_w-0)^{9.5}$
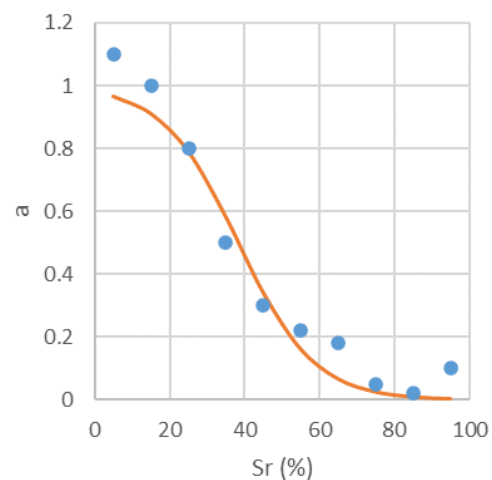
Figure 8: Boltzmann correlation of G_o and S_r by a generalised function for "a"

Using this generalised equation for G_o and plotting for compaction at constant w, as shown in Figure 9, the trial saw an initial increase in stiffness due to densification. However, consistently as S_r approaches a key range of 50% G_o plateaus before reducing. Practical applications of this process are twofold:

1. This trial's results show during compaction at fixed w, maximum G_o is found around 50% S_r, and further compaction past this range of S_r leads to a reduction in G_o.
2. Current earthwork's practices such as R44 (TfNSW, 2013), aim to achieve maximum dry density at 60-90% optimum moisture content. This process typically sees compaction undertaken across a range of S_r 40% to 70%. If attempting to use a stiffness index to monitor the compaction process, it is expected practitioners would see very little change in IC value and potentially even a reduction in measurement value.
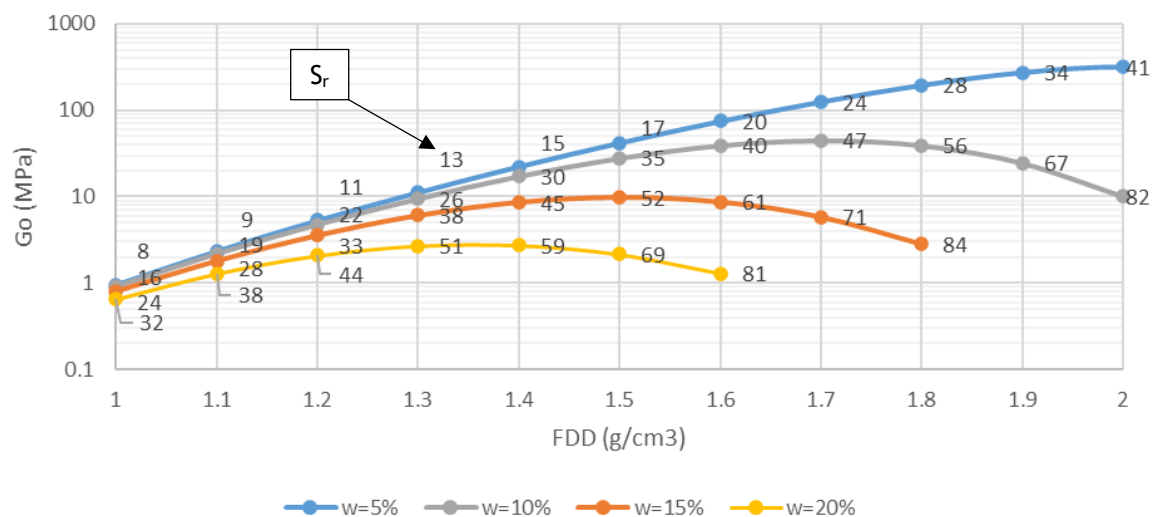
Figure 9: Calculated values of G_o during compaction for fixed w ratios[2]

[2]Note: The Boltzmann best fit equation used by Tatsuoka et al. (2021) expects that variable "a" should continue to zero for Sr > 85% in Figure 8, however, an increase is seen at Sr = 95%. This is likely due to accuracy and testing control issues as soil nears complete saturation during data acquisition. This is part of on-going research and will be investigated with a revision of this work. Results presented in Figure 9 are limited to Sr < 85%.

Tatsuoka et al (2021) have found similar correlations between soil stiffness and density when using a lightweight falling deflectometer (LWFD) and in California Bearing Ratio (CBR) tests. CBR is used as an industry standard road design parameter (from which "E=10CBR" is often adopted). However, these tests are performed using a specified relative density/moisture content followed by soaking to account

for reduced stiffness due to wetting/inundation, and thus the design stiffness is not directly related to values measured during compaction.

5   CONCLUSION

Simple application of the Proctor approach to earthworks compaction control is outdated, and it is time to upgrade. To achieve this, a more thorough understanding of soi compaction is required. Intelligent Compaction offers a promising solution to the modernising demands of the earthwork's market, however, during recent field trials, a popular Intelligent Compaction measuring unit, CMV, was found to be unusable for proving current specifications due to dry density ρ_d being independent of CMV across typical ranges of compaction.

To properly understand how stiffness indexes such as CMV are related to ρ_d, a series of laboratory-based compaction trials were conducted to test the importance of degree of saturation S_r to shear modulus G_o (a stiffness index) during the compaction process. These trials have shown G_o is empirically related to ρ_d via S_r, rather than w. The results presented in this paper show that, as expected, G_o initially increases during compaction for low S_r. However, importantly, this trial indicates that at the critical range of 50% S_r, further compaction leads to a decrease in G_o. Furthermore, when attempting to use stiffness indexes such as G_o to measure ρ_d during compaction across a typical range of 40-70% S_r, G_o will be largely independent of ρ_d, and that careful control of S_r would be required to calibrate this G_o to ρ_d relationship.

6   ACKNOWLEDGEMENTS

REFERENCES

Airey, D, Mohsin, A.K.M, (2013). "Evaluation of shear wave velocity from bender elements using cross-correlation". Geotechnical Testing Journal, Vol.36, No. 4, 2013.

Pistrol, J., Adam, D. (2021). "Lessons learned from implementation of IC in Europe". SPARC International Workshop on Intelligent Compaction 30.09.2021.

Heitor, A. (2013). "Assessment of post-compacted characteristics of an unsaturated silty sand." PhD Thesis, School of Civil, Mining and Environmental Engineering, University of Wollongong, 2013, http://ro.uow.edu.au/theses/3732

Kodikara, J, et al. (2018). "Review of soil compaction: history and recent developments", Transportation Geotechnics, https://doi.org/10.1016/j.trgeo.2018.09.006

Latimer, R, Airey, D, (2022). "Expected stiffness changes during compaction in lab and field", in preparation, Transport Geotechnics?

Proctor, R. (1933). "Fundamental principles of soil compaction." Engineering news-record 111(13).

Sutton, J., et al. (2019). "Sustainable re-use of Sydney tunnel spoil". WEC2019: World Engineers Convention 2019, Engineers Australia.

Tatsuoka, F., Correia A.G. (2018). "Importance of controlling the degree of saturation in soil compaction linked to soil structure design." Transportation Geotechnics 17: 3-23.

Tatsuoka, F., et al. (2021). "Soil stiffness as a function of dry density and the degree of saturation for compaction control". Soils and Foundations 61 (2021) 989-1002.

Transport for New South Wales, (2013). "QA Specification R44 Earthworks". TfNSW, Roads and Maritime Services

Sandström. A., (1994). "Numerical simulation of a vibratory roller on cohesionless soil". Geodynamik report, Stockholm, 22, 1994.

White, D. J., et al. (2011). "Field assessment and specification review for roller-integrated compaction monitoring technologies." Advances in Civil Engineering 2011.

PROCEEDINGS OF THE 14TH ANZ YOUNG GEOTECHNICAL PROFESSIONALS CONFERENCE
14YGPC ROTORUA, NEW ZEALAND, 2ND – 5TH NOVEMBER 2022

193

Applying 3D Geological Modelling Techniques to Geotechnical Engineering Problems – Advantages, Pitfalls, and "Getting the Geology Right"

S. M. Webber[1], K. Kijek[1]

[1]Senversa Pty. Ltd., Level 6, 15 William Street, Melbourne VIC 3000; PH +61 3 9606 0070; Email: sam.webber@senversa.com.au

ABSTRACT

The geotechnical ground model is the fundamental basis of geotechnical engineering. 3D geological modelling software is now routinely utilised to assist with solving geotechnical engineering problems – this allows rigour to be applied to ground model development, and facilitates early identification and assessment of geotechnical site issues. A good 3D conceptualisation improves connectivity between different engineering disciplines and can improve project efficiency. However, for a model to be useful, it must be founded on robust geological principles, and the value of high-quality input data and expert user guidance cannot be understated. This paper presents several project case studies from Victoria, Australia, demonstrating how the utilisation of 3D geological modelling techniques 1) expanded our understanding of the sites' geotechnical and hydrogeological ground model, 2) aided identification of the geotechnical failure model, and 3) assisted site investigations. We highlight the ways in which modelling played an essential role in clarifying the site geology, geotechnical parameters, and hydrogeology, and where it helped to refine the proposed geotechnical design. When used effectively, 3D modelling can synthesise large datasets to help identify and interpret crucial features and sources of geotechnical risk. We note that while 3D geological modelling tools are now routinely utilised on large infrastructure projects, they remain relatively under-utilised on small- and medium-sized projects, even where the geology is complex and/or the geotechnical risk is high. We demonstrate the value of 3D geological modelling combined with geological/geotechnical knowledge, and how it assists in developing ground understanding for geotechnical engineering projects of all sizes.

Keywords: 3D geological modelling, geotechnical engineering, ground model development

1   INTRODUCTION

The site ground model forms the basis for geotechnical analysis and design (Sullivan, 2010). Ground model development for geotechnical projects is now often done using 3D geological modelling software tools (e.g., Leapfrog Works), which have become increasingly affordable and user-friendly over recent years. 3D geological models are 3D interpretive representations of the earth's sub-surface geology. When used in engineering geology, they are usually deterministic ("explicit") in nature, although they may also be stochastic ("implicit;" IAEG, 2021). However, to be useful engineering tools they must utilise high-quality input data, be founded on robust geological understanding, and should be designed to address a particular engineering problem. Ideally, they should be developed in accordance with the draft guidelines laid out in IAEG (2021).

3D geological models, if used correctly, should form part of the site Engineering Geological Model ('EGM'; IAEG, 2021), which combines and evaluates all available input data to produce an interpretive understanding of the site engineering geological conditions, for the purpose of informing engineering decision-making. Therefore, 3D geological models are not merely 3D data visualisations, but are also a key input to the overall knowledge framework for the site. Key advantages include 1) improved data visualisation capabilities, 2) improved project efficiencies, and 3) improved communication. This tends to result in an improved understanding of the site ground model.

3D geological modelling tools are of most use when used on projects with a combination of 1) large or complex ground investigation datasets, 2) relatively high geological complexity, and 2) a high degree of geotechnical risk. While the up-front cost of model development can sometimes be significant – typically ~0.5–2.5% of total fees for fully-fledged models – modelling effort can be targeted, and development costs are often recuperated later in the project lifespan when efficiencies are realised. In Australia and New Zealand, 3D geological modelling is typically utilised as standard practice on larger engineering projects, where the cost of model development is relatively small compared to the total fee. However, it remains relatively under-utilised on smaller projects, even when the degree of geological complexity and/or geotechnical risk is large. This may be due to the assumption by both practitioners and clients that they are unnecessary, and that the cost of model development (as a proportion of the fee) will be

unacceptably high for smaller projects. However, as discussed in Section 4, this is not necessarily the case. The uptake of 3D geological modelling techniques by the geotechnical engineering industry has also likely been hampered to-date by 1) a general lack of applicable industry guidance for the development of 3D geological models (IAEG 2021), 2) inefficient data storage systems and relative inaccessibility of project data, and 3) discomfort with modern digital techniques compared with traditional approaches (e.g., KPMG, 2016) and a perception that models carry additional uncertainties compared to traditional 2D sections.

It is timely to summarise the key advantages and common pitfalls encountered when utilising 3D geological modeling tools, with reference to project case studies.

2   KEY ADVANTAGES

3D geological modelling packages allow for 1) visualisation of geotechnical investigation datasets, 2) 3D visualisation of published data, mapping, digital elevation models (DEMs), and aerial photography, 3) rapid statistical analysis of drilling data and geotechnical analyses, 4) recategorization, complex filtering, and querying of geotechnical investigation datasets, and 5) identification of spatial trends and patterns. Additional advantages and applications include 1) improved process efficiency (e.g., semi-automated section production, software interoperability), 2) estimation of volumes of materials, 3) developing ground profiles, 4) developing an understanding of hydrogeological behaviour, and 5) modelling contamination plumes.

3D geological modelling tools can assist with anticipating the site ground profile prior to intrusive site investigations, which can allow the scope of the drilling program to be optimised and targeted for the expected site conditions. This can help the engineer to make the best use of expensive field investigations. Unfortunately, it is common for 3D geological modelling works to be requested later in the project lifespan, once the full suite of drilling data is available, and when opportunities to adjust the site investigation and proposed design are diminished (e.g., Ranjan, 2017). However, knowledge of the ground profile is especially valuable early in the project lifespan when it is both easier (and cheaper) to adapt the site investigation program to better understand site anomalies. Improved industry awareness of the advantages of 3D geological modelling may help these tools to be more effectively utilised.

3   CASE STUDIES

We introduce three case studies from Victoria, Australia, to demonstrate the value of employing 3D geological modelling tools on small- and medium-size geotechnical engineering projects. All case studies utilise the software Leapfrog Works (version 2021.1.1), developed by Seequent. In all cases, models were primarily 'deterministic' in nature (i.e., they are fitted to the available data and guided by the modeller's understanding of the ground model). Uncertainty was not estimated directly, but was estimated and communicated on the model outputs and within the accompanying documentation.

3.1   Case Study 1: Mount Eliza Landslide

3D geological modelling can assist with slope stability modelling by improving the ability to visualise and query multiple datasets in 3D, and through improved ability to rapidly export geometries to slope stability modelling software. While this workflow is becoming fairly standard practice for slope stability analysis, it is important to emphasise that the slope stability modelling results should be fed back into the geological model to verify and improve the ground model. An example is provided below.

The project comprises a coastal multi-residential property, southeast of Melbourne. The site is located atop an active and very slow-moving landslide complex, which is related to the Manyung fault which itself bisects the site (**Figure 1**). The Manyung fault forms part of the Selwyn fault system, which is an active neotectonic feature (Geoscience Australia, 2022), although no historical ruptures have been recorded. Much of the site surface is hummocky, and numerous scarps cut the site. It had been contended by other parties that the site was previously stable but had undergone recent movements due to recent coastal foreshore erosion. We used 3D geological modelling to improve data visualisation, streamlined determination of the geotechnical failure model, and increase process efficiency through software interoperability with slope stability modelling software.

Published maps and sections for the site indicated that the site is underlain by a combination of Tertiary-aged sediments, with granodiorite and basalt expected from ~20–30 m bgl beneath the site (Gostin, 1966; Peck et al., 1992). The site foreshore comprises beach sand overlying slip debris derived from the Tertiary-aged sediments. The active Manyung fault trace, which runs NE-SW at the rear of the site

PROCEEDINGS OF THE 14TH ANZ YOUNG GEOTECHNICAL PROFESSIONALS CONFERENCE
14YGPC ROTORUA, NEW ZEALAND, 2ND – 5TH NOVEMBER 2022

195

(**Figure 1**), was originally interpreted by Gostin (1966) as a west-dipping normal fault that approximately parallels the coastline. Senversa carried out a site investigation in 2021 based on this conceptual site model to investigate slope instability. The investigation included a site geomorphological walkover, mapping of site features, and boreholes and CPTs positioned across the site with target depths nominally at 20 m bgl to confirm rock head. The deepest test location was terminated at 34 m bgl. While extremely weathered granodiorite was encountered in boreholes in the eastern part of the site, unexpectedly these passed downward into Tertiary sediments, representing an unexpected 'age reversal.' This had several important implications for the site ground model: 1) this contradicts the original interpretation of Gostin (1966) that the Manyung fault is a normal fault, 2) it requires the presence of two reverse splay faults within the site, because the location of the main Manyung fault scarp is located further to the east, and 3) the depth to bedrock may be much deeper than that predicted by Gostin (1966). As a result of this information from the 3D geological model, a thorough literature review was undertaken which identified that faults bounding the Mornington Peninsula had since been re-interpreted as reverse faults (Cayley et al., 2002), consistent with our drilling observations.
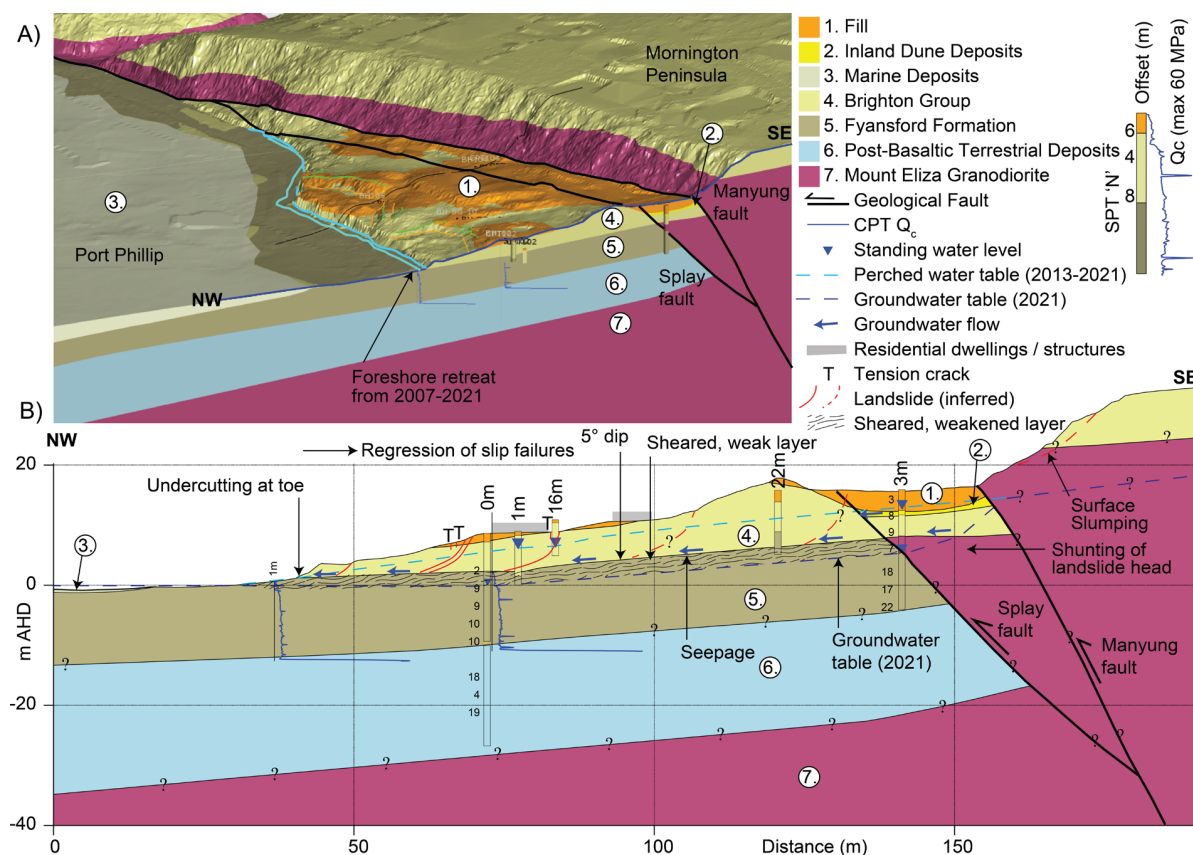
*Figure 1 – **A)** 3D geological model for the Mount Eliza site (natural scale). Note the Manyung fault and its splay fault (black lines), and the extent of foreshore retreat between 2007–2021 (light blue lines) – see text for explanation. **B)** Interpretive ground model for the site, incorporating the results of the slope stability modelling. Note the sheared, softened layer at the top of the Fyansford Formation, which defines an ancient, translational slip surface. A series of regressive, rotational slip surfaces cut the overlying Brighton Group. The Manyung fault and its splay fault define the landward limit of the landslide complex.*

Two aquifers were encountered: one perched within the upper Tertiary sediments, and another located along a softened layer (**Figure 1B**). 3D geological modelling software (Leapfrog Works) was used to visualise shoreface retreat. The literature review indicated that the rate of foreshore retreat was episodic, marked by periods of net foreshore erosion interspersed by periods of net foreshore advancement. Multiple topographic surveys (2007, 2021) were assessed to estimate the distribution of recent foreshore erosion at the site (average retreat rate of 0.2–0.3 m/yr from 2007–2021). However, historical aerial photography indicated that while net foreshore erosion had occurred between 2007–2021, foreshore erosion had been variable since 1946, with net shoreline movement sometimes being seaward.

A 3D geological model was developed for the site (**Figure 1A)** to assist with determination of the ground model and slope failure mechanism. This was useful, as the failure surface could not be definitively identified from the boreholes or CPTs, and time did not permit the installation of inclinometers. Modelling effort required was modest, incorporating both surface and sub-surface data. Cross-sections were computed along critical sections, and geometries were exported to the software GeoStudio 2021 for slope stability analysis. The slope stability model was calibrated using existing active slope failures located near the coast, and material parameters were estimated based on laboratory analyses and published correlations. Separate analyses were conducted for the 2007 and 2021 site surveys, to show the effects on slope stability of ongoing foreshore erosion and erosion of the toe over that period. The slope stability modelling showed that the ancient surface was brought closer to failure by net foreshore erosion between 2007–2021. It was also demonstrated that beach nourishment (i.e., placement of sand material on the foreshore) would slightly improve the stability of the site. The results of the slope stability modelling were then recombined with the 3D geological model to refine the model, and modelled slip surfaces were compared against the field data.

The data are consistent with a basal, ancient translational failure surface that occupies the ~5° seaward-dipping contact between two Tertiary-aged soil layers (**Figure 1B**). Repeated reactivation of that surface has resulted in development of a sheared, weakened layer there. A series of smaller, arcuate slips cut upward from the sheared layer, and are marked at the surface by back-scarps and tension cracks. Together with the historical aerial imagery, this indicates episodic movement of the landslide system. It is speculated that periods of activity on the basal, ancient landslide are triggered by a combination of 1) erosion of the landslide toe due to foreshore erosion, 2) loading of the landslide head (e.g., due to landscaping earthworks, surface slumping from the upper slope, or movement on the Manyung fault), 3) increased groundwater pressures (e.g., in response to heavy rainfall events), and 4) seismic activity or tectonic shearing (e.g., on the Manyung fault). Periods of slip on the Manyung fault would load the landslide head. Slow landslide movement results in net seaward mass movement, which loads the landslide toe. Ongoing movement on the basal landslide would then continue until the toe had been sufficiently loaded. This is followed by periods of quiescence, during which time stability is improved through shear strength healing of the softened layer (Stark and Hussain, 2010). Together, this process results in episodic periods of movement, interspersed by periods of relative stability. Based on this interpretation, Senversa was able to demonstrate that the site stability was governed by the presence of an ancient, but intermittently active, basal landslide.

3.2 Case Study 2: Brickworks Quarry
The project comprises an active quarry located in Central Victoria. Two phases of work were conducted: 1) a preliminary 3D geological model for the site was developed based on limited drilling data, and 2) the design of multiple landfill cells including a limited drilling program. The key advantages of 3D geological modelling were the ability to use the preliminary model as a data visualisation to anticipate the materials present in different parts of the site, and assistance with developing an understanding of groundwater seepage behaviour and impacts of surface water in the various quarry pits.

The site is located on a large exposure of Silurian Dargile Formation (siltstone), surrounded by Quaternary Newer Volcanic Group (basalt flows; **Figure 2A**). A preliminary 3D geological model was developed in Leapfrog Works using limited historical borehole data, geological mapping, aerial imagery, multiple topographic surveys (2007–2008, 2021), and surface water measurements. Only modest effort was required to generate the model. The two surveys were compared to determine the extent of excavation and stockpiling of fill across the site – this enabled identification of a fill embankment between the creek and the West Pit (**Figure 2B**), which had previously been incorrectly logged as alluvium.

Additional drilling was later requested by the client to investigate the ground conditions for a proposed landfill containment facility in the northern area. The location for the proposed facility had been formulated without accurate knowledge of the local ground profile – it was not known that significant filling had occurred, and the proposed footprint had been assumed to be underlain by a single stratum. However, the existing preliminary 3D geological model was able to demonstrate that the ground conditions were likely to be variable across the footprint (**Figure 2B**). This knowledge was then used to scope the drilling investigation and ensure that the thick fill and variable ground profile were adequately targeted. In this way, we were able to provide advice regarding the risks of differential settlement across the proposed footprint. Ultimately, the design solution was to strip the existing fill and adjust the proposed layout, to avoid founding partly atop fill, siltstone, and residual basaltic clay. The 3D geological model was then able to rapidly estimate the volume of fill materials to be removed.

PROCEEDINGS OF THE 14TH ANZ YOUNG GEOTECHNICAL PROFESSIONALS CONFERENCE
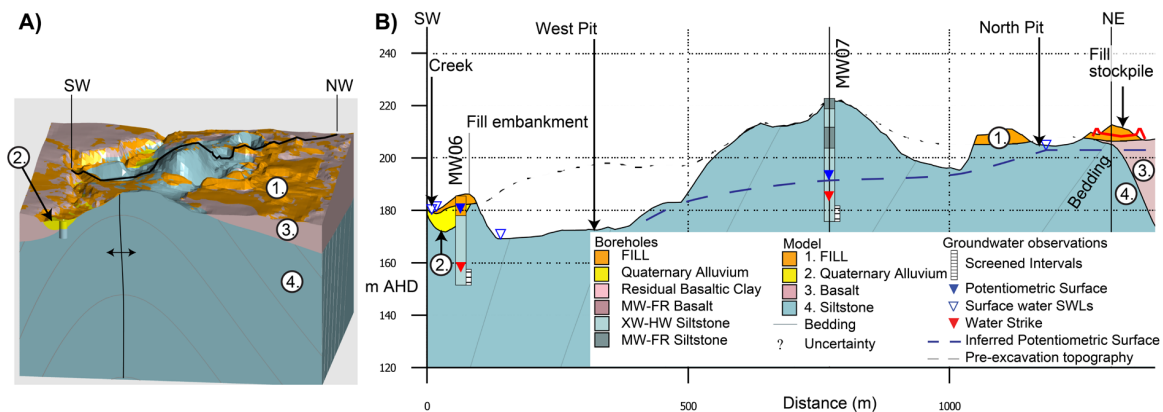14YGPC ROTORUA, NEW ZEALAND, 2ND – 5TH NOVEMBER 2022

197

*Figure 2 – **A)** 3D geological model of the brickworks quarry site (5x vertical exaggeration). Note the section alignment (black line). **B)** Cross section through the brickworks site. Note the pre-excavation topography (dashed line), present topography (black line), fill stockpiles indicated by the difference between these surfaces, and the proposed design footprint for the containment cell (red line).*

3.3   Case Study 3: Former Fire Training Facility

The project comprises an inactive former fire training facility located in Central Victoria. Pliocene basalt flows are underlain by Tertiary sediments. A 3D geological model was developed for the site to synthesise approximately 10 years' worth of site investigation data, which had previously only been reviewed in 2D. The 3D modelling enabled the extent of the geometry of a paleochannel to be rapidly determined, and assisted with planning of the ongoing drilling investigation.

A preliminary model (**Figure 3**) was developed in Leapfrog Works using 32 boreholes, supplemented by surface mapping within deeply eroded gullies to the east and west of the site. Initial model development required only modest effort, and the model was able to be updated efficiently based on subsequent rounds of drilling data. 3D visualisation of the data and ground model immediately revealed multiple paleosols developed within the basalt, separating multiple, distinct basalt flows. Paleosols have the potential to act as aquitards, and at the time it was suspected that they may control site groundwater behaviour. However, visualisation of the groundwater dataset in 3D against the paleosol layers revealed that this was not the case, and that groundwater levels were instead controlled by vertical, highly fractured zones of higher permeability in the basalt. The 3D geological model was also able to define the extent of the paleochannel, and highlighted data gaps and areas of uncertainty. This information was used to guide further site investigation works, with each phase of works being used to update the model in real-time. In this way, the locations of new boreholes were able to be optimised based on the latest understanding of the ground model. The model itself also served as an invaluable tool for guiding client presentations and discussions and improving collective understanding of the site.
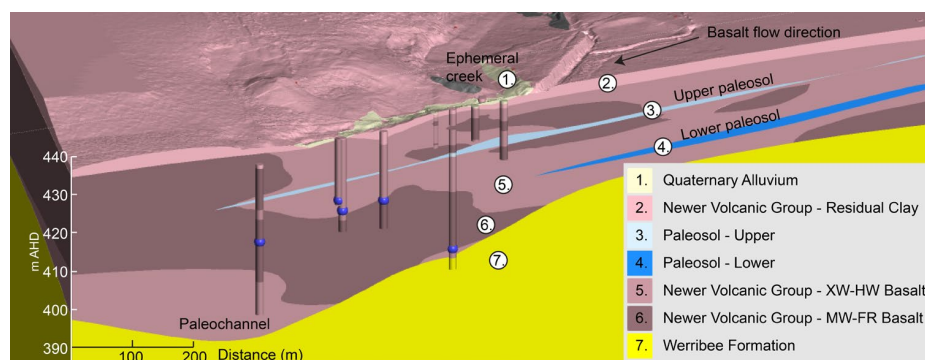
Figure 3 – 3D geological model for the former fire training facility site (5x vertical exaggeration). Note the two paleosols, paleochannel feature, and standing water levels (blue dots).

4   COMMON PITFALLS

Robust 3D geological models should incorporate geological data from a variety of sources. Typical inputs include topographic DEMs, boreholes, CPTs, piezometer data, geological maps, and aerial imagery. For sites that may have undergone cutting/filling or change over time (e.g., landsliding), multiple topographic surveys collected at various times should be used to construct the model, so that

changes to the site topography can be accurately quantified. For all three case studies described herein, multiple surveys were assessed to develop the site understanding.

3D geological modelling is not a substitute for sound engineering geology expertise. Inadequate geological understanding can limit the modeller's ability to *'get the geology right'* (e.g., Fookes, 1997), which can result in incorrect understanding of the site geotechnical risks. The modeller must have a good understanding of the geological principles and site setting, which should form the basis for the site conceptual model. The 3D geological model must be consistent with the mapped geology, and must be consistent with the geological processes and stratigraphic relationships expected at the site. For Case Study 1, lack of recognition of the "age reversal" encountered in the drilling investigation, and lack of knowledge of the Caley et al. (2002) interpretation of the Manyung Fault orientation, would have led to the assumption that the Manyung fault dipped in the incorrect direction, which would have led to a reduced understanding of the slope failure mechanism.

The modelling approach should be flexible, and the modeller should be prepared to modify the model as required by the input data (Sullivan, 2010). Multiple model hypotheses should be explored early on, and each tested, with the goal of converging on the final site conceptual model based on the evidence. The modeller also needs to understand the limitations of the dataset. It is generally unacceptable to omit data or information that do not fit the model – while 'outliers' may potentially be excluded, this must be justifiable. Ultimately, the model should be based on the facts, rather than reverse-engineering the model from a preconceived answer. Ideally, the 3D geological model should be continually refined based on the latest available data and site understanding. This is particularly the case when new data are not consistent with the predictions of the preliminary model (as was the case for Case Study 1).

It is often assumed that 3D geological modelling is unnecessary and/or too expensive for use on small- and medium-sized projects (refer Section 1). However, these techniques are potentially of great benefit to such projects if the geology is relatively complex, and if the geotechnical risk is high. It is important to note that a fully-fledged model need not be developed for all projects – the amount of modelling effort can be readily tailored to suit the project requirements, and modelling focused on key elements. For small- and medium-sized projects, it is often possible to invest only minimal modelling effort to obtain an improved understanding of the ground model. Modelling effort is regularly recuperated later in the project lifespan when additional efficiencies are realised (e.g., semi-automated section development).

5   CONCLUSIONS

3D geological modelling can be a valuable tool for geotechnical engineers. Advantages include improved site understanding, enhanced visualisation and communication, improved planning of drilling investigations, and improved efficiencies. However, 'over-enthusiastic modelling' can lead to a misuse of such tools and there are several common pitfalls, including inadequate recognition and incorporation of the available input data, and an inadequately developed site conceptual model. Finally, while 3D geological modelling tools are now routinely used on large infrastructure projects, there is significant opportunity for increased utilisation of these techniques on small- and medium-sized projects, where they can improve site understanding and improve efficiencies, in many cases with only modest modelling effort required. We argue that improved industry awareness of the key advantages (and potential pitfalls) of these tools will enable them to be more effectively utilised on small- and medium-size projects.

6   ACKNOWLEDGEMENTS

REFERENCES

Cayley, R., Taylor, D., Vandenberg, A., and Moore, D. 2002. Proterozoic – Early Palaeozoic rocks and the Tyennan Orogeny in central Victoria: the Selwyn Block and its tectonic implications. Australian Journal of Earth Sciences, 49.

Fookes, P. 1997. Geology for engineers: The Geological Model, Prediction and Performance. Quarterly Journal of Engineering Geology and Hydrogeology, 30, 293-424.

Geoscience Australia. 2022. Neotectonic Features. https://neotectonics.ga.gov.au/

Gostin, V. 1966. Tertiary Stratigraphy of the Mornington District, Victoria. Proc Royal Soc Vic, 79, 459-512.

KPMG 2017. Global Construction Survey 2016.

IAEG Commission 25 Working Group, 2021. Guidelines for the Development and Application of Engineering Geological Models on Projects (first draft 10 September 2021).

Peck, W., Neilson, J., Olds, R., and Seddon, K. 1992. Engineering Geology of Melbourne, Rotterdam, A.A. Balkema Publishers.

Stark, T., and Hussain, M. Drained Residual Strength for Landslides. In: Fratta, D., ed. GeoFlorida 2010: Advances in Analysis, Modeling & Design, 2010 Orlando, Florida. 3217-3226.

Sullivan, T. 2010. The Geological Model. 11th IAEG Congress, 2010 London. Taylor & Francis Group.

PROCEEDINGS OF THE 14TH ANZ YOUNG GEOTECHNICAL PROFESSIONALS CONFERENCE
14YGPC ROTORUA, NEW ZEALAND, 2ND – 5TH NOVEMBER 2022

199

Performance and sustainability options assessment of a building with a concrete raft foundation overlying liquefiable soil

G. McDougall[1], J. Thompson[2], M. Thomas[3], S. Van Ballegooy[4]

[1] Tonkin & Taylor Limited, PO Box 317, Tauranga, New Zealand, +6475777313, email: gmcdougall@tonkintaylor.co.nz
[2] Calibre Group Limited, Christchurch, email: Jamie.Thompson@calibregroup.com
[3] Tonkin & Taylor Limited, Auckland, email: MThomas@tonkintaylor.co.nz
[4] Tonkin & Taylor Limited, Auckland, email: svanballegooy@tonkintaylor.co.nz

ABSTRACT

Communication and interaction between the project structural and geotechnical engineers are critical to obtain an efficient building solution for the site, building owner and occupants. This is particularly important at concept development phase when building form and type is being assessed. This paper provides a case study of soil-structure interaction and the holistic concept development of a four-storey apartment type building and concrete raft foundation overlying potentially liquefiable soil. It examines how a lightweight structure can have benefits from a sustainability, seismic performance, and overall cost perspective. The site comprised liquefiable soils approximately 3 m below foundation level. The Structural Engineer and Geotechnical Engineer worked together to examine the seismic and sustainability performance of a robust reinforced concrete raft foundation for three potential superstructure types: timber, reinforced concrete and steel. For simplicity, this paper presents the two maximum and minimum structural types for seismic performance and sustainability, being reinforced concrete and timber. It was established that the seismic performance of a lightweight timber structure was significantly improved compared to a conventional concrete structure. As a result, the timber structure option only required a 400 mm thick concrete raft. Whereas the conventional concrete structure option required a 900 mm thick concrete raft with poor seismic performance, and potential for additional ground improvements. It was also assessed that the timber structure option had significantly less embodied carbon compared to a conventional concrete structure. A major contribution to this was the differences in the concrete raft thickness. The improvement in foundation design, improvement in seismic performance, and reduction in embodied carbon contributed to the building owner's selection of the timber structure concept and avoided the need for expensive ground improvement.

Keywords: liquefaction, soil structure interaction, concrete raft, sustainability, embodied carbon

1 INTRODUCTION

Sustainability and seismic performance are critical aspects of building design. The best opportunities to influence these two factors are at planning and concept development phases of a project. Carbon reduction and design changes have a lower potential for implementation later in the project. This is aligned with the MacLeamy concept.

The development described in this paper comprises several stages of apartment type buildings to be constructed in Mt Maunganui. To determine a suitable building material type for the overall development, a structural and geotechnical concept assessment of a typical four storey structure (20 m by 50 m footprint) was carried out. In this paper we look at two key issues of seismic performance and sustainability and how the geotechnical conditions, structural loads and sustainability benefits link together to inform the building owner of a suitable option to proceed with. This case study also shows the significant benefit a concept assessment can have to the overall efficiency of the building design and allows the building owner to make an informed decision about the best option to proceed with.

The ground model, based on a typical cone penetration test (CPT) from the site, is summarised in Figure 1. A simplified liquefaction and cyclic softening triggering assessment was completed using Boulanger & Idriss (2007, 2014). The liquefaction and cyclic softening factor of safety is shown in Figure 1 based on the triggering assessment for an ultimate limit state (ULS) earthquake (500 year return period, PGA=0.3g, M=5.9). Liquefaction and cyclic softening were not triggered for a serviceability limit state (SLS) earthquake (25 year return period, PGA=0.065g, M=5.9).

The generalised ground profile comprised a loose to medium dense SAND of variable density to 14 m depth overlying a firm SILT layer to 18 m depth, overlying a silty SAND to 19.5 m depth, overlying SILT to 21 m depth, overlying a medium dense SAND which becomes very dense at 25 m depth. Groundwater

was encountered at around 2.5 m to 3 m below the proposed foundation level based on 16 CPTs and 3 boreholes across the site.
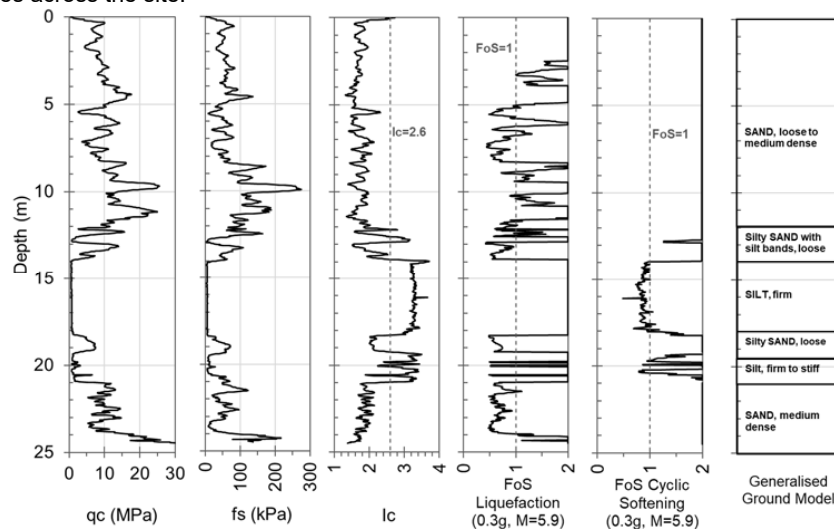
Figure 1: Summary of ground model based on typical CPT trace (CPT102)

The CPTs showed the upper sands have some level of variability in density spatially across the site and therefore there was some variation in each CPT as to the depths which were triggering liquefaction at ULS shaking intensity. However, the triggering assessment typically showed the following layers to liquefy at different earthquake intensities:

- 3 to 4 m at 500 year earthquake intensity (PGA = 0.3g, M=5.9)
- 4 to 6 m at 1,000 year earthquake intensity (PGA = 0.39g, M=5.9)
- 6 to 8 m and 12 to 14 m at 250 year earthquake intensity (PGA = 0.22g, M=5.9)

The lower firm silt layer (14 to 18 m) was also determined to trigger cyclic softening at approximately 250 year earthquake intensity (PGA = 0.22g, M=5.9). Figure 2 below also shows the development of liquefaction within different layers for three typical CPT based on shaking intensity (PGA). It shows that the predicted liquefaction triggering for the various CPT across the site is fairly consistent.
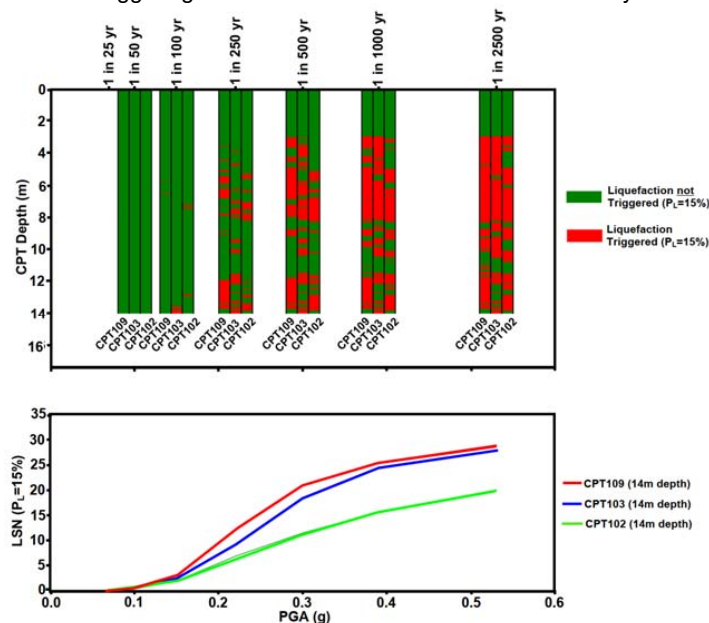
Figure 2: Liquefaction triggering plot and liquefaction severity number (LSN) based on Peak Ground Acceleration (PGA) and return period for a Mw 5.9 earthquake.

PROCEEDINGS OF THE 14TH ANZ YOUNG GEOTECHNICAL PROFESSIONALS CONFERENCE
14YGPC ROTORUA, NEW ZEALAND, 2ND – 5TH NOVEMBER 2022

201

2   INITIAL OPTIONS EVALUATION

Based on review of the ground conditions at the site, liquefaction in the upper sand layer (3 to 14 m depth) was deemed the critical geotechnical issue for the site. Given the crust thickness was only 3 m and the building loads were likely to be high for a four-storey structure, conventional shallow strip foundations were considered to have unsatisfactory performance in a large earthquake resulting in excessively large settlements and potential bearing failure. Therefore, two main options were considered:

1. Conventional heavy concrete structure with a concrete raft foundation. If a concrete raft showed unsatisfactory performance, ground improvement or screw piles to the dense sand layer at 25 m depth would be necessary. Driven piles were ruled out due to noise and vibration concerns to neighbours.
2. Lightweight timber structure (cross-laminated timber, "CLT") with a concrete raft foundation.

The option for the structure was closely linked to its mass and consequently the foundation or ground improvement option as a single system, so it was important at concept stage for the Structural Engineer and Geotechnical Engineer to collaborate closely to achieve an outcome that suited the site conditions and project objectives.

3   GEOTECHNICAL SEISMIC PERFORMANCE EVALUATION

3.1   Analysis methodology and determination of soil springs

The seismic performance of foundations for the two structural options (concrete and timber) were evaluated using an iterative soil structure interaction approach as summarised below:

- The Geotechnical Engineer provided preliminary soil spring stiffnesses ("soil springs") to the Structural Engineer.
- Bearing pressure distributions were obtained by the Structural Engineer using ETABS software and provided to the Geotechnical Engineer.
- The Geotechnical Engineer assessed settlement and stability of the raft by inputting the bearing pressures into the Plaxis 2D soil model. Soil springs were then calculated from the Plaxis model results, updated and provided to the Structural Engineer.
- The Structural Engineer updated the bearing pressures and the process above was repeated until convergence was established.

For this assessment, once the Structural Engineer used the second set of soil springs based on the Plaxis 2D model, the updated bearing pressures were within 5% of the original bearing pressures provided, and therefore convergence was achieved with a single iteration. Static SLS springs of 2000 kPa/m were determined and for the post ULS liquefied case an elastic-perfectly plastic spring was provided with a stiffness of 500 kPa/m and a pressure limit of around 80 kPa. The springs were quite "soft" due to the size of the concrete raft (50 m by 20 m) and the liquefaction issues at the site. The Structural Engineer completed a sensitivity analysis with springs that were half and double of those provided above and established that the pressure distribution and actions within the concrete raft had a low level of sensitivity to the soil spring stiffness.

3.2   Analysis cases

The Plaxis 2D analysis was completed using an elastoplastic constitutive soil model with Mohr Coulomb soil parameters. Three load and soil strength combinations were assessed for different purposes as summarised below:

1. SLS Static loading (working loads) with non-liquefied soil strength and stiffness parameters to understand the likely static settlement and global bearing capacity.
2. Seismic loading with liquefied and cyclic softened soil parameters to understand global bearing capacity (factor of safety (FoS)). Settlement was not assessed in this case as the liquefaction triggering is likely to occur toward the end of the earthquake and the loads provided by the structural engineer are transitory (occur for a short duration).
3. SLS Static loading with liquefied and softened soil parameters to understand settlements following the earthquake (primarily ULS and above).

Static strength and stiffness parameters were developed based on CPT correlations from Lunne, Robertson and Powell (1997). Liquefied soil strengths were determined using Idriss and Boulanger (2008). The CPT shaft friction was used to represent the residual cyclic softened strength at depth. The liquefied and cyclic softened stiffness was taken as 10% of the static (non-liquefied) stiffness.

3.3   Comparison of seismic performance

Figure 3 shows the global FoS for bearing/punching failure and post liquefaction settlement determined from Item 2 and 3 above using Plaxis 2D.
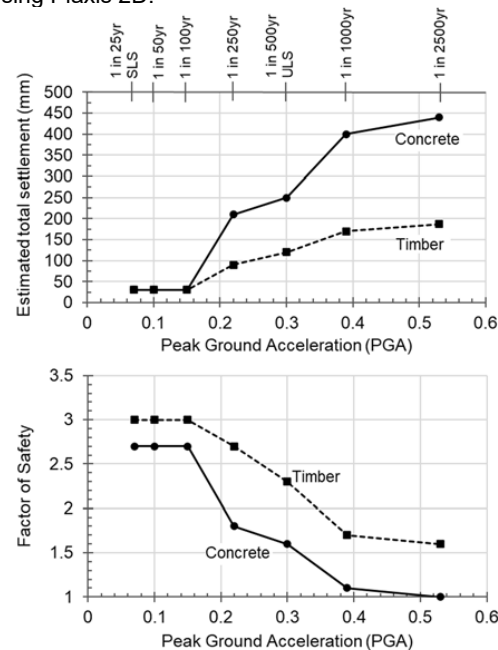
Figure 3:   Estimated foundation settlement and global bearing/punching FoS at different levels of Peak Ground Acceleration (PGA) and earthquake return period. PGA is a measure of shaking intensity.

The concrete structure option shows a significant increase in total settlement, with a sharp step change at PGA of 0.15g to 0.22g (100 year to 250 year return period). This settlement continues to rise steeply at larger levels of shaking. The reduction in FoS also shows a similar sharp reduction at 0.15g, with it approaching 1 at 0.39g (1,000 year return period). Given the uncertainties relating to liquefaction and seismic shaking, the FoS near 1 means that the estimated displacement would have a high level of uncertainty. These observations show that a concrete structure with a concrete raft foundation is likely to provide poor seismic performance. The seismic performance for the concrete structure could only be improved through ground improvement or piling which would provide a stiffer response (reduced settlement) and improve the factor of safety.

The timber structure option shows a more gradual increase in total settlement and a gradual reduction in FoS with increasing PGA (shaking intensity). This indicated significantly improved performance compared to the concrete option. Ground improvement would also have provided further improvement to performance but was considered unnecessary for the timber option based on discussions between the Structural and Geotechnical Engineer. Therefore, from a seismic performance perspective the timber structure was preferred and avoided the need for ground improvement or screw piling, which would add cost, carbon emissions, time, and disruption to the project.

4   BUILDING SUSTAINABILITY COMPARISON

An embodied carbon assessment was completed by Calibre Group using the concept structural and geotechnical design information. The purpose of the assessment was to compare the structural options and identify embodied carbon "hotspots" and opportunities for reduction. Three options were assessed. However, for simplicity, only the comparison of concrete and timber are shown here.

14th Australia & New Zealand Young Geotechnical Professionals Conference, Rotorua
2/11/2022

PROCEEDINGS OF THE 14TH ANZ YOUNG GEOTECHNICAL PROFESSIONALS CONFERENCE
14YGPC ROTORUA, NEW ZEALAND, 2ND – 5TH NOVEMBER 2022   **203**

The assessment was completed in general accordance with the MBIE document 'Whole-of life Embodied Carbon Assessment: Technical Methodology' (February 2022) using typical New Zealand-specific carbon factors for the different materials based on data published by BRANZ and specific environmental product declarations (EPDs). The carbon factors are simply multiplied by the material quantity used. Transportation carbon emissions are built into the carbon factors for each material and based on the distance from 'factory' to site. For this concept design, when this isn't known accurately, it was based on three categories of transport distance: local source (same city/town), national source, international source. The scope of this analysis covered the lifecycle stages from procurement (raw material and manufacturing) to end of construction, or modules A1-A5 in the terminology of lifecycle analysis (LCA). This is often referred to as 'up-front embodied carbon'.

Figure 4 below shows the comparison of the two options based on tonnes of embodied carbon (tCO$_2$e) to supply and build the structure and foundations, which can typically represent up to 60% of a building's embodied carbon. On the right side of Figure 4 the emissions are also normalised to gross internal floor area (GIA, kgCO$_2$e/m^2) using a GIA of 4,200 m^2 for comparison with other similar buildings. The concrete structure option shows the concrete raft contributes approximately 50% of the total embodied carbon. The concrete raft foundation was required to be larger (900 mm thick) due to the higher loads applied to the foundation (heavier structure). The timber structure option shows 40% less embodied carbon compared to concrete. A significant portion of this is from the reduction in concrete raft thickness to 400 mm, and the modification of building frame to timber from concrete.
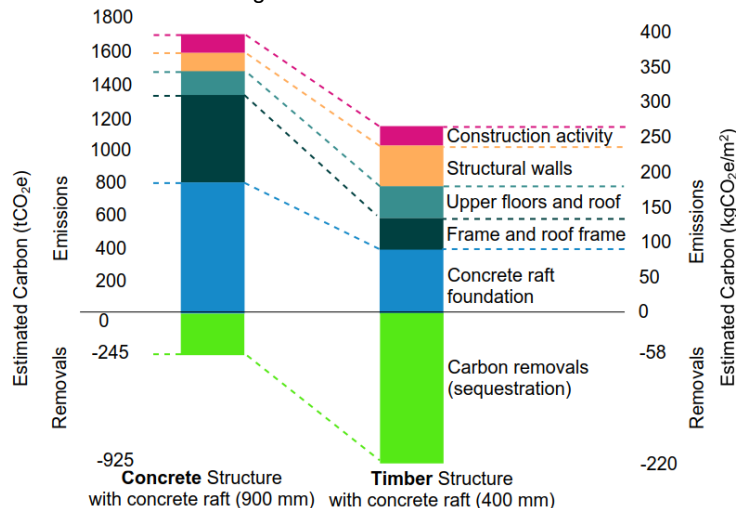
Figure 4: *Estimated embodied carbon in the structure and foundations of a four-storey building (GIA=4,200 m^2) in tCO$_2$e and kgCO$_2$e/m^2, Modules A1-A5, Raw material to end of construction (Courtesy of Calibre, graph reproduced for visual purposes)*

The timber option was estimated to contribute approximately 270 kgCO$_2$e/m^2 up to end of construction, whereas concrete was approximately 405 kgCO$_2$e/m^2. A proposed UK structural carbon benchmarking scheme (SCORS, Arnold et al. 2020) has benchmarks from A++ to G in terms of embodied carbon. This scheme would rate the concrete option as a G (high carbon intensity) and the timber option would be rated as a D (moderate carbon intensity). An A++ rating is proposed as less than 100 kgCO$_2$e/m^2. LETI (2021) has an equivalent 2020 and 2030 target of around 500 kgCO$_2$e/m^2 and 300 kgCO$_2$e/m^2 respectively, although these figures are for all building elements, not just the structure. A widely accepted carbon benchmarking scheme is yet to be established for buildings in New Zealand.

Although not included in these numbers, the timber option also has the added benefit that atmospheric carbon has been stored in the timber during the life of the tree (removals). The benefit of these removals is represented below the axis of the graph in Figure 4. The carbon emissions and removals are listed separately as there is not common agreement within the industry regarding how atmospheric carbon stored in natural materials (biogenic carbon) should be assessed in lifecycle analysis. This method allows a true comparison to be made between options, whilst still acknowledging the potential added benefit of the stored carbon in the timber.

5   CONCLUSION AND OVERALL OPTIONS EVALUATION

In conclusion, interaction between Structural and Geotechnical Engineers is critical at concept development phase to determine the most suitable building material type, foundation concept and understand the advantages and disadvantages associated with different options. This allows a more efficient building solution that is well suited to the site conditions.

For this case, Table 1 below summarises the two key considerations for the decision between a concrete and timber structure along with other considerations for this project. The main benefits were the improvement in foundation design, improvement in seismic performance, avoidance of ground improvement and reduction in embodied carbon. The builder owner also identified a programme saving with timber (approximately 1 to 2 months). These factors contributed to the building owner's selection of the timber structure option for future buildings across the site. The timber structure was therefore taken forward for development at detailed design.

Table 1:   Overall options evaluation

	Concrete structure with 900 mm thick concrete raft foundation	Timber structure with 400 mm thick concrete raft foundation
Foundation seismic performance	Poor – Large settlements and low FoS. Additional ground improvement or piling required to improve performance.	Significantly improved – Low settlements and high FoS. Ground improvement not required.
Carbon emissions	High ~ 405 kgCO$_2$/m^2	Low ~ 270 kgCO$_2$/m^2
Other considerations for this project	Larger impact on site and neighbours during construction. High durability. Low maintenance. Effective sound proofing. Higher thermal mass.	Faster construction (reduced programme). Less impact on site and neighbours during construction (less noise, dust). Sound proofing needs to be considered (i.e. between floors/walls). Typically more offsite manufactured components which reduces site impact.

6   ACKNOWLEDGEMENTS

REFERENCES

Arnold A., Cook M., Cox D., Gibbons O., Orr J. (October 2020). The Structural Engineer Article, Institute of Structural Engineers.

Boulanger R.W. and Idriss, I.M. (2007). 'Evaluation of Cyclic Softening in Silts and Clays,' Journal of Geotechnical and Geoenvironmental Engineering, 133 (6), 641–652pp.

Boulanger R.W. and Idriss, I.M. (2014). 'CPT and SPT Based Liquefaction Triggering Procedures,' Report No. UCD/CMG–14/01, Dept. of Civil & Environmental Engineering, University of California at Davis.

Idriss, I. M. Boulanger, R. W. 2008. Soil Liquefaction during Earthquakes, Monograph MNO-12, Earthquake Engineering Research Institute, Oakland, CA, 261 pp.

London Energy Transformation Initiative (2021) LETI Embodied Carbon Target Alignment, available at https://www.leti.london/carbonalignment

Lunne, Robertson and Powell (1997). Cone Penetration Testing in Geotechnical Practice, Soil Mechanics and Foundation Engineering 46(6) DOI:10.1007/s11204-010-9072-x

14th Australia & New Zealand Young Geotechnical Professionals Conference, Rotorua
2/11/2022

PROCEEDINGS OF THE 14TH ANZ YOUNG GEOTECHNICAL PROFESSIONALS CONFERENCE
14YGPC ROTORUA, NEW ZEALAND, 2ND – 5TH NOVEMBER 2022   **205**

Successful Remediation of Dual Pipeline Stress Within a Complex Landslide

C. Watson[1], D. Poh[2] and R. Satrasala[3]

[1]Engineering Geologist, Pattle Delamore Partners Ltd., Level 5, PDP House, 235 Broadway, Newmarket, Auckland; PH (+64) 27-376-4063; email: cam.watson@pdp.co.nz
[2]Geotechnical Engineer – Service Leader, Pattle Delamore Partners Ltd., Level 5, PDP House, 235 Broadway, Newmarket, Auckland; PH (+64) 27-376-4063; email: david.poh@pdp.co.nz
[3]Senior Project Manager, Firstgas, 42 Connett Road, New Plymouth, Taranaki, 4312; PH (+64) 27 958 4759; email: ramesh.satrasala@firstgas.co.nz

ABSTRACT

Intelligent "pipeline pigging" detected deflection of a 200mm high pressure gas pipeline and a 250mm petroleum products pipeline buried in the same trench, where they cross a complex landslide for a length of approximately 40m. The landslide, located in West Auckland, New Zealand, comprises two lobes and is situated within a larger relic landslide underlain by East Coast Bays Formation. Surface and subsurface geotechnical investigations, monitoring and related assessment were used to define the landslide model. Slope stability analysis and remediation optioneering had to consider the urgency of landslide stabilisation, pipelines and personnel safety during pipelines exposure (Pipeline Stress Release Trench), and stability of a nearby dwelling. Stability and health and safety risk concerns were identified for a temporary unsupported Pipeline Stress Release Trench, which required exposure of the landslide failure plane across essentially the full width of the landslide. Remedial works included installation of subsurface drainage (Stage 1) followed nine months later by exposure of the pipelines for stress relief and inspection works (Stage 2). Subsurface drainage comprised 164m of French drains, typically 2.5m deep. Inter-stage monitoring, including groundwater levels, surface changes and drain flows confirmed satisfactory drainage performance prior to Stage 2 works. Excavation and subsequent backfilling of the 3m wide by 48m long Pipeline Stress Release Trench was completed safely via a staged approach using trench shields.

Keywords: pipeline, landslide remediation, subsurface drainage, stress/strain release

1   INTRODUCTION AND BACKGOUND

The Perris Road landslide ("the site", "the landslide") is located in Henderson Valley, West Auckland, New Zealand (Figure 1B). The landslide comprises two lobes and is situated within a larger relic landslide ("relic landslide") underlain by East Coast Bays Formation (Figure 1A). Two transmission lines – a 200mm high pressure gas pipeline, and a 250mm petroleum products pipeline ("the pipelines") – are buried 2.5 – 3.1m deep in the same trench and cross the landslide for a length of approximately 40m. The high pressure gas pipeline is owned by Firstgas and supplies gas to Northland, and the Marsden Point to Auckland Pipeline (MPAP), owned by Channel Infrastructure NZ, is a 170km long pipeline which carries diesel, petrol and jet fuel in controlled batches to the Wiri fuel terminal in South Auckland.

Results from 2017/18 intelligent pigging surveys identified the landslide/strain features which were deemed to be a potential risk to the integrity of the pipelines. Intelligent pigging is an advanced robotic technique that propels a purpose-built pipeline integrity gauge (PIG) unit fitted with a variety of probes and sensors through a pipeline to detect and measure corrosion, metal loss, cracks, dents, deformations etc.

Following the identification of these features, Pattle Delamore Partners Ltd (PDP) were engaged to investigate and provide remedial options for the landslide. Investigative and remedial works were carried out over four phases, beginning with Detailed Site Investigations (DSI - Phase 1) and finishing with Remedial Works Construction and Site Reinstatement (Phase 4).

This paper presents an overview of the phases involved to successfully remediate the dual pipeline stress within the landslide through close collaboration with Firstgas, Channel Infrastructure NZ, Whitaker Civil and local landowners.
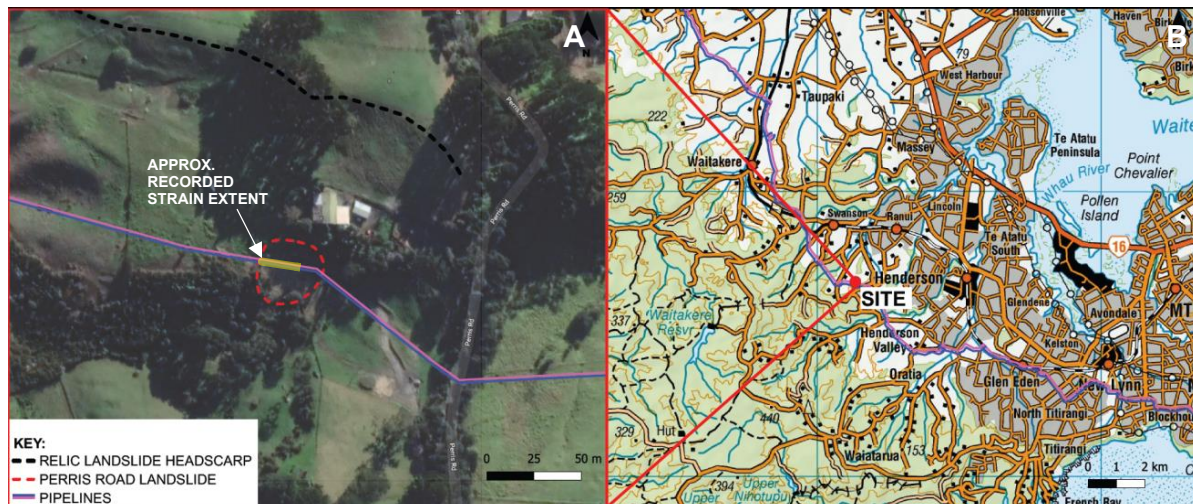
206

PROCEEDINGS OF THE 14TH ANZ YOUNG GEOTECHNICAL PROFESSIONALS CONFERENCE
14YGPC ROTORUA, NEW ZEALAND, 2ND – 5TH NOVEMBER 2022

Figure 1: (A) Overview plan of the site and landslide features; (B) Site Location

2 PHASE 1 – DETAILED SITE INVESTIGATION (DSI)

2.1 Geology

The published geology (Hayward, 1983) indicates that the site is underlain by East Coast Bays Formation (ECBF, typically sands and muds with some volcanic content and grits) of the Waitemata Group. The closest structural information indicates bedding orientations have an approximately north-south strike with shallow (6° – 10°) dips to the west-southwest. Weathered Waitemata Group is susceptible to shallow flows, slumps, or creep, particularly when saturated and on slopes steeper than 20° (Hayward, 1983).

2.2 Field Investigations

DSI field investigations were carried out in June 2019 and comprised engineering geological walkover mapping, drilling of 10 hand augerholes up to 5.0m depth (with hand held shear vane tests in cohesive material), GPS topographic survey, abney lines for engineering geological cross-section development, depth and alignment survey of the pipelines, installation of three crack monitoring lines, and installation of three hand auger piezometers/rudimentary inclinometers with level loggers to monitor groundwater levels and ground movements.

The geology encountered during the DSI was generally consistent with the published geology and consisted of landslide debris underlain by relic, blocky landslide debris most likely derived from ECBF soils described in the published geology. The recorded strain was located within the inferred mapped landslide boundaries (Figure 1). No evidence of recent instability was identified during mapping of the relic landslide (Figure 1).

2.3 Conceptual Landslide Model

An inferred conceptual landslide model for the site instability was developed based on the DSI investigations. The landslide was inferred to compose of two landslide lobes: (1) the North Landslide Lobe (NLL); and (2) the South Landslide Lobe (SLL; Figures 2 and 3). The basal landslide failure plane was inferred to have a maximum depth of 4.2m below ground level (bgl) and be within landslide debris associated with the relic landslide features present on the upper slopes (Figure 1). The landslide failure direction was inferred to be approximately south (~194°), perpendicular to the pipelines.

The failure sequence and triggering mechanisms for the landslide was inferred to be movement of the SLL first, followed by movement of the NLL either: (1) very soon afterwards (essentially a single movement event for both lobes); or (2) at a later date (separate movement events). Movement of the SLL would have partially removed toe support for the upslope NLL allowing it to retrogressively fail. Site information indicated the SLL had moved since it was first triggered with fresh tension cracks and sharp scarps in the SLL indicating that the lobe had subsequently moved, likely within the past 5 years. In contrast, the instability features associated with the NLL indicated somewhat older movement. Initial and subsequent landslide movement was inferred to have been triggered principally by elevated groundwater levels due to a combination of heavy/prolonged rainfall events.

PROCEEDINGS OF THE 14TH ANZ YOUNG GEOTECHNICAL PROFESSIONALS CONFERENCE
14YGPC ROTORUA, NEW ZEALAND, 2ND – 5TH NOVEMBER 2022

207

Figure 2: (A) Photo facing east across the landslide showing the inferred downslope deflection from assumed as-built alignment of the gas pipeline. (B) Simplified engineering geology sketch plan. Section A-A' shown on Figure 3.

2.4   Pipeline Risk

The pipelines are located within the inferred boundaries of the landslide for an approximate length of 40m (Figure 2). The inferred lateral margins of the landslide extended beyond the suspected deflection area. A suspected horizontal deflection of approximately 900mm from the assumed as-built alignment over a pipeline length of approximately 26m was inferred based on field observations (Figure 2). Based on the inferred landslide movement direction, some vertical deflection of the pipelines was also interpreted to be likely within the landslide. This is consistent with there being a vertical component of pigging strain at the site.

It was inferred that further movement of the landslide – i.e. movement of the SLL followed by re-activation of the NLL, or movement of both lobes in a single event – was possible following heavy and/or prolonged rainfall events. Potential implications for the pipelines of further movement were increased deflection and related additional strain/stress, potentially affecting the integrity of the pipelines.

3   PHASE 2 – CONCEPT DESIGN

Based on the results of the DSI, initial Conceptual Design (CD) options to stabilise the landslide and to reduce the likelihood of further land movement impacting the pipelines included: (1) Infill open tension cracks and continue to monitor the area with special site surveillance; (2) Head unload the NLL and SLL; and (3) Installation of subsurface drainage in the landslide area.

Option 1 was completed during a subsequent landslide monitoring round. The key reason for not adopting head unloading of the NLL and SLL (Option 2) was the inferred instability risk upslope of the NLL where a residential dwelling is located (Figure 1). Therefore, installation of subsurface drainage (Option 3) was the preferred remedial option to progress to Detailed Design (DD).

A pipeline strain/stress analysis, which was performed by Firstgas in parallel with the CD process, indicated the need to relieve the strain/stress in the affected section of the pipelines. This involved a Pipeline Stress Release Trench (PSRT), comprising a staged excavation to expose the pipelines to allow rebound of the deflected section of the pipelines.
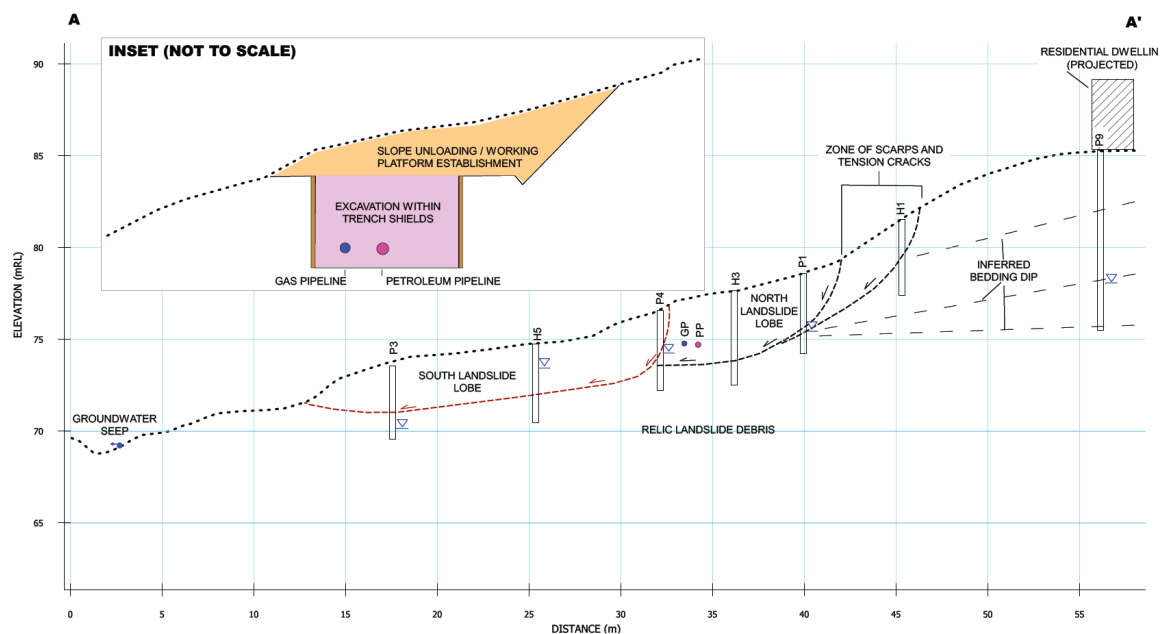
Figure 3: Engineering geological cross-section. Refer Figure 2B for section location. Inset: Simplified schematic of PSRT excavation methodology.

4   PHASE 3 – DETAILED DESIGN
4.1   Detailed Design Geotechnical Investigation
A detailed design geotechnical investigation (DDGI) was carried out to refine and update the geological ground model for DD analysis and modelling associated with the Pipeline Stress Release Trench (PSRT). The DDGI focussed mostly on the area upslope of the pipelines to provide additional ground information inputs for the stability assessment related to the PSRT excavation as well as consideration of the upslope residential dwelling. The DDGI included detailed engineering geological mapping, 13 hand augerholes to a maximum depth of 6.1m bgl (including installation of five 32mm hand auger piezometers/rudimentary inclinometers), two PQ (83mm diameter) machine drilled boreholes to a maximum depth of 10.2m bgl with piezometer installations, photogrammetry, and collection of Light Detection and Ranging (LiDAR) data to provide a detailed topographical model of the site.

Key findings from the DDGI included identification of additional NLL instability upslope of the pipelines and inferred downslope dipping bedding in the ECBF in the area upslope the landslide. Figure 3 shows an engineering geological cross-section of the updated conceptual landslide model following the DDGI works.

4.2   Slope Stability
Slope stability analysis using SLOPE/W (GeoStudio 2020) was carried out to analyse the current Factor of Safety (FoS – back analysis) of the landslide and to determine the FoS with the provision of the subsurface drainage system for groundwater control. Slope stability analyses were carried out for the long term/permanent condition i.e., on completion of the subsurface drainage system under both static and seismic conditions. The results indicated that: (1) the stability of the landslide is dependent on the groundwater levels and instability can be triggered by an increase in groundwater levels across the landslide; and (2) an acceptable FoS was met under normal (static) conditions and seismic SLS and ULS scenarios.

Based on the ongoing groundwater monitoring it was noted that the groundwater levels were highly sensitive to rainfall events and surface water recharge. Therefore, it was determined that the subsurface drainage network was required to be in place to control the groundwater levels for stability prior to the PSRT excavation.

A stability assessment for the PSRT excavation, based on a typical open cut slope excavation with subsurface drainage installed (i.e., modelled groundwater levels), yielded unsatisfactory results for temporary conditions. Subsequent discussions with Firstgas and Channel Infrastructure around safety of personnel and the pipelines, and the potential impact to the residential dwelling upslope of the work area, concluded that an open cut slope excavation approach for the PSRT was deemed high risk and therefore unacceptable. Therefore, an alternative staged excavation approach using trench shields was

introduced and the stability of the method assessed. The stability assessment achieved an acceptable FoS for the temporary conditions (i.e., during the PSRT excavation).

4.3   Subsurface Drainage

As described above, the required groundwater drawdown for the subsurface drainage system was established through a series of slope stability modelling with different groundwater levels to achieve the required FoS. Subsurface drainage coverage and layout was modelled using FEEFLOW, a computer program for simulating groundwater flow using parameters determined from the DSI and DDGI. Several configurations of the drainage layout were analysed to determine the effectiveness of the drainage systems. The modelling of the finalised layout confirmed that the subsurface drainage network would provide sufficient coverage across the landslide area for adequate groundwater drawdown.

4.4   Safety in Design and Risk Assessment

As part of the detailed design process, Firstgas/Channel Infrastructure, PDP, and Whitaker carried out a joint safety in design review process, including review of the design and the risk and hazard assessment for safe construction of the remediation works around the pipelines. For this project, the excavation was across the full width of the landslide and in places, to below the interpreted failure plane (i.e. >3m deep). The potential risks to personnel working in the trench and the integrity of the pipelines (supplying gas and petroleum products to Northland and Auckland, respectively) were of paramount importance when undertaking the safety in design review and risk assessment.

5   PHASE 4 – REMEDIAL WORKS CONSTRUCTION

The preferred remedial option (landslide drainage and PSRT) was divided into two work stages: Stage 1: Installation of landslide subsurface drainage, including a pipeline trench cut off drain east of the landslide; and Stage 2: PSRT – Excavation and exposure of the pipelines to relieve land movement related stress/strain, pipeline integrity checking, coating repair works, backfilling and reinstatement. Figure 4A shows the layout of the subsurface drainage network and the extent of the PSRT.

5.1   Stage 1: Subsurface Drainage

Subsurface drainage construction works were completed from April–May 2021 and comprised installation of 164m of 1.5–3m deep subsurface French drains, a pipeline trench cut-off drain east of the landslide, 25m of buried carrier pipes carrying the drainage discharge to three culvert drainage outlets, 13 buried drainage inlet risers at the head of subsurface drain stems, and two drain flow monitoring points. Subsurface drain pipeline crossings were installed during Stage 2 following excavation of the pipeline stress relief trench (PSRT).
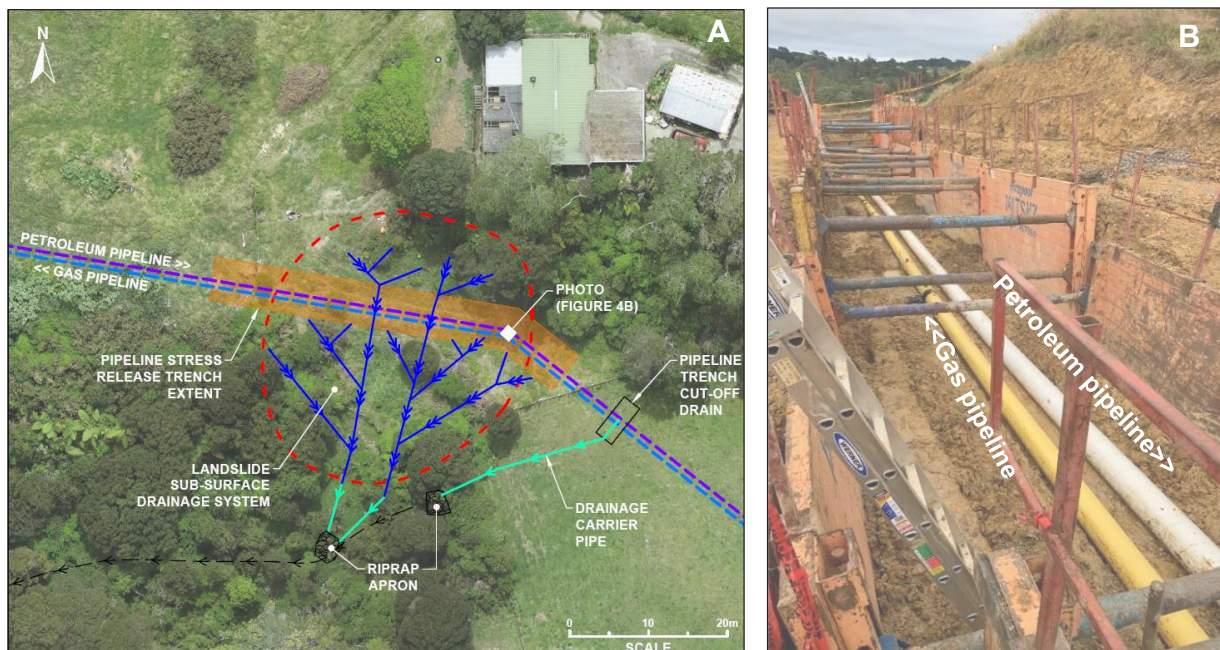

Figure 4: (A) Remedial works overview plan. (B) PSRT during Phase 4 (Stage 2) works. Photo facing west.

Monitoring of groundwater levels at 8 locations within the drainage network area of influence and drain flow measurements in the period between Stage 1 and Stage 2 works indicated effective performance. of the drainage network. Stage 2 construction works were carried out over January-March 2022. A summary of the works is provided below.

5.2   Stage 2: Pipeline Exposure and Reinstatement

The pipelines were potholed to complete a pre-excavation baseline survey. Approximately 1-2m of soil was removed from the slope in the PSRT area to form a level working platform and provide a slope unloading function (Figure 3 inset). Pipeline cover was removed to within 0.5m of the crown of the pipelines using an excavator and trench shields. The remaining 0.5m of soil overlying the pipelines was removed via hand excavation to expose the pipelines (Figure 4B). During pipeline exposure and destressing works, the pipelines moved back towards the approximate original straight-line pipeline alignment. Pipeline defects were repaired and permanent crossings underneath the pipelines were retrofitted to complete the subsurface drainage network. Trench shields were then removed, the PSRT was backfilled, and the site was reinstated.

Following the completion of the PSRT works, rock riprap aprons were placed at the base of the drainage outlets. Piezometers and groundwater monitoring equipment that was damaged or removed during the remedial works was reinstalled. In addition, a post works monitoring site visit was carried out by PDP in May 2022 to provide the landslide monitoring network baseline measurements. A monitoring plan was developed for the site going forward with the plan including rainfall trigger thresholds for monitoring site visits.

6   CONCLUSION

This project demonstrates a comprehensive phased approach for remediating pipeline stress/strain caused by landslide movement. A network of subsurface drainage installed 10 months prior to pipeline stress relief prevented the landslide from moving between the two remediation stages.

Strain assessment showed the need to relieve pipeline stress using an open excavation across the landslide. Multiple landslide lobes and potential upslope instability that could have affected a residential dwelling, together with trench safety requirements, required an alternative design for the open excavation. This design comprised trench shields for support and safe excavation of the pipelines.

Important takeaways from the project are:

- It is essential to investigate and understand site ground conditions and the landslide mechanism and its impact on key infrastructure. It is fundamental to "get the geology right" and establish a representative ground model for slope stability analysis and design of the remedial works.
- Effective and clear communication between the consultant, clients, landowners, and the contractor is essential for ensuring that the project runs smoothly. In this case, clear intention and communication between PDP, Firstgas/Channel Infrastructure and landowners were imperative in the early investigative stages of the work. In addition, close collaboration during the construction phase ensured key technical and construction issues were resolved quickly to allow smooth progress of the construction.
- The use of French drains (with associated carrier pipes and drainage outlets) is a practical and successful method for stabilising shallow landslides.
- The joint safety in design review process ensured a robust review of the design and the risk and hazard assessment for the safe construction of the remediation works around a critical lifeline infrastructure.

The remedial works effectively restored the integrity and longevity of both pipelines. This, together with the post works monitoring and maintenance plan, will prolong their operational life.

7   ACKNOWLEDGEMENTS

REFERENCES
Hayward, B.W. (1983): Sheet Q11, Waitakere. Geological Map of New Zealand 1:50,000. Map with notes, Wellington, NZ, DSIR.

PROCEEDINGS OF THE 14TH ANZ YOUNG GEOTECHNICAL PROFESSIONALS CONFERENCE
14YGPC ROTORUA, NEW ZEALAND, 2ND – 5TH NOVEMBER 2022

211

Pahoia Tephra Sequence: strength, sensitivity, and stabilisation

T.P. Robertson[1] and V.G. Moon[2]

[1]School of Science, Division of Health, Engineering, Computing and Sciences, University of Waikato, Private Bag 3105, Hamilton, 3240, New Zealand; PH +6478384026; email; thomasro@waikato.ac.nz

[2]School of Science, Division of Health, Engineering, Computing and Sciences, University of Waikato, Private Bag 3105, Hamilton, 3240, New Zealand; PH +6478384625; email; vgmoon@wakato.ac.nz

Abstract

Large, retrogressive landslides with long runouts have been attributed to the sensitive nature of quick-clay soils. In the Northern hemisphere remediation attempts have been made with chloride salt solutions. The use of potassium chloride salt has been shown to significantly reduce sensitivity *in situ* and to strengthen quick clays dominated by illite to a point where they can be regarded as stable. In Bay of Plenty, New Zealand, the Pahoia Tephra Sequence (PTS) has been identified as a sensitive soil layer, dominated by the 1:1 clay halloysite. This paper examines previously published data, together with fresh samples from the base of a recent large landslide using consolidated undrained triaxial strength testing. Initial results indicate a highly sensitive, weak layer at the base of the PTS, near the interface with the underlying Kidnappers Ignimbrite. The possibility of *in situ* stabilisation was investigated at a laboratory scale through submersion of samples in 2 molL-1 potassium acetate solution. Submersion resulted in increased shear strength and an overall reduction in sensitivity. These results are attributed to interaction between the potassium ions with the dominant halloysite clays, suggesting that there may be a method to universally increase shear strength in the sensitive soil *in situ*.

Keywords: landslide, sensitive, volcanic, slope-modelling, soil-treatment, halloysite.

1. Introduction

Large, retrogressive landslides with long runouts sourced from quick clays are a worldwide phenomenon. These events cause significant damage to infrastructure, and in some cases loss of life, and many have been directly attributed to the presence of sensitive soils (Moum *et al.*, 1968; Tavenas *et al.*, 1971). In the Northern Hemisphere it has been found that some sensitive clay soils derive from uplifted glacial outwash deposits. The leaching of sodium from glacial outwash by meteoric water causes a re-alignment of a 'house of cards' structure between the clay minerals, resulting in a drastic loss of the soil's strength upon remoulding (Locat *et al.*, 2011; Skempton & Northey, 1952).

Due to the unpredictable and highly destructive nature of quick clay slides, attempts to remediate their sensitivity have been undertaken, particularly in Norway, and to a limited extent in Italy (De Rosa *et al.*, 2016). Amelioration attempts of failures in Norway date back to the 1950's, with sodium chloride salt mixed into runout deposit debris of a large failure to strengthen and stabilise the soil (Eide & Bjerrum, 1955; Torrance, 2014). Subsequent testing in the 1960's and further re-investigation in more recent years has shown success in the use of potassium chloride salt wells to reduce sensitivity *in situ* and to strengthen illite-dominated quick-clays (Helle *et al.*, 2017; Helle *et al.*, 2015; Moum *et al.*, 1968).

New Zealand sensitive soils are generally derived from volcanic deposits in the form of ignimbrites, volcanic tuffs, and weathered or reworked tephras (Torrance, 1983). Tephra deposits with pyroclastic materials of any grain size are highly susceptible to failure, and in several cases have been responsible for catastrophic landslides (Chigira, 2014; Sidle & Ochiai, 2006). Landslides with long runouts are well documented in the North Island's Bay of Plenty region (BOP), with the Pahoia Tephra Sequence (PTS), being a significant contributor (Moon, 2016; Moon *et al.*, 2015). BOP soil sensitivity is thought to derive from the presence of large quantities of spheroidal 1:1 halloysite clay minerals (Smalley *et al.*, 1980). The minerals exhibit short range electrostatic van der Waals interactions, which upon failure and reworking cause a detachment on the clay surfaces. Edge-face charge imbalances result in an overall repulsive behaviour by the clay and leads to the large flow like nature of these deposits (Kluger *et al.*, 2017).

Halloysite, unlike illite does not preferentially strengthen with the addition of either potassium or sodium chloride salts. However, numerous studies have shown that there are distinctive changes made to the halloysite structure following the introduction of potassium acetate (K-acetate) (Garrett & Walker, 1959; Theng & Wells, 1995). These studies report that K-acetate enters the halloysite crystal lattice to form a stronger intercalate and expands the clay layers.

This paper first examines previously published data on the PTS (Wesley 2007, Mills 2016) through comparison of effective cohesion and friction angles of the soil at different BOP sites. Original results for a newly sampled layer found near to the base of the Pahoia Tephra unit, close to the interface with the Kidnappers Ignimbrite at the Kowhai Grove landslide, Ōmokoroa, are then presented. Samples were tested under consolidated undrained (CU) triaxial conditions. Finally, these data were compared with samples immersed for 1 month in a 2 MolL^{-1} potassium acetate solution in order to observe potential strength changes of the soil over time.

2. Materials and Methods
2.1 Materials – Geological Setting

The Tauranga basin, located within the BOP, is covered with a series of thick tephra and ignimbrite layers deposited within the last 3 Ma (Briggs *et al.*, 1996). Throughout the basin there are many north-northeast tending peninsulas that extend into the Tauranga harbour. These peninsulas range from 20-40 m in elevation, exhibit steep coastal slopes or cliffs, and are known to be prone to landslides. The stratigraphy is comprised of Matua Subgroup deposits (c. 2 Ma – 0.35 Ma) which consist of primary and reworked pyroclastic deposits, most notably the Pahoia Tephra Sequence (PTS c. 2.18 - 0.35 Ma), intercalated with non-welded ignimbrites (Kidnappers and Te Ranga Ignimbrites). The Matua Subgroup is usually overlain by younger airfall tephra deposits including the Hamilton Ashes (0.08 – 0.38 Ma), Rotoehu Ash and Post Rotoehu tephras (< 60,0000 years). Unit thicknesses and deposit characteristics, particularly of the Matua Subgroup materials, vary considerably throughout the Tauranga basin.

The PTS is spatially variable both horizontally and laterally, with materials within split informally into two main units (Kluger et al., 2017). The upper portion is generally made up of silty sand and sand beds (Briggs *et al.*, 1996; Oliver, 1997), while the lower unit is made up of thick halloysite-rich clay, silt, and silty clay beds. These clay-rich beds are a key contributor to instability; they generally exhibit large void ratios, very low permeability, and varying sensitivity with depth, with sensitivity ranging from 10-140 (Gulliver & Houghton, 1980; Mills & Moon, 2016).

2.2 Methods

Soil samples were collected from the Kowhai Grove landslide scarp, Ōmokoroa (see Figure 1). Determination of the layer with highest sensitivity was achieved by shear vane testing of each distinctive soil change with depth in a pit dug approximately 4 m in front of the scarp face. A highly sensitive (S_t = 28.5) layer was identified around 750 mm below the ground surface. Samples were extracted using 50 x 150 mm stainless steel push tubes as opposed to block sampling due to challenges with sample location and depth.

Water content (NMC) was determined in line with NZ standards NZ4402:1986 Test 2.1, and bulk density (ρ_d) in line with ISO 17892-2(2004). Particle density (ρ_s) was measured via a gas pycnometer using ASTM D5550-14, this was then used to determine both porosity (n) and void ratio via equations (1) (Carey *et al.*, 1996) and (2) (Jamiolkowski *et al.*, 1995).

$$Porosity(n) = \frac{dry\ bulk\ density\ (kgm^{-3})}{particle\ density} \times 100 \tag{1}$$

$$e = \frac{V_v\ (Volume\ voids)}{V\ (volume)} = \frac{n}{1-n} \tag{2}$$

PROCEEDINGS OF THE 14TH ANZ YOUNG GEOTECHNICAL PROFESSIONALS CONFERENCE
14YGPC ROTORUA, NEW ZEALAND, 2ND – 5TH NOVEMBER 2022

213

Treatment of soil was achieved through total immersion of 50 mm x 150 mm soil cores in 2 molL^{-1} K- acetate solution for a period of 1 month. Note that NWC, ρ_d, ρ_s and Atterberg limit values for treated soil have been corrected to account for the presence of salt within the soil. Triaxial tests were conducted in accordance with BS 1377-8. Confining stresses were set at points 20 and 40% lower than calculated *in situ*, pre-failure confining stress, in order to model the threshold failure point of 36% reduction in effective stress determined by (Kluger *et al.*, 2020). Effective cohesion and friction angle values have been compared with values derived by Mills (2016) and Wesley (2007) for PTS samples.

3. Results

3.1 Geomechanical properties

General geomechanical properties of the study samples are displayed in Table 1. Porosity, void ratio, and Atterberg limits for the untreated soil materials were all high which are representative of a clayey-silt with little sand, in keeping with previously published research. NWC for our untreated soil was in excess of the Liquid Limit, in keeping with soils of a sensitive nature both in New Zealand and overseas. Particle densities were higher than previous studies, the cause of which will likely require further examination through XRD testing. Shear vane measurements placed the soil within the realms of 'quick-clay' (57/2 kPa) , though it should be noted that remoulded field shear vane produced strengths higher than the 0.5 kPa required to deem a clay 'quick' in international literature (Torrance, 1983).

Table 1.Geomechanical properties of both treated (2molL^{-1} K-acetate for 1 month) and untreated soil sampled from Kowhai Grove field site. Errors were determined to one sd.

	Untreated	**Treated**
FS (kPa)	57	N/A
RFS (kPa)	2	N/A
S_t	28.5	N/A
NWC, (%)	67.3 ± 1	57 ± 0.4
ρ_d (kg m^{-3})	1576 ± 5	1628 ± 19
porosity (n) (%)	71 ± 0.1	63 ± 0.3
void ratio	2.48	1.75
ρ_s (kg m^{-3})	3282	2847
fines (<63 µm) (%)	98.4	98.6
clay (<2 µm) (%)	39 ± 8	40.2 ± 5
Liquid Limit, LL (%)	58.6 (R^2=0.99)	N/A
Plastic limit, PL (%)	45.9 ± 0.21	N/A
Plasticity index, PI (%)	12.79	N/A
Liquidity index, LI (%)	1.71	N/A
Activity, A	0.28	N/A

FS= Undisturbed field shearvane; RFS= Remolded field shear vane; St=sensitivity (FS/RFS)

3.2 Triaxial Results

Triaxial results including deviator and pore pressure paths, stress paths for untreated and 1 month treated soils are presented in Table 2 and Figure 1. For untreated soil (Fig 1A), as confining stress increased peak deviator stress similarly increased. Pore pressures at all confining stresses exhibited initial peaks prior to peak deviator stress. These were followed by slight declines in pore pressure as samples reached peak deviator stress. Upon entering into the post peak phase, deviator stresses declined noticeably. Pore pressures when entering into the post peak phase, after the slight decrease following peak deviator stress, increased when heading towards the residual, with the sample at 225 kPa confining stress showing an immediate increase in pore pressure following failure.

Table 2. Consolidated undrained triaxial results for untreated and treated samples. Note confining stresses for untreated samples are different from treated due to correction of overburden stresses following testing of untreated samples.

Sample	ECP (kPa)[a]	ε_f (%)[b]	Q_f (kPa)[c]	U_f (kPa)[d]	SS (%)[e]	c' (kPa)	Φ' (⁰)
Un-1	120	10.3	134.88	50.3	19.3		
Un-2	150	4.6	149.02	87.7	31.6		
Un-3	225	3.5	184.96	130.3	36.9	4.2	29.8
Tr-1	120	4.9	171.68	62	21.1		
Tr-2	160	3.3	201.85	86.8	31.5		
Tr-3	200	9.1	223.8	110.7	10	21.5	27.8
Mills & Moon 2016 (Ōmokoroa) (Un)						26	31
Mills & Moon 2016 (Matua) (Un)						17	32
Wesley 2007 (Un)						10	35

ECP= Effective Confining Pressure; εf=axial strain at failure; Qf=deviator stress at failure; Uf=Pore Pressure at failure; SS=strain softening; c'=effective cohesion; Φ' effective friction angle; Un=untreated soil; Tr=treated soil

Treated samples followed similar trends (Fig 1B), with declines in deviator stress and slight increases in pore pressure when heading towards a residual. Pore pressure at peak deviator stress varied with differing confining stresses. At the lowest confining stress treated samples were ~12 kPa higher treated over untreated, middle confining stresses ~1 kPa lower and approximately 20 kPa lower at the highest confining stress. It should be noted though that the middle confining stress was 10kPa higher for treated samples and 25 kPa lower for highest confining stress which has likely impacted the results slightly. Added to this is the much smaller increase in pore pressures following failure at the highest confining stress (32 kPa increase for untreated, 6 kPa increases for treated).
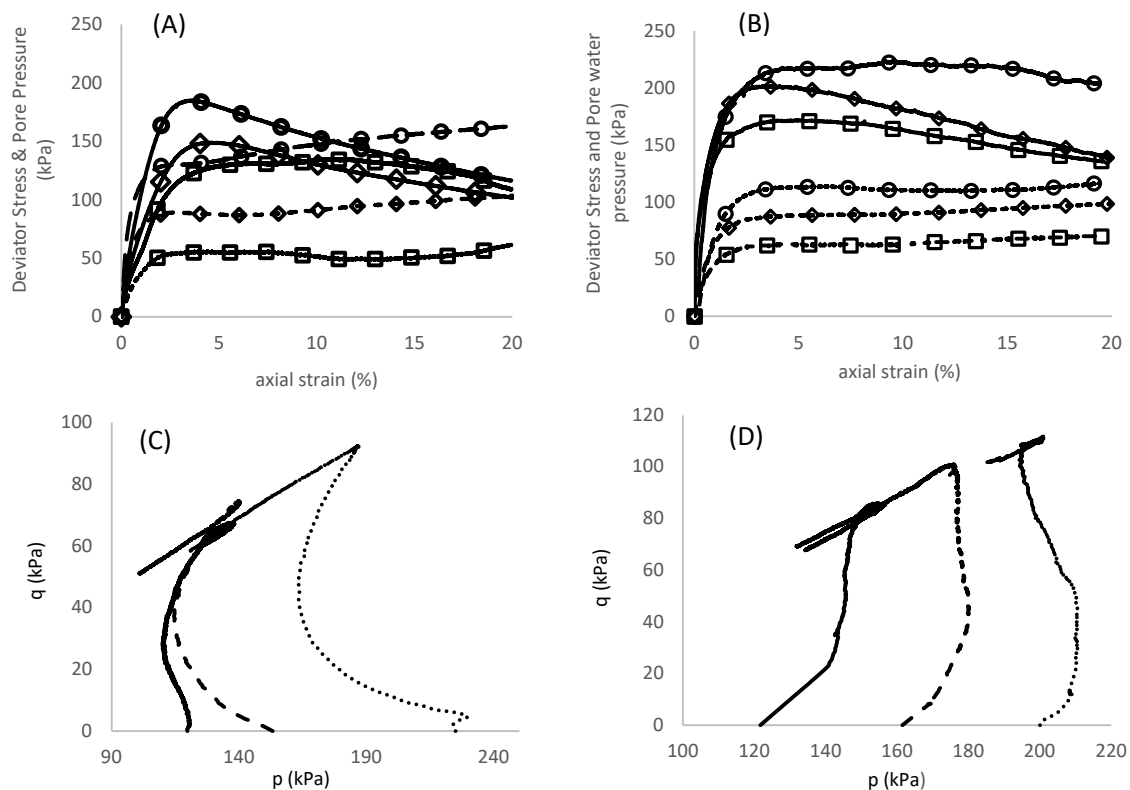
Figure 1: (A) Stress/strain (solid Lines) & Pore water/strain curves (dashed lines) for samples of untreated PTS soil at differing confining pressures. (ECP- 120=Squares, 150=diamond, 225=circle). (B) Stress/strain (solid Lines) & Pore water/strain curves (dashed lines) for samples of treated PTS soil at differing confining pressures. (ECP- 120=Squares, 160=diamond, 200=circle). (C) Stress paths for untreated PTS soil (Solid line=120, dashed line=150, dots=225). (D) Stress paths for untreated PTS soil (Solid line=120, dashed line=160, dots=200).

PROCEEDINGS OF THE 14TH ANZ YOUNG GEOTECHNICAL PROFESSIONALS CONFERENCE
14YGPC ROTORUA, NEW ZEALAND, 2ND – 5TH NOVEMBER 2022

215

One key difference was for the treated sample tested at the highest confining pressure (200 kPa). This sample had a notable reduction in strain softening as a potential result. Stress paths (Figure 1C,D) exhibited noticeable trends, with untreated samples all exhibiting an initial contraction during loading, before strongly dilating prior to reaching the CSL (Critical State Line), though once all samples reached the CSL, following failure, they proceeded to contract in the strain softening phase. Treated samples, by contrast, showed mostly straight stress paths, tending slightly to the right before proceeding left along the CSL upon failure. Untreated soil strength, c' and Φ' (Table 2), was considerably lower than those observed in Mills' 2016 study, and plotted much closer to the results of Wesley (2007). Treatment had a considerable effect on the soil strength, increasing cohesion by 17 kPa.

4. Discussion

It is vital that cohesion and friction angle are determined accurately as they are the two key parameters used in slope stability modelling and assessment. While changes in friction angle can be negligible, changes in cohesion can impact Factor of Safety (FoS) quite significantly. Some recent studies suggest an increase in cohesion of 8 kPa (8 kPa – 16 kPa) can result in increases in FoS by values of up to 0.7 in Quaternary gravels with high proportions of silt and clay, for a 4 m slope at an inclination of 1:1.25 (Harabinová & Panulinová, 2020). In the present study friction angles were somewhat lower (Un = 30° and Tr = 28°) than compared with previous studies (31 - 35°). However, our results found a significant variation in cohesion of our untreated samples (6 kPa) compared with previous studies (26 kPa).

These findings suggest that in slopes and areas where Pahoia Tephras may be present, care needs to be taken when modelling the unit. Current methods of reliance on pre-existing data, as well as regarding the PTS as a single unit may need to be reconsidered. When comparing the limited published data, it becomes clear that the Mohr-Coulomb parameters for PTS vary from site to site. As such, when creating slope stability models in future on sites where the PTS is likely to be present a series of key considerations need to be made. Firstly, if PTS is present, it is advisable to split the PTS, at the very least, into its constituent upper and lower portions to ensure the differences in two soil bodies are noted. Secondly, the values applied to these soil units need to be unique for each site. As c' and Φ' values vary markedly with location, reliance on pre-existing data for sites is likely not appropriate. Steps such as physical testing either *in situ* (i.e., CPT, Geonor vane testing) or within a laboratory setting should be taken. These steps would allow modelling of a much greater accuracy to be created and allow for a much more accurate and representative value of FoS be produced.

Examining the triaxial values it is clear that treatment of the soil with a 2 molL⁻¹ solution of potassium acetate has had a marked impact on both overall soil strength and behaviour. All samples exhibited classic post failure contractive, strain softening responses, in keeping with sensitive material tested both in New Zealand and overseas (Gylland *et al.*, 2014; Mills & Moon, 2016). However, stress paths show a clear deviation in initial loading paths between samples with pre-failure contraction then dilation in untreated soils being replaced with almost vertical paths before reaching the CSL following treatment. For treated soil, at 200 kPa there was a considerable reduction in the degree of contraction following failure of the sample, indicating a potential behaviour change of the soil at higher confining stresses. Pore pressure variations between treated and untreated soils do need to be noted, with treated soil at least at the lowest confining pressure exhibiting a much higher pore pressure at failure compared with untreated, and pore pressures at the higher confining stresses likely only lower due to the difference in confining stress. Overall strength increases are likely due to the favourable intercalation of the potassium acetate ions into the basal spaces within the halloysite, causing an expansion in the clay unit from 10 Å to 13 – 15 Å (Garrett & Walker, 1959). Furthermore, an increase in pH of the soil due to the strong alkaline nature of potassium acetate has likely caused the point zero charge (PZC) on the clay surface to shift to being negatively charged (Mitchell & Soga, 2005; Theng & Wells, 1995). This will result in much stronger van der Waals bonds between the clay spheroids, producing the significant increases in shear strength and effective cohesion we observe.

5. Conclusions

The spatial variability of the Pahoia tephra within the Tauranga basin, as well as its propensity for containing a variety of layers of significant and varying sensitivity makes it a challenge for engineers to model appropriately. With the drastic variation in c' values measured across 5 differing sites in Tauranga consideration needs to be made when creating slope stability models as to the way in which the PTS is treated. This study suggests that it may, in a number of cases, be more appropriate to break the PTS up into at the very least the upper and lower portion due to the vast differences even within the PTS at a single site. With this said, promising progress has been made on a novel method to potentially improve, strengthen and stabilise highly sensitive layers within the PTS through the use of a potassium acetate solution, with drastic changes in both cohesion and behaviour being noted following treatment.

6. References

Briggs, R., Hall, G., Harmsworth, G., Hollis, A., Houghton, B., Hughes, G., . . . Whitbread-Edwards, A. (1996). Geology of the Tauranga area, Sheet U14. *University of Waikato, Department of Earth Sciences Occasional Report, 22*, 57.

Carey, P., McLaren, R., Cameron, K., & Sedcole, J. (1996). Leaching of copper, chromium, and arsenic through some free-draining New Zealand soils. *Soil Research, 34*(4), 583-597.

Chigira, M. (2014). Geological and geomorphological features of deep-seated catastrophic landslides in tectonically active regions of Asia and implications for hazard mapping. *Episodes Journal of International Geoscience, 37*(4), 284-294.

De Rosa, J., Pontolillo, D. M., Di Maio, C., & Vassallo, R. (2016). Chemical clay soil improvement: from laboratory to field test. *Procedia Engineering, 158*, 284-289.

Eide, O., & Bjerrum, L. (1955). The slide at Bekkelaget. *Géotechnique, 5*(1), 88-100.

Garrett, W. G., & Walker, G. F. (1959). The cation-exchange capacity of hydrated halloysite and the formation of halloysite-salt complexes. *Clay Minerals Bulletin, 4*(22), 75-80.

Gulliver, C., & Houghton, B. (1980). *Omokoroa Point land stability investigation*: Tonkin & Taylor.

Gylland, A. S., Jostad, H. P., & Nordal, S. (2014). Experimental study of strain localization in sensitive clays. *Acta Geotechnica, 9*(2), 227-240.

Harabinová, S., & Panulinová, E. (2020). Impact of shear strength parameters on slope stability *MATEC Web of Conferences* (p. 00040): EDP Sciences.

Helle, T. E., Aagaard, P., & Nordal, S. (2017). In situ improvement of highly sensitive clays by potassium chloride migration (American Society of Civil Engineers.

Helle, T. E., Nordal, S., Aagaard, P., & Lied, O. K. (2015). Long-term effect of potassium chloride treatment on improving the soil behavior of highly sensitive clay—Ulvensplitten, Norway. *Canadian Geotechnical Journal, 53*(3), 410-422.

ISO. (2014). *Geotechnical investigation and testing — Laboratory testing of soil — Part 2: Determination of bulk density*. (ISO 17892-2:2014).

Jamiolkowski, M., Lancellotta, R., & Lo Presti, D. (1995). Remarks on the stiffness at small strains of six Italian clays *pre-failure deformation of geomaterials. proceedings of the international symposium, 12-14 September 1994, Sapporo, Japan. 2 vols* (

Kluger, M. O., Jorat, M. E., Moon, V. G., Kreiter, S., de Lange, W. P., Mörz, T., . . . Lowe, D. J. (2020). Rainfall threshold for initiating effective stress decrease and failure in weathered tephra slopes. *Landslides, 17*(2), 267-281.

Kluger, M. O., Moon, V. G., Kreiter, S., Lowe, D. J., Churchman, G. J., Hepp, D. A., . . . Mörz, T. (2017). A new attraction-detachment model for explaining flow sliding in clay-rich tephras. *Geology, 45*(2), 131-134.

Locat, A., Leroueil, S., Bernander, S., Demers, D., Jostad, H. P., & Ouehb, L. (2011). Progressive failures in eastern Canadian and Scandinavian sensitive clays. *Canadian Geotechnical Journal, 48*(11), 1696-1712.

Mills, P., & Moon, V. (2016). Static failure mechanisms in sensitive volcanic soils in the Tauranga Region, New Zealand *11th Australia and New Zealand young geotechnical professionals conference* (

Mitchell, J. K., & Soga, K. (2005). *Fundamentals of soil behavior* (Vol. 3): John Wiley & Sons New York.

Moon, V. (2016). Halloysite behaving badly: geomechanics and slope behaviour of halloysite-rich soils. *Clay minerals, 51*(3), 517-528.

Moon, V. G., Lowe, D. J., Cunningham, M. J., Wyatt, J., Churchman, G., de Lange, W., . . . Jorat, M. E. (2015). Sensitive pyroclastic-derived halloysitic soils in northern New Zealand: interplay of microstructure, minerals, and geomechanics *Volcanic Rocks and Soils. Proceedings of the International Workshop on Volcanic Rocks and Soils, Lacco Ameno, Ischia Island, Italy* (p. 25): Taylor & Francis, London, UK.

Moum, J., Sopp, O., & Loken, T. (1968). Stabilization of undisturbed quick clay by salt wells. *Norwegian Geotechnical Institute Publ*

Oliver, R. C. (1997). A geotechnical characterisation of volcanic soils in relation to coastal landsliding on the Maungatapu Peninsula, Tauranga, New Zealand.

Sidle, R., & Ochiai, H. (2006). Processes, prediction, and land use. *Water resources monograph. American Geophysical Union, Washington, 525*

Skempton, A., & Northey, R. (1952). The sensitivity of clays. *Geotechnique, 3*(1), 30-53.

Smalley, I., Ross, C. W., & Whitton, J. (1980). Clays from New Zealand support the inactive particle theory of soil sensitivity. *Nature, 288*(5791), 576-577.

Standards New Zealand (Te Mana Tautikanga O Aotearoa). (1986). *Test 2.1 Determination of the water content*. (NZS4402.2.1:1986).

Tavenas, F., Chagnon, J.-Y., & Rochelle, P. L. (1971). The Saint-Jean-Vianney landslide: observations and eyewitnesses accounts. *Canadian Geotechnical Journal, 8*(3), 463-478.

Theng, B., & Wells, N. (1995). The flow characteristics of halloysite suspensions. *Clay Minerals, 30*(2), 99-106.

Torrance, J. K. (1983). Towards a general model of quick clay development. *Sedimentology, 30*(4), 547-555.

Torrance, J. K. (2014). Chemistry, sensitivity and quick-clay landslide amelioration *Landslides in Sensitive Clays* (pp. 15-24): Springer.

PROCEEDINGS OF THE 14TH ANZ YOUNG GEOTECHNICAL PROFESSIONALS CONFERENCE
14YGPC ROTORUA, NEW ZEALAND, 2ND – 5TH NOVEMBER 2022

217

CMC RIGID INCLUSIONS AND GROUND IMPROVEMENT CONSIDERATIONS UNDER WIND TURBINE FOUNDATIONS

J. Jong[1] and A. Hubaut[2]

[1]Design Engineer at Menard Oceania, Sydney head office, 13-15 Lyonpark Rd, Macquarie Park NSW 2113; PH (02) 9491 7100; email: jjong@menard.com.au
[2]Design Manager at Menard Oceania, Sydney head office, 13-15 Lyonpark Rd, Macquarie Park NSW 2113; PH (02) 9491 7100; email: ahubaut@menard.com.au

ABSTRACT

Foundation systems for wind turbines are subject to large cyclic bending moments throughout their lifetime. In unfavourable ground conditions, the turbine foundation under these loads may not meet stability and serviceability requirements unless a form of foundation support is used including deep piling, stone columns, rigid inclusions, or other alternative measures which improve bearing capacity and reduce long term settlements. This paper describes the factors to be considered when choosing a foundation support option and presents a case study on the Controlled Modulus Column (CMC) rigid inclusion design supporting most of the turbine pad foundations at the Granville Harbour Wind Farm. The design of the CMC system was analysed using numerical methods which predicted that the bearing capacity, expected settlements and dynamic rotational stiffness would meet the turbine foundation design requirements.

Keywords: Ground Improvement, Wind Turbine, Rigid Inclusions, Controlled Modulus Columns

1   INTRODUCTION

Wind turbines are constructed on a range of foundation types that are chosen according to various factors including: i) if the environment is onshore or offshore, ii) ground conditions which can vary from high strength rock to soft silts, and iii) the water table elevation. Large wind turbines can also reach heights in excess of 120m causing significant bending moments to form at their base and when installed in areas with unfavourable ground conditions foundation support will likely be required. When soft ground conditions are encountered the turbines will likely be constructed on either a piled foundation (deep foundation) or a slab foundation with ground improvement supported by Rigid Inclusions or Stone Columns. This paper will address the design of such supports under onshore foundations.

In the cases where foundation support is required, choosing the most appropriate technique can be difficult due to the performance limitations, construction feasibility and cost constraints involved. This paper addresses the relevant principles and constraints for Stone Column, Rigid Inclusion and Deep Pile foundation solutions with reference to the *Recommendations for the design, calculation, installation and inspection of wind-turbine foundations* developed by the French Committee of Soil Mechanics (CFMS) in 2011. As a following case study, the design of a Controlled Modulus Column (CMC) system for the wind turbine foundations at the Granville Harbour Windfarm is described alongside the relevant strength and serviceability performance improvements.

2   DESIGN REQUIREMENTS FOR ONSHORE WIND TURBINE FOUNDATIONS

For the purpose of design, the lifecycle of a turbine can be broken into a set of critical load cases that represent the most significant conditions that the turbine will experience. These applicable load cases have been defined in the *Recommendations for the design, calculation, installation and inspection of wind-turbine foundations* (CFMS, 2011a). The *International Standard Wind turbines – Part 1: Design Requirements* IEC 61400-1: 2005 requirements are summarised in the CFMS 2011a and state that the following conditions are to be checked:

- Minimum foundation area in compression.
- Bearing capacity.
- Sliding resistance.
- Total and differential settlements.
- Stiffness;
    - Long term rotational stiffness $K_{\varphi LT}$.

- o Dynamic rotational stiffness $K_{\varphi dyn}$.
- o Stiffness requirements in displacement.
- Factor of safety against sliding and overturning.

3 GRAVITY BASES ON SOIL REINFORCEMENT BY STONE COLUMNS

Stone Columns consists of vertical columns made of cohesionless material that is driven into the ground and then compacted. This method of ground reinforcement creates a homogenous material with improved mechanical characteristics that provide greater bearing capacity, stiffness and settlement control underneath the foundation. The horizontal shear strength and internal friction angle is also improved which increases the factor of safety against sliding. Guidelines for the design of stone columns under turbine pad foundations are sourced from the CFMS 2011a and the *Recommendations for the design, calculation, construction and quality control of stone columns under buildings and sensitive structures* (CFMS, 2011b).

According to the CFMS 2011a, the Load Transfer Platform (LTP) is an important requirement below the turbine foundations supported by stone columns as it prevents subsequent construction disturbing the stone columns and ensures homogenous contact between the footing and soil. The CFMS 2011a further states that load transfer (especially shear force) must be obtained by means of a load transfer platform.

The design of Stone Columns under the turbine pad foundations rely on the principles of proportional load distribution between the soil and the Stone Columns via the LTP, as well as the limitation of the mobilised lateral earth pressure surrounding the Stone Columns. As the Stone Column behaviour depends on the soil confinement, the following limitations are noted:
- Lack of soil confinement in soft ground (undrained shear strength $C_u < 20$kPa or CPT resistance, $q_c < 300$ kPa) means it will be difficult to justify a bearing capacity greater than 250kPa at the Serviceability Limit State (SLS) or 350kPa at the Ultimate Limit State (ULS) (CFMS 2011a).
- The static deformation modulus (E) must be limited as Stone Column characteristics rely on the lateral confinement of the surrounding soil (CFMS 2011a).
- It may be necessary to include an extra row of stone columns outside of the peripheral rows under the foundation if the design relies on perfect column confinement (CFMS 2011a).
- Bulging Failure limits q_{re} must not be exceeded (CFMS 2011b).
- General Shear failure limits must not be exceeded (CFMS 2011b, Soyez 1985).
- Punching limits q_{rp} must not be exceeded for floating columns (CFMS 2011b).
- The effects of groundwater infiltration through Stone Columns should be assessed ensuring long term issues don't arise under the foundation i.e. trigger potentially collapsible material.

Due to the general limits of the soil confinement Stone Columns may not be appropriate where the ground conditions are soft or when they may form an unwanted drainage path. The significant benefits typically associated with Stone Columns are the cost advantages as both material and associated plant costs are usually low when compared to other foundation support options and with installation of the columns performed with relatively high productivity rates.

4 GRAVITY BASES ON SOIL REINFORCEMENT BY RIGID INCLUSIONS

Rigid Inclusions typically comprise of mortar or concrete elements that are bored into the ground via soil extraction or with soil displacement with the mortar or concrete cast in-situ. Rigid Inclusions may contain reinforcing steel which is installed into the wet concrete if the above methods are used. Rigid Inclusions may also be driven rather than bored using pre-cast concrete or steel columns. It should be noted that Rigid Inclusions are stated to be the preferred form of soil reinforcement when the static ground deformation modulus is less than 50MPa from the CFMS 2011a.

Rigid Inclusions are noted by the author to support the wind turbine foundations on the Fantanele & Cogealac wind farms which are currently the largest onshore wind farm project in Europe (Wind Europe 2013, Windpower Monthly 2019). These wind farms consist of 139 turbines of 2.5MW, with the turbine structures total height being about 150m above ground. The ground consisted of aeolian loss deposits over stiff clays or sandy silts underlain by rocky schist encountered down to 27m depth. Rigid Inclusions were installed at a grid between 4.5m^2 to 2.0m^2 to accommodate significant bending moments of between 35 000 to 76 000kNm (Plomteux and Ciortan, 2010).

PROCEEDINGS OF THE 14TH ANZ YOUNG GEOTECHNICAL PROFESSIONALS CONFERENCE
14YGPC ROTORUA, NEW ZEALAND, 2ND – 5TH NOVEMBER 2022

219

Rigid Inclusions reinforce the soil to deliver similar benefits as Stone Columns by improving bearing capacity, increasing overall stiffness and providing settlement control. Unlike Stone Columns, Rigid Inclusions are not limited to the lateral confinement of the surrounding soil defining the characteristics of the semi-rigid elements. However as displacement effects due to differential shortening could occur, a detailed analysis of the soil-inclusion and inclusion-soil load transfer mechanisms are required. Guidelines for the design of rigid inclusions under the turbine pad foundations are sourced from both the CFMS 2011a and the National ASIRI Project for the Recommendations for the design, construction and control of rigid inclusion ground improvements by IREX in 2012.

The design of the Rigid Inclusions relies on the principles of the structural load being distributed between the soil and rigid inclusions via the LTP including resultant displacements of the inclusions and the surrounding soil. Loads on the inclusions are also limited by the settlement that occurs on the sub-base layer under the inclusion tip and the inclusion penetrating in the load-transfer platform. In addition to the need for Rigid Inclusions to provide adequate bearing capacity, the following geotechnical and structural requirements apply:

- The geotechnical resistance of inclusions is calculated according to pressuremeter or penetrometer methods for tip resistance, R_b and Positive skin friction, q_s for friction below neutral plane (IREX, 2012).
- Negative skin friction, for friction above the neutral plane, must be verified such that the friction τ of the soil along the inclusion shaft above the neutral plane does not exceed the limit value $σ_v'$. (IREX, 2012).
- The mean compressive force at the ULS is limited to f_{cd} and the mean compressive force at the SLS is limited to the minimum of $0.3f_c^*$ and $0.45f_c$. Where f_{cd} is the inclusion design compressive strength, f_c^* is the characteristic value for concrete or grout strength and f_c is the concrete compressive strength (CFMS, 2011a).
- The structural integrity of columns under stresses calculated from combined bending actions must be verified (CFMS, 2011a).
- The structural integrity of columns in shear must be verified following the requirements of Eurocode 2 part 12 for unreinforced inclusions (CFMS, 2011a).

Without the limitations of the soil confinement preventing using Stone Columns in soft ground conditions, Rigid Inclusions provide a foundation support solution applicable in most ground conditions. Although installation costs for Rigid Inclusions may be somewhat higher than Stone Columns due to sourcing material (mortar or concrete) and plant to outlying regions, productivity rates are generally quite high for rigid inclusions which helps to balance cost. As Rigid Inclusions are able provide foundation support to a wide range of ground conditions with relatively minimal plant components, they make an ideal solution to supporting most types of turbine foundations.

5 PILED FOUNDATIONS (DEEP FOUNDATIONS)

When design requirements cannot be met with ground improvement options then piles in a deep foundation system may be necessary. Piles in the deep foundation system provide greater rigidity than ground improvement solutions through the direct connection of the foundation to the piling elements which are anchored into deeper and significantly stiffer strata, usually rock. Typically, the piling solution under turbine foundations consist of installing piles in a circular ring or rings about the perimeter of the foundation pad where stresses are highest due to the overturning moments. Drawbacks for piling solutions often involve greater cost and time implications compared to ground improvement solutions. These factors include the need to transport more expensive and heavier materials, particularly steel reinforcement, to be brought to remote areas, more plant components to move the reinforcement and slower productivity. Installation of the structural connections typically as thick pile caps between the pile and footings also contribute to additional cost expenditures and time.

A key difference between piled foundations and rigid inclusion foundations is that they result in significantly higher bending moments and vertical stresses at the head of the pile which leads to greater reinforcement requirements as demonstrated through 3D analyses conducted by Pham *et al* (2018). For the specific scenarios modelled by Pham *et al* (2018), piling options were compared to rigid inclusions with a 500mm LTP and similar replacement ratios of 2.4%, 4.8% and 7.2%. The analysis showed that although the piling option represented only about 4% to 5% (less than 5mm) of the settlements of rigid inclusions, stresses in the piles were substantially higher with bending moments more than three times that of the rigid inclusions.

6   CMC RIGID INCLUSIONS IN GRANVILLE HARBOR WINDFARM

Granville Harbour Wind Farm (GHWF) covers an area of approximately 800 hectares and is currently under construction near Zeehan, on the west coast of Tasmania. When complete, the wind farm will host 31 Vestas V126 wind turbine generators, each rated at 3.6MW with a maximum rated capacity of 111.6MW. The turbine foundation loads are shown in Table 1.

Controlled Modulus Columns (CMCs) was developed by Menard Soltraitement to support structures including wind turbines, warehouses, industrial buildings, medium weight housings, roads, railways, embankments, and storage tanks. The CMCs is predominantly used for sites with soft cohesive soils, loose sand, chalk, organic soil and peat. During the tender stage, several foundation solutions were considered including Piling, Stone Columns and Rigid Inclusions. Ultimately the solution chosen employed CMCs as Rigid Inclusions and was based on:

- High loads imposed by 3.6MW wind turbines make it difficult to justify allowable stresses in the soil and Stone Columns. This includes considering potential lateral expansion failure and punching failure of Stone Columns.
- The remoteness of the site and the expense required to control the quality of the Stone Columns in the variable ground conditions.
- Remoteness of the site means any additional machinery and materials needed, including steel for piling methods, results in significantly more expense.
- CMCs have a much faster installation rate than that of Stone Columns or Piling.
- Unlike Stone Columns made of free draining stone aggregate, CMCs do not create a preferential drainage path.

Based on the wind turbine manufacturer's specifications, the foundation solution was required to provide a rotational stiffness in dynamic conditions, $K_{\phi\text{-dyn}}$, of not less than 54GNm/rad. The ground conditions were noted to be variable across the site with groundwater levels measured from 1.8m to 17.5m with an average in the order of 10m depth below natural ground level. Although the ground conditions varied, one of the more prominent soil profiles used in the design is summarised and shown in the table below.

Calculations were performed considering the foundation base geometry with an equivalent circular base derived from the area of the octagonal foundation pad. As the octagonal pad base has an area of 338m², the diameter of the equivalent circular base is 20.75m. For the given load types in Table 1, the design cases were calculated and the minimum area requirements for the foundation in compression due to overturning were deemed acceptable in accordance with the CFMS 2011a.

Table 1: Wind turbine foundation loads

Load type SLS/ULS*	N= Vertical (kN)	H= Horizontal (kN)	M= Moment (kNm)
ULS Fundamental	5,600	900	121,200
ULS Accidental	5,600	1,000	128,200
SLS Rare	5,600	900	121,200
SLS quasi-permanent	5,700	600	73,300

*SLS: service limit state; ULS: ultimate limit state

Table 2: Soil Profile

Soil Description	Depth to top of layer (m)	E_y (MPa)	E_m (Mpa)
Silt – Stiff	0.0	6.7	3.4
Clay – Firm	3.3	3.3	2.2
Clay – Firm-Stiff	12.0	5.0	3.3
Clay – Stiff-Very Stiff	19.0	11.0	7.3
Clay – Hard (*)	22.5	20.0	13.3

(*) Anchoring layer of CMCs

PROCEEDINGS OF THE 14TH ANZ YOUNG GEOTECHNICAL PROFESSIONALS CONFERENCE
14YGPC ROTORUA, NEW ZEALAND, 2ND – 5TH NOVEMBER 2022

221

Calculations for bearing and settlement analysis however consider the reference area, S_{ref} and the corresponding reference stress, σ_{ref} which represent the relative compressed area and relative average loading which is equivalent to the compressed area, S_{comp} and the non-uniform loading over it. The reference area was derived according to the "half-moon" model defined in the CFMS 2011a. The non-uniform loadings over the compressed area S_{comp} are used for calculating local bearing capacity and allowable stress requirements for individual CMCs at each grid location. The relative compressed areas with the representation of the loadings per CMC location are shown in Figure 2, where larger circles represent a proportionally larger load at the CMC location.

Equivalent improved ground parameters were determined considering an axi-symmetrical calculation of a CMC unit cell using the quasi-permanent load case. The analysis utilised Menard in-house software that captures the distribution of the stresses and displacements from underside of the foundation slab, LTP, along the CMC, in the anchoring layer and throughout the surrounding soil. The Menard software is developed according to the analytical model MV2 explained in the ASIRI (IREX, 2012).

Stiffnesses determined and utilised in the design include the following:
- Equivalent modulus of reinforced ground: 79.8Mpa.
- Equivalent dynamic modulus of reinforced ground: 239.4Mpa.
- Long-term rotational stiffnesses in large-strain domain: 106.8GNm/rad.
- Long-term vertical stiffness: 5Mpa/m.
- Dynamic horizontal stiffness in small-strain domain: 338MN/m.
- Dynamic rotational stiffnesses in small-strain domain: 320GNm/rad > 54GNm/rad.

Global bearing capacity of the foundation system was assessed for each load case. Similarly, local bearing capacity was assessed for the most heavily loaded CMC cell. The global bearing capacity in SLS and ULS were 264kPa and 385kPa respectively.

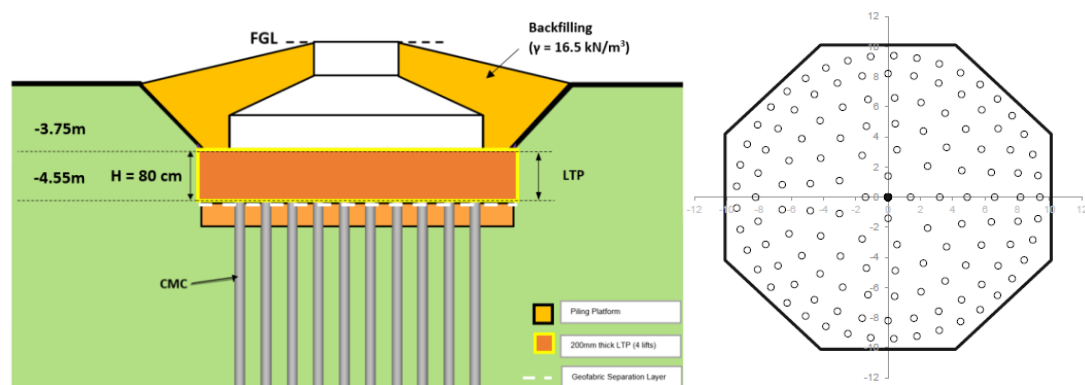Figure 1 – CMC section and arrangement under modelled turbine pad at GHWF

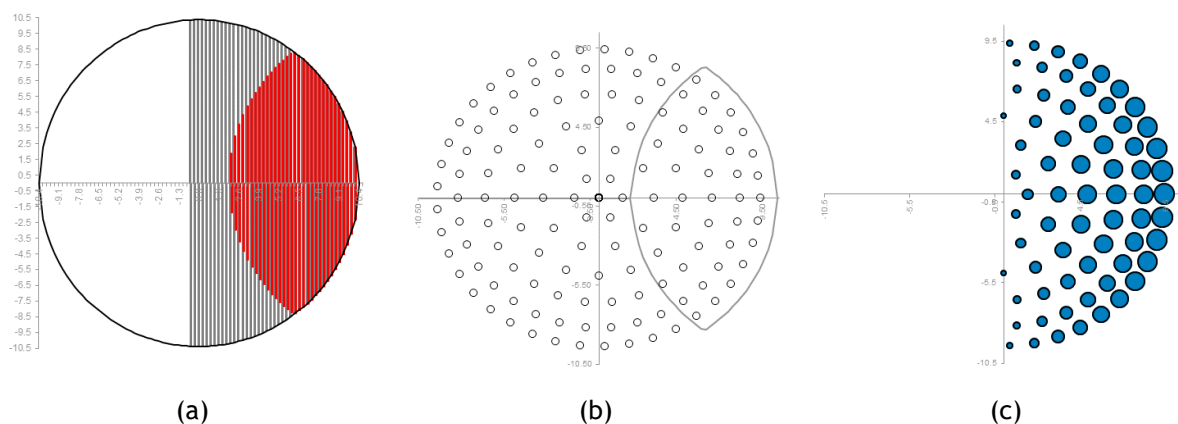| (a) | (b) | (c) |

Figure 2 – (a) Compressed area, S_{comp} in black hatching and reference area, S_{ref} in red hatching (b) Reference area, S_{ref} over CMC arrangement (c) Distributed load per CMC location over compressed area, S_{comp}

Table 3: Global Bearing Capacity Assessment

Type	Reference stress, σ_{ref} (kPa)	Reference area, S_{ref} (m^2)	Number of supporting CMCs, n	Bearing Capacity per CMC, Q_{CMC} (kN)	Mobilized load $\sigma_{ref} \cdot S_{ref}$ (kN)	Allowable bearing capacity (kN)
ULS fund$_1$	263.9	155.7	58	555	41085	59888
ULS fund$_2$	306.8	99.2	41	555	30433	40306
ULS acc	208.8	139.0	54	610	29019	60361
SLS Rare	176.1	172.9	67	431	30433	51587
SLS QP	128.9	236.5	89	352	30478	62505

1: ULS fundamental case 1, 2: ULS fundamental case 2

Settlement and rotation of the foundation system were calculated from rigidities of the improved ground for SLS quasi-permanent load. Minimum, average and maximum settlement of the foundation were calculated to be 19 mm, 26 mm and 33 mm respectively with calculations showing differential settlement would be less than 3mm/m. Once the calculations were completed the wind turbine foundation system for the described ground profile consisted of an octagonal shaped gravity-based footing with 20.2m length and 3.75m depth of embedment. Static load tests verified the performance of the inclusion-soil response where the CMC was load tested to 440kN in accordance with the testing scheme in ASIRI (IREX, 2012) resulting in a total of 2.5mm of movement.

7   CONCLUSION

Although each foundation support system has its suitability in different scenarios, care should be taken for each type of support due to the nature of the mechanisms involved including; Stone Columns for the lateral confinement pressures particularly in soft ground, Rigid Inclusions for the differential shortening of inclusion to soil and Piling solutions for the large resultant bending moments and stresses in each pile. As windfarms are usually planted in outlying areas, the benefits of each foundation system need to also be reviewed against the associated costs which can increase significantly if more material or plant is required. The ground improvement design of CMC Rigid Inclusions under the GHWF highlights the effectiveness of this foundation support for large onshore wind turbines and demonstrates the properties of the reinforced soil.

8   ACKNOWLEDGEMENTS

REFERENCES

(CFMS) Comité Français de la Mécanique des Sols et De Géotechnique (2011a) "Recommendations for the Design, Calculation, Installation and Inspection of Wind-Turbine Foundations", Revision 1.1. 109.

(CFMS) Comité Français de la Mécanique des Sols et De Géotechnique (2011b) "Recommendations for the Design, Calculation, Construction and Quality Control of Stone Columns Under Buildings and Sensitive Structures", Version No. 2

(IREX) Institute for Applied Research and Experimentation in Civil Engineering (2012) "ASIRI National Project. Recommendations for the design, construction and control of rigid inclusion ground improvements".

Frank, R. and Zhao, S, R. (1982) "Estimation à partir des paramètres pressiométriques de l'enfoncement sous charge axiale de pieux forés dans les sols fins." Bulletin de Liaison des Laboratoires des Ponts et Chaussées, 119, 17-24.

IEC 61400-1: 2005 (Wind Turbines – Part 1: Design Requirements)

Pham, H, V. Dias, D. Miranda, T. Cristerlo, N. and Araújo, N (2018) "3D Numerical Modelling of Foundation Solutions for Wind Turbines", International Journal of Geomechanics, 18(12), 04018164.

Plomteux, C. and Ciortan, R. (2010) "Integrated Ground improvement solution for the largest wind farm project in Europe", Proc 14th Danube-European Conference on Geotechnical Engineering 'From Research to Design in European Practice, 2010. Bratislava, Slovakia.

Soyez, B. (1985) "Méthodes de dimensionnement des colonnes ballastées", Bulletin de Liaison des Laboratoires des Ponts et Chaussées, 135, 35-51.

Wind Europe (2013), Ten biggest onshore wind farms in Europe, Viewed 28 February 2020, <http://www.ewea.org/fileadmin/files/library/publications/statistics/Ten_biggest_wind_farms_in_Europe.pdf>.

Windpower Monthly (2019), Ten of the best projects from the last decade, Viewed 28 February 2020, <https://www.windpowermonthly.com/article/1666828/ten-best-projects-last-decade>.

PROCEEDINGS OF THE 14TH ANZ YOUNG GEOTECHNICAL PROFESSIONALS CONFERENCE
14YGPC ROTORUA, NEW ZEALAND, 2ND – 5TH NOVEMBER 2022

223

Comparison between four quantitative goodness-of-fit criteria for acceleration time series

C. Jiang[1,2], C.P. Hayden[3], L. Wotherspoon[4]

[1]PhD candidate, Department of Civil and Environmental Engineering, The University of Auckland, Auckland, New Zealand. Tel.: +64-273530025; Email Address: zjia110@aucklanduni.ac.nz
[2]Geotechnical Engineer, Andy O' Sullivan Geotechnical Engineering, Auckland, New Zealand. Tel.: +64-273530025; Email Address: catherine@aosullivan.co.nz
[3]Lecturer, Department of Civil and Environmental Engineering, The University of Auckland, Auckland, New Zealand
[4]Associate Professor, Department of Civil and Environmental Engineering, The University of Auckland, Auckland, New Zealand

ABSTRACT

Earthquake studies often use different models to simulate acceleration time series and analyse earthquake consequences. These simulated accelerations are then generally validated against experimental data or data from recordings in the field. In order to assess the effectiveness of these simulations, a method is needed to compare between acceleration time series and quantify the similarities. Many previous studies merely qualitatively assess performance based on the match of shape and magnitude aspects. To minimize the subjective nature of these choices, various authors have proposed numerical "goodness-of-fit" criteria to quantify the similarity between two acceleration time series. This paper summarises and compares four existing goodness-of-fit criteria that have different output presentations, including parameter scores and misfit distribution over a time-frequency representation. A sensitivity analysis is used to evaluate how different factors – including amplitude, phase, and frequency – influence the criteria evaluation results. The Anderson (2004) and Olsen & Mayhew (2010) criteria both have 10 parameters and easily identify the amplitude mismatch. The Kristeková et al. (2009) criterion generates plots to visualise the envelope and phase misfit distribution over both time and frequency domains. It has two parameters that respond, independently to amplitude and phase mismatch. The Zeghal et al. (2018) criterion uses three parameters to compare the acceleration time series in the frequency domain, but the proposed metrics are not able to identify the amplitude mismatch.

Keywords: goodness-of-fit, quantitative criteria, acceleration, time-frequency representation

1 INTRODUCTION

Ground acceleration is an important parameter in evaluating the consequences of earthquakes, hence seismic analysis generally includes the study of acceleration time series. Many studies have introduced numerical modelling to simulate and analyze the ground acceleration changes over time. These models require validation against experimental data or data from recordings in the field before further investigation.

In general, researchers may compare between acceleration time series to check the accuracy of the modelling assumption or select a best-fit model. Previous studies usually qualitatively evaluate them based on the how well the overall shape and the peak ground acceleration match (Hartzell 1982; Sabetta and Pugliese 1996). However, results based on subjective judgement are generally less convincing because people may perceive different level of similarity based on the same data. Instead, a quantitative criterion is preferred to evaluate the goodness-of-fit (GOF) between acceleration time series to ensure a consistent methodological approach. Early studies suggested some straightforward methods to achieve quantitative evaluation, including using a simple difference acceleration time series defined as the difference of two acceleration time series at each time step (Aoi and Fujiwara 1999) and using the root mean square of two acceleration time series (Geller and Takeuchi 1995). However, these methods are not always appropriate, as acceleration time series are generally complicated, and it is not enough to define the similarity between two records using a single parameter. When high frequency noise is present in the data, the frequency content and spikes also need to be considered as a measure of the match between records. In addition, researchers may have different focuses when evaluating the match between acceleration time series. Some may compare based on the physical meaning, such as the measures of peak amplitudes and response spectra, while others may consider the analytical results similarity (Taborda and Bielak 2013). Therefore, the need for standard and comprehensive criteria is warranted.

In the past two decades, researchers have proposed several GOF criteria that compare acceleration time series with different output representations. The purpose of this paper is to compare four existing criteria namely: the Anderson (2004) criterion, the Olsen & Mayhew (2010) criterion, the Kristeková et al. (2009) criterion and the Zeghal et al. (2018) criterion.

2   FOUR EXISTING GOODNESS-OF-FIT CRITERIA

The criteria mentioned in the previous section are slightly modified in this paper as the outputs of the four existing criteria are not directly comparable. In particular, Kristeková et al. (2009) generates plots while the other three calculate several parameter scores. This study proposes and modifies the score equations so that all the criteria output an overall score ranging from 0 (poor match) to 10 (excellent match) for later analysis. A scale is defined as: a score over 8 is an excellent fit, a score between 6-8 is a good fit, a score between 4-6 is a fair fit, and a score below 4 is a poor fit (Anderson 2004).

2.1   The Anderson (2004) criterion

Anderson (2004) proposed ten GOF parameters: Arias duration, Energy duration, Arias intensity, Energy integral, Peak acceleration, Peak velocity, Peak displacement, Response spectra, Fourier Spectra, and Cross correlation. Most of the parameters are widely used in earthquake studies, and they comprehensively compare a pair of acceleration time series, including comparison of spectral and magnitude aspects. A generic score equation – a negative exponential function (1) – is defined to evaluate the parameter scores:

$$S(p_1, p_2) = 10\exp\left\{-\left[\frac{(p_1-p_2)}{\min(p_1,p_2)}\right]^2\right\} \tag{1}$$

Where $p_1 \& p_2$ are the parameter values of two records and S is the parameter score. Acceleration time series are evaluated by these parameters in ten frequency bands (nine narrow bands and one overall broad band) in an approximate logarithmic spacing: 0.05 – 0.1 Hz, 0.1 – 0.2 Hz, 0.2 – 0.5 Hz, 0.5 – 1.0 Hz, 1.0 – 2.0 Hz, 2.0 – 5.0 Hz, 5.0 – 10.0 Hz, 10.0 – 20.0 Hz, 20.0 – 50.0 Hz, and 0.05 – 50.0 Hz. The author recommended arithmetically averaging the parameter scores over the ten frequency bands to increase the weight of low frequencies, as they are generally more closely related to the waveform fitting.

To propose an overall score to summarize the 10 parameters, the current study proposes weighting parameters as they have different engineering significance, with Table 1 summarizing the weight allocation. Although the Fourier spectra and Response spectra are generally analysed simultaneously (Bolisetti 2015; Dang and Liu 2020), researchers usually consider the structural response more than the frequency content. Therefore, the response spectrum receives the highest weight (20%), and the Fourier spectrum receives 15%. The measures of peak amplitudes occupy a large weight (35% in total), as they are the commonly used and straightforward properties of an acceleration time series. Various studies have indicated that PGV is better correlated to earthquake destructive consequences (Orense 2005; Yaghmaei-Sabegh et al. 2011), so the weights are allocated accordingly (15% for PGV and 10% for PGA and PGD). Arias intensity and Energy integral are two pairs of parameters that highly correlate to each other, so each of them takes a relatively low weight (5%). Cross-correlation usually relates to the phase shifts, and it receives an average weight of 10%.

Table 1. The parameters and their weight allocation of Anderson (2004) and Olsen & Mayhew (2010)

Parameter number	Parameters of Anderson 2004 criterion	Weights (%)	Parameters of Olsen & Mayhew 2010 criterion	Weights (%)
1	Fourier spectrum (FS)	15	FS	15
2	Response spectrum (RS)	20	RS	10
3	Arias duration (DURA)	5	SA16	10
4	Arias intensity (AI)	5	IE ratio	10
5	Energy duration (DURE)	5	DURE	5
6	Energy integral (EI)	5	EI	5
7	Peak acceleration (PGA)	10	PGA	10
8	Peak velocity (PGV)	15	PGV	15
9	Peak displacement (PGD)	10	PVD	10
10	Cross correlation (Xcor)	10	Xcor	10

PROCEEDINGS OF THE 14TH ANZ YOUNG GEOTECHNICAL PROFESSIONALS CONFERENCE
14YGPC ROTORUA, NEW ZEALAND, 2ND – 5TH NOVEMBER 2022

225

2.2 The Olsen & Mayhew (2010) criterion

Olsen & Mayhew (2010) also defined the criterion with ten parameters, and the current study uses a weighted average as the overall score with a similar weight distribution (details shown in Table 1). Most of the parameters are the same as the previous criterion, but the authors replaced DURA and AI with SA16 and IE ratio, respectively. The SA16 is the response spectral acceleration at 16 individual periods used by recent NGA relations and IE ratio is the ratio between inelastic and elastic response spectra. The weights are modified accordingly. The SA16 and RS are both response spectra with different input periods, so they share the 20% weight. The IE ratio is of interest to structural engineers and receives 10 % weight. It then defines the error function (2) as its score equation:

$$S = A \times \text{erfc} \left[\frac{2|p_1 - p_2|}{p_1 + p_2} \right] \tag{2}$$

Where $p_1 \& p_2$ are the parameter value of two records, *S* is the parameter score, and A is the multiplier. The original study used A = 100, while the current study uses A = 10 for consistency. Figure 1 shows the score distributions of the two criteria, with normalized scores plotted against parameter ratios. A steep slope between parameter ratios 1 – 1.4 indicates that this criterion is more sensitive to small misfits, and the score changes less when the parameter ratio is greater than 2. In contrast, Anderson (2004) has a more uniform distribution as scores change almost linearly for parameter ratio values between 1.3 – 2.1.
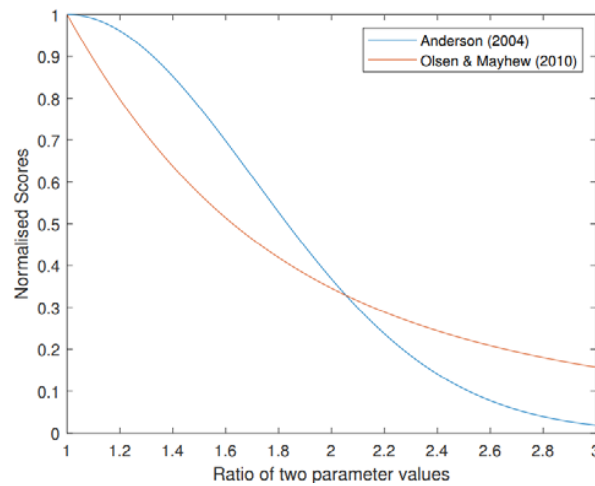

Figure 1. The plot of normalized score distribution against parameter ratio for the Anderson and the Olsen & Mayhew criterion.

2.3 The Kristeková et al. (2009) criterion

Kristeková et al. introduced a misfit criterion based on the time-frequency representations of two acceleration time series (Kristeková et al. 2006), then improved and extended the criterion (Kristeková et al. 2009). The main feature of this criterion is the visualisation of envelope and phase misfit distribution over the time-frequency (TF) representation. The authors defined a series of parameters to compare the signals. For example, the TF envelope misfit (TFEM) and TF phase misfit (TFPM) evaluate the envelope and phase differences on both time and frequency domains, and the respective GOF scores (TFEG and TFPG) are derived from them. All these parameters are matrices measuring the misfits or GOF over the time-frequency ranges, so that plots can be generated to visualise the misfit distribution. According to the definition, the parameter matrices generally have a large proportion of small misfits or high GOF, and it is difficult to summarize the parameter. Therefore, the current study modifies TFEG equation (3) and TFPG equation (4) so that they have a broader score range for later analysis and defines the overall parameter as the mean of the matrix.

$$\text{TFEG}(t, f) = A\exp\{-|\text{TFEM}(t, f) * 10|^k\} \tag{3}$$
$$\text{TFPG}(t, f) = A\exp\{-|\text{TFPM}(t, f) * 10|^k\} \tag{4}$$

Where factor A quantifies the agreement between two signals with lower misfits leading to higher GOF (e.g., when TFEM is 0, TFEG is A), and k determines the sensitivity of the GOF with respect to misfit. The following analysis uses A = 10 and k = 1.

2.4   The Zeghal et al. (2018) criterion

Zeghal et al. investigated the acceleration time series in the frequency domain by firstly converting the time series to Fourier series, and then compares them based on three aspects: phase, shape, and frequency shift. The authors defined the overall parameter d_{ij} as (5) ranging from 1 (out of phase) to 0 (in phase):

$$d_{ij} = d_{ij}^{phase} + d_{ij}^{shape} + d_{ij}^{Fshift} \tag{5}$$

The parameter d_{ij} is independent of d_{ij}^{shape} in magnitude, as d_{ij}^{shape} is deducted in d_{ij}^{Fshift} by its definition. Therefore, the current study considers d_{ij} and d_{ij}^{shape} separately. To allow a consistent scale with the other criteria, D is defined as (6) with a score range of 0 (out of phase) – 10 (in phase):

$$D = 10 \times \left(1 - d_{ij}\right) \tag{6}$$

3   SENSITIVITY ANALYSIS

To assess each criterion, a Gabor signal function (7) is used, which is a harmonic carrier with a Gaussian envelope:

$$Signal = a * \exp\left[-0.3(t - t_0)^2\right] \times \cos\left[2\pi f(t - t_0) + \varphi\pi\right] \tag{7}$$

The Reference signal has the following parameters: a = 2, t_0 = 5, f = 1, φ = 0. To evaluate how amplitude, phase, and frequency influence the criteria evaluation, three signals are defined as: a = 4 for the Amplitude signal, φ = 0.4 for the Phase signal, and f = 1.5 for the Frequency signal, while all the other parameters remain unchanged. Figure 2 presents the four signals, with each criteria used to evaluate the GOF of each modified signal against the Reference signal.
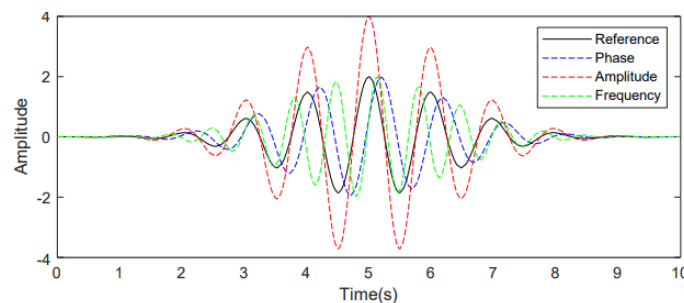

Figure 2. Test signal plots for the sensitivity analysis

Table 2 summarises the results of the four criteria and their evaluation of the GOF of the Amplitude, Phase and Frequency signals compared with the Reference signal. The first two criteria each have one overall score based on the weighted average of 10 parameters, and the last two criteria each have two parameters evaluating different aspects. Compared with a score of 9.3 for the Phase pair, Anderson (2004) gives lower scores for the Amplitude and Frequency pairs of 4.8 and 4.1, respectively. This criterion is highly sensitive to amplitude and frequency differences. Olsen & Mayhew (2010) also evaluates low scores for the Amplitude and Frequency pairs (4.8 and 4.5) compared with the Phase pair (9.1). By contrast, both parameters of Kristeková et al. (2009) give high scores for all cases (> 7). TFEG responds more to the Amplitude and Frequency pairs (8.0 and 7.5), while TFPG is more sensitive to the Phase and Frequency pairs (8.7 and 8.7). These high scores indicate that the overall parameter values are less sensitive to these changes, and it is necessary to analyze the output plots to add more information to the criterion evaluation. Figure 3 displays the TFEG and TFPG plots for the Frequency pair, with both showing a poor fit between 0.5 – 2 Hz throughout the time range, which indicates that the two signals have large misfit within the specified range and reasonable misfit outside the range. The two parameters of the Zeghal et al. (2018) perform differently, with D sensitive to the Phase (6.6) and

PROCEEDINGS OF THE 14TH ANZ YOUNG GEOTECHNICAL PROFESSIONALS CONFERENCE
14YGPC ROTORUA, NEW ZEALAND, 2ND – 5TH NOVEMBER 2022

227

Frequency (5.0) pairs compared with the Amplitude pair (9.0), while D^{shape} remains almost unchanged for all factor changes. This criterion cannot identify amplitude mismatches and D^{shape} plays a relatively unimportant role in most earthquake studies.

Table 2. Sensitivity analysis summary table

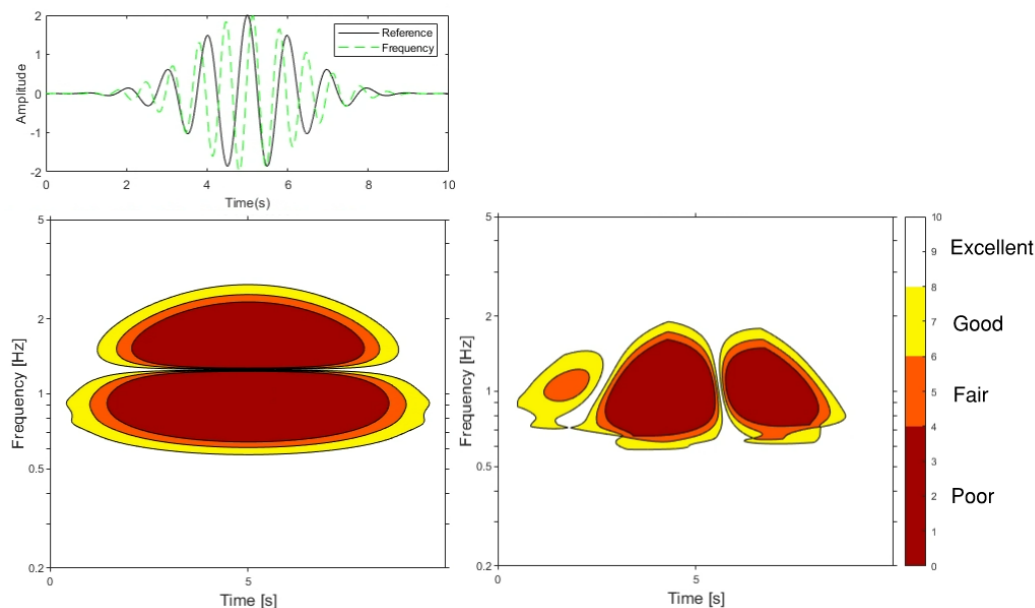| Criteria name	Score name	Score values of different cases		
		Phase	Amplitude	Frequency
Anderson (2004)	Weighted score	9.3	4.8	4.1
Olsen & Mayhew (2010)	Weighted score	9.1	4.8	4.5
Kristeková et al. (2009)	TFEG	10.0	8.0	7.5
	TFPG	8.7	10.0	8.7
Zeghal et al. (2018)	D	6.6	9.0	5.0
	D^{shape}	10.0	9.9	10.0

Figure 3. The GOF plots of the Kristeková et al. (2009) criterion comparing the Frequency signal with the Reference signal in the sensitivity analysis. (a) The Reference signal and the Frequency signal; (b) TFEG plot and (c) TFPG plot with scales.

Overall, Anderson (2004) defines frequency filtering of the acceleration time series as the first step to minimizing the influence of high and low-frequency motions which contribute less to the earthquake consequences. The parameter scores are closely related to frequency and amplitude differences, which most earthquake studies generally focus on. However, the parameter scores cannot indicate whether the simulation overestimates or underestimates the actual data and are less sensitive to small differences than significant differences as shown in Figure 1. Therefore, although this criterion is desirable to most applications, it may benefit from further improvements, such as adding signs to the scores to identify underestimation or overestimation and providing extra score equation choices according to different requirements.

Olsen & Mayhew (2010) has a higher resolution for small differences as shown in Figure 1. The sensitivity analysis shows that it responds slightly less to frequency changes as it does not include frequency filtering, and the updates to the Anderson criteria have a limited influence on the scores. Even so, structural engineers may appreciate the addition of the new parameter IE ratio to evaluate the building behaviors. This criterion is a reasonable choice for many studies, but it could be further improved by combining with the advantages of Anderson (2004).

Kristeková et al. (2009) generates plots to enable a detailed analysis of the acceleration time series comparison, as researchers can separate envelope and phase misfits and clearly visualize the misfit distribution over a time-frequency representation. However, earthquake studies usually need to compare numerous acceleration time series, so analyzing each plot individually is less efficient

compared with other criteria. As the criterion outputs matrices of scores, this study proposes an overall criterion score to summarize the performance differences between a pair of acceleration time series. In general, this criterion is desirable if it is used for specific case studies or small-scale comparisons and is helpful to improve a certain simulation as it presents the most detail, while it is less effective when used in a large scale.

Zeghal et al. (2018) compares acceleration time series based on the frequency domain. It is less applicable to earthquake studies compared with the other three criteria, as the parameters are less effective when evaluating factor changes. In the sensitivity analysis, the overall parameter responds more to phase difference compared with amplitude difference, and the shape parameter gives stable and high scores.

4   CONCLUSIONS

This paper compared four GOF criteria that quantify the similarity between two acceleration time series. The sensitivity analysis indicates that Anderson (2004) and Olsen & Mayhew (2010) are sensitive to amplitude difference. They can easily summarize the similarities between time series and suggest the one with better performance, so they are appropriate for most of earthquake studies, such as selecting a best-fit models and justifying modelling assumptions. Kristeková et al. (2009) has two parameters that measure amplitude and phase differences separately and generates several misfit distribution plots. This criterion is more suitable for specific case studies or to improve a certain model. Zeghal et al. (2018) is not very sensitive to either amplitude or frequency differences, which means the criterion is less applicable to general earthquake studies. These criteria focus on different aspects and have distinct features, so researchers can choose the most suitable one based on their requirements.

5   ACKNOWLEDGEMENTS

REFERENCES

Anderson, J. G. (2004). "Quantitative measure of the goodness-of-fit of synthetic seismograms." Proc., Proceedings of the 13th World Conference on Earthquake Engineering, International Association for Earthquake Engineering, 243.

Aoi, S., and Fujiwara, H. (1999). "3D Finite-Difference Method using Discontinuous Grids." *Bulletin of the Seismological Society of America,* 89(4), 918-930.

Bolisetti, C. (2015). *Site Response, Soil-Structure Interaction and Structure-Soil-Structure Interaction for Performance Assessment of Buildings and Nuclear Structures,* State University of New York at Buffalo.

Dang, P., and Liu, Q. (2020). "Stochastic Finite-Fault Ground Motion Simulation for the Mw 6.7 Earthquake in Lushan, China." *Nat. Hazards,* 100(3), 1215-1241.

Geller, R. J., and Takeuchi, N. (1995). "A New Method for Computing Highly Accurate DSM Synthetic Seismograms." *Geophysical Journal International,* 123(2), 449-470.

Hartzell, S. (1982). "Simulation of Ground Accelerations for the May 1980 Mammoth Lakes, California, Earthquakes." *Bulletin of the Seismological Society of America,* 72(6A), 2381-2387.

Kristeková, M., Kristek, J., Moczo, P. (2009). "Time-Frequency Misfit and Goodness-of-Fit Criteria for Quantitative Comparison of Time Signals." *Geophysical Journal International,* 178(2), 813-825.

Kristeková, M., Kristek, J., Moczo, P., Day, S. M. (2006). "Misfit Criteria for Quantitative Comparison of Seismograms." *Bulletin of the Seismological Society of America,* 96(5), 1836-1850.

Olsen, K. B., and Mayhew, J. E. (2010). "Goodness-of-Fit Criteria for Broadband Synthetic Seismograms, with Application to the 2008 Mw 5.4 Chino Hills, California, Earthquake." *Seismol. Res. Lett.,* 81(5), 715-723.

Orense, R. P. (2005). "Assessment of Liquefaction Potential Based on Peak Ground Motion Parameters." *Soil Dyn. Earthquake Eng.,* 25(3), 225-240.

Sabetta, F., and Pugliese, A. (1996). "Estimation of Response Spectra and Simulation of Nonstationary Earthquake Ground Motions." *Bulletin of the Seismological Society of America,* 86(2), 337-352.

Taborda, R., and Bielak, J. (2013). "Ground-motion Simulation and Validation of the 2008 Chino Hills, California, Earthquake." *Bulletin of the Seismological Society of America,* 103(1), 131-156.

Yaghmaei-Sabegh, S., Tsang, H., Lam, N. T. (2011). "Conversion between Peak Ground Motion Parameters and Modified Mercalli Intensity Values." *J. Earthquake Eng.,* 15(7), 1138-1155.

Zeghal, M., Goswami, N., Manzari, M., Kutter, B. (2018). "Discrepancy Metrics and Sensitivity Analysis of Dynamic Soil Response." *Geotechnical Earthquake Engineering and Soil Dynamics V: Numerical Modeling and Soil Structure Interaction,* American Society of Civil Engineers Reston, VA, 115-122.

PROCEEDINGS OF THE 14TH ANZ YOUNG GEOTECHNICAL PROFESSIONALS CONFERENCE
14YGPC ROTORUA, NEW ZEALAND, 2ND – 5TH NOVEMBER 2022

229

A particle-scale perspective on internal erosion: Observations from computational simulations and physical experiments

A. Sufian[1*], V.S.R. Annapareddy[1], Y. Zhang[1], S.A.W Holden[1], T. Bore[1], and A. Scheuermann[1]

[1]School of Civil Engineering, The University of Queensland, St. Lucia QLD 4072, Australia; PH +617 334 61352; email: a.sufian@uq.edu.au

ABSTRACT

This study presents particle-scale insights into internal erosion mechanisms using computational simulations and physical experiments. Existing design criteria to determine the susceptibility of soils to initiation mechanisms, along with filter criterion for assessing continuation have been predominantly developed based on macro-scale observations. However, limited studies have explored the underlying particle-scale mechanisms. As internal erosion involves the detachment and transport of particles due to seepage, the mechanisms that lead to the initiation and continuation of erosion are rooted at the particle-scale. Computational simulations were performed using the discrete element method which investigated the stress distribution in gap-graded soils. A key finding is that under anisotropic loading conditions, certain transitional gap-graded soils can change from being fines-dominated to coarse-dominated, and hence, their susceptibility to suffusion may change under the anisotropic loading conditions. Physical experiments were conducted using a purpose-built coaxial permeameter cell that utilised spatial time domain reflectometry, an electromagnetic observational method which enabled near-continuous measurement of local porosity during the erosion process. This enabled physical insights into the changes in the internal structure of the soil during filtration experiments. By varying particle sizes and hydraulic boundary conditions, the influence of geometric and hydraulic criteria was investigated. These particle-scale findings can improve the robustness and reliability of existing tools, whilst leading to the development of new techniques to investigate and assess internal erosion.

Keywords: internal erosion, filtration, suffusion, discrete element method, spatial TDR

1   INTRODUCTION

Internal erosion is an important element in the geotechnical design of dams, levees, and other water-retaining structures. Internal erosion occurs when soil particles within an embankment or the foundations of a structure are detached and transported by seepage flows. Internal erosion has been attributed to approximately half of all embankment dam failures globally (Foster et al., 2000). The process of internal erosion is not easily observable or measurable as it occurs within the structure and its foundations, and hence, is a poorly understood phenomenon. There is a need to move away from empirical and rule-of-thumb guidelines into a design philosophy based on underlying mechanics and a rigorous scientific process. This can be achieved by considering particle-scale observations to complement existing macro-scale knowledge, thereby providing a holistic view of the internal erosion mechanisms.

The internal erosion process can be delineated into four main phases: initiation, continuation, progression, and breach (Fell et al., 2015). Existing design approaches focus on minimising the potential for initiation mechanisms to occur and/or preventing continuation, as failure may develop quickly from initiation to breach in hours or days (Fell et al., 2009). The main design consideration to mitigate internal erosion failure is the provision of filters. Modern filter design aims to specify the range of particle sizes to prevent the erosion of soil particles, whilst maintaining sufficient drainage capacity. The performance of a filter in its retention function is clearly rooted at the particle-scale with the trapping of discrete particles. Therefore, the choice of these particle-scale characteristics of a filter is an important design consideration for protecting water retaining structures against internal erosion failure.

A recent technical bulletin summarises the current state-of-knowledge with respect to internal erosion and outlines the initiation mechanisms, including concentrated leak, backwards erosion piping, contact erosion, and suffusion (ICOLD, 2017). Concentrated leak occurs when an opening or crack is formed with subsequent expansion due to erosion of particles from the sides of the opening. Backwards erosion piping initiates at the downstream side, where the eroded particles gradually lead to the formation of a pipe structure that extends towards the upstream side of the dam or levee. Contact erosion occurs at the interface of a finer soil layer and coarser soil layer, where seepage results in the detachment and transport of finer soil particles into the pore space formed by the coarser particles. The term contact

erosion is used when seepage flow is parallel to the interface between a finer and coarser layer, while it is typically referred to as filtration when flow is perpendicular to the interface (Beguin et al. 2012). Suffusion occurs in soils with a mixture of finer and coarser soil fractions (e.g., gap-graded soils or widely graded soils) and results in preferential erosion of the finer fraction of the soil. When the fines content is relatively small, suffusion may not lead to changes in the structure or fabric of the coarser fraction, which generally only occurs at higher fines content when the finer particles are contributing to the stress transmission process. An important message to highlight is that all initiation mechanisms involve particle-scale behaviour with the detachment and transport of discrete particles. Hence, it is essential to explore particle-scale mechanisms as the internal erosion process is rooted at the particle-scale.

While the importance of particle-scale observations has been highlighted above, prior studies in the field of internal erosion have focused on macro-scale observations from physical laboratory experiments. Geometric, hydraulic, and mechanical criteria for the initiation and continuation of internal erosion have been extensively developed from macro-scale laboratory investigations. Geometric criteria have been widely used in the design of filters (Terzaghi & Peck, 1948; Sherard et al., 1984) and to assess the internal instability of soil (Kezdi, 1979; Kenney & Lau, 1985). A hydraulic criterion based on the critical seepage velocity for contact erosion was proposed by Brauns (1985), while Ziems (1969) proposed a critical hydraulic gradient for filtration. Skempton and Brogan (1994) suggested a stress reduction factor to account for the reduced effective stress carried by the finer fraction of a soil, which provided a means to understanding why suffusion initiated at hydraulic gradients less than the critical hydraulic gradient for heave failure. In addition to design criteria, observations of particle transport and changes in porosity have focused on macro-scale observations. Existing approaches to measure changes in porosity due to internal erosion have considered the cumulative loss of fine particles (Ke and Takahashi 2014; Rochim et al. 2017), or visual observation of changes in layer heights and post-test sampling (Ke and Takahashi 2012), without probing the changes in the internal structure of an eroded soil mass.

These shortcomings are a result of the available resources to probe the particle-scale characteristics of internal erosion and highlights the need to develop fundamental particle-scale understanding of internal erosion mechanisms. New experimental methods such as the application of electromagnetic observational techniques have enabled the internal structure to be observed and corresponding particle-scale mechanisms to be measured. Coupled with this is ever-increasing computing power, which has enabled large-scale simulations to uncover the influence of particle-scale interactions. This study combines computational and physical experiments to link particle-scale processes with macro-scale observations. The Discrete Element Method (DEM) was employed to enable an improved understanding of how stresses are redistributed in internally unstable soils for anisotropic stress conditions, with findings challenging the current assessment of susceptibility to suffusion. In addition, the migration of erodible particles was explored using spatial time domain reflectometry and a purpose-built coaxial permeameter cell, providing near-instantaneous and near-continuous porosity profile during the initiation and continuation phase of filtration. The combined computational and physical particle-scale observations provided a holistic view of the internal erosion process.

2   OBSERVATIONS FROM COMPUTATIONAL SIMULATIONS

In most physical experiments, it is prohibitive to obtain data regarding particle interactions, including the inter-particle contact forces, which is an important feature in understanding how stresses are transmitted through an internally unstable granular soil. The Discrete Element Method (DEM) provides a computational route to simulate the movement of individual particles according to Newtonian laws of motion (Cundall & Strack, 1979). This study presents the results of a wide range of DEM simulations on granular gap-graded soils that are susceptible to suffusion to investigate how the stress is distributed between the finer and coarser fraction of the gap-graded soil under anisotropic loading conditions.

DEM simulations of constant mean stress triaxial compression tests on idealised spherical assemblies of gap-graded soils were conducted using the open-source software LAMMPS (Plimpton, 1995). Relatively dense samples were generated with a wide range of fines content and size ratios. The particle size distributions (PSD) of the samples are shown in Figure 1. The fines content specified in Figure 1 covers gap-graded soils with an underfilled fabric through to those with an overfilled fabric. A soil with an underfilled fabric is generally observed for fines content less than 24%, and the stress is predominantly transmitted through the coarser fraction. For soils with an overfilled fabric (fines content greater than 35%), the stress is distributed among both the finer and coarser fraction. For soils with a fines content between 24% and 35%, the fabric is regarded as being transitional. In addition, the size

PROCEEDINGS OF THE 14TH ANZ YOUNG GEOTECHNICAL PROFESSIONALS CONFERENCE
14YGPC ROTORUA, NEW ZEALAND, 2ND – 5TH NOVEMBER 2022

231

ratio, defined as the ratio of the maximum to minimum particle sizes, varied from being internally unstable, borderline unstable, and internally stable according to the Kezdi (1979) criteria. This systematic approach allowed for the complete spectrum of behaviour associated with suffusive soils to be investigated. The samples comprised between approximately 68,500 particles and 3.29 million particles, depending on fines content and size ratio, making these simulations the largest conducted within the geotechnical literature (Sufian et al., 2021). A constant mean stress triaxial compression test was chosen to investigate the role of increasing deviatoric stress, as most existing studies focussed on isotropic stress conditions.
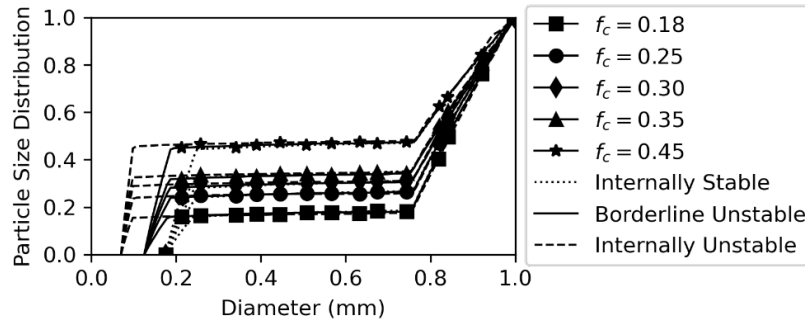

Figure 1: Particle size distribution of the samples used in DEM simulations.

A wide range of particle-based and contact-based data was generated from DEM simulations. In this study, the quantities of interest are the contact forces between particles, and the mean stress on an individual particle. For a gap-graded soil, particle-based quantities can be partitioned between the finer and coarser fraction. The mean stress carried by the finer fraction was defined by α_p. This is similar to the stress reduction factor proposed by Skempton and Brogan (1994), except that α_p is bound between $0 \leq \alpha_p \leq 1$. When considering inter-particle contacts, the mean stress can be partitioned by that transmitted at contacts between the fine-fine particles (β_p^{ff}), fine-coarse particles (β_p^{fc}), and coarse-coarse particles (β_p^{cc}), where all three β_p quantities are bound between $0 \leq \beta_p \leq 1$.

(a) Evolution of α_p
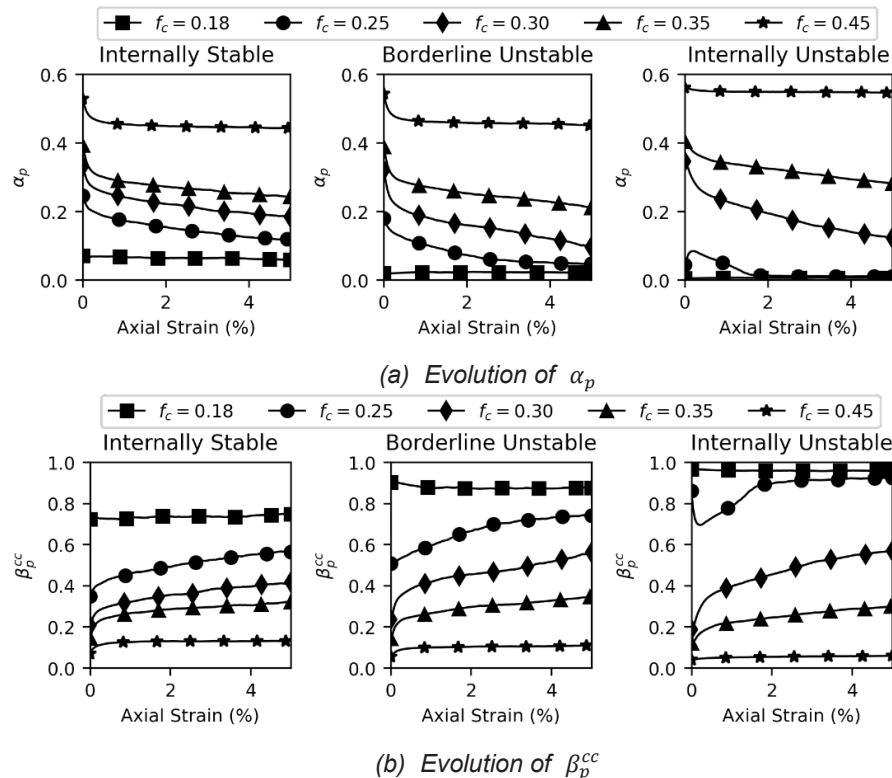
(b) Evolution of β_p^{cc}

Figure 2: Particle-scale stress distribution during constant mean stress triaxial compression tests.

232

PROCEEDINGS OF THE 14TH ANZ YOUNG GEOTECHNICAL PROFESSIONALS CONFERENCE
14YGPC ROTORUA, NEW ZEALAND, 2ND – 5TH NOVEMBER 2022

The evolution of α_p throughout the constant mean stress triaxial compression test is shown in Figure 2a. Irrespective of the degree of internal instability, the mean stress carried by the finer fraction increased with increasing fines content. For underfilled soils, α_p reduced with increasing size ratio, while for overfilled fabrics, α_p increased with increasing size ratio. For transitional soils, the trend is less clear, but there is an important observation associated with the evolution of α_p for transitional soils. While α_p changes minimally for underfilled and overfilled soils, a significant reduction in the stress carried by the finer fraction is noted for transitional soils. In some instances, an approximately 50% reduction in the mean stress can be observed. This is important because a soil is more prone to suffusion when the stress carried by the finer fraction is relatively low. The observations in Figure 2a indicate that the soils that were previously not considered susceptible to suffusion may become susceptible to suffusion when subject to anisotropic stress conditions. While internal instability is generally considered through the application of geometric criteria, these influences of the mechanical condition should be considered.

To better understand the transition from coarse dominated to fines dominated behaviour of gap-graded soils, it was necessary to investigate the evolution of β_p^{ff}, β_p^{fc}, and β_p^{cc} during the constant mean stress triaxial compression tests. The evolution of β_p^{cc} is shown in Figure 2b and exhibited an inverse trend to that observed in Figure 2a. Of particular interest was the identification of which of the three β_p were the dominant case in each simulation, from which the following characteristics were obtained:

- $\beta_p^{cc} \geq \beta_p^{fc} \geq \beta_p^{ff}$: coarse-dominated behaviour (C)
- $\beta_p^{fc} \geq \beta_p^{cc} \geq \beta_p^{ff}$: transitional coarse-dominated behaviour (TC)
- $\beta_p^{fc} \geq \beta_p^{ff} \geq \beta_p^{cc}$: transitional fines-dominated behaviour (TF)
- $\beta_p^{ff} \geq \beta_p^{fc} \geq \beta_p^{cc}$: fines-dominated behaviour (F)

While some samples remained in one of the above-listed behaviours throughout the simulation, those with a transitional fabric exhibited a tendency to become coarse dominated for anisotropic loading conditions. While only limited set of data points is available from these simulations, Figure 3 presents a preliminary chart to identify the influence of fines fraction and size ratio on the susceptibility to change behaviour under anisotropic loading conditions. Further research is required to assess and quantify the potential for transitional soils to become coarse dominated more accurately.
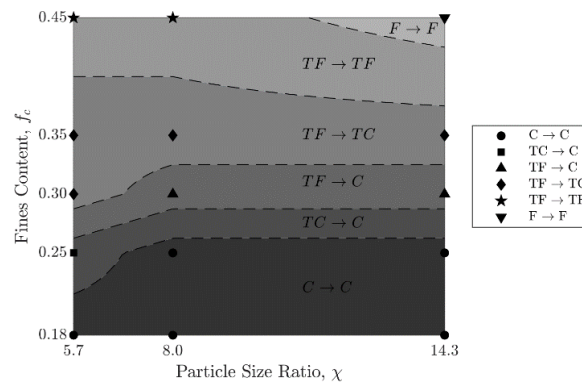

Figure 3: Redistribution of stress in gap-graded soils during anisotropic loading

3 OBSERVATIONS FROM PHYSICAL EXPERIMENTS

Internal particle-scale observations are prohibitive in most physical experiments which either measure macro-scale quantities across the complete sample or make observations of local characteristics by only considering external measurements. Given that internal erosion involves the internal change in structure of a soil, there is a need to physically observe particle-scale characteristics during the erosion process. A potential approach to investigate this is the application of spatial time domain reflectometry (spatial TDR), an electromagnetic observational method capable of measuring the water content and density (Scheuermann, 2012). The application of spatial TDR for internal erosion problems is limited and this study demonstrates how particle-scale internal observations can be inferred from spatial TDR data obtained from filtration and suffusion tests. The experiments were conducted in a purpose-built coaxial permeameter cell (Bittner et al., 2019, Sufian et al., 2022). The permeameter was copper-built with an inner and outer conductor that effectively acted as a coaxial transmission line to enable electromagnetic measurements along the length of the sample. The measured electrical signal was then

PROCEEDINGS OF THE 14TH ANZ YOUNG GEOTECHNICAL PROFESSIONALS CONFERENCE
14YGPC ROTORUA, NEW ZEALAND, 2ND – 5TH NOVEMBER 2022

233

processed via a forward inversion algorithm to obtain the local porosity along the sample. A central feature in filtration and suffusion experiments is the detachment and transport of finer soil particles through the pore space of the coarser particles. This results in a local change in porosity within the sample as the finer particles fill the pore space between coarser particles, and this local change in porosity is measured using the coaxial permeameter cell.

A set of filtration tests were conducted with a finer soil layer (base layer) underlying a coarser soil layer (filter layer) with upward flow resulting in the migration of the particles from the base to the filter layer. The experiments considered different particle sizes for the base and filter layer, along with different hydraulic boundary conditions to investigate both the geometric and hydraulic conditions on filtration. The choice of base and filter layers were such that they were incompatible and exceeded the continuing erosion boundary proposed by Foster and Fell (2001). This was deliberately selected so that the entire filtration process could be investigated from initiation to continuation to complete washout of the finer base particles, all whilst the internal structure of the soil could be measured via spatial TDR.

The principal data obtained from spatial TDR analysis of the filtration experiment is the spatial and temporal evolution of local porosity. A graphical presentation of this is shown in Figure 4a and is termed a porosity field map. From the porosity field map, three important characteristics of the filtration process can be obtained: the lower limit of the mixture zone, the upper limit of the mixture zone and the settlement line. The upper limit of the mixture zone is a result of the transport of base particles into the filter layer for upward seepage flow, while the lower limit of the mixture zone results from the concurrent settlement of the filter layer into the base layer. An outcome of overall mixing process in the settlement of the sample, which is defined by the settlement line. The porosity field maps provide a unique array of data from which a deeper understanding of the internal erosion mechanisms can be obtained.
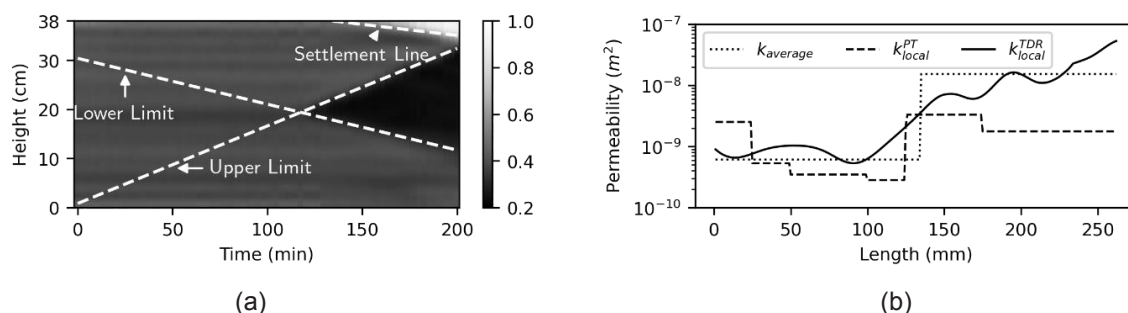

Figure 4: (a) Porosity field map data from coaxial permeameter cell. (b) Estimation of local permeability from spatial TDR data which is compared with conventional measures of permeability.

The initiation of filtration is clearly visible by the intersection of the lower and upper limits on the porosity field map, and the corresponding critical flow rate and hydraulic gradient can be readily determined. The critical flow rate showed a strong dependence on base particle size, with the critical flow rate increasing for larger base particles. In contrast, the critical hydraulic gradient exhibited a stronger dependence on the size of the filter particles, with a lower critical hydraulic gradient observed with increasing filter particle size. The continuation of filtration was also quantitatively captured in the porosity field map. A key observation was that the formation of the mixture zone was influenced by two mechanisms: (i) the transport of base particles into the filter layer due to upward seepage flows and (ii) the settlement of the filter particles into the base layer due to the reduction of the effective stress at the base–filter interface leading to partial bearing failure. Both mechanisms could be inferred from spatial TDR data by considering the differing gradients of the lower and upper limits of the mixture zones from the porosity field map. These gradients also provided quantitative insights into the continuation characteristics.

In addition to obtaining information on the local porosity, spatial TDR data can also be used to infer the local permeability. This was achieved by considering a variation on the well-known Kozeny-Carmen expression for permeability (Annapareddy et al., 2022), which incorporated the measured local porosity as well as an effective particle diameter that considered the fraction of finer and coarser particles. This enabled the local permeability measure to account for fines transport during filtration or suffusion experiments. A comparison of the local permeability obtained from spatial TDR (k_{local}^{TDR}) with the average permeability ($k_{average}$) and the local permeability obtained from pressure transducers (k_{local}^{PT}) is shown in Figure 4b. The average permeability remains constant within a layer, while the permeability obtained from pressure transducers remains constant between adjacent transducers. In contrast, the local

permeability obtained from spatial TDR shows a near-continuous variation that is reflective of the inherent variability of the soil. Ongoing research is investigating the heterogeneity of the internal erosion process using this measure of local permeability.

4   CONCLUSIONS

This study presented the findings of particle-scale computational and physical experiments on internal erosion. Computational simulations of constant mean stress triaxial compression tests on gap-graded soils were conducted using the discrete element method and demonstrated that certain types of gap-graded soils may become more susceptible to suffusion when subject to anisotropic loading conditions. Physical experiments investigated the filtration process by conducting permeameter experiments using a purpose-built coaxial permeameter that utilised spatial time domain reflectometry to take near-continuous measurements of local porosity. These observations enabled the internal structure to be quantified from initiation to continuation to complete washout of particles. These particle-scale findings provide additional data that can improve the robustness and reliability of tools used by geotechnical engineers to assess the susceptibility to internal erosion, such as the piping toolbox. Moreover, developing a fundamental mechanics-based understanding can lead to the development of new techniques to investigate and assess internal erosion.

5   ACKNOWLEDGEMENTS

REFERENCES

Annapareddy, V.S.R., Sufian, A., Bore, T., Bajodek, M. and Scheuermann, A. (2022). "Computation of local permeability in gap-graded granular soils". Géotechnique Letters, 12(1), 68-73.

Bittner, T., Bajodek, M., Bore, T., Vourch, E., and Scheuermann, A. (2019). "Determination of the porosity distribution during an erosion test using a coaxial line cell". Sensors, 19(3), 611.

Brauns, J. (1985). "Erosionsverhalten gechichteten bodens bei horizontaler durchströmung". Wasserwirtschaft, 75(10), 448-453.

Béguin, R., Philippe, P., Faure, Y.-H., and Guidoux, C. (2012). "Contact erosion between two soils". Chapter 4. John Wiley & Sons, Ltd. pp. 115-154.

Cundall, P. A., and Strack, O. D. (1979). "A discrete numerical model for granular assemblies". Geotechnique, 29(1), 47-65.

Fell, R., Foster, M., Davidson, R., Cyganiewicz, J., Sills, G., and Vroman, N. (2009). "A Unified Method for Estimating Probabilities of Failure of Embankment Dams by Internal Erosion and Piping". UNICIV Report R 446, The School of Civil and Environmental Engineering, University of New South Wales, Sydney, Australia 2052.

Fell, R., MacGregor, P., Stapledon, D., Bell, G., and Foster, M. (2015). "Geotechnical engineering of dams (2nd Edition)". CRC press.

Foster, M., and Fell, R. (2001). "Assessing embankment dam filters that do not satisfy design criteria". Journal of Geotechnical and Geoenvironmental Engineering, 127(5), 398-407.

Foster, M., Fell, R., and Spannagle, M. (2000). "The statistics of embankment dam failures and accidents". Canadian Geotechnical Journal, 37(5), 1000-1024.

ICOLD. (2017). "Internal erosion of existing dams, levees and dikes, and their foundations. Internal erosion processes and engineering assessment". International Commission of Large Dams, Volume 1.

Ke, L., and Takahashi, A. (2012). "Strength reduction of cohesionless soil due to internal erosion induced by one-dimensional upward seepage flow." Soils and Foundation, 52(4), 698–711.

Ke, L., and Takahashi, A. (2014). "Triaxial erosion test for evaluation of mechanical consequences of internal erosion". Geotechnical Testing Journal, 37(2), 347–364.

Kenney, T. C., and Lau, D. (1985). "Internal stability of granular filters". Canadian Geotechnical Journal, 22(2), 215-225.

Kezdi, A. (1979). "Soil physics – selected topics". Amsterdam, the Netherlands: Elsevier Scientific Publishing Co.

Plimpton, S. (1995). "Fast parallel algorithms for short-range molecular dynamics." Journal of Computational Physics, 117, 1–19.

Rochim, A., Marot, D., Sibille, L., and Thao Le, V. (2017). "Effects of hydraulic loading history on suffusion susceptibility of cohesionless soils". Journal of Geotechnical and Geoenvironmental Engineering, 143(7), 04017025.

Scheuermann, A. (2012). "Determination of porosity distributions of water saturated granular media using spatial time domain reflectometry (spatial TDR)". Geotechnical Testing Journal, 35(3), 441–450.

Sherard, J.L., Dunnigan, L.P., and Talbot, J.R. (1984). "Basic properties of sand and gravel filters". Journal of Geotechnical Engineering, 110(6), 684–700.

Skempton, A., and J. Brogan. 1994. "Experiments on piping in sandy gravels." Géotechnique, 44(3), 449–460.

Sufian, A., Bittner, T., Bore, T., Bajodek, M. and Scheuermann, A., (2022). "Physical observations of the transient evolution of the porosity distribution during internal erosion using spatial time domain reflectometry". Canadian Geotechnical Journal, doi: 10.1139/cgj-2021-0570.

Sufian, A., M. Artigaut, T. Shire, and C. O'Sullivan. (2021). "Influence of fabric on stress distribution in gap-graded soil." Journal of Geotechnical and Geoenvironmental Engineering, 147(5), 04021016.

Terzaghi, K., and Peck, R.B. (1948). "Soil mechanics in engineering practice". Technical Report.

Ziems, J. (1969). "Beitrag zur Kontakterosion nichtbindiger Erdstoffe". Ph.D. thesis, Verlag nicht ermittelbar.

PROCEEDINGS OF THE 14TH ANZ YOUNG GEOTECHNICAL PROFESSIONALS CONFERENCE
14YGPC ROTORUA, NEW ZEALAND, 2ND – 5TH NOVEMBER 2022

235

The Installation of Inclinometers in Saturated Granular Soils

M. Koller[1]

[1]WSP Australia, 15/28 Freshwater Place, Southbank, Victoria, 3006, Australia, +61 3 9861 1679, email: mitchell.koller@wsp.com

ABSTRACT

Level crossings at Bonbeach, Chelsea and Edithvale in Victoria were removed through grade separation of the existing road and rail. Construction at each site included sheet pile supported rail trenches within Quaternary dune sands and coastal lagoon deposits. Prior to the excavation of the rail trenches, inclinometers were installed behind the sheet pile retaining walls to measure the variation in lateral ground displacement with depth during the excavation of the rail trenches. The installation of the inclinometers was found to be challenging due to the saturated and granular nature of the surrounding soils. The boreholes drilled were vulnerable to collapse when removing the drilling casing, while a significant loss of grout was experienced through permeable soils when installing the inclinometer casing. These ground conditions made it difficult to achieve consistent contact between the permanent inclinometer casing and the surrounding soil. The drilling and inclinometer installation methodologies implemented were progressively reviewed and then modified to mitigate these construction difficulties and improve the reliability of the inclinometers installed. This paper discusses the staged installation methodology which was developed and reviews the extent to which the newly adopted methodology was able to mitigate the initial construction difficulties encountered.

Keywords: inclinometers, monitoring, retaining walls, ground displacement

1   INTRODUCTION

The Level Crossing Removal Project (LXRP) is a Victorian Government initiated program for the progressive removal of Victoria's most dangerous and congested level crossings. The Southern Program Alliance (SPA), consisting of WSP, Acciona and Metro Trains Melbourne, was engaged by LXRP to remove five dangerous and congested level crossings along the Frankston line as part of the second additional works package. Both metropolitan passenger trains and commercial freight trains operate along the Frankston line which runs parallel to Nepean Highway through congested residential and commercial areas.

The project involved the construction of new stations at Bonbeach, Chelsea and Edithvale, three road over rail bridges, station carparks, shared user paths and three sheet pile supported rail trenches within Quaternary dune sands and coastal lagoon deposits.

Prior to the excavation of the rail trenches, inclinometers were required to be installed behind the sheet pile retaining walls to measure the variation in lateral ground displacement with depth during the excavation of the rail trenches. These ground displacement measurements were then compared with trigger levels established through ground movement modelling.

The installation of inclinometers during the project was challenging due to the subsurface ground conditions encountered across the site. These ground conditions made it difficult to achieve consistent contact between the permanent inclinometer casing and the surrounding soil using the installation methodology previously adopted at other level crossing removal sites.

2   SITE CONDITIONS

2.1   Site description

The five level crossings which were removed are approximately located 31 km south-east of Melbourne's CBD, with Bonbeach, Chelsea and Edithvale train stations being approximately positioned 200 m from the beaches of Port Phillip Bay. The level crossings are located along the Frankston line

which runs parallel to the Nepean Highway and is surrounded by congested residential and commercial areas. The surrounding topography is relatively flat.

2.2 Site geology

The subsurface ground conditions encountered across the five level crossings comprise the following:

- Fill material, comprising asphalt, road base, ballast, sands and gravels.
- Quaternary age sands (dune and beach deposits), comprising poorly graded and highly permeable, loose to dense sands.
- Quaternary age coastal lagoon deposits, encountered beneath the Quaternary age sands, comprising poorly graded and highly permeable, loose to medium dense sands and highly compressible clays of high plasticity.
- Tertiary age Sandringham Sandstone (previously known as Baxter Sandstone) comprising loose to very dense clayey sands and sands, occasionally cemented and firm to very stiff sandy clays.
- Gellibrand Marl (previously known as Newport Formation), encountered beneath the Sandringham Sandstone, comprising shelly sands and carbonaceous and glauconitic silts and clays (Tmn).

An extract from the Geological Survey of Victoria 1:63,360 Cranbourne map (1967) is shown by Figure 1. A generalised subsurface ground profile encountered is shown in Table 1.

Groundwater was typically encountered across the site between 3 and 5.5 mBGL (metres below ground level).
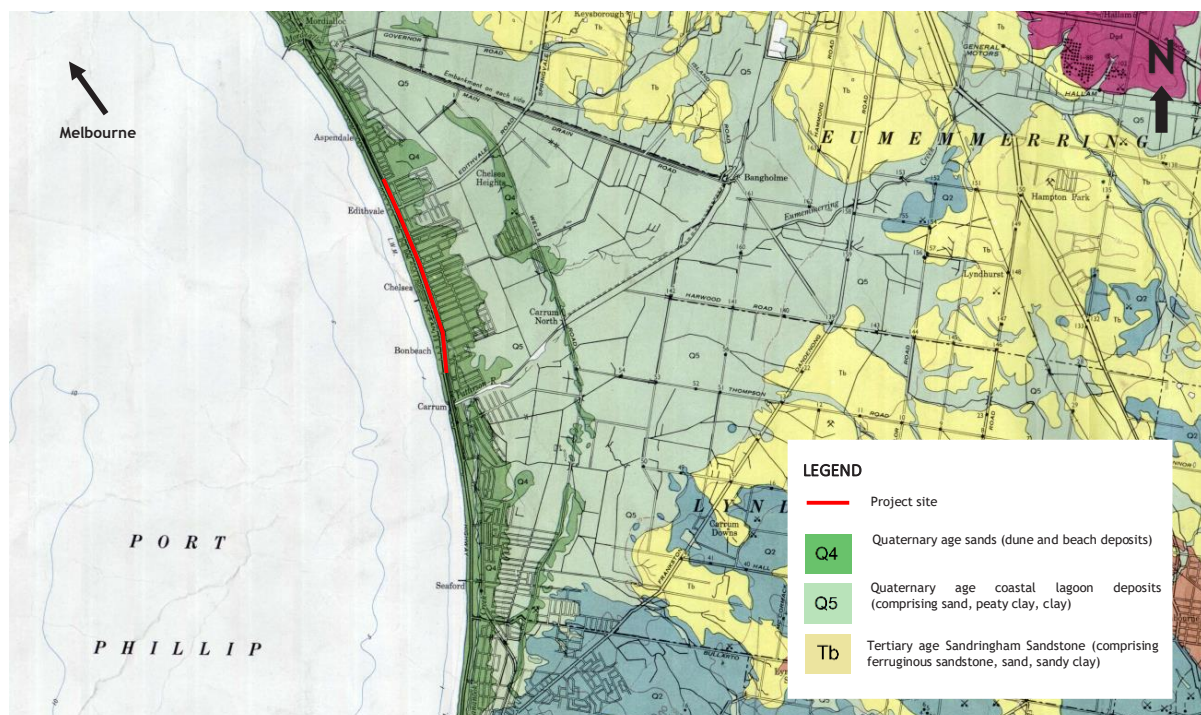

Figure 1. An extract from the Geological Survey of Victoria 1:63,360 Cranbourne map (1967)

PROCEEDINGS OF THE 14TH ANZ YOUNG GEOTECHNICAL PROFESSIONALS CONFERENCE
14YGPC ROTORUA, NEW ZEALAND, 2ND – 5TH NOVEMBER 2022

237

Table 1: A generalised subsurface ground profile encountered

Unit	Bonbeach		Chelsea		Edithvale	
	Depth to top of unit (m)	Depth to bottom of unit (m)	Depth to top of unit (m)	Depth to bottom of unit (m)	Depth to top of unit (m)	Depth to bottom of unit (m)
Fill material	0	0-1.0	0	0.1-1.2	0	0.2-0.5
Quaternary age sands	0-1.0	8.6-12.8	0.1-1.2	7.2-11.0	0.2-0.5	8.0-16.0
Quaternary age coastal lagoon deposits	8.6-12.8	10.7-15.2	7.2-11.0	11.0-14.3	8.0-9.0	9.1-13.5
Tertiary age Sandringham Sandstone	10.7-15.2	30.3*	11.0-14.3	27.0-30.5*	9.1-16.0	24.6-25.5*
Gellibrand Marl	NE	NE	27.0-29.3	NP	24.6-25.3	NP
NE= Not encountered, NP= Not penetrated, * Borehole terminated in unit						

3 INCLINOMETER INSTALLATION

The inclinometers were required to extend 3 m below the toe of the sheet pile retaining walls to ensure lateral ground displacements were captured along the entire length of the sheet piles. The length of the inclinometers varied between 19 and 21 m in length depending on the location of the inclinometer with respect to the rail trench. Due to the depth of the inclinometers, they were required to be installed across various geological units with highly variable geotechnical properties, which presented challenges during installation. The Quaternary age sands were highly permeable and vulnerable to collapse while greater borehole stability and lower permeability soils were observed throughout the Sandringham Sandstone geological unit.

The borehole drilling and inclinometer installation methodology previously implemented on other level crossing removal projects involved HQ wash boring to depth, removing the drill rods and installing the inclinometer casing in an unsupported borehole. This methodology was previously adopted due to the soils encountered predominately comprising of clay, therefore being less permeable and less vulnerable to collapse. However, inclinometer installations during this project were found to be challenging due to the saturated and granular nature of the surrounding soils. Boreholes drilled were vulnerable to collapse when removing the drilling casing, while a significant loss of grout was often experienced when installing the inclinometer casing. These ground conditions increased the risk of the inclinometer casings having poor contact with the surrounding soil and/or not reaching their proposed depths.

3.1 Drilling methodology

The drilling methodology selected is an important step in the installation process of inclinometer devices. Inclinometer boreholes are required to be drilled as vertical as possible, with minimal suspended solids and loss of soil material through the creation of voids. Ensuring minimal disturbance of the surrounding soil mass is crucial as it may potentially change the interaction between the soil mass and the inclinometer resulting in inaccurate measurements (Machan and Bennett, 2008).

As a result of shallow groundwater and loose granular soils encountered across the site, it was determined that the most suitable methodology for the drilling of the inclinometer boreholes was to use a combination of solid auguring and wash boring techniques. Solid auguring techniques were implemented down to a depth which would allow for the installation of drilling casing, after which the boreholes were drilled using PQ (OD 117.5 mm) wireline wash boring techniques. PQ wash boring techniques were adopted for the drilling of the inclinometer boreholes as the PQ drill rods ensured that the borehole walls were sufficiently supported, therefore reducing the risk of borehole collapse or loss of material resulting in voids forming during drilling and installation of the inclinometers. Highly concentrated polymer drilling mixtures were used during the drilling of the inclinometer boreholes to reduce water flush loss and to increase borehole wall stability. PQ diameter drilling was adopted instead of HQ (OD 88.9 mm), as the PVC inclinometer casing (OD 70 mm) was able to be installed within the larger diameter PQ drill rods. Once the inclinometer borehole was drilled to depth and the borehole sufficiently flushed out, the wash boring advancer was removed from the borehole using the wireline. The PQ drill casing was left in the ground to ensure that the borehole walls were adequately supported during the installation of the inclinometer casing. The PQ drill rods were removed from the ground immediately after the grout was tremie pumped into the borehole, as shown in Figure 2.

3.2 Inclinometer casing installation methodology

A flexible grouting tube was duct taped on the outside of the PVC inclinometer casing, approximately 200 mm off the end of the first casing segment to ensure that the grouting tube wouldn't get blocked by sediment at the base of the borehole. Due to ground water and drilling fluid being present at the time of installation, the PVC inclinometer casing was required to be water balanced while being installed into the borehole. Fresh water was slowly poured into the PVC inclinometer casing to reduce the positive buoyancy force which also reduced the likelihood of grout seeping from the annulus between the PVC casing and the borehole into the inclinometer casing. Sections of the PVC inclinometer casing were interlocked, and duct taped together until the casing was touching the base of the borehole with additional stickup. After the grout was tremie pumped, the flexible grouting hose was detached from the PVC inclinometer casing and removed from the borehole. The PQ drill rods were then removed from the borehole while leaving in the permanent inclinometer casing. The inclinometer casing installation methodology implemented is depicted by Figure 2.
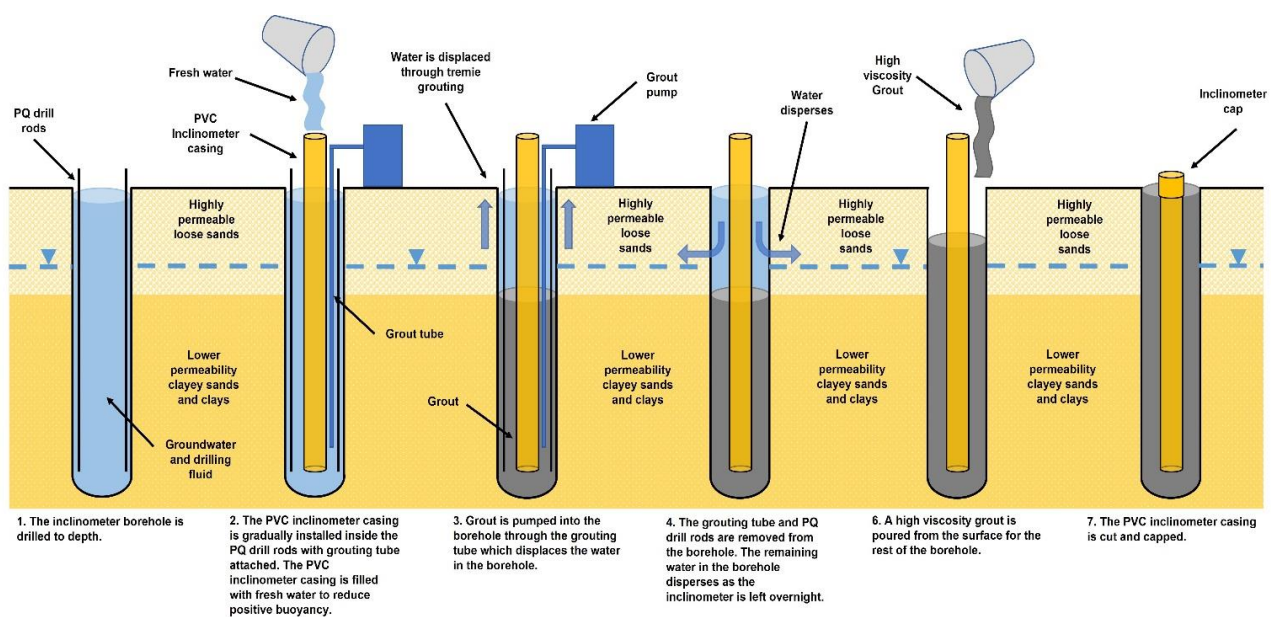

Figure 2. Inclinometer installation methodology implemented.

3.3 Selection of backfill material

The type of backfill material used to fill the annulus between the PVC casing and the borehole should ideally match the strength and stiffness of the surrounding soil mass to most accurately measure lateral ground displacements (Machan and Bennett, 2008). However, accurately matching the properties of the inclinometer backfill material to the surrounding soil can be impractical as the properties of the backfill and the surrounding soil can be significantly different, especially when installing across various geological units with varying geotechnical properties (Soil Instruments, 2014). In highly permeable ground conditions, granular backfill such as sand or gravel is preferred by some inclinometer suppliers. However, these materials can settle over time and are prone to bridging during backfilling, especially in deep inclinometers or when groundwater is encountered, due to the time taken for the backfill to settle to the base of the inclinometer (Machan and Bennett, 2008). Voids are likely to form as a consequence of the bridged backfilling material, resulting in reduced contact between the inclinometer and the surrounding soil mass. Therefore, it is preferable to select a backfill material which will completely fill the entire annulus and provide consistent contact between the inclinometer casing and the surrounding soil mass (Plinninger, et al. 2010).

Due to the varying ground conditions along the inclinometer casing and concerns of granular backfill bridging during the installation of the inclinometer, grout comprising rapid curing cement, powdered bentonite and water was used to backfill the annulus between the inclinometer casing and the borehole.

The viscosity of the grout was required to be high enough to prevent loss of grout to the surrounding soil while also low enough to allow for the grout to be pumped.

3.4 Annulus grouting methodology

Due to the permeable ground conditions encountered across the site, grout loss during inclinometer installation was a concern. The loss of grout during inclinometer installation could potentially stabilise the surrounding soil, therefore improving the ground conditions and reducing the amount of lateral displacement measured by the inclinometer. Alternatively, the loss of grout to the surrounding soil could result in voids in the inclinometer borehole if not completely backfilled with grout, resulting in improper contact between the inclinometer and the surrounding soil mass (Machan and Bennett, 2008). The highly concentrated polymer drilling mixtures used during drilling coated the borehole walls to create a semi-impermeable barrier, reducing the likelihood of loss of grout to the surrounding soil mass during inclinometer installation.

Two grout mixtures varying in viscosity were implemented to mitigate grout loss during inclinometer installation, while also allowing a portion of the grout to be tremie pumped. A 10:25:3 ratio of cement, water and powdered bentonite was typically used between 6 to 21 mBGL, where water loss during drilling was noted to be lower and where soils were generally observed to have higher relative densities or contain higher percentage of fines. These soils were typically less permeable and less vulnerable to borehole collapse. The viscosity of this grouting mixture was high enough to prevent loss of grout to the surrounding soil while also low enough to allow for the grout to be tremie pumped. The stiffness of the grouting mixture generally matched the ground conditions encountered. Soils encountered between ground surface level and 6 mBGL were generally observed to have low relative densities, contain a low percentage of fines and were vulnerable to collapse. In addition, significant water loss was observed while drilling through these highly permeable sand layers. A second higher viscosity grout was required between ground surface level and 6 mBGL to prevent grout loss through the poorly graded sands. To achieve a higher viscosity grout, a 10:25:9 ratio of cement, water and powdered bentonite was used. The second grout batch was required to be 'bucket' poured the following day as the grout mixture was too viscous to be tremie pumped. This also allowed for any remaining groundwater present above the first portion of grout in the borehole to disperse through the poorly graded sands. The grouting methodology implemented is depicted by Figure 2.

To further mitigate grout loss, the volume of grout which was tremie pumped was recorded along with the depth to which the grout was pumped to. These measurements were taken to back calculate the grout loss experienced during installation, allowing for alterations to be made to the installation methodology. Grout density tests and Marsh funnel readings were recorded to ensure the consistency of grout batches between the different inclinometers installed.

4 RESULTS

As the inclinometers are installed insitu, it is not easy to visually inspect whether the inclinometer has been installed correctly. However, the potential effectiveness of the newly adopted drilling and inclinometer installation methodology can be determined by the number of construction difficulties (loss of grout, borehole collapse, etc.) noted during installation potentially resulting in compromised data. The effectiveness of the installation methodology can also be determined by the consistency of the measured inclinometer data and the occurrence of data irregularities. If the measured inclinometer data is showing unusual results, this may potentially be a result of improper inclinometer installation. As the drilling and installation methodology was altered early in the inclinometer installation program, there is not enough inclinometer data from inclinometers which were installed using the old installation methodology. However, detailed records of any construction difficulties or as-built information were taken during the installation of the inclinometers. When comparing the newly adopted installation methodology with the previous methodology from other projects, fewer construction difficulties or issues were noted during the installation. The actual volume of grout used during the newly developed installation methodology more closely resembled the estimated required volume of grout as a result of reduced grout loss during installation. Greater borehole stability was also achieved as less borehole collapse was noted during drilling and installation, therefore resulting in a more consistent grout column around the inclinometer casing. Additional research should be conducted which compares inclinometer data from both drilling and inclinometer installation methodologies to determine their effectiveness more accurately.

5 CONCLUSION

The installation of inclinometers as part of the Bonbeach, Chelsea and Edithvale level crossing removal project was found to be challenging due to the saturated and granular nature of the surrounding soils. Drilling and inclinometer installation methodologies were developed to mitigate construction difficulties and potentially increase the reliability of the inclinometers installed. The risk of borehole collapse was mitigated through the use of PQ wash boring techniques and highly concentrated drilling polymers, while the risk of grout loss was mitigated by implementing two different grout mixes to target different geological units.

6 ACKNOWLEDGEMENTS

The author wishes to thank the Level Crossing Removal Project and the Southern Program Alliance for permission to produce this technical paper. The author also wishes to thank Richard Kaser for his assistance with the preparation of this paper.

REFERENCES

Dunnicliff, J., Green, G. E. (1993). "Geotechnical instrumentation for monitoring field performance", John Wiley & Sons, Inc., New York, USA.

Durham Geo Slope Indicator. "Grout mixing - Soil Instruments Knowledge Base", <https://soilinstruments.helpdocs.com/inclination/grout-mixing> [Accessed 25 July 2022]

HMA Geotechnical (2018). "Inclinometer casing installation manual", model 7040, <http://hmagrp.com/wp-content/uploads/2016/11/GEO-ML-0001-Inclinometer-Casing-Installation-Manual.pdf> [Accessed 20 July 2022]

Jenkin, J. J., Keble, R. A., Gostin, V., Thomas, D. E. (1967). "1:63,360 Cranbourne map", Geological Survey of Victoria, Department of Mines Victoria.

Kane, W.F. (2000). "Monitoring slope movement with time domain reflectometry",

Geotechnical Field Instrumentation: Applications for Engineers and Geologists, Washington, USA.

Machan, G., Bennett, V. G. (2008). "Use of inclinometers for geotechnical instrumentation on transportation projects", Transportation Research Circular E-C129, Transportation Research Board, Washington DC, USA.

Plinninger, R. J., Alber, M., Düllmann, J. (2010). "The influence of casing and backfilling materials on inclinometer measurements", Geologically Active - Proceeding's 11th IAEG Congress, Auckland, New Zealand, pp. 2361-2367.

Sargand, S. M., Sargent, L. and Farrington, S. P. (2004). "Inclinometer - time domain reflectometry comparative study", Ohio Research Institute for Transportation and Environment, Ohio University, Ohio, USA, pp. 4, 12-13.

Soil Instruments (2014). "Bentonite pellets/cement grout", user manual, <http://www.itmsoilsupport.com/manuals/Man171_Bentonite_Pellets.pdf> [Accessed 25 July 2022]

PROCEEDINGS OF THE 14TH ANZ YOUNG GEOTECHNICAL PROFESSIONALS CONFERENCE
14YGPC ROTORUA, NEW ZEALAND, 2ND – 5TH NOVEMBER 2022

241

14th YGPC 2022 Paper
Anchor investigation in weak, soft, mudstone to assess the impacts of flush type and potential of underream methods

D.B.Beasant

[1]Mount Messenger Alliance (MMA) comprising Downer Enterprises Ltd, HEB Construction Ltd, Tonkin & Taylor Ltd and WSP Opus New Zealand Ltd, in association with Waka Kotahi NZ Transport Agency.
[2]Tonkin & Taylor Ltd, Christchurch.

ABSTRACT

When installing anchors in weak argillaceous rocks selecting appropriate ultimate grout to ground bond strength parameters can be challenging, yet critical to ensure safe and rational anchor design. Literature notes groundwater and/or drill flush type can influence the ultimate bond strength due to water softening effects. One tool which can be deployed to increase the capacity of an anchor in weak rock is underreaming, locally increasing the diameter of the anchor fixed length. This paper summarises anchor investigation tests undertaken in the Mount Messenger Formation in North Taranaki. It compares the ultimate capacities of straight shafted anchors drilled with air and water flush, in addition to an underream anchor. The data presented may support anchor practitioners working in similar 'papa' lithologies, or equivalent Late-Miocene soft rocks in New Zealand and internationally.

Keywords: anchor, investigation, mudstone, underream, water-softening.

1   INTRODUCTION

1.1   Project requirements

Mount Messenger is a remote area 50 km north-east of New Plymouth in Taranaki, NZ. The existing section of State Highway (SH3) in Mount Messenger is steep, narrow and winding. The Te Ara o Te Ata: Mt Messenger Bypass project provides a new 6 km upgrade improving safety and resilience. A temporary cableway is required to provide early access for critical path construction activities. This is a significant engineering feat with heli-access constraints and anchor demands of approximately 4.5 MN.
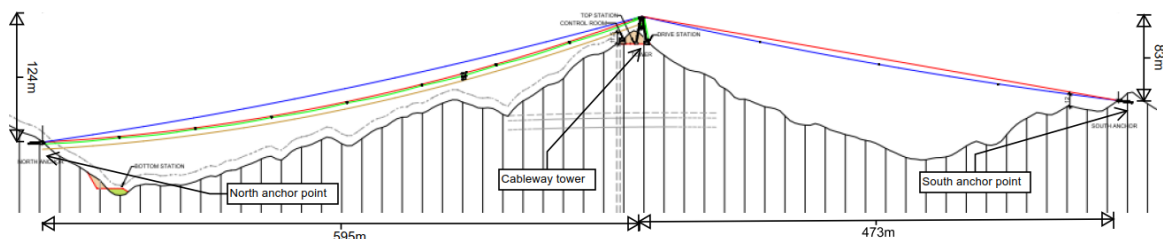

Figure 1: Cableway general arrangement with the north anchor block, the south anchor block and the tower.

An investigation was carried out to confirm both the ultimate bond strength parameters appropriate for design and the constructability of the anchors with the plant and equipment proposed.

1.2   Ground conditions

The host rock in the area is known as the Mount Messenger Formation (11-9 Ma). These typically soft rocks include a continuum of silty, fine grained sandstones to silty mudstones. Bedding is typically thick to massive dipping gently (around 2 to 4°) towards the west.

Table 1: Summary of typical engineering parameters of the Mount Messenger Formation (MMF).

Bulk density (t/m³)	UCS (MPa)	Moisture content (%)	RQD %	GSI	RMR	E (GPa)	SPT (N value)
2.1 to 2.25	1 to 5	13 to 22	75 to 90	70 to 80	41 to 60 (fair rock)	0.1 to 1.0	>50 for 15 to 40 mm

There is little published data for anchor testing in similar 'papa' lithologies in the Taranaki area, or equivalent Late-Miocene soft rocks in New Zealand, and internationally.

2   LITERATURE REVIEW

A literature review was undertaken to assist in designing the anchor investigation in the MMF. Part of this is presented below.

The simple design equation for calculating the ultimate capacity of an anchor in rock is:

$$T_{ult} = \pi \cdot d \cdot L_{fix} \cdot \tau_{ult} \quad [Eqn. \ 1]$$

where: d = anchor diameter, L_{fix} = anchor fixed length and τ_{ult} = ultimate bond stress.

Equation 1 above assumes a uniform load distribution at the grout-ground interface and ignores the progressive debonding phenomena which occurs on longer anchor fixed lengths.

Littlejohn (1980) found that the bond mobilised at the grout-ground interface is unlikely to be uniform unless the rock is soft and/or the modular ratio (E_{Grout}/E_{Rock}) is > 10.

Progressive debonding occurs due to differing elastic properties of the tendon, grout and ground. Barley (1995) notes this phenomenon to be negligeable in short anchors and only relevant to longer fixed lengths. The mechanism of progressive debonding is depicted in Figure 2 below.
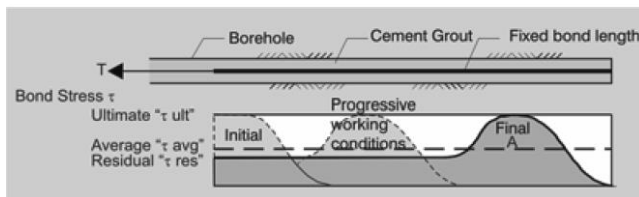

Figure 2: Development of bond stress distribution along a fully bonded fixed anchor length (Barley, 1995).

Numerous authors have undertaken research and proposed efficiency factors to account for progressive debonding on anchors with longer fixed lengths. However, efficiency factor studies are generally limited to investigations of anchor performance in sands and clays.

$$T_{ult} = \pi \cdot d \cdot L_{fix} \cdot \tau_{avg} \qquad [Eqn. \ 2]$$

Minor modification to Equation 1: $\tau_{avg} = \tau_{ult \ x \ f_{eff}}$ = average bond stress mobilised along fixed length at the ultimate load.

Water softening can occur in fine grained argillaceous rocks resulting in reduced grout to rock bond strength. Barley (1988) and Weersinghe (1993) noted water to cause softening of borehole walls in mudrocks. The standard BS 8081 (2018) notes the time between drilling and grouting to be of vital importance in materials susceptible to water softening.

Weersinghe (1993) in his study on behaviour of anchorages in weak mudstone notes there are two ways to enhance the capacity of weak rock anchorage systems:
1. Distribute load in fixed length uniformly e.g. SBMA or multi-stage anchors.
2. Increase mechanical interlock at grout-ground interface e.g. underreams.

Weersinghe & Littlejohn (1997) found a single underream in weak mudstone increased anchor capacity by 145% in comparison to that of a straight shafted anchor. BS 8081 (2018) provides the following equation to calculate the ultimate grout-ground resistance of underream anchors:

Ultimate geotechnical capacity = side shear underream + end bearing + side shear (no underream).

$$R_{GG;calc} = \pi D L_{fixed(U)} c_s + \frac{\pi}{4} (D^2 \text{-} d^2) N_c c_b + \pi d L_{fixed(NU)} c_a \qquad [Eqn. \ 3]$$

Where; D and d, are diameter of straight shaft and enlarged lengths, $L_{fixed(u)}$ and $L_{fixed(Nu)}$ are fixed lengths of underream and non-underream lengths, c_s c_b and c_a are average bond strength(s) and Nc is the bearing capacity factor.

3   ANCHOR INVESTIGATION

3.1   Aim
The aims of the anchor investigation were:
1.   Confirm the ultimate grout-ground bond strength of a 200 mm diameter bore in the MMF.
2.   Drill anchors with air flush and water flush to investigate impact on bond strength.
3.   Install an underream to assess suitability of this method for anchoring in the MMF.
4.   Drill anchors with a helicopter portable rig to confirm constructability.

PROCEEDINGS OF THE 14TH ANZ YOUNG GEOTECHNICAL PROFESSIONALS CONFERENCE
14YGPC ROTORUA, NEW ZEALAND, 2ND – 5TH NOVEMBER 2022

243

3.2 Construction and testing

Three test anchors were installed in April 2022 using a rubber tracked mini skid steer (Vermeer S925TX) with a drill mast attachment (combined weight of 1.5t). Two Atlas Copco (XAS400) compressors provided air flow (800 CFM) to the drill string. Where water flush was used it was delivered at 60 to 80 L/M (Litres per Minute). All three anchors were drilled 15° below the horizontal with down the hole camera inspections completed prior to installing Titan Ishbeck (103/51) bar tendons. All anchors were grouted using a hydraulic powered twin bowl shear mixer grout plant within 3 hours of the fixed length being drilled and flushed clean. Investigation testing was undertaken in accordance with BS EN 1537 (2013) using Test Method 1 as outlined in ISO 22477-5 (2018).
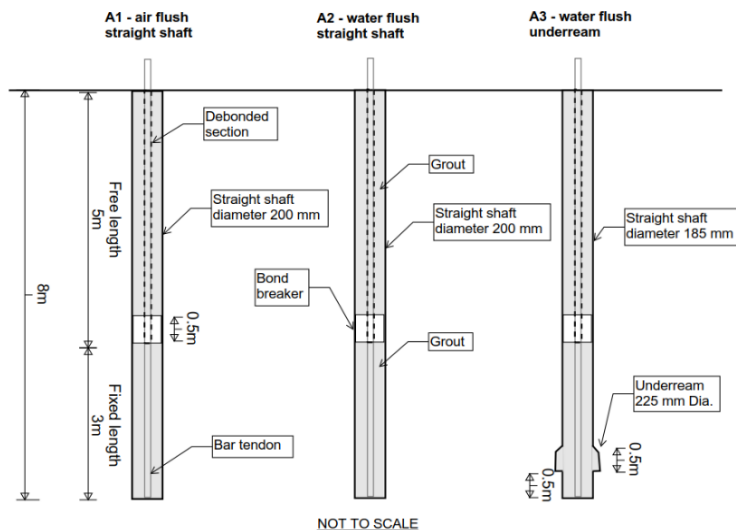

Figure 3: Sketch of the three investigation anchors installed in the Mount Messenger Formation.

Figure 4 below presents photos of the drilling equipment and demonstrates investigation activities.

a. The 200 mm diameter Poly Crystalline Drill (PCD) bit.

b. The 185 mm diameter drag bit.

c. The 225 mm diameter underreamer with blades 'flared' behind the drag bit.

d. Installing a 7 m long bar tendon section.

e. Grout flowing out of proximal end of the anchor hole.

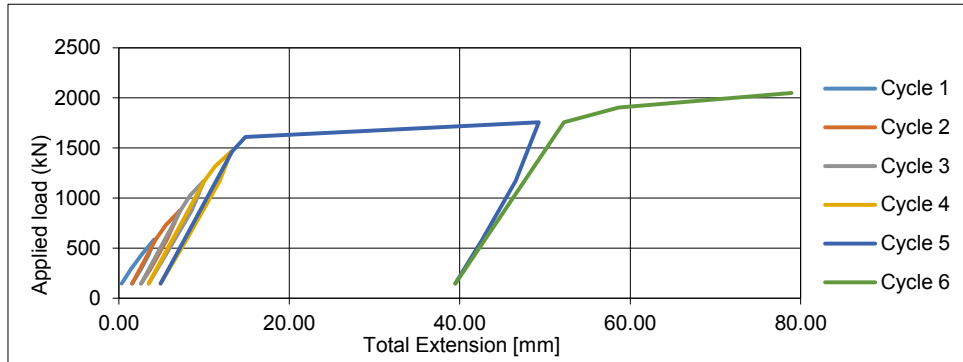*f. Typical anchor investigation test set up.*

Figure 4: Construction and testing photos from investigation trial.

3.3 Results

Investigation tests were designed to fail at the grout-ground interface over nine incremental load cycles to a proof load (2,928 kN).

3.3.1 Test data

The investigation test data is presented below for the three anchors.

Figure 5: Anchor A1 (air flush) investigation test failed on creep on the sixth load cycle.

Upon building to the peak load increment of cycle 5 with anchor A1, approximately 30 mm displacement occurred before stabilising at the peak load. A release of friction between the bar and whaler is suspected to have caused the excessive displacement as damage to the underside of bar was identified post-test.
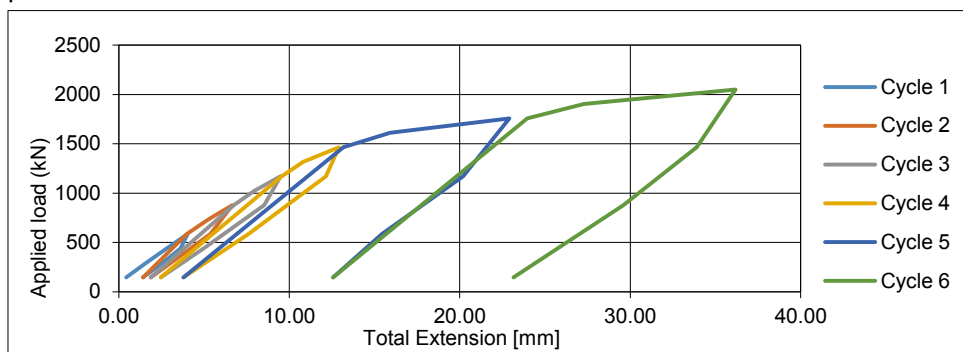
Figure 6: Anchor A2 (water flush) investigation test failed on creep on the sixth load cycle.

After creep failure was noted and cycle 6 was completed, the anchorage was overloaded in a 7th cycle to investigate the peak load and residual capacity. The peak load sustained by the anchor was 2,685 kN with a gradual pull-out noted (no sudden release). After approximately 50 mm of additional displacement, the residual load recorded was 2,600 kN. The load-displacement readings from the overload test are not presented in Figure 6.
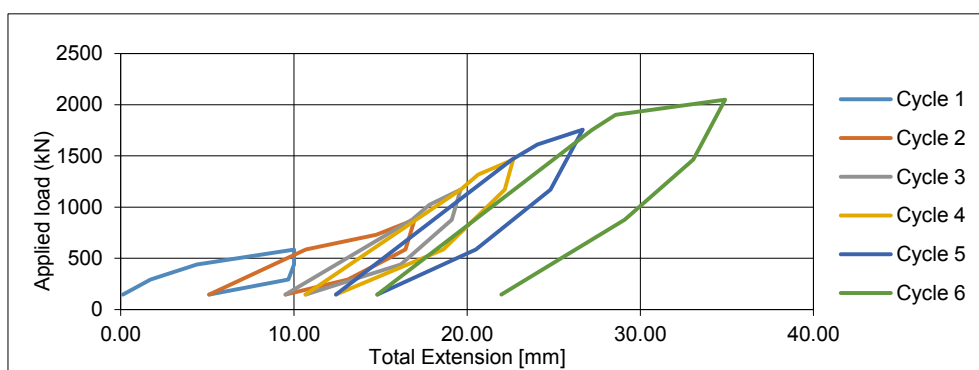
Figure 7: Anchor A3 (underream) investigation test failed on creep on the sixth load cycle.

Issues with the test set-up on Anchor A3 resulted in irregular displacement readings in cycle 1 to 2. The waler did seat properly until higher loading, as evident in Figure 8 (cycle 3 onward). After creep failure was noted in cycle 6, anchor A3 was overloaded in a 7th cycle with a peak load of 2,685 kN held. This was followed by a sudden release and drop in load to 2,300 kN. This residual load of 2,300 kN was held by the anchor after an additional 50 mm of displacement. The load-displacement readings from the overload test are not presented in Figure 7.

PROCEEDINGS OF THE 14TH ANZ YOUNG GEOTECHNICAL PROFESSIONALS CONFERENCE
14YGPC ROTORUA, NEW ZEALAND, 2ND – 5TH NOVEMBER 2022

245

3.3.2 Data interpretation

Apparent tendon free lengths were found to be generally in accordance with ISO 22477-5 (2018) indicating the anchors had well-formed free lengths. The geotechnical resistance Ultimate Limit State (ULS) criteria for Test Method 1 was used in the creep assessment. A creep ($\alpha 1$) limit of 2 mm was adopted as specified in EC7 (2013). Ultimate loads are determined graphically in Figure 8 below.
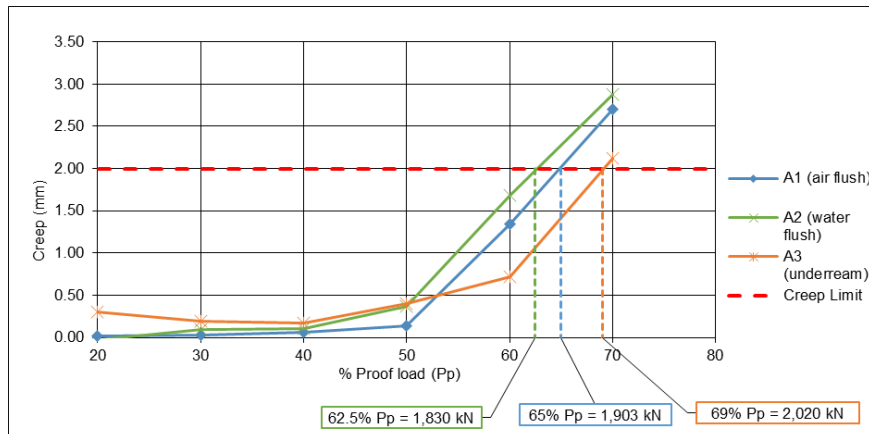

Figure 8: Graph of proof load vs creep showing the geotechnical ultimate capacities derived for each anchor.

A creep displacement vs log time plot is presented below for test cycles 4 (1,464 kN) and 5 (1,757 kN) to compare creep rates at the load cycles prior to failure (cycle 6). The creep rate at 1,464 kN has been extrapolated to estimate creep displacements over a one-year period.
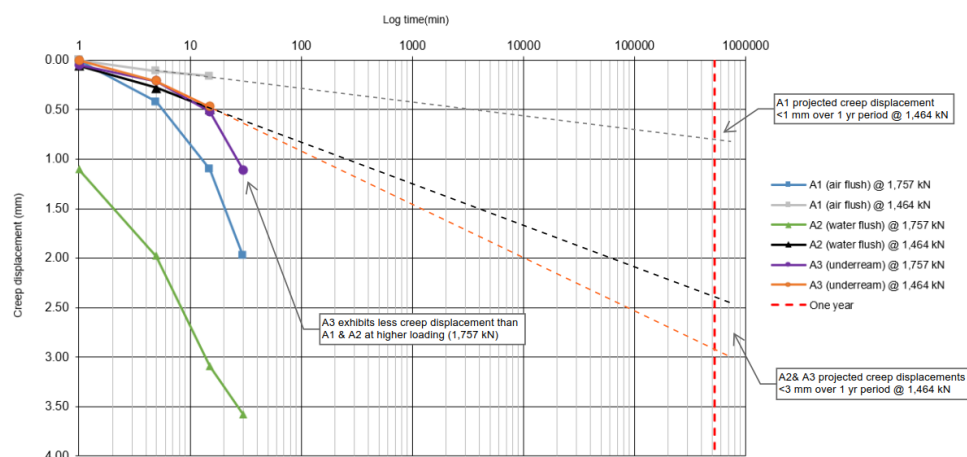

Figure 9: creep displacement vs log-time plot.

The anchor test results are summarised in Table 2 below.

Table 2: Summary of anchorage investigation test results.

Anchor ID	Bond length (m)	Bond area (m²)	Failure mechanism	Failure load (kN)	Ultimate bond capacity (kPa)
A1 (air flush)	3.0	1.885	Creep	1903	1010
A2 (water flush)	3.0	1.885	Creep	1830	971
A3 (water flush, underream)	[1]3.0	[2]1.806	Creep	2020	1,118

Table notes:

1. The bond length of anchor A3 comprised a 185 mm diameter, 2.5 m long straight shaft section and a 0.5 m underream length approximately 7.0 to 7.5 m into the anchor.
2. The down the hole camera footage indicates the underream may have had a smaller area due to tapered edge at the proximal end. This would result in a conservative ultimate bond capacity being calculated for A3.

4   DISCUSSION

The investigation tests indicate the principal mode of failure in the MMF is creep. This mechanism may also be dominant in other similar 'papa' lithologies or equivalent Late-Miocene soft rocks.

The underream anchor (A3) demonstrated a higher ultimate capacity than the two straight shafted anchors. Due to a reduced straight shaft diameter the capacity is not readily comparable to anchors A1 and A2. Installing a single 225 mm diameter underream in a 185 mm straight shaft anchor increased the load capacity by approximately 120% (π x 0.185 m x 3.0 m x 971 kPa = 1,693 kN).

Weersinghe & Littlejohn (1997) underream investigation in weak mudstone proved a 145% increase in capacity however it is noteworthy their underream to straight shaft (D/d) diameter ratio was >2.0 (280/130mm). The D/d ratio in this trial was ~ 1.22. A higher D/d ratio is expected to translate to increased capacity through additional end bearing.

The creep log-time plot (Figure 9) was used to compare creep rates at the peak load increment of cycle 4 (1,464 kN) and cycle 5 (1,757 kN). During cycle 4 it is noteworthy that the creep rate when extrapolated to one year, indicates water flush anchors (A2 & A3) may creep 2-3 times more than the anchor drilled with air flush. A longer hold period would have been required to confirm this trend.

The creep log-time plot shows at higher loads (cycle 5) the underream anchor (A3) creeped the least. This indicates the benefit of underreams are realised at higher loads after load-displacement of the proximal fixed length above. Anchor overload investigations (post creep failure) indicate residual loads in MMF to be high.

The straight shafted anchors (A1 & A2) pulled out slowly, whereas the underream anchor (A3) exhibited a sudden release. Using Equation 3 (Section 2) to estimate the ultimate design resistance of the underream anchor the estimated capacity is 2,279 kPa. This is 10% higher than the failure load determined (2,020 kN). There are two inaccuracies which may have contributed to this over-prediction:

1. The underream has a tapered edge rather than the cylinder assumed.
2. Grout-ground capacities (c_a, c_b and c_s) were assumed to be equal (971 kPa).

Based on the more sudden failure mode witnessed with A3 during the trial, the author suspects the load was concentrated in the underream and the 0.5 m long, 185 mm diameter straight shafted section beneath the underream was sheltered from applied loads. Assuming this 0.5 m section provided negligeable contribution to the design resistance prior to failure, the estimated capacity is:

$$R_{GG;calc} = [\pi \text{ x } 0.225 \text{ m x } 0.5 \text{ m x } 971 \text{ kPa}] + [\frac{\pi}{4} (0.225^2 \text{-} 0.185^2) \text{ x } 42 \text{ x } 971 \text{ kPa}] + [\pi \text{ x } 0.185 \text{ m x } 2.0 \text{ m x } 971 \text{ kPa}]$$

$$= 1,997 \text{ kN. (Estimated capacity 2)}$$

Underream anchor (A3) estimated capacity 2 is within 1% of the value proven in the trial.

5   CONCLUSION

The findings of this investigation are strictly only applicable to the MMF. Geological engineering parameters are presented (Section 1.2) for the host rock to enable other anchor practitioners to assess the relevance of this investigation to their projects. Despite the limited number of investigation tests undertaken, the author hopes this case study will help the industry optimise anchor performance in similar very weak, soft, mudstones.

Conclusions are presented as follows:
- Ultimate grout to ground bond strengths in the MMF were found to be similar (within 5%) when using air or water flush drilling techniques [τult = 1,010 kPa (dry), τult = 970 kPa (wet)].
- Potential water softening effects from drilling with water flush can be controlled in the MMF if bores are flushed with clean water (multiple times) at 70 litres/minute and anchors are grouted within 3 hours of drilling.
- Anchors drilled with water flush may exhibit more creep displacement over time in comparison to those drilled with air flush.
- A single underream installed at the distal end of a 3 m anchor fixed length in the MMF increased the ultimate load capacity by approximately 20%.

6   ACKNOWLEDGEMENTS

PROCEEDINGS OF THE 14TH ANZ YOUNG GEOTECHNICAL PROFESSIONALS CONFERENCE
14YGPC ROTORUA, NEW ZEALAND, 2ND – 5TH NOVEMBER 2022

247

A Case Study on Dispersive Soils – Saraji Mine, Dysart (QLD)

M.I.B. Wijekoon[1], MIEAust

[1]Jacobs Group (Australia) Pty Ltd, Level 12, 452 Flinders Street, Melbourne VIC 3000; PH +61 499 202 888; email: maneesha.wijekoon@jacobs.com

ABSTRACT

The presence of excess exchangeable sodium ions is one of the main causes of dispersive behaviour in clayey soils. However, the presence of excess exchangeable cations other than sodium can also promote dispersion in soils. In this paper, the effect of the presence of excess exchangeable magnesium and sodium ions in dispersive soil were investigated and an assessment on the effectiveness of using the Australian Standard Emerson Class Number (AS ECN) testing standard to identify dispersive soil was undertaken. This case study was based on geotechnical investigations undertaken for the design of Coolibah Dam and Drain at Saraji Mine, Dysart. Laboratory testing undertaken on various samples collected during investigations completed for the dam and drain confirmed the presence of sodic and abnormal levels of magnesic soils. Although it's well established that sodicity is a main driver of dispersion, effect of magnesicity in soils is not well defined. Further laboratory testing suggested the presence of magnesic soil may also promote dispersion. Dispersive soil samples were treated with gypsum to reduce the amount of exchangeable sodium and magnesium based on the cation exchange capacity. Whilst gypsum treatments chemically stabilised the soil, they failed to satisfy the visual based criteria from ECN testing as defined in the Australian Standards (AS). The presence of excess exchangeable sodium and magnesium ions has been identified as a likely factor promoting dispersion. Furthermore, a review of the current AS ECN testing standard is suggested as it does not effectively amalgamate the chemical properties of soil which effect soil dispersion.

Keywords: Dispersive soil, sodic soils, magnesic soils, Emerson Class Number, Modified Emerson Aggregate Test, gypsum treatment

1 INTRODUCTION

Dispersion is the phenomenon of clay particles detaching from adjacent clay particles in a soil when exposed to wet conditions. This detachment causes the clay aggregates to structurally breakdown which presents a plethora of problematic properties in the soil. High erodibility can create rill and gully erosion on surfaces, piping and tunnel erosion below the surface, poor soil stability, chemical imbalances in the soil resulting in low soil fertility and extremely poor plant growth (vro.agriculture.vic.gov.au, 2019).
Research has clearly identified that the presence of excess exchangeable sodium ions in clayey soils results in the phenomenon of dispersivity. According to Northcote and Skene (1972), soils with an Exchangeable Sodium Percentage (ESP) greater than 6% of the Cation Exchange Capacity (CEC) are known as 'sodic soils' and those with an Exchangeable Magnesium Percentage (EMP) excess of 15% are 'strongly sodic soils'. According to data published by the Queensland Government (2014), sodic soils are known to be problematic throughout North and Central QLD and approximately 45% of soils in QLD are considered to be sodic.

Similar to sodic soils, soils with an EMP greater than 25% of the CEC are known as magnesic soils. It has been further identified that magnesic soils can also become unstable under wet conditions and have the potential to promote dispersion when the magnesium ion concentration is high in relation to other cations. Although the contribution of magnesic soils towards soil dispersion has been identified, it has not been defined to the level of the effects of sodic soils (Upjohn et al., 2005).

To reduce the effects of sodic soils it is generally recommended that the cation balance be altered by increasing the relative proportion of calcium in the soil while reducing the relative proportion of exchangeable sodium. This is usually achieved by the introduction of gypsum ($CaSO_4.2H_2O$) into the problematic soil, which is favoured due to its solubility, low price and it does not alter the soil pH (vro.agriculture.vic.gov.au, 2019).

The Emerson Aggregate Test (EAT) (Emerson, 1967) which in its current Australian Standard form in AS 1289.3.8.1: 2017 titled "Determination of Emerson Class Number" (AS ECN) is the most common test referred by engineers for identifying dispersive soils. Although the determination of CEC and Exchangeable Cations (i.e. ESP and EMP) are the most accurate chemical testing methods to identify

sodic, magnesic and potentially dispersive soils, AS ECN testing is commonly used as a cheaper screening method to identify whether the soils are likely to be dispersive and therefore identify a need for further, more expensive chemical testing to confirm soil dispersivity.

The degree of dispersion in the EAT test depends not only on ESP, but also on the relative Exchangeable Calcium Percentage (ECP) and EMP (Emerson, 1983). Furthermore, sodic soils with high EMP are more susceptible to dispersion than those with high ECP. Loveday and Pyle (1973) refined Emerson's test by subdividing the classes and taking the rate and degree of dispersion into account. Their test was highly correlated with ESP. However, their testing was limited to soils from certain areas of Central West NSW and did not correlate ESP to Emerson's original classes.

Numerous other researchers have related observed dispersion to ESP (Emerson, 1983). However, all of these studies were conducted on a small range of soils or on artificially prepared soils with specific ESP, mineralogy and solution composition.

2   METHODOLOGY

Samples from the footprints of the Coolibah Dam and Drain were obtained during geotechnical investigations undertaken in 2018 during the design phase of the project. The investigation comprised five (5) test pits excavated within the proposed Coolibah Dam footprint and four (4) test pits excavated along the Coolibah Drain alignment. All the test pits were excavated to a target depth of 4m. The collected samples were subjected to four phases of laboratory testing as described below.
Phase 1 of the laboratory testing included AS ECN and Particle Size Distribution (PSD) testing and was used to identify whether the soils were likely to be susceptible to dispersion and erosion. Two (2) samples each from the Coolibah Dam and Drain sites were used for this phase of testing. Results of Phase 1 testing identified that all the soil samples had an AS ECN of 2 and were therefore likely susceptible to dispersion. Further testing was required to understand the cause/s of the observed AS ECN values.

Phase 2 of the laboratory testing included chemical testing in addition to the AS ECN and PSD testing, specifically: Exchangeable Cations, CEC, Chloride Content, Electrical Conductivity (EC) and pH Value. These chemical tests were used to determine the chemical properties of the soil samples which demonstrated likely dispersive characteristics. Nine samples, namely one from each test pit were submitted for Phase 2 testing. An additional 27 gypsum treated samples (created by mixing the soils with gypsum at rates of 0.5%, 1.0% and 1.5% (by mass) were subjected to the same suite of chemical testing. The gypsum dosage rates were initially calculated based on the requirement to neutralise the ESP (based on the total CEC of the soil) which was initially thought to be the dominant factor which promotes dispersion in a soil. The mixing of gypsum with the relevant soil samples was undertaken using minimal amounts of water to make small, plasticine-like aggregates for testing. Results of Phase 2 testing indicated that the addition of gypsum showed minor improvement in the AS ECN of the treated soil samples. Out of the total nine (9) samples tested during this phase only two (2) samples showed a significant improvement where the AS ECN increased from 2 to 4. According to the results of Phase 2 testing, it was understood that it is likely that the added amount of water may not have been the optimal amount required for the gypsum to properly dissolve in order to facilitate the migration of calcium ions into the soil sample and/or to react with adequate amounts of sodium ions on the colloidal surfaces. Also, the duration assigned for the reaction to take place during the experiment may not have been sufficient for the gypsum to completely react during this phase of testing. These shortfalls were rectified in the next two phases of laboratory testing.

Phase 3 of the laboratory testing was undertaken by using the same gypsum rates with a more rigorous mixing procedure to better enable the chemical reactions to take place. This was also undertaken to replicate the possible field methodology used during the construction phase of the project. The material was initially broken down to <2mm particle size and then the gypsum was added to the soil along with enough distilled water to create a slurry. The soil was then soaked for 3 days, mixed with a hydrometer mixer in an effort to speed up the gypsum–water–soil chemical reactions and allowed to sit for a minimum of 24 hours prior to drying in a 45°C oven for a day. After the slurry had dried, some of the sample was broken apart for AS ECN testing. In addition to AS ECN testing, the same suite of chemical testing undertaken during Phase 2 was carried out at this phase. Gypsum addition rates of 1.0% and 1.5% (by mass) were trialled during this phase. Also, samples subjected to AS ECN tests were photographed to enable further visual based analysis of the dispersive behaviour of soil. The results of

PROCEEDINGS OF THE 14TH ANZ YOUNG GEOTECHNICAL PROFESSIONALS CONFERENCE
14YGPC ROTORUA, NEW ZEALAND, 2ND – 5TH NOVEMBER 2022

249

Phase 3 indicated only minor improvement in the AS ECN, even after following the more vigorous mixing methodology. However, the chemical testing undertaken during this phase revealed that all the gypsum treated samples were within the accepted criteria for chemically stable and productive soils (detailed further in Section 3) and therefore likely non-dispersive. Although chemical tests revealed the soils were chemically stable and productive and likely non-dispersive, soil samples were put through a final phase of testing (Phase 4) to gain further understanding of the dispersive behaviour still observed in the AS ECN testing on the gypsum treated samples.

Phase 4 laboratory testing was undertaken by using the same rigorous mixing procedure whilst increasing the gypsum addition rates to 2.5%, 5.0% and 10.0% (by mass). The AS ECN results of these samples increased to 4 for the samples which were mixed with 10% (by mass) gypsum. As the chemical composition of samples tested in Phase 3 were within the acceptable range for non-dispersive soils, additional chemical testing was not undertaken in this phase of testing. Similar to Phase 3 testing, samples subjected to AS ECN tests were photographed to enable further qualitative visual based analysis of the dispersive behaviour of soil. A visual assessment was undertaken using the photographs of the samples from Phases 3 and 4. The assessment was based on the modified EAT classification method provided in the Queensland Department of Transport and Main Roads (QDTMR) Road Drainage Design Manual (RDDM) from June 2002 (now superseded) which provides three additional subclasses for AS ECN 2 and two additional subclasses for AS ECN 3. The probability of sodicity occurring within these sub-classes are in the following order: 2(3) > 2(2) > 2(1) > 3(4) > 3(3) > 3(2) > 3(1).

3   DISCUSSION

Results obtained from the chemical testing were compared based on a set of desirable common indicators utilised to define chemically stable, non-dispersive and productive soils (soils which supports plant growth) which were developed from the data of Reuter and Robinson (1997), Peverill et al. (1999), Standards Australia (2003), Incitec Pivot Ltd (2008), Hazelton and Murphy (2007) and QDTMR (2017). Table 1 provides a summary of the desirable values of the indicators utilised to define stable productive soils. It should be noted that the analysis undertaken for this case study was based only on the main indicators which influence the characteristics of stable productive soils. Other indicators such as Electrical Conductivity (EC), Chloride Content and soil pH have not been taken into consideration during the assessment undertaken within this case study.

Table 1:   Desirable values of the indicators (i.e. Exchangeable Cations (ESP and EMP), CEC and AS ECN) for stable productive soils.

Parameter		Desirable range	Unit
Exchangeable Cations Proportions	Exchangeable Sodium percentage (ESP)	<6	%
	Exchangeable Magnesium percentage (EMP)	15 – 25	%
Exchangeable Cations Abundance	Cation Exchange Capacity (CEC)	>6	meq/100g of soil
	Exchangeable Magnesium	>0.2	meq/100g of soil
Australian Standards Emerson Class Number (AS ECN)		≥4	-

3.1   Exchangeable Cations
3.1.1   Exchangeable Sodium Percentage (ESP)

Results of Phase 3 testing obtained from untreated samples showed high ESP values which lay well outside the desirable range for ESP < 6% for a non-dispersive soil. These high ESP values in untreated soil suggested that soils from the Coolibah Dam and Drain sites are highly sodic. Hence, the treatment of soil with gypsum was introduced, in order to reduce the high ESP values to obtain non-dispersive characteristics and to chemically stabilise the soil. Figure 1 shows the variation of ESP of multiple samples with gypsum treatment rates varied between 0.0%, 0.5%, 1.0% and 1.5% by mass added to the soil to determine the optimum amount of gypsum required. The results shown in Figure 1 suggest that the ESP of the majority of the samples are reduced to the desirable range at a gypsum treatment rate of between 0.5% and 1.0%.
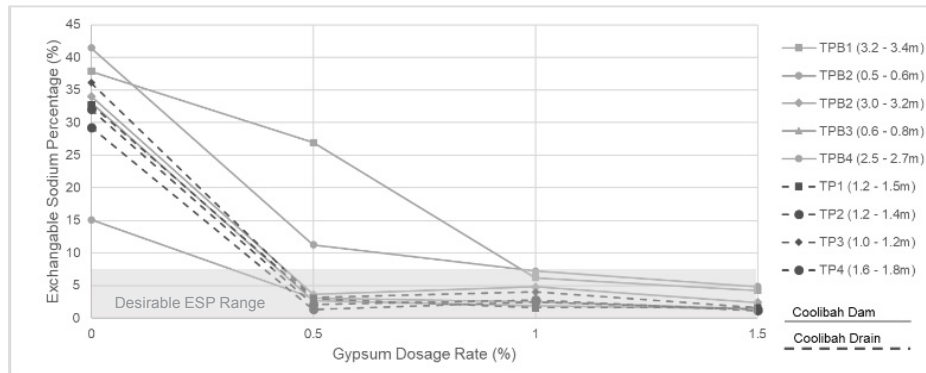
Figure 1. ESP vs Gypsum Rate

3.1.2   Exchangeable Magnesium Percentage (EMP)

Untreated soil samples at Coolibah Dam and Drain showed EMP values above the recommended range for non-dispersive soils which support plant growth. This indicated that the soils are highly magnesic and that the presence of high levels of exchangeable magnesium could also be a cause soil dispersion (in addition to the more common cause attributed to high ESP which is further discussed in Section 3.2). The variation of EMP of the soils with gypsum treatment rates of 0.0%, 0.5%, 1.0% and 1.5% by mass are depicted in Figure 2.
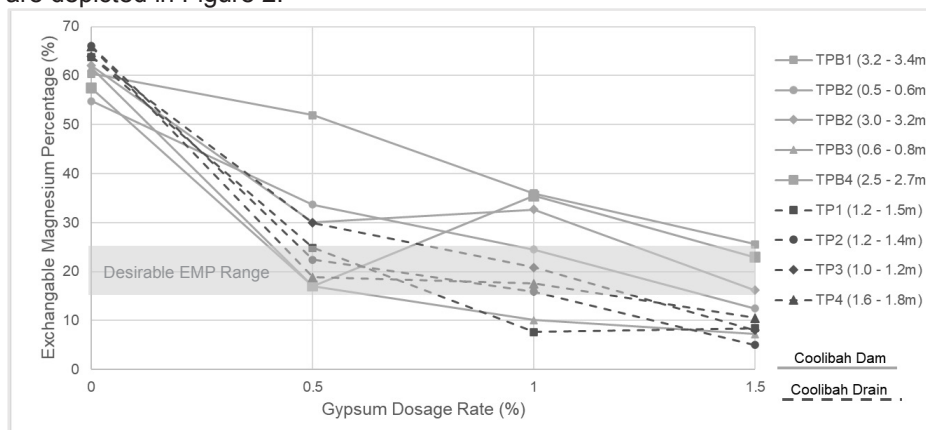

Figure 2. EMP vs Gypsum dosage rate.

With the application of gypsum, the EMP of the soil samples reduced significantly. The EMP of the majority of the soil samples fell below the desirable range by a gypsum rate of 1.5%. Although the EMP fell below the desirable range at this gypsum rate, a conclusion could not be categorically made that the ameliorated soil would not support plant growth because the exchangeable magnesium abundance requirement for non-dispersive soils which supports plant growth (being >0.2meq/100g) was fulfilled in all instances based on the laboratory test results. Accordingly, the optimum gypsum dosage rate (considering only ESP and EMP criteria for non-dispersive soils) to reduce excess sodium and magnesium in these soil samples lies between 1.0 and 1.5%. It should be noted that the results for cation abundance testing are not presented due to page limit limitations of this paper.

3.2   Cation Exchange Capacity (CEC)

CEC is the total capacity of a soil to hold exchangeable cations. According to the laboratory results shown in Figure 3, the results indicated that the CEC which was previously below the desirable range in many samples could be improved to be within the desirable range by the treatment with 1.5% (by mass) gypsum to the soil samples being assessed.

As discussed in Section 3.1, the ESP of the soil samples were reduced to the recommended range at a gypsum treatment rate of 1.0% (by mass). Although the ESP levels were satisfied, as shown on Figure 3, the CEC of some of the soil samples at this gypsum treatment rate did not necessarily lie within the recommended range. This suggested the presence of additional exchangeable cations which influenced

PROCEEDINGS OF THE 14TH ANZ YOUNG GEOTECHNICAL PROFESSIONALS CONFERENCE
14YGPC ROTORUA, NEW ZEALAND, 2ND – 5TH NOVEMBER 2022

251

the CEC of the soil other than sodium in some of the soil samples. In this case it was quite evident that the additional exchangeable cations were the excess magnesium observed in these samples of soil. Hence, it was understood that the excess magnesium and sodium present in the soil were likely factors promoting dispersion.

This was further validated by analysing the CEC and EMP levels at a gypsum rate of 1.5% (by mass). With the reduction of excess magnesium in the soil samples at a gypsum rate of 1.5% (by mass), the CEC of the samples improved to the recommended range as shown in Figure 3. Subsequently, it appeared that a gypsum treatment rate of 1.5% (by mass) was necessary to achieve the desirable criteria for ESP, EMP and CEC to produce chemically stable and productive soils (that are also likely to be non-dispersive).
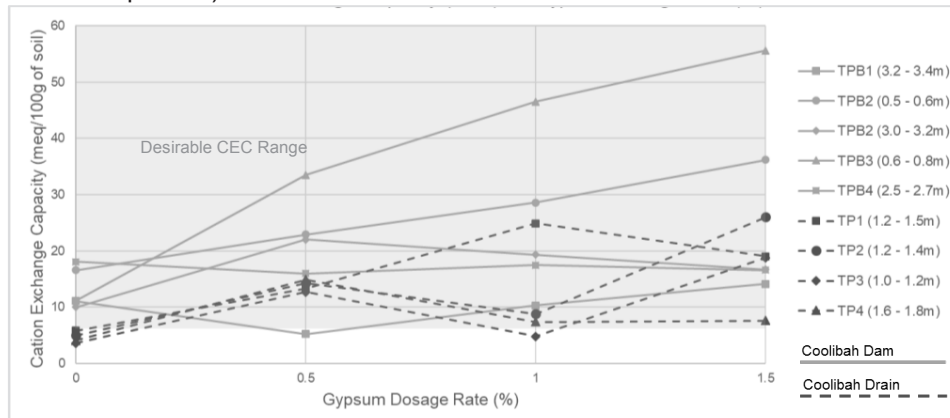

Figure 3. Cation Exchange Capacity vs Gypsum Rate.

3.3 Emerson Class Number (ECN)

The AS ECN tests undertaken on the natural soil samples as well as those treated with gypsum by up to 5.0% (by mass) showed little or no improvement from their original dispersive state with AS ECN values of 2 which suggested the soil was susceptible to dispersion. Only under the application of an abnormally high gypsum dosage rate of 10% (by mass) did the AS ECN of each of those samples improve to 4 (which suggests the treated material is non-dispersive at this dosage).

The AS ECN test results for soils treated with various gypsum dosages when compared with the visual-based assessment using the modified EAT classes, resulted in many of the test results having a lesser likelihood of being sodic and therefore a less damning view on the degree of dispersion. Further interrogation of Phase 3 AS ECN testing indicated that at a gypsum rate of 1.5%, the soil samples showed a modified EAT of 2(2) or 2(1). According to the modified EAT definitions describing the likelihood of being sodic, the samples were highly likely to be sodic (2(2)) or might be sodic (2(1)). Phase 4 testing revealed that the modified EAT of 50% of the samples treated with 2.5% gypsum (by mass), improved to 3(1) or 4 and the remaining samples improved to 2(1). Overall, the results indicated that 50% of the samples are unlikely to be sodic whilst the rest of the samples might be sodic, thus showing minimal dispersive characteristics. With an increase of the gypsum treatment to 5.0% gypsum (by mass), the percentage of samples with an EAT of 3(1) or 4 increased to 80%, which means most of the samples can be classified as 'unlikely to be sodic'. Treating the samples with 10% gypsum (by mass) resulted in all modified EAT results becoming 4 or 3(1) which indicated that all the treated soil samples were 'unlikely to be sodic' and likely non-dispersive.

As discussed in Section 3.2 the exchangeable cation data following gypsum treatment offers evidence of the soils becoming non-sodic and non-magnesic. This outcome further validates observations made by the modified EAT assessment, that a 2.5% gypsum (by mass) dosage is likely to largely reduce the dispersion and the likelihood of the soil being sodic from 'highly likely' or 'almost certainly' to 'might be' or 'unlikely'. It is therefore apparent that the inclusion of the modified sub-classes provides a more practical outcome which can be better corelated to the chemical properties of the soil than the AS ECN testing standard which is currently in use.

4   CONCLUSION

An assessment was undertaken to identify the percentage of gypsum (by mass) required to provide a chemically stable and productive soil that may also show non-dispersive behaviour. The initial assessment indicated that the soils were not only sodic but abnormally magnesic as well. Chemical testing showed that treatment with 1.5% gypsum (by mass) was likely to be optimal for providing a chemically stable and productive soil which is likely to be non-dispersive. The assessment indicated that the presence of excess cations such as sodium and magnesium are likely to promote soil dispersion. It is acknowledged that whilst there is more information regarding sodic soils nowadays, further research is required with regards to magnesic soils and the testing done during this study is only based on a limited number of samples.

Whilst the chemically tested gypsum treated soil samples (to 1.5% gypsum (by mass)) indicated that the soils were likely to be desirable in terms of being chemically stable, productive and non-dispersive, the AS ECN testing on the same treated samples indicated that there was no apparent change from testing undertaken on the untreated samples (an AS ECN of 2). In fact, the AS ECN test results on the soils only increased to the desired value of 4 after the addition of 10% (by mass) gypsum. However, further careful visual assessment undertaken with consideration of the modified EAT classes (presented on the now superseded QDTMR (2002) Road Drainage Manual) in conjunction with the evidence of desirable chemical testing results (of ESP, EMP and CEC etc), revealed that the soil could be deemed non-dispersive with less gypsum additive (2.5% by mass).

The results indicated that the removal of the sub-classes and associated visibly descriptive behaviours from the modified EAT classes (from QDTMR (2002) Road Drainage Manual) to the current day test method that further identify the degree of dispersion and likelihood of being sodic as being a significant factor which prevents the current day AS ECN test method from providing practical outcomes. Indeed, the ability for a soil to be chemically stable and productive for the purpose of providing vegetative cover is equally as important (if not more) for the soil to be non-dispersive. Therefore, the importance of undertaking quality chemical testing trials in addition to the ECN testing (incorporating the modified EAT classes) are vitally important to achieving practical and beneficial outcomes on projects where dispersive (and sodic) soils are a problem.

5   ACKNOWLEDGEMENTS

REFERENCES

Emerson, W.W. (1967). "A classification of soil aggregates based on their coherence in water." Australian Journal of Soil Research, CSIRO, Melbourne, Victoria.

Emerson, W.W. (1983). "Soils – An Australian Viewpoint (Chapter 31 – Interparticle Bonding)." Division of Soils, CSIRO, East Melbourne, Victoria.

Hazelton, P.A., and Murphy, B.W. (2007). "Interpreting soil test results: What do the numbers mean?" CSIRO Publishing, Collingwood, Victoria.

Incitec Pivot Ltd (2008). "Agronomy Advantage." A training course for the professional farm adviser, Incitec Pivot Ltd, 70 Southbank Boulevard, Southbank, Yarra, Victoria, 3006 (unpublished).

Loveday, J. and Pyle, J., (1973). "The Emerson dispersion test and its relationship to hydraulic conductivity." Division of Soils - CSIRO Australia.

Northcote, K.H. and Skene, J.K.M. (1972). "Australian soils with saline and sodic properties." Soil Publication, CSIRO Australia.

Peverill, K.I., Sparrow, I.I., and Reuter, D.J. (1999). "Soil Analysis: An Interpretation Manual." CSIRO Publications, Collingwood, Victoria.

QDTMR (2017). "Technical Specification, MRTS16 Landscape and Revegetation works", <https://www.tmr.qld.gov.au/business-industry/technical-standards-publications/specifications/3-roadworks-Drainage-culverts-and-geotechnical#mrts16> (Oct. 15, 2019).

QDTMR (2002). "The Modified EAT Classes." Road Drainage Design Manual, 2-51 pp (now superseded).

Queensland Government (2014). "Soil Sodicity", <https://www.qld.gov.au/environment/land/management/soil-properties/sodicity> (Oct 15, 2019).

Reuter, D.J., and Robinson, J.B. (1997). "Plant analysis: An Interpretation Manual". CSIRO Publishing, Collingwood, Victoria.

Standards Australia (2003). "AS 4419: Soils for landscaping and garden use." Standards Australia, 16-20 Bridge Street, Sydney, NSW 2000.

Standards Australia (2017). "AS 1289.3.8.1:2017: Methods of testing soils for engineering purposes – soil classification tests – Dispersion – Determination of Emerson class number of a soil". Standards Australia, 16-20 Bridge Street, Sydney, NSW 2000.

Upjohn, B., Fenton, G. and Conyers, M. (2005). "Soil acidity and Liming." Agfact AC.19, Department of primary Industries NSW.

Victorian Resources Online (2019). "Dispersion", <http://vro.agriculture.vic.gov.au/dpi/vro/vrosite.nsf/pages/soilhealth_soil_structure_dispersion> (Nov. 30,2019).

PROCEEDINGS OF THE 14TH ANZ YOUNG GEOTECHNICAL PROFESSIONALS CONFERENCE
14YGPC ROTORUA, NEW ZEALAND, 2ND – 5TH NOVEMBER 2022

253

Landslide Damage to Road Networks in the 2021 Marlborough Storm

G. M. Yukich[1], BE (Hons), BA and M. L. Pittar[2], BE (Hons)

[1]WSP Nelson, Level 1 Morrison Square, 77 Selwyn Place, Nelson, 7010; PH (027) 559 7303; email: gina.yukich@wsp.com
[2]WSP Nelson, Level 1 Morrison Square, 77 Selwyn Place, Nelson, 7010; PH (027) 242 8382; email: margeaux.pittar@wsp.com

ABSTRACT

A large storm occurred in Marlborough in July 2021, causing widespread damage and severe disruption to the Marlborough Sounds road network from landslides, flooding, scour, and failure of retaining walls. Comparison of rainfall gauge data and historical records indicate that the average recurrence interval (ARI) of the storm was between a 15 and 40-year event, though hourly rainfall intensities may have had higher ARIs. Poor drainage and early road construction practices contributed to the damage, and the impacts were exacerbated by the narrow road corridors and lack of alternative routes. Initial rapid route assessment was carried out in the week after the storm to triage landslide damage and over 1500 network faults were recorded. Of these, 165 significant geohazard sites were added to a monitoring regime across three key roads in the Marlborough Sounds. The observed landslide mechanisms included debris flows, deep rotational slides, shallow planar slides, and rock falls. Evacuation of historic side-cast fill deposits was frequently observed, and scour and backfill loss was the primary cause of retaining wall failure. Subsequent weekly and post-rainfall inspections of the worst-affected roads have been carried out from October 2021 to March 2022. This paper presents a categorisation of the observed failures and observations on the ongoing behaviour of slip-damaged sites.

Keywords: Landslide; Rainfall; Road networks; Retaining Walls; Marlborough

1 INTRODUCTION

Transportation routes are critical lifelines for the community, particularly in the event of natural hazards. New Zealand has rugged terrain, which means that engineered cut and fill slopes are required to form transportation routes. In 2021 a heavy rainfall event occurred between the 16th and 19th July, affecting the upper South Island. The flooding and landslides that resulted caused severe damage to road networks, including key roads in the Marlborough Sounds ("the Sounds") region. The recovery effort to restore the road network is the second largest post-disaster recovery for a local road network, after the Christchurch earthquake damage (Marlborough District Council, 2022).

Understanding the mechanisms and distribution of failures, and relating these to the impacts on infrastructure, is important for emergency response planning and for implementing measures to enhance the resilience of the roads. This storm provides a valuable opportunity to document slope failures along the road corridors and their consequent effects on the network. This paper provides a summary of the landslide damage observed on these key roads in the Sounds, and the impact this damage had on the road network in the year since the event. Data capture and analysis of landslide damage occuring from mid-July 2022 onwards has not been incorporated into this paper.

2 SETTING

2.1 Geology and Geomorphology
The Sounds are located in the upper South Island and are characterised by submerged valleys and steep surrounding topography. The bedrock of the Sounds is mapped as undifferentiated Caples terrane TZII schist. The schist generally has a deep and intense weathering profile, with completely weathered rock breaking down to a soil which displays clay-like properties. Strongly foliated schist is commonly found at depths greater than two metres deep and ranges from extremely weak to strong. The schist is jointed, with occasional crushed zones and clay-infilled seams. Large areas of the Sounds are also mapped as undifferentiated Pleistocene – Holocene landslide deposits ranging from coherent shattered masses of rock to unsorted fragments in a fine-grained matrix (GNS Science, 2013).

2.2 Historical Development and Road Formation
The majority of land in the Sounds is sloped at greater than 25°, with significant areas in the western end of the Sounds of very steep slopes (>35°) (Wolter, et al., 2022). Given the steep, topography and

remote location, road networks were originally developed for farming and forestry purposes with a standard width of 4m and grades of less than 8H:1V (Miller, 2015). This involved significant construction of sidling fills, with anecdotal evidence for an unengineered construction methodology involving cutting of the slopes on the uphill side of the road and side-casting this material over the pre-existing slopes on the downhill side. As the population has grown in Marlborough and the use of the Sounds for residential and recreational purposes has increased, the roads have been widened and sealed to accommodate the additional traffic. Records on MobileRoads (2022) suggest that much of QCD and Kenepuru Road (to Portage) were sealed in the 1970s.

3   JULY 2021 STORM EVENT

3.1   Rainfall

The storm event occurred over the weekend of 17 to 19 July 2021. Marlborough District Council (MDC) collects and records rainfall data in 24 hour increments across a number of rainfall gauges in the Sounds (Marlborough District Council, 2022). Data from the most relevant rainfall gauges is presented in Table 1. These gauges are located at Kenepuru Heads (intersection of Kenepuru and Titirangi roads) and south of Havelock on the Kaituna River.

Table 1:   HIRDS v4 Rainfall for Kenepuru Head and Kaituna (source: (NIWA, 2017)

Rainfall Gauge	24 hr max rainfall	HIRDS ARI[a]	48 hr max rainfall	HIRDS ARI[a]
Kenepuru Head	196 mm	15 years	271 mm	30 years
Kaituna @ Higgins Bridge	154 mm	15 years	229 mm	40 years

[a] Average Recurrence Interval

Analysis of Metservice rain radar data by GNS Science indicated that there were large areas across the Sounds that received high intensity (>25mm/hr) and large overall depths of rainfall (>400mm) that were not well captured by the MDC rain gauge network (Wolter, et al., 2022). Based on their analysis, GNS reports that the storm in the Kenepuru Head area had an ARI of ~100 years over 48 hours. Localised areas of high intensity rainfall are expected to have occurred around the centre of Kenepuru Sound.

3.2   Road closures

The storm event caused over 1,500 faults on the road network, including landslides, rock falls, debris flows, flooding, scour, underslips, tree falls and damage to retaining walls and bridges. Kenepuru Road, Queen Charlotte Drive (QCD) and Moetapu Bay Road (MBR) were all closed to traffic immediately following the storm due to overslip debris. Work to reopen the roads proceeded straight away, with different levels of prioritisation for each road based on their One Network Road Classification (ONRC)(Waka Kotahi NZ Transport Agency, 2022). At the time of writing (July 2022) ongoing recovery works mean that Kenepuru Road and MBR are still subject to frequent day-time closures. Works on QCD are typically within one-lane closures. The locations of failures on this part of the Sounds network are shown in *Figure 1*.

Queen Charlotte Drive (QCD)
Overslips were cleared quickly on QCD, allowing access for residents within 4 days, with the exception of a debris flow and underslip site near Havelock which remained closed for all traffic for 2 months. While access along QCD was possible, there was still significant debris and silt on the road surface, with water overtopping the road in several locations due to culvert blockage. Overslip clearance to reinstate two lanes was prioritised on this road and took place throughout August and September 2021.

Kenepuru Road
On Kenepuru Road, single lane access past overslips was also quickly reinstated, however the available corridor tended to be narrower and ongoing movement of overslip debris meant that many sites were initially only passable for 4WD or high clearance vehicles. A significant rockfall at RP19.660 (nicknamed "The Rock") blocked the road completely until November, which meant there was boat access only for residents of the outer Sounds. Underslips along Kenepuru Road also restricted access; heavy vehicles could not traverse past narrow underslip sites at RP12.8 and RP28.50, and significant deformation of the road surface due to 'global' slope deformations also required a 4WD vehicle in several locations.
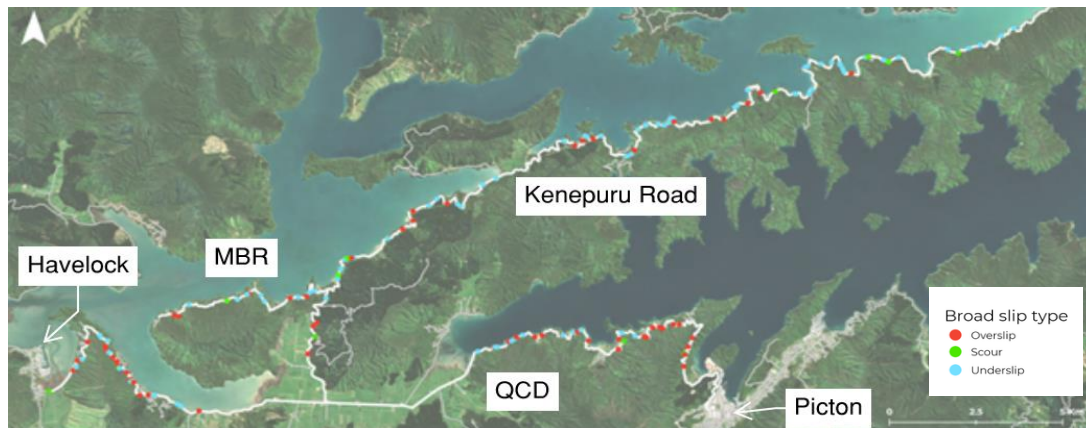
PROCEEDINGS OF THE 14TH ANZ YOUNG GEOTECHNICAL PROFESSIONALS CONFERENCE
14YGPC ROTORUA, NEW ZEALAND, 2ND – 5TH NOVEMBER 2022

255

Figure 1. Locations of slope failures on the road network

Over the 12 months following the storm, there was also more notable deterioration of sites along Kenepuru Road resulting in closures being introduced at RP19.6 (Mistletoe Bay underslip) and RP20.5 (Watertank underslip). As Kenepuru Road provides the sole vehicle access to the outer Sounds, road retreat into the hillside around the more significant underslips was prioritised.

Moetapu Bay Road (MBR)
Access along MBR was restricted by underslips at RP0.5 and RP3.0 as well as by several significant debris flows and overslips. The two major underslips limited access for heavy vehicles until a road retreat could be carried out, which in turn prevented the clearance of the debris flows and overslips. Single lane access was open for vehicles within a week after the event, and debris clearance from the overslips began in February 2022, following earthworks to retreat the road at RP0.5 and RP3.0.

Table 2:   Timeframes for road reopening from storm event (17th July – including weekends)a

	Controlled resident access restored	Public access restored
QCD (Picton - Linkwater)	4 days	42 days (28th August 2021)
QCD (Linkwater - Havelock)	60 days	61 days (20th September 2021)
Kenepuru Road	4 months, 13 days	~ 8 months (11th March 2022)
Moetapu Bay Road	10 days	~ 12 months (7th July 2022)

a Some dates are based on the timing of regular road inspections, therefore may not exactly reflect when the road status changed.

4   SLOPE FAILURE MECHANISMS

4.1 Overslips
Overslips range from small slumps and rock falls to large volume landslides on the hillslopes above the roads. Overslips were the principal cause of the immediate road closures in the Sounds, but single-lane access was typically reinstated within 2 to 7 days, with priority given to reopening QCD as a Primary Collector Route (the highest category route for the Sounds). The key characteristics of overslips observed in the Sounds are described below.

4.1.1   Debris and mud flows
Debris and mud flows occurred in high steep catchments, most frequently on the western end of QCD (Mahakipawa hill) and along Kenepuru Road (Figure 2A). Flows occurred in both clear-felled, mature forestry and native bush catchments. The liquefied flow material frequently blocked culverts and redirected surface water where they crossed the road corridor, consequently triggering underslips and scour damage below the road. Large volumes and high saturation of the debris resulting from flow failures meant these sites took longer to clear than any other form of overslip.

4.1.2   Rock fall
Rock falls were common from steep cut slopes formed in the weathered schist bedrock throughout the Sounds. These failures tended to have a minor impact on the road network overall as they resulted in smaller volumes of debris and often only extended partially into the road lane (Figure 2B). One significant exception to this was 'the Rock' site, where a car-sized boulder toppled and blocked the road (Figure 2D). Clearing the boulder took several weeks, however this site was part of an extended unstable slope and was closed to all traffic till November while additional earthworks were carried out.

4.1.3   Undifferentiated slides

There were a variety of mechanisms seen in sliding failures of overslips above the road. Some examples include planar slides along soil-rock interfaces and along dipping foliation planes, rotational slumps in over-steep cut slopes and compound slides in rock slopes (Figure 2C). Slides on high hillslopes would often transition into debris and mud flows by the time they intersected the road corridor. The impact of overslips typically depended on their size and location, rather than failure mechanism.

Small to medium volume overslips occurring from steeper natural slopes and cut batters were fast to clear but often failed again, depositing small quantities of debris on the roadside regularly after rainfall. Larger failures in locations with thicker soil deposits and deeper weathering profiles often required more extensive initial earthworks as the slopes would regressively fail as the slip debris was removed from the toe. Benching slopes was an effective way of reducing the quantity of debris that reached the road, though benches would often 'fill up' with debris and lose their effectiveness over time (Figure 2E).
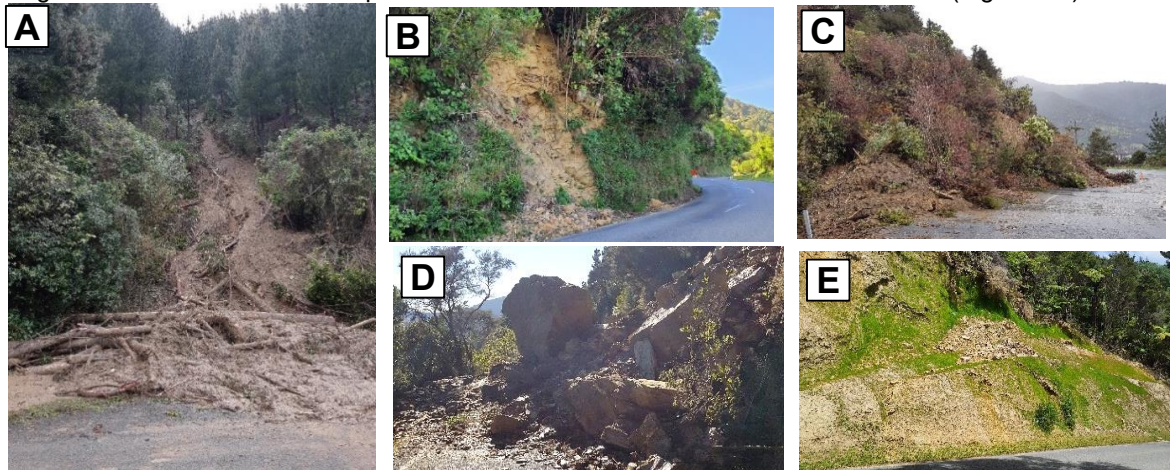

Figure 2. Typical examples of overslips. (A) Debris flow. (B) Small rock fall from a cut in weathered schist. (C) Undifferentiated slide (D) Large rock fall at The Rock (E) Ongoing failure of benched slope.

4.2 Underslip Failures

Landslides below the road caused the most significant outage, due to their greater complexity to fix than overslips. At the time of writing, 26 single lane closures due to underslips remain in place. The characteristics of underslip failures are described below, and examples are shown in Figure 3.

4.2.1   Shallow planar slides

Shallow planar slides typically occurred on slopes >30° and involved the surficial layers of colluvium and residual soil with an estimated depth of <1-2m (Figure 3A). The debris from these slides frequently developed into flows, often extending down to sea level. These types of failures typically occurred in road shoulders and showed minimal signs of regression after the initial event, though the exposed soil was vulnerable to scour.

4.2.2   Side-cast fill failures

Typically developing as planar slides, side-cast fill failures occur in the outer road lane, often developing initially as cracking and subsidence at the edge of seal where water runoff saturates the soil. Side-cast fill failures can be difficult to differentiate from planar slides occurring on natural slopes, as the resulting damage is similar, however, these slips tend to extend further into the road corridor resulting in greater impact on the road network. In 12 months, 3 sites that initially consisted of cracking and subsidence of the road edge developed into fully evacuative failures (Figure 3B). The evacuation occurred rapidly following rainfall, with no notable deterioration of the site pre-rainfall which would have predicted the failure.

4.2.3   Rotational slides

Rotational soil slides are characterised by semi-circular head scarps that have developed in the shoulder or road lane. Most of these slips tend not to have not fully evacuated, with the bulk of the slip mass is still in place with a steep semi-circular head scarp. Where the slip extended into the road, they tend to remain un-remediated 12 months after the storm with single lane closures still common, particularly on Kenepuru Road. Regular inspections showed that the slip masses settled and cracks widened in the

PROCEEDINGS OF THE 14ᵀᴴ ANZ YOUNG GEOTECHNICAL PROFESSIONALS CONFERENCE
14YGPC ROTORUA, NEW ZEALAND, 2ᴺᴰ – 5ᵀᴴ NOVEMBER 2022

257

first few months following the July storm, however, over summer the displacement ceased. At the sites that did evacuate (Figure 3C) the deep slip surface resulted in steep slip scarps greater than 3 m which limited heavy vehicle movement on the narrow road for over 6 months.

4.3 Retaining Wall Damage

In general, retaining walls performed well during the July storm event. The observed damage to the most common wall types is described below.

4.3.1 Driven rail-iron retaining walls

The most common form of retaining wall in the Sounds, rail-iron walls are formed from driven rail iron piles with timber lagging. They have a typical height of 1.5-3.5m and are frequently tied-back to a deadman pile below the road. Where tie-backs were present, these walls typically performed well during the storm. The primary form of damage was the formation of large voids behind the timber lagging. This was initially attributed to scour, however following inspection it was found that voids were forming below the base of the timber lagging due to underslips in front of the wall (Figure 3D & 3E). These voids allowed the loose backfill to migrate out from behind the wall. At several retaining walls, the geotextile wrapped around the base of the backfill was the only thing preventing further creation of voids behind the wall.

Figure 3. Typical examples of underslips and wall failures. (A) Planar soil slide. (B) Side-cast fill failure into a planar slide. (C) Rotational slide at MBR RP3.0. (D) Void behind rail iron retaining wall. (E) Loss of backfill below lagging. (F) Global slope deformation.

4.3.2 Gabion retaining walls

Gabion walls in use in the Sounds tend to be 1-2 m high and used for widening of the road shoulder and around culvert outlets. It is anticipated that they were frequently installed on poor foundations of side-cast fill or soft soil. Undermining and collapse of gabion walls was noted in 5 locations. The loss of the wall was typically accompanied by a shallow, planar slide on the steep slope below the road. Tie-backs were observed inconsistently at different failures. Less common forms of failure noted included cracking in the seal due to settlement and overturning of the entire wall due to bearing failure. Several large, well-engineered gabion walls (>3 m) are present in the network and showed no sign of damage following the event.

4.4 Slope Deformation

Deformation related to large, deep-seated movements of hillsides encompassing the whole road bench were noted in 11 locations after July 2021. Common damage observed was transverse cracking across the road, with large vertical distortion in the pavement, indicating a slip surface which passed below the road (Figure 3F). Often these slips were accompanied by smaller overslips or underslip / toe failures, while culvert disjointing and tomo-formation was also common. None of these slips were seen to have fully evacuated, and the slope deformation consisted of limited displacement of the landslide mass. These movements were traversable by 4WD vehicles immediately after the storm, and due to the scale they are typically managed by re-leveling and monitoring the road. These slope deformation features were typically located in areas mapped by GNS as Pleistocene-Holocene landslide deposits. The movements are expected to reflect re-activation of lobes of large relict landslides, occurring due to elevated ground water after prolonged rainfall.

4.5 Scour Damage and Culvert Failure

The context of local road networks in the Sounds (as low volume roads surrounded by steep, heavily vegetated slopes) result in stormwater infrastructure which is often undersized and difficult to maintain. Culvert failure was generally a result of corrosion of corrugated iron culverts or disconnection of butt-jointed concrete culverts. Failure resulted in backfill loss behind retaining walls, piping erosion and formation of 'tomos', and sometimes contributed to the development of larger failures. Without remediation, scour and underslips that resulted from culvert failures tended to worsen over the monitoring period. Scour damage unrelated to culverts was less common. It tended to result where a debris flow or large overslip had blocked and diverted existing water courses into roadside channels, resulting in much larger water volumes than would usually be experienced.

5 OBSERVATIONS FROM ONGOING MONITORING

Visual monitoring of landslides was carried from October 2021 to July 2022, which allowed deterioration or head scarp regression to be monitored over an extended period. It was observed that over half of the monitored landslides deteriorated to some degree within the 9 months, and with the most significant deterioration of the landslides occurring in the initial 3 months following the storm event while the soils were still saturated.

The overslips tended to be the most active of the slips monitored, with approximately 66% showing instability over the year to July 2022. This is likely due to the easy recognition of activity from these slips (i.e. failed material on the road or table drains). In contrast, just under half of the underslips worsened. This was largely noted as minor regression of the scarp, minor settlement of the road edge, or an increase in cracking within the seal. Ongoing failure of overslip sites was more common on slopes with more highly weathered rock and thicker overlying soil deposits. These sites were reprofiled with benches to catch debris, and while there were ongoing failures of the upper batter slopes these had minimal impact on the road as the debris collected on the benches.

6 CONCLUSIONS

The damage caused by the landslides across the Marlborough Sounds provided valuable lessons on the impact of road performance in a remote setting. Damage to the network was widely spread across the three key roads within the Sounds. Overslips were the most widely distributed but tended to be easiest to clear, while underslips have resulted in the longest outages, with single lane sections still remaining on all key roads at the time of writing. Underslips required considerable time to proceed through to construction; requiring stages for options assessment, investigation, design, tendering and procurement all before construction could commence. The overall scale of the damage distributed across a highly constrained road network through steep and unstable terrain meant that significant landside damage remains un-remediated 12 months following the storm.

Regular monitoring and post-rainfall inspections provided insight into how the landslide sites deteriorated over time. Overall, the monitoring showed that very few sites worsened significantly during the monitoring period. Ongoing damage generally consisted of minor regression of slip scarps or small overslips. Exceptions to this were several notable rapid failures of underslips, which were originally expressed as minor cracking in the outer road lane in the July 2021 event, and regressive failures of large overslip sites which required more significant earthworks and benching to reduce the road impact.

This paper was written at the beginning of July 2022 to record the status of the road network in the 12 months following the July 2021 storm. Since writing, Blenheim has been reported as experiencing its wettest month on record in July (Stuff, 2022) and then suffered a larger storm event on August 17th-18th. There has been significant damage to the road network in the Sounds and quantifying the impact of these storm events on the network will take some time.

7 ACKNOWLEDGEMENTS

Erionite in New Zealand: A Risk Assessment for Central Interceptor

M.A.F. Blakemore

[1]Jacobs NZ Limited, 12-16 Nicholls Lane, Parnell, Auckland 1010. Phone: 0212270090. Email: max.blakemore@jacobs.com

ABSTRACT

Erionite is a naturally occurring asbestiform zeolite mineral. The main geological occurrences of zeolites are in tuff, tephra and volcaniclastic rocks deposited in deep ocean basins subject to low temperature hydrothermal alteration or burial diagenesis. An emerging body of research in Europe and North America has established erionite as carcinogenic to humans. Inhalation exposure to erionite fibres may result in increased risk of malignant mesothelioma. In Auckland, the presence of erionite in tuffaceous and volcaniclastic layers of Waitemata Group sedimentary rocks has been known since the late 1970s, however, neither an occupational exposure limit nor an approved code of practice for handling and disposing of erionite containing materials have been developed in New Zealand or internationally. Watercare's Central Interceptor project is one of several large infrastructure projects in Auckland that handles and disposes of large volumes of Waitemata Group rocks. In the absence of approved guidance, Watercare commissioned Jacobs New Zealand to establish the risks erionite posed to the project. Borehole logs and photographs from the Central Interceptor were reviewed to identify samples with the highest probability of containing erionite for laboratory testing. The accuracy of laboratory tests available in New Zealand and internationally were assessed against the soil guideline values for friable asbestos. Quantitative X-Ray Diffraction testing was considered suitable to screen samples for the presence of erionite. Quantitative X-Ray Diffraction identified one possible occurrence of erionite from thirty-seven samples tested. Consequently, the Central Interceptor project implemented a series of recommendations to limit inhalation exposure of erionite fibres to site workers during construction. Fluidized Bed Asbestos Segregator (FBAS) sample preparation techniques, developed in the United States, used with Transmission Electron Microscopy (TEM) offer detection of erionite in concentrations comparable to soil guideline values established for asbestos. FBAS with TEM may prove fundamental in assessing presence of erionite in the future, once an occupational exposure limit and an approved code of practice for handling and disposing of erionite containing materials have been developed.

Keywords: Risk Assessment, Erionite, Central Interceptor, Auckland, New Zealand.

1   INTRODUCTION

Erionite is a naturally occurring asbestiform zeolite mineral (Brook, 2019). The main geological occurrences of zeolites are in tuff, tephra and volcaniclastic rocks deposited in deep ocean basins subject to low temperature hydrothermal alteration or burial diagenesis (Christie, 2002; Hay and Sheppard, 2001; Marantos *et al.,* 2012). An emerging body of research in Europe and North America has established erionite as carcinogenic to humans (Carbone *et al,* 2011; Van Gosen *et al,* 2013: Giordani *et al.,* 2017). In Auckland, the presence of erionite in tuffaceous and volcaniclastic layers of Waitemata Group sedimentary rocks has been known since the late 1970s (Sameshima, 1978), however, neither an occupational exposure limit nor an approved code of practice for handling and disposing of erionite containing materials have been developed in New Zealand or internationally (Brook, 2019). In light of the emerging research and the significant volume of tunnelling and excavation programmed within Waitemata Group rocks the Ministry of Business, Innovation and Employment awarded the University of Auckland funding to investigate the risks posed by erionite on a national scale (MBIE, 2020) and Watercare Services Limited (Watercare) commissioned Jacobs New Zealand Limited (Jacobs) to establish the risks erionite posed on a project-scale for the Central Interceptor. The aim of the project-scale study was to: establish how erionite forms, understand where erionite is distributed in the Auckland region, identify risks erionite posed to the project, and recommend practical risk mitigation controls that could be implemented during construction.

2   ZEOLITES

2.1   What are zeolites?

Erionite is a naturally occurring asbestiform mineral that belongs to a group of alumino-silicate minerals called zeolites (Brook, 2019). Natural zeolites form where volcanic rocks and ash layers react with alkaline groundwater. Zeolites also crystallize in post-depositional environments as secondary minerals

during burial diagenesis and low-grade metamorphism at temperatures below 200°C (Fuoco, 2012). In mafic rocks, rich in iron and/or magnesium, zeolites occur as cavity infills as a result of deposition by fluids or vapours (Rafferty *et al*., 2020). In sedimentary rocks, zeolites occur as alteration products, cementing detrital material together (Iljima and Utada, 2006).

2.2 Where do zeolites form?

The main global geological occurrences of natural zeolites are in tuffs, tephra and volcaniclastic rocks deposited in deep ocean basins (Hay and Sheppard, 2001). Railton and Watters (1990) assert zeolites hosted in sedimentary rocks are found in three main geological settings in New Zealand: (1) Altered rhyolitic tuffs in lake beds of Quaternary age in the Taupo Volcanic Zone; (2) Marine tuffs and volcaniclastic sandstones of Miocene age in Northland and Auckland; and (3) Weakly metamorphosed marine tuffs and volcaniclastic sandstones of Triassic and Jurassic age in Southland and Southwest Auckland. Only zeolite deposits associated with sedimentary rocks in Northland and Auckland were reviewed, as these formations will be encountered during tunnelling and shaft excavation on CI.

2.3 Why is erionite a concern?

Erionite is an asbestiform fibrous zeolite mineral that is known to be carcinogenic to humans with the potential to cause respiratory disease similar to asbestosis (Brook *et al,* 2020). If inhaled, erionite fibres can become lodged in various organs of the body such as the linings of the lungs, abdomen, and heart resulting in increased risk of mesothelioma. Compared with other asbestiform minerals, erionite has been shown to have a greater potential to cause fatal respiratory disease than common asbestos minerals typically encountered in industrial use (Rezvani and Bolduc, 2014). At the time of writing, there was no known occupational exposure limit (OEL) for erionite in New Zealand or internationally (Brook *et al, 2020)*.

3 GEOLOGY ALONG THE CENTRAL INTERCEPTOR ALIGNMENT

Understanding the geology along the CI alignment was critical to qualifying the risks erionite posed to the project, as the diagenetic history of Auckland determined how and where zeolites form.

3.1 Provenance of the Waitemata Group

The East Coast Bays Formation (ECBF) of the Waitemata Group is a thick sequence of Miocene-aged sedimentary rock (Edbrooke, 2001) that underlies the entire CI alignment and forms the predominant tunnelling and excavation substrate. ECBF rocks are interpreted as turbidite deposits (flysch) and are characterised by alternating sandstones and siltstones, in various proportions, with less common coarse-grained volcaniclastic sandstones and conglomerates, commonly referred to as Parnell Volcaniclastic Conglomerate (PVC). The origin of the flysch deposits are submarine debris flows, most likely resulting from periodic flank collapse and/or volcanic eruptions along the two bounding volcanic arcs; one currently submerged off the west coast and one to the east, comprising the Coromandel Volcanic Arc (Shane *et al.,* 2010). Significantly, these volcanic arcs and resulting debris flows provided the volcanic ash and andesitic source materials for the formation of zeolite minerals within the ECBF.

3.2 Induration of the Waitemata Group

Though relatively old (approximately 20 million years), ECBF rocks are poorly indurated. Evidence suggests these rocks have not been very deeply buried – perhaps to a maximum depth of 300 m (Edbrooke *et al.,* 1988). Consequently, the materials have never been subjected to the high temperatures and pressures required to fully indurate the sediments. The rocks have been subjected to early rock-forming processes, called diagenesis, which started to break down the constituent sediment components and form a matrix of clay with cementation by zeolites (very low-grade metamorphic minerals) and calcite.

3.3 Known sources of zeolites in the Waitemata Group

Sameshima (1978) noted that zeolites are common throughout Waitemata Group rocks, with the most common occurrence within volcaniclastic and tuffaceous beds and are mainly present as a matrix cement. The most intense zeolitisation occurs in the coarse-grained volcaniclastic sandstones and conglomerate units. Known sources of erionite within Waitemata Group rocks, include: Puketotara, in the Kaipara area, associated with a 90 cm thick tuff bed in the deep marine Timber Bay Formation (Sameshima, 1978); The Tor, Torbay associated with channelised coarse-grained volcaniclastic sandstone deposits: and Caster Bay, Auckland, associated with channelized coarse-grained volcaniclastic sandstone deposits (Rod, n.d.).

PROCEEDINGS OF THE 14TH ANZ YOUNG GEOTECHNICAL PROFESSIONALS CONFERENCE
14YGPC ROTORUA, NEW ZEALAND, 2ND – 5TH NOVEMBER 2022

261

4   REVIEW OF EXISTING CENTRAL INTERCEPTOR GROUND INVESTIGATION DATA

Geotechnical investigations commissioned to inform detailed design of CI incorporated petrographic (thin section) and X-Ray Diffraction (XRD) analysis to determine bulk mineralogical properties of the tunnelling substrate. The tests were not commissioned specifically to look for zeolites but results from coarse-grained volcaniclastic sandstone were re-analysed to establish whether there was evidence of erionite in the existing dataset.

4.1   Petrographic review
A review of previous petrographic data was inconclusive. Very few samples of conglomeritic sandstone were examined at sufficient magnification to understand the mineralogy of the finer grains. Consequently, it was impossible to distinguish matrix zeolites from other forms of clay matrix (such as illite). While there was no conclusive petrographic evidence for erionite in the historical CI samples, there was evidence to suggest that zeolite minerals could be present. Many of the volcaniclastic sandstones and conglomerates contained highly altered clasts which represents a potential formation environment for erionite.

4.2   X-Ray Diffraction Review
XRD analysis undertaken for detailed design showed little evidence for zeolites (and therefore erionite), potentially due to the low numbers of samples tested. The XRD results indicated the presence of zeolite minerals chabazite and clinoptilolite in coarser volcaniclastic units, but it was difficult to establish the concentration of zeolite minerals within the sample as the analysis was not quantitative.

5   ERIONITE-SPECIFIC TESTING

5.1   Sampling criteria
CI borehole core logs and photographs were reviewed to identify samples to test for the presence of erionite. Based on the desktop study review, layers of volcanic ash (tuff) deposited within the East Coast Bays Formation and channelised deposits of volcaniclastic sandstone and conglomerates (PVC) have the highest potential to contain zeolites and erionite. Only one possible lens of tuff was identified in CI borehole logs and was sampled for testing. Samples of PVC were selected regardless of whether they were encountered in the tunnel horizon or shaft footprints. Tunnel and shaft excavation could intersect channelised deposits of PVC at any location outside the limits of what is known from current investigation data. A series of control samples were also selected to test for the absence of erionite, the samples were chosen based on their provenance, which was believed to have a low probability of containing erionite.

5.2   Testing methodology
The risks associated with erionite were not widely known when Watercare awarded the Contract to construct CI. This study was commissioned after the contract had been awarded; commencement of shaft excavation was imminent, consequently, a quick turnaround of test results and findings was paramount to establish risks and controls to the project. A survey was undertaken to identify laboratories in New Zealand that could undertake suitable testing to avoid delays associated with international couriering. Panda GeoScience Limited (New Zealand) offered quantitative XRD testing with a detection limit for erionite of 1% weight for weight (w/w) - taken as the weight of the mineral with reference to the weight of the sample tested. Panda GeoScience Limited confirmed quantitative estimates of mineral abundances in terms of major (>20%), minor (~5-20%), and trace (>1% w/w to<~5%) was available via XRD, based on relative peak heights in each sample (Panda GeoScience, 2020). Quantitative XRD was considered suitable for the purpose of the initial screening study, to establish whether erionite might be present in any of the samples and provide an indication to the amount of erionite present.

5.3   Results
Possible erionite was identified in a trace amount (>1% w/w to <5% w/w) in one of the thirty-seven samples tested using quantitative XRD (Panda GeoScience, 2020). The sample (BH 308, 35.6 m to 36.05 m) was obtained from a borehole drilled near the centre of the Manakau Harbour from a depth outside the tunnel horizon. The sample was categorised as PVC and described as slightly weathered, massive, dark grey speckled pink and brown, matrix supported, volcaniclastic CONGLOMERATE, very weak (Jacobs, 2017a). The sample was not considered physically distinguishable from other PVC samples tested. In the other thirty-six samples tested, erionite was not identified above its detection limit, but could perhaps be present in concentrations less than 1% w/w.

6   DISCUSSION

The results indicated erionite could be present in trace amounts (>1% w/w to <5% w/w) in PVC. To qualify the potential risk erionite posed to the project, it was important to understand: the construction techniques proposed for CI, to identify sources of dust; the distribution of PVC along the CI alignment and compare the concentrations of erionite detected against the detection limits and occupational exposure limits for asbestos.

6.1   Central Interceptor construction methodology

CI is a new 14.7km long, 4.5m internal diameter wastewater tunnel. The project also incorporates two link sewers adding a further 4.5km of smaller diameter tunnels. The CI alignment is constructed using a closed-face earth pressure balance (EPB) Tunnel Boring Machine (TBM). The link sewers are pipe jacked using an EPB TBM cutter head. The closed-face EPB TBM removes the tunnel spoil as a wet slurry reducing the amount of dust in the tunnels. Seventeen shafts are to be excavated along the tunnel and link sewer alignments. Conventional earthworks excavators are planned to excavate soil and ECBF rock within shaft footprints, with the exceptions of Keith Hay Park shaft and Walmsley Park shaft, for which shaft drilling techniques are proposed (Jacobs, 2019).

6.2   Distribution of Parnell Volcaniclastic Conglomerate

The distribution of PVC was baselined in the CI Contract Documents, which informed the Contractor to anticipate PVC along 5% of the CI Main Tunnel Alignment and 2% of the Link Sewers. Lenses of PVC, in the order of 5m thick, were encountered in boreholes near Mangere Pump Station Shaft, Walmsley Park Shaft, Haverstock Road Shaft and Haydock Road Shaft. The Contractor should expect to encounter lenses of PVC in the order of 5m thick within the ECBF in these shaft locations. Whilst PVC was not encountered in boreholes near other shaft locations, the Contractor can expect to encounter 5% by volume of moderately strong coarse-to-cobble sized volcanic conglomerate within the ECBF (Jacobs, 2019).

6.3   Comparison of detection limits for erionite and asbestos.

The detection limit for erionite in Quantitative XRD analysis was 1% w/w, which is orders of magnitude greater than the detection limit for friable asbestos or asbestos fines (BRANZ, 2017). The soil guideline values for friable asbestos and asbestos fines in New Zealand is 0.001% w/w i.e., any site with fibrous asbestos >0.001 % w/w requires further assessment (BRANZ, 2017). The guideline value for asbestos fines is orders of magnitude lower than the detection limit for erionite quoted by Panda Geoscience for their XRD-analysis.

7   RISK ASSESSMENT

In light of the results, the anticipated distribution of PVC throughout the scheme, and the proposed closed-face tunnelling methodologies, the probability of encountering airborne erionite in concentrations greater than 1% w/w during tunnelling was considered low. The probability of encountering airborne erionite mineral fibres in concentrations greater than 1% w/w within shaft excavation footprints was considered higher than anticipated in tunnels, primarily because conventional excavators were proposed without dust suppression. The presence of erionite indicated in one sample and the disparity between the detection limits for erionite versus asbestos created uncertainty and warranted construction controls to be implemented during shaft excavation.

8   RECOMMENDATIONS

Construction recommendations were made based on the findings of this study. At the time of writing, there was no known detection limit or occupation exposure limit for erionite in New Zealand or internationally. If an occupational exposure limit for erionite is established during construction, then the controls should be reviewed and amended, as necessary.

8.1   Further testing

It is acknowledged that the number of samples tested was statistically small. To improve the reliability of the test results, Jacobs recommended re-testing at least ten existing samples via Quantitative XRD, one sample must include the sample in which erionite was detected. The Contractor was also advised to collect samples of PVC and tuff encountered during shaft excavation to send for Transmission Electron Microscopy (TEM) testing to further quantify the risks erionite posed to the project team.

PROCEEDINGS OF THE 14TH ANZ YOUNG GEOTECHNICAL PROFESSIONALS CONFERENCE
14YGPC ROTORUA, NEW ZEALAND, 2ND – 5TH NOVEMBER 2022

263

8.2 Geological field mapping

The Contractor had undertaken additional site investigation since the CI Contract was awarded. The Contractor was advised to undertake a thorough review of the new (and existing) borehole logs around each shaft location to understand where PVC and tuff is likely to be encountered to enable controls to be implemented in due time. A suitably qualified engineering geologist should be on site during shaft excavation to accurately identify the ground conditions and ensure controls are implemented.

8.3 Air quality monitoring

Jacobs recommended the Contractor contact an IANZ accredited (or equivalent) laboratory capable of undertaking ambient air testing in accordance with ISO 14966:2019 (British Standards Institute, 2019) to see whether the test was suitable for identifying the numerical concentration of erionite fibres during shaft excavation through PVC and tuff. If suitable, periodic air-quality testing was recommended at ventilation egress points to monitor the composition of airborne dust. Similar air quality testing could be undertaken at temporary and permanent spoil sites to identify whether erionite became airborne as spoil heaps dried out. Until an approved code of practice is developed for erionite, the Contractor was advised to review their results of air quality testing against WorkSafe's (2016) approved code of practice for the management and removal of asbestos.

8.4 Dust Suppression

The traditional excavation techniques proposed to excavate shafts did not supress dust. To minimise inhalation exposure to erionite dust, the Contractor was advised to: use water jets whilst breaking or ripping PVC or tuff beds, cover and moisten temporary stockpiles of spoil, and engage a suitably qualified engineering geologist to accurately identify when the Contractor is encountering PVC or tuff beds.

8.5 Personal Protective Equipment

The Contractor was recommended to seek the advice of an occupational hygienist to establish a suitable face filtering piece (face mask) for staff to wear whilst working with PVC and tuff, which may contain erionite.

8.6 Spoil Disposal

The Contractor was advised to keep spoil moist and covered to minimise dust and was reminded that spoil disposal must meet local authority requirements and resource consent conditions; the presence of erionite in PVC warranted spoil to be disposed of in a landfill licensed to receive asbestos.

9 FUTURE INVESTIGATION

Quantitative XRD offered detection of possible erionite to 1% w/w. Low level detection of mineral fibres has been accomplished using polarized light microscopy (PLM) providing detection limits around 0.25% w/w (Berry *et al.*, 2019). Fluidized Bed Asbestos Segregator (FBAS) sample preparation techniques, developed in the United States, used with Transmission Electron Microscopy (TEM) offer detection of erionite in concentrations of 0.0003% w/w (Berry *et al*, 2019), which is comparable to soil guideline value established for asbestos fines 0.0001% w/w (BRANZ, 2017). Moreover, FBAS with TEM enables the distinction between fibrous and crystalline erionite, which is key, as only fibrous erionite is classified as a carcinogen (Berry *et al*, 2019). FBAS with TEM may prove fundamental in assessing concentrations of erionite in the future, once an occupational exposure limit and an approved code of practice for handling and disposing of erionite containing materials have been developed.

10 CONCLUSION

The desktop study review indicated coarse grained volcaniclastic sandstones and conglomerates within the Waitemata Group have the highest potential to contain zeolite minerals. Borehole core logs were reviewed to identify samples of coarse grained volcaniclastic sandstone to screen for the presence of erionite. Thirty-seven samples were tested via Quantitative XRD, one sample detected a trace amount (>1%w/w <5%w/w) of erionite. The distribution of coarse grained volcaniclastic sandstones across the project footprint was estimated to be less than 5% of the total excavation volume. Exposure to dust on CI is suitably mitigated during tunnelling by using an earth pressure balance tunnel boring machine, but workers would be exposed to dust during traditional shaft excavation. Whilst the probability of encountering fibrous erionite in concentrations greater than 1% w/w was considered to be low, the possible presence of erionite in one sample, the disparity between the detection limits for asbestos

versus erionite via XRD testing and the lack of approved guidance created uncertainty. Consequently, the Central Interceptor project proactively implemented a series of construction controls during shaft construction through PVC and tuff, to mitigate the risks associated with inhalation exposure to erionite. To improve the reliability of future erionite investigations, investigators are recommended to obtain robust data sets, test samples using a range of techniques (XRD, PLM and FBAS TEM) and compare results against known reference materials which have been well classified.

11 ACKNOWLEDGEMENTS

12 REFERENCES

Berry, D., Januch, J, M. Woodbury, L. and Kent, D. (2019). Detection of Erionite and Other Zeolite Fibres in Soil by the Fluidized Bed Preparation Methodology. Microscope. 2019; 67(4): 147–158.

BRANZ. (2017). New Zealand Guidelines for Assessing and Managing Asbestos in Soil. New Zealand, Print link. BRANZ Limited.

British Standards Institute. (2019) Ambient air. Determination of numerical concertation of inorganic fibrous particles. Scanning electron microscopy method. BS ISO 14966:2019. BSI.

Brook, M.S., Black, P.M, Salmond, J., Dirks, K.M., Berry, T.A. and Steignhorn, G. (2020). Erionite in Auckland bedrock and malignant mesothelioma: an emerging public and occupational health hazard? New Zealand Medical Journal, Volume 133. No. 1518. New Zealand Medical Association.

Brook, M.S. (2019). Exposure to erionite: health effects and implications for geotechnical risk management in the New Zealand construction sector. NZ Geomechanics News. Issue 98.

Carbone, M., Baris, Y.I. and Bertino, P., Brass, B., Comertpay, S., Umran Dogan, A., Gaudino, G., Jube, S., Kanodia, S., Partridge, C.R., Pass, H.I., Rivera, Z.S., Steele, I., Tuncer, M., Way, S., Yang, H. and Miller, A. Erionite exposure in North Dakota and Turkish villages with mesothelioma. Proceedings of the National Academy of Sciences of the United States of America 108(33): 13618–3623.

Christie, T., Braithwaite, B. and Thompson, B. (2002). Mineral Commodity Report 23 - Zeolites. NZ Mining, Volume 31, 16-24.

Davidson, K.J.; Black, P.M. (1994). Diagenesis in Early Miocene Waitemata Group sediments, Upper Waitemata Harbour, Auckland, New Zealand. Geoscience Reports. Shizuoka University, 20: 135-142.

Edbrooke, S.W., Crouch, E.M., Morgans, H.E.G., Sykes, R. (1998). Late Eocene-Oligocene Te Kuiti Group at Mount Roskill, Auckland, New Zealand. New Zealand Journal of Geology and Geophysics, 85-93.

Edbrooke, S.W. (2001). Geology of the Auckland Area. Lower Hutt: Institute of the Geological and Nuclear Sciences.

Fuoco, D. (2012). A new Method for Characterisation of Natural Zeolites and Organic Nanostructure using Atomic Force Microscopy. Nanomaterials 2012, 2, 79-91.

Giordani M, Mattioli M, Ballirano P, Pacella P, Cenni M, Boscardin M, Valentini L. (2017). Geological occurrence, mineralogical characterization and risk assessment of potentially carcinogenic erionite in Italy. Journal of Toxicology & Environmental Health B 20: 81-103.

Hay, R.L. (1978). Geologic occurrence of zeolites. In: Sand, L.B.; Mumpton, FA. (eds), Natural zeolites - occurrence, properties, use, Pergamon Press,135-143.

Hay, R.L. and Sheppard, R. A. (2001). Occurrence of zeolites in sedimentary rocks: an overview. In Bish. D. L. and Ming, D. W. (Eds) Natural zeolites: occurrence, properties, applications. Reviews in Mineralogy and Geochemistry, Volume 45, Mineralogical Society of America, 217-243.

Iljima, A. and Utada, M. (2006). Zeolites in sedimentary rocks, with reference to the depositional environments and zonal distribution. Sedimentology. 7(4): 327-357. Wiley Online Library.

Jacobs New Zealand Limited. 2017a. Central Interceptor Main Project Works Detailed Design Geotechnical Factual Report.

Jacobs New Zealand Limited. 2019. Central Interceptor Main Project Works Detailed Design Geotechnical Baseline Report.

Kermode, L. (1992). Geological of the Auckland Urban Area Sheet R11 Scale 1:50,000, IGNS Geological Map 2

Langella, A., Cappelletti, P., de Gennaro, M. (2001): Zeolites in closed hydrologic systems. In: Bish; D.L., Ming, D. W. (eds), Natural zeolites: occurrence, properties, applications. Reviews in Mineralogy and Geochemistry, volume 45. Mineralogical Society of America, pp. 235-260.

Marantos, I., Christidis, G.E. and Ulmanu, M. 2012. Zeolites Formation and Deposits. Handbook of Natural Zeolites. 2012, 28-51.

Ministry of Business, Innovation and Employment [MBIE]. (2020). 2020 Endeavour Fund Successful Proposals. [Online]. [Accessed 2022.09.30]. Available from: https://www.mbie.govt.nz/

Panda Geoscience Limited. (2020). XRD study of 37 samples from the Central Interceptor for Watercare.

Rafferty, J.P., Augustyn, A., Lotha, G., Mahajan, D., Rodriguez and Tikkanen, A. (2020). "Zeolite". Encyclopaedia Britannica, 17 Jan. 2020.

Railton, G.L.; Watters, W.A. (1990). Minerals of New Zealand. New Zealand Geological Survey bulletin 104.

Rezvani, N., and Bolduc, D.L. (2014). Erionites. Encyclopaedia of Toxicology (Third Edition), Academic Press, 2014, 448-452.

Rod, M. (n.d.) Zeolites and associated minerals from Parnell Grit beds of the East Coast Bays Formation, Auckland. Essence of Microscope (NZ)

Sameshima, T. (1978). Zeolites in tuff beds of the Miocene Waitemata Group, Auckland Province, New Zealand. P. 309-317, In: Sand, L.B.; Mumpton, F.A. (eds), Natural zeolites, occurrence, properties and uses. New York, Pergamon Press.

Shane, P., Strachan, L.J., Smith, I. (2010). Redefining the Waitemata Basin, New Zealand; A new tectonic, magmatic, and basin evolution model at a subduction terminus in the SW pacific. An Electronic Journal of The Earth Sciences.

Van Gosen B, Blitz TA, Plumlee GS, Meeker GP, Pierson MP. (2013). Geologic occurrences of erionite in the United States: an emerging national public health concern for respiratory disease. Environmental Geochemistry & Health 35: 419–430.

WorkSafe. (2016) Approved Code of Practice: Management and Removal of Asbestos.

14TH AUSTRALIA & NEW ZEALAND YGP CONFERENCE

Field Trip Guide

5 November, 2022

Bradley Scott
GNS Science, Wairakei Research Centre, Taupo

INTRODUCTION

The purposes of this excursion are to illustrate:

- The complexity of the interactions between tectonic and volcanic processes in the northern Taupo Volcanic Zone (TVZ),
- The association of geothermal surface features to Rotorua Caldera,
- The large volumes of extruded lava in the Okataina Volcanic Centre, diversity of eruption sizes and styles,
- The extent of extensional faulting south of the Okataina Volcanic Centre,
- The development of the geothermal resources,
- The dependence of our awareness of volcanic hazards on the information available in the geological record

These notes are intended to be a brief guide to the localities of geological interest that are visited during this field trip to the Rotorua area. The notes are not all-encompassing, but I have referenced some topics as a starting point for further reading that you might like to pursue. The field trip will visit localities associated with the Rotorua and Okataina Volcanic Centres. It will not pass through the Taupo Fault Belt south of Rotorua, but notes are included. The bias of the trip is to the broad geomorphic structures in this area – at best a small snapshot of this interesting area.

FIELD TRIP ITINERARY

This field trip is focused on caldera volcanism (explosive and effusive) in the northern TVZ that has occurred in the last 450 kyr. During this time period there have been several large caldera forming events especially in the 350 to 280 ka period and intra caldera eruptions the last ~60 kyr (the Modern TVZ of Wilson et al., 1995).

      Leave 8.30 am.
1) Rotorua Caldera over view (Tihiotonga reserve).
2) Kuirau Park geothermal features.
3) Blue Lake caldera boundary, moat lake.
4) Lunch stop, Stony Bay Lake Tarawera
5) Mt Tarawera 1886 overview.
6) *Return to Rotorua.*

BACKGROUND

The Bay of Plenty – Waikato regions are highly vulnerable to volcanic activity, due to their locations within the Taupo Volcanic Zone (TVZ), the focus of intense volcanic activity that extends from White Island in the north to Tongariro National Park in the south. Volcanic activity within the TVZ is characterised by an enormous range of eruption magnitudes, as indicated by the volumes of erupted material. The larger events have ejected 200-700 km^3 of pyroclastic material, whilst the smallest produced less than 0.001 km^3 (Houghton et.al 1995, Wilson et. al 1984) The duration of eruptive episodes is also highly variable, ranging from a few hours to months, through to sustained intermittent activity for several centuries.

Two dominant types of volcano are present in the TVZ; cones like Ruapehu, White Island and Ngauruhoe, which erupt small volumes on a geologically regular basis (5-20years); and the major caldera volcanoes which erupt significantly less frequently (1000-5000 years) but their eruptions, would be regionally catastrophic.

A lesser known source of volcano hazard is 'Caldera Unrest'. This is where a volcano shows signs of unrest, but these may not lead to an eruption. The unrest creates uncertainty and brings about costs. Episodes of heightened caldera unrest have occurred frequently across the globe, including in New Zealand. Unrest in the form of seismicity, deformation and hydrothermal activity can be indicative volcanic phenomena. This style of unrest is commonly recorded at calderas; however, there is uncertainty over when the activity increases from "background" levels to "volcanic unrest" and an eruption threat.

GEOTHERMAL ACTIVITY

There are approximately 20 known geothermal systems, over half have been explored by drilling down to a maximum depth of ~ 3500 m (Figure1). In the central TVZ, hydrothermal systems are regularly spaced (10 to 20 km apart) and separated by zones of recharge. The main control on their distribution is uncertain though a few systems are clearly related to either major fault structures e.g. Orakeikorako, Te Kopia, Waikite or caldera boundaries e.g. Waimangu, Waiotapu (Wood, 1995). Most modern hydrothermal systems have been active for at least 10,000 years and possibly more than 300,000 years. The total estimated heat flow, due to hydrothermal convection, ranges between 2000 and 4000 MW, within an order of magnitude of that contributed by volcanism (last 200,000 years), 500 to 1000 MW.

Figure 1.   Distribution of active geothermal systems in the TVZ.

PROCEEDINGS OF THE 14TH ANZ YOUNG GEOTECHNICAL PROFESSIONALS CONFERENCE
14YGPC ROTORUA, NEW ZEALAND, 2ND – 5TH NOVEMBER 2022

267

Rotorua Caldera

The Rotorua Caldera in its present form dates back about 240 000 years to the major ignimbrite eruptions that formed the Mamaku plateau. A large volume of magma rose under Rotorua to occupy shallow magma chambers. Following the large scale 'Mamaku eruptions' the roof of the magma chamber was weakened and collapsed to form the Rotorua basin (caldera) as we know it today (Figures. 2, 3, 4 and 5). There were also similar large eruptions to the south centred on the Artiamuri area, generating a complex eruption sequence between the two areas.
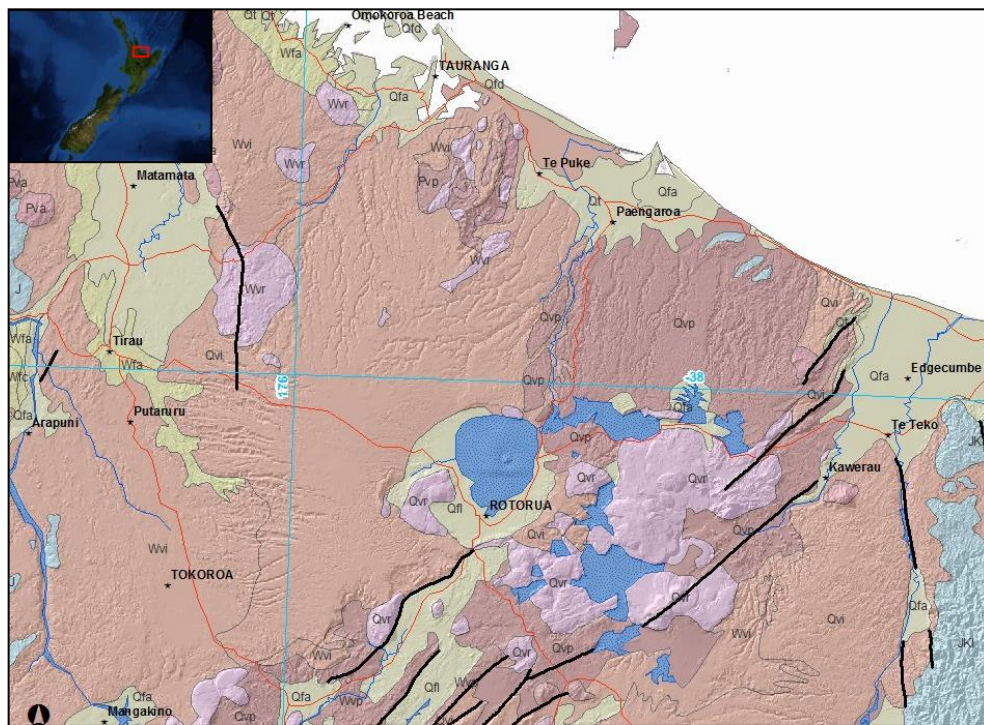

Figure 2.　　　A view from the Tihi o Tonga stop, showing the caldera basin.
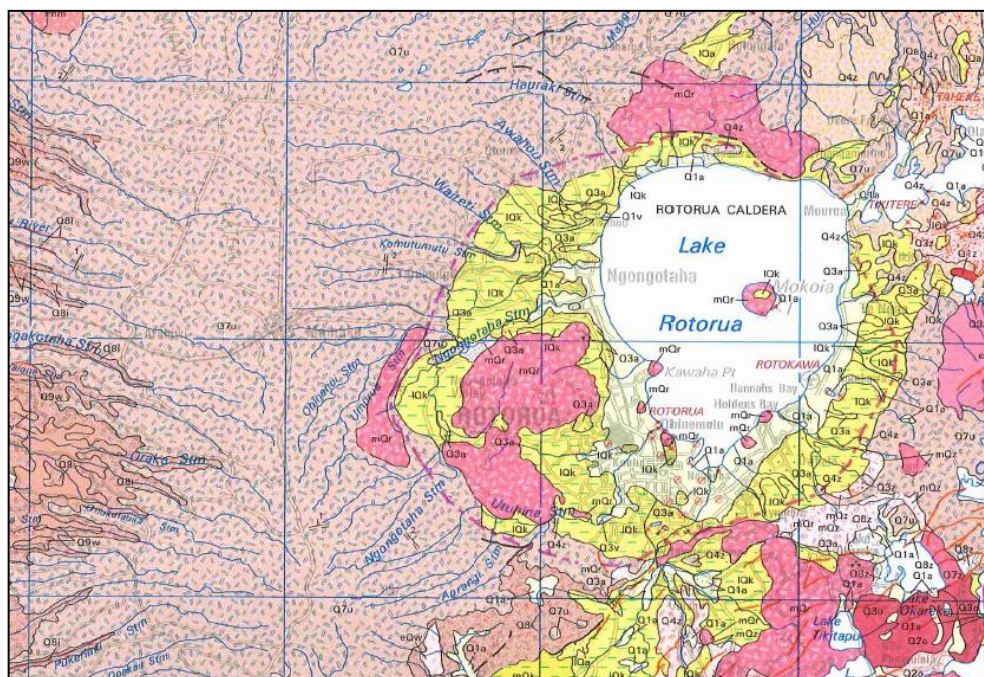

Figure 3.　　　Aerial view of Rotorua Caldera from the north (DB Townsend).

**Figure 4**   Simplified regional geology, Rotorua District (QMap).

Post formation of the caldera basin lava domes have grown within the caldera, like Mt Ngongotaha, Mokoia Island (Figures 4 and 5). Lave dome growth had stopped by about 80 – 50 000 years ago.

Figure 5.   Simplified geology of the Rotorua Caldera (QMap).

PROCEEDINGS OF THE 14TH ANZ YOUNG GEOTECHNICAL PROFESSIONALS CONFERENCE
14YGPC ROTORUA, NEW ZEALAND, 2ND – 5TH NOVEMBER 2022

269

Discharge energy	1. Geysers	4. Intermittent or active hydrothermal eruption craters	7. Mud geysers	10. Fumaroles
High ↕ Low	2. Flowing springs	5. Mixed springs	8. Ejecting mud pots	11. Steaming ground
	3. Non flowing pools	6. Mixed pools	9. Mud pools	12. Heated ground
	Primary geothermal fluid	*Mixed/diluted geothermal fluid*	*Mixed/diluted steam heated fluid*	*Steam Fed*
Geothermally-influenced aquatic habitat				
Geothermal habitat on heated/acid dry ground				
Habitat dependent on geothermally-altered atmosphere overlays all types (warm air, frost-free)				

Figure 7.   A schematic representation of surface geothermal features (BOPRC 2014, after Scott 2012). Note the inclusion also of three broad categories of habitat (atmosphere, aquatic and heated ground).
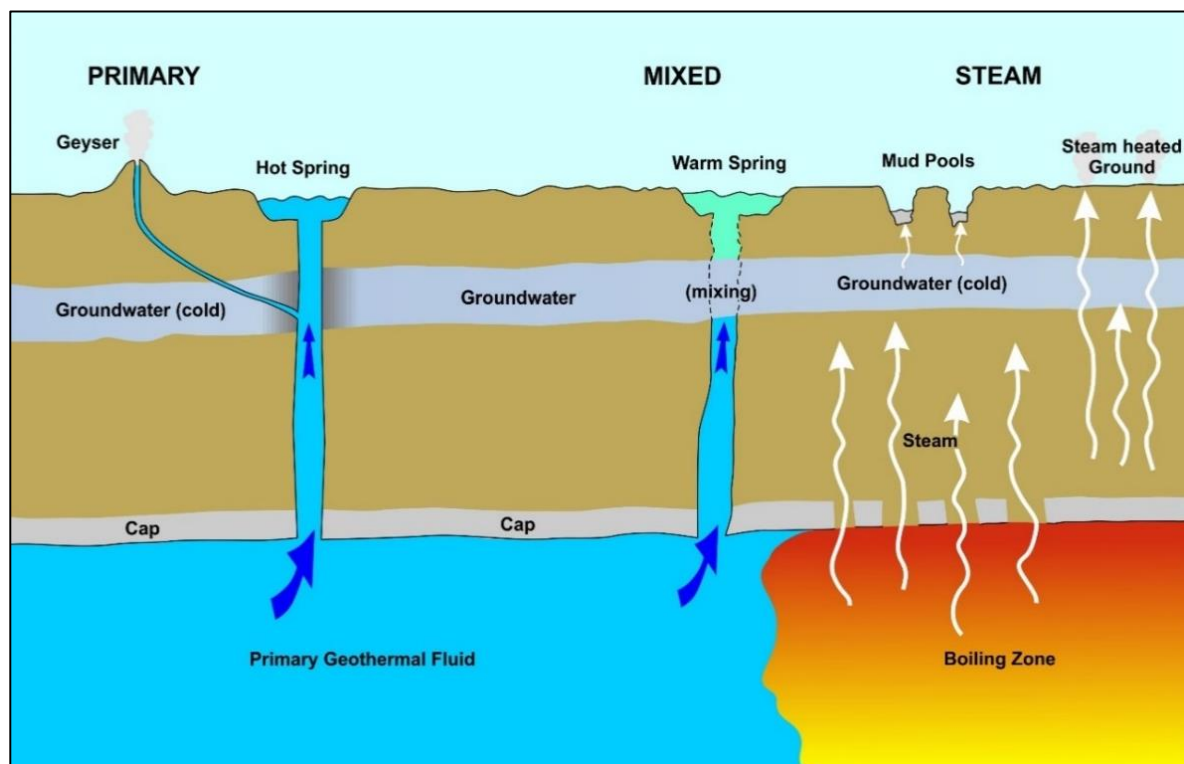
Figure 8.   Schematic relationship between the various types of geothermal surface features and process's that support them.

Figure 9. Impacts of a small scale hydrothermal eruption in Rotorua City.

PROCEEDINGS OF THE 14TH ANZ YOUNG GEOTECHNICAL PROFESSIONALS CONFERENCE
14YGPC ROTORUA, NEW ZEALAND, 2ND – 5TH NOVEMBER 2022

271

Okataina Volcanic Centre

Okataina Volcanic Centre (OVC) is located east of Rotorua city and south-west of Kawerau (Figures 10, 11). OVC consists of a series of vents along two lineations, magma has erupted from multiple vents along both lineation's (Nairn, 1989, 2002). OVC has undergone some very large and explosive eruptions, which have caused pyroclastic flows and deposited large amounts of ash and pumice over the Bay of Plenty. Historically, in 1886 Mount Tarawera underwent a short but explosive basalt eruption (Figures 16, 17), depositing scoria and mud across the Bay of Plenty and blocking the outlet to Lake Tarawera, which subsequently caused a dam-break flood that flowed through the Kawerau area in November 1904 (Nairn 1979, 1986 2002; Nairn et. al 2001, 2003; Leonard et. al 2002).
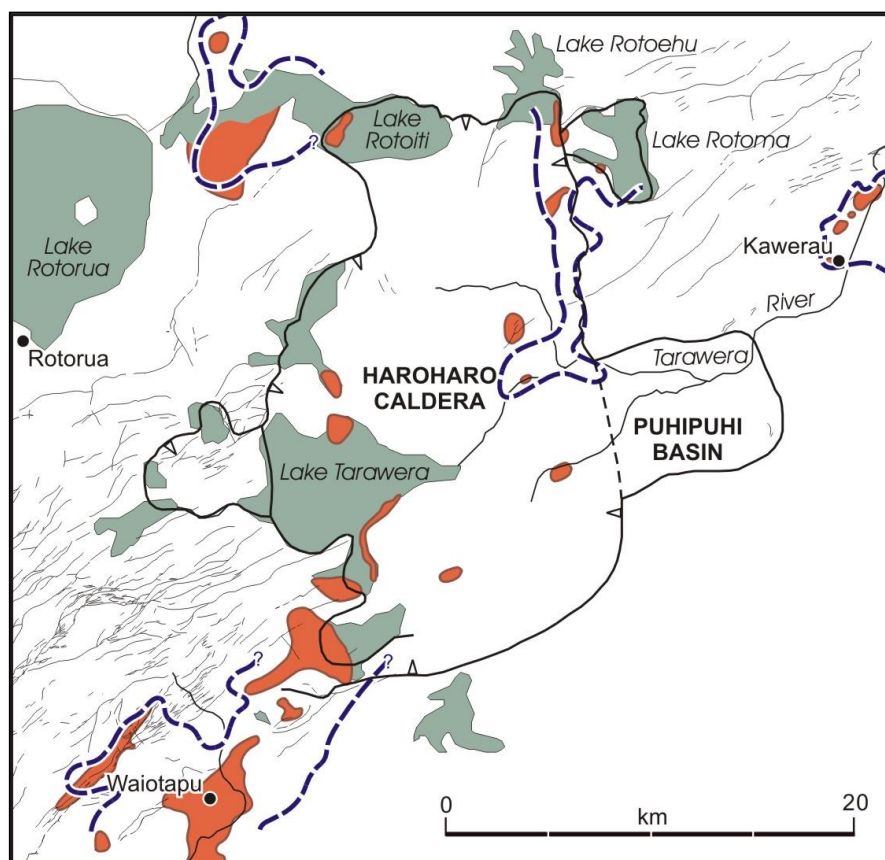

Figure 10.   Simplified structure map of the Okataina Volcanic Centre, showing the caldera boundary (black), major faults (grey) and geothermal systems (orange). After Nairn 2002.

The topography and lakes of the Rotorua District are controlled by the activity from the Okataina Volcanic Centre (Figure 10, 11). Many of the lakes are trapped as moats around the caldera edges (Rotoiti, Tarawera, Okataina, Blue and Green Lakes) while others are part of eruption sources/craters (Rotoma, Okareka) and others form behind lava flows which have dammed valleys (Rotoehu, Green Lake).

The Okataina Volcanic Centre has erupted about 80 km^3 of lava and pumice in the last 22,000 years (Table 1; Figure 11). A very active volcano system.
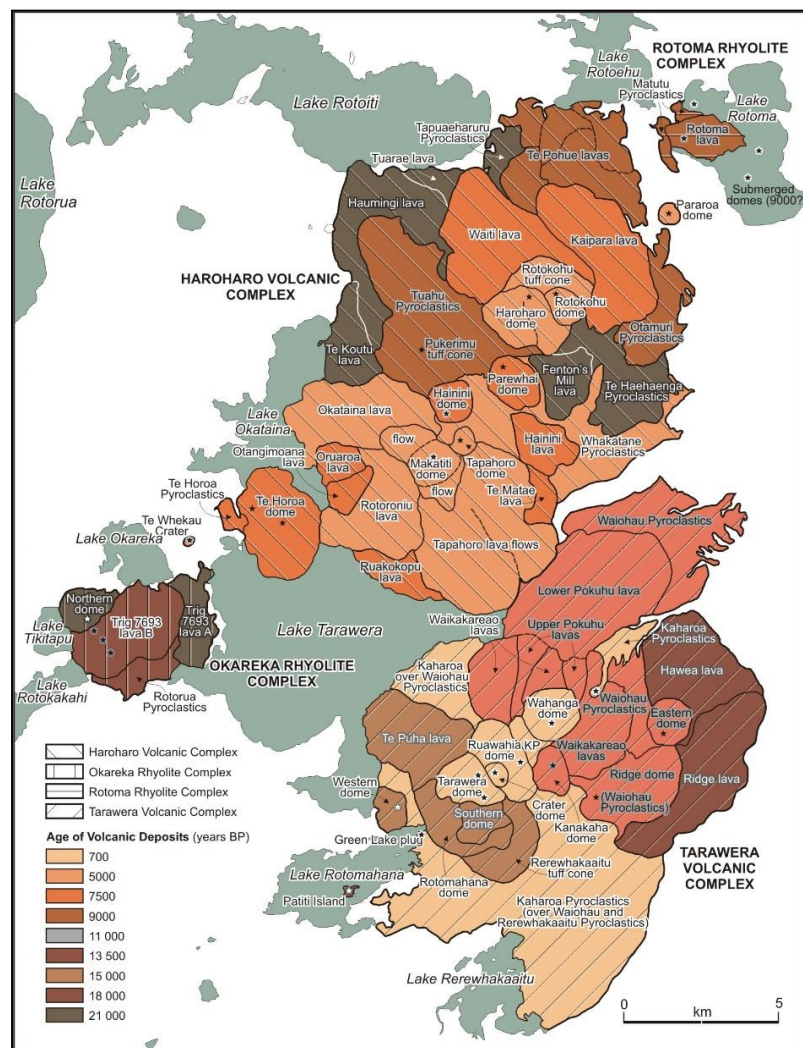
Figure 11. Simplified geological map of the Okataina Volcanic Centre, showing the ages of the major lava domes (after Nairn 2002).

Table 1. Sequence of OVC eruptions and volumes (after Nairn 2002).

Eruptive Episode	Age (ka)	Lava Volume km³	Pumice Volume km³
Tarawera	1886 AD	-	2
Kaharoa	0.7	2.5	5
Rotokawawau	3.4	-	0.7
Whakatane	5	9	10
Mamaku	7.5	15	6
Rotoma	9	2	13
Waiohau	11	4	15
Rotorua	13.5	1	7
Rerewhakaaitu	15	2	6
Okareka	18	5	6
Te Rere	21	10	5

PROCEEDINGS OF THE 14TH ANZ YOUNG GEOTECHNICAL PROFESSIONALS CONFERENCE
14YGPC ROTORUA, NEW ZEALAND, 2ND – 5TH NOVEMBER 2022

273

Earthquake Flat volcano

On the south western boundary of the Okataina Volcanic Centre lies Earthquake Flat volcano (Figure 12). About 50 km^3 of unwelded ignimbrite was erupted from here about 60,000 years ago. This is a typical example of an explosive rhyolite volcano, low angle cone, shallow summit crater.

Figure 12. Aerial view of Earthquake Flat Volcano, looking north northwest towards Rotorua.

FAULTING

The Taupo Volcanic Zone is an area of crustal extension. It is characterised by numerous normal faults (Villamor et. al 2001, 2011). These are best seen in the Ngakuru and Waikite Valleys and north east of Earthquake Flat (Figures 13, 14 and 15). Spreading of the TVZ is happening at about 7-9 mm/yr and subsidence is at about the same rate. The largest Fault structures are the Paeroa, Ngapouri, Tumunui, Whirinaki and Horohoro.

None of these fault structures can be traced into the Okataina Volcanic Centre or directly align with the vents within the caldera. However we do see faulting associated with the eruptive episodes (Figure 14, 15).
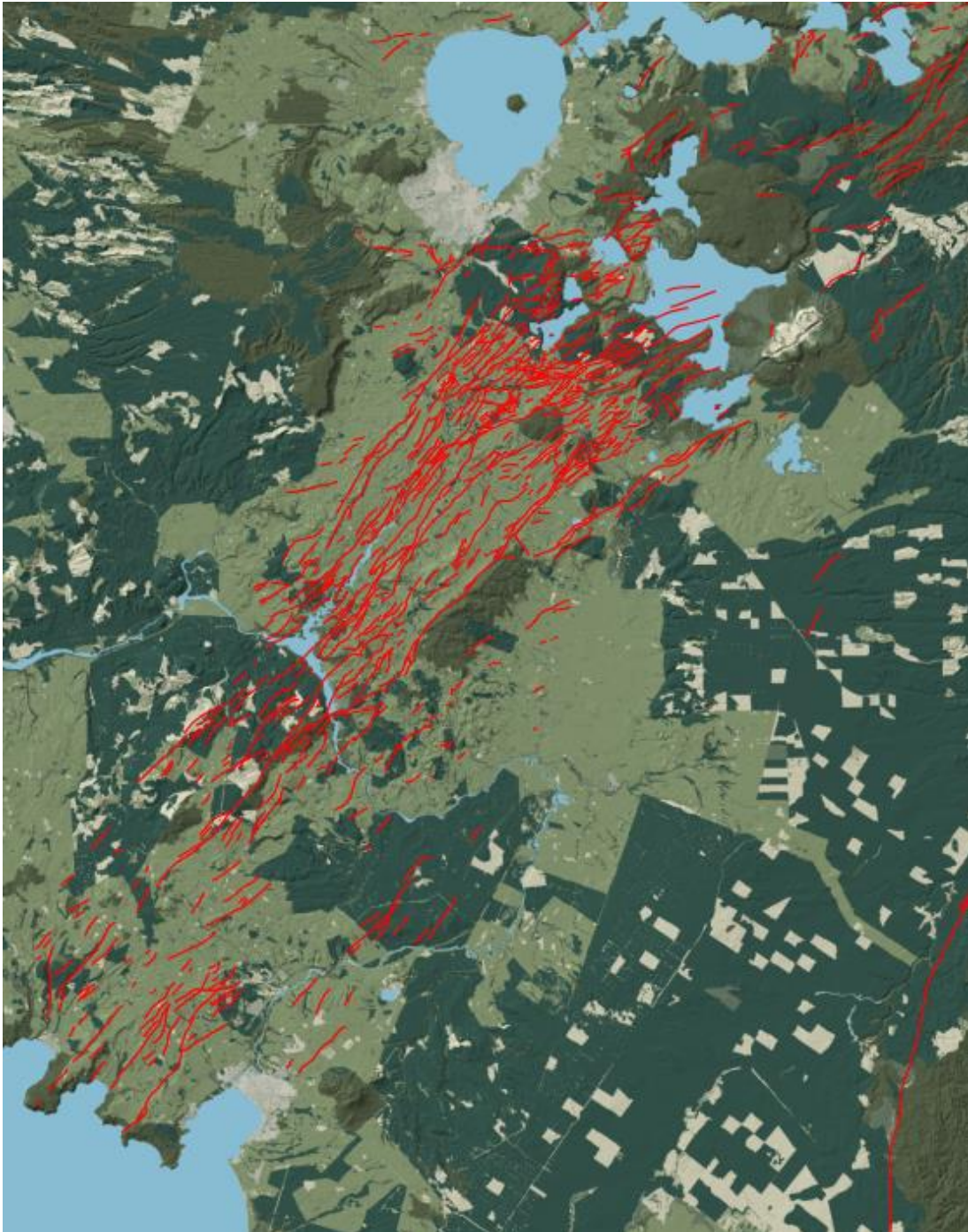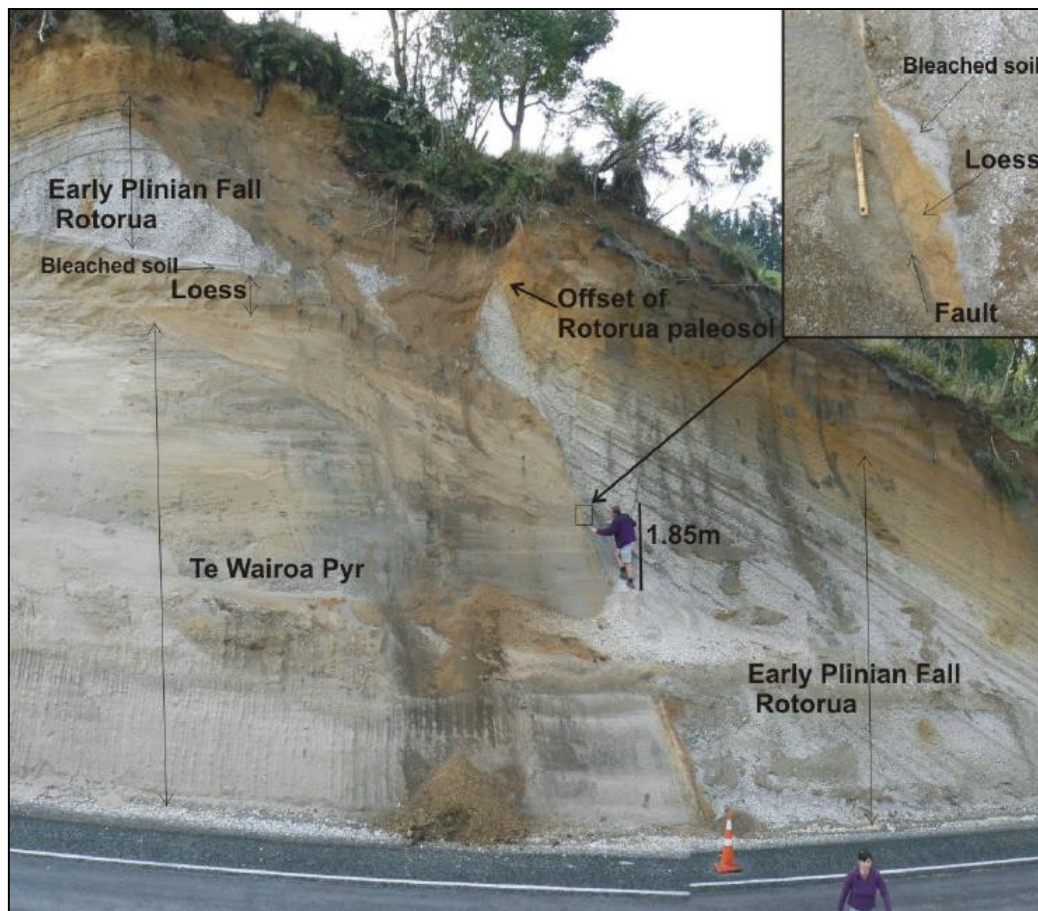

Figure 13. Map showing the faulting in the Rotorua-Taupo area. After NZ Active Faults database.

PROCEEDINGS OF THE 14TH ANZ YOUNG GEOTECHNICAL PROFESSIONALS CONFERENCE
14YGPC ROTORUA, NEW ZEALAND, 2ND – 5TH NOVEMBER 2022

275

Figure 14.   Exposure of the Opawhero Fault on Tarawera Road, showing the large displcemnt (~ 6m) of the Rotorua ash (13.5 ka).


Figure 15.   Active fault scarp on Waimangu Loop Road (Earthquake Flat).

Tarawera-Waimangu-Rotomahana

The Okataina Volcanic Centre is the most recently active one in the TVZ with pyroclastic and dome building events occurring about 650 years ago within the Tarawera complex (Nairn et al., 2003, Leonard et. al 2002). However, the youngest event was the 1886 basaltic eruption from a south-west trending line of vents, extending from the summit of Mt. Tarawera to the Waimangu Valley (Nairn 1979, 2002).

The Waimangu-Rotomahana hydrothermal system is located along the southern margin of the Okataina Volcanic Centre (Figures 16, 17).
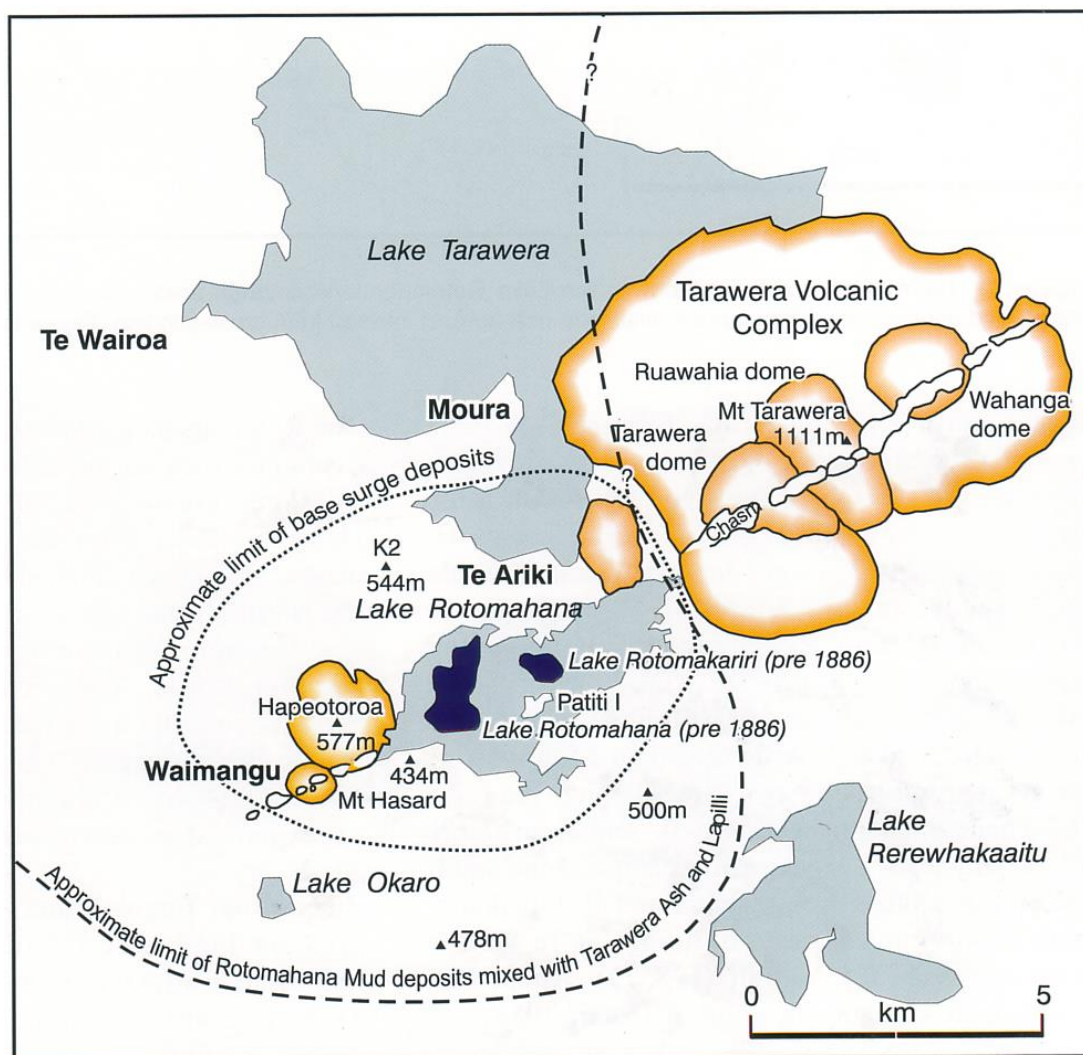
Figure 16. Map of the Tarawera-Rotomahana-Waimangu area showing the 1886 rift, Tarawera domes, limits of surge and airfall deposits and sites of pre and post eruption lakes (after Nairn, 2002).

PROCEEDINGS OF THE 14TH ANZ YOUNG GEOTECHNICAL PROFESSIONALS CONFERENCE
14YGPC ROTORUA, NEW ZEALAND, 2ND – 5TH NOVEMBER 2022

277

Figure 17.   View along the Tarawera vent lineation from Waimangu, across Lake Rotomahana, to Tarawera and Mt Edgecumbe. Photo D.L. Homer.

Volcanic Hazards

Hazard maps (Figure 18) and scenarios have been developed for Okataina Volcanic Centre (Johnston and Nairn, 1993; Scott and Nairn, 1998) and it is noted that a number of smaller settlements are located within destructive volcanic hazard areas (e.g. Lake Okareka, Lake Tarawera). Hazards expected from OVC include ash fall, pyroclastic flows, lava flows,

hydrothermal eruptions, volcanic gases, lahars and floods and volcanic earthquakes. The types of hazards expected at OVC are often compared with those experienced during and after the 1991 Pinatubo eruption in the Philippines.
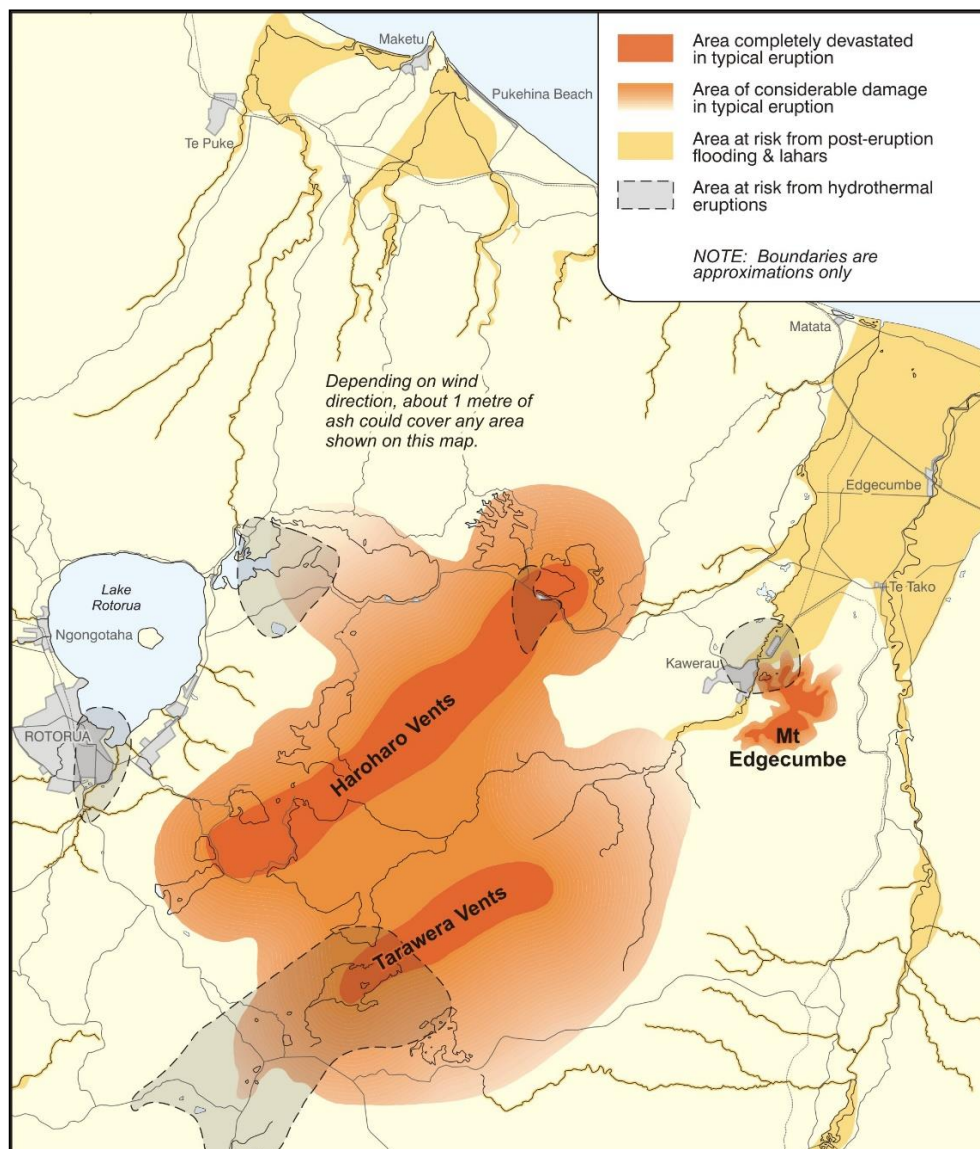
Figure 18. Volcanic hazard map of the Okataina Volcanic Centre (in Nairn, 2002 and adapted from Scott and Nairn, 1998).

References

Brooker, M.R.; Houghton, B.F.; Wilson, C.J.N.; Gamble, J.A. 1993. Pyroclastic phases of a rhyolitic dome-building eruption: Puketarata tuff ring, Taupo Volcanic Zone, New Zealand. Bulletin of Volcanology, 55(6): 395-406

Chambefort I, Lewis B, Wilson CJN, Rae A, Coutts C, Bignall G, Ireland T, 2014. Stratigraphic and structure of the Ngatamariki geothermal system from New zircon U-Pb geochronology: Implications for Taupo Volcanic Zone evolution. Journal of Volcanic and Geothermal Research. 274:51-70.

PROCEEDINGS OF THE 14TH ANZ YOUNG GEOTECHNICAL PROFESSIONALS CONFERENCE
14YGPC ROTORUA, NEW ZEALAND, 2ND – 5TH NOVEMBER 2022

279

Houghton, B.F., Wilson, C.J.N., McWilliams, M., Lanphere, M.A., Weaver, S.D., Briggs, R.M. and Pringle, M.S., 1995. Chronology and dynamics of a large silicic magmatic system: Central Taupo Volcanic Zone, New Zealand: Geology, v. 23: 13-16.

Johnston, D.M.; Nairn, I.A. 1993. Volcanic impacts report: the impact of two eruption scenarios from the Okataina Volcanic Centre on the population and infrastructure of the Bay of Plenty, New Zealand. Whakatane: Environment BOP. Resource planning publication / Bay of Plenty Regional Council 93/6. vi, 153 p.

Leonard, G.S., Cole, J.W., Nairn, I.A. and Self, S., 2002. Basalt triggering of the c. AD 1305 Kaharoha rhyolite eruption, Tarawera Volcanic Complex, New Zealand. Jour. Volc. & Geothermal Research 115: 461-486.

Nairn, I.A., 1979. Rotomahana-Waimangu eruption, 1886: base surge and basalt magma: NZ Jour. Geology and Geophysics, v. 22: 363-378.

Nairn, I.A., 1986. Volcanism in the Taupo Volcanic Zone: Part 2. Okataina Volcanic Centre: in Guide to the Active Epithermal Systems and Precious Metal Deposits of New Zealand (eds R.W. Henley, J.W. Hedenquist, P.J. Roberts) Monograph Series Mineral Deposits, Gebruder Borntraeger, Berlin, n. 26: 29-36.

Nairn, I.A., 1989. Mt Tarawera: Geological Map of New Zealand, 1:50 000, Sheet V16 AC.

Nairn, I.A., 2002. Geology of the Okataina Volcanic Centre, 1:50 000. Institute of Geological and Nuclear Sciences Geological Map 25.

Nairn, I.A., Self, S., Cole, J.W., Leonard, G.S. and Scutter, C., 2001. Distribution, stratigraphy and history of proximal deposits from the c. AD 1305 Kaharoa eruptive episode at Tarawera Volcano, New Zealand. NZ Jour. Geol. & Geophys. V44: 467-484.

Nairn, I.A., Shane, P.R., Cole, J.W., Leonard, C.J., Self, S., Pearson, N., 2003. Rhyolite magma processes of the ~AD 1315 Kaharoa eruption episode, Tarawera volcano. JVGR 2732: 1-30.

Scott, B.J.; Cody, A.D. 2000. Response of the Rotorua geothermal system to exploitation and varying management regimes. Geothermics, 29(4/5): 573-592

Scott, B.J.; Nairn, I.A. 1998. Volcanic hazards: Okataina volcanic centre. Scale 1:100,000. [Whakatane]: Bay of Plenty Regional Council. Resource planning publication / Bay of Plenty Regional Council 97/4. 1 map

Villamor, P.; Berryman, K.R. 2001 A Late Quaternary extension rate in the Taupo Volcanic Zone, New Zealand, derived from fault slip data. New Zealand Journal of Geology and Geophysics, 44(2): 243-269.

Villamor, P.; Berryman, K.R.; Nairn, I.A.; Wilson, K.J.; Litchfield, N.J.; Ries, W. 2011 Associations between volcanic eruptions from Okataina Volcanic Center and surface rupture of nearby active faults, Taupo rift, New Zealand: insights into the nature of volcano-tectonic interactions. Geological Society of America Bulletin, 123(7/8): 1383-1405.

Wilson, C.J.N., Rogan, A.M., Smith, I.E.M., Northey, D.J., Nairn, I.A., Houghton, B.F., 1984. Caldera volcanoes of the Taupo Volcanic Zone, New Zealand: Jour. Geophys. Res., v. 89 B10: 8463-8484.

Wilson, C.J.N., Houghton, B.F., McWilliams, M.O., Lanphere, M.A., Weaver, S.D. and Briggs, R.M., 1995. Volcanic and structural evolution of Taupo Volcanic Zone, New Zealand: A review. Jour. Volc. Geothermal Res., v. 68: 1-28.

Wood, C.P., 1995. Calderas and geothermal systems in the Taupo Volcanic Zone, New Zealand. In proceedings of the World Geothermal Co

NOTES

PROCEEDINGS OF THE 14TH ANZ YOUNG GEOTECHNICAL PROFESSIONALS CONFERENCE
14YGPC ROTORUA, NEW ZEALAND, 2ND – 5TH NOVEMBER 2022

281